Studies in Antarctic Meteorology (1966)

Pages
242

Size
7 x 10

ISBN
0309359708

Morton J. Rubin, Editor; American Geophysical Union; National Research Council

Volume 9

ANTARCTIC
RESEARCH
SERIES

Studies in Antarctic Meteorology

Morton J. Rubin, *Editor*

Published with the aid of a grant from the National Science Foundation

PUBLISHER
AMERICAN GEOPHYSICAL UNION
OF THE
National Academy of Sciences–National Research Council
Publication 1482
1966

Volume 9 | ANTARCTIC RESEARCH SERIES

STUDIES IN ANTARCTIC METEOROLOGY

Morton J. Rubin, *Editor*

Suite 506, 1145 Nineteenth Street, N. W.
Washington, D. C. 20036

Library of Congress Catalog Card No. 66-65798

List Price, $14.00

Printed by
The William Byrd Press, Inc.
Richmond, Virginia

THE ANTARCTIC RESEARCH SERIES

During the International Geophysical Year discussions were held among geophysicists, biologists, and geologists aimed at developing a medium for the publication of the papers resulting from the intensive research work being done in Antarctica. The Antarctic Research Series is designed to provide this medium, presenting authoritative work with uniformly high scientific and editorial standards from leading scientists engaged in antarctic research.

In a sense the series continues a tradition dating from the earliest days of geographic exploration and scientific expeditions—the tradition of the expeditionary volumes which set forth in rich detail everything that was seen and studied. But in much of the present antarctic work one expedition blends into the next, and it is no longer scientifically meaningful to separate them. However, antarctic research in all disciplines has a large degree of coherence and deserves the modern counterpart of the expeditionary volumes of past decades and centuries.

Papers appearing in the series represent original contributions too lengthy or otherwise inappropriate for publication in the standard scientific journals. The material published is directed not only to scientists actively engaged in the work but to graduate students and scientists in closely related fields as well. The series will serve as a source of information both for the specialist and for the layman versed in the biological and physical sciences. Many of the early volumes are cohesive collections of research papers grouped around a central theme. An editor for each book is drawn from the discipline it represents, as are the reviewers on whom each editor relies.

Early in 1963 the National Science Foundation made a grant to the American Geophysical Union to initiate the series, and a Board of Associate Editors was appointed to implement it. To represent the broad nature of the series, the members of the Board were chosen from all fields of antarctic research. At the present time they include Eugene L. Boudette, representing geology and solid Earth geophysics; Martin A. Pomerantz, aeronomy and geomagnetism; A. P. Crary, seismology and glaciology; George A. Llano, botany and zoology; Waldo L. Schmitt, marine biology and oceanography; and Morton J. Rubin, meteorology. Earlier members of the Board, since resigned, were Harry W. Wells and Jarvis B. Hadley. AGU staff members responsible for the series are Judith S. McCombs, managing editor, and Marie L. Webner, style editor.

MORTON J. RUBIN
Chairman, Board of Associate Editors
Antarctic Research Series

ANTARCTIC RESEARCH SERIES

American Geophysical Union

Volume 1
BIOLOGY OF THE ANTARCTIC SEAS
Milton O. Lee, *Editor*

Volume 2
ANTARCTIC SNOW AND ICE STUDIES
Malcom Mellor, *Editor*

Volume 3
POLYCHAETA ERRANTIA OF ANTARCTICA
Olga Hartman

Volume 4
GEOMAGNETISM AND AERONOMY
A. H. Waynick, *Editor*

Volume 5
BIOLOGY OF THE ANTARCTIC SEAS II
George A. Llano, *Editor*

Volume 6
GEOLOGY AND PALEONTOLOGY OF THE ANTARCTIC
Jarvis B. Hadley, *Editor*

Volume 7
POLYCHAETA MYZOSTOMIDAE AND SEDENTARIA OF ANTARCTICA
Olga Hartman

Volume 8
ANTARCTIC SOILS AND SOIL FORMING PROCESSES
J. C. F. Tedrow, *Editor*

Volume 9
STUDIES IN ANTARCTIC METEOROLOGY
Morton J. Rubin, *Editor*

PREFACE

Since the beginning of the International Geophysical Year in 1957, a new phase of scientific exploration has turned Antarctica into a unique laboratory. Earlier concepts of Antarctica had been mainly preliminary, even confused, having been based upon intermittent, noncontemporaneous, and insufficient observations limited mainly to the periphery of the continent. Through programs supported by international activity, a coordinated and well-founded effort has been directed to the observation, analysis, and interpretation of a broad spectrum of geophysical and biological phenomena and processes. Man began to open up new horizons in his quest for understanding and mastery of Nature.

For meteorology, as for other scientific disciplines, Antarctica has provided conditions not found elsewhere on this planet: a high circumpolar continent, very low ambient temperatures, a seemingly limitless expanse of snow and ice almost completely devoid of exposed rock, soil, and vegetation. Even before the IGY it was realized that these circumstances would provide an unexcelled opportunity to study atmospheric turbulence and energy exchanges, radiative fluxes, snow drift, precipitation mechanisms and accumulation, and other significant physical and dynamical phenomena. The continuing and varied observational and analytical studies soon began to clarify the earlier concepts, substantiating some and correcting others.

This volume is the first collection of meteorological studies in the *Antarctic Research Series*. As the reader will see, they are based upon data obtained by laborious and exacting field work, some of it by the authors themselves. These illustrate clearly, as do other recent studies, the magnitude of the advance of knowledge and the extent to which our understanding of antarctic meteorological phenomena and processes has developed in a few short years.

The first paper (by Lettau) describes and explains a rare phenomenon on the polar plateau, katabatic flow. It is based upon data obtained from a micrometeorological program at South Pole, the broader results of which are presented in the second paper (by Dalrymple, Lettau, and Wollaston). In that paper the authors discuss the features of the wind and temperature profiles, surface friction, eddy flux, heat flux, and the surface energy budget. The third paper (by Budd) extends the theory of steady-state turbulent snow drift to snow consisting of particles of different sizes. In the fourth paper, Budd, Dingle, and Radok describe the techniques used in a study of 129 snow drift gagings at Byrd station and analyze the results in terms of wind profiles, roughness profiles, and snow surface texture.

The fifth paper (by Vickers) is an attempt to determine the distribution of snow accumulation in western Antarctica and to relate it to synoptic meteorological factors; it is a good example of the interrelationship between glaciological and meteorological phenomena. In the sixth paper, Bull describes the climatological characteristics of the ice-free Wright and Victoria valley systems, a relatively unique phenomenon in Antarctica, and accounts for the continued ice-free nature of the region. Dalrymple, in the last paper, presents a regional climatic classification for the interior of Antarctica and discusses the micrometeorology of the region.

MORTON J. RUBIN

A CASE STUDY OF KATABATIC FLOW ON THE SOUTH POLAR PLATEAU

HEINZ H. LETTAU

University of Wisconsin, Madison

Abstract. Micrometeorological wind and temperature profile data obtained by Dalrymple at Amundsen-Scott station during 1958 indicate that katabatic flow on the gently sloping central Antarctic Plateau can occur, but that it is an extremely rare phenomenon. An interesting case of katabatic flow structure (with the speed maximum at about 4 meters above ground level) on September 17, 1958, is discussed and analyzed. Hourly means of low-level wind and temperature profiles were found to correspond, at a surprisingly close degree, with distributions predicted by Prandtl's elementary theory of steady katabatic winds. The surface energy budget under katabatic flow conditions is investigated. There are indications of an inherent instability of this flow type. The breakdown of katabatic flow structure was found to be accompanied by an abrupt temperature decrease (of about 4°C) in the air layer from 2 to 8 meters above the ground. It is shown that the probable cause of such abrupt changes in air temperature (decreases as well as, on other occasions, increases) is a local mesoscale convergence (or divergence) in the low-level wind field, and the resulting vertical advection of heat.

1. INTRODUCTION

During the period February through November 1958, an extensive program of micrometeorological wind and temperature profile observations was carried on by the U. S. Quartermaster Corps at Amundsen-Scott station at 90°S. A data report describing the instrumentation and the observation schedule was published by *Dalrymple* [1961]. For an analysis of the dynamical structure of micrometeorological wind and temperature profiles under the prevailing condition of strong to moderate inversion and for an evaluation of the energy budget of the south polar snow surface, see *Dalrymple et al.* [1966].

In the vicinity of 90°S the Antarctic Plateau is remarkably flat and approximates an inclined plane. From various traverses that have arrived at, or departed from, the south pole, *Dalrymple et al.* [1966, section 4] have derived that, for radial distances of approximately 200 km from Amundsen-Scott station, the average ascendent vector of the terrain is 1.76 ± 0.26 m/km, directed toward 152° ± 23° longitude east of Greenwich. In the practical terminology of polar synoptic analysis this direction is referred to as SSE.

A study of surface wind direction frequencies for the period of Dalrymple's micrometeorological observations (February through November 1958) at Amundsen-Scott station showed that about 50% of the time the wind direction was NNE to NE, whereas SSE winds occurred only 0.1% of the time, and all wind directions from SE to S had a relative frequency of no more than 1.3%. Thus, we must conclude that truly downslope motion, which is the prerequisite for katabatic flow, appears to be extremely rare on the central Antarctic Plateau. Consistent with this is another result derived by *Dalrymple et al.* [1966, section 4]. They found that, at the south pole, the difference vector between the wind velocity at the top of the inversion layer and the wind velocity in the surface layer gives evidence not only of a systematic frictional backing of wind direction with height, but also of an additional prevailing tendency toward a cross-slope motion. In other words, there appears to exist a physical cause that tends to make the air motion in the surface layer an ENE wind regardless of the velocity vector in the free atmosphere.

An obvious explanation presents itself in the thermal wind effect, or the geostrophic balance between a force due to gravity and a horizontal density gradient, and the Coriolis force, which accompanies the resulting equilibrium motion of the air. Namely, the prevailing condition of a substantial ground-inversion layer of several 100 meters thickness, on a sloping boundary, must of

necessity mean that the temperature increase normal to the snow surface sets up a horizontal temperature increase in the air away from higher ground. The large horizontal extent of the sloping plateau provides sufficient opportunity for the Coriolis force to develop the balance, because, at a mean speed of 5 m/sec, it would take nearly a full day to traverse a distance of 400 km. In conclusion, it can be said that the surface wind distribution at the south pole is primarily caused by geostrophic motion above inversion height, which is modified by a prevailing thermal wind (due to systematic horizontal density gradients in the sloping inversion layer) as well as by surface friction.

However, among the rare cases of surface winds from SSE at Amundsen-Scott station, the observations in the early GMT hours on September 17, 1958, are interesting for two reasons. First, it appears that during this limited period the large-scale pressure gradient was exceptionally weak, which permitted the development of a truly katabatic wind on the antarctic polar incline. It will be shown that, for several hours, the observed micrometeorological profiles of wind speed and air temperature corresponded very closely to a simple theoretical model of steady katabatic flow. Second, the breakdown of this flow type was accompanied by an abrupt lowering of air temperature, which amounted to approximately 5°C cooling at the 8-meter level. It will be shown that the sudden temperature change can be explained by local or mesoscale convergence of the low-level air flow, which produced a piling-up of cold surface air. Correspondingly, sudden warming, also observed occasionally at Amundsen-Scott station, is probably caused by local divergences of the low-level air flow, i.e., under both conditions by vertical advection of heat.

It can also be mentioned that micrometeorological observations made by Dalrymple in 1957 at Little America V station (78°10′S, 162°13′W) indicate a relatively high frequency of katabatic winds. To establish the procedure for an appraisal of the significance of katabatic motion for energy budget studies, a review of a theoretical model of katabatic flow appears to be in order.

2. THEORETICAL BACKGROUND

A relatively complete theoretical model of steady katabatic (or anabatic) air flow was presented by L. Prandtl in 1942 in his renowned textbook *Fuehrer durch die Stroemungslehre;* reference can also be made to *Defant* [1951], who has reviewed Prandtl's theory and extended it to include nonsteady cases. Both authorities, however, have treated only a laminar flow problem and have assumed for the mathematical solution of the problem that the diffusivity of the air is independent of height. In the following the basic theory will be developed in a more general form, so that an extension to turbulent flow is possible, i.e., under consideration of height dependency of eddy diffusivity.

The general assumption underlying the model of katabatic flow is that gravity (g) is the only external acceleration. As in other types of gravity-induced currents, the Boussinesq-Rayleigh assumption is introduced; i.e., the air density (ρ) is considered a variable only in the product $g\rho$ and assumed to be a constant (ρ_0) in all other terms of the fluid dynamics equations. In comparison with the intensity of boundary heating or cooling rates ($\pm Q_0$) and the resulting heat advection and heat diffusion, the effect of any internal heat source or sink (especially, effects of infrared radiation-flux divergence, or heat generated by dissipation of mechanical energy) is considered negligible. Then, the equations of continuity, momentum, and energy are

$$\nabla \cdot \mathbf{V} = 0 \tag{1}$$

$$\rho_0 \, d\mathbf{V}/dt + \nabla p + \mathbf{k} g\rho = \mathbf{F} \tag{2}$$

$$d\theta/dt = \partial\theta/\partial t + \mathbf{V} \cdot \nabla\theta = H/c_p\rho_0 \tag{3}$$

where $\mathbf{V}$ = vector of motion, p = atmospheric pressure, $\mathbf{k}$ = vertical unit vector, $\mathbf{F}$ = vector of frictional force per unit volume, θ = potential temperature, c_p = specific heat of air, and H = rate of heating per unit volume, by the process of heat diffusion.

The discussion will be restricted to two-dimensional motion in the vertical plane parallel to the fall line of a uniformly flat slope. Let $\mathbf{V}$ be independent of the lateral horizontal, or cross-wind, coordinate. In order to eliminate pressure gradient effects, we take the curl of equation 2 and consider the lateral component (η) of vorticity, whereupon (2) yields the following equation for the vorticity in the x, z plane:

$$\rho_0 \, d\eta/dt - g \, \partial\rho/\partial x = \mathbf{j}(\nabla \times \mathbf{F}) \tag{2'}$$

when $\mathbf{j}$ = unit vector in the lateral horizontal direction.

We want to apply the system of equations to steady-state conditions in potential temperature and lateral vorticity, i.e., for $\partial\theta/\partial t = 0$ and $\partial\eta/\partial t = 0$. Moreover, it will be assumed that the vector of motion is completely described by the component parallel (or antiparallel) to the fall line of the slope.

We introduce a new system of rectangular coordinates, n (normal to the slope and positive into the air) and s (parallel to the slope and positive toward higher ground). Let the slope inclination be given by the constant angle ϵ. This angle is assumed to be sufficiently small so that $\tan\epsilon = dz/dx \approx \epsilon$ and, also, $\sin\epsilon = dz/ds \approx \epsilon$, when ϵ is expressed in radians. It follows from simple geometry that, together with $dz = \epsilon\, ds$, we have also that $dn = -\epsilon\, dx$. This means that in equation 2′ we may write $-\epsilon\,\partial\rho/\partial n$ in place of $\partial\rho/\partial x$. Considering that the air moves parallel to the fall line of the slope, the wind speed is $ds/dt = u$. It is assumed that u is only a function of the independent variable n, so that $\eta = \partial u/\partial n$ and $\mathbf{V}\cdot\nabla\eta = 0$. The frictional force will be acting parallel to the fall line, or to the vector of motion, and its intensity is given by $\partial\tau/\partial n$, where τ = shearing stress. Thus, in equation 2′, $\mathbf{j}(\nabla \times \mathbf{F}) = \partial^2\tau/\partial n^2$; in equation 3 we have, correspondingly, that $H = -\partial Q/\partial n$, where Q = heat flux in the normal direction, positive when directed upward.

With all the above assumptions the system of equations 1 to 3 can be reformulated as

$$\partial u/\partial s = 0 \tag{4}$$

$$g\epsilon\,\partial\rho/\partial n = \partial^2\tau/\partial n^2 \tag{5}$$

$$c_p\rho_0 u\,\partial\theta/\partial s = c_p\rho_0\epsilon u\,\partial\theta/\partial z = -\partial Q/\partial n \tag{6}$$

Concerning the temperature field, Prandtl assumed that potential temperature is initially a linear function of height (z) and that a disturbance (ϑ), which is exclusively a function of the normal coordinate (n), is superimposed so that, with γ = constant > 0,

$$\theta = \theta_0 + \gamma z + \vartheta(n) \tag{7}$$

Furthermore, consistent with the above restrictions it is assumed that the density disturbance is related to the temperature disturbance by the simplified version of the equation of state $d\rho/\rho_0 = -d\theta/\theta_0$, where θ is in degrees Kelvin. Thus, equations 5 and 6 become

$$-\epsilon\rho_0 g\,\partial\theta/\partial n = \theta_0\,\partial^2\tau/\partial n^2 \tag{8}$$

$$c_p\rho_0 u\epsilon\gamma = -\partial Q/\partial n \tag{9}$$

The physical meaning of equation 5 or 8 is that vorticity diffusion (as represented by the right-hand side) is balanced by vorticity generation through gravity and the density-temperature disturbance (as represented by the left-hand side). The physical meaning of equation 9 is that heat advection balances heat diffusion. Note that the expression of heat advection on the left-hand side of equation 9 is exact so long as air motion is actually restricted to being downslope or upslope without having any component normal to the ground surface. In as much as $\partial\vartheta/\partial s = 0$ and $u = ds/dt$, only the initial vertical temperature gradient (γ) contributes to the advection process, so that $\mathbf{V}\cdot\nabla\theta = u\epsilon\gamma$. Obviously, any disturbance that will deflect the vector of motion from the direction parallel to the slope will result in advection terms involving ϑ and its gradient. Such disturbances of katabatic flow can actually occur, as will be shown in section 6.

Assuming gradient-type diffusion, we have as the defining equations of the effective diffusivities, K for momentum, and K_H for heat,

$$\tau = \rho_0 K\,\partial u/\partial n \tag{10a}$$

$$Q = -c_p\rho_0 K_H\,\partial\theta/\partial n \tag{10b}$$

Now, we multiply both sides of equation 8 by $c_p K_H$ and consider equation 10b; then, we differentiate equation 9 once with respect to the independent variable n, multiply both sides of the resulting relation by K, and consider equation 10a. After slight rearrangement of terms the following is obtained:

$$\epsilon g Q/c_p\theta_0 = K_H\,\partial^2\tau/\partial n^2 \tag{11a}$$

$$\epsilon c_p\gamma\tau = -K\,\partial^2 Q/\partial n^2 \tag{11b}$$

Here, shearing stress and heat flux are the dependent variables, the normal distance from the sloping boundary is the independent variable, and the diffusivities can be either height-dependent coefficients or constants.

It is useful to transform the variables and the equations into dimensionless forms. Let X denote a parameter having the physical dimension of length, so that $n/X = \xi$ is a dimensionless form of the independent variable. Differentiations with respect to ξ will be denoted by primes. Dimensionless expressions of the dependent variables, including heat flux (q), shearing stress (r), wind speed (U),

and temperature disturbance (W), and also a dimensionless momentum diffusivity (y) and heat diffusivity (y_H) are defined by the following identities:

$$q = Q/Q_0 \tag{12a}$$

$$r = \tau/\tau_0 \tag{12b}$$

$$U = u\rho_0 K_1/\tau_0 X \tag{13a}$$

$$W = c_p\rho_0\theta K_1/Q_0 X \tag{13b}$$

$$y = K/K_1 \tag{14a}$$

$$y_H = yP_1/P \tag{14b}$$

where $P = K/K_H$ = generalized Prandtl number, which may or may not be a function of ξ, and P_1 is its value at $\xi = 1$.

In addition to scale height X, two pairs of other scale or reference values are introduced in the system (12a) through (14b); the first pair consists of the boundary values of shearing stress (ground drag) and heat flux (rate of surface heating or cooling), τ_0 and Q_0, respectively; the second pair of scale values consists of K_1 which is the value of momentum diffusivity at $\xi = 1$ (or $n = X$), and P_1 which is the Prandtl number at $n = X$. Upon inserting the expressions for Q, τ, K, and K_H as given by (12a and b) and (14a and b) into equations 10a and b, the following interrelationships between the scale values Q_0, τ_0, K_1, and X are obtained:

$$X^4 = \theta_0 {K_1}^2/g\epsilon^2\gamma \tag{15}$$

$$Q_0/\tau_0 = c_p(\theta_0\gamma/g)^{1/2} \tag{16}$$

This produces dimensionless forms of equations 11a and 11b

$$q = y_H r'' \tag{17a}$$

$$r = -yq'' \tag{17b}$$

which can be referred to as the characteristic equations of the katabatic flow problem. The corresponding dimensionless forms of equations 10a and b, $r = yU'$ and $q = -y_H W'$, transform, with the aid of equations 17a and b, into

$$U' = r/y = -q'' \quad \text{or} \quad U - U_0 = -q' \tag{18a}$$

$$W' = -q/y_H = -r'' \quad \text{or} \quad W - W_0 = -r' \tag{18b}$$

where U_0 and W_0 are integration constants or boundary values to be determined later.

Thus, the problem is to solve the scalar system of two differential equations of second order (17a and b), which is equivalent to one scalar fourth-order differential equation

$$q = -y_H(yq'')'' \quad \text{or} \quad r = -y(y_H r'')'' \tag{19}$$

Note that equations 18a and b illustrate that dimensionless wind speed (U) is directly related to vertical divergence of heat flux (q'), and that dimensionless temperature disturbance (W) is directly related to the frictional force per unit volume, or the vertical momentum flux divergence (r'). Such interrelationships are typical for natural, or gravity-buoyancy-induced, flow of which katabatic wind is an interesting example.

Obviously, the solution depends exclusively on the analytical formulation of the height dependency of diffusivities, i.e., the ξ dependency of the functions $y(\xi)$ and $y_H(\xi)$. The simplest possible case, $y = y_1$ = constant = y_0 (or $y' = 0$), together with P = constant, results in the classical Prandtl solution as will be demonstrated in section 3.

It is highly interesting that, for constant Prandtl number (P = constant) but height-varying diffusivity ($y' = y_H' \neq 0$), the characteristic equations 19 of katabatic flow represent formally the same mathematical problem as the characteristic equations of the planetary boundary layer in a barotropic atmosphere. (See equations 3b in *Lettau* [1962a, p. 197].) In other words, the computation of vertical profiles of the two rectangular components of horizontal shearing stress in the barotropic (thermally neutral) planetary boundary layer corresponds exactly to the computation of the vertical profiles of unidimensional shearing stress and heat flux of katabatic motion in diabatic states. The classical solution (i.e., for $y = y_0 = y_1$ = constant) leads in the former case to the Ekman spiral. The mathematical structure of Prandtl's classical solution for the katabatic flow (see equations 22a and b) is, indeed, obviously closely related to the well-known Ekman-spiral solution.

In view of this similarity, it is immediately possible to apply to the katabatic flow problem any of the variety of known wind-spiral solutions reported in the literature, for a certain choice in the mathematical formulation of the function $y(\xi)$. For y being a linear or exponential function, or a power law of ξ, closed solutions exist and are given by Bessel functions (Hankel functions). For y being a quadratic function of ξ, the closed solution

is expressed by elementary functions and results in 'equiangular' spirals [*Lettau*, 1962*b*]. However, as was pointed out earlier (see *Lettau* [1962*a*, p. 197]), none of these solutions, or related solutions, using preconceived explicit formulations of $y(\xi)$, has produced satisfactory agreement with observational results concerning boundary layer structure, and similar shortcomings must be expected for katabatic flow structure.

The universal solution of atmospheric boundary layer flow presented by *Lettau* [1962*a*] rests essentially on the concept that the absolute value of the shearing velocity $(\tau/\rho)^{1/2}$ decreases monotonically with height, and enters as a factor in the formulation of the height-dependent eddy diffusivity for momentum. The other factor of K is a height-dependent length scale of turbulent eddies. This model has an inherent nonlinearity and cannot be applied directly to katabatic flow, because the typical feature here is that wind shear goes through zero at a relatively low level, $z^* = n^*$, whereas the structure of the temperature profile at such relatively close proximity to the ground indicates that heat conduction is finite and certainly not zero at this level. This requires that the thermal diffusivity of the air cannot be taken as being proportional to the local shearing velocity, which, in turn, may still be proportional to the local wind shear. In other words, an assumption must be made about a mathematical formulation of height dependency of the generalized Prandtl number. At the present time no universally accepted principle that could be used for a solution of this problem is known. On the other hand it is not unsound physically to expect that for the main layer of katabatic flow, i.e., in the stratum of air centered about the level of maximum wind speed, the diffusivities are, to a tolerable degree, independent of the distance from the ground. This is strictly true for laminar flow and molecular diffusivities; for turbulent flow the eddy diffusivities should be proportional to the molecular values. This condition was assumed by Prandtl, and it will be shown in the following sections that Prandtl's model leads to some acceptable results.

3. THEORETICAL MODELS OF KATABATIC FLOW

The transformation of the dimensional dependent and independent variables of the katabatic flow problem into nondimensional variables was achieved and defined in section 2 in a rather general form, without the introduction of convenient numerical factors. In Prandtl's original discussion, a slightly different definition of the scale height (which here will be denoted by Z) was used, so that, in comparison with equation 15

$$Z^4 = 4X^4/P_1 \tag{20}$$

In this discussion, the Prandtl number, $P = P_1$, is height independent and equals, for laminar flow, the physical constant ν/κ, where ν = molecular kinematic viscosity and κ = molecular thermal diffusivity. For consistency, let the new dimensionless independent variable be $\zeta = n/Z$. Then, the characteristic equations 19 simplify greatly, owing to $y = 1$, and may as well be written in terms of the dimensional dependent variables u (wind speed) and ϑ (temperature disturbance)

$$\partial^4 u/\partial\zeta^4 = -4u \tag{21a}$$

$$\partial^5\vartheta/\partial\zeta^5 = -4\,\partial\vartheta/\partial\zeta \tag{21b}$$

The boundary conditions are

at the interface ($\zeta = 0$):

$$u = u_0 = 0 \qquad \vartheta = \vartheta_0 \neq 0$$

at large normal distance ($\zeta \gg 1$):

$$u = u_\infty = 0 \qquad \vartheta = \vartheta_\infty = 0$$

A solution satisfying these conditions is

$$u = u_i e^{-\zeta} \sin\zeta \tag{22a}$$

$$\vartheta = \vartheta_0 e^{-\zeta} \cos\zeta \tag{22b}$$

where the two integration constants u_i (cm/sec) and ϑ_0 (°C) are interrelated by

$$u_i = \vartheta_0(g/\gamma\theta_0 P_1)^{1/2} \tag{23}$$

The mathematical structure of Prandtl's classical solution for katabatic flow, equations 22*a* and *b*, is obviously the same as that of the well-known Ekman-spiral solution of the two-dimensional wind profile in the planetary boundary layer.

When the effective Prandtl number is unity, relations 23, 20, and 15 produce a very convenient simple relation for the eddy diffusivity:

$$K_1 = K_0 = 0.5\epsilon Z^2\sqrt{g\gamma/\theta_0} \tag{24}$$

Surface stress (τ_0) and boundary value of heat flux (Q_0) follow from the defining equations 10*a* and *b*

which yield, with the aid of the above relations

$$\tau_0 = \rho_0 K_0 u_i / Z \tag{25a}$$

$$Q_0 = -c_p \rho_0 K_0 (\gamma + \vartheta_0 / Z) \tag{25b}$$

A characteristic of katabatic flow is that the wind profile must show a maximum speed (u^*) at a relatively small normal distance (n^*) from the interface. For a sufficiently small value of slope inclination, the normal distance (n) is practically indistinguishable from the vertical distance (z). Thus, at a given micrometeorological mast installation on the sloping surface, we can also say that a maximum wind speed (u^*) will occur at a certain height (z^*). The differentiation of the wind profile equation 22 once with respect to ζ produces the shear profile equation:

$$\begin{aligned} \partial u / \partial \zeta &= u_i e^{-\zeta} (\cos \zeta - \sin \zeta) \\ &= Z \, \partial u / \partial n \approx Z \, \partial u / \partial z \end{aligned} \tag{26}$$

It follows that the first level of maximum wind speed (i.e., where $\partial u / \partial \zeta = 0$) occurs at $\zeta^* = \pi/4 \approx z^*/Z$. The original wind profile equation 22a then gives the maximum speed

$$u^* = u_i e^{-\pi/4} \sin \pi/4 = 0.323 u_i \tag{27}$$

It is usually concluded that inspection of an observed wind profile (which is supposed to be katabatic) will directly yield a pair of u^*, z^* values; consequently, $u_i = u^*/0.323$, and $Z = 4z^*/\pi$. Together with other independent information about the values of the external parameters ϵ, θ_0, γ, and g, the knowledge of u_i and Z appears to be sufficient for the verification of equations 23 through 25.

In a decisive test of the katabatic nature of an observed flow case, however, we must also consider the thermal structure of the lower atmosphere. The observed vertical temperature profile must agree with equation 22b and the model relationship equation 7, namely

$$\theta = \theta_0 + \gamma z + \vartheta_0 e^{-\zeta} \cos \zeta; \quad \vartheta_0 = u_i \sqrt{\gamma \theta_0 / g} \tag{28}$$

when u_i and $Z = z/\zeta$ are the same as derived from wind profile data with the aid of Prandtl's model.

Furthermore, the Q_0 value estimated with the aid of equation 25b must satisfy energy budget requirements, established by independent determination of the boundary values of net radiation (R_0), subsurface heat flux (S_0), and heat of evaporation-condensation (E_0), in the balance equation

$$Q_0 = R_0 - S_0 - E_0 \tag{29}$$

Finally, the relative curvature of katabatic profiles will be expressed, using as a convenient measure the Deacon numbers of the wind profile (De) and of the potential temperature profile (DE). It follows from the definition of the Deacon number, and equations 22a, 22b, 26, and 28, that

$$De = -\frac{\partial \log (\partial u / \partial \zeta)}{\partial \log \zeta} = \frac{2\zeta}{(1 - \tan \zeta)}$$

$$DE = -\frac{\partial \log (\partial \theta / \partial \zeta)}{\partial \log \zeta} = \frac{2\zeta}{(1 + \cot \zeta - Z\gamma e^{\zeta} / \vartheta_0 \sin \zeta)}$$

Although both Deacon numbers are zero at the interface, De goes through $\pm \infty$ at $z = z^*$. DE will remain relatively small in the same region. This behavior is significantly different from the curvature conditions in ordinary surface layers, where De and DE are unity at the surface and remain bounded (for details see *Dalrymple et al.* [1966, section 3]).

F. Defant [1951] has made the statement, based on previous work by A. Defant, that there will be a critical value of slope inclination. For $\epsilon \geq \epsilon_{crit} \approx 1/100$, the katabatic motion can become unstable. It was mentioned in section 1 that the slope of the central Antarctic Plateau is of the order of 10^{-3} and, according to Defant, should permit stable katabatic flow. However, owing to large Reynolds number, the motion will not be laminar, which will justify the assumption that the effective Prandtl number is unity.

Ball [1960] has approached the problem of katabatic flow along different theoretical lines from Prandtl, using bulk coefficients of surface friction and bulk dimensions of the inversion layer, rather than investigating wind and temperature profile structure in detail. Emphasis was given to the strong to severe types of katabatic winds observed so frequently at the coastal region of Antarctica and to the effects of synoptic pressure distribution, Coriolis force, and deflection by local topography. This approach has led to practical formulations of relations among bulk wind speed, inversion height, and slope inclination. If Ball's diagram is applied for the conditions on the central Antarctic Plateau near the south pole, a bulk speed of katabatic wind of about 2 m/sec can be expected. This appears to be the correct order of magnitude, as can be seen in Figure 1. However, the study of details of profile

structure will always be necessary for a more complete understanding of katabatic motion and its significance for local heat budget studies on sloping surfaces.

4. SUMMARY OF OBSERVATIONAL DATA

As was mentioned in the introduction, one of the rare cases of SSE winds at the south pole occurred in the early GMT hours of September 17, 1958. The U. S. Weather Bureau aerovane (on a 10-meter mast) recorded calm conditions. Micrometeorological profile data taken from the report by *Dalrymple* [1961] are plotted in Figure 1. The graphs show that the profiles during the hours 02 to 06 GMT are of the same type. Since tendency toward a wind maximum at the 4-meter level is evident, the profiles may be katabatic. Wind data for the hour 04 to 05 GMT are not available in the report. Three-hourly profile means, computed for the period 02 to 06 GMT, are summarized in Table 1.

Supporting U. S. Weather Bureau station data are as follows: net radiation $R_0 = -2.2$ ly/hour; air density at the surface $\rho_0 = 0.00112$ g/cm^3. Data on inversion heights and inversion temperatures from prior and later (02 and 11 GMT) radiosonde observation soundings on September 17, 1958, are somewhat conflicting. A representative temperature gradient through the inversion of $\gamma = 5°C/100$ meters, which is about 3 times the monthly average for September 1958, will be assumed [*Dalrymple et al.*, 1966, section 3].

5. ANALYSIS OF DATA

Figure 2 illustrates the averages of wind speed and air temperature as presented in Table 1. For the theoretical analysis, equation 28 was considered first. With $\gamma = 5 \times 10^{-4}$ °C/cm, and $\theta_0 = -55.0°C = 218°K$, it was found that the values of $\vartheta_0 = -10.54°C$ and $Z = 700$ cm produced a satisfactory fit between actual temperature distribution and Prandtl's theory of katabatic flow. Consequently, for $g/\gamma\theta_0 = 9000$, or $(g/\gamma\theta_0)^{1/2} = 94.9$ cm/sec °C, using equations 23 and 27, we obtain $u_4 = 1000$ cm/sec, or $u^* = 323$ cm/sec. Figure 2 shows that sufficient agreement between the actual wind data and the theoretical profile for katabatic flow is obtained. The largest discrepancies occur at the lower levels, presumably related to the fact that here the assumption of height independency of eddy diffusivity will least probably hold true. Employing the above-quoted parameters, and $\epsilon = 0.00176$, Prandtl's theory (see equation 24) gives $K_0 = 20.4$ cm^2/sec.

Assuming that the representative Reynolds number of katabatic flow is $Re = u^*Z/\nu$, we obtain for Re the order of 10^6. In view of the generally accepted value of a critical Reynolds number of the order of 10^3, it must be concluded that the case of katabatic flow under discussion cannot be truly laminar. An effective Reynolds number can be defined as $RE = Re\ \nu/K_0$. With the above value of K_0 we find that RE is of the order of 10^4. This is still significantly in excess of the commonly quoted critical value of 10^3, and it may indicate an in-

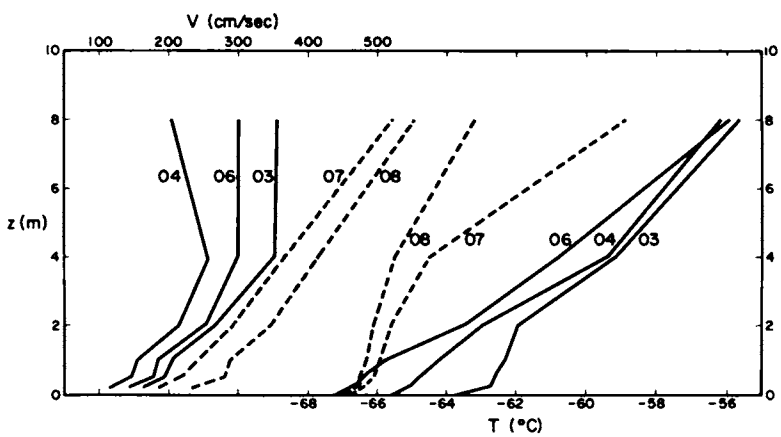

Fig. 1. Hourly means of wind and temperature profiles at the south pole, September 17, 1958. The hourly means are for 60-minute periods ending at the indicated hour of GMT.

herent instability of the flow conditions as illustrated in Figure 2. In fact, there is evidence in Figure 1 that the flow persisted only for a few hours, whereupon a radical change took place, after which, for the following 2 hours, the wind profile resembled a more conventional type of surface layer structure. The accompanying change in the temperature profile is very interesting (see Figure 1)—a general lowering of temperature together with a significant reduction in vertical temperature gradients. This makes it impossible to interpret the breakdown of the observed katabatic flow as a change related to vertical instability and mixing. Advective processes could be involved. More details will be discussed in section 6.

TABLE 1. Three-Hourly Profile Means, Amundsen-Scott Station, 02 to 06 GMT on September 17, 1958

Three-hourly means of wind speed (V), potential air temperature (θ), snow temperature (T), and rate of change of $T(\delta T)$, at indicated nominal distance (z) from the air-snow interface.

z, m	Wind Speed V, cm/sec	Potential Air Temperature θ, °C	Nominal Distance z, cm	Snow Temperature T, °C	Rate of Snow Temperature Change δT, °C/hr
8	286.8	−55.89	0	−65.53	−1.15
4	301.4	−59.76	− 2	−63.60	−1.02
2	244.4	−62.78	− 5	−62.67	−0.70
1	180.5	−64.16	−10	−59.23	−0.40
0.5	173.7	−64.60	−25	−56.83	−0.25
0.25	139.9	−64.77	−50	−56.17	−0.01
0.12	—	−64.87	—	—	—

For the hours of presumable katabatic flow condition on September 17, 1958, the surface stress and the surface heat flux are obtained, with the aid of equations 25*a* and *b*, as $\tau_0 = 0.033$ dyne/cm² and $Q_0 = -0.856 \times 10^{-4}$ ly/sec $= -0.3$ ly/hour, respectively. Because net radiation was $R_0 = -2.2$ ly/hour, and heat of sublimation or rime deposition was presumably negligible (which is supported by the extremely low level of absolute temperature), the heat flux (S_0) from the subsurface snow layer to the snow surface must have supplied −1.9 ly/hour to satisfy the energy balance equation, $R_0 = S_0 + Q_0$, with the above theoretical $Q_0 = -0.3$ ly/hour.

The average volumetric heat capacity of the uppermost 50 cm of snow at the south pole is $C = 0.15$ ly/deg cm [*Dalrymple et al.*, 1966, Table 22]. Using this C value, and assuming that the heat flux in the snow layer from 0 to −50 cm goes asymptotically to zero at −50 cm, the numerical integration of the rates of snow temperature change listed in

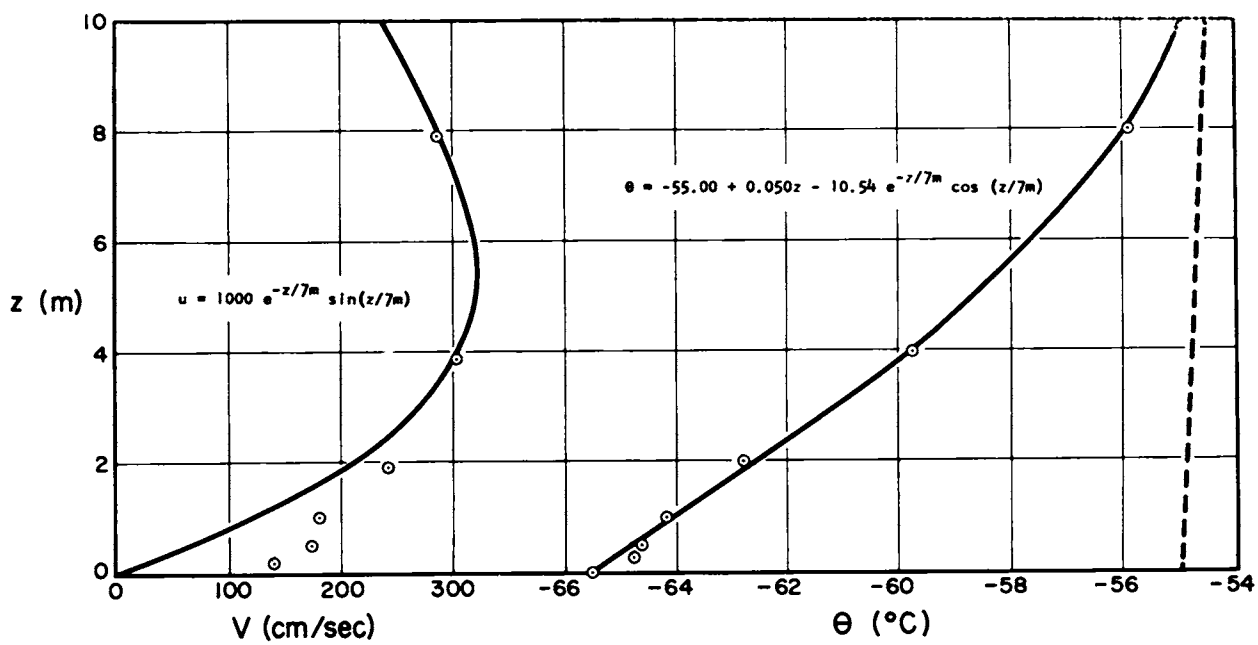

Fig. 2. Wind and potential temperature data at the south pole, September 17, 1958; averages for 02 to 06 GMT, in comparison with theoretical profiles in katabatic flow.

Table 1 indeed gives —1.9 ly/hour. In comparison with monthly averages of S_0 at the south pole (which were never during the sunless period in excess of —10 ly/day, which is approximately —0.4 ly/hour), the above S_0 of —1.9 ly/hour is quite extreme, and it cannot be expected that S_0 will be maintained at this high value for more than a few hours. See also *Hanson and Rubin* [1962]. The close agreement found between S_0 and $R_0 - Q_0$ may be fortuitous, but, during the period under investigation, the micrometeorological conditions at Amundsen-Scott station seem to have been really exceptional and anomalous.

6. POSSIBLE CAUSES OF ABRUPT CHANGES IN SURFACE LAYER STRUCTURE

Figure 1 shows that there was a marked and rather abrupt change in surface layer structure between the 60-minute periods ending at 06 and 07 hours GMT. Before the change, the wind and temperature profiles appear to correspond to a truly katabatic flow type. After the change, the wind has generally speeded up, especially in the 4- to 8-meter layer, and the air is much colder than before; for example, at the 4-meter level the temperature went down by 3.7°C from one hourly mean to the next. It was mentioned in section 5 that vertical mixing must be ruled out because it should cause at least a partial warming in the lowest layers, and this did not occur. Horizontal advection of cold air can likewise be ruled out because it would require the existence of horizontal temperature differences along the sloping interface, which can hardly be expected in the polar region, owing to the unsurpassable degree of uniformity of surface conditions.

There remains another cause that can explain temperature changes in direct relation to the simultaneous wind changes evidenced on Figure 1. Namely, vertical advection due to convergence of horizontal flow can account for the observed cooling. For simplicity the terms 'horizontal' and 'vertical' will be used in the following discussion, although 'tangential' and 'normal' to the interface would be the correct terminology.

A conventional, usually tacitly made, assumption about the interpretation of local time changes, like $\partial u/\partial t$, at a micrometeorological site is that, for a sufficiently large region surrounding the station, they are the same for any x (or s). Preferably, we deal with steady-state mean conditions; that is, $\partial u/\partial t = 0$. However, nothing prevents us from assuming instead that the total time derivative is zero; that is, $du/dt = 0$. For the simplified type of flow under investigation (see section 2) this means that

$$\partial u/\partial t = -u\,\partial u/\partial x \tag{30}$$

In other words, the observed local time change of 'mean' wind speed is now interpreted as being caused by the passage of volumes of air, each having a characteristic velocity and velocity distribution. Obviously, the dimensions (especially the horizontal extent in the downwind direction) of these volumes of air must be larger, by several powers of 10, than the scale of eddies of ordinary turbulence; they may belong to what in meteorology has been termed mesoscale phenomena. Nothing can be said about the lateral, or horizontal, cross-wind extent of these disturbances; they may or may not be truly two-dimensional, similar to ocean swell. Since compressibility effects can be safely neglected, continuity of motion (see equation 1) will require that

$$\partial u/\partial x = -\partial w/\partial z \tag{31}$$

when the lateral component of air motion is zero, or constant, at all lateral distances, and w is the vertical component of air motion. Writing δu for the time change (per hour, or any other convenient time increment) of horizontal component (u), the combination of equations 30 and 31 gives

$$w = \int_0^z (\delta u/u)\,dz \tag{32}$$

If the initial state is that of steady katabatic flow, there is only horizontal advection, as represented by the term $u\epsilon\gamma$, which is balanced by vertical diffusion of heat (see equation 9). However, this holds true only when the vertical (normal) component w is zero. If equation 32 gives $w \neq 0$, it is reasonable to assume (in view of the slowness of radiative cooling rates) that the total time derivative $d\theta/dt$ will be zero. In the terms of the above simplified model this means that

$$\partial\theta/\partial t = -w\theta' \tag{33}$$

where θ' stands for $\partial\theta/\partial z$. Writing $\delta\theta$ for the rate of time change (per hour) of temperature, we obtain finally from equations 32 and 33

$$\delta\theta = -\theta' \int_0^z (\delta u/u)\,dz \tag{34}$$

Equations 32 and 34 were applied to the micrometeorological conditions illustrated in Figure 1. As the initial state, the 60-minute means of wind speed (assuming $V = u$) and of temperature of the period ending at 04 GMT were taken from the data report by *Dalrymple* [1961] and were contrasted against the corresponding values of the 1-hour period ending at 08 GMT. The basic data and the computational results are summarized in Table 2. The agreement between the directly observed rates of temperature drop and those computed from horizontal convergence and subsequent vertical advection (compare the sixth and the last columns of Table 2) appears fair enough. The computed vertical velocities (w) can be interpreted as vertical displacements of air per hour. This displacement is generally about 20% of actual height. It is due solely to the extremely strong inversional temperature gradient of the initial katabatic flow structure that such weak vertical displacements can produce a temperature change of the order of 1°C per hour, or per any other convenient time increment.

7. CONCLUSIONS AND OUTLOOK FOR FUTURE WORK

It can be concluded that the kinematics of the investigated phenomenon of abrupt temperature decrease has been clarified as that of convergence, or 'piling up,' of air which had originally been cooled by close contact with the radiating snow-air interface. This may be related to an inherent instability of katabatic flow. An investigation of the dynamics of the breakdown must be postponed, however, owing to lack of information on the horizontal variability of surface layer structure. It must be mentioned that the reverse process, abrupt warmings in the layer of micrometeorological measurements, has also been reported by Dalrymple at Amundsen-Scott station [*Dalrymple et al.*, 1966, section 2]. It is self-suggestive to conclude that a rapid warming will be caused by a local divergence of horizontal flow and the resulting subsidence of air toward the surface, as a counterpart to the above-discussed case of local convergence and induced upward motion of surface air.

On the status of the theory of katabatic flow, it can be concluded from the discussion at the end of section 2 that new concepts must be explored to solve the problem in a realistic manner. One purpose of this discussion was to outline the background and limitation of the existing theory and to demonstrate the need for continuation of theoretical efforts. Steps in this direction have been taken at the University of Wisconsin. Theoretical models

TABLE 2. Basic Data and Computational Results Amundsen-Scott Station, September 17, 1958

Nominal Height z, cm	Height Increment Δz, cm	Wind Speed* V, cm/sec	Vertical Temperature Gradient* θ', °C/cm	Average Rate of Change of Wind Speed† δV, cm/sec/hr	Average Rate of Temperature Change† $\delta\theta$, °C/hr	Computed Height Increment Δw, cm/hr	Computed Vertical Motion w, cm/hr	Theoretical Temperature Change $\delta\theta_{comp}$ °C/hr
800		203	0.009	62	−1.8		164	−1.5
(600)	400					93		
400		254	0.012	40	−1.5		71	−0.9
(300)	200					32		
200		214	0.015	34	−0.6		39	−0.6
(150)	100					19		
100		153	0.012	34	−0.2		20	−0.2
(75)	50					11		
50		149	0.013	33	−0.1		9	−0.1
(37.5)	25					6		
25		117	0.013	30	−0.0		3	−0.0
(12.5)	25					3		
0		0	—	0	—		0	—

* 03 to 04 GMT.
† 07 to 08 GMT minus 03 to 04 GMT.

are being investigated by means of numerical integration methods similar to those employed by *Lettau* [1962*a*] for the boundary layer problem.

Another purpose of this preliminary discussion is to appeal to observers. For the conclusive testing of any theoretical model of steady katabatic flow it is desirable that details of wind and temperature profiles, including turbulence structure, together with surface heat budget determinations, are procured in higher resolution and with greater representativeness than before. The most promising locations for improved observations of this flow type should be found on the sloping plateaus of Greenland and Antarctica, at a sufficient distance from the coastlines.

An improved understanding of the steady-state problem of katabatic flow is also prerequisite for the discussion of the development, i.e. onset and decay, of unsteady katabatic flow, including the question of inherent instability, possibly related to the existence of a critical value of slope inclination as discussed by *Defant* [1951], and the vehement nature of this flow type when influenced by topography as recently investigated by *Ball* [1960], at the rim of the Antarctic Plateau.

Acknowledgments. I thank Dr. Dalrymple and Miss Wollaston for supplying information and advice in the preparation of this study.

The research for this investigation would not have been possible without my affiliation as consultant to the U. S. Army Natick Research Laboratories, Earth Sciences Division, and as codirector of the Climatic Research Center, University of Wisconsin, supported by the Atmospheric Sciences Section, National Science Foundation, grant GP-444.

REFERENCES

Ball, F. K., Winds on the ice slope of Antarctica, in *Antarctic Meteorology,* Proceedings of the Symposium in Melbourne, February 1959, pp. 9–16, Pergamon Press, New York, 1960.

Dalrymple, P., South pole micrometeorology program, 1, Data presentation, Natick, Mass., Earth Sciences Div., Hq., QM R&E Command, *Tech. Rept. ES-2,* October 1961.

Dalrymple, P., H. Lettau, and S. Wollaston, South pole micrometeorology program: Data analysis, *this volume,* 1966.

Defant, F., Local winds, in *Compendium of Meteorology,* p. 655, American Meteorological Society, Boston, Mass., 1951.

Hanson, Kirby J., and Morton J. Rubin, Heat exchange at the snow-air interface at the south pole, *J. Geophys. Res., 67,* 3415–3424, 1962.

Lettau, H., Theoretical wind spirals in the boundary layer of a barotropic atmosphere, *Beitr. Physik Atmosphaere, 35,* 195–212, 1962*a*.

Lettau, H., Equiangular wind and current spirals, *Final Rept., contract DA-36-039-SC-80282* (USEPG, Fort Huachuca, Arizona), pp. 159–172, University of Wisconsin, 1962*b*.

Prandtl, L., *Fuehrer durch die Stroemungslehre,* pp. 373–375, Vieweg & Sohn, Braunschweig, 1942.

SOUTH POLE MICROMETEOROLOGY PROGRAM: DATA ANALYSIS[1]

PAUL C. DALRYMPLE,[2] HEINZ H. LETTAU,[3]
SARAH H. WOLLASTON[2]

Abstract. At the South Pole station in 1958 observations of wind and temperature in the lowest 8 meters of the atmosphere and of temperature in the upper 8 meters of the snow were recorded. The curvature characteristics of wind and air-temperature profiles (as measured by Deacon numbers) were analyzed in great detail; to express stability (and its change with height), Richardson number computation was employed, because it takes into account wind shear as well as temperature lapse rate. It was found that moderate to extreme stability represents the average condition at South Pole, resulting in a significant tendency to suppress mechanical turbulence. The maximum inversion was 14.7°C in the lowest 8 meters. Stability tends to be greatest in the early winter and at periods with lowest temperatures. A new method was developed for evaluation of the aerodynamic roughness parameter from wind data showing stability-affected profile curvature. The computed z_0 for the snowfield near South Pole has a mean value of 0.014 cm and is nearly constant for a wide range of bulk stability. In general the wind profile curvature decreases as stability increases. However, with great bulk stability, the wind profile Deacon number as a function of height reaches a minimum near 0.25 and then increases upward, in spite of height-increasing Richardson number. Temperature profile Deacon numbers do not show this behavior, indicating that the change of shearing stress with height (relative to the ground drag) must be an important factor in wind profile structure.

An analysis of the relation between winds near the snow surface and at the top of the inversion (on the average near 600 meters above ground, using aerological soundings) demonstrates that air motion in the lower atmosphere is controlled by surface friction and by the wind in the free atmosphere, modified by thermal winds due to horizontal temperature gradients resulting from the general slope of the terrain.

Eddy heat flux was computed, on the basis of estimated surface stress (using Kármán's constant, with Deacon-number-corrected wind shear) and vertical differences of potential temperature and wind speed, in the lowest layers where a similarity requirement was satisfied. To obtain representative climatological means of eddy heat flux, a statistical relationship was established between Quartermaster observations (concerning profile structure versus bulk stability) and U. S. Weather Bureau standard observations, using conveniently defined coefficients of stability and transfer of momentum and heat. For February through November, monthly values of surface stress ranged from 0.825 to 0.103 dyne/cm^2, monthly values of eddy heat flux from 0.0052 to −0.0239 ly/min.

Heat movement in the substratum was investigated by harmonic (Fourier) analysis of snow-temperature variations. A new method was derived which permits us to determine the layers in which genuine conduction of heat prevails. At South Pole it was found that the upper 4 meters of snow respond to other influences (radiation absorption, packing, etc.) in addition to genuine heat conduction.

To establish the surface energy budget, hourly values of net radiation from the U. S. Weather Bureau net radiometer were used. Monthly means of net radiation (R_0) were compared with those of eddy heat flux (Q_0) and heat flux in the snow (S_0) (which is a relatively small term). The latent heat flux (E_0), when treated as a remainder in the balance, indicates slight but significant deposition of hoarfrost in midwinter at South Pole, as illustrated by the following mean values: $R_0 = -56.5$, $Q_0 = -51.0$, $S_0 = -2.5$, $E_0 = -3.0$, all in ly/day. The error tolerances and possible systematic effects in these estimates are discussed, and a comparison is given for three other antarctic stations.

[1] Quartermaster Research and Engineering Center, Technical Report ES-7, Ohio State University Research Foundation project 1362, supported by National Science Foundation grant G19630.

[2] Quartermaster Research and Engineering Center, Natick, Massachusetts.

[3] University of Wisconsin, Madison, Wisconsin.

1. INTRODUCTION: SOURCE OF DATA AND PLAN OF ANALYSIS

Data analyzed in this report were obtained by the Quartermaster Corps during 1957 and 1958 at Little America V and Amundsen-Scott (South Pole) station on the continent of Antarctica, as part of the glaciology program of the International Geophysical Year. The data have been published as a Quartermaster Research and Engineering Center Technical Report [*Dalrymple*, 1961].

It was believed that the absence of direct diurnal influences would permit determination from the antarctic data of the interrelationships between fully developed low-level wind and temperature profiles for strong inversions above uniformly smooth surface areas of large extent. Consequently, computations were to be made of Richardson numbers, Deacon numbers, roughness parameters, and surface shear stresses in order to study interrelationships between stability, profile curvature, and effects of roughness and of friction produced by the snow surface. It was also planned to compute the vertical transfer of sensible heat and to relate it to general meteorological and glaciological conditions of the energy budget at the interface. Finally, temperature profile data were to be analyzed to determine a climatology of the air temperature in the 8-meter-deep surface layer, the environmental layer for most human ground activities.

2. MICROCLIMATIC DATA AT LITTLE AMERICA V AND SOUTH POLE[4]

General character of the data. Little America V is located at 78°10′S and 162°13′W, 3 km south of Kainan Bay on the Ross Ice Shelf. The range of temperature is large and changes are abrupt, owing to exposure to both marine and continental air masses. Large surface inversions occur with the advection of moderately cold air from the Ross Sea; the maximum difference between the surface and 8 meters in 1957 was 19.3°C; between the surface and 2 meters, 14.0°C, observed about 6 weeks after final sunset. Surface inversions are larger and of a more uniform character at Little America V than at South Pole.

Amundsen-Scott station is located at the geographical south pole, 2800 meters above and 1235 km away from the open sea. Mean temperatures are significantly lower than at Little America V. The midwinter monthly (June) temperature range in 1958 was 35°C (−39° to −74°C), considerably larger than the 11°C (−19° to −30°C) range in midsummer (December). In summer there is a relatively high frequency of low wind speeds; however, the maximum gust of 22 m/sec occurred in January. The maximum inversion from the surface to 8 meters was 14.7°C and occurred in April. Temperature changes with height within the first meter are usually relatively small, although occasionally very steep gradients occur for short periods. For example, on May 7, 1958, a temperature difference of 6.2°C existed between 50 and 100 cm. Figure 1 illustrates an abrupt change of temperature distribution at all levels in the lowest 8 meters. Abrupt changes were observed a number of times during the winter night: twice on May 5, on May 8, May 26, June 21, June 22, and on September 17 and 19, 1958. The change on September 17 was most extreme, with a fall of 9°C in 3 minutes at 8 meters. A fall of 3.8°C in 3 minutes at 2 meters occurred on October 6 and a fall of 4.1°C in 3 minutes at 2 meters on October 7, 1958.

Wind and temperature profile data reduction. At Little America V, a total number of 1,145 hourly wind profiles were measured on 157 days, and air temperature profiles were recorded for approximately 3,000 hours on 150 days. At South Pole, 1,416 hourly wind profiles (based on six anemometer levels) were obtained on 303 days. Temperature profiles (based on nine thermocouple levels) were recorded for approximately 5,750 hours on 278 days. Snow-temperature measurements at 7 depths and a surface-temperature measurement were also obtained. All temperatures have been transformed from millivolt readings on strip charts to degrees Celsius on punch cards. The sampling rate was 18 per hour at each level. The data reduction was accomplished through an automatic readout system especially designed for the project by *Dillon and Arbarchuk* [pending publication]. Data reduction was reproducible 99% of the time to ±0.1°C.

[4] *Symbols used in this section*:

- g, acceleration of gravity (982 cm/sec²).
- z, height (cm).
- θ, potential temperature (deg† Kelvin).
- T, temperature (deg)†.
- V, wind speed (cm/sec).

† The abbreviation 'deg' stands for degrees Celsius, whereas 'Deg' is used for degrees of an arc.

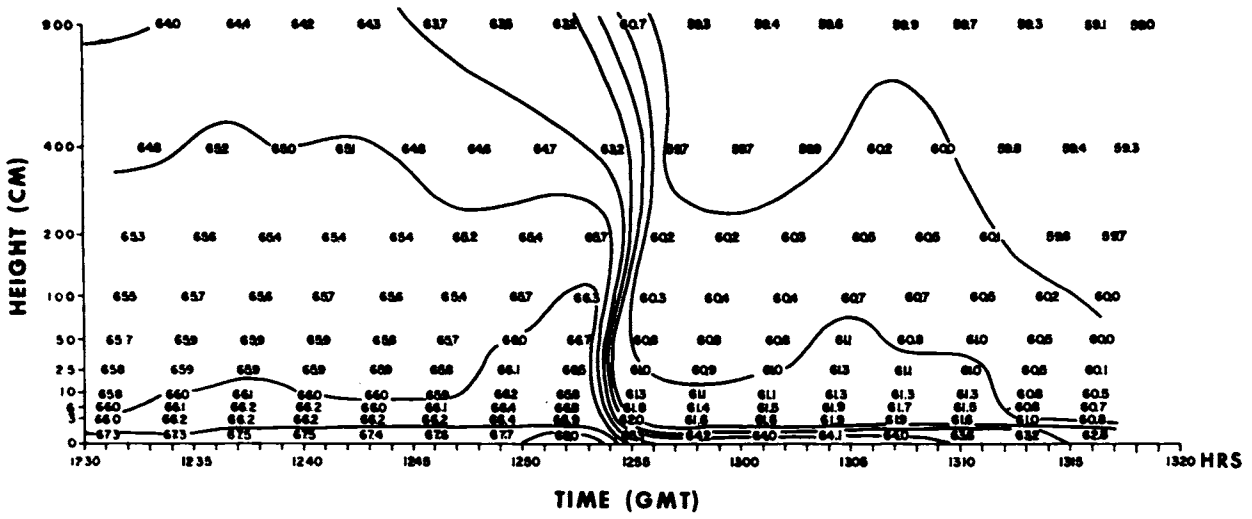

Fig. 1. Rapid change of temperature, —°C, South Pole, May 8, 1958.

Tabulations of these data (105,080 IBM cards of Little America V profile data; 210,622 IBM cards of South Pole profile data) were critically reviewed and edited, and summary and mean cards were transcribed for each hour and day. Hourly averages of wind speed at six heights (geometrically spaced from 0.25 to 8.0 meters) were expressed in centimeters per second and were punched onto IBM cards (517 cards for Little America V; 1,088 for South Pole).

Computation of Richardson numbers. Using all periods when both wind and temperature profiles were available, 1,050 Richardson number profiles were computed for South Pole and 580 Richardson number profiles for Little America V. Most of the wind profiles used were for 1-hour intervals, but all wind profile observations of at least 40-minute duration, and some of 2- or 3-hour duration, were included. Average temperatures were computed, to 0.01°C, for the same levels and approximately the same periods as the wind measurements. Using wind and temperature data at 800, 400, 200, 100, and 50 cm, gradient Richardson numbers (Ri) at 400, 200, and 100 cm were computed from

$$Ri = (g\ \Delta z\ \Delta\theta)/[T_m(\Delta V)^2] \qquad (1)$$

where T_m = layer mean temperature (deg Kelvin) obtained by averaging the temperature at the 5 levels. Three overlapping differences (800 to 200, 400 to 100, and 200 to 50 cm) were used, resulting in three Ri values (i.e., a Richardson number profile) at geometric mean levels of 400, 200, and 100 cm.

A detailed description of the collection and reduction of the South Pole profile data has been published [*Dalrymple,* 1961]. Since the 1958 data for South Pole are superior in many respects to the data for Little America V (1957), owing partly to the experience gained during the earlier year and to the improved instrumentation, a detailed investigation of the wind, temperature, and Richardson number profiles is limited in this report to the approximately 10 months of observation at South Pole. Additional climatic analysis of a less specialized character will be included in a study on antarctic climatology (this volume).

3. ANALYSIS OF PROFILE STRUCTURE AT THE SOUTH POLE[5]

Determination of radiation errors. Laboratory tests were conducted by *Portman* [1961] in an effort to establish correction formulas for the radiation errors that occurred at South Pole during the

[5] *New symbols used in this section*:

- H, height of top of inversion (m).
- U, wind speed (USWB observations).
- S, dimensional stability coefficient (°F/kt²).
- β, Deacon number.
- z_0, aerodynamic roughness length (cm).
- d, zero displacement (cm).
- D, zero displacement parameter (cm) = $d + z_0$.
- τ_0, surface stress (dynes/cm²).
- Q, eddy heat flux (ly/time, where ly = langley = cal/cm²).
- k, Kármán constant (~0.4).

antarctic summer. It was determined that radiation errors were a function of solar angle, solar intensity, wind speed, and wind direction. These errors were most pronounced in the observations below 25 cm. These observations were not used in the micrometeorological analysis, because it had not been possible to measure wind speed and temperature at identical heights at these low levels. Radiation errors above 25 cm were considered inconsequential, and no corrections were applied.

Classification of profiles by bulk Richardson number, Ri'. Bulk Richardson numbers, Ri', provide a measure of the general stability of the air layer under consideration. Values were obtained by summing the Ri values computed for 400, 200, and 100 cm and dividing the result by the sum of the heights (i.e. 700 cm). Hourly profiles were arranged in order of Ri' and grouped into 10- and 30-run groups. The method is essentially the same as that introduced by *Lettau* [1957]. In view of the existing near-to-linear structure of individual Ri profiles, it is found that, to a fair approximation, $Ri = z \cdot Ri'$; specifically, Ri' given in 10^{-3}/m can conveniently be taken as 10^{-3} $Ri_{100\,cm}$ which has sometimes been used as a stability parameter.

After averaging wind and temperature data, local Richardson numbers Ri were computed for the group averages. This grouping was done (as the data were reduced) for three seasonal divisions, but later, since similar results were appearing in each division, all seasonal divisions were ignored. After elimination of questionable hourly profiles, 665 were used, broken down into five 10-run, one 15-run, and twenty 30-run groups. Ri' values for the groups range from −18 to 110 in units of 10^{-3} per meter, which is the same as 1 unit per kilometer. There is only one unstable group ($Ri' = -18$); it contains 15 hours but will hereafter be referred to as though it were another 10-run group. Cases of negative Ri', indicating lapse conditions, are infrequent; they occur mostly during the polar day but occasionally also during the period without Sun, probably owing to long-wave radiation from overrunning warm air.

TABLE 1. Seasonal Variation of External Parameters and Stability

Bulk Richardson number (Ri', 10^{-3}/m); number of test cases (n) used to calculate Ri'; monthly mean wind speed at 10 m (U_{10}, m/sec); monthly mean temperature at 2.5 m ($T_{2.5}$, °C); monthly mean height of the inversion layer (H, m); monthly mean total temperature difference (ΔT, °C); and monthly mean temperature gradient ($\Delta T/H$, °C/100 m) within the inversion layer at South Pole.

Date	Ri'	n	U_{10}	$T_{2.5}$	H	ΔT	$\Delta T/H$
Dec. 1957	...	...	...	...	408	0.9	0.22
Jan. 1958	...	...	...	...	370	1.7	0.46
Feb. 1958	13.4	36	4.3	−35.3	524	4.9	0.94
Mar. 1958	30.6	83	5.8	−54.0	611	11.1	1.82
April 1958	30.4	100	5.7	−62.1	589	14.3	2.43
May 1958	17.5	55	8.1	−56.9	587	10.7	1.82
June 1958	23.8	85	7.2	−61.1	655	11.8	1.80
July 1958	23.3	42	8.8	−55.1	626	9.2	1.47
Aug. 1958	31.0	51	6.3	−61.7	538	12.7	2.36
Sept. 1958	25.0	44	6.6	−56.2	580	9.9	1.71
Oct. 1958	22.5	104	7.1	−49.2	495	7.9	1.60
Nov. 1958	12.3*	70*	4.4*	−39.4*	535	5.0	0.93

* Nov. 1–22, inclusive.

Variation of external parameters with Ri' and season. Average monthly values of Ri' for South Pole were computed using all hours for the 10- or 30-run groups. This measure of the 10-month course of bulk stability for that particular year (1958) as obtained from the test hours is shown in Table 1. It is compared with the monthly average wind speed (U_{10}, m/sec) and temperature ($T_{2.5}$, °C) from the U. S. Weather Bureau (USWB) observations at the South Pole station. The table also includes the monthly means of the height (H, m) of the inversion layer, the total temperature difference (ΔT, °C), and the average gradient ($\Delta T/H$, °C/100 m) within the inversion layer; these data were derived from the aerological soundings at South Pole reported by the USWB.

The most frequent stability class interval for the 10-month period was $Ri' = 11$ to 20, with the 21 to 30 interval more frequent in March and April and the 1 to 10 interval more frequent in October and November.

A dimensional stability coefficient, S, was computed from USWB data for February 1958–January 1959, inclusive:

$$S = (T_{10} - T_{2.5})/(U_{10})^2 \qquad (2)$$

For convenience the USWB data were used in units in which they were recorded. Temperature (T) is in °F, and wind speed (U) is in knots at the height (in meters) indicated in the subscripts. Thus S is expressed in °F/kt². The frequency distribution of class intervals of S, by months, is shown in Table 2.

TABLE 2. Seasonal Variation of the Dimensional Stability Coefficient, S (°F/kt²)
(As number of hours per month, according to class intervals of S, where i is the lower limit of the interval, from USWB data at the South Pole.)

	1958										1959
i	Feb.	Mar.	Apr.	May	June	July	Aug.	Sept.	Oct.	Nov.	Dec.	Jan.
$< -.01$	28	22	0	0	4	0	6	9	136	108	19	81
$-.01$	103	16	30	76	58	128	86	202	363	158	90	158
0.00	190	320	157	469	413	506	309	325	181	182	164	271
$+.01$	91	102	215	76	135	65	147	44	24	58	75	78
$+.02$	43	68	122	33	44	27	63	26	14	36	44	30
$+.03$	27	37	56	23	21	10	49	21	1	24	27	13
$+.04$	16	38	33	11	13	7	17	7	4	12	19	8
$+.05$	10	26	27	13	13	3	15	8	3	13	6	1
$+.06$	6	12	13	11	10	5	12	7	2	10	5	3
$+.07$	14	11	11	7	5	1	7	11	1	4	3	2
$+.08$	11	11	13	3	0	2	5	1	0	9	5	2
$+.09$	9	10	4	5	0	2	3	3	2	3	1	0
$+.10$	8	9	0	2	0	1	3	6	0	4	8	1
$+.11$	5	3	5	0	0	1	1	1	2	2	5	1
$+.12$*	118	37	11	8	4	4	15	53	8	48	23	25

* ($+.12$ to ∞)

The empirical relationship between Ri' and S is illustrated in Figure 2. As shown in Table 2, May, June, and July had pronounced peaks of more than 400 hours for the class interval 0.000 to +0.01; these three months had the highest average wind speeds. The greatest variation of S occurred during months with Sun, November through February. The most unstable month was October, the first complete month of the antarctic spring with Sun. For 1958 at least, April, the first complete month after sunset, was the most stable. These results from the larger body of data are in agreement with those shown in Table 1 for the test data.

Figure 3 illustrates the variation with bulk stability Ri' of wind speed, temperature, total sky cover, opaque sky cover, height (H) of the inversion above the surface, the total temperature difference (ΔT) and the lapse rates within the inversion layer. These elements are taken, for the hours of detailed profile data, from the USWB observations of instantaneous wind speed, temperature at 2.5 meters as measured by a 'thermohm' in an aspirated shield, eye observations of sky conditions, and the radiosonde ascents. It can be seen from Figure 3 that ΔT increases with Ri' at about the same rate as the temperature at 2.5 meters decreases, and a tabulation of the temperature at the top of the boundary layer inversion versus bulk stability Ri' indicates that the low-level bulk stability is independent of the temperature at the top of the inversion. Mean temperature versus wind direction frequency at South Pole is shown in Figure 4 for the

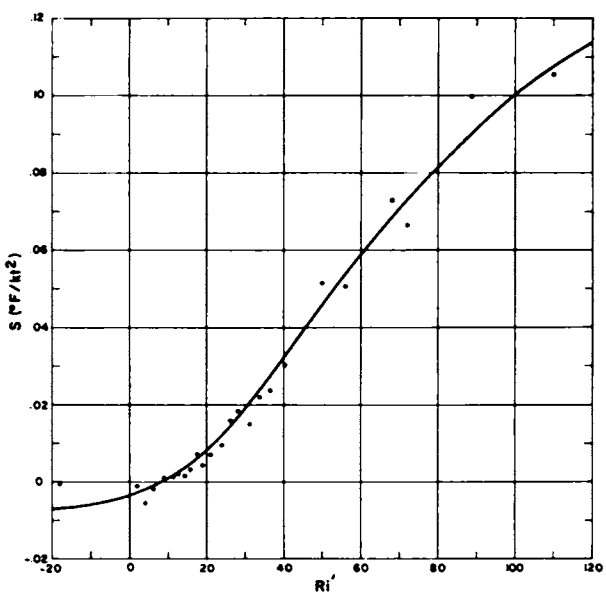

Fig. 2. Stability coefficient S versus bulk Richardson number Ri', South Pole.

period when the Sun was below the horizon (March to September).

Variation of Richardson number. A plot of the Richardson number Ri versus height for selected 10- and 30-run groups (665 profiles) is shown in Figure 5. In view of the gain of reliability due to averaging, the computation was based on the five differences between adjacent levels. A systematic change of Ri with height in the lowest 4 meters is evident. For all groups, Ri can be assumed to equal zero at the surface. The over-all height gradient of Ri corresponds rather closely to the group values of Ri'. However, increasing gradient with height, or a slight curvature of the Ri profile, seems to exist for extreme cases at the higher levels of the profile.

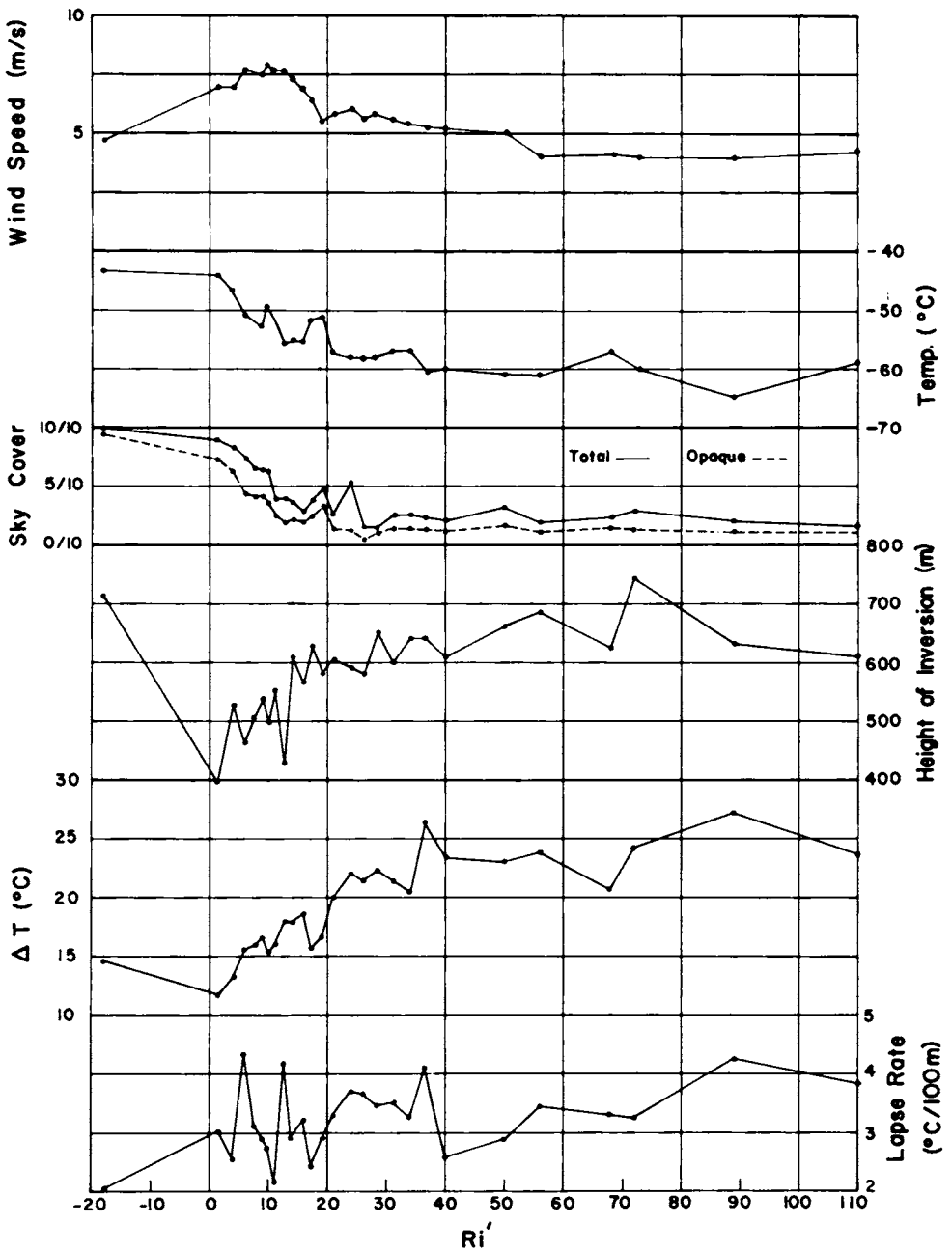

Fig. 3. Variation of external parameters with stability, South Pole.

An inspection of the seasonal divisions shows that, for extreme bulk stability in winter, Ri increases with height slightly less rapidly in the lower 2 meters than in spring and fall.

Computation of wind profile curvature and zero displacement parameter. The Deacon number of the wind profile β_v is a measure of profile curvature. For its definition, reference is made to *Lettau* [1957]. β_v was computed for the 10- and 30-run groups of South Pole profiles using overlapping differences in the following equation:

$$\beta_v = \frac{\Delta \log \Delta z - \Delta \log \Delta V}{\Delta \log (z + D)} \tag{3}$$

The zero displacement d corrects for irregularities of the terrain in the direction from which the wind is blowing and for shiftings of snow at the site, which produced uncertainty concerning the elevation of the anemometers above the average surface. At the site, the arms of the anemometer mast were adjusted periodically, when the snow accumulation raised the height of the surface.

For the adiabatic surface layer the zero displacement d can be determined with the aid of a least-squares fit to the logarithmic wind law; *Robinson* [1962] describes a program for automatic computation of D, z_0, and the surface stress τ_0. This method cannot be applied for diabatic conditions, since it is known that the logarithmic law holds true only in adiabatic surface layers.

A new approach is used here. The Deacon numbers for the group analysis were computed using adjacent as well as overlapping height intervals and

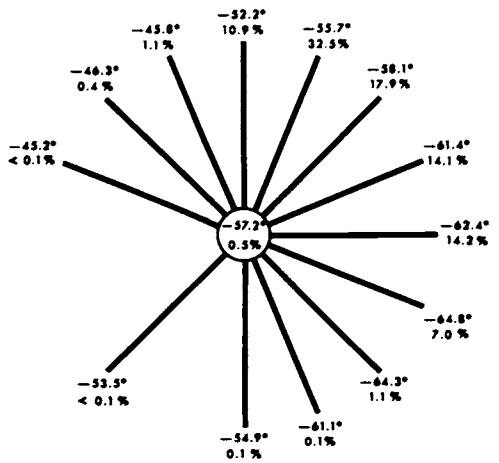

Fig. 4. Mean hourly temperatures (°C) and wind direction frequency (%), South Pole, March-September 1958.

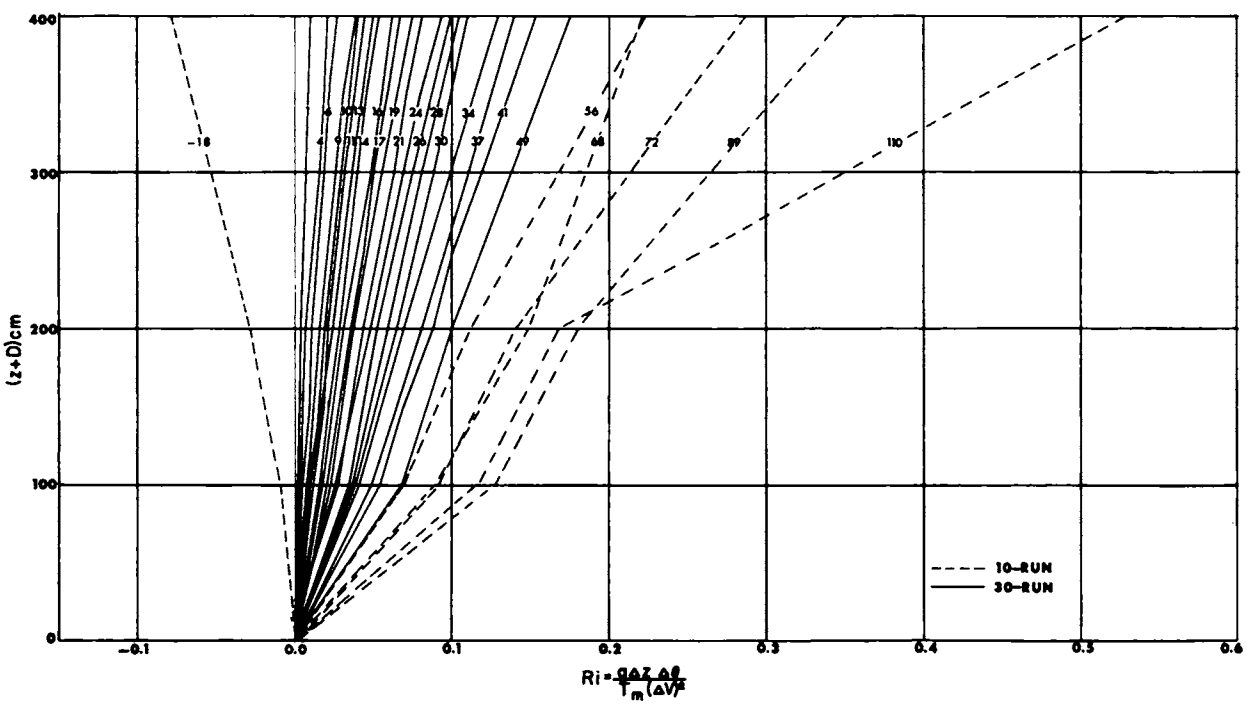

Fig. 5. Ri versus height for indicated Ri', South Pole.

assuming a sequence of tentative D values (i.e., first $D = 0$; then $D = -5, -10, -15$ cm; then $D = 5, 10, 15$ cm, etc.). For each group, resulting β_v values (at nominal heights of 100, 141, 200, 283, 400 cm) were plotted against height in linear coordinates. It was assumed that at $z = 0$ the Deacon number equals unity. The D value that produced the least change of curvature with height in the β_v profile was selected. By applying the D value, the systematic change of β_v profiles with bulk stability (see Figure 6) was considered. It was found that in the lowest 1- to 2-meter layer the absolute value $|1 - \beta_v|$ was always directly proportional to the distance from the actual surface. For the 10- and 30-run averages, D was occasionally as large as 15 cm and could be either positive or negative; it might be larger for individual runs.

Variation of wind profile curvature. The dependency of β_v profile structure on bulk stability (bulk Richardson number) is shown in Figure 6. In a neutral case β_v should equal unity in the lowest atmosphere, provided that the wind profile is exactly logarithmic. Figure 6 shows that, for surface heating, β_v tends to be greater than unity and increases with height; for surface cooling (inversion), β_v tends to be smaller than unity and decreases generally with height. At the South Pole there were no differing roughness characteristics upwind that might explain the change of β_v with height, as suggested by *Sutton* [1953].

In stable cases, β_v becomes less than unity and decreases with height as long as Ri' is only moderately large. It is extremely interesting to note that as bulk stability increases further, that is for Ri' greater than approximately 50, the decrease of β_v is very strong only in the lowest part of the layer under investigation. The β_v profiles begin to show a minimum level which seems to subside gradually to about 1.5 meters for the extreme stability observed. Above this minimum level, β_v increases rapidly with height and may exceed the surface value of unity.

When the groups are divided according to season, less curvature of the stable wind profile (values of β_v nearer 1) occurs for the same bulk stability (Ri')

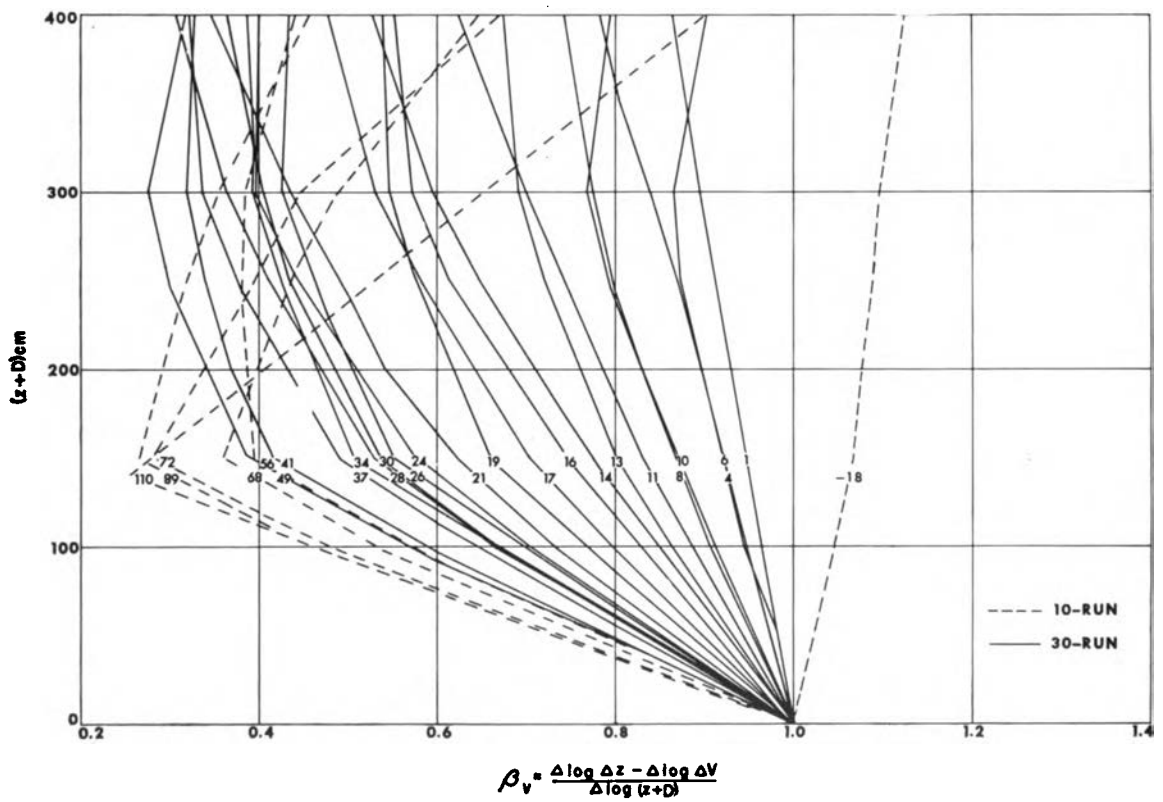

Fig. 6. β_v versus height for indicated Ri', South Pole.

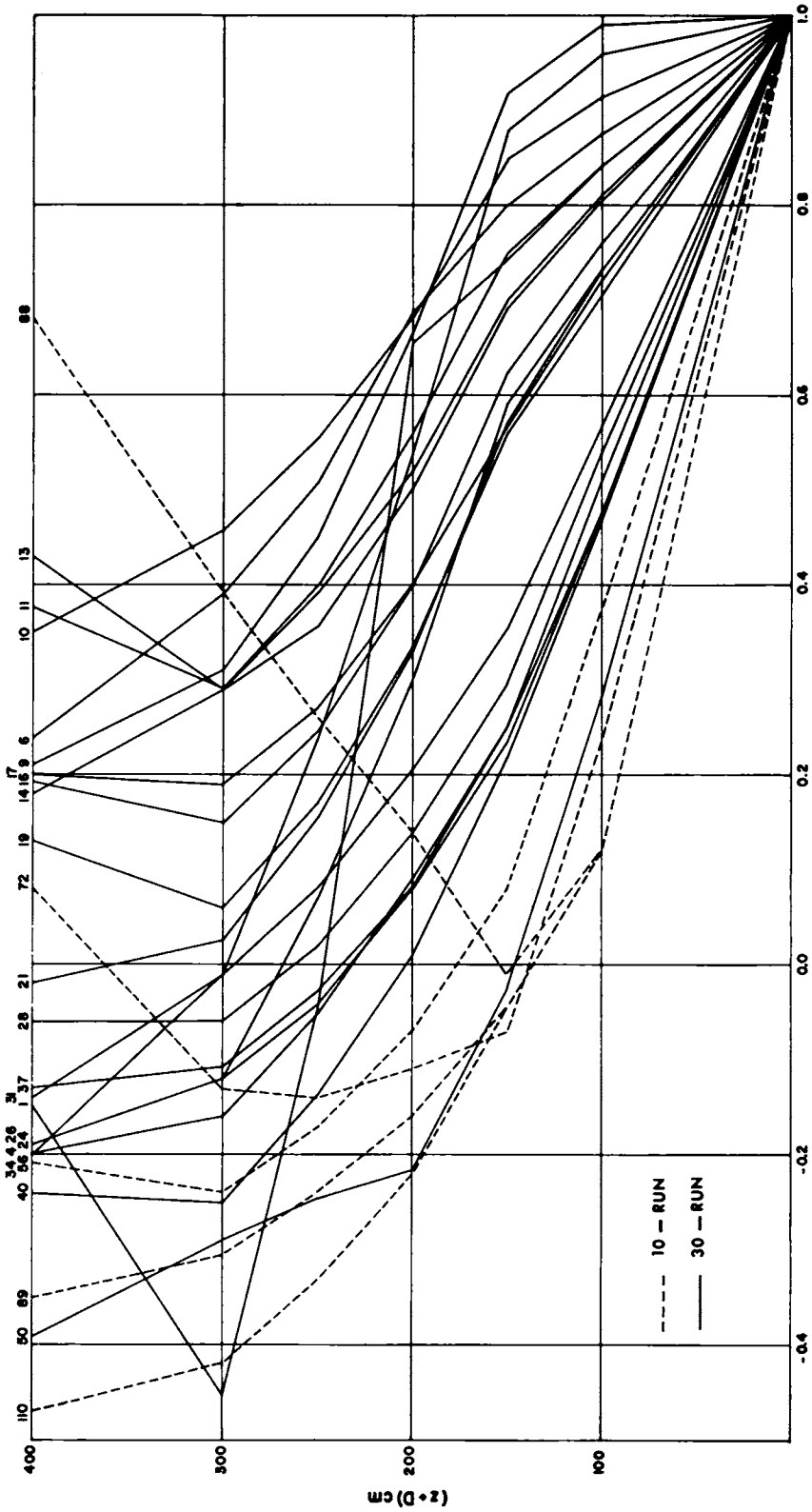

Fig. 7. β_θ versus height for indicated Ri', South Pole.

in winter, and the decrease of β_v with height is slightly less in the lower 2 meters than in spring and fall.

The most interesting and significant feature of the Deacon number variations with height evident in Figure 6 is that, in stable cases, β_v does not become zero but, even with great bulk stability, goes only to approximately 0.25 and then recurves. This recurvature is most likely due to vertical gradient of shearing stress, that is, to the increasing importance of the effect of the ratio $(\partial \log \tau / \partial \log z)$ on the wind profile curvature, where τ is the shearing stress. In other words, it is suggested that the thickness of the surface layer decreases with increasing stability, so that it becomes less than 2 meters for $Ri' > 50$.

Temperature profile curvature and the interdependence between Deacon numbers and Richardson numbers. The curvature of the profile of potential temperature, β_θ, was computed from 10- and 30-run mean vertical differences, $\Delta\theta$, grouped in the same manner as β_v. Figures 7 and 8 show that β_θ is similar to β_v only at the lower levels. For strong bulk stability the β_θ profiles do not recurve but go through zero to negative, at levels above 1 to 2 meters. At the lowest levels, near the adiabatic, β_θ appears to be unexpectedly large (Figure 7), indicating low temperatures at 50 cm. Actually, at these low levels, the temperature differences amount to only a few hundredths of a degree and may be affected by instrumental errors, which make the curvature computation (β_θ) highly unreliable.

The different behavior of β_v and β_θ profiles at strong bulk stability suggests that the surface layer of the temperature field must be significantly thicker than that of the wind field. In other words, relative momentum-flux divergence is greater than relative heat-flux divergence at a few meters above the antarctic snowfield. This is consistent with the basic equations of motion and energy in that $\partial\tau/\partial z$ is essentially given by the geostrophic departure (which will be relatively large, owing to low velocities, even though τ_0 is small), whereas $\partial Q/\partial z$, the change of eddy heat flux with height, is essentially given by the time derivative of mean temperature (which is relatively small).

Almost all existing theories of the diabatic wind profile structure are based on the assumptions that vertical flux divergence is negligible and that $\beta_v = \beta_\theta$. Also, the working hypothesis is usually made

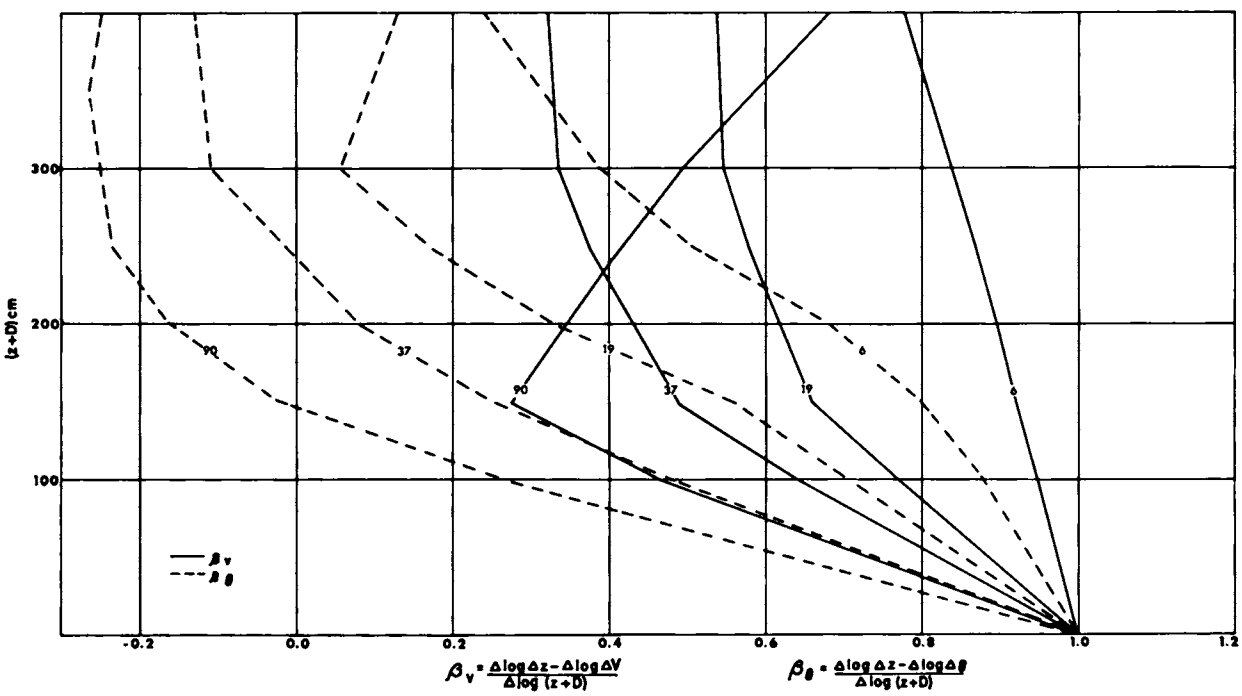

Fig. 8. β_v and β_θ versus height for indicated Ri', South Pole.

that

$$\frac{(z + D)k}{(\tau_0/\rho)^{1/2}} \cdot \frac{\partial V}{\partial z} = (1 + bRi)^a \qquad (4)$$

where a, b = numerical constants. It follows directly from equation 4 and the definition of β_v, equation 3, that

$$\beta_v = (1 + bRi)/[1 + b(1 + a)Ri] \qquad (5)$$

in view of $\partial \log Ri/\partial \log (z + D) = 2\beta_v - \beta_\theta = \beta_v$, if $\beta_v = \beta_\theta$. For $|b\ Ri|$ large in comparison to unity, β_v in equation 5 will approach asymptotically the constant of $1/(1 + a)$. According to *Priestley* [1959], this asymptotic value exists for $Ri < 0$ and equals 4/3, which requires that $a = -1/4$. *Panofsky et al.* [1960] suggest that $b = -18$, and thus the theoretical relationship in equation 5 results in

$$\beta_v = (1 - 18Ri)/(1 - 13.5Ri) \qquad (6)$$

The empirical relationship between β_v and Ri for South Pole is illustrated in Figure 9. The theoretical relationship in equation 6 describes the data reasonably well for slightly stable conditions, but predicts $\beta_v = 0$ when $Ri = 1/18 = 0.0555$. As shown in Figures 6, 8, and 9, the observed β_v does not become zero as Ri increases but recurves and increases again beyond $Ri = 0.15$. This appears to illustrate the effect of divergence of momentum flux, and it evidences again the above-quoted limitations of existing theories of diabatic profile structure.

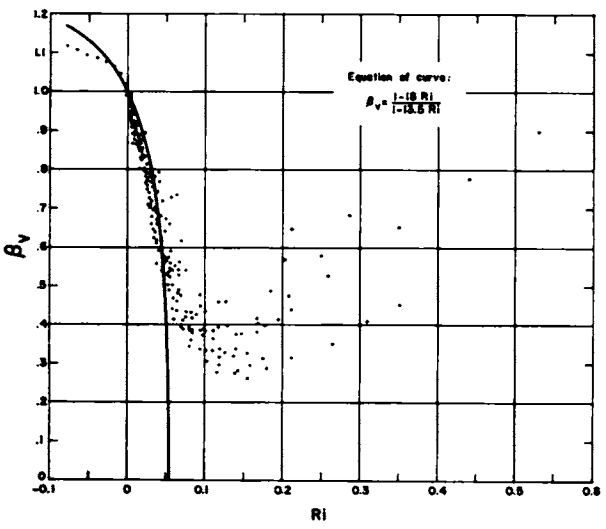

Fig. 9. Wind profile curvature β_v versus Richardson number Ri, South Pole.

β_θ is plotted versus Ri in Figure 10. β_θ does not become greater than unity for negative values of Ri as does β_v, but it must be realized that the computations for the few (and absolutely very weak) heating cases are not very reliable. In contrast to wind profile curvature, β_θ does not become double-valued with great bulk stability.

Lettau [1962] presents a quantitative explanation of the observed height variation of Deacon number β_v, with the aid of diabatic wind profile structure. In this explanation the surface theory for a horizontal surface of the Earth is considered. The following section will be devoted to an analysis of the effect of the terrain in the vicinity of the South Pole station.

4. STATISTICAL ANALYSIS OF AIR MOTION IN THE INVERSION LAYER AT THE SOUTH POLE IN RELATION TO LARGE-SCALE TERRAIN SLOPE[6]

Description of terrain and estimate of slope inclination approximately 250 km around South Pole. The terrain around South Pole appears from the air and from the surface as a relatively flat plain. This appearance is deceptive, since vehicles going to and coming from the station dip down into depressions out of sight of the base and then come back into view. These depressions are more than 10 km from camp and are of the order of tens of meters in local relief. Over distances of 200–300 km and more, the terrain shows a systematic slope, evidenced by elevation determinations during the various traverses coming into the station.

At 800 km from South Pole, and even as close as 450 km, the highest land is about 70° ± 10° azimuth. Although contours in East Antarctica are the result of a few oversnow and several airborne traverses and are subject to revision, there is no ques-

[6] *New symbols used in this section*:

G,	intensity (m/km) of ascendent vector of snow plain.
γ,	azimuth (Deg)† of ascendent vector of snow plain.
α,	wind direction (Deg)†.
S,	surface.
N,	frequency (%).
v^*,	frictional wind speed (m/sec).
U,	thermal wind vector (m/sec).
f,	Coriolis parameter (sec^{-1}).
V_g,	geostrophic wind speed (m/sec).
σ,	deviation angle of the wind (Deg)†.

† The abbreviation 'deg' stands for degrees Celsius, whereas 'Deg' is used for degrees of an arc.

tion but that the highest elevations are near the Pole of Maximum Inaccessibility. It appears that the station at the geographical south pole is lower than any site in East Antarctica within 450 km.

In the following paragraph, a method is discussed by which the general slope of the terrain can be evaluated.

Let G = intensity (m/km, or 10^{-3}) and γ = azimuth (Deg) of the ascendent vector of the snow plain in the vicinity of South Pole. For any route, i, leaving the station in azimuth α_i, the observed inclination along this route will be

$$G_i = G \cos(\alpha_i - \gamma) \quad (7)$$

If two G_i values for two different routes α_1 and α_2 have been found from elevation changes along the route, the unknown G and γ can be determined. The following relationships can be derived from elementary trigonometric and arithmetical transformations

$$G \sin\gamma = (G_1 \cos\alpha_2 - G_2 \cos\alpha_1)/\sin(\alpha_1 - \alpha_2) \quad (8)$$

$$G \cos\gamma = (G_2 \sin\alpha_1 - G_1 \sin\alpha_2)/\sin(\alpha_1 - \alpha_2) \quad (9)$$

whereupon

$$G = [(G \sin\gamma)^2 + (G \cos\gamma^2]^{1/2} \quad (10)$$

$$\gamma = \tan^{-1}(G \sin\gamma / G \cos\gamma) \quad (11)$$

Obviously, the computation of the G value will be most reliable when $\alpha_1 - \alpha_2$ is closest to ± 90 or ± 270 Deg,

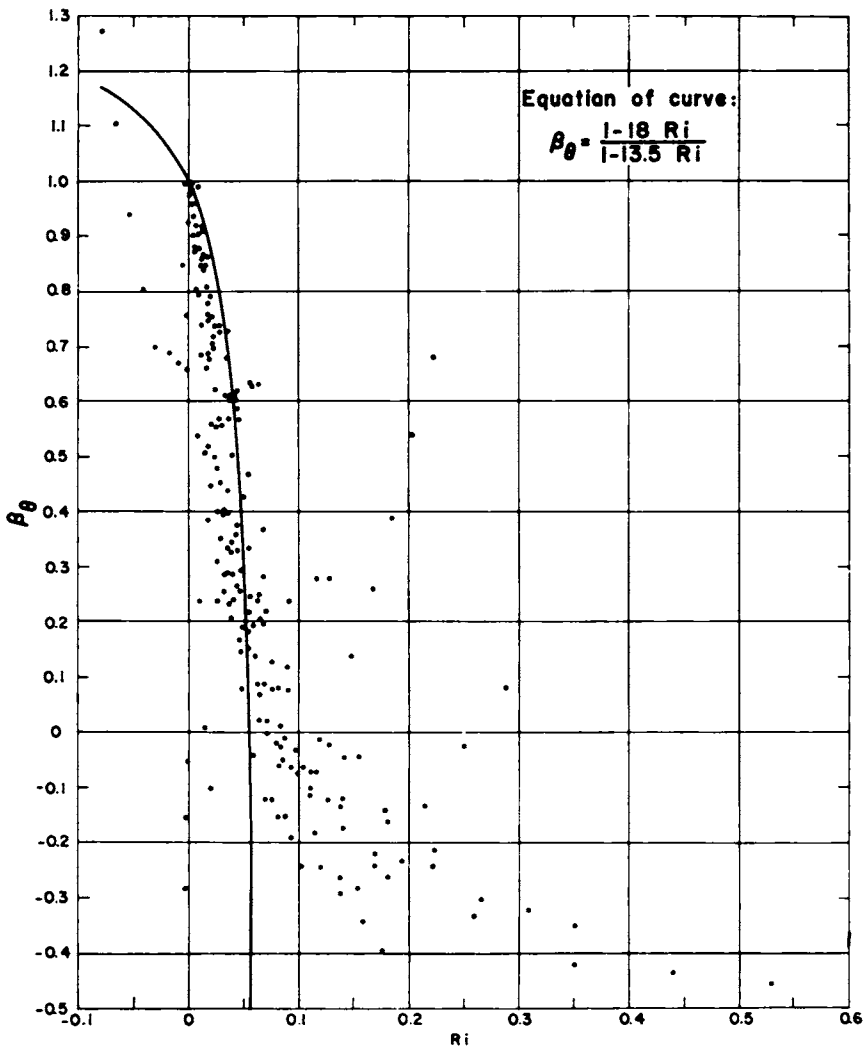

Fig. 10. Potential temperature profile curvature β_θ versus Richardson number Ri, South Pole.

and it will be unreliable when the azimuth difference of two routes is close to zero or ±180 Deg.

Basic data for slope computation are listed in Table 3. Estimates of average G_i values were obtained after reading 2–4 elevations marked on the antarctic map prepared by the American Geographical Society for the U. S. Antarctic Program. Four traverses and distances of 200–300 km out of camp were used. Of the possible 6 combinations of pairs of traverses, the one combining the inward and outward routes of the Commonwealth Trans-Antarctic Expedition cannot be used because the azimuth difference is too close to 180 Deg. The results of computation for the 5 remaining combinations are summarized in Table 4. Within tolerable error limits, the slope of the terrain (representative at a scale of an area of approximately 400-km diameter) has a magnitude of 1.76 m/km and is directed toward the meridian of 152 Deg longitude east of Greenwich.

Statistics of wind data at the top of the inversion and at the surface. Wind direction and speed at the surface (S) and top of the boundary layer inversion (H) were read from microfilms of the U. S. Weather Bureau rawinsonde data (WBAN-20 forms) for 1958, and the angle between the two ($\alpha_S - \alpha_H$) was tabulated for the sunless period,

TABLE 3. Observed Average Inclination (along Indicated Routes) of the Terrain Surrounding South Pole
(As determined from 2 to 4 spot readings at distances up to 300 km from South Pole station.)

No., i	Route	Route Azimuth, α (Deg)	Route Inclination, G_i(m/km)
1	Commonwealth Trans-Antarctic Expedition (1957–1958) (in)	330	−1.18
2	Commonwealth Trans-Antarctic Expedition (1957–1958) (out)	140	1.71
3	USSR Traverse (1959–1960)	107	1.30
4	McMurdo-South Pole Traverse (1960–1961)	202	1.10

The routes named above are indicated by numbers 1 through 4 under the general symbol 'i' (first column of table). This symbol is then used as a subscript (last column of table) to indicate that each of the inclinations listed applies along that particular route.

TABLE 4. Computed Intensity and Direction (Azimuth) of the Ascendent Vector of the Terrain Surrounding South Pole
(From indicated pairs of routes as listed in Table 3.)

Route Combination	Azimuth Difference between Routes $\alpha_1 - \alpha_2$ (Deg)	Computed Ascendent Vector: Intensity G(m/km)	Computed Ascendent Vector: Azimuth γ (Deg)
1–3	223	1.35	121
1–4	128	2.17	192
2–3	33	1.73	148
2–4	−62	1.74	151
3–4	−95	1.79	150
Representative mean:		1.76	152
Standard deviation:		±0.26	±23

March 22–September 24, as a function of wind direction at the top of the inversion (Table 5). Class intervals of 22.5° width were used in tabulating the number of cases; the 16 classes are listed in the table according to the azimuth of the middle of the interval. The difference ($\alpha_S - \alpha_H$) is considered positive for counterclockwise turning from S to H. A systematic variation with top-of-the-inversion wind direction is obvious. Table 6 shows the mean wind speed at the top of the inversion for the cases in each interval of Table 5; Table 7 shows the difference between the mean wind speed at the surface and that at the top of the inversion. These tables are used in the following section to investigate whether the topography at South Pole causes a katabatic effect (low-level winds tending to be downslope) or a thermal wind effect (low-level winds tending to be cross-slope).

The angle between the surface wind direction and that at the top of the inversion is tabulated by 10° class intervals for each month of 1958 in Table 8. The spread is large and the peak value of the distribution lies in the interval 51 to 60 Deg.

Table 9 shows wind speed versus direction for the year 1958. The wind direction frequency is also illustrated for the sunless period by Figure 4. The data shown in Figure 4, when compared with the direction of 152 Deg for the ascendent vector of the terrain as derived in Table 4, indicate that the prevailing surface winds are cross-slope rather than downslope, although the coldest winds are downslope, as would be expected. For both cross-slope

TABLE 5. Frequency Distribution

Wind direction at top of inversion (α_H, Deg) versus angle between wind direction at the surface (α_S, Deg) and at top of inversion, using counterclockwise turning with height as positive.

	α_H															
$\alpha_S - \alpha_H$	112	135	157	180	202	225	247	270	292	315	337	360	22	45	67	90
0	1												1			1
22					1			1			2	8	3	1	3	1
45										8	29	19	9	9	3	2
67						1		2	13	26	13	14	10	6		
90				1		1	1	9	14	9	3	2	1			
112						1	4	2	2	4						
135						5		3	1							
157					1	4	1	2								
180						2	1									
202						1										
225						1										
247				1		1										
270	1															
292		1	1													1
315	1	1		1												
337	1															
Total no. of cases	4	2	1	3	2	17	7	19	30	47	47	43	24	16	6	5
%	1.5	0.7	0.4	1.1	0.7	6.2	2.6	7.0	11.0	17.2	17.2	15.7	8.8	5.9	2.2	1.8

Total cases = 273

TABLE 6. Mean Wind Speed (V_H, m/sec) at Top of Inversion

(For 16 classes of α_H (Deg), according to classes of ($\alpha_S - \alpha_H$), using counterclockwise turning with height as positive.)

	α_H															
$\alpha_S - \alpha_H$	112	135	157	180	202	225	247	270	292	315	337	360	22	45	67	90
0	6.6												8.4			4.0
22					10.6			20.8			15.6	14.5	12.4	15.7	9.3	5.0
45										14.9	11.4	10.4	9.7	7.9	8.3	11.4
67						3.9		17.2	14.1	11.6	10.5	6.6	8.3	9.0		
90				5.0		15.6	16.1	11.7	10.1	8.6	4.7	6.0	10.0			
112						20.0	11.1	8.8	4.2	5.2						
135						6.1		6.7	6.7							
157					7.7	5.4	3.4	4.5								
180						5.9	4.9									
202						2.3										
225						8.9										
247				4.3		8.9										
270	2.3															
292		2.3	3.2													4.8
315	7.4	1.7		4.7												
337	3.0															
Total no. of cases	4	2	1	3	2	17	7	19	30	47	47	43	24	16	6	5
%	1	1	0	1	1	6	3	7	11	17	17	16	9	6	2	2

Total cases = 273

TABLE 7. Mean Wind Speed Difference (m/sec) between Surface and Top of Inversion
(For 16 classes of α_H (Deg), according to classes of ($\alpha_S - \alpha_H$), using counterclockwise turning with height as positive.)

	α_H															
$\alpha_S - \alpha_H$	112	135	157	180	202	225	247	270	292	315	337	360	22	45	67	90
0	+1.4												−2.4			+1.7
22					−8.6			−13.8			−4.6	−4.3	−3.5	−8.2	−2.3	−5.0
45										−5.3	−2.7	−1.9	−2.5	−0.6	−2.6	−2.4
67						+1.1		−10.4	−6.1	−3.5	−3.2	−0.2	−1.8	−2.9		
90				−1.5		−9.6	−13.6	−5.1	−3.7	−2.5	+1.0	+0.4	−3.0			
112						−11.0	−5.5	−3.8	+1.3	−0.3						
135						−2.4		−2.0	−2.2							
157					−0.7	−1.3	+0.6	−1.5								
180						−2.4	+0.1									
202						+1.7										
225						−6.9										
247				−1.3		−6.9										
270	+3.7															
292		+1.2	+1.8													+0.2
315	−1.4	+2.3		+0.3												
337	+1.5															
Total no. of cases	4	2	1	3	2	17	7	19	30	47	47	43	24	16	6	5
%	1	1	0	1	1	6	3	7	11	17	17	16	9	6	2	2

Total cases = 273

TABLE 8. Frequency Distribution of Angle between Wind Direction at Surface (α_S, Deg) and at Top of Inversion (α_H, Deg)
(By months, using counterclockwise turning with height as positive.)

$\alpha_S - \alpha_H$	Jan.	Feb.	Mar.	April	May	June	July	Aug.	Sept.	Oct.	Nov.	Dec.	Total No. of Cases
0– 10	1	4		1				1			2		9
11– 20	3	3	2	2		1			1	2		1	15
21– 30	2	1		1	4		3		2	2	2	2	19
31– 40	6	4	4		8	5	11	2	4	9	1	2	56
41– 50	1	5	6	3	7	6	10	9	2	14	1	4	68
51– 60	4		7	4	9	6	12	8	4	4	10	2	70
61– 70	1	2	4	6	6	11	7	8	9	7	5	1	67
71– 80	1	4	2	4	4	4	2	9	6	4	1	2	43
81– 90		2	4		2	7	2	8	5	2	3		35
91–100			2		3	1	5	4	3		2		20
101–110				3	1	3		2	1	3	3		16
111–120				1		1		1	2	2	1		8
121–130			1		1		1			2			5
131–140			1	2					1	2			6
141–150	1			1		1				1			4
151–160	1		2	1									4
161–170						1							1
171–180		1	1	1					2				5
Negative	4	6	2	2	1			3	1		3	1	23
Total	25	32	38	32	46	47	53	55	43	54	34	15	474

and downslope winds, the agreement is within about 30 Deg.

Data transformation and analysis of effects of thermal winds in the inversion layer. With the aid of information summarized in Tables 5–7, the mean speed at the top of the inversion layer and the two rectangular components (tangential and normal to V_H) of the surface wind vector were computed for each of the 16 individual classes of α_H. The frequencies of individual subclasses of $\alpha_S - \alpha_H$ (see Table 5) were taken into consideration in performing the computation. Results are listed in Table 10 and illustrated in Figures 11 and 12. For brevity, the wind vector at the top of the inversion for any of the 16 α_H classes will be referred to as 'inversion wind.' In the following, smoothed distribution data will be used, i.e., values from the columns of Table 10 that are labeled 'ave.'

Figure 11 is self-explanatory; Figure 12 shows the distribution of inversion winds (same as in Figure 11) as background and illustrates mainly the 16 difference vectors between inversion wind and surface wind. The surface wind vector that belongs to any inversion wind could be obtained by connecting the small circle (at the end of an individual difference vector) with the zero point of the diagram. The asymmetry of the arrangement of the difference vector endpoints on Figure 12 demonstrates clearly that there must be a systematic deflection vector superimposed on the surface winds

TABLE 9. Frequency Distribution of Surface Wind Speed versus Surface Wind Direction

Wind Dir., Deg	Wind Speed, m/sec														
	1	2	3	4	5	6	7	8	9	10	11	12	13	14	15
000	2	8	19	15	31	30	38	28	14	13	13	5	5	1	1
020	1	10	19	29	46	50	59	70	49	41	20	13	11		
040	5	7	17	29	31	30	44	29	18	4	1	3			
070		5	18	21	36	34	36	13	11		1				
090	4	6	15	33	40	47	29	13	4	1					
110	1	7	8	8	13	19	17	7	3	3					1
140	2	2	4	1	1	2	2	2							
160			1												
180		2													
200		2	1												
250		1	2												
270		2	1	1	2		1								
290		1			1	1	1		1						
310		1		3	6	4	1	5		1					
340		1	3	4	7	1	4	5		1		1			1

TABLE 10. Inversion Winds

Relative frequency (N, %) and speed (V_H, m/sec) of inversion winds as a function of azimuth (α_H, Deg); also, computed components of surface wind ($v_{S,t}$, $v_{S,n}$, m/sec) tangential and normal to V_H at indicated α_H for South Pole, 273 cases, March 22 to September 24, 1958.

α_H	N	V_H		$v_{S,t}$		$v_{S,n}$	
		dir.	ave.	dir.	ave.	dir.	ave.
0	15.7	9.66	10.13	5.18	4.90	5.60	5.69
22.5	8.8	9.38	9.43	4.25	4.73	5.12	5.41
45	5.9	8.81	9.11	4.25	4.39	5.24	4.94
67.5	2.2	8.80	8.55	5.25	4.67	3.34	4.30
90	1.8	7.32	7.27	5.20	4.93	2.40	1.33
112.5	1.5	4.82	5.45	4.10	4.27	−2.98	−0.55
135	0.7	2.00	3.71	2.05	3.29	−3.00	−3.29
157.5	0.4	3.20	3.50	1.90	1.50	−4.60	−2.33
180	1.1	4.67	5.83	0.80	−0.17	−0.93	−0.83
202.5	0.7	9.15	7.10	−2.35	−2.04	1.75	1.50
225	6.2	7.30	8.08	−2.47	−2.46	1.94	2.34
247.5	2.6	9.71	9.28	−2.43	−1.58	3.57	3.58
270	7.0	10.90	10.96	−0.47	0.13	5.04	5.72
292.5	11.0	11.30	11.09	1.10	1.57	6.63	6.49
315	17.2	11.03	11.06	2.70	3.17	6.86	6.48
337.5	17.2	10.91	10.58	4.96	4.26	6.05	6.18

Note: Values in column 'dir.' are computed directly from data listed in Tables 5–7. Values in column 'ave.' are 3-value running means using indicated frequencies (N) of α_H classes as weight factors.

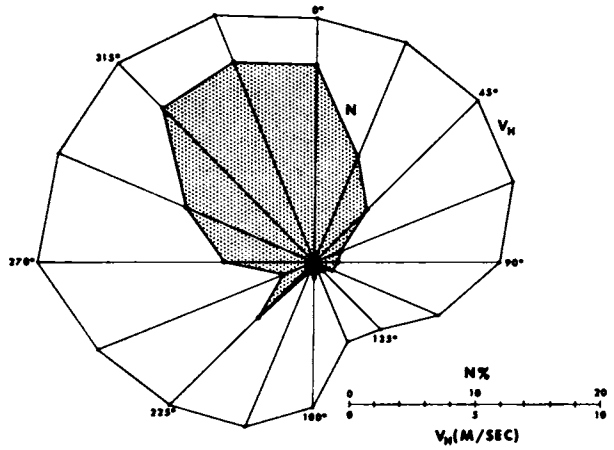

Fig. 11. Relative frequency (N, %) and speed (V_H, m/sec) of winds at the top of the inversion as a function of azimuth (α_H, Deg) at South Pole (273 cases, March 22 to September 24, 1958).

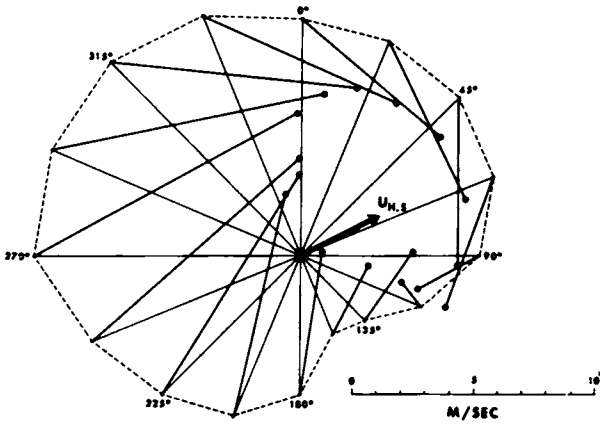

Fig. 12. Thermal wind in the inversion layer ($U_{H,S}$) constructed from mean vector differences between wind at surface (V_S) and at top of the inversion (V_H, m/sec) as a function of azimuth α_H, Deg) at South Pole (273 cases, March 22 to September 24, 1958).

at South Pole relative to the inversion winds. In the following analysis it shall be shown that this systematic deflection is very probably due to the superposition of a persistent thermal wind in the inversion layer between surface and height H.

Obviously, Figure 12 suggests some kind of 'focusing' effect in that, for inversion wind from the wide azimuth sector 22°–112°, the accompanying surface wind directions are only between 67° and 112°; or, for inversion winds in the azimuth sector 202°–315°, the surface wind directions range only from 330° to 20°, approximately. This effect will explain the differences in the over-all frequency distribution of surface winds (see Figure 4) and inversion winds. Details of analysis follow.

Let us assume that there exists a thermal wind that is persistent and independent of the inversion wind. Then it follows from vector geometry that the thermal wind effect will exactly cancel out when pairs of wind distributions for opposite azimuth directions α_H are averaged. The results of such procedures are given in Table 11. It will be assumed that the possibly existing thermal wind in the inversion layer above the South Pole region has been eliminated by this averaging. Hence, purely 'frictional' surface wind components (tangential and normal to the inversion wind V_H) for each of the 16 α_H classes can be obtained as

$$v_{S,t}^* = \bar{v}_{S,t} V_H / \bar{V}_H \qquad (12)$$

$$v_{S,n}^* = \bar{v}_{S,n} V_H / \bar{V}_H \qquad (13)$$

where the barred valued are those given in Table 11 for 8 pairs of α_H values, whereas V_H is the series of the 16 values listed in Table 10. Finally, the thermal wind components (tangential and normal to the inversion wind V_H) can be restored and are obtained as

$$u_t = v_{S,t} - v_{S,t}^* \qquad (14)$$

$$u_n = v_{S,n} - v_{S,n}^* \qquad (15)$$

The angle between the thermal wind vector and the inversion wind is given by $\tan^{-1}(u_n/u_t)$. Thus, the thermal wind has the true azimuth of $180 + \alpha_H + \tan^{-1}(u_n/u_t)$, and the intensity of $(u_t^2 + u_n^2)^{1/2}$.

The results of computation of the direction and intensity of the thermal wind are summarized in Table 12. It can be seen that the obtained azimuth values are indeed fairly constant, averaging 241.5 Deg with a standard deviation of ±9.0 Deg, with

TABLE 11. Inversion Winds, Averages

Average of inversion wind speed ($\bar{V}_H$, m/sec) and surface wind components ($\bar{v}_{S,t}$, $\bar{v}_{S,n}$; m/sec), from Table 10, for indicated pairs of opposite azimuth values (α_H, Deg).

α_H	$\bar{V}_H$	$\bar{v}_{S,t}$	$\bar{v}_{S,n}$
0 and 180	7.98	2.36	2.43
22.5 and 202.5	8.26	1.34	3.46
45 and 225	8.60	0.97	3.64
67.5 and 247.5	8.92	1.55	3.94
90 and 270	9.12	2.56	3.52
112.5 and 292.5	8.27	2.92	2.94
135 and 315	7.38	3.23	1.60
157.5 and 337.5	7.04	2.88	1.92

TABLE 12. Inversion Wind and Thermal Wind

Speed of inversion wind (V_H, m/sec), estimated frictional components of surface wind ($v^*_{s,t}$, $v^*_{s,n}$; m/sec), estimated components of thermal wind (u_t, u_n; m/sec), also magnitude ($(u_t^2 + u_n^2)^{1/2}$, m/sec) and azimuth ($180 + \alpha_H + \tan^{-1}(u_n/u_t)$, Deg) of thermal wind between surface and top of the inversion at South Pole, as a function of azimuth (α_H, Deg).

α_H	V_H	$v^*_{s,t}$	$v^*_{s,n}$	u_t	u_n	$(u_t^2 + u_n^2)^{1/2}$	$\tan^{-1}\frac{u_n}{u_t}$	$180 + \alpha_H + \tan^{-1}\frac{u_n}{u_t}$
0.	10.13	2.99	3.08	1.91	2.61	3.24	53.9	234
22.5	9.43	1.53	3.95	3.20	1.46	3.52	24.5	226
45	9.11	1.04	3.86	3.35	1.08	3.52	17.9	243
67.5	8.55	1.47	3.78	3.20	0.52	3.24	9.2	257
90	7.27	2.04	3.81	2.89	−2.48	3.81	−40.8	229
112.5	5.45	1.82	1.82	2.45	−2.37	3.41	−44.1	248
135	3.71	1.62	0.81	1.67	−4.10	4.43	−67.8	247
157.5	3.50	1.43	0.95	0.07	−3.28	3.28	−88.8	249
180	5.83	1.73	1.78	−1.90	−2.61	3.23	−116.1	234
202.5	7.10	1.15	2.97	−3.19	−1.42	3.49	−156.1	226
225	8.08	0.92	3.42	−3.38	−1.08	3.55	−162.3	243
247.5	9.28	1.61	4.10	−3.19	−0.52	3.23	−170.8	257
270	10.96	3.08	4.24	−2.95	1.48	3.30	−206.7	243
292.5	11.89	3.70	3.74	−2.13	2.70	3.44	−231.7	241
315	11.06	4.05	2.40	−0.88	4.08	4.17	−257.9	237
337.5	10.58	4.35	2.09	−0.09	4.09	4.09	−268.7	249
Mean and standard deviation						3.56 ± 0.32		241.5 ± 9.0

an average magnitude of the thermal wind of 3.56 ± 0.32 m/sec. This vector $U_{H,S}$ is indicated on Figure 12. It remains to be proven that it really does represent a thermal wind.

It has been demonstrated that, for about 200- to 300-km radius about South Pole, the terrain has a general ascendent vector in the direction of 152 ± 23 Deg. Assuming relatively uniform surface temperature and inversion layer thickness, this must imply that there is in the lower atmosphere a horizontal temperature gradient parallel to the ascendent vector. It follows from elementary dynamics of the atmosphere that a thermal wind must result in the direction of 152 + 90 = 242 Deg, which is equal to the average azimuth of the vector $U_{S,H}$ derived in Table 12.

However, estimates of the theoretical magnitude of the thermal wind produce a result that is less satisfying than the above.

It follows from Table 1 that from March through September the temperature difference $T_H - T_S$ averages 11.4°C. The intensity of the ascendent vector of the terrain was determined in Table 4 as $G = 1.76 \times 10^{-3}$. Assuming uniformity of inversion layer structure along the slope, the horizontal temperature gradient in the middle of the inversion layer will be approximated by 11.4 G/H = 0.020 deg/H, where H = height of the inversion above the surface. Values of monthly means of H are also listed in Table 1 but will not be needed for the following discussion. The thermal wind in the layer from the surface to H will be proportional to H multiplied by the horizontal temperature gradient. Thus, with the proper coefficient of proportionality

$$U_{H,S} = g(T_H - T_S)G/T_m f = 6.1 \quad \text{m/sec} \qquad (16)$$

where T_m = average absolute layer temperature = 220°K.

Considering the computational value of the standard deviation of the G determination (1.76 ± 0.26 m/km), the above theoretical result of 6.1 ± 0.9 m/sec does not compare favorably with the average of 3.6 ± 0.3 m/sec derived in Table 12. However, the uncertainties due to the assumption of a uniform inversion layer structure may account for a factor of nearly 2. It is difficult to improve the basis of computation without direct knowledge of actual conditions in the environment of South Pole.

Finally, an attempt was made to investigate certain characteristics of surface friction in the south pole region from the data analyzed above.

It is assumed that the inversion wind corresponds to the geostrophic wind at height H. When the thermal wind components for individual inversion wind directions (α_H) are known it is easy to subtract the thermal wind vector from the inversion wind. This procedure results in the angular deviation ($\sigma_{g,0}$) from the inversion wind direction (α_H) of the geostrophic wind at the surface

$$\tan \sigma_{g,0} = u_n/V_H \tag{17}$$

and the intensity ($V_{g,0}$) of the geostrophic wind at the surface

$$V_{g,0} = [(V_H + u_t)^2 + u_n^2]^{1/2} \tag{18}$$

The deviation angle σ_S from α_H and the intensity (V_S) of the surface wind are

$$\tan \sigma_S = v_{S,n}/v_{S,t} \tag{19}$$

$$V_S = [v_{S,n}^2 + v_{S,t}^2]^{1/2} \tag{20}$$

Since σ_S and $\sigma_{g,0}$ both measure deviation from α_H, their difference represents the angular deviation of the observed surface wind from the surface geostrophic wind, which would be parallel to the isobars

$$\alpha_0 = \sigma_S - \sigma_{g,0} \tag{21}$$

This deflection (α_0) of the surface wind from the isobars, together with the wind ratio ($V_S/V_{g,0}$), shows the effect of surface friction. These quantities have been computed for 8 directions of the inversion wind (α_H) and are shown in Table 13. Only these 8 α_H data produced coherent results. The other 8, probably due to low relative frequency and low wind speeds, gave erratic and widely scattered results.

Summary of analysis. The significant result of the analysis of statistical wind data from the South Pole region is that no evidence of katabatic air flow has been found. The results do indicate that the air motion in the lower atmosphere is controlled by surface friction and by the geostrophic motion in the free atmosphere above the inversion layer, modified by thermal winds due to horizontal temperature gradients which result from the general slope of the terrain.

For a sloping plain of the extent of 200- to 300-km radius, equilibrium with the Coriolis acceleration is likely because, at an average speed of 6 m/sec or 20 km/hr, it would take a full day to traverse this region.

Since this analysis does not indicate that the observed profile structure at South Pole reflects katabatic winds even partly, it has eliminated a possible cause of the observed profile structure which might have invalidated the previous conclusions concerning the vertical profile of Deacon numbers.

5. ROUGHNESS LENGTH[7]

Computation of roughness length from wind profiles. The conventional method of z_0 determination is based on the logarithmic wind profile which will exist only in an adiabatic surface layer [*Lettau*, 1957]. In view of the extreme rareness of neutral conditions at South Pole, a new method of profile analysis was introduced which permits computation of roughness length, z_0, from diabatic profiles. Supported by the facts illustrated in Figure 6, the assumption is made that $(\beta_v - 1)$ varies in direct proportion to height, at least in the lowest layer. Then, using the equation defining β_v, it follows upon integration that

$$\log z_0 = \log (z + D) - 0.4343 [\alpha^{-1} e^{(1-\beta_v)} - (1 - \beta_v) - 0.25(1 - \beta_v)^2 \cdots] \tag{22}$$

where common logarithms are used and the profile contour number α equals $\Delta \log V/\Delta \log (z + D)$. Since D was obtained independently, equation 22

TABLE 13. Surface-Geostrophic Wind

Speed ($V_{g,0}$, m/sec) and deviation angle ($S_{g,0}$, Deg) of the surface-geostrophic wind estimated from inversion wind, V_H, and thermal wind components, u_t, u_n (see Table 12). Also speed (V_S, m/sec) and deviation angle (σ_S, Deg) of the surface wind (from Table 10), and ratio $V_S/V_{g,0}$, and deflection angle $\alpha_0 = S_S - S_{g,0}$. Data are listed as a function of the azimuth (α_H, Deg) of the inversion wind at South Pole for 8 classes of α_H.

α_H	$V_{g,0}$	$S_{g,0}$	V_S	σ_S	$V_S/V_{g,0}$	α_0
292.5	9.2	14	6.6	76	0.72	62
315	10.8	20	7.2	64	0.67	44
337.5	11.3	21	7.5	55	0.66	34
0	12.4	14	7.5	49	0.60	35
22.5	12.8	9	7.2	49	0.56	40
45	12.6	7	6.6	48	0.52	41
67.5	11.9	3	6.4	43	0.54	40
90	10.7	−19	5.1	15	0.48	34
Mean	11.46		6.76		0.594	41.2

[7] *New symbols used in this section*:

α, profile contour number.
ρ, air density (g/cm³).
ν, molecular kinematic viscosity (cm²/sec).

can be solved for any level where α and β_v are known.

The mean z_0 was obtained from all data levels, or, in the more stable cases, from at least the three lowest levels. The D value in one case was adjusted to obtain more reasonable values of z_0, keeping the measure of the profile curvature β_v, however, in line with curves for adjacent Ri' classes.

Magnitude and variation of roughness length. The aerodynamic roughness length z_0 of the South Pole region was found to be nearly constant at about 0.014 cm for a wide range of bulk stability (Figure 13).

The low value is consistent with other measurements over snow. *Liljequist* [1956–1957] at Maudheim (71°03′S, 10°56′W) obtained an average of 0.012 cm for winds between 5 and 15 m/sec at 10-meter height. *Rusin* [1960] found the roughness parameter less than 0.01 mm at the Soviet temporary portable stations, and he attributes the minimum values to streamlining of the surface caused by blowing snow. *Deacon* [1953] gave 0.005 cm for smooth snow on short grass, and 0.1 cm from Priestley's measurements over snow in Canada. Deacon states that a z_0 independent of bulk stability is consistent with small variation of β_v with height; actually at South Pole there was considerable variation of β_v with height and z_0 appears to be constant.

Roughness lengths that increased slightly with instability and with extreme stability are questionable because the instances are so few. However, Lilje-

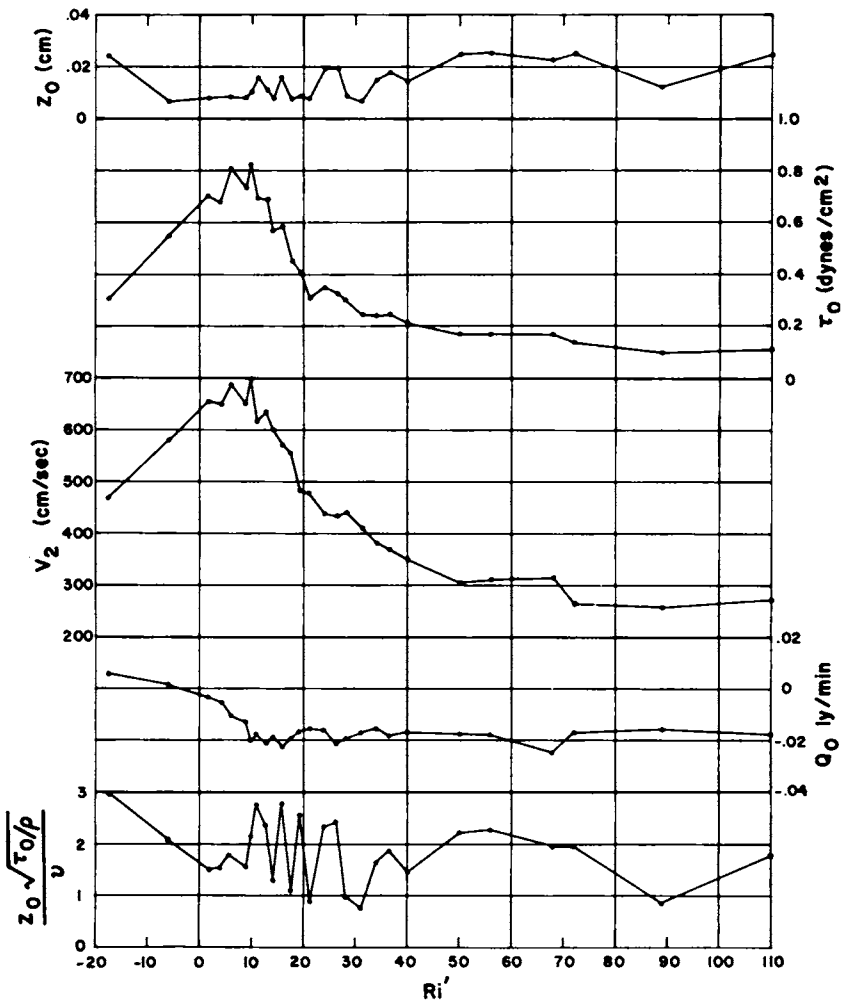

Fig. 13. Variation with stability of roughness length z_0, surface stress τ_0, 2-meter wind speed V_2, eddy heat flux Q_0, and $z_0[(\tau_0/\rho)^{1/2}/\nu]$, South Pole.

quist obtained similar results at Maudheim (71° 03′S, 10°56′W). The very small increase at extreme bulk stability could be due to difficulty in obtaining the best values of D, where β_v profiles begin to show curvature at relatively low elevation. Also, Liljequist suggests that flow that is near the laminar and includes molecular effects may cause increase of z_0 with decreasing wind speed. However, if the requirement for truly laminar flow is assumed to be a strictly linear wind profile, i.e., $\beta_v = 0$, one must conclude from Figure 6 that truly laminar flow never occurred at South Pole.

Sastrugi greater than 20 cm were always removed from the mast area. Since the snow is frequently drifting and sastrugi migrating during high winds, the surface is of a different character from the usual land surface, perhaps more like an ocean surface or one with flexible roughness elements like bending grass blades. The roughness length was computed for several days in May with wind speeds near 10 m/sec at the 8-meter level, and the surface under and near the mast covered with sastrugi that had not been disturbed. In this case, large D values are necessary to obtain good fits of the wind profile curvature, and z_0 is small. It appears, in fact, that z_0 decreases with increasing wind speed instead of increasing, as was expected. D values used and roughness length are shown in Table 14 for 6 hours of May 14–17.

To obtain cases with still higher wind speeds it is necessary to use the observations that had been omitted because simultaneous wind and temperature profiles are not available. From these observations it becomes evident that z_0 does increase under unstable conditions when wind speed is high enough (about 13 m/sec at 8 meters) to produce an increase of β_v with height throughout the 0.5- to 8-meter layer. The flow is then fully rough, but even at slightly lower speeds an inversion still exists in the lowest meter. Liljequist considers the increase in z_0 with increase in wind speed, at higher wind speeds, as due primarily to surface friction from drifting snow, a theory that may well be valid at South Pole.

When z_0 was computed for 2 individual hours per month, on separate days, in the Ri' range near 20, no reliable seasonal variation was detectable. Although stability does vary somewhat throughout the year, z_0 seems to vary little with change in stability, and, therefore, little change in z_0 with season would be expected from this cause. Day to day variations in the profiles apparently are greater than change induced by variations in the character of the snow surface with season.

Roughness length, z_0, was multiplied by friction velocity, $(\tau_0/\rho)^{1/2}$, and the product divided by molecular kinematic viscosity ($\nu = 0.14$ cm^2/sec). This ratio is conventionally taken as a measure of the aerodynamical nature of the flow. Smooth flow usually is assumed to exist when $z_0(\tau_0/\rho)^{1/2}/\nu$ is smaller then 0.2, whereas fully developed rough flow requires that $z_0(\tau_0/\rho)^{1/2}/\nu$ be larger than 2.5. Nearly all stability classes except the most unstable 15-run group fall between the two limits, as shown in Figure 13.

6. SHEARING STRESS AND EDDY HEAT FLUX[8]

Friction velocity, surface stress, and drag coefficient. The friction velocity $(\tau_0/\rho)^{1/2}$, was computed from the grouped data, using a formula that is valid for the same assumptions that underlie equation 22, namely $\partial\beta_v/\partial z =$ constant, and $\beta_{v,0} = 1$.

$$(\tau_0/\rho)^{1/2} = 0.4343\, ke^{(\beta_v - 1)} \cdot \frac{\Delta V}{\Delta \log (z + D)} \qquad (23)$$

where common logarithms and a value of the Kármán constant $k = 0.40$ are used.

Surface stress, τ_0, was determined by averaging values of $(\tau_0/\rho)^{1/2}$ for the lower levels where the profile curvature always seems to vary such that $(1 - \beta_v)$ is directly proportional to height. Air

TABLE 14. Roughness Length with Higher Wind Speeds
Wind speed at 4 meters (V_4, m/sec); displacement parameter (D, cm); and roughness length (z_0, cm), May 14–17, 1958, at South Pole.

V_4	D	z_0
8.4	45	0.0009
9.2	10	0.0013
4.9	0	0.0080
4.8	−20	0.0106
5.6	−30	0.0014
6.1	−25	0.0009

[8] *New symbols used in this section*:
c_p, specific heat of dry air at constant pressure (cal g^{-1} deg^{-1}).
λ, dimensionless momentum transfer coefficient.
Φ, dimensionless heat transfer coefficient.
Λ, heat transfer coefficient [cm(°F) min^{-1} kt^{-2}].

density, ρ, was computed from the USWB station data, using their 3-hourly observations of temperature, pressure, and pressure tendency. For these lower levels, stress (τ) is considered independent of height. The surface stress for the grouped data ranges from 0.103 dyne/cm^2 at $Ri' = 89$ to 0.825 at $Ri' = 10$. The results are illustrated in Figure 13, as is the wind speed at 2 meters, which the stress variations follow closely.

A convenient drag coefficient (as defined by the dimensionless ratio $[(\tau_0/\rho)^{1/2}/V_4]$ is nearly independent of bulk stability and averages 0.039.

Eddy heat flux. Eddy heat flux Q_0 was computed using a similarity relation, based on vertical differences of wind speed and potential temperature from all 5, or in cases of extreme stability, the lowest 4 or 3 heights.

$$Q_0 = -c_p\tau_0(\Delta\theta/\Delta V) = -14.4\tau_0(\Delta\theta/\Delta V) \qquad (24)$$

This involves the assumption that the eddy diffusivities for heat and horizontal momentum are the same. A sign convention is chosen so that heat flowing in the direction of increasing z values (upward) corresponds to positive Q_0, whereas the heat flux accompanying inversional temperature gradients is in the downward direction and, therefore, a negative Q_0. Eddy heat flux for the grouped data ranges from —0.0239 ly/min at $Ri' = 68$ to 0.0052 ly/min at $Ri' = -18$ (Figure 13), although, above $Ri' = 10$, no consistent variation is apparent.

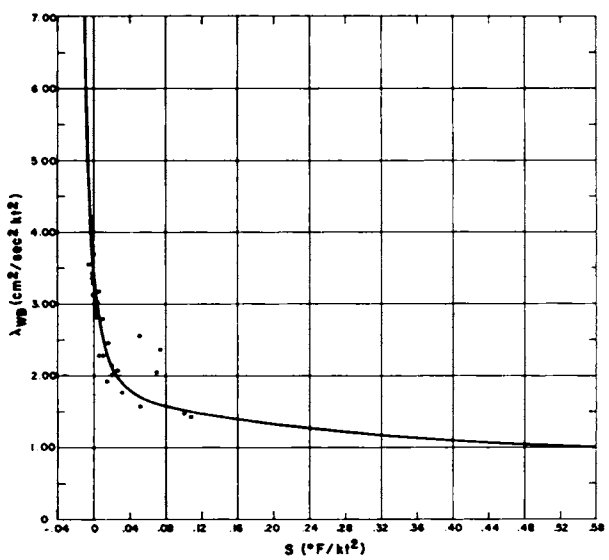

Fig. 14. Momentum transfer coefficient λ_{WB} (USWB data) versus stability coefficient S, South Pole

Coefficients of momentum transfer and heat transfer. A dimensionless momentum transfer coefficient is defined and computed from

$$\lambda = \tau_0/\rho(V_2 - V_{0.5})^2 \qquad (25)$$

and a corresponding dimensionless heat transfer coefficient from

$$\Phi = -Q_0/c_p\rho(V_2 - V_{0.5})(\theta_2 - \theta_{0.5}) \qquad (26)$$

Since it had been assumed in computing the eddy heat flux Q_0 that $\tau_0/Q_0 \sim \Delta V/\Delta\theta$, the two coefficients produce similar curves when plotted against Ri', both showing a nonlinear decrease with bulk stability. Since the ratio of friction velocity to wind speed shows relatively little variation with bulk stability and wind speed, a more convenient coefficient of momentum transfer is defined as

$$\lambda^* = \tau_0/\rho(V_4)^2 \qquad (27)$$

and a heat transfer coefficient, for consistency, as

$$\Phi^* = -Q_0/c_p\rho(V_4)(\theta_2 - \theta_{0.5}) \qquad (28)$$

Hourly values of shearing stress and heat flux from USWB observations. In order to estimate hourly values of shearing stress and the heat flux for the entire period, it is necessary to establish an empirical relationship between measures of bulk stability and the coefficients of momentum transfer and heat transfer for hours when temperatures at two levels and wind speed at one are available from both Quartermaster and USWB observations. The relationship of the bulk stability coefficient Ri' from Quartermaster data to the stability coefficient S from USWB data (equation 2) is shown in Figure 2.

For the 26 groups of 665 hours, coefficients of momentum transfer λ_{WB}, and heat transfer, Φ_{WB}, were computed from

$$\lambda_{WB} = \tau_0/[\rho(U_{10})^2] \qquad (29)$$

and

$$\Phi_{WB} = -Q_0/[c_p\rho(U_{10})(T_{10} - T_{2.5})] \qquad (30)$$

using τ_0 and Q_0 for the groups, as computed from the Quartermaster data, wind speed at 10 meters (U_{10}), and temperatures at 10 and 2.5 meters (T_{10} and $T_{2.5}$) from USWB observations.

By plotting λ_{WB} versus S for the 26 groups, the curve in Figure 14 was obtained. When Φ_{WB} was plotted versus S, however, an unsatisfactory curve was obtained, because Φ_{WB} becomes infinite when $S = 0$, i.e., when the temperature gradient between 10 and 2.5 meters is zero. By studying the curve, it was found that the product $S \cdot \Phi_{WB}$ appeared to be a linear function of S. Putting $S \cdot \Phi_{WB} = \Lambda$, the new heat transfer coefficient Λ was computed for the Quartermaster eddy heat flux data (for the 26 groups) and plotted against the stability coefficient S (Figure 15). Although there is considerable scatter, the relationship does appear to be linear, and the equation of the resulting straight line is

$$\Lambda = 0.04 + 3S \qquad (31)$$

with Λ in cm(°F) min^{-1} kt^{-3}. From equations 2 and 30 it follows that Λ is inversely proportional to the cube of wind speed. The use of a wind speed to the third power in dimensionless relationships between heat flux and stability is suggested by the theory as originally proposed by *Lettau* [1952].

Since the slope was increasing rapidly in the direction of instability in Figure 14, the graphs in Figures 14 and 15 were not extended beyond $S = -0.01$. The slope in Figure 14 becomes very slight with great stability; therefore the graph was extended to $S = 0.56$, assuming for λ_{WB} an asymptotic value of unity. λ_{WB} was read from Figure 14 for each hour of the 1958 data when S was available, excluding hours with calm winds (which would give infinity for S). Λ was computed from equation 31. The surface stress was obtained by using equation 29, and the eddy heat flux by using equation 30, with c_p, the specific heat of dry air at constant pressure, as 0.13 cal/g(°F). After U, S, ρ, λ_{WB}, and Λ were punched on cards, the multiplications were done by machine.

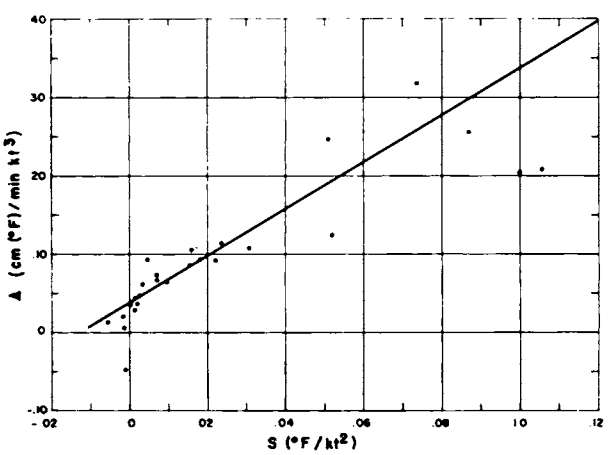

Fig. 15. Eddy heat transfer coefficient, Λ (USWB data) versus stability coefficient S, South Pole.

7. HEAT FLUX IN THE SNOW[9]

Temperature patterns at Maudheim and South Pole. The heat flux in the snow (S_0) is an important constituent of the heat budget at the snow-air interface. For South Pole, information on subsurface temperature and snow density is available in the glaciological data report by *Giovinetto* [1960], particularly in Table 20, p. 84. Similar information for Little America V is included in a report by *Crary* [1961].

The seasonal variation of S_0 may be obtained from a harmonic (Fourier) analysis of snow-temperature records. To develop and test a suitable and objective procedure for obtaining S_0, with full consideration of the inhomogeneity of the snow, data published for Maudheim (71°03′S, 10°56′W) by *Schytt* [1960] were used. Temperatures at the various depths for both Maudheim and South Pole were tabulated, centered on 24 equally spaced dates throughout the year, using April 1 as the zero date. The temperatures published for Maudheim are 10-day running means. Down to and including the 4-

[9] *New symbols used in this section:*

- S_0, vertical heat flux in the snow at the interface (ly/time).
- n, frequency.
- A, amplitude of the harmonic wave of temperature (deg)†.
- α, phase lag of the harmonic wave of temperature (Deg)†.
- t, time.
- B, amplitude of the harmonic wave of vertical temperature gradient (deg)†.
- β, phase lag of the harmonic wave of vertical temperature gradient (Deg)†.
- γ, phase difference between waves of temperature and vertical temperature gradient (Deg)†.
- K, thermal diffusivity of the snow (cm^2/sec).
- F, flux of heat (ly/time).
- λ, heat conductivity (ly $time^{-1}$/deg m^{-1}).
- ρ, snow density (g/cm^3).
- C, heat capacity (cal deg^{-1} cm^{-3}).
- T', partial differentiation of temperature with respect to time.
- T'', vertical temperature gradient, i.e., partial differentiation of temperature with respect to depth.
- σ, phase lag of the harmonic of the heat flux (Deg)†.
- ϵ, phase difference between harmonic waves of heat flux and vertical temperature gradient (Deg)†.

† The abbreviation 'deg' stands for degrees Celsius, whereas 'Deg' is used for degrees of an arc.

meter level, 3-value running means of these published temperatures were computed. Below 4 meters only 12 values per year are given. The intermediate temperatures were obtained by graphical interpolation, and no further smoothing was used (Figure 16).

For South Pole, the subsurface spot-reading temperatures at 1.0-, 1.5-, 2-, 3-, 5-, and 12-meter depth were taken from *Giovinetto* [1960]. With the division of the year into 24 equally spaced periods, some interpolations are necessary when using this table, regardless of the zero date chosen. As in the case of Maudheim data, April 1 was used as zero

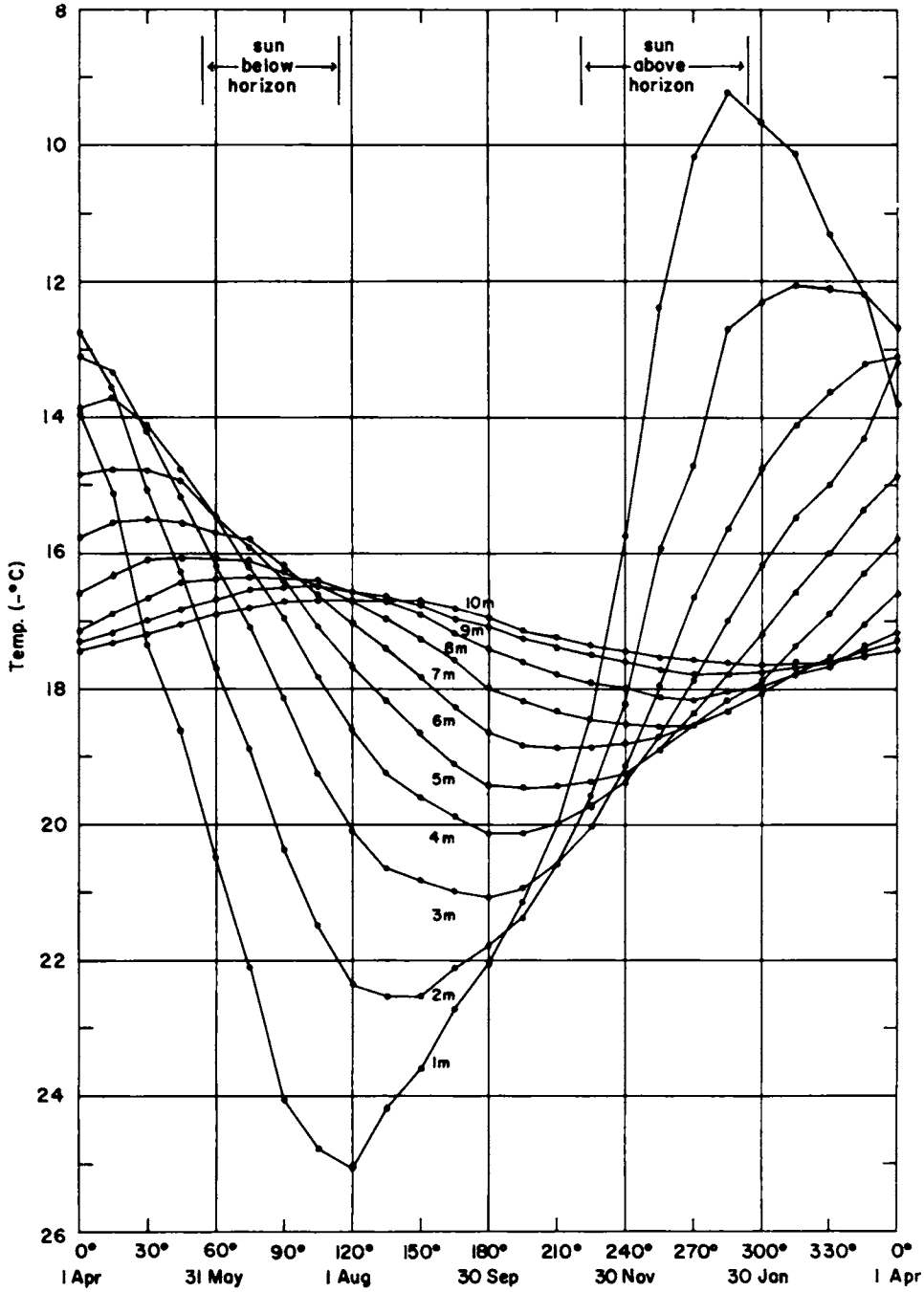

Fig. 16. Subsurface temperature versus time at Maudheim (1950 and 1951).

date. Daily means were computed for subsurface data from —2 to —50 cm, and 7-day running means were determined for —250 and —800 cm. The simultaneous appearance of small fluctuations at the various levels, as contrasted with the slow and progressive penetration of the annual temperature wave, made it possible to identify and eliminate, at —250 and —800 cm, the irregularities that were caused by recorder drift, reference ice-bath changes, and electric power fluctuations (Figure 17).

Seven-day running means of Quartermaster observations of temperature at 200 cm, at the surface, and at —10 cm and below were plotted. Where data were missing for a day or two, they were interpolated graphically, occasionally with some guidance from the USWB thermohm reading at 2.5 meters. Interpolation over a relatively long period during the summer was necessary, since only ten months of Quartermaster observations are available for South Pole. This interpolation was limited to the following levels: 200 cm, surface, —50 cm and below. Three-value running means were used to smooth all temperatures except those below 500 cm. By graphing these temperatures and subsurface temperatures form Giovinetto's table, annual smoothed curves were obtained (Figure 18), and temperatures read for the dates when observations were missing.

Isotherms, or temperature isopleths in a time-depth coordinate system for South Pole are shown in Figure 19. This figure depicts the penetration of the temperature wave to greater depths.

Figure 20 covers the period March 1 to October 31. Triple minima, at approximately 2-month intervals, occur at 200 cm, the surface, —10, —25, and —50 cm. At —250 cm there is a single minimum in late September. For that year (1958) at least, air temperatures do not exhibit a smooth annual course, with a single minimum just before sunrise and a sharp rise thereafter, but show the flat winter minimum, with reversals of the temperature trend typical of polar regions in both hemispheres.

Tautochrones showing temperature versus depth at a given time were plotted for both Maudheim and South Pole. For Maudheim (Figure 21) a wider scale was used, giving the appearance of a wider 'basket' than for South Pole. At lower depths at both stations, the tautochrones tend to become symmetric and approach the vertical. Using the temperature at 8 meters as a measure of the long-term mean annual temperature, the mean for South Pole is —50.8°C, and the mean for Maudheim —17.2°C. It appears significant that the tautochrone pattern near the surface is very symmetrical at Maudheim, but at South Pole (Figure 22) it shows relatively intense and rapid warming for a few months, followed by rapid cooling for a few months and slower cooling for the remainder of the year.

In 1958, by March 1, at South Pole, there was cooling to 1.5 meters, while farther below the temperature was still rising. This pattern replaced the incoming radiation-type temperature versus depth

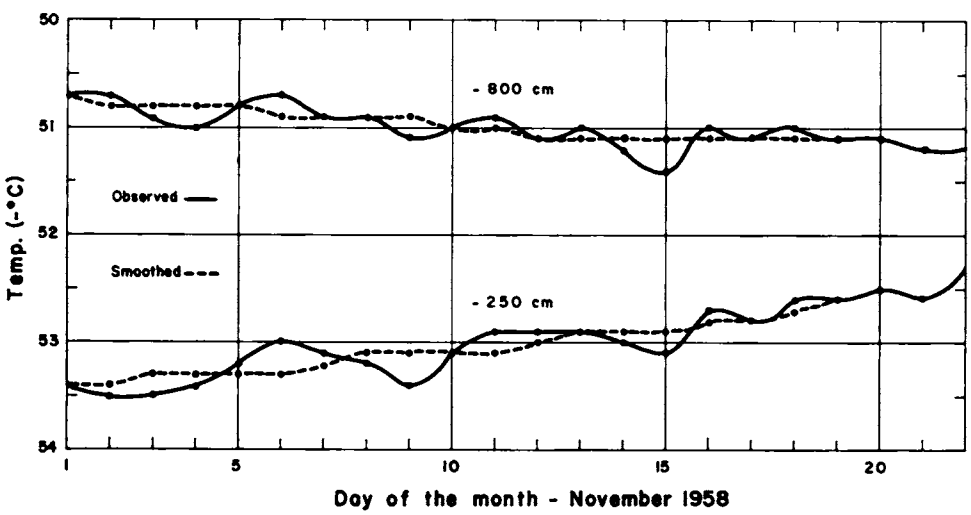

Fig. 17. Deep thermocouple fluctuations, South Pole.

curve, and produced a level of minimum temperature at 1.5 meters. As this minimum moved farther down it became less distinct, appearing at 2 meters by April 1, 3 meters by May 1, 5 meters by May 31, and 8 meters by August 1. Thus a nearly uniform temperature gradient in the 8-meter layer was established about 1 month before sunrise. Then the cycle reversed. Warming above and continued cooling below caused a level of maximum temperature at 1-meter depth by September 30, 2-meter by October 31, 3-meter by November 30, 5-meter by December 31, and 8-meter by January 30. These

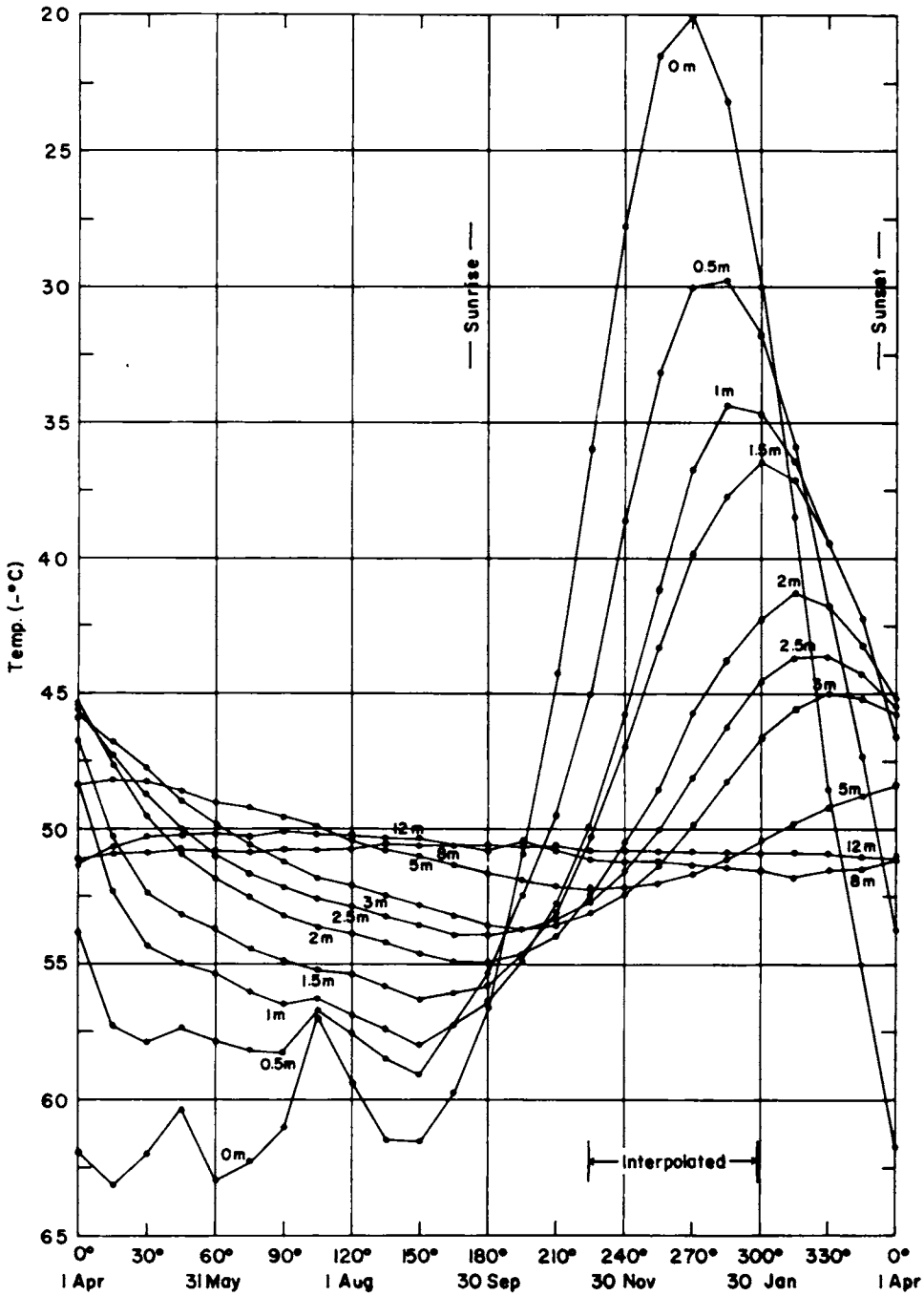

Fig. 18. Subsurface temperature versus time at South Pole, 1958.

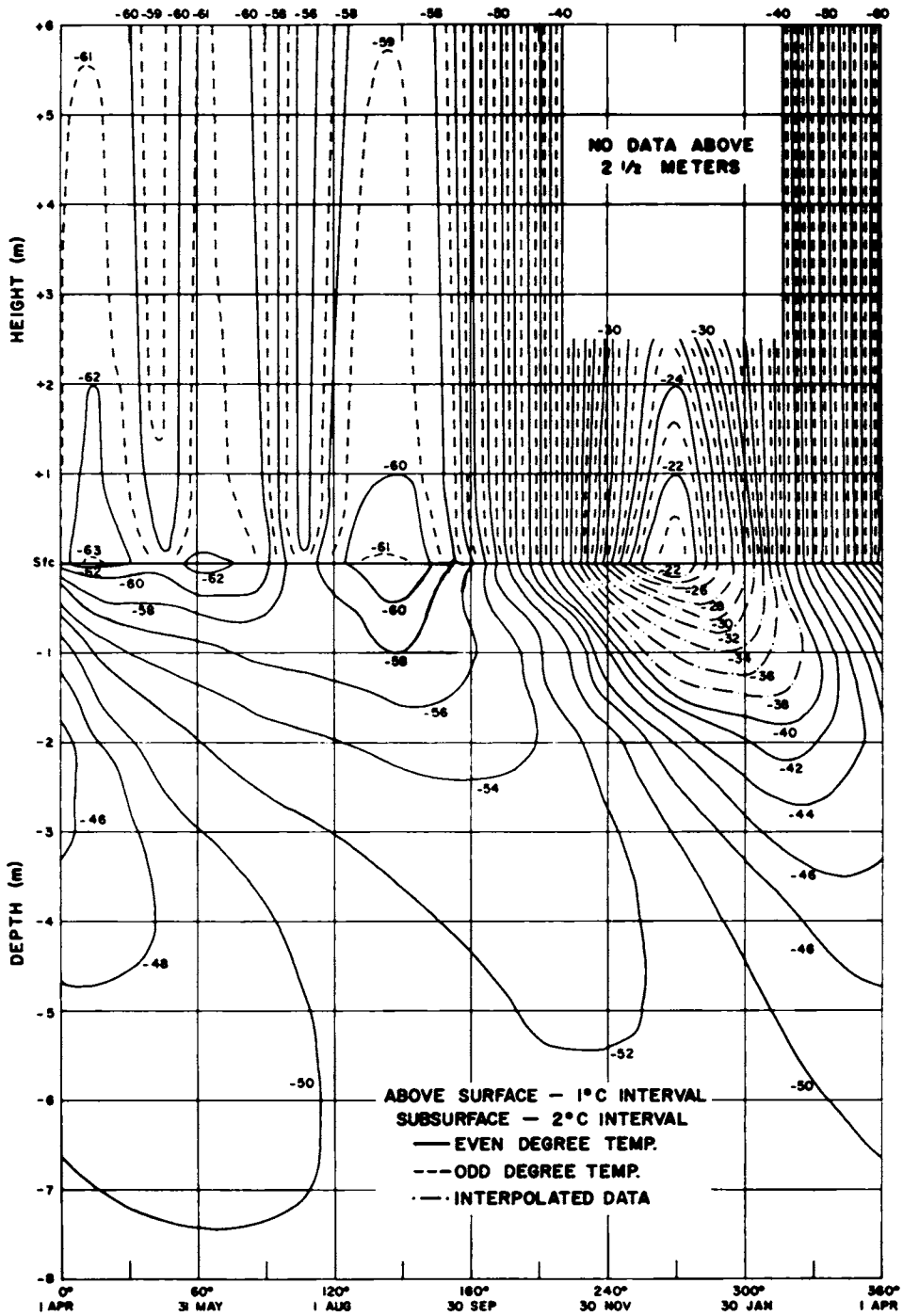

Fig 19. Isotherms, South Pole.

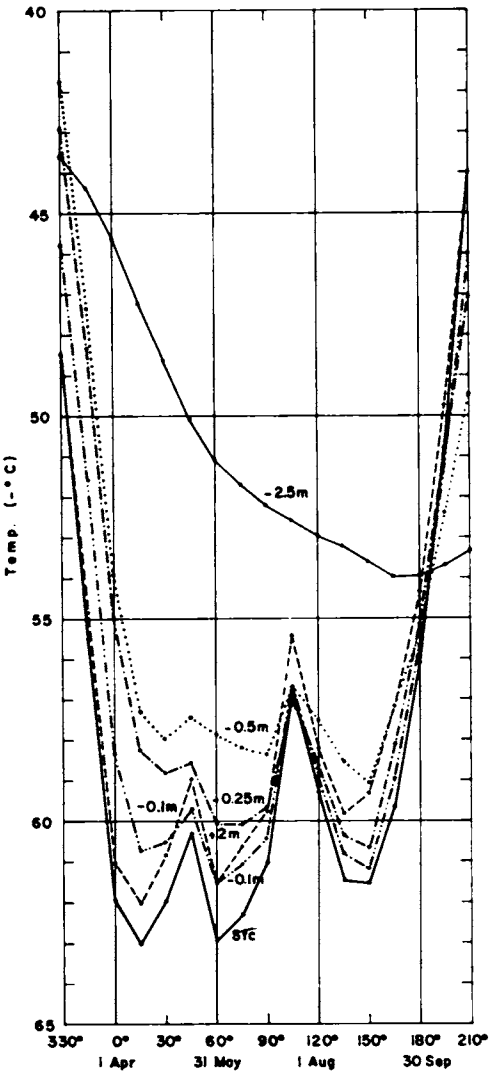

Fig. 20. Winter minima, South Pole.

changes and their times of occurrence are similar to those at Maudheim.

Descriptive analysis of snow temperature variations. For the sake of consistency with previous work in the literature in the fields of surface layer turbulence as well as subsurface heat diffusion, it is unavoidable that certain mathematical symbols (such as α, β, λ, etc.) in this section must be used with a different meaning than in previous sections. See list of symbols and units in footnotes to this report. Natural logarithms are used and abbreviated by 'ln.'

The method of snow-temperature analysis used is similar to that described by *Lettau* [1954] for soil-temperature analysis. Before applying it to South Pole data, the method will be discussed and illustrated, using a harmonic analysis of Schytt's data over the two years 1950 and 1951 for the mean annual variation of subsurface temperature at Maudheim. The zero date of the cycle is taken as April 1, whereas Schytt considered a zero date of January 1.

Let n = frequency of the annual cycle = $2\pi/365$ = 0.0172 rad/day. The first and second harmonic of the annual variation of temperature is described by

$$T = T_m + A_1 \cos(nt - \alpha_1) + A_2 \cos(2nt - \alpha_2) \tag{32}$$

where subscript m denotes the annual mean. The use of the cosine function (rather than the sine function) together with the minus sign of the phase lag in equation 32 is for convenience. This α value yields directly the time of occurrence of the extreme phase, at zero date plus α/n. This time is the minimum value, since all temperatures are negative and the Fourier analysis is performed without carrying the minus sign of temperatures.

Table 15 lists the results of a re-analysis for ten equidistant levels at Maudheim. Only the first harmonic was considered, owing to the insignificance of higher harmonics; A and α are hereafter written in place of A_1 and α_1. Data on mean snow density and volumetric heat capacity are also included.

Let differentiation with respect to depth (z) be indicated by primes. Then it follows from equation 32 that, for the first harmonic

$$T' = T_m' + A' \cos(nt - \alpha) + A\alpha' \sin(nt - \alpha) \tag{33}$$

Since we want to express the seasonal variation of the vertical temperature gradient T' by a simple harmonic, we define amplitude B and phase lag β in the identity

$$T' \equiv T_m' - B \cos(nt - \beta) \tag{34a}$$

or, upon introducing $\gamma = \alpha - \beta$ = phase difference between the waves of temperature and vertical temperature gradient

$$\begin{aligned} T' &= T_m' - B \cos(nt - \alpha + \gamma) \\ &= T_m' - B \cos\gamma \cos(nt - \alpha) \\ &\quad + B \sin\gamma \sin(nt - \alpha) \end{aligned} \tag{34b}$$

Upon comparison of terms in equations 33 and 34*b*, it

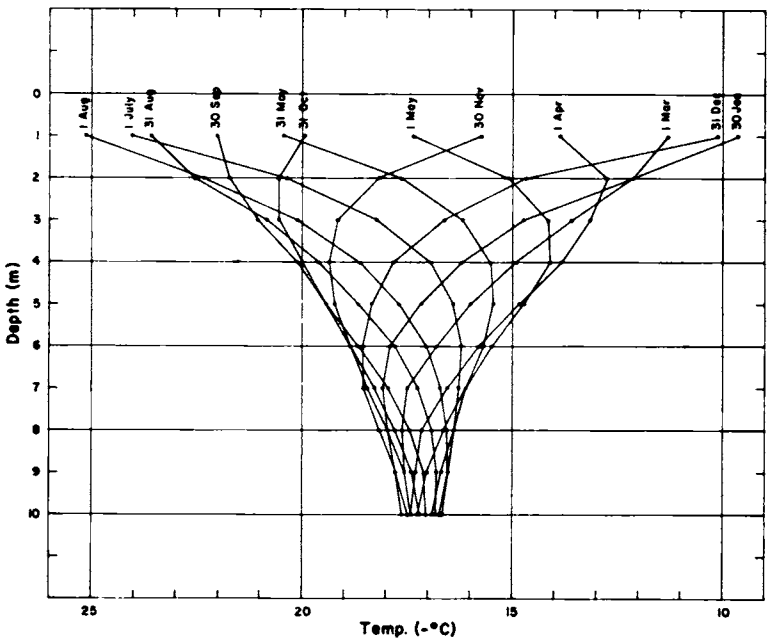

Fig. 21. Tautochrones, Maudheim.

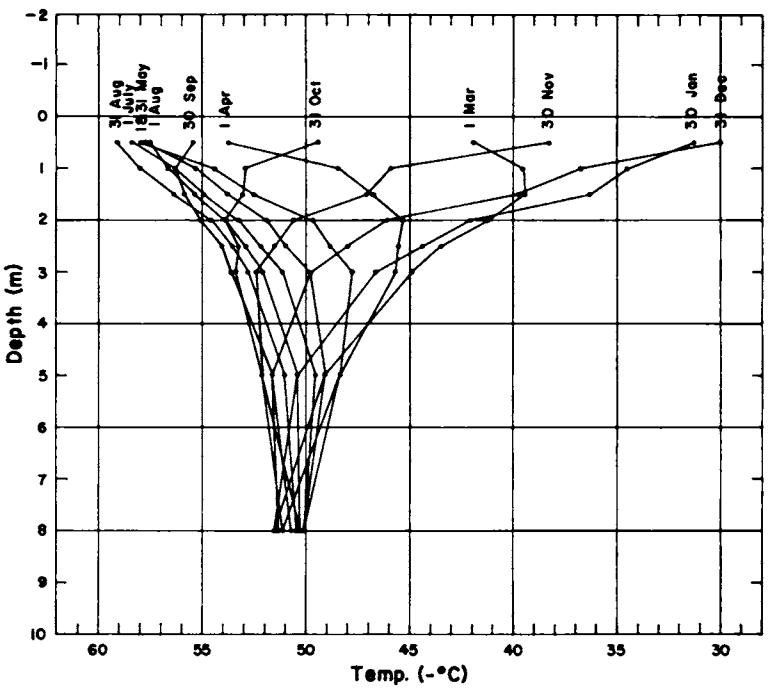

Fig. 22. Tautochrones, South Pole.

TABLE 15. Fourier Analysis in the Upper Ten Meters of the Snow at Maudheim, 1950–1951

Mean snow density (ρ, g/cm³); mean volumetric heat capacity (C, cal deg^{-1} cm^{-3}); annual mean temperature (T_m, deg); and amplitude (A, deg) and phase lag (α, Deg and rad) of the first harmonic of annual variation of snow temperature at indicated depth (z, m).

z	ρ	C	T_m	A	ln A	α, Deg	α, rad
0	0.380	0.180	−17.90	10.8	2.380	96.5	1.683
1	0.415	0.200	−17.66	7.48	2.013	126.8	2.212
2	0.430	0.218	−17.46	5.60	1.723	148.1	2.584
3	0.489	0.232	−17.34	4.23	1.443	167.9	2.930
4	0.527	0.244	−17.27	3.22	1.171	186.2	3.250
5	0.508	0.256	−17.25	2.39	0.870	204.1	3.562
6	0.546	0.264	−17.24	1.73	0.546	222.7	3.886
7	0.557	0.268	−17.24	1.25	0.220	241.3	4.212
8	0.571	0.270	−17.23	0.899	−0.106	260.0	4 538
9	0.576	0.270	−17.23	0.649	−0.432	278.7	4.864
10	0.575	0.270	−17.23	0.469	−0.758	297.4	5.190

follows that

$$B = -(A'/\cos\gamma) = (\alpha' A/\sin\gamma) \tag{35}$$

and

$$\begin{aligned}\tan\gamma &= -(\alpha A/A') \\ &= -[\alpha'/(\ln A)'] = -[d\alpha/d(\ln A)]\end{aligned} \tag{36}$$

Equations 35 and 36 can be used to compute first γ, then B and β from the empirical depth functions A and α, employing numerical differentiations to obtain $(\ln A)'$ and α' as functions of depth. For the classical case of a homogeneous conductor, it follows that $\gamma =$ constant $= 45°$, or $d\alpha = -d(\ln A)$.

Figures 23–25 illustrate that the snow at Maudheim is homogeneous only below approximately 5 meters. Closer to the surface, $d\alpha/d(\ln A)$, the ratio of the change of the phase angle to the change of the logarithm of the amplitude, deviates systematically from minus unity, indicating a degree of inhomogeneity which increases toward the surface. Slightly smoothed values of these changes with height, $(\ln A)'$ and α', together with subsequent values of the phase difference, γ, $\beta = \alpha - \gamma$, and β', and also the resulting thermal diffusivity K are listed in Table 16.

Using Lettau's theoretical model, the thermal diffusivity is obtained as a function of depth by the equation

$$K = (n \sin\gamma \cos\gamma)/(\alpha'\beta') = (n \sin 2\gamma)/(2\alpha'\beta') \tag{37}$$

As an average 'effective diffusivity,' *Schytt* [1960] quoted a value of 0.00827 cm²/sec, which was derived using the questionable assumption that $\gamma =$ 45°. Table 16 shows that Schytt's estimate is too low for depths beyond 3.5 meters and much too high closer to the snow surface.

To obtain the annual variation of heat flux, all that remains to be done appears to be the combining of the local values of the temperature gradients (as given by equation 34*a* or 34*b*) and the computed values of $B = -A'/\cos\gamma$ and β with that of heat conductivity as given by the product KC. This procedure leads, however, to certain discrepancies. Their causes and the method used to eliminate them will be discussed in the theoretical analysis.

In view of the glaciological structure of the snow, an increase of thermal diffusivity with depth ($K' > 0$) is the condition that should have been expected. For any inhomogeneous but genuine conductor, however, it should be expected theoretically that $\gamma < 45°$ for $K' > 0$; correspondingly, $\gamma > 45°$ for $K' < 0$. However, Table 16 shows for the snow at Maudheim that $K' > 0$ is accompanied by $\gamma >$ 45°. This result suggests lack of genuine conduction.

Theoretical analysis of snow-temperature variations. It must be borne in mind that the thermal diffusion model used above rests on the assumption of genuine heat conduction: that is, at any time and anywhere in the conductor the flux of heat (F, ly/time) should be directly proportional to the vertical temperature gradient (T')

$$F = -\lambda T' \tag{38}$$

The factor of proportionality λ, which is defined as

the coefficient of heat conductivity of the medium ($\lambda = KC$, where C = heat capacity), can be a function of depth. Furthermore, it is assumed that no internal sources or sinks of heat exist in the conductor. Therefore, the equation of heat continuity is

$$F' = -CT^{\cdot} \tag{39}$$

where the dot denotes partial differentiation with respect to time.

When equation **32** is differentiated with respect to time, it follows from equation **39** that

$$F' = -CT_m^{\cdot} + nCA \sin(nt - \alpha) \tag{40}$$

Upon expansion, assuming that $T_m^{\cdot}$ is negligible and remembering that equation **34***b* gives $\alpha = \beta + \gamma$

$$F' = nCA \cos\gamma \sin(nt - \beta) - nCA \sin\gamma \cos(nt - \beta) \tag{41}$$

On the other hand, equation **38**, when combined with equation **34***a*, yields, upon differentiation

$$F' = -(\lambda T_m')' + (\lambda B)' \cos(nt - \beta) + \lambda B\beta' \sin(nt - \beta) \tag{42}$$

The first term on the right-hand side of equation **42** is assumed to be negligible. A comparison of terms of equation **42** and **41** yields

$$\lambda B\beta' = nCA \cos\gamma \tag{43a}$$

and

$$(\lambda B)' = -nCA \sin\gamma \tag{43b}$$

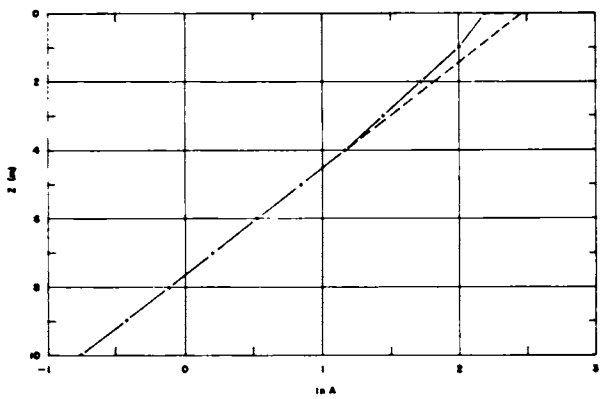

Fig. 23. Log amplitude versus depth.

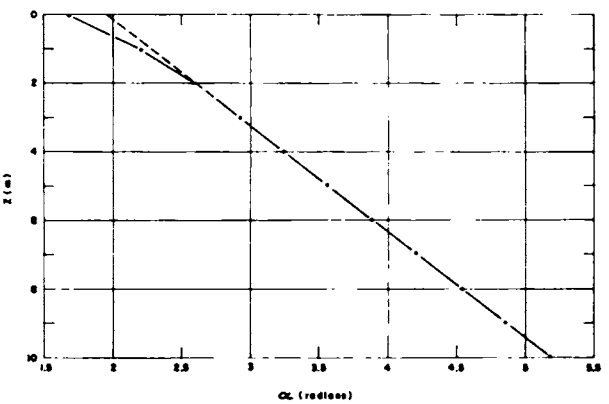

Fig. 24. Phase angle versus depth.

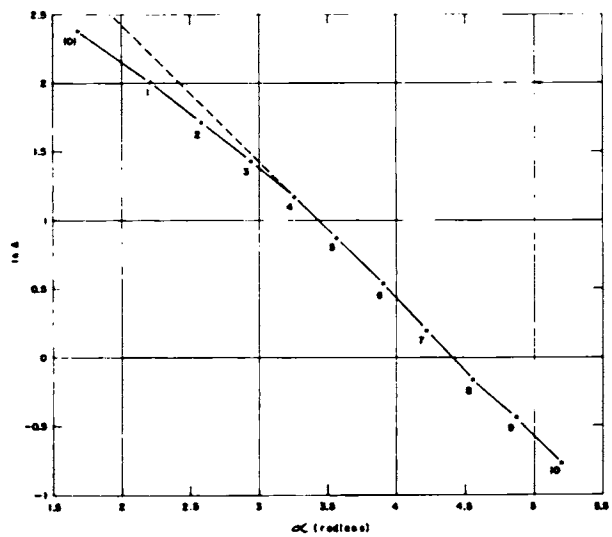

Fig. 25. Log amplitude versus phase angle at indicated depth (meters).

Figs. 23–25. Snow temperature at Maudheim, first harmonic, annual wave.

TABLE 16. Thermal Diffusivity (K, cm²/sec) of the Snow at Maudheim, 1950–1951

Computed as a function of depth (z, m) with the aid of *Lettau*'s [1954] method, from smoothed values of logarithmic amplitudes and phase lags, their derivatives $(\ln A)'$ and α', and subsequent angular functions γ, β, β', using the first harmonic of annual snow-temperature variation reported by *Schytt* [1960]; data for $z = 0$ are obtained by extrapolation.

z, m	$\ln A$	$-(\ln A)'$, rad/m	α, Deg	α', rad/m	γ, Deg	β, Deg	β', rad/m	K, cm²/sec
0	2.380	0.382	96.5	0.560	55.7	40.8	0.664	0.00250
1	2.013	0.328	126.8	0.450	53.9	72.9	0.486	0.00444
2	1.723	0.285	148.1	0.359	51.6	96.5	0.395	0.00684
3	1.443	0.276	167.9	0.338	50.7	117.2	0.367	0.00787
4	1.171	0.286	186.2	0.316	47.8	138.4	0.362	0.00867
5	0.870	0.312	204.1	0.318	45.5	158.6	0.343	0.00912
6	0.546	0.325	222.7	0.325	45.0	177.7	0.330	0.00928
7	0.220	0.326	241.3	0.326	45.0	196.3	0.326	0.00936
8	−0.106	0.326	260.0	0.326	45.0	215.0	0.326	0.00936
9	−0.432	0.326	278.7	0.326	45.0	233.7	0.326	0.00936
10	−0.758	0.326	297.4	0.326	45.0	252.4	0.326	0.00936

When equation 43*a* is combined with equation 35, the term B can be eliminated and we can solve for $\lambda/C = K$, the result being equation 37, which is valid for any variation of thermal diffusivity with depth. Thus, when C is known, λ can be obtained as KC and equation 43*a* can be used to calculate directly the amplitude of heat flux (λB) at any depth, which, together with the previously derived phase constant β from equation 35 and $\beta = \alpha - \gamma$, permits us to calculate the heat flux F.

However, equations 43*a* and 43*b* must hold true simultaneously. Equation 43*b* permits us to calculate λB indirectly but independently of (43*a*), using

$$\lambda B = (\lambda B)_1 + \int_{z_1}^{z} (\lambda B)'\, dz = (\lambda B)_1 - n \int_{z_1}^{z} CA \sin\gamma\, dz \qquad (44a)$$

Upon dividing equation 43*b* through equation 43*a*, a slightly simplified version is obtained:

$$\ln(\lambda B) = \ln(\lambda B)_1 + \int_{z_1}^{z} \frac{(\lambda B)'}{\lambda B}\, dz = \ln(\lambda B)_1 - \int_{z_1}^{z} \beta' \tan\gamma\, dz \qquad (44b)$$

If they apply anywhere in the medium, the assumptions of genuine conduction, absence of external sources and sinks of heat, or both, will hold at great depth; for example, at and below 7 meters at Maudheim. In Table 17 we have listed amplitude values of heat flux (λB), calculated directly from equation 43*a* and also by numerical integration from equation 44*b*, assuming $z_1 = 7.0$ meters.

Table 17 shows quite strikingly that the two equations do not produce identical results. The differences increase with the approach toward the surface. This must mean that at least one, if not all, of the assumptions underlying the model will not hold true for conditions in the snow. Most questionable is the assumption concerning internal heat sources. Certainly, short-wave radiation penetrates into the snow; reference is made to *Liljequist* [1956]. Radiation absorption will be supplementary to the conduction of heat in the snow, thus requiring a modification of equation 39. Other effects include

TABLE 17. Amplitude of Heat Flux (λB, ly/day) at Maudheim, 1950–1951

Calculated as a function of depth by two formulas that should produce identical results if genuine conduction prevails.

z	from Equation 43*a*	from Equation 44*b*
0	2.85	10.19
1	3.11	7.77
2	3.30	5.90
3	2.91	4.42
4	2.51	3.27
5	2.14	2.40
6	1.68	1.74
7	1.25	1.25
8	0.90	0.90
9	0.65	0.65
10	0.47	0.47

convection in the upper layers of the snow, heat release by packing, evaporation, and recondensation processes in pores, etc. Additionally, uncertainties regarding actual depth of the thermometers as snow accumulates on the surface may be important.

To avoid the ambiguity of the results of the snow-temperature analysis, the following more universally valid method is proposed:

1. Determine the lower region ($z > z_1$), where genuine heat conduction without external or internal sources and sinks of heat applies; this determination is achieved with the aid of equations 43*a* and 43*b* by locating layers where $CA \sin \gamma$ agrees sufficiently closely with $-[(CA \cos \gamma)/\beta']'$. For the annual wave at Maudheim, this appears to be true below 7 meters.

2. Compute K, and $\lambda = KC$, using equation 37 at and below z_1 only, and obtain the heat flux at $z = z_1$ from B_1 and β as

$$S_1 = \lambda_1 B_1 \cos (nt - \beta_1) \qquad (45a)$$

3. Calculate the effective heat flux at $z < z_1$ strictly on the basis of the equation of heat continuity

$$S = S_1 - \int_{z_1}^{z} CT' \, dz \qquad (45b)$$

which, for harmonic temperature variations as given by equation 32, yields

$$S = S_1 + n \int_{z_1}^{z} CA \sin (nt - \alpha) \, dz \qquad (45c)$$

TABLE 18. Calculated Values of Heat Conductivity [λ (ly/day)/(deg/m)] at Maudheim, 1950–1951

Amplitude (ΔS, ly/day) and phase angle (σ, Deg) of the first harmonic of the subsurface heat flux, and phase difference ($\epsilon = \sigma - \beta$) between the harmonic waves of heat flux and vertical temperature gradient, as a function of depth (z, m).

z	ΔS	σ	ϵ	λ, Equation 37	λ, Effective Value
0	8.27	71.5	30.7	0.389	0.969
1	6.88	90.5	17.6	0.748	1.587
2	5.47	107.6	11.1	1.288	2.098
3	4.23	124.2	7.0	1.578	2.176
4	3.18	141.1	2.7	1.828	2.321
5	2.36	158.7	0.1	2.02	2.21
6	1.712	177.2	−0.5	2.12	2.15
7	1.242	196.0	−0.3	2.17	2.16
8	0.900	215.0	0.0	2.18	2.18
9	0.650	233.7	0.0	2.18	2.18
10	0.470	252.4	0.0	2.18	2.18

TABLE 19. Heat Flux (S_0, ly/day) at the Surface of the Snow at Maudheim, 1950–1951

(From the equation for the first harmonic, at the first day of each month.)

Month	S_0	Month	S_0
Jan	7.78	July	−7.85
Feb.	5.28	Aug.	−5.43
Mar.	1.74	Sept.	−1.52
April	−2.62	Oct.	2.70
May	−6.15	Nov.	6.30
June	−8.11	Dec.	8.12

Specifically, at the surface

$$S_0 = S_1 + n \int_{z_1}^{0} CA \sin (nt - \alpha) \, dz \qquad (45d)$$

The actual heat flux distribution given by equation 45*c* may be expressed as

$$S = S_m + \Delta S \cos (nt - \sigma) \qquad (46)$$

where ΔS = amplitude and σ = phase lag.

For Maudheim the first harmonic of heat flux at the surface was derived by numerical integration for $0 \leq z \leq z_1 = 7$ meters, in the above-described manner. Assuming a zero value for the annual mean of S_0 and substituting in equation 46, the result is

$$S_0 = -8.27 \cos (nt - 71.5)$$

in ly/day, with $nt = 0$ at April 1 (Table 18). This procedure produces at the first day of each month the series of values shown in Table 19. A sign convention is chosen corresponding to that for Q_0 in the earlier section on coefficients of momentum transfer and heat transfer. Heat flowing in the direction of increasing depth (i.e. downward, away from the surface) is denoted by a positive S_0 value, whereas negative S_0 denotes upward heat flux (toward the surface).

Summarizing from Tables 16 and 18, we find at Maudheim that $\alpha_0 = 96.5$ Deg, $\beta_0 = 40.8$ Deg, and $\sigma_0 = 71.5$ Deg. With the zero date for the first harmonic of April 1 ($n = 360$ Deg/365 days), we thus obtain extreme (minimum) surface values of temperature at July 8, vertical temperature gradient at May 12, and heat flux at June 13. The discrepancy between the last two dates illustrates again the importance of nonconductive processes in the snow at Maudheim.

TABLE 20. Preliminary Fourier Analysis in the Upper Twelve Meters of the Snow at South Pole, 1958

Annual mean temperature (T_m, deg); amplitude (A, deg) and phase angle (α, Deg) of the first and second harmonics of annual variation of snow temperature at indicated depth (z, m).

z	T_m	A_1	α_1	A_2	α_2
0.5	−49.13	13.49	99.0	5.76	21.2
1.0	−49.56	10.65	116.8	4.12	44.3
1.5	−49.23	9.11	123.5	3.38	53.2
2.0	−49.82	6.23	143.1	1.98	81.8
2.5	−49.94	4.81	151.6	1.46	97.9
3.0	−50.05	4.04	168.2	1.11	114.4
5.0	−50.31	1.88	212.3	0.33	171.2
8.0	−50.80	0.68	289.3	0.20	281.8
12.0	−50.78	0.16	339.8	0.05	428.2

Results of analysis of snow temperature at South Pole. The snow-temperature data described earlier were harmonically analyzed using April 1 as the zero date. The results of the Fourier analysis are summarized in Table 20.

Obviously, amplitude and phase angles at 8 and 12 meters are unreliable, owing to the small magnitude of amplitudes and the fact that data for only one year are available. Consequently, the discussion is restricted to the first 5-meter layer of snow. Interpolated and slightly smoothed amplitudes and phase angles for the first two harmonics for every ½ meter are listed in Table 21. The degree of smoothing can be judged from Figures 26–31.

It seems justified to assume that the snow at South Pole is a homogeneous conductor below 4 meters. It is especially noteworthy that thermal diffusivity computed by equation 37 is practically the same using the first and the second harmonic (see Table 22). Also, it can be concluded from the listings in Table 23 (cf. Table 17) that the effect of nonconductive processes at South Pole seems to be important for a shallower depth (approximately 3–4 meters) than at Maudheim (approximately 6–7 meters) and to be limited to the first harmonic. The latter result appears to indicate that radiation penetration is the major cause of nonconductive processes, in view of the dominant single annual variation of radiation at South Pole.

In the terms of equations 43a and 43b the ratio

$$r = 1 - (CA \cos \gamma/\beta')'/(CA \sin \gamma) \qquad (47)$$

can be taken as a convenient dimensionless measure of the effect of nonconductive processes, r being equal to zero for genuine conduction. Table 24 provides information on r values for the uppermost 4.5 meters of snow at South Pole, in comparison with values for Maudheim. It can be concluded that only the second harmonic of snow-temperature variation is sufficiently close to genuine conductor conditions.

The evaluation of heat-flux variation with depth was computed for the first harmonic using the method outlined in the section on the theoretical analysis of snow-temperature variations; direct evaluation was used for the second harmonic (Table 25). The last column gives representative values of heat conductivity obtained as the arithmetric average of λ_{eff} for the first harmonic and λ from equation 37 for the second harmonic. The average probable error of λ_{rep} can be estimated as less than $\pm 10\%$. For the first harmonic the extreme value of the vertical temperature gradient occurs on May 8 (since $\beta_0 = 37.7$ Deg). The extreme value of vertical heat flux lags by 9 days (i.e., $\epsilon_0 = 9.1$ Deg) and occurs on May 17 (since $\sigma_0 = 46.8$ Deg).

Finally, assuming no annual mean heat flux into the snow, it follows at $z = 0$, using equation 46, that

$$S_0 = -6.79 \cos (nt - 46.8) - 4.02 \cos (2nt + 43.9)$$

in ly/day, with the zero date of April 1 as at Maudheim in 1950–1951. This relation will be used in the

TABLE 21. Fourier Analysis in the Upper Five Meters of the Snow at South Pole, 1958

Interpolated and slightly smoothed values of mean snow density (ρ, g/cm³); mean volumetric heat capacity (C, cal deg^{-1} cm^{-3}); annual mean temperature (T_m, deg); amplitudes (A, deg) and phase angles (α, Deg) of the first and second harmonics of annual variation of snow temperature at indicated depth (z, m).

z	ρ	C	T_m	A_1	α_1	A_2	α_2
0	0.354	0.147	−49.33	17.86	83.7	9.00	−1.3
0.5	0.373	0.155	−49.13	13.51	100.2	4.83	22.0
1.0	0.379	0.157	−49.56	10.40	115.6	3.91	43.3
1.5	0.377	0.156	−49.23	8.13	129.9	2.75	62.7
2.0	0.381	0.158	−49.82	6.43	143.4	1.99	80.8
2.5	0.393	0.163	−49.94	5.14	156.2	1.46	97.9
3.0	0.406	0.168	−50.05	4.15	168.5	1.09	114.5
3.5	0.413	0.171	−50.13	3.38	180.4	0.819	130.9
4.0	0.420	0.174	−50.19	2.76	192.0	0.616	147.1
4.5	0.422	0.175	−50.26	2.26	203.5	0.465	163.3
5.0	0.430	0.178	−50.31	1.85	215.0	0.351	179.9

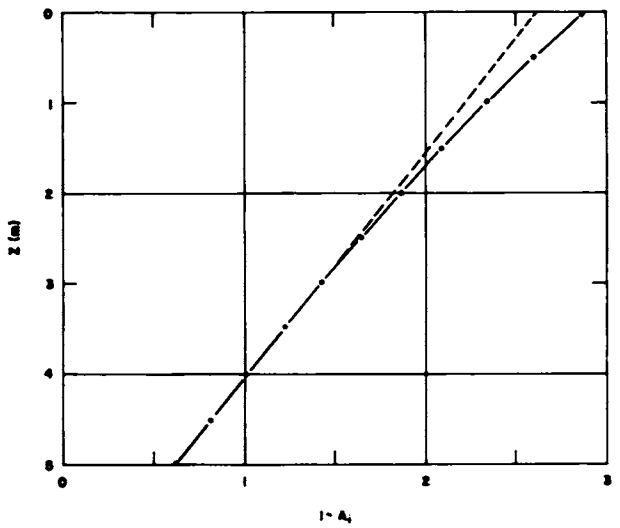

Fig. 26. Log amplitude versus depth.

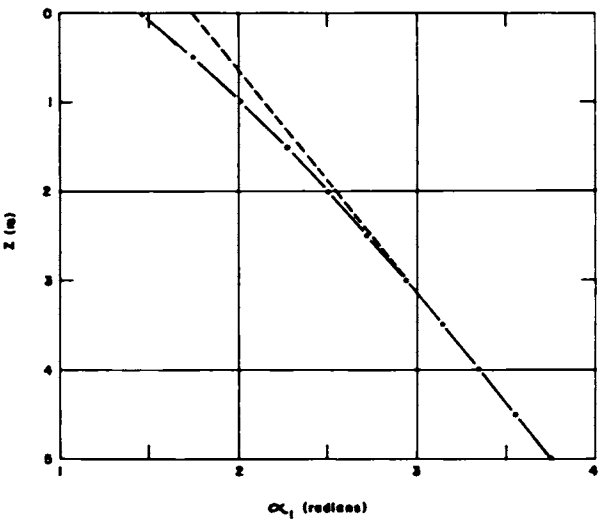

Fig. 27. Phase angle versus depth.

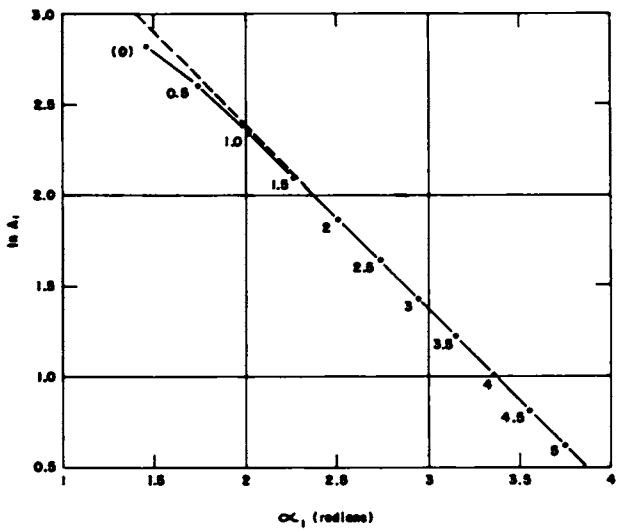

Fig. 28. Log amplitude versus phase angle at indicated depth (meters).

Figs. 26–28. Snow temperature at South Pole, first harmonic, annual wave.

following section for the study of the heat budget at the snow-air interface at South Pole, in terms of monthly means. If S_0 is desired for shorter periods (5-day means, daily or hourly means) the representation by the first two harmonics of the annual trend will not be sufficient. For shorter periods it is necessary to use the temperature integral method directly or, alternatively, mean vertical gradients of snow temperature, extrapolated to $z = 0$, in combination with the representative λ values listed in Table 25. The accuracy of short-time S_0 estimates will not, however, be very great.

8. SURFACE ENERGY BUDGET[10]

[10] *New symbols used in this section*:

R_0,	net radiation at the interface (ly/time).
E_0,	flux of latent heat at the interface (ly/time).
L,	latent heat of sublimation (cal/g).
r_B,	Bowen ratio $\equiv Q_0/E_0$.
q,	specific humidity.
e_{s_i},	saturation vapor pressure (mb) at top of inversion.
p,	atmospheric pressure (mb).
K_Q,	eddy diffusivity for heat (cm²/sec).
K_M,	eddy diffusivity for horizontal momentum (cm²/sec).
γ,	K_Q/K_M.

†The abbreviation 'deg' stands for degrees celsius, whereas 'Deg' is used for degrees of an arc.

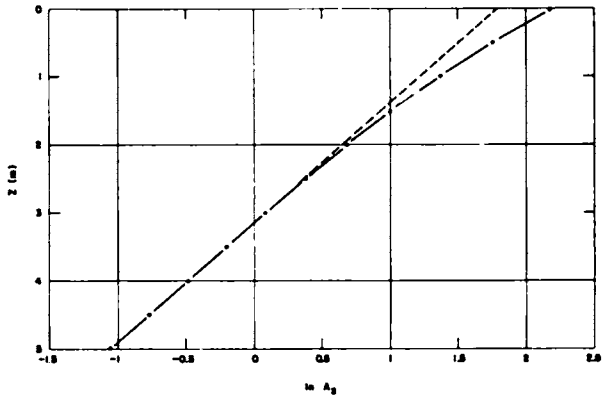

Fig. 29. Log amplitude versus depth.

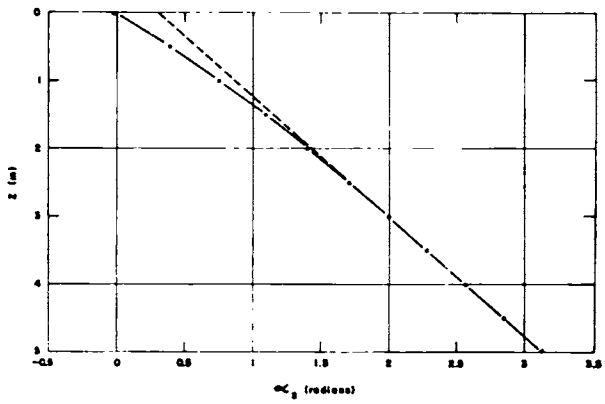

Fig. 30. Phase angle versus depth.

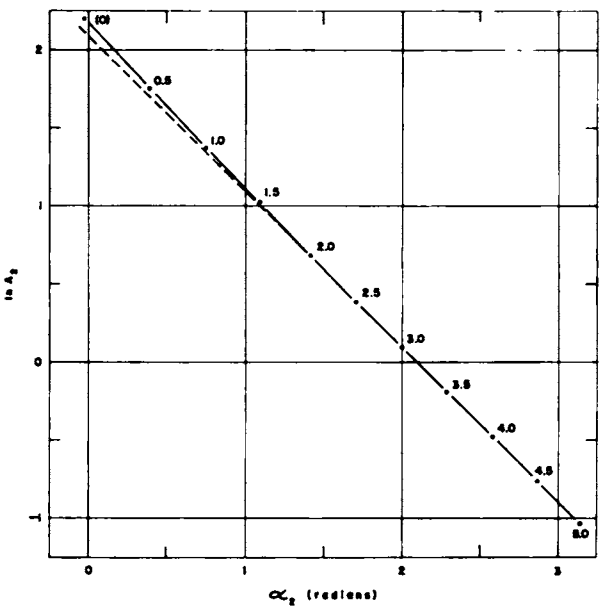

Fig. 31. Log amplitude versus phase angle at indicated depth (meters).

Figs. 29–31.—Snow temperature at South Pole, semiannual wave.

Definitions, and example for Maudheim. The equation of the energy budget at the snow-air interface will be considered in the form

$$R_0 = Q_0 + S_0 + E_0 \qquad (48)$$

where R_0 = radiation balance, or net radiation at the interface.
Q_0 = eddy heat flux at the interface.
S_0 = snow heat flux at the interface.
E_0 = latent heat flux at the interface.

All terms are expressed in ly/time, where ly = langley = g cal/cm^2. Convenient units are either ly/day or ly/hour. The sign convention for the three fluxes (Q_0, S_0, and E_0) is such that transport away from the interface has the positive sign. Net radiation is defined as positive when more radiation energy is received than emitted from the interface. Thus, a positive R_0 indicates an energy source at the interface (usually requiring the presence of solar radiation); a negative R_0 indicates an energy sink at the interface and will result in negative fluxes directed toward the surface for balance requirements.

A different sign convention for the constituents of the surface energy equation is sometimes used in the literature. For example, *Liljequist* [1956] defines the

TABLE 22. Thermal Diffusivity (K, cm²/sec) of the Snow at South Pole, 1958

Computed as a function of depth (z, m) by equation 37 from interpolated and slightly smoothed values of logarithmic amplitudes and phase lags, their derivatives ($\ln A$)′ and α'; and subsequent angular functions γ, β, β'.

z, m	$\ln A$	$-(\ln A)'$, rad/m	α, rad	α', rad/m	γ, Deg	β, Deg	β', rad/m	K, cm²/sec
				First Harmonic				
0.0	2.883	0.576	1.460	0.596	46.0	37.7	0.594	0.00282
0.5	2.604	0.540	1.748	0.556	45.8	54.4	0.564	0.00317
1.0	2.342	0.508	2.017	0.520	45.6	70.0	0.526	0.00364
1.5	2.095	0.480	2.267	0.486	45.4	84.5	0.492	0.00416
2.0	1.861	0.456	2.503	0.460	45.2	98.2	0.468	0.00466
2.5	1.638	0.436	2.727	0.438	45.1	111.1	0.444	0.00512
3.0	1.424	0.420	2.941	0.420	45.0	123.5	0.426	0.00557
3.5	1.217	0.408	3.148	0.408	45.0	135.4	0.412	0.00593
4.0	1.015	0.402	3.351	0.402	45.0	147.0	0.402	0.00616
4.5	0.815	0.400	3.550	0.400	45.0	158.5	0.400	0.00622
5.0	0.615	0.400	3.750	0.400	45.0	170.0	0.400	0.00622
				Second Harmonic				
0.0	2.197	0.930	−0.025	0.855	42.6	−43.9	0.834	0.00279
0.5	1.757	0.833	0.384	0.781	43.2	−21.2	0.764	0.00334
1.0	1.364	0.746	0.745	0.710	43.6	−0.3	0.696	0.00402
1.5	1.011	0.678	1.094	0.654	44.0	18.7	0.642	0.00475
2.0	0.686	0.631	1.410	0.615	44.3	36.5	0.606	0.00534
2.5	0.380	0.599	1.709	0.589	44.5	53.4	0.582	0.00581
3.0	0.087	0.580	1.999	0.575	44.7	69.8	0.570	0.00608
3.5	−0.200	0.571	2.284	0.568	44.9	86.0	0.565	0.00620
4.0	−0.484	0.566	2.567	0.565	44.9	102.2	0.563	0.00625
4.5	−0.766	0.564	2.849	0.564	45.0	118.3	0.563	0.00627
5.0	−1.048	0.564	3.131	0.564	45.0	134.4	0.563	0.00628

fluxes by the opposite sign, net radiation by the same sign. For the purpose of comparison, monthly means of net radiation and estimated eddy heat flux at Maudheim are taken from Liljequist's data and listed in Table 26, using the sign convention and the symbols explained in the preceding paragraph. Also listed are S_0 values derived from the re-analysis of the Maudheim data, with the aid of the harmonic expression derived from equation 46:

$$S_0 = -8.27 \cos (nt - 71.5)$$

in ly/day, valid for a zero date ($t = 0$) of April 1. S_0 data for midmonths were computed and listed in the table.

The latent heat flux (E_0) is obtained with the aid of equation 48 as the remainder which makes the budget complete. For temperature below freezing, a negative E_0 indicates deposition (i.e., the vapor phase transforms directly to solid ice; for example, as hoarfrost); a positive E_0 indicates sublimation (i.e., the ice evaporates, without intermediate liquid phase). This nomenclature phase change of H_2O was suggested by *MacDonald* [1958].

Table 26 shows that positive E_0 (evaporation or sublimation) occurs only during the three core months of the antarctic summer. From February through October there is deposition at the surface. The annual mean of this deposition can be converted to a mass flux density, or cm of liquid water per time, considering the latent heat (L) of the vapor-to-ice phase equal to 667 cal/g. Thus 5 ly/day, which corresponds to 1825 ly/year, corresponds to a water equivalent of 2.7 g/cm² per year, which is 27 mm of water per year. A value of this order of magnitude was also computed and discussed by *Liljequist* [1956].

It could be argued that only the harmonics of R_0, Q_0, and S_0 should be compared and used for estimating the first harmonic of E_0. The equation for $E_0 = R_0 - Q_0 - S_0$ can be obtained in the following manner:

TABLE 23. Amplitudes of Heat Flux (λB, ly/day) at South Pole, 1958

Calculated as a function of depth (z, m) for the first and second harmonic by two formulas that should produce identical results if genuine conduction prevails.

	First Harmonic		Second Harmonic	
z	Eq. 43a	Eq. 44b	Eq. 43a	Eq. 44b
0	5.29	7.43	4.02	4.48
0.5	4.45	5.97	2.46	3.27
1.0	3.74	4.82	2.20	2.47
1.5	3.11	3.93	1.65	1.85
2.0	2.65	3.23	1.28	1.40
2.5	2.29	2.66	1.00	1.07
3.0	1.99	2.19	0.78	0.82
3.5	1.71	1.80	0.60	0.62
4.0	1.45	1.48	0.48	0.47
4.5	1.20	1.22	0.35	0.36
5.0	1.00	1.00	0.27	0.27

$$R_0 = -24.9 - 4.4\cos(nt) - 30.8\sin(nt)$$
$$-Q_0 = 19.8 - 0.7\cos(nt) + 6.7\sin(nt)$$
$$-S_0 = 0.0 + 2.6\cos(nt) + 7.8\sin(nt)$$
$$E_0 = -5.1 - 2.5\cos(nt) - 16.3\sin(nt)$$
$$= -5.1 + 15.5\cos(nt - 260.7)$$

Net radiation at the south pole. Radiation values for the South Pole station were supplied by the U.S. Weather Bureau; observational equipment and procedures are described by *Hanson* [1960]. Hourly values of net radiation were obtained with a Beckman and Whitley net exchange radiometer which measured the total (short-wave and long-wave) radiation balance between incoming and outgoing solar and atmospheric radiation on a horizontal surface (short- and long-wave). The outgoing radiation consists of short-wave radiation reflected from the ground and long-wave radiation emitted by the ground.

Net radiation (R_0) data are available for the period February–November 1958 for most of the hours for which the USWB stability coefficient could be computed; values are not available for December 1958 and January 1959. The orientation of the radiometers was changed to a downwind position at the end of March, and the data are believed to be of superior quality thereafter.

R_0 was punched onto the IBM cards that already

TABLE 24. Nonconductive Processes in the Snow

Relative significance in the upper 5 meters at Maudheim and South Pole; listed are ratios (r) defined in equation 47 at indicated depth (z, m).

	Maudheim	South Pole	
z	First Harmonic	First Harmonic	Second Harmonic
0.5	1.11	0.40	0.03
1.5	0.92	0.30	0.10
2.5	0.74	0.35	0.15
3.5	0.64	0.23	0.06
4.5	0.39	0.07	0.02

TABLE 25. Calculated Values of Heat Conductivity [λ, (ly/day)/(deg/m)] at South Pole, 1958

Amplitude (ΔS, ly/day) and phase angle (σ, Deg) of the first and second harmonics of the subsurface heat flux and phase difference ($\epsilon = \sigma - \beta$) between harmonic waves of heat flux and vertical temperature gradient, as a function of depth (z, m). The last column gives representative λ values for South Pole.

	First Harmonic					Second Harmonic				
z	ΔS	σ	ϵ	λ Eq. 37	λ_{eff}	ΔS	σ	ϵ	λ Eq. 37	λ_{rep}
0	6.79	46.8	9.1	0.359	0.452	4.02	−43.9	0.0	0.354	0.393
0.5	5.58	61.8	7.4	0.425	0.528	2.46	−21.2	0.0	0.448	0.488
1.0	4.59	75.9	5.9	0.494	0.603	2.20	− 0.3	0.0	0.545	0.574
1.5	3.81	89.0	5.5	0.562	0.683	1.65	18.7	0.0	0.640	0.661
2.0	3.17	101.2	3.0	0.636	0.762	1.28	36.5	0.0	0.728	0.745
2.5	2.63	112.9	1.8	0.720	0.827	1.00	53.4	0.0	0.818	0.822
3.0	2.18	124.3	0.8	0.808	0.886	0.78	69.8	0.0	0.882	0.884
3.5	1.80	135.8	0.4	0.877	0.918	0.60	86.0	0.0	0.917	0.917
4.0	1.49	147.1	0.1	0.926	0.955	0.48	102.2	0.0	0.940	0.947
4.5	1.22	158.4	0.0	0.940	0.953	0.35	118.3	0.0	0.949	0.951
5.0	.99	169.9	0.0	0.956	0.956	0.27	134.4	0.0	0.967	0.961

TABLE 26. Energy Fluxes at Maudheim, 1950–1951

Average monthly heat budget constituents (ly/day) at the snow-air interface: net radiation (R_0); eddy heat flux (Q_0) from *Liljequist* [1956]; snow heat flux (S_0) from re-analysis of snow-temperature variations as presented by *Schytt* [1960]. $E_0 = R_0 - Q_0 - S_0$ = remainder term.

Month	R_0	Q_0	S_0	E_0
Jan.	11	−11	7	15
Feb.	−16	−14	4	−6
Mar.	−36	−19	0	−17
April	−43	−22	−4	−17
May	−48	−24	−7	−17
June	−46	−27	−8	−11
July	−46	−25	−7	−14
Aug.	−47	−24	−4	−19
Sept.	−34	−22	0	−12
Oct.	−17	−19	4	−2
Nov.	−4	−17	7	6
Dec.	27	−14	8	33
Mean	−25	−20	0	−5

contained surface stress (τ_0) and eddy heat flux (Q_0). The eddy heat flux was based on wind and temperature computed from USWB observations, with the stability coefficient S (USWB), and heat transfer coefficient Λ, obtained by comparison with the Quartermaster values of eddy heat flux and surface stress for the 665 test hours. Using the hours when τ_0, Q_0, and R_0 were all available, 5-day means were computed and listed by the Quartermaster Computer Branch.

In Figure 32 ($R_0 - Q_0$) and τ_0 are plotted for 5-day and 30-day periods. The 30-day means were computed from six 5-day totals. Owing to the extreme cold and the long winter, the predominant direction of ($R_0 - Q_0$) during the February through November period was negative, requiring a flux toward the surface for balance. Since $R_0 - Q_0 = S_0 + E_0$, this balance would be supplied by the sum of the subsurface heat flux and the flux of latent heat. Figure 32 illustrates that, during the sunless period, as the surface stress increases ($R_0 - Q_0$) becomes less negative and occasionally positive. The periods with τ_0 strong and ($R_0 - Q_0$) positive, requiring a flux away from the surface for balance, are also the warmer periods of the sunless season.

Surface heat budget, evaporation estimate. Monthly means of R_0 and Q_0 were computed from the same listing used for 5-day means. S_0 was computed from equation 46 using the surface values of amplitude (ΔS) and phase lag (σ) for the first and second harmonics at South Pole. By substituting R_0, Q_0, and S_0 in equation 48, the remainder E_0 was obtained for each of the ten months. The monthly values of the four constituents of the energy balance are shown in Table 27 and plotted in Figure 33.

Table 27 may be compared with Table 26, which shows the same quantities for Maudheim. Note, however, that Maudheim observations are for 1950–1951 and the South Pole observations for 1958. Both stations have values of E_0 indicating deposition during the winter night. Although deposition seems reasonable and is confirmed by hoarfrost observations at coastal stations, it was not expected in much quantity because of the low moisture content of the air on the inland plateau. It is difficult to account for a moisture source that would produce hoarfrost in quantity equal, in the winter season, to that at Maudheim. Certainly, the air will hold much less moisture at South Pole, where the mean temperature was about −49°C, than at Maudheim, where it was −17°C. It appears necessary to test the result. This will involve comparison with other findings and also a critical review of the assumptions that underlie the computation.

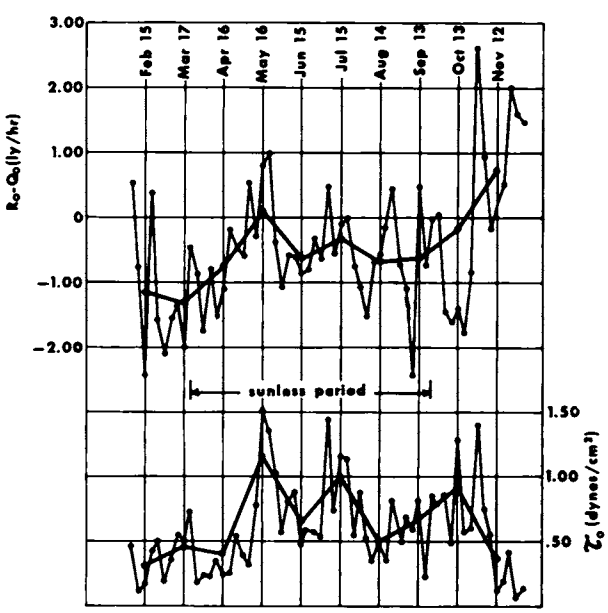

Fig. 32. Annual variation of difference between net radiation flux and eddy heat flux ($R_0 - Q_0$) and of surface stress τ_0, South Pole.

TABLE 27. Energy Fluxes at South Pole, 1958

Average monthly heat budget constituents (ly/day) at the snow-air interface: Net radiation (R_0) and eddy heat flux (Q_0) from USWB and QM data, snow heat flux (S_0) from USWB, QM and Arctic Institute of North America glaciological data. $E_0 = R_0 - Q_0 - S_0$ = remainder term.

Month	R_0	Q_0	S_0	E_0
Jan.			+ 4	
Feb.	−40	−16	− 3	−21
Mar.	−65	−32	− 7	−26
April	−60	−32	− 7	−21
May	−54	−56	− 4	+ 6
June	−54	−39	− 2	−13
July	−59	−50	− 3	− 6
Aug.	−50	−33	− 3	−14
Sept.	−46	−32	− 1	−13
Oct.	−31	−28	+ 5	− 8
Nov.	+14	− 8	+10	+12
Dec.			+10	

S_0 was obtained for South Pole in 1958 by *Hanson and Rubin* [1962] by summing month-to-month energy change profiles. Compared with the results from harmonic analysis, more heat flux toward the surface in winter, especially immediately after sunset, is indicated. In their study of the heat exchange at South Pole, they treat the sensible and latent heat exchange with the atmosphere as a residual of the net radiation and the heat flux in the snow.

While a light deposit of hoarfrost was occasionally observed on the anemometers at South Pole in 1958, it was less in quantity and less frequent in occurrence than at Little America V in 1957. The heat budget constituents computed by *Hoinkes* [1961] for Little America V data of 1957, with revised net radiation figures received later

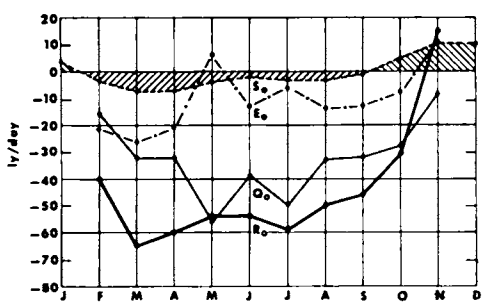

Fig. 33. Seasonal trends in energy budget terms of the snow surface at South Pole, 1958. $R_0 = Q_0 + S_0 + E_0$.

TABLE 28. Energy Fluxes at Little America V, Winter, 1957

Average monthly heat budget constituents (ly/day) at the snow-air interface: net radiation (R_0), eddy heat flux (Q_0), and snow heat flux (S_0), from *Hoinkes* [1961]. $E_0 = R_0 - Q_0 - S_0$ = remainder term.

Month	R_0	S_0	Q_0	E_0
April (21–30)	−30.4	−14.9	−12.0	− 3.5
May	−41.1	− 9.1	−10.8	−21.2
June	−30.2	4.4	− 9.4	−25.2
July	−34.7	− 9.6	−13.5	−11.6
Aug. (1–20)	−31.4	− 4.1	−14.3	−13.0

by personal communication, are shown in Table 28 in the notation and form used for Table 27 (South Pole). Deposition during the winter night is indicated in an amount slightly greater than at Maudheim.

Energy fluxes at Mirnyy (66°33′S, 93°01′E) in 1957, as reported by *Kopanev* [1960] are shown in Table 29. The monthly values given by Kopanev in large calories/cm² have been converted to ly/day by multiplying by 1000 and dividing by the number of days in the month. For all four months E_0 is positive (evaporation or sublimation). A summary of data for the four stations is presented in Table 30.

Too exacting a comparison of the data is not justified because instrumentation used to measure radiation varies, methods of computing it do not agree in all details, and two of the stations measured net radiation directly and two computed it. Net radiation amounts were measured by a Beckman and Whitley net radiometer at South Pole and a Schulze net radiometer at Little America V, and any small systematic error might be sufficient to change the latent heat flux from a small deposition to a small sublimation.

TABLE 29. Energy Fluxes at Mirnyy, 1957

Average monthly heat budget constituents (ly/day) for two winter and two summer months at the snow-air interface: net radiation (R_0), eddy heat flux (Q_0), and snow heat flux (S_0) from *Kopanev* [1960].

Month	R_0	Q_0	S_0	E_0
June	−57	−83	−3	29
July	−45	−71	−3	29
Nov.	30	−33	1	62
Dec.	84	−26	6	104

TABLE 30. Summary of Midwinter Energy Fluxes at Four Antarctic Stations (Average of June and July Values)
Mean station temperature (T_m, °C) and surface energy budget constituents (ly/day): net radiation (R_0), eddy heat flux (Q_0), and snow heat flux (S_0). $E_0 = R_0 - Q_0 - S_0$ = remainder term.

Station (Altitude, m)	Year	T_m	R_0	Q_0	S_0	E_0
South Pole (2800)	1958	−58.1	−56.5	−44.5	−2.5	− 9.5
Mirnyy (35)	1957	−16.4	−51.0	−77.0	−3.0	+29.0
Maudheim (37)	1950–51	−26.7	−46.0	−26.0	−7.5	−12.5
Little America V (44)	1957	−21.6	−32.5	−11.4	−2.6	−18.5

Liljequist computed net radiation at Maudheim from frequent, carefully controlled measurements, taken under different conditions of cloudiness. Monthly values were based on the resulting relationships and observations of cloudiness. The short-wave radiation balance was obtained from global radiation (direct plus diffuse, with direct radiation computed under various conditions of cloudiness) and the upward short-wave radiation measured by a Moll-Gorczynski pyranometer. The net long-wave radiation balance was measured by an Angstrom pyrgeometer, again using a frequency distribution of net long-wave radiation under different cloud conditions.

At Mirnyy the net radiation balance was computed rather than measured by net radiometer, using the net long-wave and net short-wave balances but with some differences in instrumentation and in details of computation.

The winter net radiation flux is negative at all stations (away from the surface) and shows the extreme value at South Pole (Table 30). With a mean temperature at Mirnyy as high as −16.4°C, higher values of R_0 might be expected. However, lack of a severe winter temperature regime at Mirnyy is attributed by *Rusin* [1958] to the foehn wind, other effects of which are high wind speeds, low humidity, and clear skies.

Heat release from the snow is the smallest term at all stations. At Mirnyy the eddy heat flux toward the surface in winter is very large, and, according to *Kopanev* [1960] the latent heat flux is directed upward at Mirnyy, whereas all other authorities obtain the opposite direction (downward) for the latent heat flux. Although its intensity may be uncertain, it must be said that downward flux of moisture (deposition) is much more likely for the mean antarctic winter condition than upward flux (sublimation). The reason for the statement in support of deposition is the strong inversion existing over the continent. The foehn wind at Mirnyy may explain the differences in the energy balance from that at the other coastal locations.

Estimates of monthly mean values of the latent heat flux E_0 at South Pole were obtained by two other methods, for comparison with the values obtained by the heat budget residual method.

Let the subscript i denote the value of a meteorological element at the top of the inversion. Assuming similarity between the mechanism of vertical transfer for heat and moisture, an application of the Bowen ratio concept provides an estimate if the ratio r_B, in

$$Q/E = c_p(T_i - T_0)/L(q_i - q_0) \approx Q_0/E_0 \equiv r_B \quad (49)$$

Since the density of a gas is proportional to its molecular weight, the specific humidity is given by $q = 0.622\ e/p$, where e/p is the ratio of vapor pressure to atmospheric pressure. We minimize r_B by determining q_i from the saturation pressure e_{si} at T_i and by letting $q_0 = 0$. Thus, we write in a first approximation

$$r_B = c_p(T_i - T_0)p_i/0.622\ Le_{si}$$

For average winter values at South Pole ($T_i - T_0 = 18.9$°C, $p_i = 615$ mb, $e_{si} = 0.138$ mb), a value of $r_B = 48.7$ is obtained.

The energy budget equation 48, when combined with equation 49 can be solved for E_0:

$$E_0 = (R_0 - S_0)/(1 + r_B) = Q_0/r_B \quad (50)$$

In Table 31 estimates of E_0 based on equation 50 are compared with the previous results, based on the residual method, and independent Q_0 values in equation 48. In general, the Bowen ratio method produces much smaller deposition rates.

Another quasi-independent estimate can be made by assuming similarity between the mechanism of vertical transfer for moisture and (horizontal) momentum throughout the entire inversion layer, using the

estimated τ_0 values, in the approximate relation

$$E_0 = -\tau_0 L(q_i - q_0)/(V_i - V_0)$$
$$\approx -0.622\tau_0 L e_{si}/p_i V_i \qquad (51)$$

when $V_0 = 0$ and, as before, q_0 are neglected in comparison with $q_i > 0.662 e_{si}/p_i$. Monthly averages of the basic data, $(T_i - T_0)$, T_i, e_{si}, p_i, V_i, and τ_0 at South Pole and resulting E_0 values are listed in Table 31.

Hanson [1960] has computed the energy balance for four periods of several hours each on September 18–19, 1958, at the South Pole station. During the first period with clear skies and cold temperatures, deposition was indicated; during the last period, with temperature rise, slight sublimation was obtained. The rate of deposition during the first period was 0.15 mm per day in water equivalent; E_0 from Table 27 equals −13 ly/day in September, which is an average of 0.19 mm per day. It is interesting that the surface temperature during the last period was only slightly warmer than during the first period and the general shape of the temperature profile differed little. To have an upward flux of latent heat in the last period, one would have expected the surface temperature to have been considerably warmer than in the first period. In 1958, periods of warming in the winter months of May and July at South Pole apparently produced conditions favorable for sublimation (positive E_0). In fact, in May slight sublimation was the average condition. In July the average for the month showed only half as much deposition as in June or August.

It may very well be that the uncertainty of all terms in equation 48 is such that the remainder computation is accurate only within ±10 ly/day, which is the same as ±0.007 ly/min. In view of the comparatively large deposition obtained as $E_0(a)$ in Table 31, a new latent heat flux value has been computed, taking $E_0 = [E_0(a) + E_0(b) + E_0(c)]/3$, and is shown in Table 32. The remainder $\Delta_0 = R_0 - (Q_0 + S_0 + E_0)$ has been treated as the error term (systematic and random).

In completing the discussion of the heat balance, it appears appropriate to investigate critically some of the model assumptions involved in the estimate of eddy heat flux from profile data. The similarity assumption introduced in the section on eddy heat flux can be formulated more generally by consideration of the ratio $\gamma = K_Q/K_M$, where K_Q is the eddy diffusivity for heat and K_M that for horizontal momentum. Although equation 24 is true for $\gamma = 1$, a more general form of this equation would be

$$Q_0 = -c_p \gamma \tau_0 \, \Delta\theta/\Delta V$$

In spite of the efforts of many investigators, the true dependency of γ on bulk stability is still a matter of controversy. It is frequently suggested that $\gamma < 1$ applies for inversion cases. However, if this were true, the magnitude of Q_0 would be reduced in the above equation for inversion conditions. With the given values of R_0 and S_0 at South Pole, the result would be that the computed depo-

TABLE 31. Latent Heat Flux (E_0, ly/day) at South Pole, 1958

Estimate of monthly mean values using three methods: (*a*) heat budget residual method, (*b*) similarity between heat and moisture transfer, and (*c*) similarity between momentum and moisture transfer. Also indicated are temperature difference ($T_i - T_0$, °C) through the inversion, temperature (T_i, °C), saturation pressure (e_{si}, mb), atmospheric pressure (p_i, mb), wind speed (V_i, cm/sec), and surface stress (τ_0, dynes/cm²).

Month	$T_i - T_0$	T_i	e_{si}	p_i	V_i	τ_0	$E_0(a)$	$E_0(b)$	$E_0(c)$
Jan.	3.1	−22.1	0.794	657					
Feb.	8.8	−26.3	0.555	640	7.2	.310	−21	−5.4	−1.3
Mar.	20.0	−33.7	0.257	624	7.8	.437	−26	−2.0	−0.8
April	25.8	−36.8	0.183	624	6.9	.339	−21	−1.0	−0.5
May	19.3	−36.8	0.183	623	10.9	.928	+ 6	−1.3	−0.9
June	21.2	−39.4	0.137	615	8.9	.655	−13	−0.9	−0.6
July	16.6	−39.2	0.140	615	11.9	.986	− 6	−1.3	−0.7
Aug.	22.8	−39.2	0.140	620	9.1	.500	−14	−0.8	−0.4
Sept.	17.9	−37.9	0.162	616	11.6	.660	−13	−1.1	−0.5
Oct.	14.2	−34.8	0.228	624	9.0	.869	− 8	−1.6	−1.3
Nov.	9.1	−30.3	0.368	634	6.9	.349	+12	+0.4	−1.0
Dec.	16.1	−24.2	0.685	661					

TABLE 32. Average Monthly Heat Budget Constituents and Error (systematic and random) at the Snow-Air Interface at South Pole, 1958

Net radiation (R_0, ly/day); eddy heat flux (Q_0, ly/day); snow heat flux (S_0, ly/day); latent heat flux ($\bar{E}_0$, ly/day), where $\bar{E}_0 = [E_0(a) + E_0(b) + E_0(c)] \div 3$ from Table 31; and remainder (Δ, ly/day) where $\Delta = R_0 - (Q_0 + S_0 + \bar{E}_0)$ = error.

Month	R_0	Q_0	S_0	$\bar{E}_0$	Δ
Jan.			+ 4		
Feb.	−40	−16	− 3	− 9	−12
Mar.	−65	−32	− 7	−10	−16
April	−60	−32	− 7	− 8	−13
May	−54	−56	− 4	+ 1	+ 5
June	−54	−39	− 2	− 5	− 8
July	−59	−50	− 3	− 3	− 3
Aug.	−50	−33	− 3	− 5	− 9
Sept.	−46	−32	− 1	− 5	− 8
Oct.	−31	−28	+ 5	− 1	− 7
Nov.	+14	− 8	+10	+ 4	+ 8
Dec.			+10		

sition rate would be larger than for $\gamma = 1$. This result appears highly unrealistic, and it must be concluded that $\gamma = 1$ is the better assumption.

If, in addition to eddy diffusion, heat would be transferred from layer to layer by infrared radiation, an apparent γ larger than unity could be expected. However, radiational transfer of heat must be proportional to both absolute temperature and moisture of the air. Both factors are extremely low at South Pole, and a significant contribution of radiation to the heat transfer within the lowest few meters can be ruled out.

The other possible source of error in the model used is the exact value of the Kármán constant (k) used in the estimate of τ with the aid of equation 23 before being used in equation 24. It can be seen that k^2 is a factor in the estimate of Q_0. All computations for South Pole were made using $k = 0.40$. However, the numerical value of Kármán's constant is, unfortunately, not known with the desirable precision. Values used in the literature range from 0.38 to 0.45. A re-analysis of Nikuradse's experiment by *Lettau* [1961] produced, as the best value, $k = 0.428$ rather than 0.40. Corrected values of Q_0 computed for South Pole, obtained by multiplying the values presented in Table 27 by the factor $(0.428/0.4)^2 = 1.145$, are given in Table 33, as are the resulting values of the remainder term E_0. The 10-month deposition rate for South Pole is reduced to approximately one-half its former value. Liljequist and Hoinkes used $k = 0.40$, whereas Kopanev used $k = 0.38$ in computing Q_0. Revised values for the midwinter energy fluxes at the four antarctic stations, using $k = 0.428$, are given in Table 34. The amount of deposition is reduced at South Pole, Maudheim, and Little America V, while sublimation is greater at Mirnyy. In view of many error sources it is still difficult to arrive at a precise value of the deposition rate for South Pole.

9. CONCLUSIONS

At South Pole, moderate to extreme stability represents the average condition for the 10-month period, February through November 1958, with greater stability on the average in the early winter and in the months with the lowest average wind speed and coldest average temperature. During the sunless period, wind prevailed from 20° east of Greenwich. Temperatures show a flat winter minimum, with reversals of the temperature trend, typical of polar regions in both hemispheres.

The Richardson number changes systematically with height in the lowest 4 meters, decreasing under unstable conditions and increasing under stable conditions. Wind profile curvature decreases with increasing stability. A highly significant feature appears to be that the wind profile Deacon number does not become zero with increasing bulk stability but reaches a minimum (near 0.25) and then in-

TABLE 33. Revised Energy Fluxes at South Pole, 1958

Average monthly heat budget constituents (ly/day) at the snow-air interface: net radiation (R_0) and eddy heat flux (Q_0) from USWB and QM data, using $k = 0.428$, snow heat flux (S_0) from USWB, QM, and Arctic Institute of North America glaciological data. $E_0 = R_0 - Q_0 - S_0$ = remainder term.

Month	R_0	Q_0	S_0	E_0
Jan.			+ 4	
Feb.	−40	−18	− 3	−19
Mar.	−65	−37	− 7	−21
April	−60	−37	− 7	−16
May	−54	−64	− 4	+14
June	−54	−45	− 2	− 7
July	−59	−57	− 3	+ 1
Aug.	−50	−38	− 3	− 9
Sept.	−46	−37	− 1	− 8
Oct.	−31	−32	+ 5	− 4
Nov.	+14	− 9	+10	+13
Dec.			+10	

TABLE 34. Revised Summary of Midwinter Energy Fluxes at Four Antarctic Stations (Average of June and July Values)
Mean station temperature (T_m, °C) and surface energy budget constituents (ly/day): net radiation (R_0), eddy heat flux (Q_0), using $k = 0.428$ and snow heat flux (S_0). $E_0 = R_0 - Q_0 - S_0$ = remainder term.

Station (Altitude, m)	Year	T_m	R_0	Q_0	S_0	E_0
South Pole (2800)	1958	−58.1	−56.5	−51.0	−2.5	− 3.0
Mirnyy (35)	1957	−16.4	−51.0	−97.7	−3.0	+49.7
Maudheim (37)	1950–51	−26.7	−46.0	−29.8	−7.5	− 8.7
Little America V (44)	1957	−21.6	−32.5	−13.1	−2.6	−16.8

creases with height, probably owing to increasing importance of change of shearing stress with height. In other words, thickness of the surface layer appears to become less than 2 meters with extreme stability. Temperature profile curvature decreases with height and stability, but the recurvature shown by the graph of the wind profile curvature does not occur. The different behavior of wind and temperature profile curvature at strong bulk stability suggests that relative momentum-flux divergence is greater than relative heat-flux divergence a few meters above the antarctic snowfield.

Analysis of statistical wind data from the South Pole region indicates that the air motion in the lower atmosphere is controlled by surface friction, and by the geostrophic motion in the free atmosphere above the inversion layer, modified by thermal winds due to horizontal temperature gradients which result from the general slope of the terrain.

The new method that permits computation of aerodynamic roughness length from diabatic wind profiles yields a value of 0.014 cm for a large range of bulk stability, which is consistent with other measurements over snow. For hourly data classed by bulk stability into 30-run groups, surface stress ranges from 0.825 to 0.103 dyne/cm^2, and eddy heat flux from 0.0052 to 0.0239 ly/min, where the negative sign indicates flux toward the surface.

Fourier analysis of the subsurface temperatures at South Pole indicates that genuine heat conduction prevails below 4 meters but that other influences are present in the upper layers. Heat flux at the surface is calculated by numerical integration of the energy-change equation.

The energy budget at the snow-air interface is considered in the form that net radiation is equal to the sum of the eddy heat flux, the heat flux in the snow, and the latent heat flux. The latent heat flux, when treated as a remainder, indicates deposition in midwinter in quantities equal to that at the coastal stations of Maudheim (1950–1951) and Little America V (1957). Approximate monthly values for latent heat flux at South Pole by two other methods also indicate deposition in midwinter but yield smaller deposition rates. The uncertainty of all terms in the heat budget equation may be such that the latent heat flux, computed as a remainder, is accurate within only ±10 ly/day.

Acknowledgments. The late Richard Hubley served as coordinator for the micrometeorological programs conducted in the polar regions by the glaciologists of the USNC-IGY, and he is responsible for setting up the original program. The Quartermaster Research and Engineering Center purchased the instruments, established and carried out the programs at two antarctic sites (Little America in 1957 and South Pole in 1958). The data reduction and analysis have been performed at the Quartermaster Research and Engineering Center under sponsorship of both the National Science Foundation and the Quartermaster Research and Engineering Center. The Ohio State University Research Foundation administered two NSF grants that covered a period of 42 months.

Richard P. Goldthwait, glaciologist, Ohio State University Research Foundation (OSURF), served as project supervisor; Paul C. Dalrymple, meteorologist, Quartermaster Research and Engineering Center, served as principal investigator; Sarah Wollaston, meteorologist, both OSURF and Quartermaster Research and Engineering Center, conducted most of the analyses; and Heinz H. Lettau, University of Wisconsin, served both as an OSURF consultant and as a Quartermaster Research and Engineering Center expert.

In addition to the above persons, many others contributed to the data analysis program. Donald Portman, University of Michigan, who served in 1958–1959 as Quartermaster Research and Engineering Center consultant in micrometeorology, was responsible in a large degree for the initial planning of the data reduction and analysis, and he was instrumental in drafting the proposal to the National Science Foundation. Dorothy DesRoches and Barbara O'Neill, mathematicians, initiated the data analysis program and computed the Richardson numbers for many

of the South Pole profiles. Leonora Kundla, key punch operator, assisted in many small but essential tasks in the later stages of the analysis. James Dillon, Management Division, was responsible for programming some of the computations, through the Quartermaster Research and Engineering Center Computer Branch. Aubrey Greenwald, Pernel Leuvelink, and William Loughlin (Cartographic Branch, Earth Sciences Division) prepared the figures for reproduction.

The cooperation and support given by the Polar Meteorology Research Project, Environmental Science Services Administration, has been deeply appreciated. Past and present members of the project who have materially aided in making data available are Morton Rubin, William Weyant, Kirby Hanson, and Edwin Flowers.

Mirnyy data (USSR) were made available by the IGY World Data Center A: Glaciology, at the American Geographical Society. Maudheim data were obtained from the classic volumes by Gosta Liljequist (1956) and Valter Schytt (1960). Little America V energy budget data were obtained from Herfried Hoinkes (1961).

REFERENCES

Crary, A. P., Glaciological studies at Little America station, Antarctica, 1957 and 1958, *IGY Glaciological Rept. 5, A, Glaciology*, New York, American Geographical Society, IGY World Data Center, March 1961.

Dalrymple, P. C., South Pole micrometeorology program, 1, Data presentation, *Tech. Rept. ES-2*, Earth Sciences Division, Quartermaster Research and Engineering Center, Natick, Mass., October 1961.

Deacon, E. L., *Verticle Profiles of Mean Wind in the Surface Layer of the Atmosphere, Geophysical Memoirs, 91*, Meteorological Office, London, 1953.

Dillon, J. J., and J. Arbarchuk, A strip chart data reduction system, to be published, Quartermaster Research and Engineering Center, Natick, Mass.

Giovinetto, Mario, USNC-IGY antarctic glaciological data, field work 1958 and 1959 (South Pole station), *Ohio State Univ. Rept. 825-2-part IV, IGY Proj. 4.10, NSF grant Y/4.10/285*, April 1960.

Hanson, K. J., Radiation measurements on the antarctic snowfield, a preliminary report, *J. Geophys. Res., 65*, 935–946, March 1960.

Hanson, K J., and M. J. Rubin, Heat exchange at the snow-air interface at the south pole, *J. Geophys Res., 67*, 3415–3424, August 1962.

Hoinkes, H. C., Studies in glacial meteorology at Little America V, Antarctica, *Symposium on Antarctic Glaciology, IUGG International Association of Scientific Hydrology, Publ. 55*, 29–48, 1961.

Kopanev, I. D., *Snow Cover of the Antarctic*, 113 pp., Chief Administration of the Hydrometeorological Service, Leningrad, 1960.

Lettau, H. H., The present position of selected turbulence problems in the atmospheric boundary layer, *Geophys. Res. Papers, 19*, section 1.3 of *International Symposium on Atmospheric Turbulence in the Boundary Layer*, edited by E W. Hewson, Geophysical Research Directorate, Air Force Cambridge Research Center, Cambridge, Mass., 1952.

Lettau, H H., Improved models of thermal diffusion in the soil, *Trans. Am. Geophys. Union, 35*, 121–132, February 1954.

Lettau, H. H, *Exploring the Atmosphere's First Mile*, vol. 1, Pergamon Press, New York and London, 1957.

Lettau, H. H., A generalized mathematical model of the mean-velocity distribution in fully turbulent duct flow, section 8, *Annual Rept. (contract DA-36-039-SC-80282)*, University of Wisconsin, Madison, August 1961.

Lettau, H. H., Notes on diabatic profile structure, section 10, *Final Rept. (contract DA-36-039-SC-80282)*, pp. 195–226, Madison, Wisconsin, 1962.

Liljequist, G. H., Energy exchange of an antarctic snowfield, *Norwegian-British-Swedish Antarctic Expedition, 1949–1952, Scientific Results*, part 1, vol. 2, Oslo, 1956–1957.

MacDonald, J. E., 'Deposition'—A proposed antonym for 'sublimation,' *J. Meteorol., 15*, 245–247, April 1958.

Panofksy, H. A, A. K. Blackadar, and G. E. McVehil, The diabatic wind profile, *Quart. J. Roy. Meteorol Soc., 86*, 390–398, 1960.

Portman, D. J., An investigation of some heat-transfer characteristics of two thermocouple probes, *Final Rept. (Natl. Sci. Found., IGY grant Y/21.13/336)* Meteorological Laboratories, University of Michigan, Ann Arbor, September 1961

Priestley, C. H. B., *Turbulent Transfer in the Lower Atmosphere*, 130 pp., University of Chicago Press, Chicago, Ill., 1959.

Robinson, S. M., Computing wind profile parameters, *J. Atmospheric Sci., 19*, 189–190, March 1962.

Rusin, N. P., Meteorological processes in the surface layer of the atmosphere in Antarctica, Hydrometeorological Service, Leningrad, pp. 5–25, 1958; *Trans. Office Climatology, U. S. Weather Bureau*, February 1960.

Schytt, Valter, Snow and ice temperatures in Dronning Maud Land, *Norwegian-British-Swedish Antarctic Expedition 1949–1952, Glaciology II, A-C, D, vol. 4, Scientific Results*, Oslo, 1960.

Sutton, O. G., *Micrometeorology*, 333 pp., McGraw-Hill Book Company, New York, 1953.

THE DRIFTING OF NONUNIFORM SNOW PARTICLES[1]

W. F. Budd

Antarctic Division, Department of External Affairs, Melbourne, Australia

Abstract. The theory of steady-state turbulent snow drift is extended to the case of snow consisting of a distribution of particles of different sizes. We make the following *assumptions:* (1) snow particle fall velocities are proportional to their effective diameters; (2) the distribution of particle diameters at a given height can be approximated by a gamma variate; (3) particles of the *same* fall velocity are distributed along the vertical according to the steady-state turbulent drift theory; (4) particles of *different* fall velocities act independently.

On the basis of these assumptions, the following *conclusions* are reached: (1) The particle fall velocities at a given height are also distributed as a gamma variate. (2) The fall velocities at any arbitrary height z are distributed as a third gamma variate, and the mean particle size decreases with height. (3) The drift density falls off less rapidly with height than it would for uniform drift; the deviation is greater the larger the variance of the particle size distribution, but it decreases as wind speed increases. (4) The decrease in particle size with height is less for high winds, and the greater the variance to the mean of the original distribution, the greater the rate of decrease of particle size with height.

The predicted conclusions are found to agree satisfactorily with the empirical results from measurements of drift density and particle sizes at Byrd and other stations in Antarctica.

1. INTRODUCTION

Measurements of snow drift are beset with natural difficulties and the consequent inaccuracies. As a result, only few of the data published on snow drift in Antarctica and elsewhere have been such as to permit even the most cursory check of theoretical predictions, which therefore had to be based on the simplest of assumptions. A considerable advance came with the measurements made during 1962 at Byrd station (80°01′S, 119°32′W) [*Budd et al.*, 1966]. Although not final in any respect and severely limited in some (especially with regard to the wind range explored), these data were sufficiently extensive and precise to bring out systematic deviations from the predictions based on the turbulent exchange theory of snow drift, first formulated independently by *Shiotani and Arai* [1953] and *Loewe* [1956]. It was concluded that explaining these discrepancies required the dropping of either or both of two simplifying assumptions made: the constancy of the particle fall velocity and the existence of steady-state conditions. The present paper explores the consequences of relaxing the first of these restrictions and thus deals with drift snow composed of irregular particles of different sizes. The theoretical laws applying to such snow conglomerates are deduced and tested in particular by application to the Byrd results, which included detailed particle size data.

[1] See report on the Byrd snow drift project, pp. 71–134.

2. THEORY OF NONUNIFORM SNOW DRIFT

Introductory remarks. The existing theory of turbulent snow drift [*Shiotani and Arai*, 1953; *Loewe*, 1956; *Mellor and Radok*, 1960; *Dingle and Radok*, 1961] assumes uniform constant fall velocity (w). For drift made up of nonuniform particles this assumption is somewhat artificial in view of the presence of w in the relation for the drift density n_z as a function of height z

$$n_z = n_{z_1}(z/z_1)^{-w/ku_*} \tag{1}$$

where u_* is the shear velocity of the logarithmic wind profile and k is Kármán's constant.

Equation 1 shows clearly that, since particles of different sizes have different fall velocities, they will distribute themselves differently in the vertical and therefore will produce a change in the particle size distribution as well. To understand the effect of particles of different sizes, then, it will first be

necessary to inquire into the relation between particle size and fall velocity. Given such a relation, equation 1 can be applied to particles of the same velocity. Then, by combining the independent results over the entire fall velocity distribution, the drift density and particle size distribution can be derived as a function of height and wind velocity.

Particle size and fall velocity. Empirical measurements [*Baumeister and Marks*, 1958] indicate that the fall velocity of particles in the atmosphere for diameters between 1 and 0.1 mm can be expressed by the relation

$$V_n = K' S^{2/3} \rho^{-1/3} \eta^{-1/3} D$$

where S is the particle specific gravity, ρ is the air density, η is the air viscosity, D is the particle diameter (in microns), and V_n is the particle fall velocity (in ft/min). (Note: 1 ft/min = 0.508 cm sec^{-1}.) For typical air conditions this expression reduces to $V_n = k_2 S^{2/3} D$, where k_2 is a shape factor varying from 0.81, for spherical particles, to 0.51, for irregular shapes.

For ice $S^{2/3} \approx (0.917)^{2/3} \approx 0.944$, we take $k_2 =$ 0.81, 0.51, in turn, for snow drift particles, and obtain

$$w = 3880x \qquad k_2 = 0.81$$

or

$$w = 2440x \qquad k_2 = 0.51$$

respectively, where w is fall velocity in cm sec^{-1} and x is the particles' effective diameter in cm.

Hence, for particles in this size range the fall velocities will be considered directly proportional to the diameters.

For particle diameters above 2 mm the fall velocity is proportional to $(D)^{1/2}$ [*Baumeister and Marks*, 1958], and for smaller diameters (2 to 50 microns) the fall velocity is proportional to D^2, following Stokes' law.

From measurements of snow drift particles [*Dyunin*, 1956; *Lister*, 1960; *Budd et al.*, 1966] only a very small proportion of drift particles have projective diameters less than 0.05 mm, so that the simple proportionality relationship will be adopted here. However, as the size of the drift particles (0.04 to 0.30 mm) merges into the transition region, between direct proportionality and Stokes' law, discrepancies may be expected for the very small particles and low velocities. This effect will be discussed further in section 4.

Drift density and particle-size distribution as a function of height. If the distribution of particle diameters at a certain height is known, then a correction can be made to the drift profile given by equation 1. Furthermore, the distribution of particle diameters and fall velocities at all heights can be calculated.

Suppose the snow particles at a particular height have diameters, x, distributed with a frequency function $f(x)$ (the form of this frequency function will be discussed later). Since the fall velocities are related to diameters by a relationship of the form

$$\kappa w = x \qquad (\kappa \approx 1/3880 \text{ to } 1/2440 \text{ sec}) \tag{3}$$

the frequency function for fall velocities at height z will be given by

$$g(w)\, dw = f(x)\, dx$$

therefore

$$g(w) = \kappa f(x) \tag{4}$$

In unit volume of drift at height z_1, let $\Lambda_{z_1 w}$ be the *mass* of particles with fall velocity between w and $w + dw$; Λ_{z_1}, the *total mass* of particles of all fall velocities; and Λ_{z_1}, the total *number* of particles. The mass of a particle of fall velocity w is $K_1 w^3$, where, for spherical particles, $K_1 = \rho \kappa^3 \pi / 6$ but may also depend on the particle shape. Then

$$\Lambda_{z_1 w} = K_1 w^3 N_{z_1} g(w)\, dw \tag{5}$$

and

$$\Lambda_{z_1} = N_{z_1} K_1 \int_0^\infty g(w) w^3\, dw \tag{6}$$

From equation 6, if the drift density Λ_{z_1} at height z_1 is known, the number of particles N_{z_1} per unit volume at z_1 can be calculated.

Now it will be assumed that particles of the same fall velocity are distributed along the vertical according to equation 1 and also that particles of different fall velocities act independently. Then from equations 1 and 5 the mass of particles at height z with velocities between w and $w + dw$ is given by

$$\Lambda_{zw} = N_{z_1} K_1 w^3 g(w) e^{aw}\, dw \tag{7}$$

where $a = -(1/ku_*) \log_e z/z_0$ and the total drift

density at height z is given by

$$\Lambda_z = \int_0^\infty N_{z,1} K_1 w^3 g(w) e^{\alpha w}\, dw \tag{8}$$

To obtain the mean particle diameter at an arbitrary height z, we first obtain the frequency distribution of fall velocities at height z, i.e., the *proportion* of particles at height z with fall velocities between w and $w + dw$. This proportion is given by the ratio of the number of particles per unit volume with fall velocity between w and $w + dw$ (N_{zw}) to the total number per unit volume for all velocities (N_z).

Since the mass of a particle of fall velocity w is $K_1 w^3$, we see from (7) that

$$N_{zw} = N_{z,1} g(w) e^{\alpha w}\, dw \tag{9}$$

and

$$N_z = N_{z,1} \int_0^\infty g(w) e^{\alpha w}\, dw \tag{10}$$

Hence from (9), the proportion of particles with fall velocities between w and $w + dw$ is

$$(N_{z,1}/N_z) g(w) e^{\alpha w}\, dw = h(w)\, dw \tag{11}$$

and $h(w)$ is then the frequency function of the particle fall velocities at height z. The mean particle diameter $\bar{x}_z$ may be obtained from the mean of this distribution by a simple transformation of the form (3), viz. $\bar{x}_z = \kappa \bar{w}_z$.

3. SPECIAL CASE: GAMMA DISTRIBUTION OF SNOW PARTICLE DIAMETERS

Choice of gamma variate. In order to take the discussion one step further, some particular form must be specified for the frequency function $f(x)$ [and hence $g(w)$] which is in accord with the observed snow particle diameters at some standard height. The theory of breakages [*Aitchison and Brown*, 1957] suggests that the log normal distribution may be the most appropriate form. This conjecture is supported by the results of *Dyunin* [1956] and *Lister* [1960] for drift particles and will also be shown to be in accord with the Byrd results. The distribution of aggregates of other types of smaller particles also seem to fit the log normal model [*Krumbein and Pettijohn*, 1938; *Herdan*, 1953].

The log normal form is awkward, however, when applied to the relations derived in the preceding section. For the following analytical treatment a more suitable form of distribution has been found to be the two-parameter gamma distribution defined by

$$P\{x < \xi < x + dx\} = \frac{1}{\beta^\alpha \Gamma(\alpha)} e^{-x/\beta} x^{\alpha-1}\, dx = \gamma_{\alpha\beta}(x)\, dx \tag{12}$$

with mean $\alpha\beta$ and variance $\alpha\beta^2$.

It will be shown in section 4 that such a distribution provides a good fit for the observed effective diameters of the drift particles. We shall next explore the result of assuming a gamma distribution for the particle sizes according to the previously described theory.

Snow drift density as a function of height. If the diameters x, at height z_1, are distributed as $\gamma_{\alpha_1\beta}(x)$ with mean fall velocity w, and, if the drift density Λ_{z_1} is known, then the variation in drift density and particle size with height may be obtained from the results given in section 2.

From equation 4 the frequency function for fall velocities at height z_1, is

$$g(w) = \frac{1}{\beta_1^{\alpha_1}\Gamma(\alpha_1)} \kappa^{\alpha_1} e^{-(\kappa/\beta_1)w} w^{\alpha_1-1} = \gamma_{\alpha_1\beta_2}(w) \tag{13}$$

where $\beta_2 = \beta_1/\kappa$. To obtain the drift density Λ_z at any height we require the number of particles per unit volume at z_1 (i.e. $N_{z,1}$). We note from (5)

$$\Lambda_{z_1 w} = K_1 N_{z,1} \frac{1}{\beta_2^{\alpha_1}\Gamma(\alpha_1)} e^{-(w/\beta_2)} w^{(\alpha_1+3)-1}$$

and hence

$$\Lambda_{z_1} = K_2 \int_0^\infty \gamma_{\alpha_2\beta_2}\, dw \tag{14}$$

where $\alpha_2 = \alpha_1 + 3$ and $K_2 = N_{z,1} K_1 [\Gamma(\alpha_1+3)/\Gamma(\alpha_1)]\beta_2^3$.

As the integral in (14) is unity, we see $\Lambda_{z_1} = K_2$ and hence

$$N_{z_1} = (\Lambda_{z_1}/K_1)[\Gamma(\alpha_1)/\Gamma(\alpha_1 + 3)]\beta_2^{-3}$$

From (14) and (7) we see

$$\Lambda_{zw} = K_2 \gamma_{\alpha_2\beta_2}(w) e^{\alpha w}\, dw = K_2 \frac{1}{\beta_2^{\alpha_2}} \frac{1}{\Gamma(\alpha_2)} e^{-(w/\beta_2)} w^{\alpha_2-1} e^{\alpha w}\, dw = K_3 \gamma_{\alpha_2\beta_2}(w)\, dw$$

where $\beta_3 = \beta_2/(1 - a\beta_2)$ and $K_3 = K_2(\beta_3^{\alpha_2}/\beta_2^{\alpha_2}) = K_2(1 - \beta_2 a)^{-\alpha_2}$. Hence

$$\Lambda_z = K_3 \int_0^\infty \gamma_{\alpha_2,\beta_2}(w)\, dw$$

$$= K_3 = K_2(1 - \beta_2 a)^{-\alpha_2}$$

and since $K_2 = \Lambda_{z_1}$, we obtain

$$\Lambda_z = \Lambda_{z_1}(1 - \beta_2 a)^{-\alpha_2} \qquad (15a)$$

By rearranging and taking logs of both sides we find

$$\log (\Lambda_z/\Lambda_{z_1}) = -\alpha_2 \log |1 - \beta_2 a|$$

and, provided $|\beta_2 a| < 1$, we can expand the right-hand side as a power series, giving

$$\log (\Lambda_z/\Lambda_{z_1}) = \alpha_2\beta_2 a + \tfrac{1}{2}\alpha_2\beta_2^2 a^2 + \tfrac{1}{3}\alpha_2\beta_2^3 a^3 + \cdots$$

or

$$\log \frac{\Lambda_z}{\Lambda_{z_1}} = -\frac{w'}{ku_*} \log \frac{z}{z_1} + \frac{1}{2}\frac{\alpha_2\beta_2^2}{(ku_*)^2} \log^2 \frac{z}{z_1} + \cdots \qquad (15b)$$

since $a = -(1/ku_*) \log z/z_1$ and $w' = \alpha_2\beta_2 = \bar{w}[(\alpha_1 + 3)/\alpha]$.

The first term on the right of equation 15*b* is the log of the drift density ratio $(\Lambda_z/\Lambda_{z_1})$ as given by the simple drift theory with constant fall velocity w'. The second term is a correction term depending firstly on the variance $\alpha_2\beta_2^2$ of the original particle distribution. Secondly, it should be noted that u_*, the friction velocity in the logarithmic wind profile, is proportional to the wind speed at a given level (for roughness length z_0 constant as assumed here). This means that the second term in (15*b*) decreases with increasing wind velocity (or becomes less for strong winds). For a given logarithmic wind profile the correction term varies with height z, as the square of log (z/z_1). The effects of higher terms in the series will be discussed in section 4.

Variation of particle size and fall velocity with height. To find the change in particle size with height, we see from equation 11, for the frequency function of particle fall velocities, that we require the number of particles per unit volume at height z, N_z.

From equations 10 and 13

$$N_z = N_{z_1} \int_0^\infty \gamma_{\alpha_1,\beta_1} e^{\alpha w}\, dw$$

$$= N_{z_1}\left(\frac{\beta_3}{\beta_2}\right)^{\alpha_1} \int_0^\infty \gamma_{\alpha_1,\beta_3}(w)\, dw$$

$$= N_{z_1}(\beta_3/\beta_2)^{\alpha_1}$$

and since $\beta_3 = \beta_2/(1 - a\beta_2)$.

$$N_z = N_{z_1}(1 - a\beta_2)^{-\alpha_1}$$

or

$$N_z = N_{z_1}[1 + (\beta_2/ku_*) \log (z/z_1)]^{-\alpha_1}$$

Incidentally, this quantity would be important when considering drift density estimates associated with counts of particles caught on slides exposed for a short time.

In particular we have

$$N_{z_1}/N_z = (\beta_2/\beta_3)^{\alpha_1}$$

Now the frequency function for all velocities for (11) and (13) is given by

$$h(w) = (N_{z_1}/N_z)\gamma_{\alpha_1,\beta_3}(w)e^{\alpha w}$$

$$= (\beta_2/\beta_3)^{\alpha_1}(1/\beta_2^{\alpha_1})[1/\Gamma(\alpha_1)]e^{-w[(1/\beta_3)-\alpha]}w^{\alpha_1-1}$$

$$= (\beta_2/\beta_3)^{\alpha_1}\frac{\beta_3^{\alpha_1}}{\beta_2^{\alpha_1}}\gamma_{\alpha_1,\beta_3}(w)$$

Hence $h(w) = \gamma_{\alpha_1,\beta_3}(w)$ is the frequency function for particle fall velocities at height z. This has the mean

$$\bar{w}_z = \alpha_1\beta_3 = \alpha_1\beta_2/(1 - \beta_2 a)$$

therefore

$$\bar{w}_z = \frac{w_{z_1}}{1 + (\beta_2/ku_*) \log z/z_1} \qquad (16a)$$

since $\bar{w}_{z_1} = \alpha_1\beta_2$ and $a = -(1/ku_*) \log (z/z_1)$. It follows from equation 4 that the mean particle diameter is given by

$$\bar{x}_z = \frac{\bar{x}_{z_1}}{1 + (\beta_1/ku_*) \log (z/z_1)} \qquad (16b)$$

From equation 16*a* it can be seen that the mean particle fall velocity (and hence diameter) decreases logarithmically with height for a given wind profile. The greater β_2 (i.e., the ratio of the variance to the mean of the fall velocities), the more rapid the decrease in particle size with height. For high wind speeds (u_* large) the decrease in particle size with height is less pronounced.

The variance of the distribution is given by

$$\alpha_1\beta_3^2 = [\alpha_1\beta_2^2/(1 - \beta_2 a)^2]$$
$$= [\alpha_1\beta_2^2/(1 + (\beta_2/ku_*) \log z/z_1)^2]$$

Taking the square root it can be seen that the standard deviation varies with height and wind speed just as does the mean.

It must be noted here that, because of the skew distribution of particle diameters, the mean mass of the particles $\bar{M}$ is not the same as the mass of the particle of mean diameter m but is in general larger. This fact becomes important when calculating the number of particles in a given mass. Similarly, the mean surface area $\bar{S}$, as distinct from the surface area s of the particle of mean diameter, becomes important when considering drift gages of the photoelectric type.

For gamma distribution, m, $\bar{M}$, s, $\bar{S}$ are related by

$$\bar{M} = m[1 + (3/\alpha) + (2/\alpha^2)]$$

and

$$\bar{S} = s[1 + (1/\alpha)]$$

(Note that for Byrd particle distribution $\alpha \approx 15$.)

The next stage will be to compare the predicted results, in paricular those of equations 16 and 15, with the results of available drift and particle size data.

4. APPLICATION OF THEORY TO DRIFT AND PARTICLE SIZE OBSERVATIONS

The theoretical results of the preceding section will be tested in the main by means of the data of the Byrd drift project [*Budd et al.*, 1966], but other observations will also be referred to where applicable. The following separate aspects will be treated: (1) the theoretical and empirical distributions of particle sizes, (2) the expected and observed variation of mean particle diameter with height and wind speed, (3) the expected and observed variation of mean particle fall velocity with wind speed, (4) the effect of the nonuniformity of drift snow on the drift density as a function of height and wind speed.

Theoretical and empirical distribution of snow particle sizes. In the course of the Byrd drift project, Dingle succeeded in obtaining a large number of snow particle casts on Formvar-coated slides exposed at the levels of the drift gages. Subsequently he measured the projected areas of some 2500 of

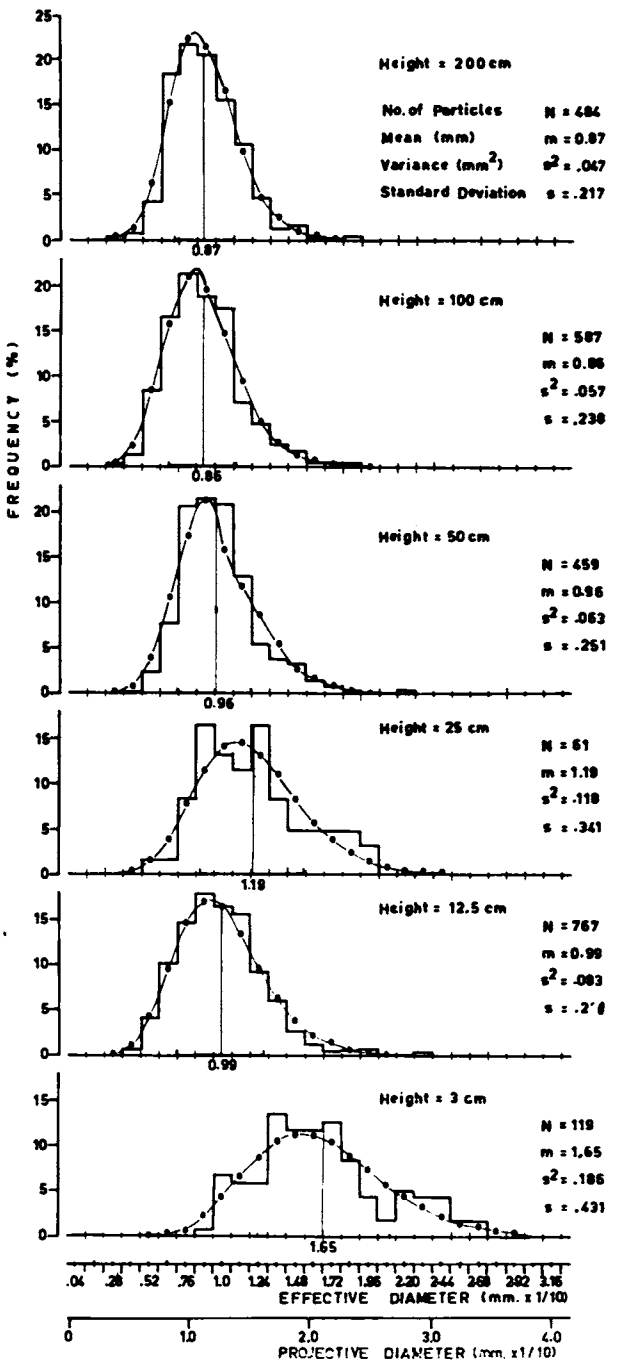

Fig. 1. Histograms for the frequency distribution of snow particle sizes at various heights above the surface. The corresponding theoretical gamma distributions are shown by dots connected by solid lines.

these particle replicas by approximating each particle by a rectangle of the same area. From the sides l and b of these rectangles the 'effective' diameters were next computed as $D_e = (lb)^{1/2}$ on an electric computer and arranged into size frequency distributions for the different levels (viz., 3, 12.5, 25, 50, 100, 200 cm). Finally, the means and standard deviations were computed for each of these distributions.

It should be noted here that the 'projective diameter' D_p, which is defined as the diameter of the *circle* with same area as the projective area of the particle, is related to D_e above by

$$D_p = (4/\pi)D_e \qquad 4/\pi \approx 1.27$$

This relation emphasizes the problem of a shape factor when attempting to represent the size of an irregular particle by a single dimension. Since spheres have the *maximum* fall velocity for a given volume, irregular particles will have an 'effective diameter' for fall velocity calculations less than the projective diameter.

Timbrell [1954] and *Robins* [1954] show values of the ratio D_p/D_s, where D_s is the 'Stokes' diameter,' i.e., the diameter of the sphere that falls with the same terminal velocity as the particle, to range between 1.3 and 1.6. for different types of irregular particles. For this reason the effective diameter as defined above has been used as the linear dimension typical of the particle for fall velocity calculations.

The empirical distributions are shown as histograms in Figure 1, together with distributions of the $\gamma_{\alpha\beta}$ type computed from the means and variances of the respective empirical distributions.

The theoretical curves appear to provide a satisfactory fit to the observations at all levels where large numbers of particles were obtained. This provides sufficient justification for applying the theory of section 3.

The validity of the approximation of the observed frequency distributions of particle sizes by gamma distributions can be further judged from Figure 2, which shows the observed distribution of effective diameters for the 12.5-cm level, together with three theoretical distributions (viz., normal, log normal, and gamma).

There seems little to choose between the log normal and gamma distributions, both of which provide as good a fit as could be expected on the basis of two parameters. The log normal distribution lies below the empirical frequencies for small effective diameters. This implies that the empirical distribution, when plotted on a logarithmic scale, is skew toward the small diameters. This feature seems to be characteristic of small particle aggregate distributions [*Lister*, 1960; *Bagnold*, 1941; *Krumbein and Pettijohn*, 1938].

Accepting the gamma variate as a sufficiently close approximation, for theoretical purposes, to the observed particle size distributions leaves the

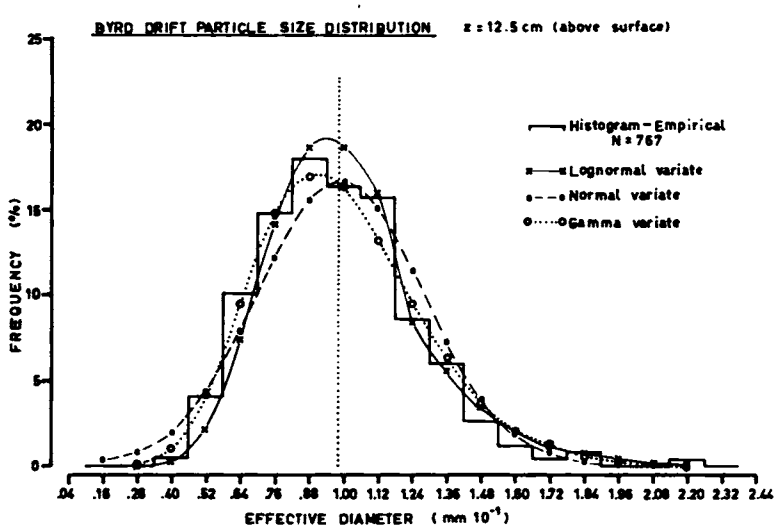

Fig. 2. Comparison between the empirical distribution, at the 12.5-cm level, and the three theoretical distributions (normal, log normal, and gamma) of the same mean and variance. $z = 12.5$ cm (above surface).

difficulty that the range of the particle sizes is from 0.04 to 0.3 mm, to some extent in the transition zone between the regions of validity of Stokes' law ($w \propto D^2$) and a linear relation between particle diameter and fall velocity. This leads us to expect certain discrepancies between theoretical and observed results for the smaller particles, which predominate at greater heights and lower wind speeds.

Variation of mean particle size with height and wind speed. Equation 16*b* suggests that the mean particle diameter should tend to decrease with height but depend also on wind speed (i.e., u_*) and the variance to the mean β of the particle size distribution.

The particles collected at Byrd were obtained over a wide range of wind speeds on a number of different occasions. The over-all mean diameters, averaged over all wind speeds, for each level have been plotted in Figure 3, together with two curves derived from equation 16*b* for two values of wind speed, and using $z_1 = 50$ cm. The average wind speed for the particles collected at 50 cm was 17.5 m sec^{-1}, and this value is used for the calculation of the full curve in Figure 3.

The greatest discrepancies between theory and observations in Figure 3 occur at the 3- and 25-cm levels, at which only 119 and 61 particles, respectively, were measured.

The scatter between measurements on different occasions was comparatively large and is believed to be due to past meteorological conditions such as wind speed, temperature, and the amount of new snow available.

For further comparison, two profiles of mean particle size with height for South Ice are plotted on the same diagram. These were computed from the histograms given by *Lister* [1960] and show a similar general decrease of size with height, as well as having an absolute size range in close agreement with the results from Byrd.

The theoretical curve has been extrapolated down to the level of the mean roughness length ($z_0 = 0.015$ cm) of the Byrd wind profiles, giving a maximum particle size of 0.33 mm. The validity of this may be judged by reference to the size of snow particles on the surface. No direct measurements were made of snow particle size at Byrd. However, some 200 saltating particles collected through an open hatch level with the surface gave an average size of 0.18 mm, which corresponds on the extrapolated curve to a height of about 1.0 cm. *Kotlyakov* [1961] quotes average sizes of drift snow particles on the surface at Vostok (78°28′S, 106°48′E) ranging between 0.2 and 0.4 mm. *Dyunin* [1956] quotes snow drift particles at the surface ranging from 0.32 to 0.36 mm and occasionally, after being reduced by wind action, to between 0.2 and 0.3 mm. This suggests that the theoretical extrapolated value given above is not too unrealistic.

The expected variation of particle size with wind speed may be obtained from equation 16*b*. This equation indicates that, if the mean particle size at the surface were constant, then the mean size at all other levels would increase with wind speed (i.e., u_*, which is assumed to be linearly related to the wind speed at a given level). From the Byrd results

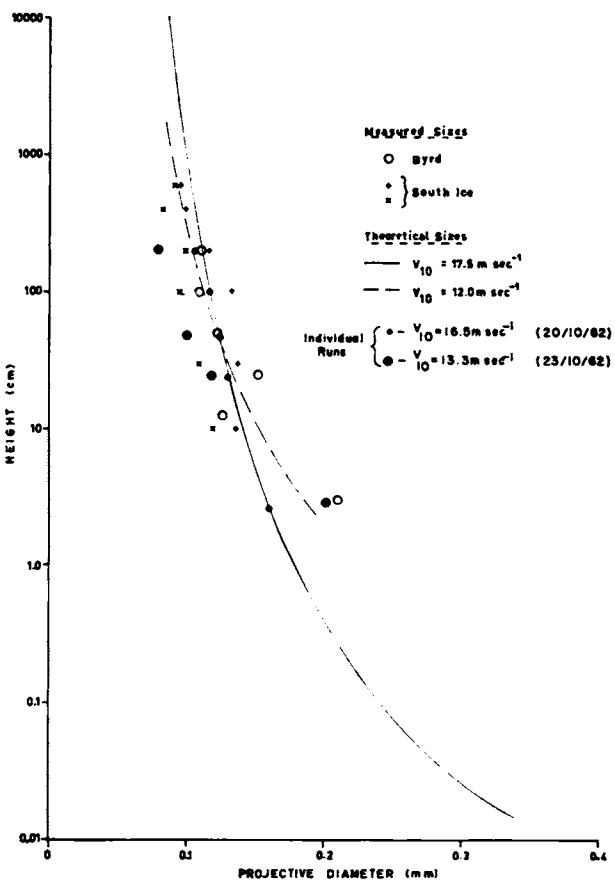

Fig. 3. The measured mean particle size variation with height for Byrd and South Ice compared with the theoretical curves for two different wind speeds, calculated from equation 16*b* for $z = 50$ cm. The continuous curve uses the average wind speed for the particles collected at this level.

it is evident that the average size on the surface is not constant but varies greatly from one occasion to another. Consequently, no significant variation with wind speed was found for the lower levels (3 and 12.5 cm). For the higher levels (100 to 200 cm), however, the average increase of size with wind speed was considerable and has been plotted in Figure 4. This figure shows reasonable agreement between the observed variation of particle size with wind speed and that predicted by equation 16*b*.

Variation of particle fall velocity with height and wind speed. The particle fall velocity is difficult to measure directly but can be computed from the drift densities measured at the different levels. From equation 15*a* it follows that

$$\Lambda_z = \Lambda_{z_1}[1 - (\beta_2/ku_*) \log (z/z_1)]^{-\alpha_2}$$

since the mean fall velocity at height z is given by $w_z = \alpha \beta_2$, which from equation 15*a* is

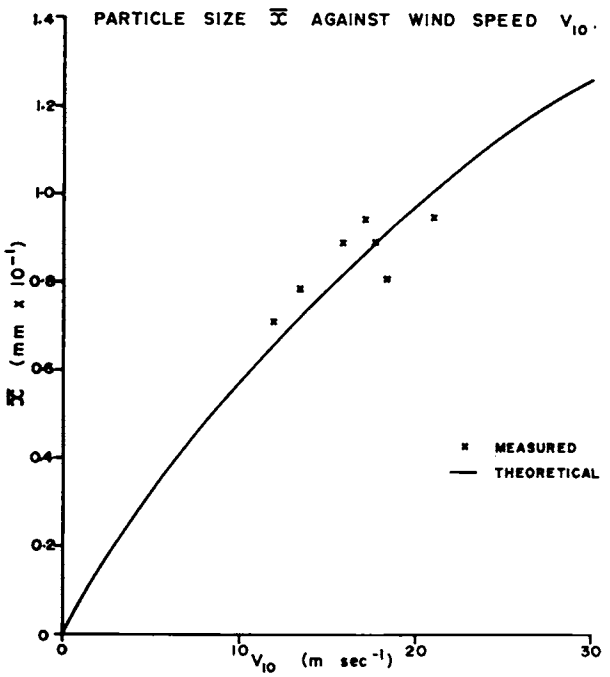

Fig. 4. The increase in particle mean size with wind speed from the measured drift particles at the 100- and 200-cm levels from Byrd is compared with the theoretical curve

$$\bar{x}_z = \frac{\bar{x}_{z_0}}{1 + (\beta/ku_*) \log (z/z_0)}$$

assuming a constant size distribution at the surface (z_0) and a linear variation of u_* with the wind speed at the 10-meter level (V_{10}).

$$w_z = \frac{\alpha_2 k u_* [(\Lambda_z/\Lambda_{z_1})^{(1/\alpha_2)} - 1]}{\log z/z_1} \qquad (17)$$

This result differs only slightly from the result for constant w, viz.

$$w_z = kn_* \frac{\log (\Lambda_z/\Lambda_{z_1})}{\log (z/z_1)}$$

provided z is near enough to z_1, e.g. for two adjacent levels of the drift gaging measurements at Byrd.

From equation 17 the mean fall velocity at each level was computed for six wind speeds from 11 to 22 m sec^{-1}. Figure 5 shows how these mean fall velocities vary with height, for different wind speeds. Theoretical curves obtained from equation 16 are also shown for comparison. Figure 5 clearly confirms the expected decrease of fall velocity with height and its reduction with increasing wind speed.

Figure 6 shows how the mean fall velocity increases with wind speed for several different levels. The theoretical curve from equation 16*a* for the 50-cm level is shown for comparison. This assumes constant z_0 and $\bar{w}_{z_0}$ (i.e., a constant particle size at the surface) and indicates that the rate of increase of mean fall velocity with wind speed (under these conditions) is not linear, but that w tends to a maximum value which would correspond to that of the particles at the surface (strictly z_0). From Figure 6 and the extrapolated particle size curve of Figure 3, the surface particles should have mean fall velocity of about 80 cm sec^{-1}.

Figure 6 also shows that the measured fall velocities at the 50-cm level are less than the theoretical values for the low wind speeds. This is due to the particles being smaller at the lower wind speeds and to the smaller particles not obeying the simple proportionality between size and fall velocity which was assumed in the derivation of equation 16. The same effect is brought out more clearly in Figure 7, which shows the relation between fall velocity and particle size.

The curves in Figure 7 give the linear relations from *Baumeister and Marks* [1958] for spherical and irregular particles above 100 μ, the corresponding Stokes' law relations for particles below 50 μ, and the transition zone between the two size ranges. For each level the mean particle size from Figure 3 is plotted against the mean fall velocity for the corresponding mean wind speed. These values agree well with the chosen linear relation

$$w_z = 3100 x_z$$

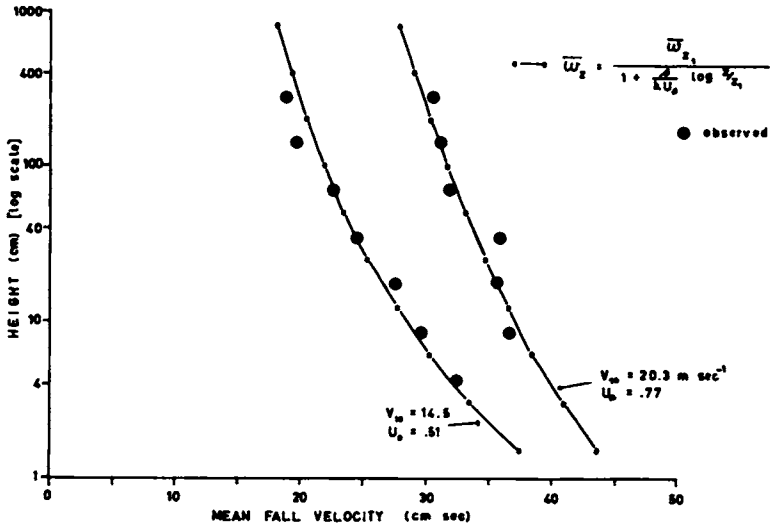

Fig. 5. Snow particle mean fall velocities for various heights, calculated from the vertical drift density profile, and for various wind speeds. The theoretical expected curves are calculated from the mean and variance of the particle size distribution at the 50-cm level, and the linear relation between fall velocity and wind speed.

shown as the heavy line, except for the 3- and 25-cm levels, where the particle sizes were larger than expected, probably due to the small number of particles collected at these levels. The measured fall velocities of the 50-cm level are also given in Figure 7. These show that the lower velocities, i.e. for the smaller particles, diverge from the linear relation in the transition zone. The results suggest that there is a smooth transition from the linear to the square relation for the fall velocity.

The effect of the nonuniformity of the drift snow on the drift density as a function of height and wind speed. It remains to consider the effects of the distribution of particle sizes on the drift density profile itself. The predicted variation of drift density

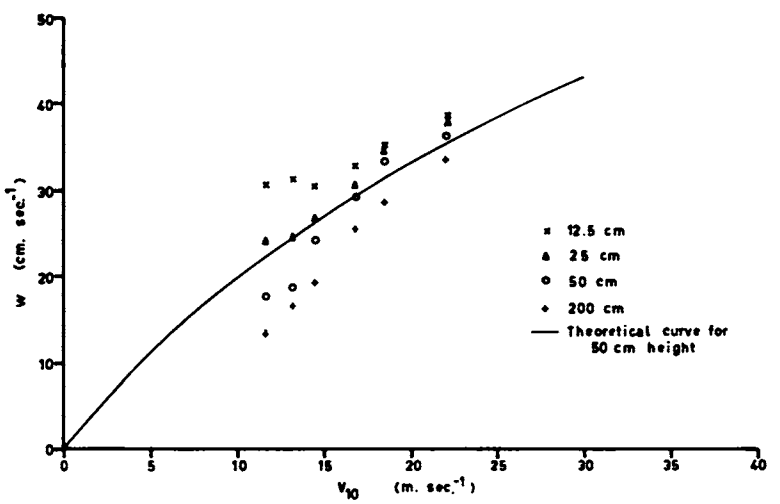

Fig. 6. The variation of the mean particle fall velocity at all levels and with wind speed, as calculated from the drift density profile. The theoretical curve was obtained from the relation in equation 16*a*, assuming u_* varies linearly with V_{10} (wind speed at 10-meter level).

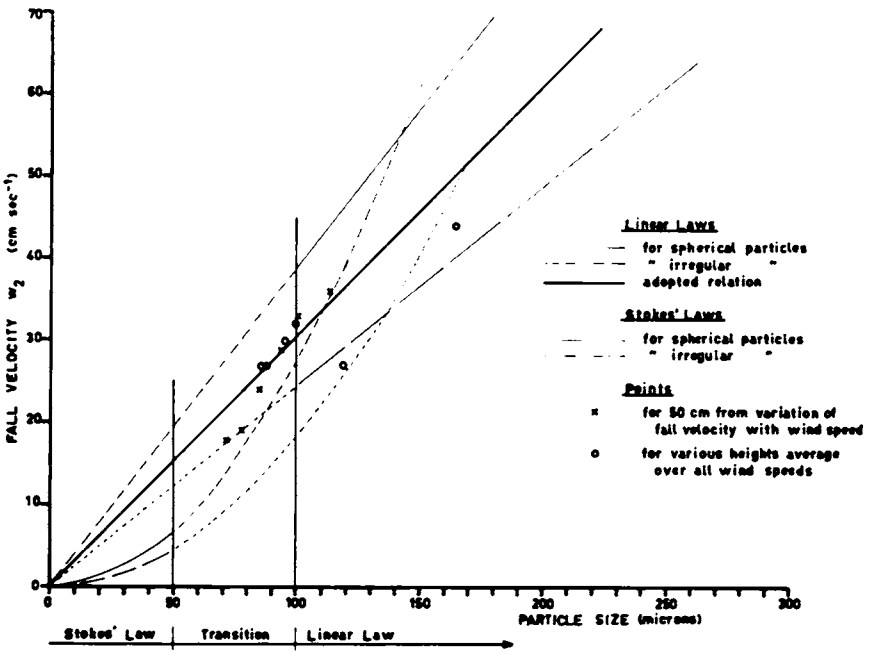

Fig. 7. The mean particle size for each level (from Figure 1) plotted against mean fall velocity (from Figure 5), for wind speed corresponding to mean speeds at which particles were measured. Measured fall velocities from Figure 6 for the 50-cm level, correspond to theoretical curve which uses the adopted straight line relation. Other straight lines and curves are drawn from empirical laws quoted by *Baumeister and Marks* [1958].

with height was given by equation 15*b*. By combining the first term on the right with that on the left we obtain directly the deviation from the straight-line log density-log height relation predicted by the basic theory for uniform snow in the form

$$\log \frac{\Lambda_z}{\Lambda_{z_1}} - \frac{w'}{ku_*} \log \frac{z}{z_1} = \frac{1}{2} \frac{\alpha\beta^2}{(ku_*)^2} \log^2 \frac{z}{z_1} - \frac{1}{3} \frac{\alpha\beta^3}{(ku_*)^3} \log^3 \frac{z}{z_1} + \cdots$$

In this expression the square term predominates and the deviations therefore would be expected to vary approximately parabolically with log distance from the mean height.

Figure 8 shows the observed mean drift density deviations from the straight line, in a log height-log density coordinate system, together with the theoretical deviation curves given by equation 15*c* for three different wind speeds represented by u_*. This parameter appears as a square term in the denominator of the principal correction term and has the effect of drastically reducing the size of the deviation for higher wind speeds; thus, for strong winds the results obtained with a constant fall velocity represent a good approximation to reality.

The effect of the cubic term (numerically approximately an order smaller than the square term) is to make the parabolic variation slightly asymmetric, adding to the mean deviations below the mean height and subtracting from those above.

The theoretical deviations from the straight line log height-log drift density relation are shown (Figure 8) to agree well with those observed deviations, at all levels except at 3 cm.

The measurements at this lowest level were made with a special type of trap which appears to have a collection efficiency slightly different from that of the standard Mellor trap [cf., *Budd et al.*, 1966]. Pending a more precise calibration, the lowest-level values carry little weight and do not detract from the general agreement between the observed and theoretically predicted drift density profiles for different wind speeds.

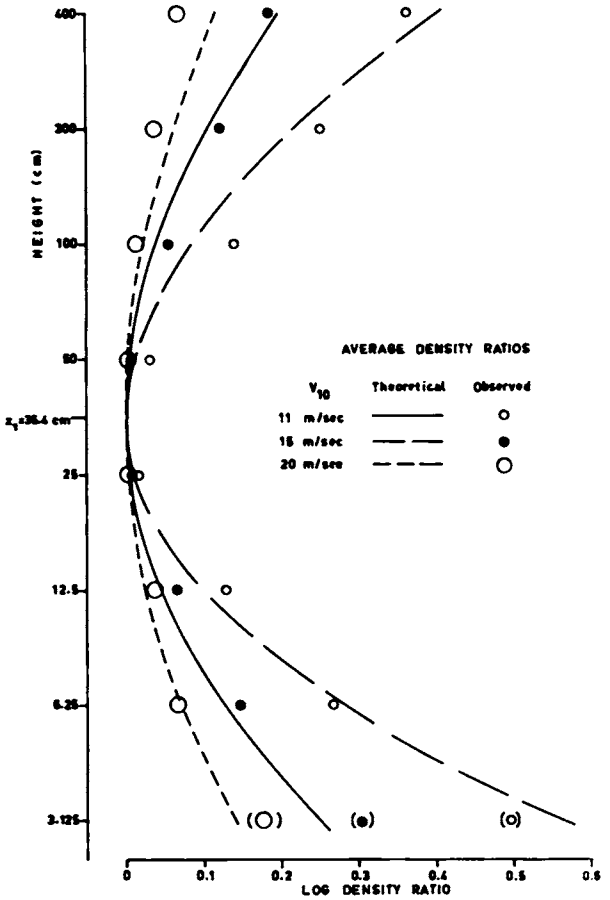

Fig. 8. Average deviation in measured drift density values from the linear log density-log height relation for each level and for three wind speeds. Theoretical curves calculated for corresponding wind speeds from parameters α, β of the particle size distribution at the 50-cm level (near the mean height) and the relation

$$\Delta = \log(\Lambda_s/\Lambda_s) - (w/ku_*)\log(z/z_1)$$

$$\approx \frac{1}{2}\frac{\alpha\beta^2}{(ku_*)^2}\log^2(z/z_1) - \tfrac{1}{3}[\alpha\beta^3/(ku_*)^3]\log^3(z/z_1)$$

5. CONCLUSION

The analysis presented in this paper shows that:

1. The *distribution* of snow drift particle size can be closely approximated by a gamma variate.

2. In drifting snow the *mean particle size* decreases with increasing height, depending on the wind speed, and the size distribution at the surface.

3. The *fall velocity* of snow drift particles is approximately linearly related to the particle size, but for the smaller particles the fall velocity decreases more rapidly as the particle size approaches the range in which Stokes' law becomes applicable. The average fall velocity of the particles decreases with increasing height, as does the mean particle size, also depending on wind speed. The average fall velocity *increases* with *wind speed* at all levels.

4. The existence of a diversity of particle sizes and fall velocities in drifting snow accounts for the bulk of the discrepancies between the measured vertical *drift density* profile and the predictions of the basic steady-state drift theory, which assumes uniform snow of constant fall velocity.

Acknowledgments. The author wishes to thank R. Dingle for making the numerous exacting measurements used in the paper, various staff members of the Meteorology Department, University of Melbourne, for assistance in the reduction of data, Judith Martin for drawing the diagrams, and U. Radok for critically reviewing the manuscript. Thanks are also due to the Director, Antarctic Division, Australia, for permission to publish this paper.

REFERENCES

Aitcheson, J., and J. A. C. Brown, *The Log Normal Distribution*, Cambridge University Press, New York and London, 1957.

Bagnold, R. A., *The Physics of Blown Sand and Desert Dunes*, Methuen & Company, London, 1941.

Baumeister, T., and L. S. Marks, Gas cleaning, dusts, clouds, smokes, in *Mechanical Engineers Handbook*, McGraw Hill Book Co., New York, 1958.

Budd, W., W. R. J. Dingle, and U. Radok, The Byrd snow drift project: Outline and basic results, *this volume*, 1966.

Dingle, W. R. J. and U. Radok, Antarctic snow drift and mass transport, General Assembly of Helsinki, International Association of Scientific Hydrology, 1961.

Dyunin, A. K., Struktura metelevogo snega i zakonomernosti snegovogo potoka (The structure of blowing snow and the laws governing its flow), *Questions of the Utilisation of Snow*, Institut Geografii Akademii Nauk, SSSR, 1956.

Herdan, G., *Small Particle Statistics*, Elsevier Publishing Co., Amsterdam, 1953.

Kotlyakov, V. M., Results of a study of the processes of formation and structure of the upper layer of the ice sheet in eastern Antarctica, General Assembly of Helsinki, International Association of Scientific Hydrology, 1961.

Krumbein, W. C., and F. J. Pettijohn, *Manual of Sedimentary Petrography*, D. Appleton-Century-Crofts, New York, 1938.

Lister, H., Glaciology, 1: Solid precipitation and drift snow, *Trans-Antarctic Expedition 1955–1958, Scientific Reports 5*, London, 1960.

Loewe, F., *Études de Glaciologie en Terre Adélie, 1951–1952*, Hermann, Paris, 1956.

Mellor, M., and U. Radok, Some properties of drifting snow, Symposium on Antarctic Meteorology, Melbourne, Pergamon Press, London, 1960.

Robins, W. H. M., The significance and application of shape factors in particle size analysis: The physics of particle size analysis, *Brit. J. Appl. Phys.* (*Suppl. 3*), 1954.

Shiotani, M., and H. Arai, A short note on the snow storm, *Proceedings of Second Japanese National Congress for Applied Mechanics*, 1953.

Timbrell, V., The terminal velocity and size of airborne dust particles, The physics of particle size analysis, *Brit. J. Appl. Phys.* (*Suppl. 3*), 1954.

THE BYRD SNOW DRIFT PROJECT: OUTLINE AND BASIC RESULTS

W. F. BUDD,[1] W. R. J. DINGLE,[2] AND U. RADOK[3]

Respectfully Dedicated to Fritz Loewe on the Occasion of His 70th Birthday

CONTENTS

Abstract. Equipment and techniques used in a study of drifting snow at Byrd station during 1962–1963 are described. Basic data obtained consist of 129 snow drift gagings with Mellor drift traps at eight levels between 400 and 3.125 cm above the snow surface, simultaneous wind measurements at five or six of these levels, 32 sets of upper-wind observations by means of accelerated radiotheodolite readings, and 7 sets by means of rocket trail photography. Auxiliary observations in the form of accumulation and visibility measurements in the test area and Formvar replicas of drift snow particles collected at various heights above the surface are also presented. The theory of steady-state drifting of uniform snow is reviewed and tested by means of the observations. The wind profiles in the lowest 4 meters closely approximate the logarithmic form, which frequently is also a reasonable approximation up to 300 meters, throughout the layer of snow drifting. The roughness height of the snow surface appears to be unaffected by macrofeatures like dunes and sastrugi, but it is larger for smooth soft than for smooth hard snow; it bears no relation to the amount of drift snow in the air. The vertical drift density profile is found to deviate significantly from that predicted by the theory; the cause of this deviation is traced back to the nonuniformity of drift particle size. The theoretically expected exponential relation between drift density and reciprocal wind velocity at a given level is found to hold to a reasonable degree of accuracy, making possible a single specification of drift density in terms of both height and wind speed. On the other hand, the observed total drift contents and drift transports change with wind speed in a manner very different from that predicted by the theory. The observed drift snow transports in the layer from 1 mm to 300 meters above the snow surface, $Q_{10\text{-}3}^{300}$ (g m^{-1}sec^{-1}), can be represented by the relation

$$\log Q_{10\text{-}3}^{300} = 1.1812 + 0.0887 V_{10}$$

[1] Antarctic Division, Australian Department of External Affairs, Melbourne, Australia.
[2] Commonwealth Bureau of Meteorology, Australia.
[3] Project Leader, Department of Meteorology, University of Melbourne, Australia.

where V_{10} is the wind velocity at the 10-meter level. This relation accounts for over 90% of the variance of the transports computed from five-run average winds and drift densities and has been used to compute monthly and annual net drift snow transports through a vertical east-west plane at Byrd. The annual transport is approximately 3×10^9 g m^{-1} and equals 5% of the net accumulation of a 1-meter strip extending 300 km northward from Byrd to the ridge between the Crary Mountains and the Executive Committee Range. It also equals the mass in a column of 1 m^2 cross sectional area extending vertically through the ice cap at Byrd.

> There is one thing of special interest to the Glacialist—the transportation of snow on the ice-cap by the wind. . . .
>
> *Lt. E. A. Peary, U. S. Navy, 1898*

1. INTRODUCTION

Drifting snow is an ubiquitous phenomenon in cold regions that has attracted the attention of numerous investigators. The majority of these investigators have been concerned with the practical problems of 'drifts,' the depositions resulting from snow drift, but attempts to measure the snow concentration in the air during snow drift also go back at least to the first polar year [*Andrée*, 1886] and became widespread in Antarctica during the IGY [*Averyanov*, 1959; *Rusin*, 1959; *Lister*, 1960; *Garcia*, 1960; *Mellor* 1960]. The significance of snow drift for the mass budget of an ice cap was discussed for Greenland by *Loewe* [1933], who later also made the first numerical estimates of the snow drift contribution to the antarctic mass balance; and quite recently *Black and Budd* [1964] pointed out the possible relevance of snow drift as an explanation for the wavy irregularities found on otherwise featureless expanses of the antarctic and Greenland ice caps. Thus Peary's statement prefacing this paper remains fully valid today.

Until now measurements of drifting snow have employed almost exclusively the principle of trapping the wind-blown snow in some form of container or 'drift trap.' The great variety of shapes and sizes of these traps has made it difficult to compare their results. Also different authors have used the term 'drift' for a number of different concepts. Both circumstances have so far prevented a unified discussion of the extensive information on snow drift now in existence both for coastal antarctic stations (Port Martin[4] [*Barré*, 1954; *Loewe*, 1956], Mawson[5] [*Mellor and Radok*, 1960], and Mirnyy[6] [*Kotlyakov*, 1961; *Rusin*, 1961]), and for the interior of Antarctica (Vostok I[7] [*Averyanov*, 1959], South Ice[8] [*Lister*, 1960], Charcot[9] [*Garcia*, 1960; *Lorius*, 1962], and Wilkes satellite station S2[10] [*Budd*, 1965]).

Such a comprehensive discussion of snow drift must evidently rest on an adequate physical theory of the snow drift process. One possible approach to such a theory, suggested by the work of *Bagnold* [1941] for sand, has indeed been explored for snow [*Mellor and Radok*, 1960; *Lister*, 1960; *Strom et al.*, 1962; *Jenssen*, 1964]. The main progress in understanding the physics of blown snow did not, however, come from this work or from the somewhat empirical eddy-model discussion by *Dyunin* [1959] but from the application of turbulent transfer theory initiated independently by *Shiotani and Arai* [1953] and *Loewe* [1956]. The soundness of this approach is borne out by the adequate explanation it provides for the low-level wind profile in terms of momentum transfer. Its validity for the transfer of drift snow was confirmed by multilevel drift measurements made at Wilkes (66°15′S, 110° 35′E) [*Dingle and Radok*, 1961], which also accounted for the discrepancies between empirical drift-wind relationships obtained by earlier authors. At the same time the analysis of the Wilkes data raised the first questions regarding the adequacy of a drift theory assuming uniform snow and steady-state conditions.

The Byrd (80°01′S, 119°32′W) drift project was undertaken in 1962–1963 to produce drift data capable of answering these questions for the interior of West Antarctica, where snow drift may have been the principal agent in forming the extremely thick ice cap [*Wexler*, 1961].

[4] 66°49′S, 141°24′E.
[5] 67°36′S, 62°53′E.
[6] 66°33′S, 93°01′E.
[7] 72°09′S, 96°37′E.
[8] 81°56′S, 29°30′W.
[9] 69°22′S, 139°01′E.
[10] 66°28′S, 112°17′E.

This paper is an attempt to present the essential facts about the Byrd drift project and its basic results as they appear against the background of the drift theory available when the project began. In section 2 the technical and operational aspects are outlined; copies of a detailed operations report and of the raw data are held by the U. S. Weather Bureau and the Meteorology Department in the University of Melbourne. Section 3 discusses the basic concepts of snow drift and their laws as predicted by the theory of turbulent transfer in the boundary layer. Section 4 presents the basic wind and drift density profile data against the background of the theory; relevant accumulation and drift particle size results are also considered in this section. Section 5 deals with the integrated drift quantities (drift content and drift transport) and culminates in an estimate of the total snow drift transport at Byrd. Section 6 summarizes the results and indicates further work needed to explain finer details beyond the scope of this first survey of the Byrd drift data.

2. METHODS AND EQUIPMENT

2.1 *Snow Drift Gaging—General*

The drift measurements were made in the undisturbed or 'science' quadrant bearing north to east from the new Byrd station. The wind regime of the region ensured that practically all winds giving rise to snow drift reached the drift installation from an unlimited expanse of undisturbed plateau. The layout of the drift installation can be seen in Figure 1. It consisted of a mast for exposing traps and anemometers, located some 75 meters from an underground cold room used for weighing the snow traps and for housing the anemometer counters. The mast was linked to the cold room by a line of snow poles spaced at 9-meter intervals and used for visibility estimates. The area northwest of the drift mast was used for accumulation measurements. Although the installation of the cold room box by a Peter plough drastically altered the snow structure in the vicinity of the cold room, great care was taken to preserve the original conditions far-

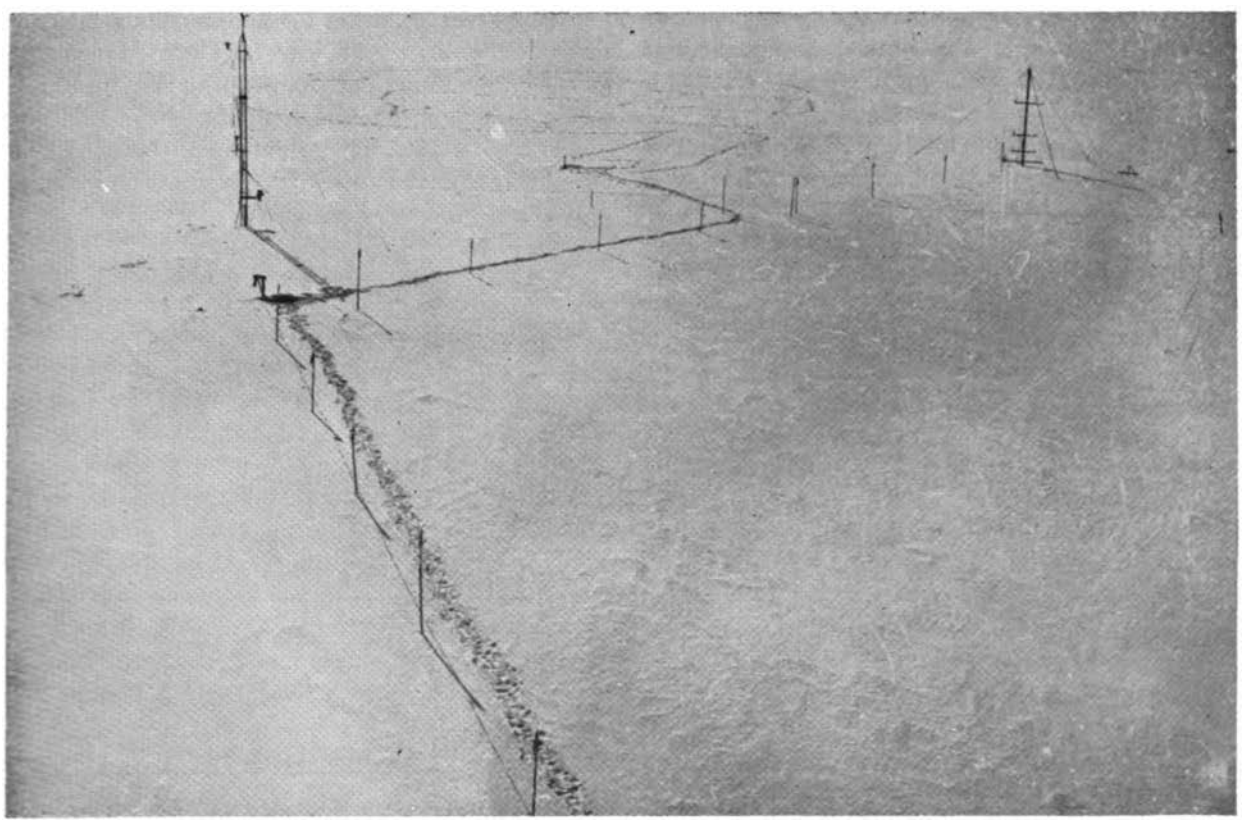

Fig. 1. Drift gaging installation at the new Byrd station. The line of snow poles links the drift gaging mast (right rear) to the undersnow shelter (marked by ventilation pipe). The mast on the left carries the station anemometer.

ther out, especially beyond the drift mast and in the accumulation area.

2.1.1 *Snow traps.* The traps used for the drift gagings were essentially of the type developed during the IGY at Mawson [*Mellor,* 1960] and used for subsequent drift studies at Wilkes [*Dingle and Radok,* 1961; *Budd,* 1965].

For the lowest level (nominally 3.125 cm, less than one-half the trap diameter above the surface) a distorted rocket trap was constructed by D. Williams and became known as the 'Williams Special.' It took the place of the smaller 'saltation' type traps used at low levels in the Wilkes drift studies. Although uncertainties introduced by the shorter operating time of the saltation traps were eliminated in this way, the collection efficiency of the Williams Special trap turned out to be different from that of the standard Mellor trap. This difference forms part of the general calibration problem considered in the next section.

2.1.2 *Trap characteristics.* The determination of the collection efficiency of drift snow traps in some respects represents the hard core of the problem of measuring snow drift. A good deal of thought was devoted throughout the project to this problem, which requires discussion in some detail.

An ingenious method for calibrating the Mellor drift snow trap in the wind tunnel was developed by *Pound* [1958]. It permits us to measure the aerodynamic efficiency of the trap, defined by

$$\eta_a = 4q/\pi d^2 V \qquad (1)$$

where q (cm^3 sec^{-1}) is the volume of air passing through the trap inlet in unit time, d is the inlet diameter (cm), and V (cm sec^{-1}) is the wind tunnel flow velocity.

Two of the modified Mellor traps were calibrated in this manner during the preparatory stage of the Byrd snow drift project and were found to have the same efficiency characteristics as the traps of the original design. After the Byrd measurements further wind tunnel calibrations were undertaken for a variety of drift trap designs of other workers, which had been compared with the Mellor trap at Byrd. One of the Mellor traps was included in these postoperational calibrations and was found to have a somewhat higher aerodynamic efficiency than suggested by the earlier tests. A further set of tests was then carried out on six more Mellor traps. The results of all these wind tunnel calibrations are summarized in Figures 2 and 4.

Figure 2 suggests that the aerodynamic efficiency of the Mellor drift traps used for the Byrd measurements varied somewhat from trap to trap, probably owing to minor differences in the shape and size of the trap outlets. The relevance of the wind tunnel curves for the snow drift results, however, is

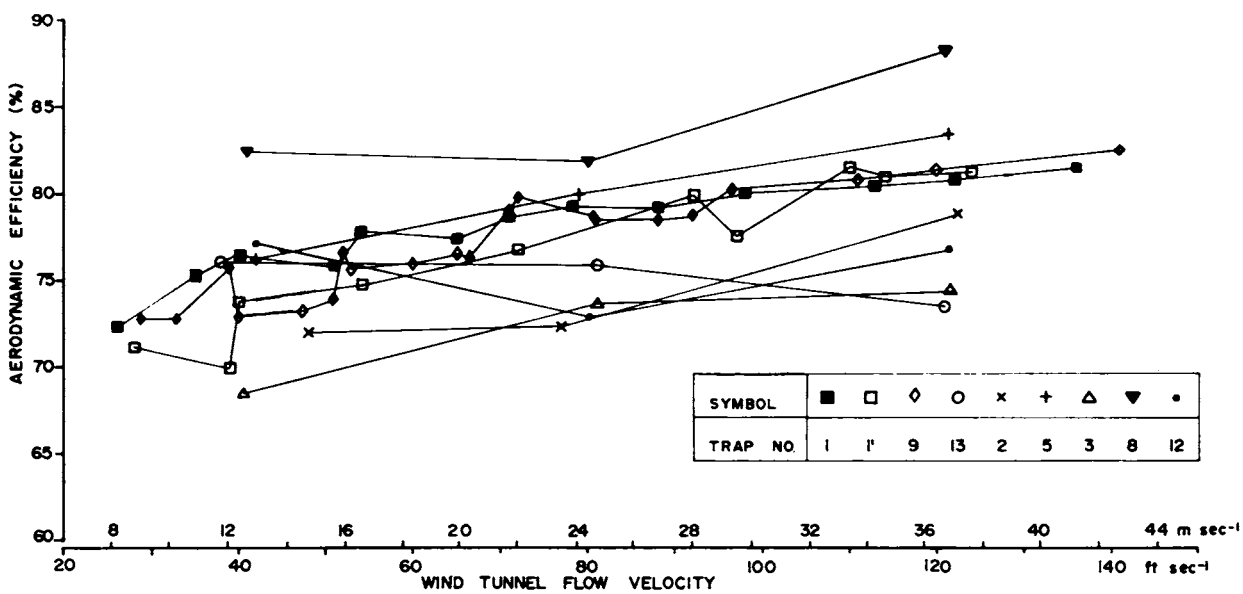

Fig. 2. Results of wind tunnel tests of Mellor snow traps. Note especially the differences between traps 5 and 13. Trap 1' was identical with trap 1 except for a fairing.

not clear. It seems not inconceivable that owing to the inertia effects near the relatively restricted inlet of the Mellor trap the quantity of drift snow entering the trap could equal or even exceed the amount of snow geometrically in line with the trap inlet before the trap inlet started to deflect some of the streamlines, producing the reduced aerodynamic efficiencies indicated by the wind tunnel tests. For trap designs with wide inlets this effect should be less marked or absent.

For the Mellor traps a test of this hypothesis can be made by comparing measurements obtained with individual traps. In anticipation of the discussion of sections 3 and 4, the drift concentration per unit volume of air, n_z, or 'drift density,' is used for this purpose. Figure 3 compares five-run average values of n_z for three levels, obtained with traps 1 and 8 (400 cm), 2 and 9 (200 cm), and 5 and 13 (50 cm), respectively. The last of these pairs exhibited particularly large differences in the wind tunnel tests (cf. Figure 2). Nevertheless, the measured drift densities reveal no sign of similar differences in the operational collection efficiencies.

The above is confirmed by the results of operational comparisons of different drift trap designs at Byrd and later at Mawson. The following drift traps were compared with the Mellor trap: *Lister*'s [1960] South Ice trap, *Garcia*'s [1960] Charcot trap, and the USSR VO 2 trap.[11] A series of comparative measurements was also made using SIPRE snow samplers as drift snow collectors, but the results will not be discussed here, although they may well be relevant to a discussion of earlier French drift measurements made with Nescafé tins [*Barré*, 1954; *Lorius*, 1962].

The Byrd drift trap comparisons were made throughout at the 1-meter level. The results of the comparisons for the different trap types can be expressed by regression equations listed in Table 1 for the drift density as measured by the Mellor trap (M) in terms of the corresponding density suggested by the other traps.

Assuming that for the drift traps with wide inlets the aerodynamic efficiency equals the operational drift snow collection efficiency, defined by

$$\eta_0 = 4Q/\pi d^2 n V \qquad (2)$$

where Q is the snow quantity collected in unit time (g sec^{-1}) and n is the drift density (g m^{-3}), the operational collection efficiency of the Mellor trap should result from applying the factors of Table 1 to the *aerodynamic* efficiencies of the other traps. Figure 4 shows the aerodynamic efficiency curves for the VO 2 (USSR), South Ice (Lister), and Williams Special traps, and the operational efficiency curve of the Mellor trap deduced in the above manner. It is interesting that the three transposed curves agree quite well in placing the operational efficiency of the Mellor trap around 110%.

This result has subsequently received direct confirmation from extensive calibrations made by Budd at Mawson with the help of a self-regulating version of the Russian 'cyclone' snow trap [*Govorukha and Kirpichev*, 1961; *Barkov*, 1963] developed in Australia [*Landon-Smith*, 1964]. This trap is designed to have isokinetic entry and therefore 100% efficiency. Full details of Budd's measurements are not yet available, but his over-all result places the average collection efficiency of the Mellor trap at 115%. Allowing for minor snow losses likely to occur in operational drift runs, we are then justified in regarding the drift densities measured with the Mellor trap as representative of the true drift snow concentrations in the air, and no corrections for collection efficiency will be applied in the following to the measurements with the Mellor trap.

2.1.3 *Drift mast and cold room arrangements.* The exposure of a battery of snow traps and anemometers for drift measurements presents the problem of providing each trap and anemometer with its prescribed height above the irregular snow surface, which undergoes substantial changes with time. At Byrd this was achieved with an arrangement developed in 1959 at Wilkes by Dingle and further improved by H. P. Black in 1960.

The drift assembly is shown in Figure 5. It consisted of the exposure rack, with movable cross arms, which could be secured at spacings providing the prescribed distances between exposure levels, and the main mast, which held the rack in the vertical position and was firmly planted and guyed at the exposure site. The vertical displacement of the exposure rack to provide the correct height for a datum line above the snow surface (and thereby the prescribed heights for all the cross arms with their traps and anemometers) was achieved by

[11] We are grateful to Professor P. A. Shumskiy for making drawings of the USSR snow trap available.

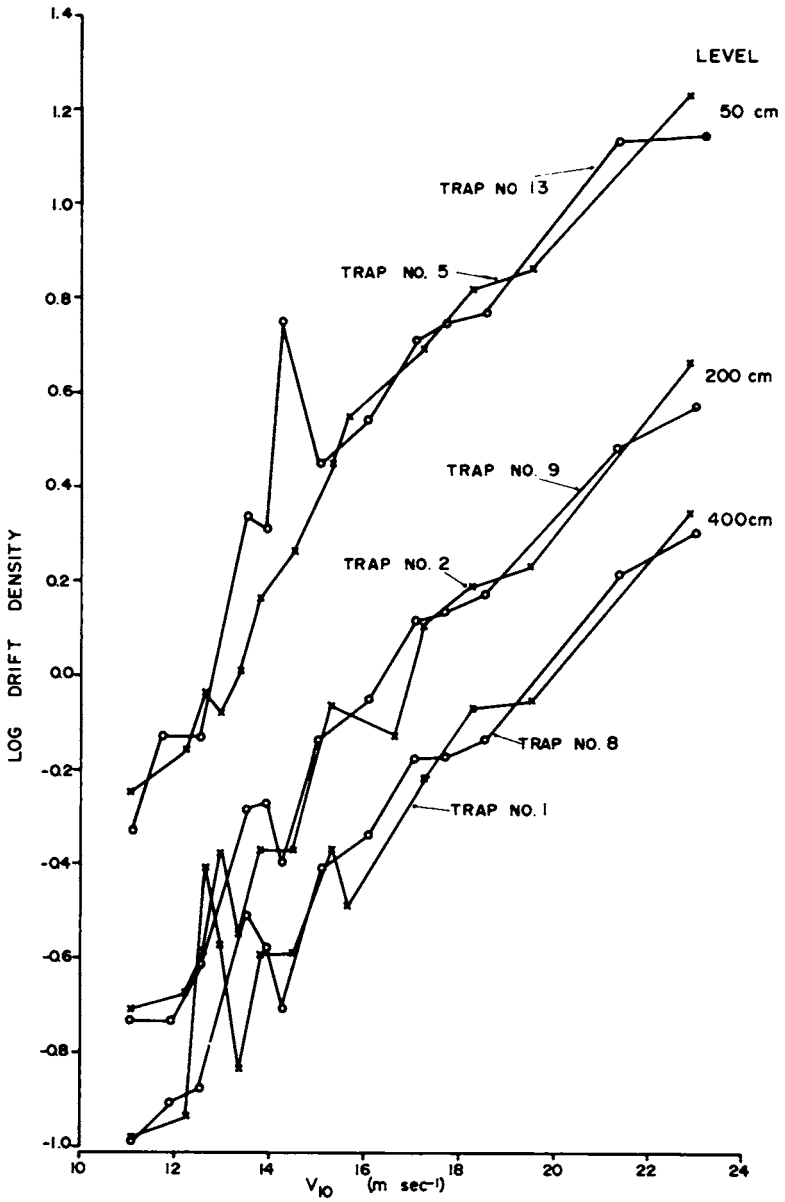

Fig. 3. Snow trap comparison in terms of actual drift measurements.

TABLE 1. Comparisons between the Mellor and Other Drift Traps, Byrd, 1962

Trap Type	Regression Equation for Drift Density (M = Mellor density g m^{-3})	No. of Points	Wind Range, m sec^{-1}
Williams Special (WS)	M = 0.21 + 0.7 WS	10	7.3–16.8
Lister [1960] (L)	M = −0.15 + 1.47 L	4	9.3–14.0
VO 2 (U. S. S. R.) (V)	M = 1.37 V	5	9.3–14.0
French [*Garcia*, (G) 1960]	M = 0.40 + 2.94 G	17	8.1–11.5

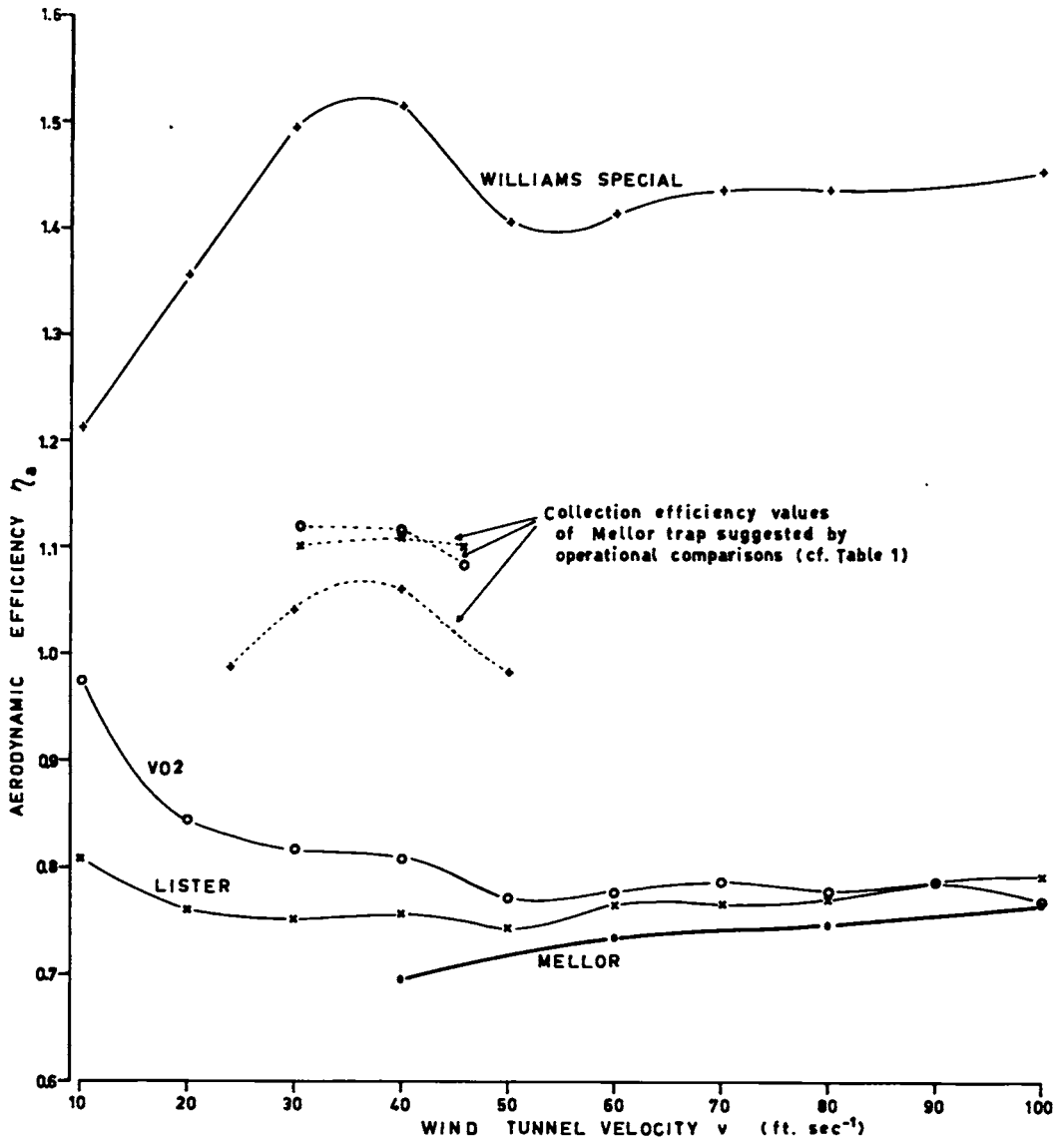

Fig. 4. Wind tunnel calibration results for different snow trap designs. The dotted lines give the estimated collection efficiency of the Mellor trap, derived by applying the factors of Table 1 to the aerodynamic efficiency curves shown.

means of a small wire strainer. Once the correct height and orientation into the wind direction were achieved, the rack was secured by means of spacing blocks and clamps.

Special brackets were provided for the exposure of low-level traps and anemometers. The top of the drift mast carried a downward-directed searchlight to facilitate the measurements during darkness.

Access to the cold room, some 75 meters from the drift mast, was provided by a roof hatch and ladder. The cold room contained a work bench with a triple-beam sliding-weight balance on which the drift traps were weighed before and after each run. After being weighed with drift snow inside it, each trap was placed into the containers shown in Figure 6, where the snow was melted by means of an electric heating tape (arrow). The meltwater drained into a cup below the trap container and provided a means of checking the drift quantity obtained by weighing.

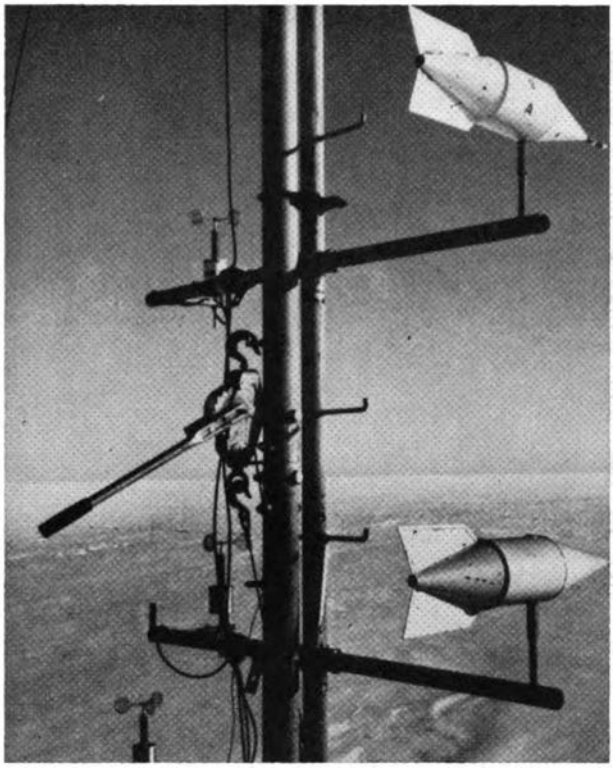

Fig. 5. Drift gaging mast section showing wire strainer used for lifting instrument rack to the correct level and U bolt for securing it in position.

The cold room also housed the recording section of the anemometer system (cf. 2.2) in an insulated box constantly heated by means of a 40-watt light globe.

2.2. *Wind Measurements—General*

For the purposes of the Byrd drift project, measurements of the Byrd wind velocity and its change in the vertical (which the theory shows to be crucial) ranked equal in importance with measurements of the drift snow themselves. Whereas the drift measurements were restricted by technical difficulties to the lowest 4-meters above the snow surface, every effort was made to extend the wind measurements through and beyond the layer believed to contain appreciable quantities of drifting snow. The upper boundary of that layer is not known with certainty, but aircraft have reported plumes of drift snow rising to a height of a thousand meters or more. Wind measurements over such an extended height range called for a variety of equipment and techniques which will now be considered.

2.2.1 *Low-level winds.* The wind velocities near the snow surface were measured by means of the Beckman and Whitley anemometer installation previously employed at the south pole by Dalrymple. Five anemometers were constantly located at the following levels: 400, 200, 100, 50, and 25 cm; the sixth was operated at the 12.5-cm level on some occasions and at 6.25 cm on others. Attempts to measure the wind velocity at the lowest drift trap level, 3.125 cm, proved unsuccessful, a circular ridge tending to form in the snow below the rotors. The operation of an anemometer in an inverted position so as to bring the rotor close to the snow surface also proved unsatisfactory.

It was usual practice to dismantle and inspect each anemometer after 3 hours' exposure under working conditions. Anemometer housings, rotor shafts, and rotors were interchangeable, and no single component was ever associated with a par-

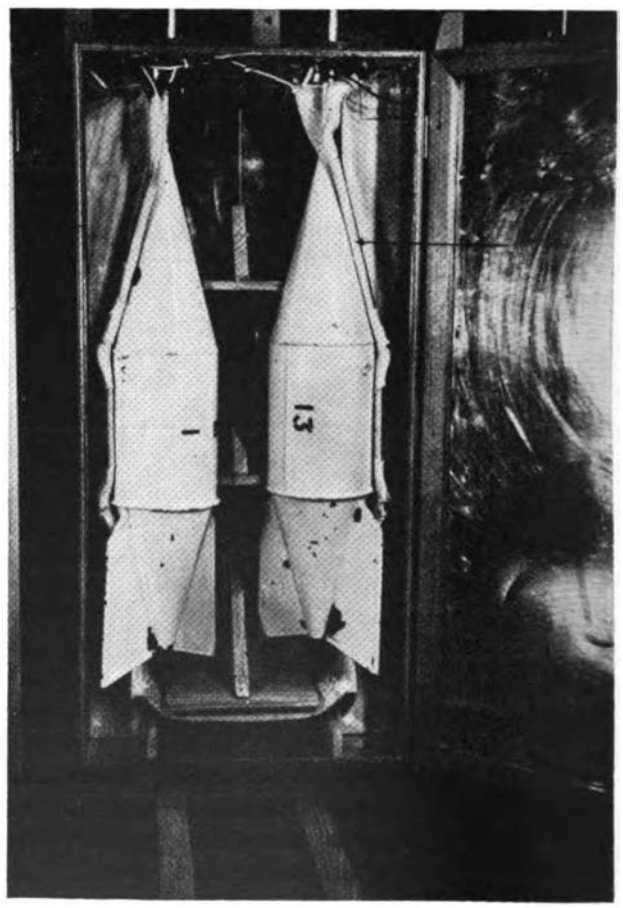

Fig. 6. Undersnow shelter arrangement for emptying snow traps by means of heating tape (arrow).

ticular instrument or circuit. This somewhat haphazard grouping of component parts and the subsequent random selection of exposure heights for individual anemometers eliminated the need for periodic calibration checks throughout the year.

2.2.2 *Upper winds.* The significant contribution made to the total drift transport by layers above the 4-meter level, even on the most conservative assumptions about the vertical wind profile and the height of the low-level wind maximum, had become abundantly clear from the Wilkes drift results [*Dingle and Radok*, 1961]. Hence at Byrd a special effort was made to obtain detailed wind information for the lowest kilometer or so above the ice cap surface. The basic upper-wind procedure, developed by Dingle and the American meteorologists at Wilkes in 1959, was to operate the radiotheodolite printout at top speed during the first 4 minutes of radiosonde ascents in drift conditions. This provided angles of azimuth and elevation every 6 seconds or, with a rate of ascent around 210 m/min, at vertical intervals of approximately 20 meters. The corresponding temperatures could be read off the radiosonde trace. A total of 32 sets of these 'rapid-run' wind observations were obtained at Byrd during or close to drift measurements. The laborious evaluation of these measurements was made by Dingle partly at Byrd and partly in Melbourne after the completion of the operational phase of the project.

A second technique for measuring the upper winds was employed in an impromptu fashion, when a dozen wind-finding rockets and accessory equipment were made available to the project by the Australian Weapons Research Establishment. The technique in question was developed and described by *Cooke* [1962]; an improved rocket type has been suggested recently by *Gill et al.* [1963]. The performance of the technique under antarctic conditions was uncertain, and, since no provision existed in the original project plan for this work, a good deal of on-the-spot improvisation was needed to make the twelve firings possible. There is no need to emphasize the wasteful nature of such an enterprise, which probably could not be justified even by the need to obtain the maximum of information while the project was operational. Therefore Radok's apologies to all concerned are expressly recorded here. The rocket firings produced little quantitative wind information but were useful in revealing the complex nature of the wind profile in the lowest kilometer above the ice cap, and small-scale turbulence details (through the rate of broadening of the vapor trails).

2.3 *Accumulation—General*

In an area of net accumulation like the high antarctic plateau snow drift is the major factor determining the shape of the snow surface and local differences in the rate of surface rising or lowering. Conversely, we may suspect that information about the drift process can be deduced from a study of local accumulation and ablation rates. *Black and Budd* [1964] have suggested that large local differences in net accumulation on the undulating surface of the ice cap south of Wilkes could be due to changes in the drift snow capacity of the katabatic wind passing over the surface undulations, which as a result appear to be moving upwind at speeds of the order of 100 meters a year. In general, detailed measurements of accumulation over a limited area during a period of snow drift should reveal whether the surface flow could be regarded as super- or subsaturated with respect to drift snow. The accumulation measurements for the Byrd project were made with this in view.

For the determination of accumulation rates in the area of drift measurements at Byrd, a micro-accumulation network of ¼-inch-diameter cane stakes was set up northwest of the drift mast in an area closed to vehicular and foot traffic. The stake system consisted of nine permanent or principal stakes set in the form of a square with 24-meter sides with 12-meter intervals between stakes. Each of the principal stakes was supplemented by two further stakes planted not more than 2 meters away in a square of 3-meter sides centered on the principal stake. The supplementary stakes were repositioned from time to time at randomized distances measured in the north-south and west-east directions from the principal stakes. Stake readings were taken as far as possible before and after periods of snow drift, and snow density determinations were made in the area just south (i.e. generally downwind) of the accumulation field.

The moving stakes were replanted at monthly intervals during the period of the actual drift measurements, which ended with the cessation of heavy drift in November 1962. During the summer

period from November 27, 1962, to February 22, 1963, the replanting of stakes was discontinued and visits to the accumulation area were restricted to the absolute minimum. Precipitation during this period was unusually heavy, and soft snow compacted into footprints tended to remain long after the surrounding undisturbed snow had been removed by wind action. This gave rise to parasitic sastrugi, which in turn interfered seriously with the natural behavior of the accumulation area. However, these difficulties did not assume serious proportions until the drift measurements had ended.

During winter and spring the system of fixed and moving stakes provided information on both temporal and local variations in accumulation or ablation rates as well as comparatively precise estimates of the mean rates for the test area as a whole. This type of experimental arrangement was developed originally by *Wilm* [1946] for the measurement of rainfall in forests, but it is of quite general validity.

For the present first analysis P. Morgan computed for each accumulation interval the regression of the average accumulation values recorded with pairs of moving stakes, x_i, on their associated principal stake, X_i, using all stakes and the entire length of record. The resulting regression coefficient b, say, provides a corrected mean of the average local accumulation in the ith time interval according to the relation

$$\bar{x}_i' = \bar{x}_i + b(\bar{X}_i - \bar{X}) \qquad (3)$$

The $\bar{x}_i'$ can be regarded as a good estimate of the mean accumulation rate of the drift project area as a whole even in periods when sastrugi made single stake readings almost meaningless.

2.4 *Drift Particle Measurements—General*

The size and shape of drift snow particles are of basic importance for the study of snow drift. It will be seen in section 3 that the particle fall velocity, which depends on both shape and size, is one of the principal parameters in the theory of turbulent snow drift. Shape and size of the drift snow particles might be expected to be related to the state of the snow surface and hence to have a bearing on the question of steady-state versus transient-state snow drift. Moreover, *Lister* [1958] has pointed out that microscopic examination of snow particle shapes may permit drift particles to be distinguished from precipitating snow and hence provide estimates of snow precipitation amounts, notoriously difficult to measure by other means in windy conditions.

The standard method for the study of particle shapes and sizes is the Formvar technique first suggerted by *Schaefer* [1942]. In theory this technique produces durable plastic casts or 'replicas' of the original particles for examination at leisure. In practice it has proved difficult to apply under snow drift conditions. Numerous workers have found that even the briefest exposure of a Formvar-coated slide produces a conglomeration of particles that is almost impossible to analyze. A great deal of devel-

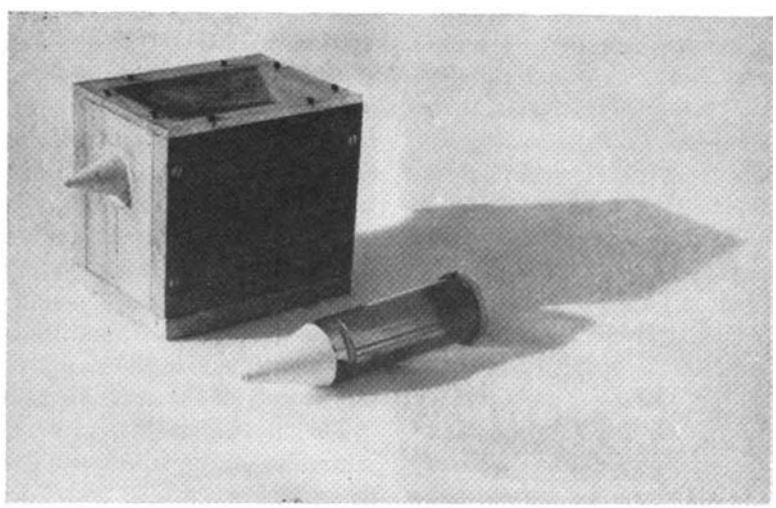

Fig. 7. Snow particle replica collectors.

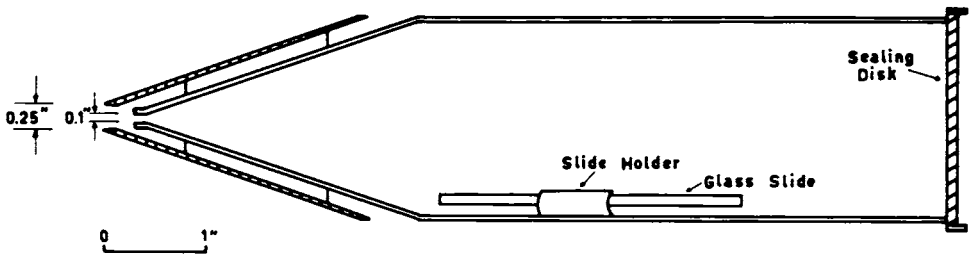

Fig. 8. Low-level replica collector Byrd, 1962, for use in strong winds and heavy drift.

opment work was necessary before a satisfactory collection technique was discovered by Dingle.

Two collector models are shown in Figure 7. One of the collectors, used mainly in the heavy drift near the surface (3–15 cm), was built around the cone-shaped, clear plastic shell of an unserviceable U. S. Army radiosonde transmitter type T 304/AMT-4A. Limitation of flow into the collector, without restriction of the inlet diameter to a point where the larger snow particles would be shattered on entry, was achieved by the addition of a second cone with a larger opening (Figure 8). Most of the snow flowing through this fairing tended to be deflected away from the inlet orifice of the actual collector, and exposures from 1 to 5 seconds would produce well-separated replicas even in heavy drift.

The second collector was basically a wooden box with a removable base and a Plexiglass window which made it possible to terminate the particle collection when a satisfactory cover of the Formvar-coated slide had been obtained. This collector was used at heights between 25 and 200 cm.

Particle sizes were determined for all isolated replicas on a large proportion of the 133 slides obtained during the project, a total of some 3000 replicas being measured. Only very small replicas of indefinite shape, measuring less than 0.02 by 0.02 mm, were omitted from this first analysis. The dimensions of the remainder were found with a 100× micrometer by visually remolding each particle into an imaginary square or rectangle. Figure 9 illustrates this process with some typical shapes encountered; Figure 10 shows actual drift particle replicas and the separation achieved with Dingle's collectors.

2.5 *Sundry Measurements*

In addition to the main measurements discussed above a number of subsidiary sets of observations were made in the course of the Byrd snow drift project. They included observations of visibility by means of the marker stakes spaced at 9-meter intervals between the cold room and the drift mast (cf. Figure 1), temperatures at the snow surface and at the levels of the drift traps during drift conditions (by means of 'thermohms'), and detailed records of the state and nature of the snow surface —in short, all information that could conceivably be relevant to the understanding of the snow drift transport at Byrd. In view of their subsidiary nature these observations will not be further discussed here but will be elaborated as needed by the main discussion, which now turns to the theory of the snow drift process.

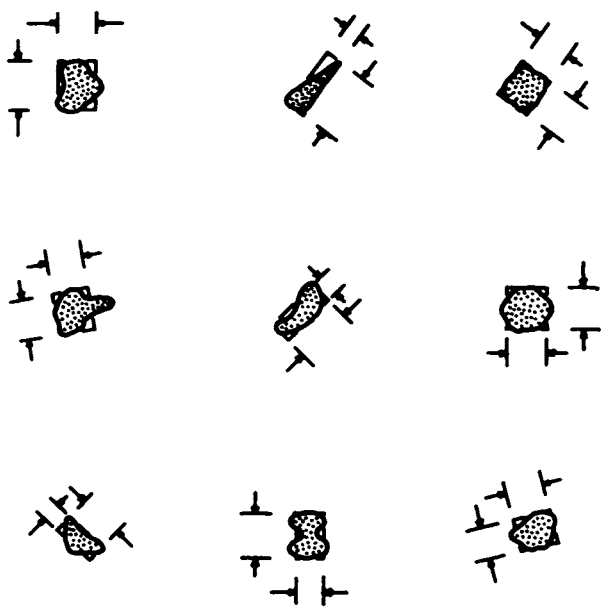

Fig. 9. Determination of effective drift particle size $(l \times b)^{1/2}$.

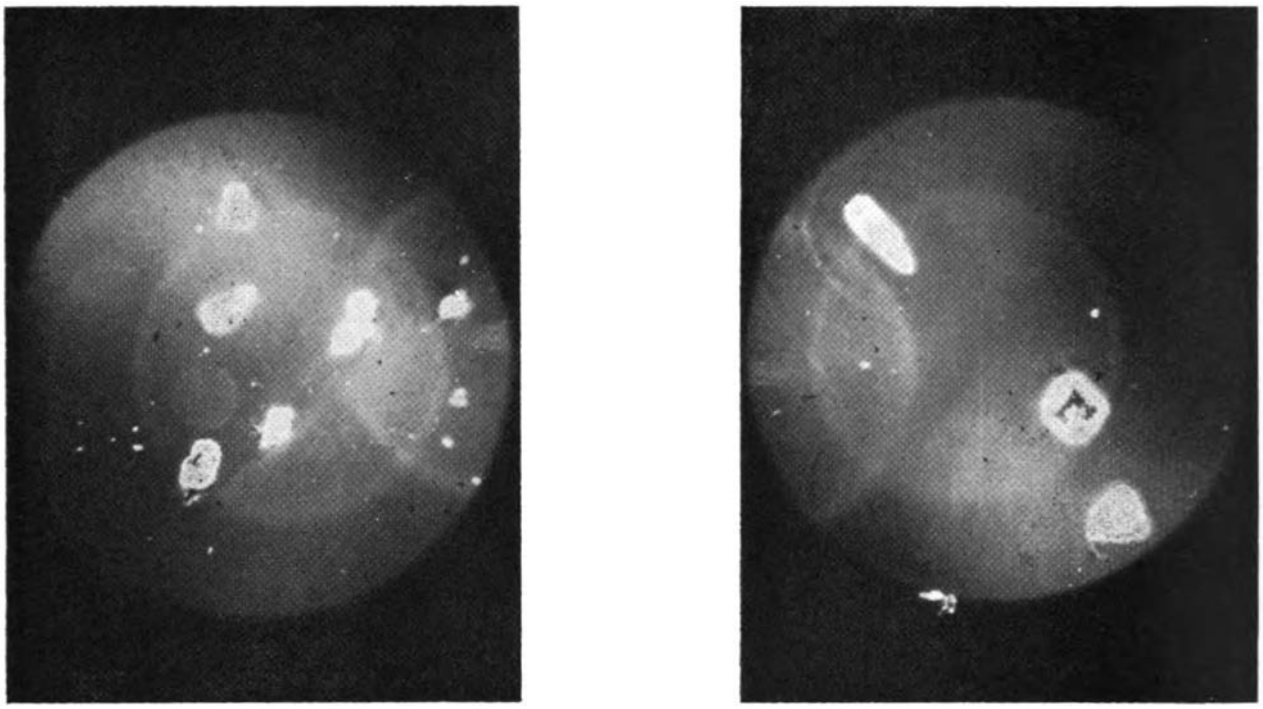

Fig. 10. Drift particle replicas. Magnification approximately 100×.

3. THEORY—GENERAL

Before summarizing the theory of turbulent snow drift that formed the basis for planning the Byrd snow drift project, it will be desirable to define the principal concepts to be used. Quite apart from the fact that drift can also mean a solid deposition of snow, different students of the transport of snow by the wind have used the word 'drift' for a variety of physical quantities.

Loose snow, having been lifted from the surface by the wind, is carried past an observer at a rate proportional to the wind velocity and the drift snow concentration in a unit volume. We shall denote that concentration by 'drift density' n_z (g m^{-3}), where the subscript z refers to the level of observation. The actual drift measurements then give the 'drift flux' F_z defined by $F_z = n_z V_z$ (g m^{-2} sec^{-1}) where V_z stands for the wind velocity at the level z. Whereas the drift density can in the future be measured directly by means of the optical drift gage developed by *Landon-Smith and Woodberry* [1964], existing methods, including those used for the Byrd snow drift project, have made it necessary to divide F_z by V_z in order to obtain n_z. Integration of the drift density n_z over a specified height range gives the total 'drift content' of a vertical column; this will be denoted by Γ and has the dimension g m^{-2}. Similarly, integration of the drift flux leads to the 'drift transport' Q (g m^{-1} sec^{-1}) in unit time through a vertical surface of unit width at right angles to the wind.

Kotlyakov [1961] has considered F alone, whereas *Lister* [1960] proceeded from F to Q by statistical methods. Estimates of the drift transport Q form the major aim of snow drift studies but cannot safely be obtained from measurements of the drift flux F_z at a few levels without an understanding of the interpolation and extrapolation rules to be used. This makes it essential to start from the drift density n_z, which is the basic quantity from the theoretical point of view and provides the means of testing the theory itself.

The theory of turbulent snow drift begins with the observation [cf., e.g., *Liljequist*, 1957] that the low-level profile of winds strong enough to produce snow drift closely approximates a logarithmic form

$$V_z = c + d \log_{10} z \qquad (4)$$

Prandtl [1925], the first to explain this wind

profile in terms of a downward flux of momentum (which makes itself felt as a constant shearing stress in the surface layer), showed that the general relation for the shearing stress in terms of the vertical wind gradient,

$$\tau = \rho K \, \partial V_z/\partial z \tag{5}$$

is compatible with (4) provided the eddy viscosity K has the form

$$K = k(\tau/\rho)^{1/2} z \tag{6}$$

where $(\tau/\rho)^{1/2}$ is commonly denoted by u_*, the friction velocity, and $k = 0.4$ is von Kármán's constant. With this interpretation the logarithmic wind profile is usually written in the form

$$V_z = (u_*/k) \log_e z/z_0 \tag{7}$$

The empirical constants in (4) are then related to those in (7) by

$$\begin{aligned} d &= \frac{u_* \log_e 10}{k} \quad \text{or} \quad u_* = \frac{kd}{\log_e 10} \\ c &= d \log_{10} z_0 \quad \text{or} \quad z_0 = 10^{c/d} \end{aligned} \tag{8}$$

u_* measures the vertical gradient of V_z on the height scale of $\log_e z^{1/k}$, and z_0 is the roughness height at which the wind velocity as given by (7) vanishes.

The closeness with which this wind profile is realized during snow drift conditions at Byrd will be demonstrated in section 4. Anticipating the fact, it seems reasonable to assume that the turbulence responsible for momentum transport also creates the steady upward transport of drift snow needed to balance the steady fallout of drift snow (fall velocity w) caused by gravity. This assumption leads at once to the balance relation of steady-state snow drift [*Shiotani and Arai*, 1953; *Loewe*, 1956]

$$K \, \partial n_z/\partial z = -w n_z \tag{9}$$

with $K = ku_*z$, the value explaining the wind profile, as an obvious first and simplest guess for the eddy diffusivity.

For uniform drift snow or constant fall velocity w, equation (9) can be integrated immediately over a height range from z_1 to z_2 to give the ratio of the drift densities at the two levels in the form

$$n_{z_1}/n_{z_2} = (z_1/z_2)^{-w/ku_*} \tag{10}$$

We shall write w_* for the non-dimensional fall velocity w/ku_*, which governs the vertical distribution of drift snow according to (10).

It would seem profitable to choose the roughness height z_0 as one of the two levels, but in practice the formal advantages of this choice are offset by the large scatter of the surface drift density values n_{z_0}, which must be determined by downward extrapolation from levels where measurements are possible. Thus the simple relations resulting from the choice of z_0 as reference level will be quoted merely as curiosities in the following discussion of drift quantities as functions of height and wind speed.

3.1 *Drift Quantities as Functions of Height*

For the drift density n_z equation 10 indicates in the case of constant fall velocity w a linear dependence of $\log n_z$ on $\log z$. The hyperbolic relation, zn_z = constant, claimed by *Rusin* [1961], evidently holds only for the special case of $w_* = 1$ or $w = ku_*$.

Since the slope of the $\log n_z$-$\log z$ line is proportional to the particle fall velocity w, the particle fall velocity can be estimated for any layer from the drift densitities at its boundaries by means of the relation [*Dingle and Radok*, 1961].

$$w_{z_1}^{z_2} = ku_* \log (n_{z_1}/n_{z_2})/\log (z_2/z_1) \tag{11}$$

The drift content $\Gamma_{z_1}^{z_2}$ of a column extending from z_2 down to z_1 is obtained by integration of (10); for constant w_* it takes the form

$$\Gamma_{z_1}^{z_2} = \frac{1}{1 - w_*} (z_2 n_{z_2} - z_1 n_{z_1}) \tag{12}$$

For $w_* = 1$ this expression becomes indeterminate (since then $z_2 n_{z_2} = z_1 n_{z_1}$). However, the drift content in this case is readily computed as

$$(\Gamma_{z_1}^{z_2})_{w_*=1} = z_1 n_{z_1} \int_{z_1}^{z_2} \frac{dz}{z} = z_1 n_{z_1} \log_e \frac{z_2}{z_1} \tag{13}$$

Budd [1965] has pointed out that, when $z_2 \to \infty$, the drift content becomes infinite for $w_* \geq 1$, whereas for $w_* < 1$ we obtain simply

$$\Gamma_{z_1}^{\infty} = \frac{z_1 n_{z_1}}{1 - w_*} \tag{14}$$

Similar considerations apply to the drift transport $Q_{z_1}^{z_2}$ in the layer between z_2 and z_1 . Following *Dingle and Radok* [1961] this is given by

$$Q_{z_1}^{z_2} = \int_{z_1}^{z_2} n_z V_z \, dz = q_{z_2} - q_{z_1} \tag{15}$$

where

$$q_z = \frac{z n_z u_*}{(1 - w_*)^2} \left((1 - w_*) \log_e \frac{z}{z_0} - 1 \right) \qquad w_* \neq 1 \tag{16}$$

or

$$q_z = \frac{zn_z u_*}{k} \log_e z \log_e \frac{z}{z_0} \left[1 - \frac{\log_e z}{2 \log_e \frac{z}{z_0}}\right] \qquad w_* = 1 \tag{17}$$

For subsequent purposes we note the full expression for Q in terms of z and u_*, viz.,

$$Q_{z_1}^{z_2} = \frac{ku_*^2}{ku_* - w} \log_e \left\{\frac{(z_2/z_0)^{z_2 n_{z_2}}}{(z_1/z_0)^{z_1 n_{z_1}}}\right\} - \frac{k^2 u_*^3}{(ku_* - w)^2} (z_2 n_{z_2} - z_1 n_{z_1}) \tag{18}$$

For $w_* < 1$ the drift transport remains finite as $z_2 \to \infty$, and for $z_1 = z_0$ it takes the simple form [*Budd*, 1965]

$$(Q_{z_0}^{\infty})_{w_*=1} = z_0 n_{z_0} ku_*^3/(ku_* - w)^2 \tag{19}$$

This completes the survey of the height dependence of drift quantities for the case of constant fall velocity. All the relations given in this section can also be interpreted in terms of wind speed, as is shown in the next section.

3.2 *Drift Quantities as Functions of Wind Speed*

The wind speed plays two separate roles in snow drift. It is obvious that quantities like the drift flux and the drift transport, which contain wind speed as a factor, should increase with wind speed. In addition it will be seen that increasing wind speed has the effect of increasing both the amount of snow in the air and the uniformity of its distribution along the vertical.

It follows from the logarithmic wind profile (7) that for a constant roughness height z_0 the wind speed at a given level z is proportional to the shear velocity u_*, so that we can replace u_* in the formulas of section 3.1 by

$$u_* = \left(\frac{k}{\log_e (h/z_0)}\right) V_h \tag{20}$$

The level h will in general be identified with that of the standard anemometer installation, 10 meters.

With the substitution of (20) in the equations of section 3.1, these equations link the variation of various drift quantities at a fixed level or in a fixed layer with changes in wind speed from occasion to occasion. At first sight this seems somewhat surprising, since the basic turbulence relation (10) provides no information on the absolute quantity of snow drift in the air but only on the vertical distribution of the available snow. (This difficulty has been pointed out by Dr. C. H. B. Priestley.) The relations derived in section 3.1, however, contain as variables (apart from w and z_0, which have already been assumed constant) only u_* and the drift snow density near the surface, n_{z_1}. Hence the interpretation in terms of wind velocity will be quite legitimate provided that the drift density at the roughness height, or at some constant height above the snow surface, does not vary appreciably with wind velocity. The validity of this assumption, like that of all others made here (steady-state drift, constant fall velocity, constant roughness height), must evidently be confirmed by means of the observations; but it seems plausible that the absolute drift density close to the surface should depend primarily on the amount of loose snow available rather than on the wind velocity, which must vanish close to the surface no matter how great it may be higher up.

When u_* is substituted in equation 10, from equation 20 the drift density takes the wind-dependent form

$$n_z = n_{z_1} e^{-w \log_e (z/z_1) \log_e (h/z_0)/k^2 V_h} = n_{z_1} e^{a_{1,h}/V_h} \tag{21}$$

where $a_{1,h} = -(w/k^2) \log_e (z/z_1) \log_e (h/z_0)$ is a constant for a given level z and reference level h. It is especially convenient to chose h equal to z and z_1 equal to z_0, since then $a_{00} = -(w/k^2) \log_e^2 (z/z_0)$ and the drift density at the level z is a simple exponential function of the reciprocal wind velocity at that level.

In its essentials equation 21 was first obtained by *Dingle and Radok* [1961], who showed that it explains the height variation of the exponent γ in empirical power laws of the form

$$n_z \propto (V_z - B)^{\gamma}$$

suggested by various workers for the relationship between wind speed and drift density or drift flux. Equation 21 reveals above all that with increasing wind speed (and provided the low-level drift density remains unchanged) the drift snow distribution along the vertical tends to become uniform.

The drift flux $n_z V_z$ can be written in the wind-dependent form

$$F_z = n_{z_0} V_z e^{a_{00}/V_z} \tag{22}$$

indicating that for quasi-constant n_{z_0} the drift flux should be proportional to the wind speed both for low levels (small a_{00}) and for high wind speeds.

Turning next to the drift content $\Gamma_{z_1}^{z_2}$, we find from equations 12 and 20 that its wind-dependent form is

$$\Gamma_{z_1}^{z_2} = \left(1 - \frac{w \log_e (h/z_0)}{k^2 V_h}\right)^{-1} (z_2 n_{z_2} - z_1 n_{z_1}) \qquad (23)$$

For $V_z \to \infty$ it follows from (21) that $n_z \to n_{z_1}$ and hence that $\Gamma_{z_1}^{z_2} \to n_{z_1}(z_2 - z_1)$.

The drift transport $Q_{z_1}^{z_2}$ is a rather complicated function of wind speed. Substitution for u_* from (20) in (18) gives the expression

$$Q_{z_1}^{z_2} = \frac{k^3 V_h^2}{\log_e h/z_0 \,(k^2 V_h - w \log_e h/z_0)} \cdot \log_e \left\{\frac{(z_2 - z)^{z_2 - z}}{(z_1/z_0)^{z_1 - z_0}}\right\} - \frac{k^5 V_h^3}{\log_e (h/z_0)(k^2 V_h - w \log_e h/z_0)^2} \cdot (z_2 n_{z_2} - z_1 n_{z_1}) \qquad (24)$$

but this is not yet the full story, since the wind speed occurs implicitly also in the drift density at the upper boundary n_{z_2}, which in general will be strongly wind dependent. Equation 24 is therefore difficult to interpret except for small and for very great wind velocities. For small V_h the drift transport is approximately proportional to the third power of the wind speed, as has been suggested on empirical grounds by several workers [*Lister*, 1960; *Rusin*, 1961; *Kotlyakov*, 1961; cf. also *Bagnold*, 1941]. For $V_h \to \infty$ the drift transport in the layer from z to z_1 approaches the limiting value

$$\lim_{V \to \infty} Q_{z_0}^{z} \to \left[\frac{n_{z_0} z(\log_e (z/z_0) - 1)}{\log_e (z_1/z_0)}\right] V_z, \qquad (25)$$

i.e., linear increase in drift transport with wind velocity! That this must be so was first pointed out by *Budd* [1965]; it follows immediately from equation 21 which show the drift snow density to become uniform with height for very large wind velocities. Equation 25 can in fact be derived directly in the form $Q = n_{z_0} z \bar{V}$, where $\bar{V}$ is the mean velocity computed for the logarithmic wind profile over the layer from the surface to height z. Since, in practice, the ratio $(\log_e z/z_0 - 1)/(\log_e z_h/z_0)$ does not differ greatly from unity, the slope of the drift transport asymptote is approximately

$$z n_{z_0} \ (\mathrm{g\ m^{-1}\ sec^{-1}/m\ sec^{-1}} = \mathrm{g\ m^{-2}}).$$

As a curiosity we may note that, for a 300-meter drift layer and a surface drift density of the order of 3×10^3 g m^{-3}, the drift transport would ultimately increase at the rate of 1 ton m^{-1} sec^{-1} for each meter per second increase in wind velocity, but also that this state of affairs is approached only for wind speeds of the order of 10^3 m sec^{-1}. The theoretical drift transport relations (18) and (24) for constant fall velocity bear in fact little relation to observed drift transports, as will be brought out by the discussion of the Byrd observations in the remainder of this paper.

4. BASIC RESULTS OF THE BYRD SNOW DRIFT MEASUREMENTS—GENERAL

In this section the results derived from the Byrd measurements concerning the wind and drift density profiles will be presented. The theoretical relations of section 3 will provide the background and determine to some extent the quantities evaluated and the coordinate systems used for their display. However, a good deal of detailed numerical information is presented in the appendices to this paper so as to enable other 'glacialists' to improve on our treatment and conclusions. Appendix A provides general information on each of the 129 drift runs. Appendix B gives the detailed low-level wind information for each drift run. Appendix C contains a summary of the main features of the rapid-run wind measurements in the lowest kilometer above the ice cap. Appendix D gives individual drift density values for all runs and levels. Finally, Appendix E presents the drift contents and transports to be discussed in section 5. Further reference to these tables will be made as the various variables are considered.

4.1 *The Wind Profile during Snow Drift at Byrd*

As indicated in section 2.2 the wind observations made during the Byrd project fall into two separate groups. The first covers the layer between the surface and the 4-meter level. This group poses the question whether a logarithmic wind profile exists and, if so, the question of the dependence of its parameters on wind speed and surface conditions. The second group of wind observations covers the layer from approximately 30 to 1000 meters; here the mathematical form of the wind profile has not yet been determined and presents a major problem outside the scope of this paper. We shall be mainly

concerned with finding an approximate form for use in the drift transport calculations; we shall also use the upper-wind observations to determine the upper limit of the layer of appreciable snow drift.

4.1.1 *The low-level wind profile.* Each of the 129 sets of wind measurements made during the drift runs at levels between 400 cm and 12.5 or 6.25 cm above the snow surface has been fitted with a regression line using $\log_{10} z$ as independent variate. The regression coefficients provide the shear velocities and roughness heights in accordance with equation 8 of section 3. The individual values of u_* and $-\log_{10} z_0$ are listed in both Appendix B and Appendix D.

Prior to a discussion of these parameters characterizing the logarithmic wind profile (7), the validity of this profile must be tested for the present observations. Such a test has been made by means of the differences between the observed and log z regression wind speeds for all levels and drift runs (cf. Appendix B). Figure 11 shows the average vertical profile of these differences, which represents the over-all mean deviation of the observed winds from the logarithmic wind profile. It appears that on the average there is no systematic trend in the deviations from the logarithmic wind profile. Such trends would be expected to show up most clearly in a comparison of winds observed for differ-

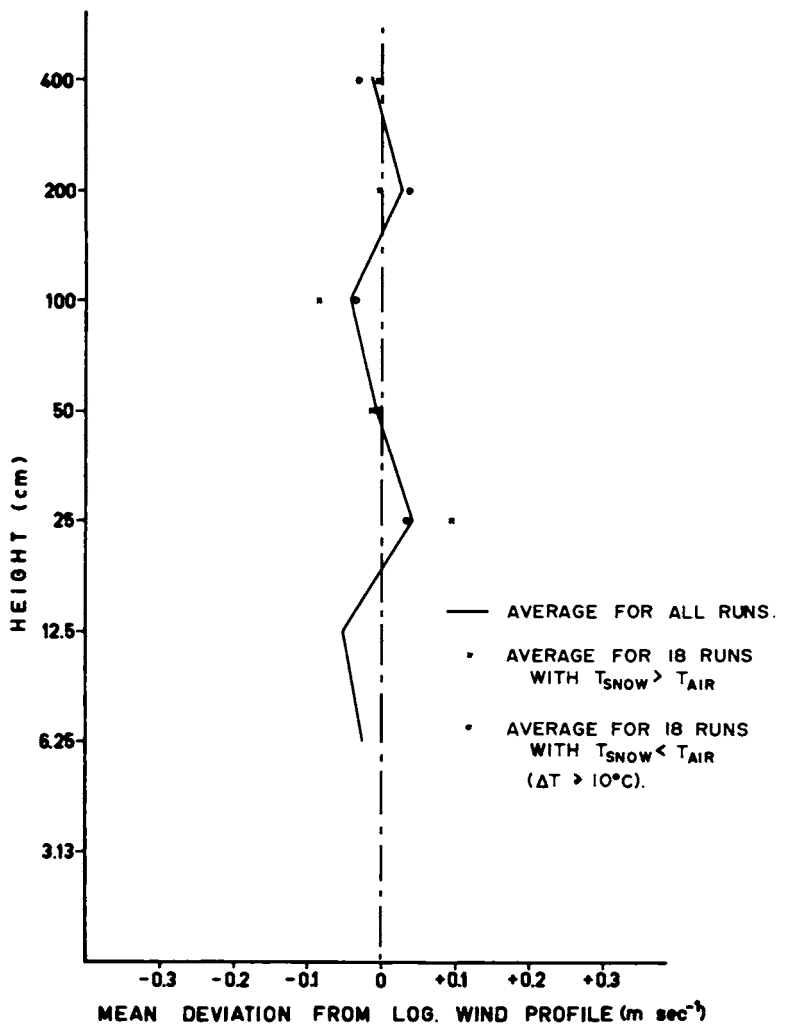

Fig. 11. Test of the validity of the logarithmic wind profile for snow drift conditions. Mean velocities range from 8 m sec^{-1} at 6 cm to 15 m sec^{-1} at 400 cm. For explanation see text.

ent stability conditions. Although the temperature measurements made during the drift runs at Byrd cover too small a height range for the computation of reliable values of the Richardson number for individual runs, a broad separation of cases of contrasting static stability can be made on the basis of the snow-air temperature difference. In 18 of the 129 drift runs this difference was distinctly positive, temperature differences between the snow surface and the air at the level of the 100-cm trap ranging from close to zero to more than 7°C. For the remaining 111, the same temperature difference was either very small (2 cases) or distinctly negative, exceeding −10°C in the 18 most extreme cases.

The average wind profile deviations for the two sets of 18 cases with snow warmer or much colder than the air are shown as crosses and circles, respectively, in Figure 11. Again no systematic trend with altitude or away from the general average is apparent. We are then entitled to conclude that during snow drift conditions at Byrd the wind profile has the logarithmic shape (7).

This conclusion is further confirmed by the average wind profiles computed for different mean wind velocities at the 10-meter level (Figure 12). The most significant feature of these profiles, apart from their linearity, is their tendency to rotate around a focus located near the point $z = 1$ mm, $V_z = 2$ m sec^{-1}. This produces a systematic increase with wind velocity in the roughness height z_0, the

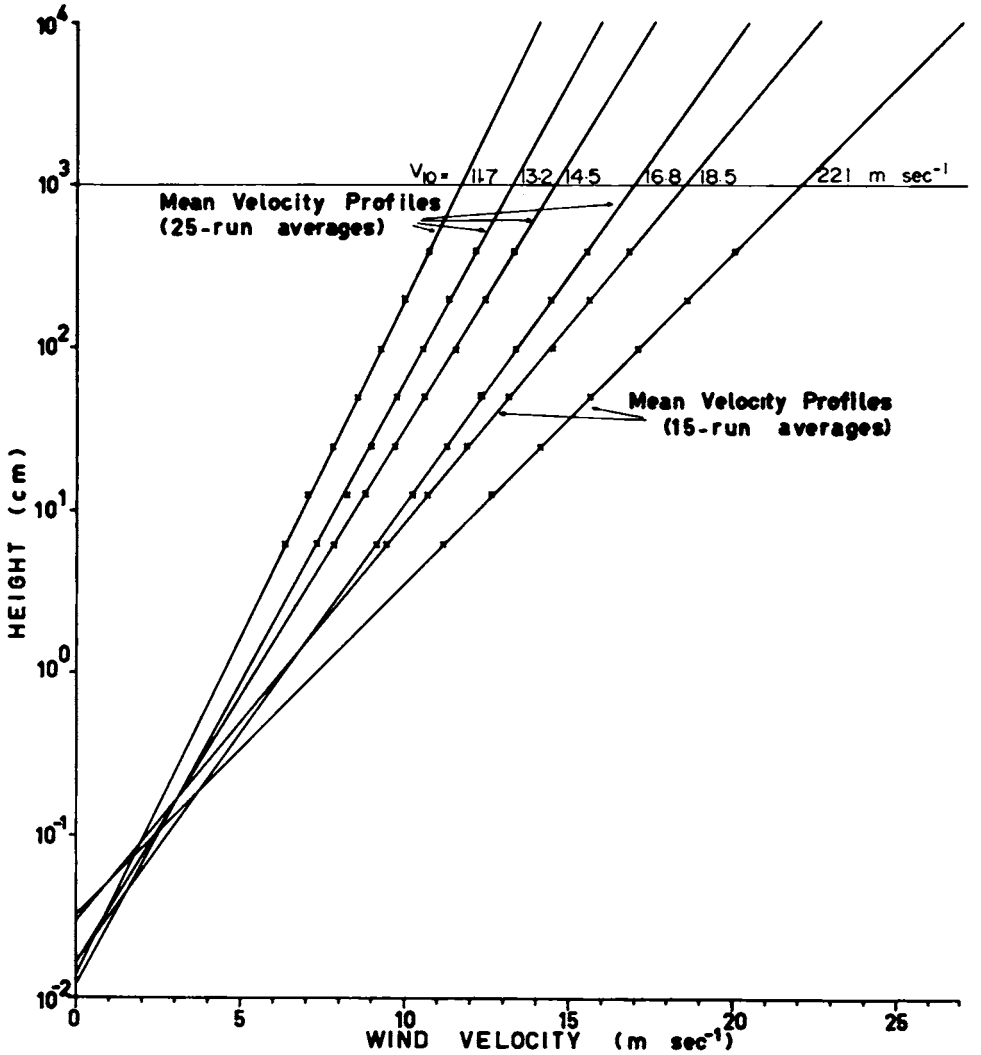

Fig. 12. Mean low-level wind profiles.

intercept of the straight lines with the ordinate axis. Similar features noted by *Bagnold* [1941] for drifting sand and by *Liljequist* [1957] for snow drift have been ascribed by these authors to the increased shearing stress created by the drift. It will be seen in section 4.1.2 that the Byrd data do not support this view but suggest instead genuine changes in roughness as the wind velocity increases.

Details of the shear velocity u_* and the roughness height z_0 are given in Figure 13 which gives averages computed from sets of five wind runs with approximately the same 10-meter wind velocity. The roughness height shows a slight tendency to increase with wind speed; the reality of this effect is confirmed by the systematic deviation of the u_* values from the straight line of best fit through the origin.

In addition to the roughness heights derived from the Byrd measurements Figure 13 contains a number of other z_0 values reported for the south pole by *Dalrymple et al.* [1963], for Mirnyy by *Rusin* [1961], for Maudheim by *Liljequist* [1957], and for the Wilkes satellite station S2 by *Budd* [1965*a*]. The Mirnyy values, although smaller throughout than those found at Byrd, show a similar trend with wind velocity, whereas the trend in the Maudheim roughness heights is very much more pronounced. The z_0 values for Wilkes reported by *Dingle and Radok* [1961] as being of the order of 5×10^{-3} mm are at the other extreme and must be regarded with some doubt, being based on wind measurements at three levels only. It will be seen in section 5.1 that these excessively small roughness heights have tended to inflate drift transport estimates for Wilkes.

The scatter of the z_0 values in Figure 13 arises evidently from changes in surface conditions and processes, which are considered in the next section.

4.1.2 *Snow surface conditions and their effects on the low-level wind profile.* The accumulation-ablation history of the drift project area at Byrd station is summarized in Figure 14. Two separate estimates are given for the mean accumulation: the first has been obtained by simple averaging of the accumulation on the nine principal stakes; the second represents corrected values deduced from the

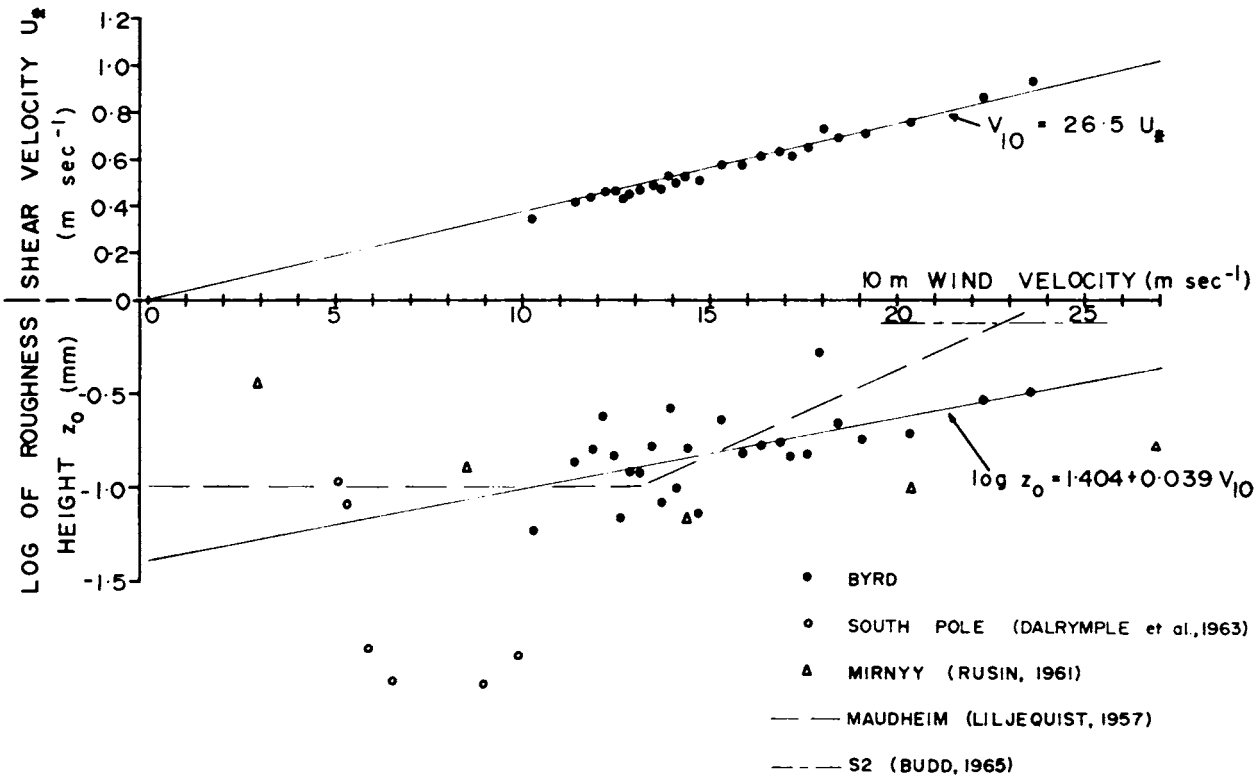

Fig. 13. Mean values of shear velocity (top) and roughness height (bottom) for Byrd and other antarctic stations. The Byrd values represent averages of 5 wind runs each.

regression of the moving stake accumulation rates on those of the principal stakes, in accordance with the discussion in section 2.3.2. The accumulation values indicated by the two extreme stakes of the network are also shown, to illustrate the dangers of relying on isolated stakes. The remaining curves in Figure 14 give the mean surface densities and the average wind velocities for the periods between accumulation readings.

The information in Figure 14 is supplemented by the detailed surface conditions on the occasions of drift measurements (given in Appendix A). During the winter months the snow surface tended to be mostly hard and smooth. Occasionally, however, during periods of moderate to heavy drift (in association with suspected precipitation) the appearance and texture of the surface snow constantly changed. Shallow layers of soft snow, of unknown areal extent, would develop on the more usual hard flat winter crust and would disperse at frequent intervals during the half-hour to hour occupied by a drift run. Occasionally after heavier precipitation a substantial layer of new soft snow would form on the hard winter crust. Winds in excess of 8 m sec^{-1} would then start the formation of shallow dunes and barchans, both formations advancing downwind

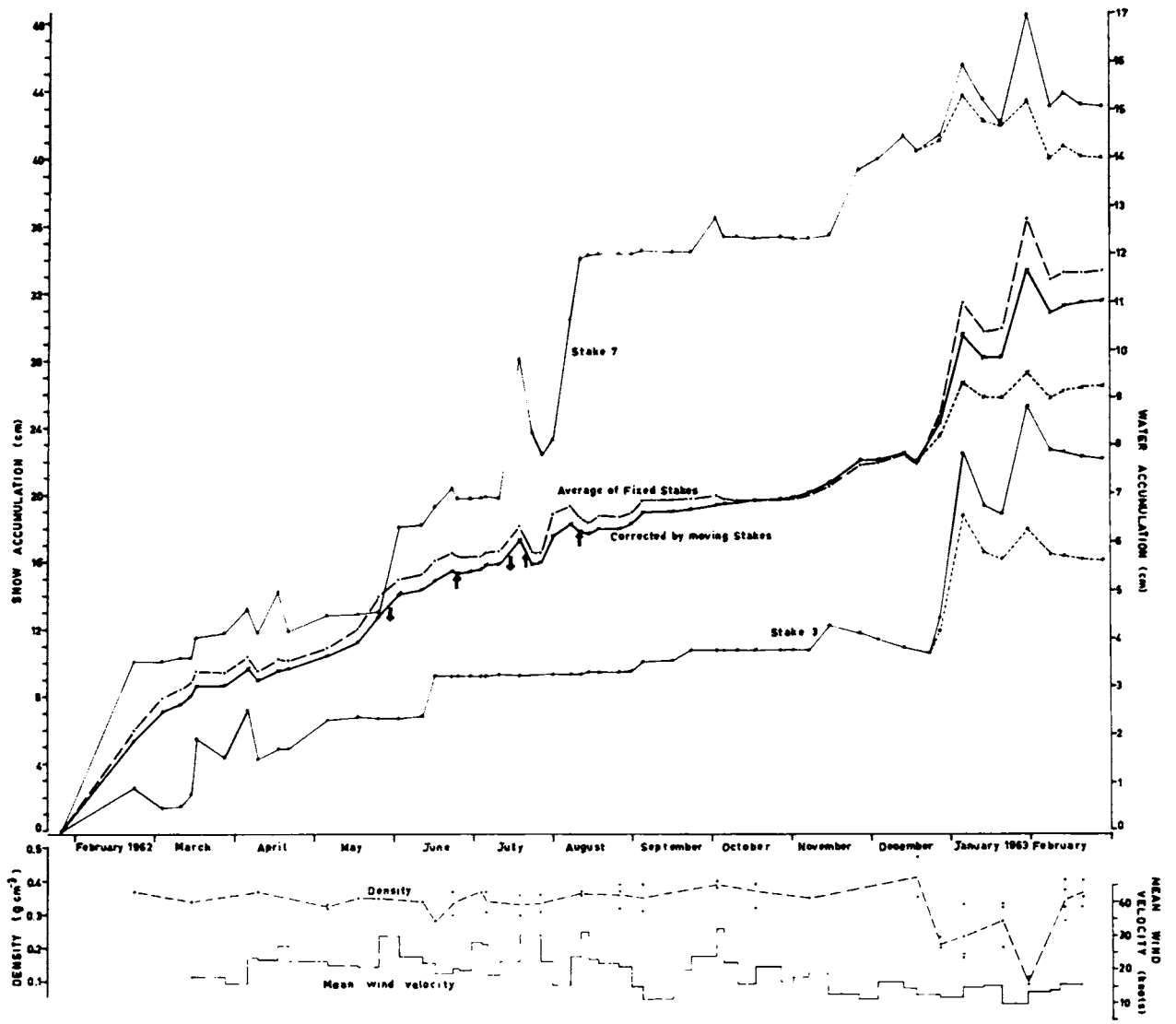

Fig. 14. Snow accumulation and related parameters for Byrd 1962–1963. For details see text. The arrows show the expected direction of the net drift transport for the occasions tested in Figure 20.

TABLE 2. Frequency of Different Surface Conditions at Byrd 1962–1963

	Type of Surface						
	Hard Smooth	Macrodisturbances		Soft Snow			Detail Uncertain, (Poor Visibility)
		Dunes, Barchans	Sastrugi	General Cover	Patches	Rippled Surface	
No. of drift runs	35	46	11	14	13	5	5

owing to the constant movement of snow particles from the exposed windward side of the formation to the sheltered downwind side. This process became much more common during the summer period, which was marked by relatively heavy precipitation and complete absence of heavy drift.

After extended periods of surface winds too light to produce drifting, a thin protective crust tended to form on the existing snow surface. Dune and barchan formations that had been exposed to this process at any stage of their life tended to resist surface winds of up to 13 m sec^{-1}, retaining both their shape and location. Winds in excess of 14 m sec^{-1}, however, tended to undercut and distort the windward side of such formations and to create for a time sastrugi patterns separated by patches of hard and flat winter snow. During the winter these sastrugi represented transient conditions, as can be seen from Table 2, which gives the numbers of drift runs made with different types of surface.

A full understanding of drift features will require an analysis of the surface history preceding each individual run. In the present context we merely examine average values of surface roughness and shear velocity for occasions of hard smooth snow, soft smooth snow, and macrodisturbances (dunes, barchans, sastrugi). These averages are given in Table 3 (where drift density averages for the 12.5-cm level have also been included, in anticipation of section 4.2.1). To make the wind and drift parameters referring to different surface conditions strictly comparable they have been computed from sets of drift gagings with closely similar 10-meter wind velocities; this procedure is of general utility in dealing with strongly wind-dependent phenomena and will be referred to as 'wind-matching' in the following.

Table 3 shows that hard smooth surfaces on the average had the lowest values of roughness height and shear stress (u_*), whereas the largest values occurred in the presence of smooth soft snow rather than with macrodisturbances such as dunes, barchans, and sastrugi. Although for the small samples in question the differences are not statistically significant, they make physical sense and agree with previous results for Wilkes [*Dingle and Radok*,

TABLE 3. Shear Velocity, Roughness Height and Low-Level Drift Density Averages for Different Surface Conditions (Computed from 22 wind-matched drift runs in each group)

Type of Surface	$\bar{u}_*$, m sec^{-1}		$-\overline{\log z_0}$, mm		$\bar{z}_0$, mm	$\bar{n}_{12.5}$, g m^{-3}
A Hard smooth snow	0.533		0.926		0.119	16.78
B Dunes, barchans, sastrugi	0.545		0.835		0.146	16.20
C Soft snow	0.554		0.658		0.220	17.76
Differences	Mean	Standard Deviation of Mean	Mean	Standard Deviation of Mean	Mean	Standard Deviation of Mean
C–A	0.021	0.011	−0.268	0.103	0.98	1.342
C–B	0.009	0.01	0.177	0.097	1.56	1.28
B–A	0.012	0.005	−0.091	0.124	−0.58	0.96

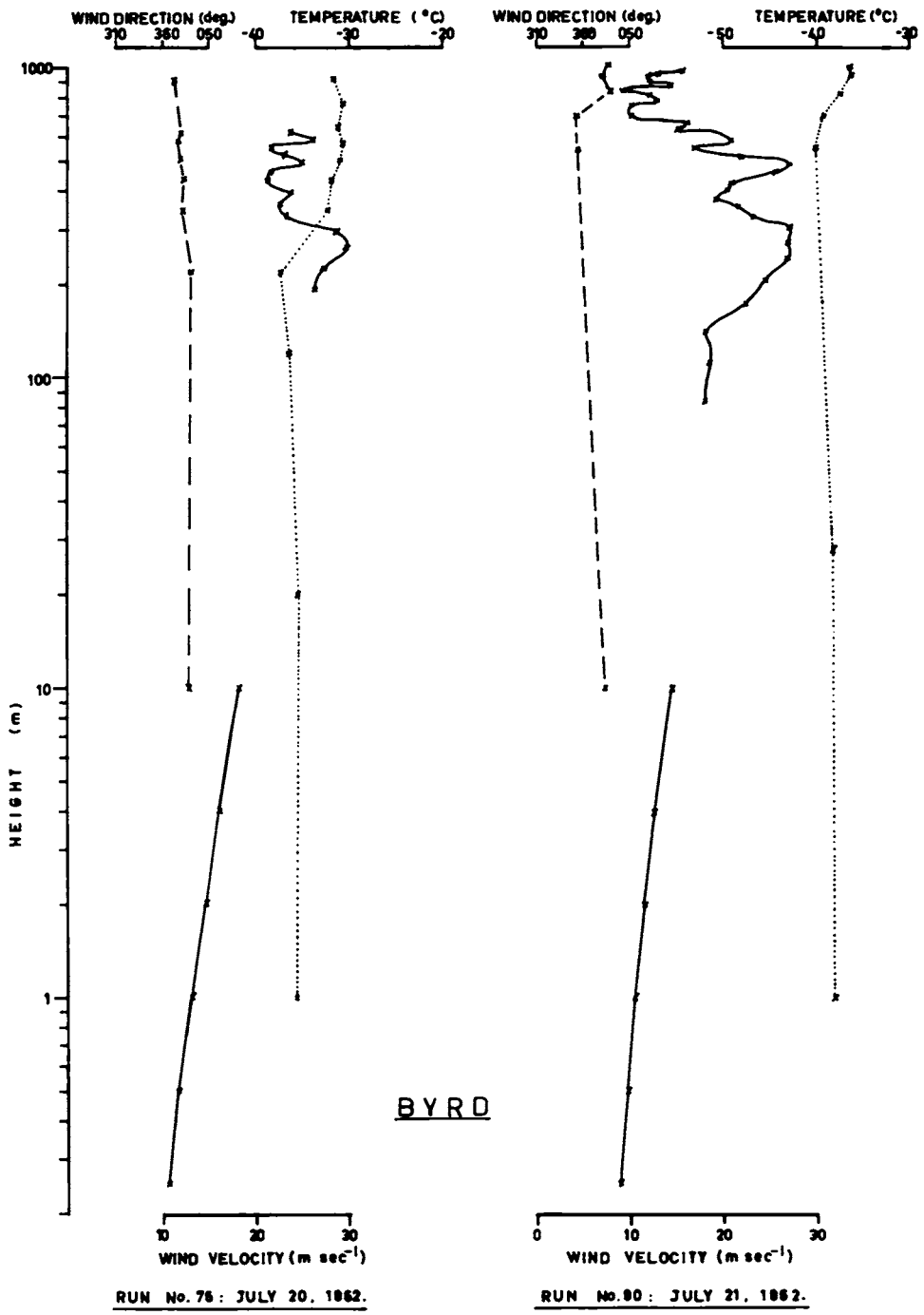

Fig. 15. Wind and temperature profiles determined from rapid-run radiosoundings (logarithmic height scale).

1961]. The macrodisturbances apparently are shaped by the wind so as to minimize their wind resistance, and the effective roughness of a snow surface, like that of water waves, is then determined mainly by its micro features.

It has been suggested [*Liljequist*, 1957] that an additional factor determining the effective roughness of polar snow surfaces is the drift snow itself, which through its momentum requirements is supposed to add to the shear stress. As pointed out by *Lister* [1960], such an effect should leave its mark also on the *form* of the wind profile, rather than produce the simple rotation around a low-level 'focus' observed (cf. Figure 12). Without probing too deeply into the postulated semi-intuitive physical process, however, the present data permit a direct test for a relation

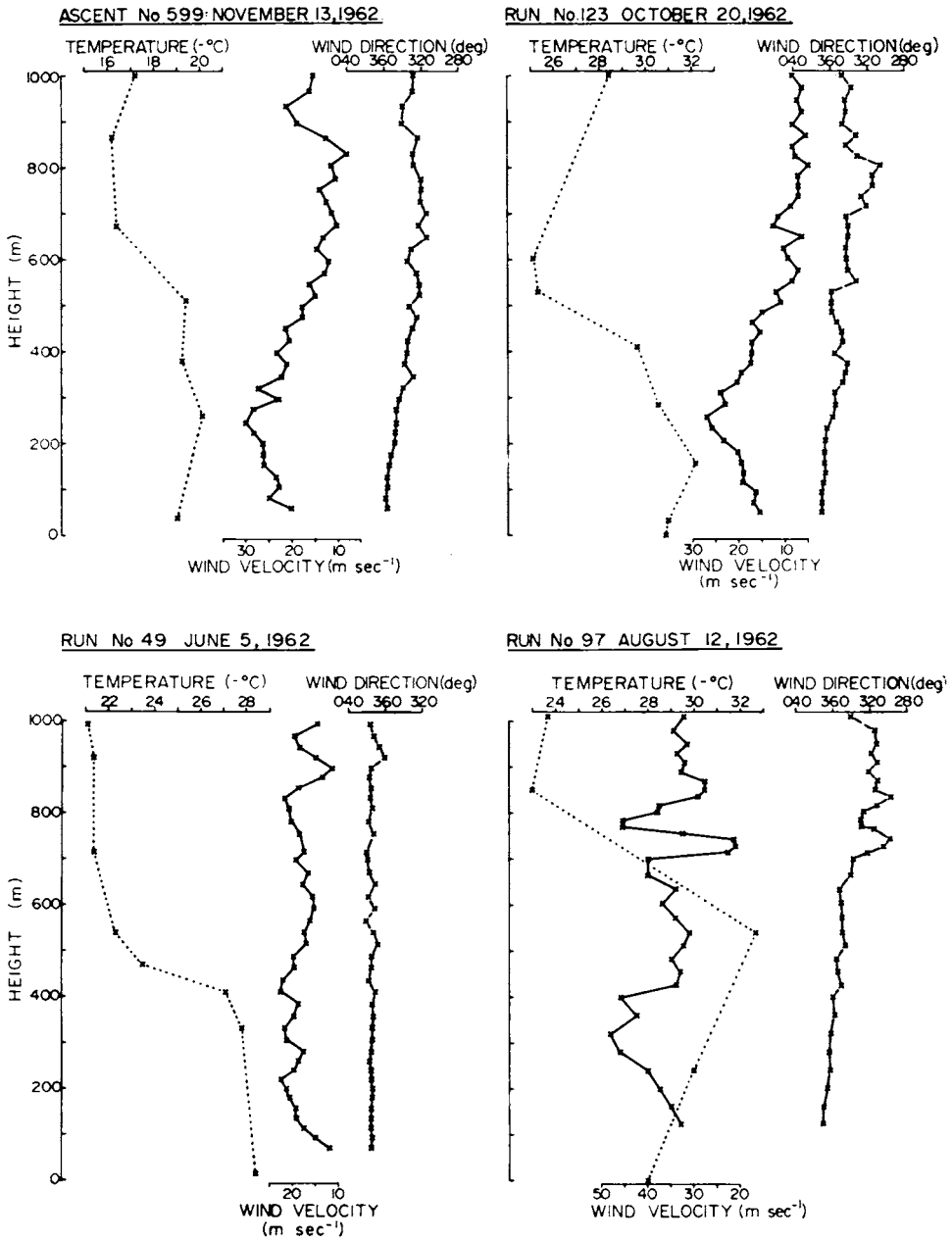

Fig. 16. Wind and temperature profiles determined from rapid-run radiosoundings (linear height scale).

between drift density and roughness height. Such a test is provided by the correlation between log z_0 and a low-level drift density such as $n_{12.5}$ for all cases of drift in the presence of a hard smooth snow surface, which is unlikely to be made rougher by a moderate increase in wind speed. For the 35 drift runs made on a hard smooth surface the total correlation was found to be 0.222, well below the 0.1 level of significance; above all the partial correlation $r_{\log z_0,\, n_{12.5},\, V_{10}}$, eliminating the remaining effects of changes in wind velocity, was found to be -0.076. In combination with the absence of any significant deviations from the logarithmic form of the observed wind profiles this seems to rule out an effective contribution of snow drift surface friction to surface roughness.

In conclusion we note for later use several periods, marked by arrows in Figure 14, during which the snow surface either rose or descended at an appreciable rate. The drift runs made in these intervals may be expected to differ in essential features if the imbalance of upward transport and settling of drift snow had been sufficiently marked to affect the validity of the steady-state assumption made in section 3. This matter will be examined as part of the discussion of drift density profiles in section 4.2.1. Here we now consider the upper winds.

4.1.3 *Upper-wind features during snow drift.* Our knowledge of upper-wind features during snow drift at Byrd rests mainly on the results of the 32 rapid runs (Appendix C) with the radiotheodolite (cf. 2.2.2). Although the photogrammetry of rocket trails is potentially superior for this purpose, it could not be tried at Byrd until the drift conditions had effectively come to an end. Examples of the rapid-run wind and temperature profiles are shown on a log height scale in Figure 15 and on a linear height scale in Figure 16.

Figure 15 illustrates the fact that occasionally the logarithmic wind profile of the immediate surface layer persists upward to almost the level of the first wind maximum. The sample wind profiles shown on the linear height scale in Figure 16 have been chosen to illustrate the variety of profile forms encountered under snow drift conditions. Although low-level wind maxima predominate, they are not always pronounced, and on some occasions the influence of the large-scale pressure field is clearly dominant (cf., e.g., the flight of November 13).

Rusin [1961] has interpreted Mirnyy soundings in terms of idealized wind profiles representing pure cyclonic and katabatic conditions as well as transitions from each to the other. These profiles are reproduced in Figure 17. According to Rusin, the true katabatic flow ('stok') is quite shallow, and the wind profile with a pronounced maximum at an altitude of a few hundred meters represents a transition from the cyclonic to the katabatic profile. Rusin's description of both this transition and the transition in the opposite sense deserves being quoted in extenso:

> . . . When the transition is from cyclonic to katabatic flow the larger velocities observed under cyclonic conditions persist only in the layer from 200 to 500 or 600 meters. One gets the impression that the katabatic starts as it were from

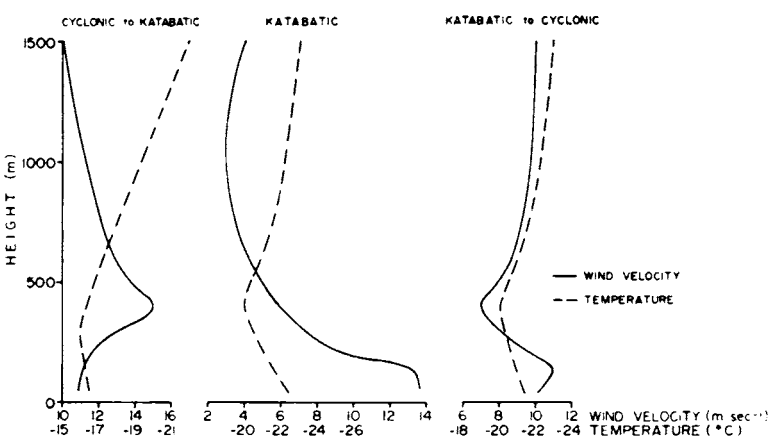

Fig. 17. Schematic wind and temperature profiles characterizing katabatic and transitional conditions [after *Rusin*, 1961].

above. At the surface the wind velocity falls sharply. The air temperature (at this stage) decreases with altitude, as under cyclonic conditions, but in the surface layer the lapse rate is small, and sometimes almost isothermal conditions are found there.

A completely different picture is observed in the transition from katabatic to cyclonic flow. At the surface large velocities persist, with a maximum near 100 meters. Above this level the wind velocity decreases sharply as during katabatic flow, up to heights of the order of 300 to 500 meters, to increase again still higher. Now the cyclonic flow overcomes, as it were, the katabatic beginning in the upper levels, but lacks the strength to check the katabatic near the surface, where it attains its full downslope intensity. The air temperature still rises in the surface layer under these conditions. The strongest inversion is observed in the first hundred meters; above the inversion the lapse rate, as formerly, decreases with height, and the stratification becomes almost isothermal around 400 or 500 meters. Above this level the normal temperature decrease with height is

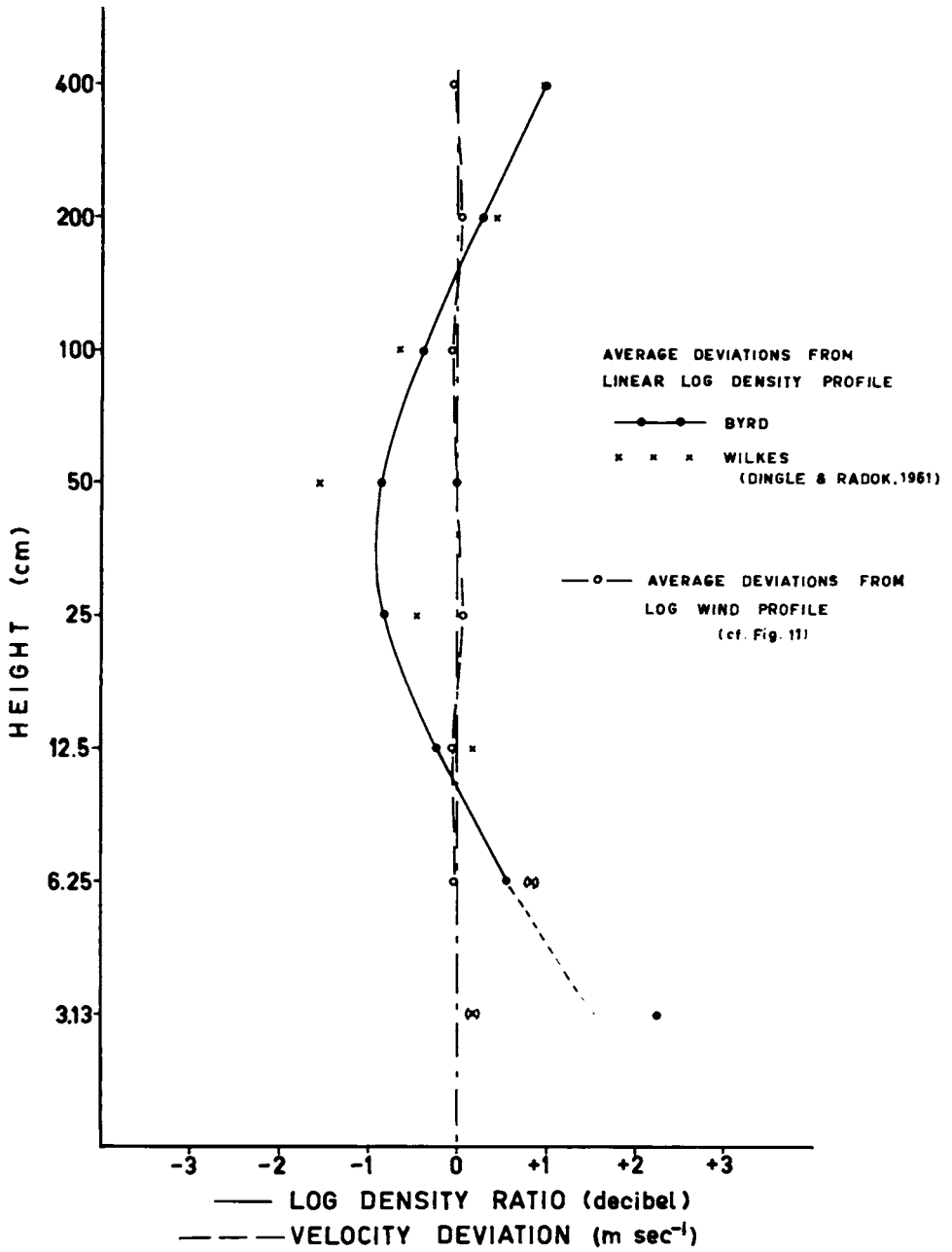

Fig. 18. Test of linearity of log n_z versus log z.

resumed, just as in the case of katabatic flow. [Translated from *Rusin* (1961), pp. 74–76.]

For Byrd we have no fully comparable wind data, but the wind profiles in Figure 16 could be interpreted along similar lines as arising from the combination of katabatic and large-scale pressure gradient effects. The absence of clear correspondence between the levels of maximum wind velocity, temperature inversion, and onset of marked wind direction changes, brought out by Figure 16 and especially by Appendix C, supports *Lettau's* [1963] contention that other factors such as the surface heat budget must play a vital role in shaping the wind profile under these conditions.

For the purpose of the present paper we have now some justification for assuming that in drift conditions the wind profile does not deviate markedly from the logarithmic form up to the level of the first velocity maximum. Table 3 shows the average height of that maximum to be 250 meters; the average upper limit of the drift layer will therefore be not far from 300 meters, the level suggested by *Prudhomme and Boujon's* [1952] observations in the Adélie Coast and also used in drift transport calculations for Wilkes by *Dingle and Radok* [1961].

This completes the discussion of the wind observations made during the Byrd project; we turn now to the actual snow drift measurements.

4.2 *Snow Drift Density*

A complete summary of the drift density values computed from the Byrd measurements of drift flux and the regression (logarithmic profile) winds of Appendix B is given in Appendix D. This information is homogeneous with the exception of the values for the lowest level (3.125 cm). These values were computed from measurements with the Williams Special trap but have not been brought into line with the Mellor trap measurements (cf. section 2.1.2), since the trap comparisons at Byrd were not sufficiently extensive (especially as regards range of wind speeds) to warrant much reliance on the trap conversion factors in Table 1. Further work by Budd at Mawson has suggested that the Williams Special trap is only slightly (4%) more efficient than the Mellor trap. Until Budd's full results become available, the drift densities at the lowest

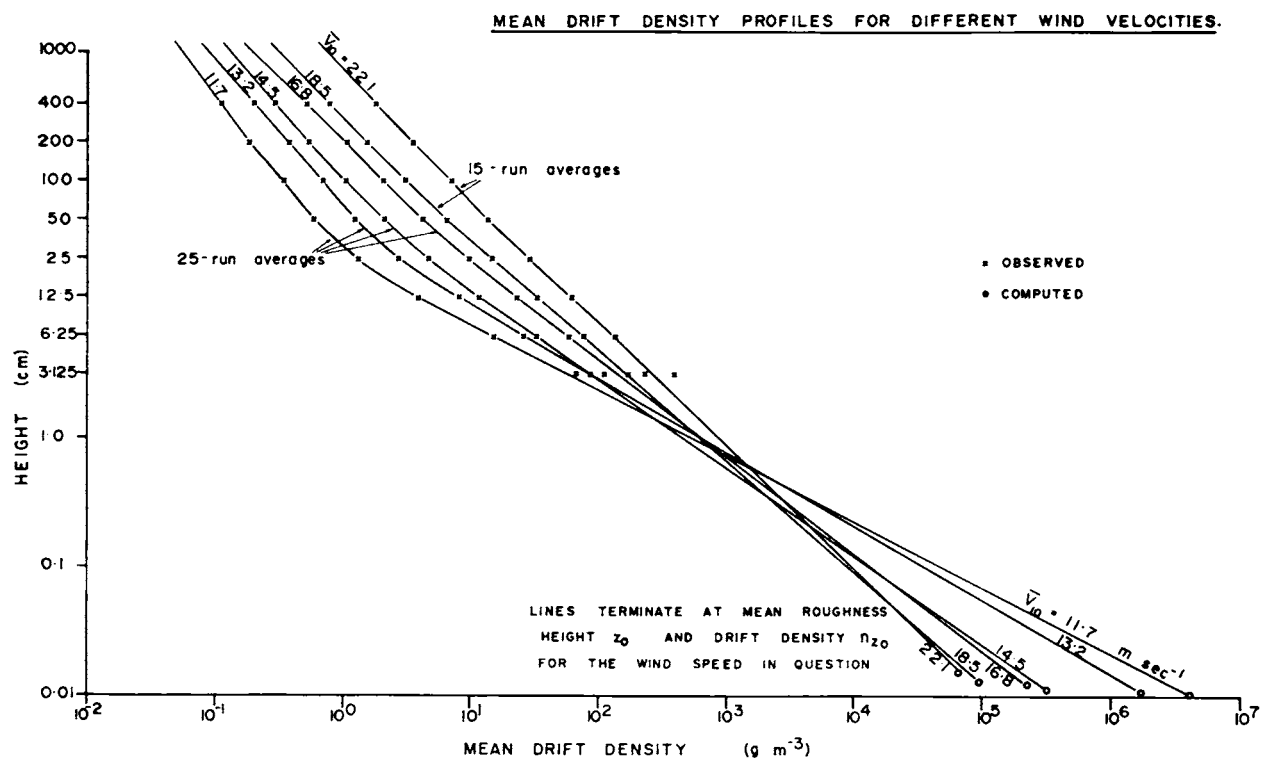

Fig. 19. Snow drift density as a function of height.

level remain in some doubt, and for the purpose of this paper all extrapolations to surface values of drift density have been made by means of the observations at the 12.5- and 6.25-cm levels.

The main theoretical predictions for the drift density are that, for a given logarithmic wind profile (i.e. z_0 and u_*) and fall velocity w, the logarithm of the drift density, log n_z, should vary linearly with log z; furthermore, for a given height log n_z should vary linearly with V_*^{-1} in the absence of significant changes in z_0 and n_{z_0} with wind velocity. The first of these predictions will be tested in the next section; the wind-dependence of drift density is treated in section 4.2.3.

4.2.1 *Drift density as function of height.* The validity of the linear log n_z profiles is tested in Figure 18 in the same manner as in section 4.1 for the logarithmic wind profile. The 3-cm density values have not been considered in fitting the regression lines. The average wind deviations of Figure 11 are reproduced in Figure 18 on a relative scale broadly equivalent to that used for the density deviations in order to demonstrate the magnitude and systematic trend of the density deviations. These average drift density deviations from the expected straight log n_z–log z relation suggest strongly that the fall velocity changes with height (as was noted by *Dingle and Radok* [1961], whose deviations are reproduced as crosses in Figure 18), and in fact that the change is continuous rather than abrupt. This interpretation is supported by Figure 19 which shows mean vertical drift density profiles for a number of representative wind velocities. Each of the profiles in Figure 19 is curved; the average density at each level increases with wind speed; both the vertical density gradient and the profile curvature decrease with increasing wind speed.

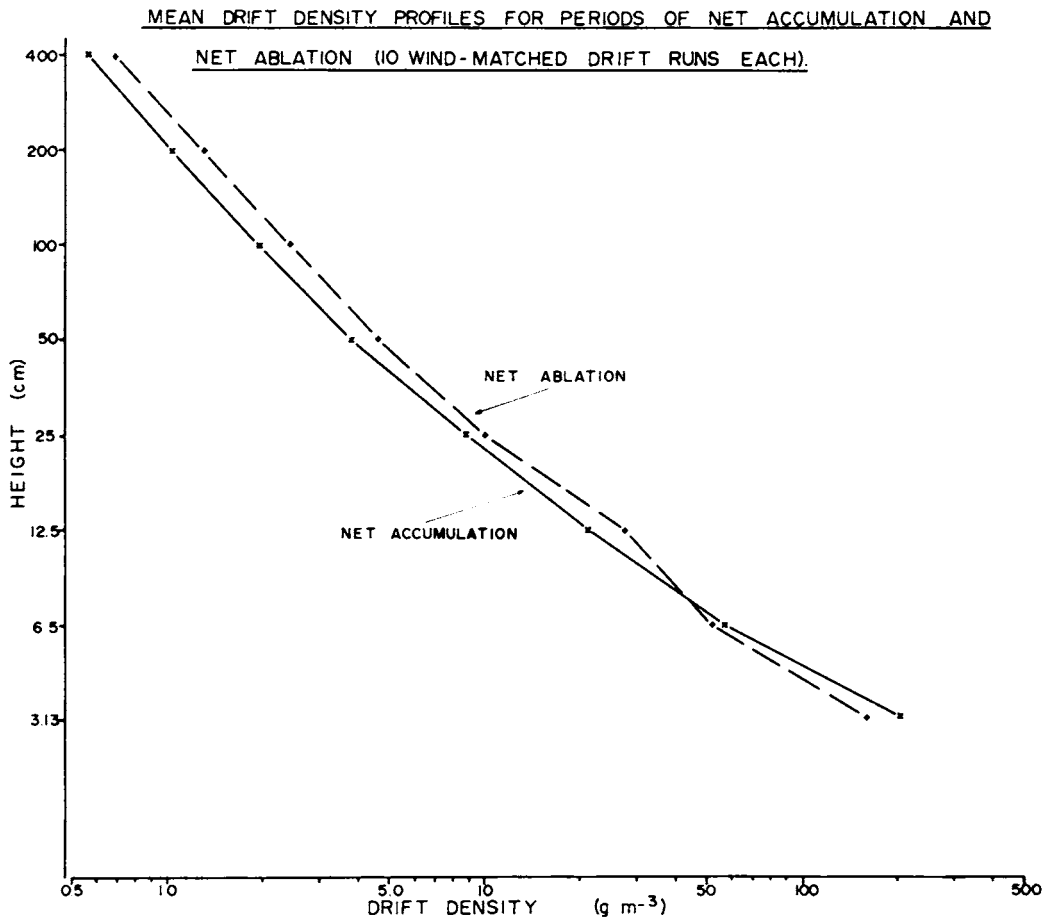

Fig. 20. Mean drift density profiles for periods marked by arrows in Figure 14.

TABLE 4. Mean Log Drift Density Deviations from Linear log n_z − log z Relations for Wind-Matched Occasions of Net Accumulation and Ablation
(10 cases each)

	Level, cm							
	400	200	100	50	25	12.5	6.25	3.125
Net accumulation	0.1067	0.0238	−0.0400	−0.0991	−0.0868	−0.0507	0.0856	0.0707
Net ablation	0.0597	0.0242	−0.0301	−0.0713	−0.0432	−0.0029	0.0383	0.0350
Δ log deviations	0.0470	−0.0004	−0.0099	−0.0278	−0.0436	−0.0478	0.0473	0.0357
Standard deviations of Δ log deviations	0.027	0.018	0.014	0.024	0.025	0.030	0.024	0.029

Figures 18 and 19 together make it clear that the simple drift theory of section 3 represents at best a first approximation to the truth. Although there is a strong suggestion that the assumption of uniform drift snow (with constant fall velocity) may be mainly responsible, it cannot be ruled out that deviations from steady-state conditions also play a significant part. In order to confirm or eliminate this possibility we consider first the drift density profiles for the occasions of appreciable net accumulation or ablation, marked by arrows in Figure 14.

In this connection it is again essential to use wind-matched data. Figure 20 shows the mean drift profiles for net accumulation and ablation computed in each case from ten drift runs, and Table 4 gives the corresponding mean deviations from the linear log drift density versus log height relation and their standard errors. It is evident from these results that with a rising snow surface the drift density tends to be relatively larger near the surface and smaller at the higher levels than during net ablation. Although statistically the differences

TABLE 5. Percentage Frequency Distributions of Particle Sizes, Byrd 1962–1963

Level, cm	Surface	3.125	12.5	25	50	100	200
No. of Measured Particles	231	119	767	61	459	587	484
Size Ranges, mm							
Less than 0.034	0.86		0.01			0.17	0.21
0.034–0.046	···	—	0.52			1.19	0.83
0.047–0.058			4.05	1.69	2.18	8.18	4.13
0.059–0.070	1.30		10.05	1.69	7.63	16.54	18.20
0.071–0.082	3.90		14.75	8.20	20.50	21.15	21.70
0.083–0.094	8.23	0.84	17.87	16.40	21.35	18.76	21.30
0.095–0.106	12.57	6.72	16.30	13.12	20.70	17.56	15.30
0.107–0.118	13.00	5.88	15.65	11.47	12.85	7.00	10.53
0.119–0.130	11.70	5.88	8.61	16.40	5.23	4.61	4.75
0.131–0.142	11.70	13.45	6.00	8.20	3.70	2.22	1.03
0.143–0.154	9.96	11.76	2.74	4.92	3.27	1.71	1.65
0.155–0.166	9.96	11.76	1.17	4.92	1.31	0.34	0.21
0.167–0.178	6.50	12.60	0.39	4.92	0.87	0.34	—
0.177–0.190	5.20	8.41	0.52	4.92	—	0.34	0.21
0.191–0.202	1.72	4.20	0.78	3.28	—	—	—
0.203–0.214	0.86	1.68	—	—	—		
0.215–0.226	0.86	5.04	0.01		0.22		
0.227–0.238	0.43	4.20	0.39		—		
0.239–0.250	0.43	4.20	—		—		
0.251–0.262	0.43	1.68			0.22		
greater than 0.262	0.86	1.68					
$\bar{X}$	0.132	0.165	0.099	0.119	0.096	0.086	0.087
S^2	0.00147	0.00186	0.000829	0.00118	0.000634	0.000573	0.000473

TABLE 6. Means and Mean Squares of Drift Particle Sizes for Individual Drift Runs

	Temperature °C						Particle Size	
V_{10}, m sec^{-1}	Air	Snow	Date 1962	Drift Run No.	Level, cm	No. of Particles Measured	Mean $\bar{X}$, 10^{-1} mm	Mean Square S^2, 10^{-2} mm^2
11.87	−36.8	−39.6	9/29	112	200	26	0.940	0.787
					100	50	0.581	0.074
					12.5	60	0.708	0.610
					Surface	61	1.1338	0.1388
12.10	−20.1	−24.2	10/25	126	200	6	0.768	0.135
12.43	−26.0	−31.7	8/30	110	200	20	0.727	0.291
					100	41	0.952	0.646
					12.5	47	1.266	1.380
					Surface	50	1.432	1.815
12.53	−30.8	−30.3	10/20	123	25	20	1.109	1.432
					12.5	20	1.247	0.762
					3	30	1.496	1.119
13.28	−18.9	−24.4	10/23	124	200	8	0.787	0.976
					100	15	0.993	0.595
					50	10	1.077	1.142
					25	11	1.118	1.098
					3	19	2.084	2.168
14.59	−39.4	−37.8	10/1	116	200	28	0.719	0.093
					12.5	80	1.011	0.707
14.86	−37.2	−37.9	10/1	115	100	62	0.792	0.385
					50	52	0.894	0.289
16.51	−29.6	−30.3	10/20	122	200	20	0.984	0.383
					100	24	1.151	0.442
					50	24	1.226	0.890
					25	30	1.266	0.911
					3	30	1.593	1.214
16.91	−38.9	−39.1	10/3	117	50	79	0.928	0.520
					12.5	46	0.885	0.379
					12.5	89	0.818	0.360
17.04	−26.9	−39.6	9/30	113	200	19	0.719	0.192
					100	10	0.724	0.186
17.07	−22.7	−32.2	8/25	109	200	54	0.974	0.478
					100	65	0.965	0.179
					50	114	0.985	0.349
17.25	−18.9	−21.7	11/12	128	200	15	1.005	0.236
					3	40	1.667	1.752
17.51	−19.1	−32.2	8/25	108	200	46	0.865	0.310
					100	61	0.867	0.507
					12.5	103	1.121	0.339
17.79	−22.8	−27.9	10/4	121	200	40	0.861	0.205
					100	20	0.935	0.221
					50	26	1.100	0.719
					12.5	30	1.128	0.692
					Surface	60	1.488	0.105
18.57	−26.6	−34.4	8/23	105	100	37	0.848	0.534
					12.5	64	1.116	0.911
18.65	−37.4	−37.9	10/3	118	200	108	0.778	0.333
					100	112	0.812	0.375
					50	70	0.818	0.375
					12.5	106	0.844	0.383
19.39	−28.2	−39.3	9/30	114	50	49	0.949	0.331
					12.5	124	1.022	0.545
19.81	−25.6	−30.7	10/4	120	200	50	0.953	0.381
					100	41	0.948	0.543
					50	42	1.060	1.338
22.08	−29.1	−33.2	10/4	119	200	44	0.979	0.604
					100	42	0.992	0.717

are barely significant for the small sample utilized in Figure 20 and Table 4, their consistency suggests physical reality.

The deviations from the theoretical drift density profile are more pronounced during occasions of net accumulation than of net ablation. The same type of departure is evident, however, on both occasions. Hence, although the existence of unbalanced drift conditions can be demonstrated, they do not provide the explanation for the inadequacy of the simple drift theory. For such an explanation we turn therefore to the measurements of drift particle sizes.

4.2.2 *Drift particle size and the drift density profile.* Before the Byrd collection of snow drift particle replicas only *Lister* [1960] seems to have succeeded in making measurable Formvar casts under snow drift conditions. Lister's particle size distributions failed to reveal any clear trends with height but amply demonstrated the presence of a wide range of particle sizes, and hence fall velocities, in drifting snow.

Results of the Byrd measurements of particle size (cf. section 2.4.1) are summarized in Tables 5 and 6. In addition to frequency distributions of particle size for different levels, the means and standard deviations are given for different runs, in order of wind velocity.

A full discussion of this material is beyond the scope of this first survey of the Byrd results, and only features bearing on the problem of the drift density profile will be considered. In contrast to *Lister*'s [1960] particle size data, the Byrd measurements indicate a distinct height variation in average particle size; cf. Table 7. A variation with wind speed is brought out by Figure 21, which shows the individual mean particle sizes available for the 100- and 200-cm levels where Table 7 indicates no significant height variation.

Apart from a trend to larger drift particles for stronger winds Figure 21 illustrates the great variability in particle size from occasion to occasion. Table 6 shows, in fact, that the variability is of the same order as the change in particle size with height on a given occasion. Under the circumstances it is difficult to advance beyond the point reached with Table 7 and Figure 21 without a thorough examination of the particle size frequency distributions. We may, however, turn back to the drift densities of section 4.2.1 to see whether the variation of the profile slope with height and wind speed, when interpreted as change in fall velocity by means of equation 11, is in general agreement with the particle size trends deduced above. Figure 22 shows isopleths of fall velocity constructed from the six mean profiles of drift density in Figure 19. We note that the variation of w with wind speed is most marked at the highest levels, whereas the variation of w with height is most pronounced at low wind speeds. This is precisely what we would expect from Table 7 and Figure 21.

A satisfactory theory of the snow drift process must evidently account for the joint variation of drift particle size and drift density with both height and wind speed. Such a theory developed and verified by means of the Byrd data by *Budd* [1966] appears elsewhere in this volume. For our present purpose the drift density features at variance with the theory of section 3 may now be regarded as explained, so that henceforth we shall be concerned with how much, not whether, the observed drift quantities differ from the theoretical predictions of section 3. One of these predictions, which concerned a linear dependence of log n_z on the reciprocal wind velocity V_z^{-1} at the same level will be examined in the next section.

4.2.3 *Drift density as function of wind speed.* Although the surface drift densities resulting from the extrapolation to z_0 of the mean drift density profiles in Figure 19 show a marked decrease with increasing wind speed, there appears to exist near the 1-cm level a layer in which the drift density is largely independent of wind speed. This makes it

TABLE 7. Means and Standard Deviations of Average Particle Size for Different Levels

Level, cm	Surface Drift	3.125	12.5	50	100	200
No. of particles	231	119	767	459	587	484
Mean, mm	0.132	0.165	0.0986	0.0964	0.0863	0.0869
Standard deviation of mean, mm	0.004	0.004	0.001	0.001	0.001	0.001

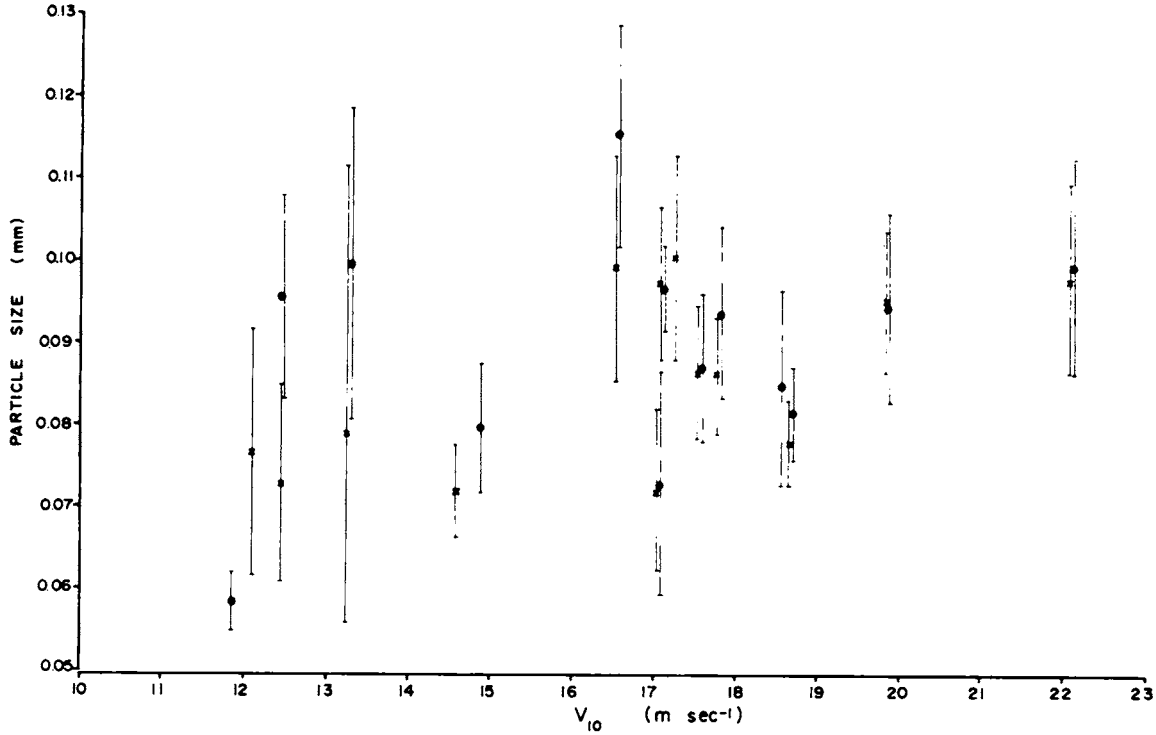

Fig. 21. Mean particle sizes at 200 cm (*cross marks*) and at 100 cm (*solid dots*) as a function of wind speed (lines give $2\delta_s$).

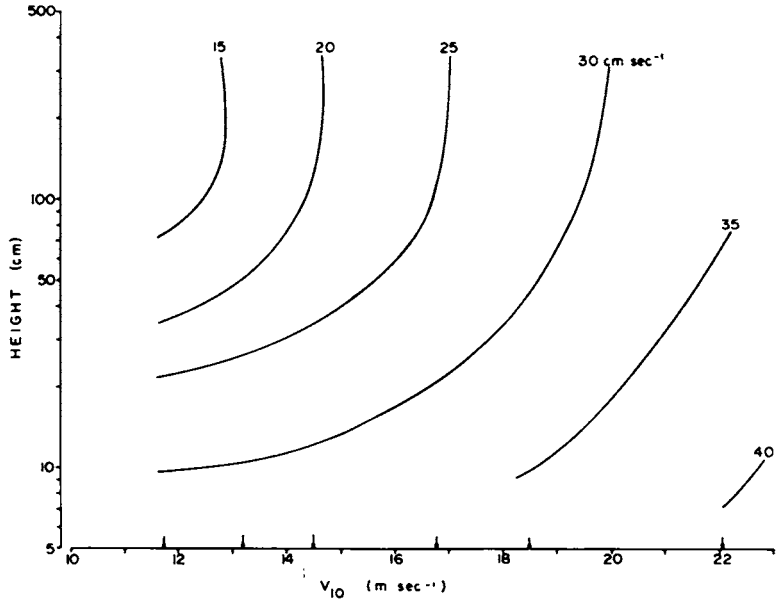

Fig. 22. Drift particle fall velocity isopleths determined from equation 16.

worth while to examine changes in drift density at a fixed level as a function of wind speed alone, despite doubts about the validity of such a move (cf. section 3.2).

To justify beyond doubt such comparisons between drift measurements on different occasions, the individual drift density values for all runs and selected levels have been plotted against their relevant reciprocal wind speeds in Figure 23. The surprisingly small scatter around the least squares regression lines lends support to the view that the absolute drift snow quantities present on any occasion depend more on the state and history of the snow surface than on the wind velocity.

It must be expected that the *mean* drift densities of Figure 22, when plotted in the fashion of Figure 23 against $\bar{V}_z^{-1}$, will again deviate from the theoretical straight line. Figure 24 confirms this to be so but for some unknown reason at the lowest and highest levels only. In the center of the height range covered by the measurements, the $\overline{\log n_z} - V_z^{-1}$ relations are very well represented by straight lines that intersect the ordinate axis in the region of 500 to 600 g m^{-3}. This drift density might then be regarded as a rough estimate of the hypothetical uniform drift density expected from equation 21 for very large wind velocities. Comparison with Figure 19 shows that the extrapolation of the mean drift density profiles down to z_0 leads to surface drift densities two orders of magnitude larger than the 'terminal' (infinite wind speed) value derived from the central lines in Figure 24; on the other hand, the surface drift density agrees well with the mean drift density near the 1-cm level in the layer little affected by changes in wind speed, both being of the order of 10^3 g m^{-3} or approximately equal to the air density. Thus the simple theory of section 3 appears to work passably well in the present context—owing presumably to mutual cancellation of some of the effects that produced the marked discrepancies between the theoretical and observed vertical drift density profiles (section 4.2.1).

In more general terms the regular variation from occasion to occasion in the drift density at a given level suggests that snow drift characteristics of different antarctic regions might be rendered comparable merely by making allowance for differences in their wind regimes. Unfortunately, published information on wind and snow drift has rarely been sufficiently detailed for testing this possibility, and the only interstation comparisons we have been able to make are based on the Mellor trap measurements by Dingle at Wilkes and by Budd at the Wilkes satellite station S2 (situated 80 km east-south-east of Wilkes at an elevation of 1170 meters). It is fortunate that together with the Byrd measurements these data cover the main regional contrasts of interest, between the coast, the coastal

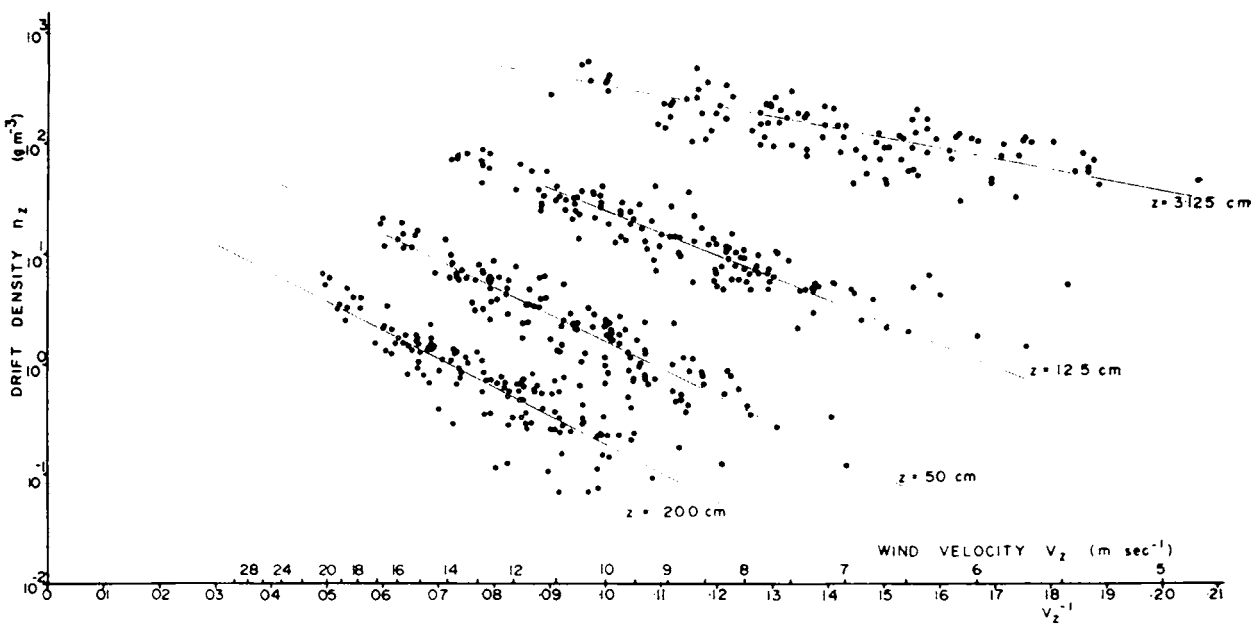

Fig. 23. Drift density for selected levels as a function of reciprocal wind speed at those levels.

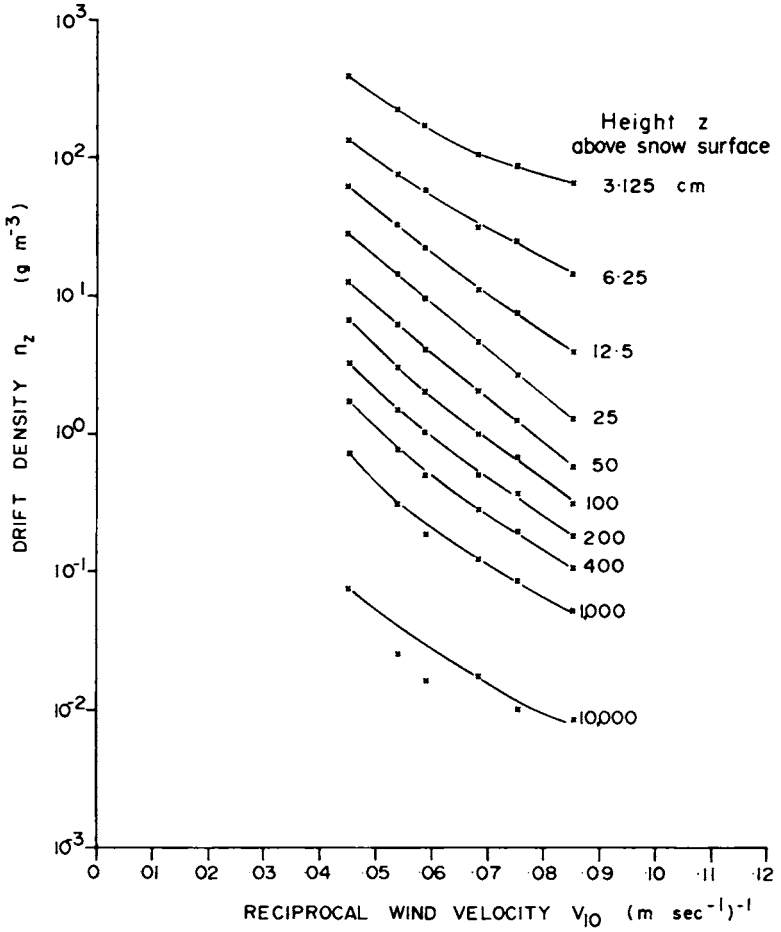

Fig. 24. Mean drift density for different levels as a function of the reciprocal 10-meter wind speed.

plateau slopes, and the interior of Antarctica (outside the most central part where snow drift becomes a rare phenomenon; cf. Table 8 of section 5.2).

Figure 25 shows mean drift densities for three levels as a function (reciprocal) of the 10-meter wind speed. Byrd and Wilkes agree surprisingly well, whereas with increasing height the S2 curves drop more and more below the other two. *Budd* [1965*a*] has interpreted the discrepancies between the S2 and Wilkes drift densities as being due to the presence of larger particles at S2; a full explanation must await the more detailed examination of individual cases and clarification of the dependence of absolute drift snow concentrations on past and present surface weather conditions.

To encourage further comparisons of this type we finally present the Byrd data in the form most likely to be directly useful to other students of the snow drift process wishing to test their own unpublished data: viz., as mean drift *flux* profiles, Figure 26. As an example we have added *Averyanov's* [1959] values for the surface drift flux at Vostok 1, which seem quite compatible with the Byrd curves.

4.2.4 *Drift density isopleths and visibility in snow drift conditions.* With drift density established as a function of both height and wind speed it is possible to construct isopleths of this basic snow drift parameter in a log $z - V^{-1}$ coordinate system for use in various considerations involving the order of magnitude of the snow concentration in the air. Such isopleths constructed from the drift density averages of Figure 19 are shown in Figure 27. As

an illustration of their use we consider briefly the visibility observations made in conjunction with the snow drift measurements.

The relation between drift density and visibility was studied by *Liljequist* [1957], who used an ingenious argument involving the wind dependence of both visibility and roughness height to confirm his theoretical result indicating that the visibility should be proportional to the drift density at eye level. The Byrd data permit this confirmation to be made directly. Figure 28 shows the mean drift densities of Figure 19 for the 200-cm level plotted against the average reciprocal visibilities measured by means of the stake line between the cold room and the drift mast (cf. Figure 1). We see that with sufficient accuracy the visibility

$$D = 100/n, \quad \text{meters} \tag{26}$$

This relation makes it possible to interpret the drift density isopleths of Figure 27 as visibility isopleths in the log z–V_{10} coordinate system, an operationally useful result of the Byrd drift project.

This completes the discussion of the basic results derived from the Byrd drift measurements, and we shall now consider quantities derived in turn from these results by height integration, viz. the drift snow content of a vertical column and the drift transport through a vertical plane at right angles to the wind.

5. DRIFT CONTENT AND TRANSPORT—GENERAL

The calculation of the drift content $\Gamma = \int n_s\, dz$ and the drift transport $Q = \int n_s V_s\, dz$ from equations 12 and 16 or 17 appears to be straightforward once the

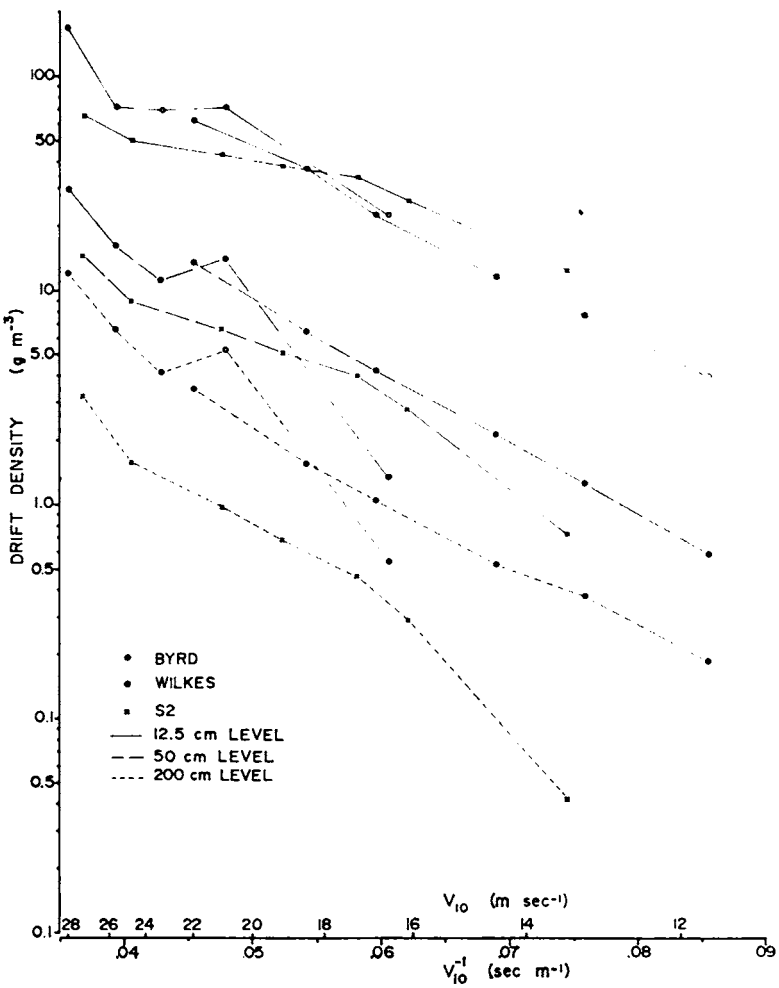

Fig. 25. Comparison of mean drift densities for Byrd, Wilkes, and S2.

limit heights are chosen. Near the snow surface the large variability of the roughness height z_0 (which must be found by extrapolation of the wind profiles, cf. Figure 15) makes z_0 unsuitable as the lower limit; it is preferable to chose instead a constant height near the level where both V_z and n_z have minimum variability. We shall follow *Dingle and Radok* [1961] in placing the lower limit at the 1-mm level and the upper limit at 300 meters (cf. also section 4.13). The main problem arises from the fact that both Γ and Q represent essentially small differences of two large numbers, especially when w_* is close to unity. The discussion of the drift density profiles in section 4.2.1 showed that in general w_* changes with height for a given wind profile. It is therefore inevitable that the values of drift content and transport computed with the assumption of constant fall velocity will be in error. By dividing the total height range from 1 mm to 300 meters into a number of layers with constant w_*, it is possible to approximate the observed density profile to any desired degree of accuracy; yet the accuracy of the computed differences representing drift content and transport will tend to decrease with the size of these layers.

To find the optimum subdivision and to establish the deviations of the observed drift contents and transports from the value predicted by the simple theory of uniform drift, estimates have been computed in a number of different ways. Six sets of averages, each representing 25 drift runs (4 sets) or 15 drift runs (2 sets), taken in order of increasing 10-meter wind velocity (cf. Appendix D), were used. The results of these calculations are shown in Figures 29 and 30.

The curves labeled 'w = const' in Figures 29 and 30 have been computed from equations 12 and 16 with constant w and z_0 equal to the overall means of these parameters for all drift runs ($\bar{w} = 0.257$ m sec^{-1}, $\bar{z}_0 = 0.174$ mm). The remaining curves have been computed using means of the observed values of $w_* = w/ku_*$ and V_{10} for each set of averages; for the sake of consistency the relevant values of z_0 have been determined from the logarithmic wind profile relation as

$$\bar{z}_0 = 10^{-5.76\bar{\Gamma}_{10}/\bar{u}_*} \tag{27}$$

where $5.76 = k \log_e 10$.

The outstanding feature of Figures 29 and 30 is the marked divergence between the uniform drift

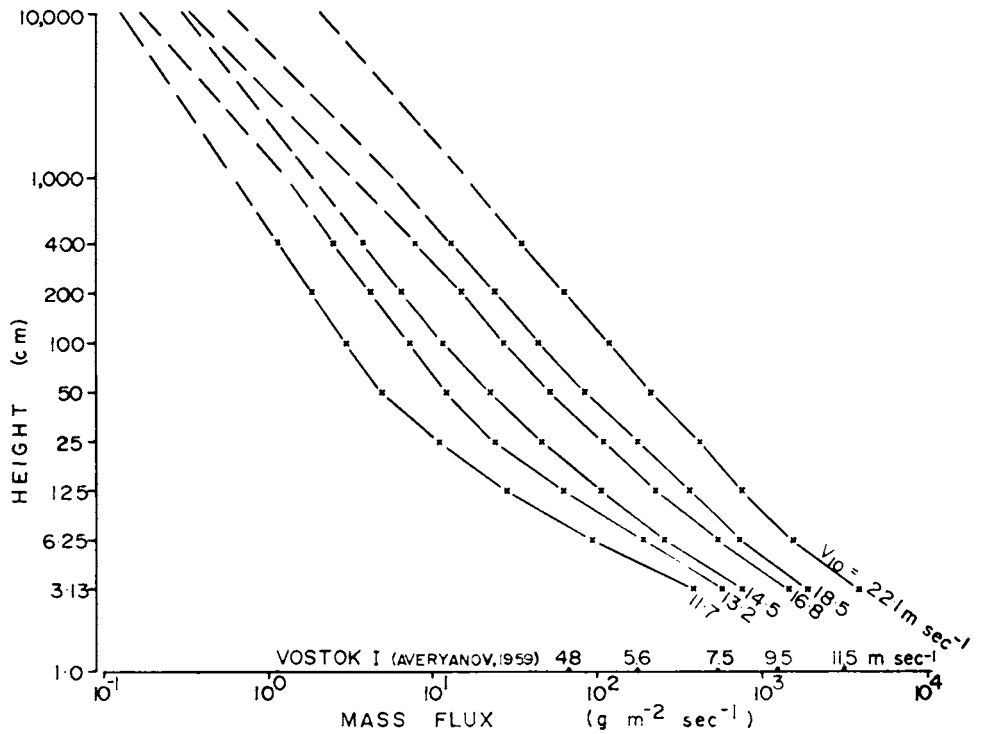

Fig. 26. Mean drift flux F as a function of wind speed for Byrd.

curves and the various approximations to the observed drift content and transport curves. Evidently the comparatively slight deviations of the observed drift density profiles from the straight log n_z versus log z relation, valid for uniform drift, become greatly accentuated in the height integration of both drift density and flux. The uniform drift estimates therefore cannot serve even as first approximation to the true drift contents and transports as function of wind velocity.

The various estimates using observed values of w_* and z_0 differ substantially for low wind velocities but tend to converge for increasing V_{10}, in accordance with simultaneous trend to diminished curvature in the drift density profiles noted in section 4.2.1. Keeping in mind the reduced accuracy expected

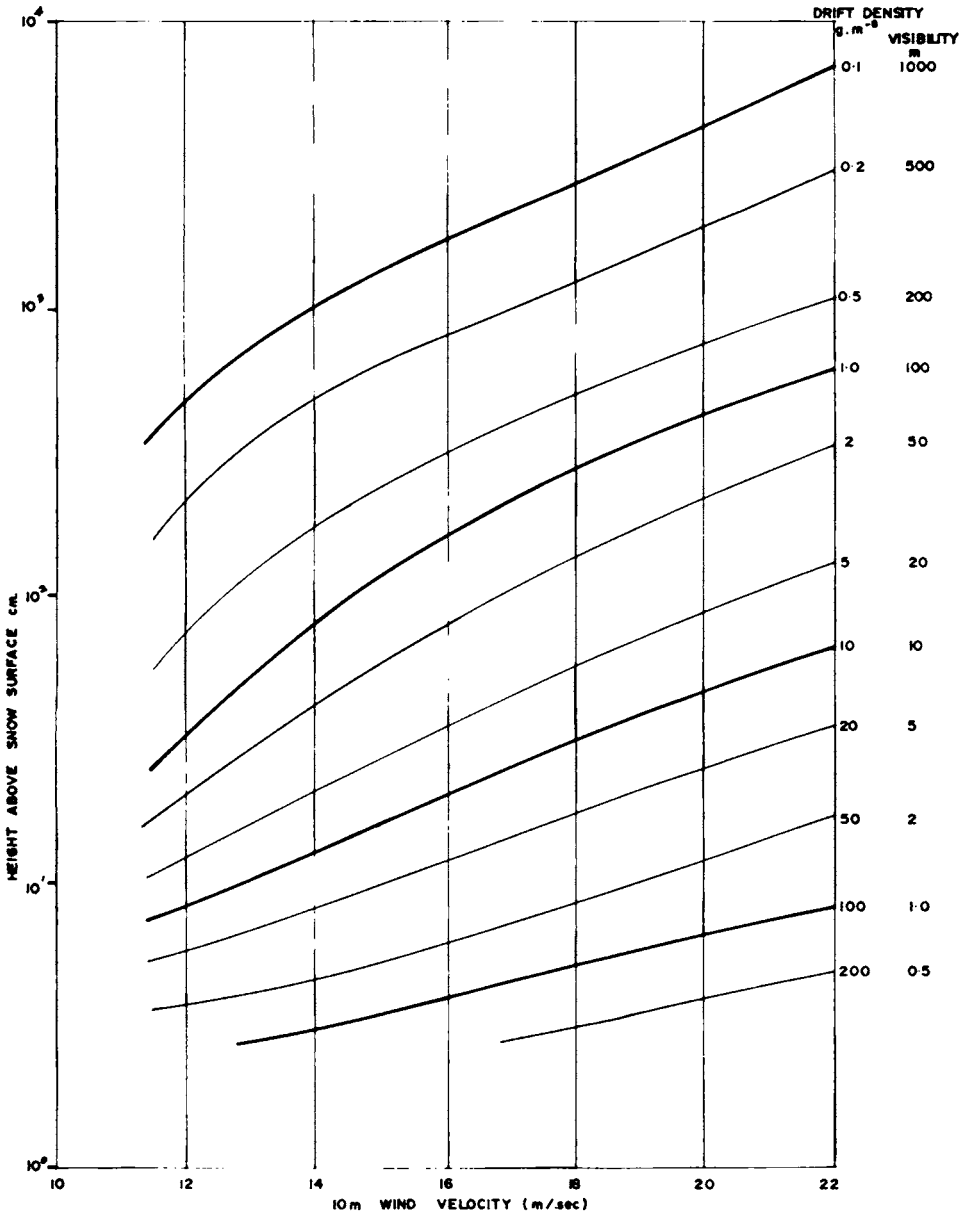

Fig. 27. Drift density and visibility isopleths constructed from the mean drift densities in Figure 19.

for thinner layers, we seem to have little to chose between the four- and six-layer models. Since the calculations for the four-layer model amount to only two-thirds of those involved in the six-layer model, the model dividing the total drift layer into four sublayers has been adopted for the more detailed drift content and transport calculations of section 5.1.

Figure 29 needs little discussion, but attention might be drawn to the isolated drift content estimate for Greenland, marked by a circle; this estimate was obtained by *Loewe* [1933] from observations made by A. Wegener and an intuitive judgment about the efficiency of Wegener's drift snow collecting device. The agreement between this estimate and the values measured for similar wind speeds at Byrd 30 years later has seemed sufficiently impressive to be placed on record here.

Figure 30 contains a number of additional curves requiring discussion. The curve labeled

$$\sum^{8} n_s \bar{V}_s \Delta z$$

has been computed from the products of drift density and wind velocity for the levels of actual drift and wind measurements, the product for the

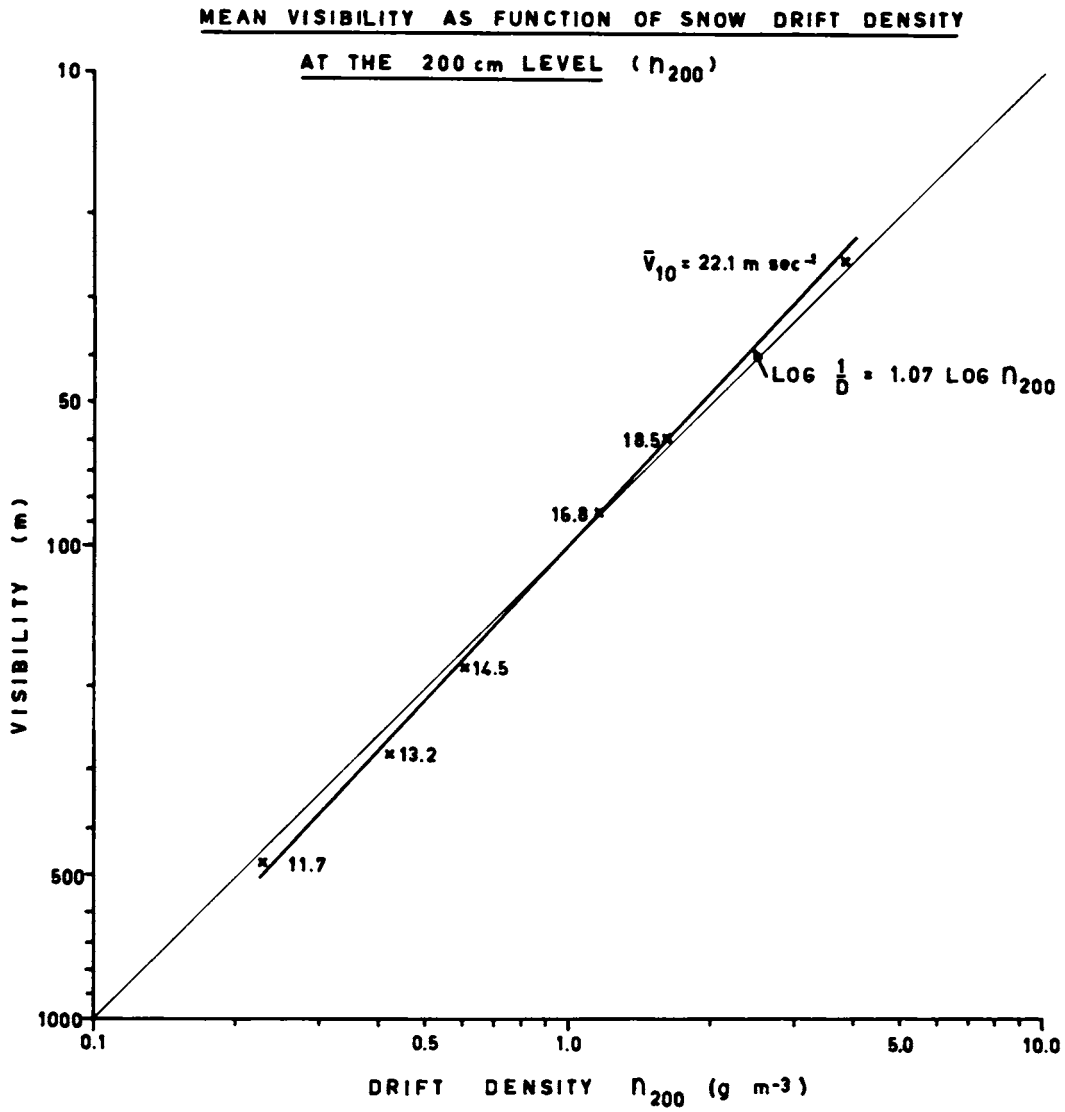

Fig. 28. Dependence of visibility on drift density.

level z_i being interpreted as the average transport for the layer between $(z_i z_{i-1})^{1/2}$ and $(z_i z_{i+1})^{1/2}$. The remainder of the drift layer has been represented by densities and winds extrapolated to the levels $[(4\times 8)^{1/2}\times 300]^{1/2}$ meter and $[(3\frac{1}{8}\times 1\frac{9}{16})^{1/2}\times 0.1]^{1/2}$ cm. Owing to the curvature of the actual drift density profile, this procedure tends to overestimate the transport in each layer. Figure 30 shows the resulting total transport values to be substantially larger than the estimates based on equation 18. This illustrates the danger of computing drift transports directly from the measurements at a few levels.

The curve labeled 'Wilkes model' in Figure 30 has been computed precisely in the manner described by *Dingle and Radok* [1961], who assumed a linear decrease in eddy viscosity from $100ku_*$ at 100 meters to a residual value of $50/\rho$ cm sec^{-2} (ρ = air density) at 300 meters. The resulting drift transport estimates should be strictly comparable with the values found by Dingle and Radok for Wilkes, represented in Figure 30 by their straight line of least squares fit. These curves suggest that the drift transports at Byrd amount to only a fraction of those observed at Wilkes for the same wind velocity. The chief reason for this is to be found in the very small roughness height values used in the Wilkes calculations (cf. section 4.1.1); these values must have markedly increased both the nondimensional fall velocities w_* and the wind velocities in the layer of densest drift below the 10-meter level at Wilkes in comparison with Byrd. We cannot, therefore, draw any firm conclusions from Figure 30 as to the relative magnitude of the drift transports at Byrd and Wilkes without further confirmation of the Wilkes wind profiles. Unpublished wind measurements made at Wilkes in 1960 by H. P. Black at five levels between 860 and 6 cm above the snow surface showed a substantial proportion of curved profiles, which would have suggested excessively small roughness heights unless a more involved evaluation procedure (such as that given by *Dalrymple et al.* [1963]) had been applied. On this limited evidence, then, the Wilkes transport values seem likely to be somewhat inflated.

A more definite comparison of drift snow transports can be made for the layers of actual drift measurements at Byrd and S2 [*Budd*, 1965]. Figure 30 shows the Byrd drift transport in the layer between 400 and 3 cm above the snow surface to be appreciably larger than the corresponding transport at S2. A small part of these differences may have arisen from Budd's use of a constant particle fall velocity for the entire height range, but there remains clear evidence that the snow drift transport at S2 is on the whole less intense, for a given wind velocity, than at Byrd (especially at higher levels; cf. section 4.2.3).

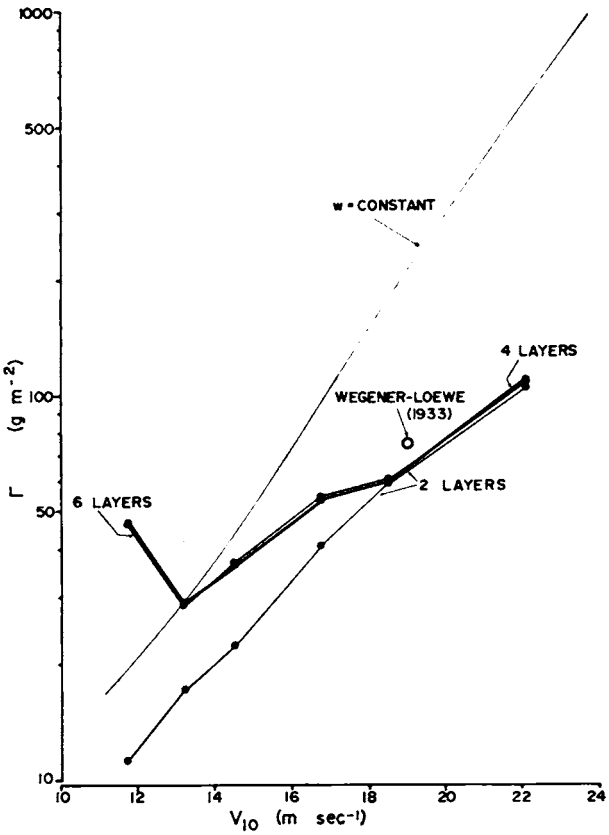

Fig. 29. Comparison of drift content estimates based on equation 12 (thin line) and on different subdivisions of the layer from 1 mm to 300 meters above the snow surface.

For other inland stations, such as South Ice, Charcot, or Vostok I, not enough information has been published for tests of this kind. The drift snow transport estimates of *Lister* [1960] and *Lorius* [1962] have been included in Figure 30 to show that they agree in order of magnitude with the Byrd and S2 estimates for the layer of dense drift near the surface. Lorius' values do in fact refer to such a layer, and the same applies to the curve constructed by means of the semiempirical drift transport formula of D. M. Mel'nik (quoted by *Dyunin* [1954]).

5.1 *Snow Drift Content and Transport as Function of Wind Speed*

In accordance with the conclusions reached in the preceding section detailed drift content and transport estimates have been computed on the basis of the four-layer subdivision, using 26 sets of five-run averages. The results are given in Appendix E separately for each of the four layers used (1 mm to 12.5 cm; 12.5 to 50 cm; 50 to 200 cm; 200 cm to 300 meters) and for the entire drift layer. Figure 31 shows the total transport values on a logarithmic scale plotted against V_{10}, together with a straight regression line of best fit which has the form

$$\log Q_{10\text{-}300} = 1.1812 + 0.0887 V_{10} \qquad (28)$$

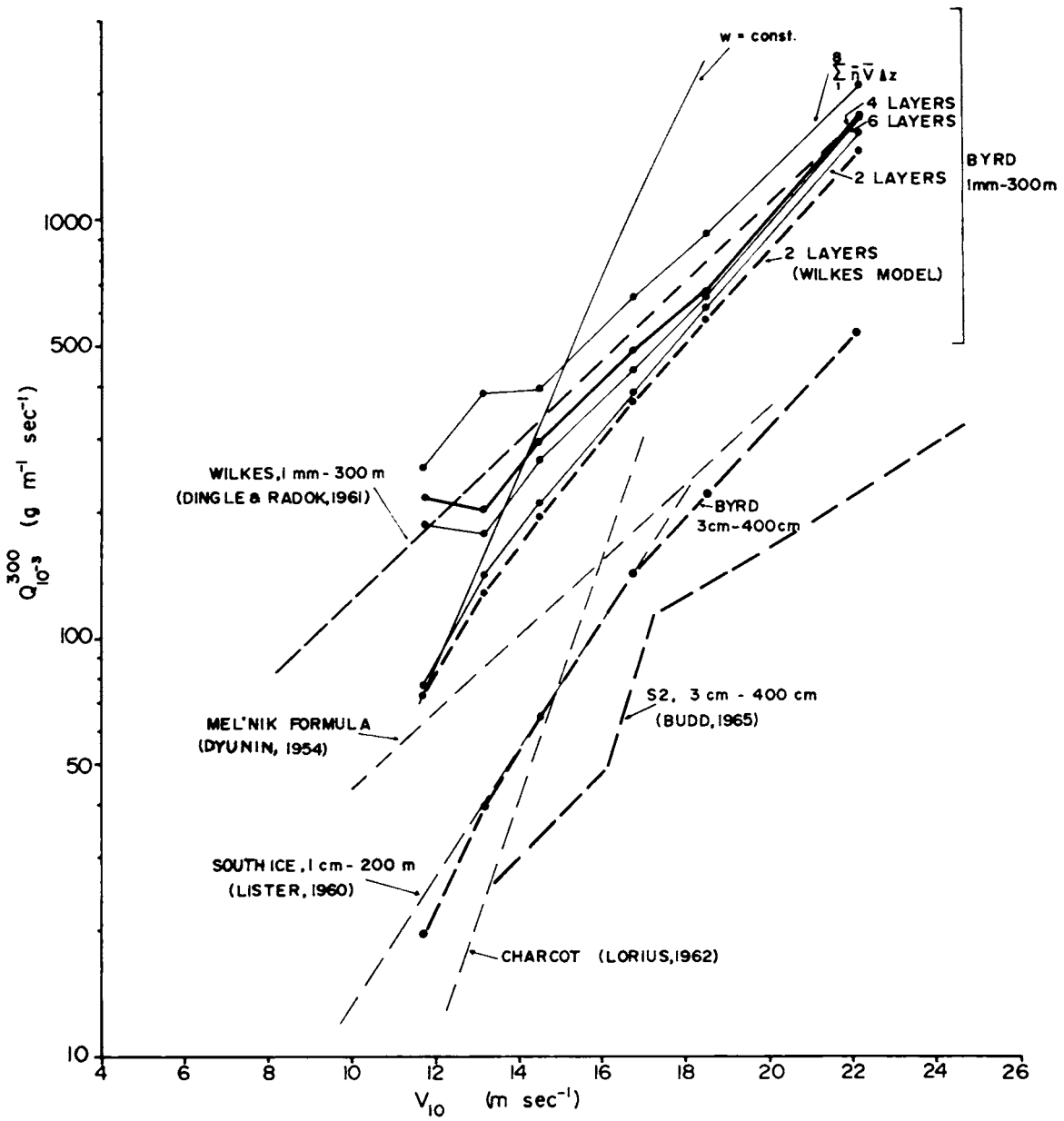

Fig. 30. Comparison of drift snow transport estimates based on equation 16 (thin full curve) and on different subdivisions of the drift layer. For details see text.

The form of this relation is difficult to explain theoretically. An idea of its complex background is provided by Figure 32, which shows the values of $w_* = w/ku_*$ for the different layers used in calculating the transport values of Figure 31. The curves in Figure 32 give the dependence of w_* on wind speed or u_* expected for uniform drift (w = constant). The best approximation to such conditions is seen to exist in the lowest layer, where the equations of section 3 would therefore have their greatest degree of validity; at the highest levels w_* tends to be constant over a substantial part of the wind range, implying a linear change in particle transport with wind velocity. For the total transport the exponential transport versus wind relation equivalent to (28) accounts for just over 90% of the total variance (as compared with 87% for a power law). Although caution is needed outside the wind range covered by the Byrd measurements (9.6 to 24.0 m sec^{-1} at the 10-meter level) relation (28) provides a basis for estimating the total net monthly and annual drift snow transport past Byrd station. As a preliminary for these calculations we consider next the surface wind regime at Byrd.

5.2 *Surface Wind and Frequency of Snow Drift at Byrd*

The available surface wind information for Byrd is summarized in Figure 33 and 34 giving direction and speed histograms for several years including the period of the drift project (March 1, 1962, to February 28, 1963; heavy lines). Although this representation provides no clue to the link between direction and speed, it suffices for the present purpose to state that almost all strong winds at Byrd come from the northern sector, the direction of the

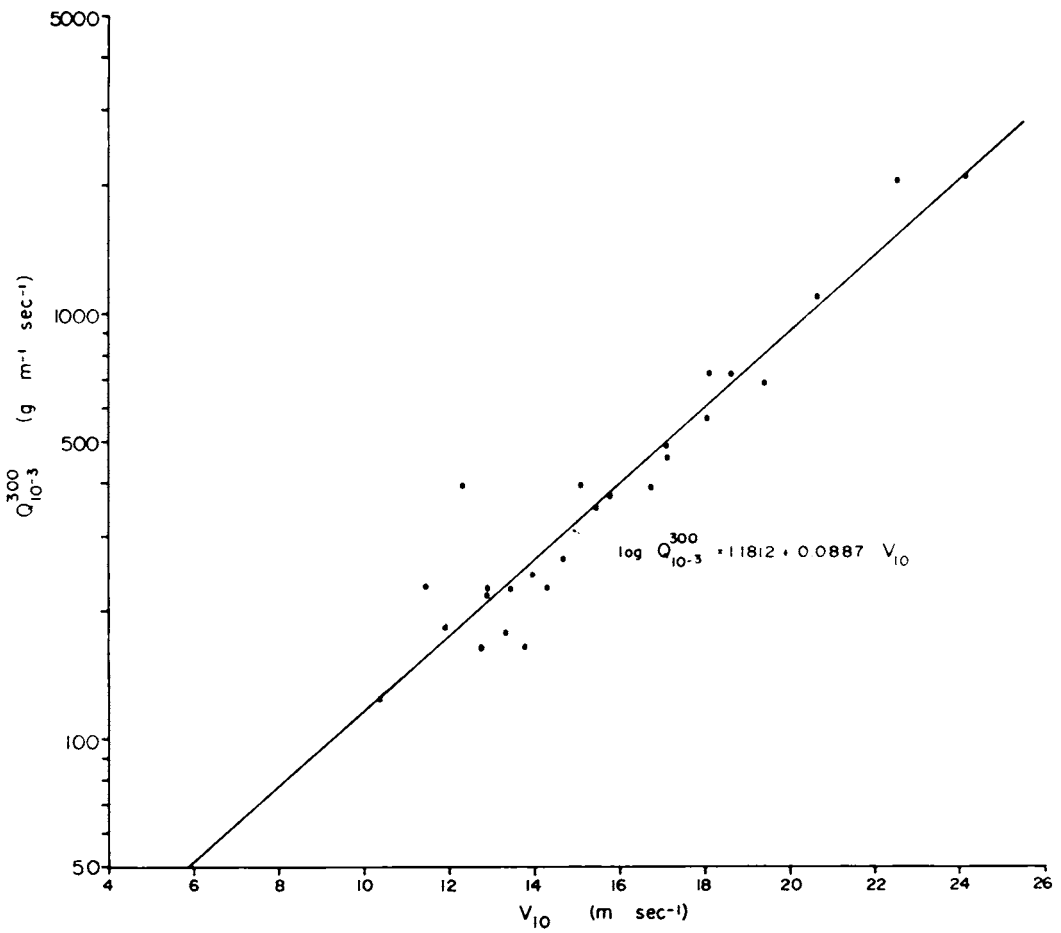

Fig. 31. Snow drift transport in the layer from 1 mm to 300 meters above the snow surface as a function of 10-meters wind speed. Dots are 5-run average transports.

most frequent wind. In calculating the net drift transport, therefore, it is reasonable to consider a vertical surface of unit width (1 km, say) orientated west-east and extending in the vertical from 1 mm to 300 meters above the snow surface.

The wind information for earlier years permits a judgment as to whether the transports computed for 1962–1963 can be regarded as representative. A striking feature of Figure 33 is the steady change to more easterly directions in the predominant wind at the old Byrd station during the three years of its existence. By contrast the first year of observations at the new Byrd station suggested due north as the predominant wind direction. It is tempting to ascribe these differences to the accumulation of drift snow that occurred above the old station and caused its abandonment just before the start of the drift project. The anemometer at old Byrd was located on the western side of the station 'tell,' where a

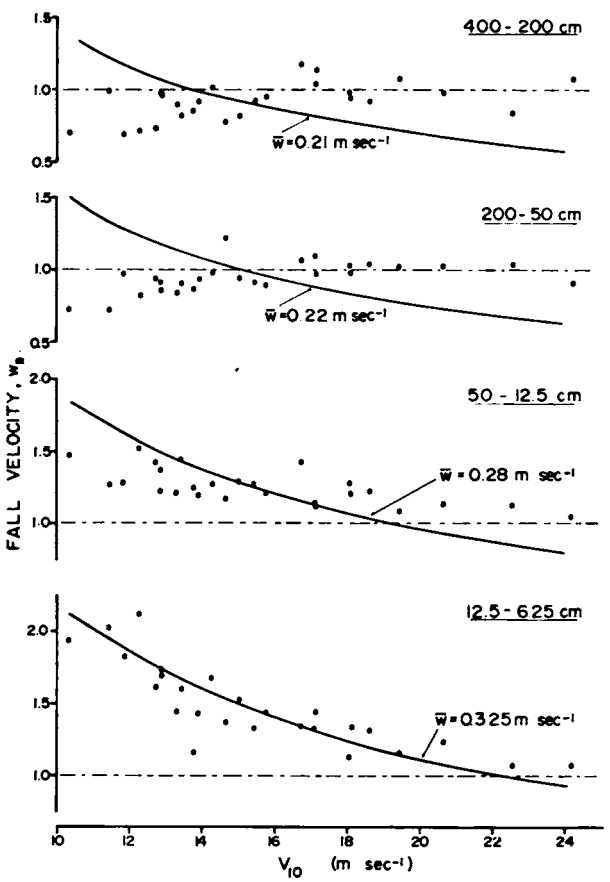

Fig. 32. Average values of $w_s = w/ku_*$ (5 drift runs each) for different layers The curves give the variation expected for constant fall velocity.

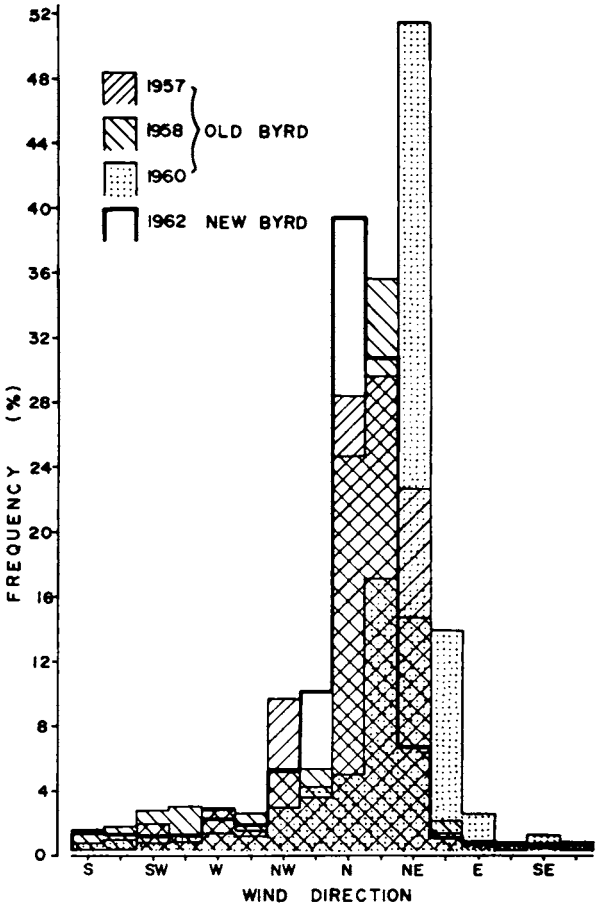

Fig. 33. Surface wind direction statistics for Byrd.

deflection of the wind to a more easterly direction seems reasonable enough. The predominant northerlies at new Byrd on the other hand should be viewed against the large-scale topography of the area, which shows the greatest elevations some 200 km north and east of Byrd, raising again the suggestion of a katabatic element in the blizzard winds at Byrd.

The wind speed histograms suggest that the year of the drift project was reasonably representative of normal conditions, to the extent these are defined by the existing observations, although the number of occasions in the velocity range 20–30 knots was somewhat higher and that of winds between 10 and 20 knots somewhat lower than in previous years. A comparison in terms of snow drift frequency is more difficult since no fully objective criterion exists for distinguishing snow drift from ice fog or precipitation. Table 8 gives the monthly numbers of

snow drift reports (ww = 36–39) at Byrd in 1962–1963, expressed as percentage of the total number of 3-hourly weather reports in each month. Comparative figures for Byrd 1958 and 1959 have been taken from a report by *Herman* [1965], and for a number of Russian stations in East Antarctica from Table 37 in *Rusin* [1961].

Table 8 suggests that September 1962 and the entire summer of 1962–1963 may have had fewer than the normal number of snow drift occasions. However, the annual drift frequencies for the two complete years of record show complete agreement, and there is no reason to doubt that transport figures derived from the 1962–1963 drift measurements are representative for Byrd. As regards other antarctic stations, the USSR values suggest a gradual decline in snow drift toward the center of East Antarctica. The Byrd frequencies fit in somewhere between Pionerskaya (69°44′S, 95°31′E) and Vostok (78°28′S, 106°48′E) and may in fact be not far from average for the entire continent.

5.3 *Monthly and Annual Snow Drift Transports*
Estimates of the net monthly and annual snow drift transports through a vertical east-west plane 1 meter wide and extending from 1 mm to 300 meters above the ice cap surface at Byrd are given in the first line of Table 9. These estimates have been obtained by converting individual 3-hourly wind observations to drift transports by means of equation 28 and multiplying each of these transports by $1.08 \times 10^4 \cos D$, where D is the wind direction and the factor represents the number of seconds in 3 hours. Separate estimates are given for all winds above 10 knots and for occasions when the meteorological observer reported snow drift. The only other monthly values have recently been publishd by *Barkov* [1963] on the basis of measurements at Mirnyy with a 'cyclone' drift trap; these values are also given in Table 9. In addition annual transport estimates for Adélie Coast [*Loewe*, 1956] and Mac. Robertson Land [*Mellor*, 1959], and for the Budd Coast and the S2 satellite station near Wilkes [*Budd*, 1965], are listed in Table 9 together with the average annual drift transport estimated for Byrd.

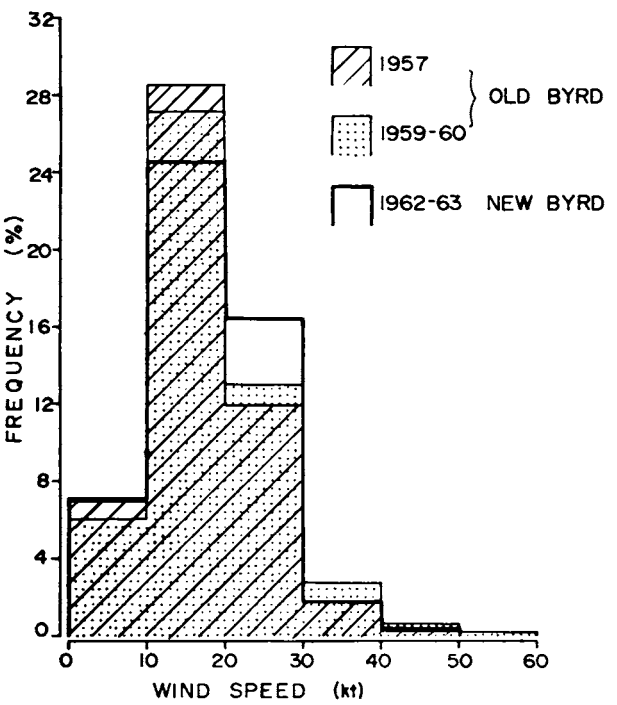

Fig. 34. Surface wind speed statistics for Byrd.

These annual transports provide the clearest comparison. At extremely windy places like Port Martin (annual mean wind 17.8 m sec^{-1}) or Mawson (10.7 m sec^{-1}) the drift transport is an order of magnitude larger than at less windy parts of the coast like Wilkes (5.5 m sec^{-1}) or at inland stations like S2 (10.7 m sec^{-1}) and Byrd (7.6 m sec^{-1}). No corrections have been applied for trap collection efficiency (these should not amount to more than 10% except in the Port Martin estimate, which probably should be doubled to be comparable to the others).

It remains to discuss the significance of the Byrd snow drift transport of at least 2.4×10^9 g m^{-1} year^{-1}. The annual accumulation at Byrd has been estimated at 13.5 cm of water or 1.35×10^5 g m^{-2} [*Mellor*, 1961]. Hence the drift transport is equivalent to the total net accumulation of a belt extending 22 km to the north of Byrd station. A more rational interpretation would be that the drift snow originates in a belt extending part way or all the way to the ridge between the Crary Mountains and the Executive Committee Range some 300 km north of Byrd. If the entire belt contributes to the drift transport at Byrd, its total accumulation must be some 5% larger than its average net accumulation of approximately 20 cm of water. In the lower region between Byrd and the pole the drift transport could be nearer to 10% of the net accumulation. Both figures represent minimum estimates and

TABLE 8. Percentage Frequency of Snow Drift at Byrd and Other Antarctic Stations

	Jan.	Feb.	Mar.	Apr.	May	June	July	Aug.	Sept.	Oct.	Nov.	Dec.	Year
Byrd, 1962–1963	15.3	18.8	13.7	38.3	47.3	18.7	34.5	38.8	7.1	19.4	15.8	17.8	23.8
Byrd, 1958*				20.2	29.0	1.9	16.5	12.6	20.8	24.4	17.2	14.9	
Byrd, 1959*	5.2	16.3	20.7	18.0	23.0	37.9	31.6	42.2	35.4	24.9	23.4	6.6	23.8
Mirnyy, 1957–1960†	12.9	32.0	32.3	56.7	71.2	70.1	83.9	77.6	70.1	55.0	33.3	29.1	52.2
Pionerskaya, 1956–1958†	64.7	63.6	71.2	86.8	77.6	66.7	71.2	77.6	76.7	74.3	66.7	55.0	71.0
Vostok I 1957†	—	—	—	43.3	48.5	53.3	42.0	67.8	36.7	35.5	20.0	···	—
Vostok, 1958–1959†	0	3.6	22.6	10.0	6.5	16.7	22.6	12.9	16.7	12.9	10.0	0	11.3
Sovietskaya, 1958†	—	0	0	6.7	3.2	3.3	3.2	0	6.7	0	3.3	3.2	2.7

* *Herman* [1963].
† *Rusin* [1961].

would have to be increased if the drift transport affected a more limited area.

To put the foregoing into perspective we note that a vertical column of 1 m^2 cross section extending right through the ice at Byrd represents a mass of approximately 2.4×10^9 grams, the same as the minimum annual drift transport, Q_{min}. Hence if v is the ice flow velocity in meters year^{-1}, the mass transport due to ice flow is vQ_{min}, or at least one order of magnitude larger than that due to snow drift. It follows that *Peary*'s [1898] view of snow drift as 'one of the most potent factors in preventing the increase in height of the ice cap' is not sustained by the Byrd results. The evidence presented, however, suggests that snow drift plays a substantial role in equalizing the accumulation of West Antarctica.

6. CONCLUSIONS AND PLANS

The results and conclusions drawn from this first survey of Dingle's snow drift measurements at Byrd can be summarized as follows:

(*a*) *Wind profiles.* No evidence has been found of any significant deviations, in the lowest 4 meters, under snow drift conditions, from the logarithmic wind profile. A slight tendency for the roughness height to increase with wind speed apparently cannot be explained by friction due to the drift snow itself. For a given wind speed the roughness height tends to be larger when the surface consists of smooth soft snow than when it is smooth hard snow; the presence of macrofeatures like dunes and sastrugi appears to produce no significant increase in the roughness height.

At higher levels the wind profile during snow

TABLE 9. Monthly and Annual Snow Drift Transports (10^8 g m^{-1}) at Byrd and Other Antarctic Stations

	Jan.	Feb.	Mar.	Apr.	May	June	July	Aug.	Sept.	Oct.	Nov.	Dec.	Year
Byrd, 1962–1963 (10^{-3}–300 m)	1.19	1.59	1.23	3.82	5.68	3.57	7.25	5.01	2.31	4.52	2.00	1.61	39.77
					All winds ≥ 10 knots								
Occasions of drift	0.46	0.64	0.85	2.43	4.25	1.28	5.45	3.61	0.47	2.54	1.05	0.66	23.69
Mirnyy, 1960 (0–5 m) [*Barkov* 1963]						3.30	4.50	2.23	10.80	6.25			

	Port Martin [*Loewe*, 1956]	Mawson [*Mellor*, 1959]	Wilkes [*Budd*, 1965*a*]	S2 [*Budd*, 1965*a*]	Byrd (Average)
Annual transport estimates	200	200	21	35	32

drift often shows a velocity maximum and a layer of accelerated backing, but there appears to be no strong link between these two features or with the elevated temperature inversion also characteristic of snow drift conditions. The average height of the velocity maximum is 250 meters, so that the upper limit of significant drift may be placed at around 300 meters, the level suggested by direct observations in Adélie Coast and elsewhere.

(*b*) *Snow drift density as function of height.* The vertical profile of drift density n_z deviates significantly from the linear log n_z-log z relationship predicted by the theory of uniform steady-state snow drift. The observed profiles exhibit a steady curvature rather than the abrupt change of slope deduced from more restricted data for Wilkes by *Dingle and Radok* [1961]. The profile curvature decreases with height for a given wind speed and with wind speed in a given layer.

The nature of the snow surface in the immediate surroundings of the drift installation show little relation to the absolute quantity of drift snow in the air, but during periods of net accumulation the drift density is found to be slightly larger near the surface and smaller at levels above 25 cm than during net ablation. Similar minor differences occur in the deviations from the linear log n_z-log z relation, but the same form of curved profile remains in evidence during both net accumulation and net ablation. This eliminates nonsteady drift conditions as principal explanation of the discrepancies between theory and observations.

On the other hand the analysis of drift particle replicas collected on Formvar-coated slides at different levels during snow drift conditions shows a wide range of particle sizes and, presumably, particle fall velocities. The average size tends to decrease with height at a rate which itself decreases with height and wind speed. Similarly, as the wind speed increases, the mean particle size also increases but at a decreasing rate. These effects are partly obscured by a large variability in the over-all average particle size from occasion to occasion, but they suggest strongly that the nonuniformity of drift snow provides the explanation for the deviations of observed density profiles from the linear log n_z-log z form.

(*c*) *Snow drift density as a function of wind speed.* The exponential relation between drift density at a given level and reciprocal wind speed, which should exist according to the theory of uniform steady-state drift if the drift density close to the surface were largely independent of wind speed, is found to be surprisingly well realized. This may be due to the fact that several effects not considered by the theory tend to cancel one another. The practical result is that drift density isopleths can be constructed in a height versus wind velocity coordinate system; these isopleths have an immediate interpretation in terms of visibility in snow drift. At the same time the deviations from the linear log $n_z - V^{-1}$ relationships provide part of the raw material for a study of the effects of meteorological and snow surface conditions on the absolute snow drift density.

(*d*) *Drift content and drift transport as function of wind speed.* In contrast to the simple dependence of drift density at one level on the wind velocity at that level, total drift content and drift transport vary with wind speed in a manner very different from that predicted by the simple drift theory, although the theoretical relation is usable for the layer next to the snow surface, owing to the relative constancy of the size of the particles forming the surface drift. Realistic values of the total drift transport have to be computed separately for a number of layers with approximately constant fall velocity yet of sufficient vertical extent to prevent excessive errors in the transport calculation (which involves small differences of two large numbers). In practice, a subdivision into four layers, with the boundaries, respectively, at 1 mm, 12.5 cm, 50 cm, 2 meters, and 300 meters, is found to be most appropriate.

The drift transports computed in this manner are found to be significantly larger than those measured for similar wind velocities at the Wilkes satellite station S2; they can be represented by a single exponential function of wind velocity, which explains more than 90% of the total scatter, when the calculations are based on averages of sets of five drift runs for similar wind velocities. Although of limited validity, owing to the present imperfect understanding of the upper-wind features, this relation makes it possible to estimate the monthly and annual drift transports at Byrd, which according to the available information on wind direction frequencies are all directed toward the pole. The annual drift transport in the layer from 1 mm to 300 meters above the snow surface is between 2.4×10^9

and 4.0×10^9 g m^{-1} and bears a reasonable relation to estimates published for other antarctic stations.

These results raise a number of other questions which will have to be answered by further analysis of the Byrd material and possibly by additional measurements. The most immediate need is for a theory of nonuniform steady-state snow drift; such a theory has already been formulated by *Budd* [1965*b*] and is presented elsewhere in this volume. Other investigations will cover the following aspects:

1. Wind profiles in the lowest kilometer above the ice cap as a katabatic wind problem.
2. Detailed analysis of the complete accumulation data and of the precision obtainable with the Wilm type accumulation network.
3. Dependence of drift particle size and shape distributions, drift density, and drift content on contemporary and previous meteorological and snow surface conditions.

This list shows that the present paper has made no more than a beginning with the evaluation of the data obtained during the Byrd snow drift project. At the same time we hope that Peary's opinion prefacing the paper has been provided some support by the results here described.

Acknowledgments. It is impossible to acknowledge in detail all the help given to the Byrd snow drift project; a few names must suffice. The initial step toward the project was taken by the late Dr. H. Wexler at the suggestion of E. Vollprecht and W. J. Gibbs. Preparations received constant support from M. J. Rubin in the United States and at various stages from D. J. Williams, H. P. Black, Diane Lemair, R. Griess, and T. Pound in Australia, and from P. A. Shumskiy in the U.S.S.R. E. E. Goodale saw to it that the equipment reached Byrd on time and made many subsequent arrangements, especially in connection with the rocket wind program which could not have been conducted without the extensive help of M. Mellor and his SIPRE colleagues or that of the Australian Weapons Research Establishment and the Royal New Zealand Air Force. For the evaluation of the data we had the help of P. J. Morgan, Judith Martin, Joyce Poppins, Ruth Chalmers, and various students of the Meteorology Department in the University of Melbourne. Finally, Dingle's thanks go to the Director of Meteorology for leave to carry out the work at Byrd; and Budd's, to the Director of the Antarctic Division for permission to contribute to this paper.

The Byrd drift project was made possible by a grant from the U. S. Weather Bureau to the University of Melbourne, as part of a research project supported by the National Science Foundation.

REFERENCES

Andrée, S. A., Sur le chasse-neige dans les régions arctiques, *Arch. Sci. Phys. Nat., Genève, 15,* 523–533, 1886.

Averyanov, V. G., Dinamika snezhnogo pokrova na stantsii Vostok I (Snow cover dynamics at station Vostok I), *Inform. Bull. Soviet Antarctic Expeditions,* no. 6, 19–26, 1959.

Bagnold, R. A., *The Physics of Blown Sand and Desert Dunes,* Methuen and Company, London, 1941.

Barkov, N. I., Metelemernaya ustanovka 'tsiklon' i opyt raboty s nei v observatorii Mirnyy (The 'cyclone' snow trap and experience with it at Mirnyy Observatory), *Inform. Bull. Soviet Antarctic Expeditions, 42,* 51–55, 1963.

Barré, M., *Propriétés électriques du blizzard,* Expédition Polaire Française, Paris, 1954.

Black, H. P., and W. F. Budd, Accumulation in the region of Wilkes, Wilkes Land, Antarctica, *J. Glaciol. 5*(37), 3–16, 1964.

Budd, W. F., M. Sc. thesis, unpublished, 1965 (published as *ANARE Publ. 88,* 1966).

Budd, W. F., The drifting of nonuniform snow, *this volume,* 1966.

Cooke, T. H., A smoke-trail technique for measuring wind, *Quart. J. Roy. Meteorol. Soc., 88,* 83–88, 1962.

Dalrymple, P. C., H. H. Lettau, and Sarah H. Wollaston, South pole meteorology program: Data analysis, *this volume,* 1966.

Dingle, W. R. J., and U. Radok, Antarctic snow drift and mass transport, *Intern. Assoc. Sci. Hydrology Publ. 55,* 77–87, 1961.

Dyunin, A. K., Solid flux of snow-bearing air flow, *Trudy Transportno-Energicheskogo Instituta, 4,* 71–88, Tech. Transl. 1102, NRC, Canada, 1954.

Dyunin, A. K., Fundamentals of the theory of snow drifting, *Izv. Sibirsk. Otdel. Akad. Nauk SSSR 12,* 11–24, Tech. Transl. 952, NRC, Canada, 1959.

Garcia, R., Mesures du transport de neige par le vent à la Station Charcot, *La Météorologie, 57,* janvier–mars, 1960.

Gill, G. C., E. W. Bierly, and J. N. Kerawalla, An inexpensive rocket technique for obtaining low level wind profiles, *J. Appl. Meteorol., 2,* 457–462, 1963.

Govorukha, L. S., and E. F. Kirpichev, Pervye rezultaty metelemernykh nablyudenii s pomoshtsh'yu metelemera 'tsiklon' (First results of snow drift measurements with the 'cyclone' snow trap), *Inf. Bull. Soviet Antarctic Expeditions, 26,* 22–25, 1961.

Herman, J. R., Precipitation static and electrical properties of blowing snow at Byrd station, Antarctica, *Geomagnetism and Aeronomy, Antarctic Research Series, 4,* pp. 221–236, American Geophysical Union, Washington, D.C., 1965.

Jenssen, M. J. D., Ph.D. thesis, unpublished, 1964.

Kotlyakov, V. M., Snezhnyi pokrov Antarktidy i ego rol' v sovremennom oledenii materika (The snow cover in the Antarctic and its role in the modern glaciation of the continent), *Results of the IGY, Glaciology, 7,* Akademiya Nauk, Moscow, 1961.

Landon Smith, I. H., M. Sc. thesis, unpublished, 1964.

Landon Smith, I. H., and B. Woodberry, The photoelectric metering of wind-blown snow, *Interim Report, Series A (IV), Glaciology, Publ. 79,* 18 pp., Antarctic Division, Department External Affairs, Melbourne, 1965.

Lettau, H. H., Preliminary note on the theory of steady katabatic flow for height-dependent eddy diffusivity, *Ann. Rept. Dept. Meteorol., Univ. Wisconsin,* 139–149, 1963.

Liljequist, G., Energy exchange of an antarctic snow field, *Norwegian-British-Swedish Antarctic Expeditions 1949–1952, Sci. Res., 2,* part 1c, 1957.

Lister, H., Glaciology (1): The balance sheet *or* the mass balance, in *Venture to the Arctic,* pp. 179–180. Pelican Book no. A432, 1958.

Lister, H., Glaciology (1): Solid precipitation and drift snow, *Trans-Antarctic Expedition 1955–1958, Sci. Rept. 5,* 1960.

Loewe, F., Die Bedeutung des Schneefegens für den Massenhaushalt von Inlandeisen, *Meteorol. Z., 50,* 434–436, 1933.

Loewe, F., *Études de Glaciologie en Terre Adélie, 1951–1952,* Hermann, Paris, 1956.

Lorius, C., Contributions to the knowledge of the antarctic ice sheet: a synthesis of glaciological measurements in Terre Adélie, *J. Glaciol., 4*(31), 79–92, 1962.

Mellor, M., Mass balance studies in Antarctica, *J. Glaciol., 3*(26), 522–533, 1959.

Mellor, M., Gauging antarctic drift snow, in *Antarctic Meteorology,* pp. 347–354, Pergamon Press, Oxford, 1960.

Mellor, M., The antarctic ice sheet, *Cold Regions Science and Engineering, I-Bl,* U.S. CRREL, 1961.

Mellor, M., and U. Radok, Some properties of drifting snow, in *Antarctic Meteorology,* pp. 333–346, Pergamon Press, Oxford, 1960.

Peary, E. A., Journey in north Greenland, *Geograph. J. 11,* 213–240, 1898.

Pound, T. N., Calibration of snow gauges, *Tech. Mem. 139, Aero. Res. Labs.,* Melbourne, 1958.

Prandtl, L., Bericht über Untersuchungen zur ausgebildeten Turbulenz, *Z. Angew. Math. Mech., 5,* 136–139, 1925.

Prudhomme, A., and A. H. Boujon, Sur les tempêtes observées en Terre Adélie, *La Météorologie, 31,* juillet–septembre, 1952.

Rusin, N. P., Gorizontal'nyi perenos snega v Antarktide (Horizontal snow transport in Antarctica), *Tr. Gl. Geofiz. Observ. Vyp., 96,* 1959.

Rusin, N. P., *Meteorologicheskii i radiatzionnyi rezhim Antarktidy* (Meteorological and radiation regime of Antarctica), Gidrometeorologicheskoe Izdatel'stvo, Leningrad, 1961.

Schaefer, V. J., Preparation of snow particle replicas, *Nature, 149,* 81, 1942.

Shiotani, M., and H. Arai, A short note on the snow storm, *Cong. Appl. Mech.,* Science Council of Japan, 1953.

Strom, G. H., G. R. Kelly, E. L. Keitz, and R. F. Weiss, Scale model studies on snow drifting, *U. S. Army Snow, Ice and Permafrost Establishment Res. Rept. 73,* 1962.

Wexler, H., Growth and thermal structure of the deep ice in Byrd Land, Antarctica, *J. Glaciol., 3,*(30), 1075–1087, 1961.

Wilm, H. G., The design and analysis of methods for sampling micro climatic factors, *J. Am. Statist. Assoc., 41,* 221–232, 1946.

APPENDIX A. General Information on Snow Drift Runs, Byrd, 1962

No. of Run	Date	Time		Temperatures, −°C		Wind Direction, deg	Wind Speed, m sec^{-1}	Drift Run Average Speed (10 m), m sec^{-1}	Remarks
		Start	Finish	Air (100 cm)	Snow				
1	3/23	0815	1005	25.3		030	13	11.07	Generally hard packed with smooth even surface.
2	3/26	0950	1050	31.4		360	13.5	12.97	Relatively hard packed snow with tendency for ripple formations to windward of exposure mast. Low-level collectors exposed on flat smooth surface.
3	3/26	1425	1525	27.1		360	13	13.39	Hard packed snow with smooth flat surface except where occasional barchan formations developing to windward of mast.
4	3/26	1900	2005	26.7		360	16	15.02	Hard packed snow with smooth flat surface.
5	4/3	1045	1145	42.8		030	12.5	11.17	Generally hard packed snow with several large barchans scattered throughout snow transport area. One barchan immediately below collectors and exposure heights for collectors listed against measured weights.

APPENDIX A. *(Continued)*

No. of Run	Date	Time		Temperatures, −°C		Wind Direction, deg	Wind Speed, m sec^{-1}	Drift Run Average Speed (10 m), m sec^{-1}	Remarks
		Start	Finish	Air (100 cm)	Snow				
6	4/3	1550	1650	42.3		030	12.5	11.93	Generally hard packed snow; barchans still evident in snow transport area with previous monster located below collectors some 5 feet downwind of mast. Surface snow generally rough upwind of mast.
7	4/6	0940	1120	28.4		030	10	9.60	Generally hard packed snow with saw tooth formations in previous barchan localities. Soft snow in immediate vicinity of mast, which necessitated raising mast during run.
8	4/6	1458	1558	28.1		040	18	16.54	Generally hard packed with most barchan formations dispersing, leaving surface more or less flat.
9	4/7	0953	1058	32.2		030	11.5	10.19	Generally hard packed snow with relatively smooth surface. Raised footprints to windward of mast leveled down to surrounding surface before start of run.
10	4/7	1445	1545	29.9		030	13	11.64	Generally hard packed with good even surface.
11	4/10	0938	1038	36.1		020	12.5	11.31	Hard packed snow with barchan formations developing to windward of mast (nearest approximately 50 yards north).
12	4/12	1135	1335	26.3		030	11	9.78	Hard packed snow with good even surface.
13	4/12	1435	1635	26.4	28.1	030	13	12.08	Hard packed snow; good even surface.
14	4/13	1621	1721	26.3	28.6	030	14.3	12.41	Hard packed snow with barchan formations developing.
15	4/19	1003	1133	38.6	36.0	020	15	12.56	Hard packed snow; good even surface.
16	4/19	1615	1700	31.1	34.8	020	13	12.56	Hard packed snow with good even surface.
17	4/19	2045	2135	32.2	34.2	020	15	13.40	Hard packed snow with good even surface.
18	4/20	0210	0310	32.0	33.9	020	14.5	13.80	Hard packed snow with good even surface.
19	4/20	1055	1135	24.0	30.3	040	19.0	17.98	Hard packed snow with good even surface.
20	4/20	1450	1520	23.4	29.1	040	21.5	20.17	Hard packed snow with raised footprints on surface.
21	4/30	1012	1112	33.9	37.8	360	15.0	14.17	Hard packed snow with good even surface.
22	4/30	1453	1553	28.8	34.9	360	15.0	14.05	Hard packed snow with good even surface.
23	4/30	2210	2310	29.1	33.8	360	15.5	13.62	Hard packed snow with good even surface.

APPENDIX A. *(Continued)*

No. of Run	Date	Time Start	Time Finish	Temperatures, −°C Air (100 cm)	Temperatures, −°C Snow	Wind Direction, deg	Wind Speed, m sec^{-1}	Drift Run Average Speed (10 m), m sec^{-1}	Remarks
24	5/1	0520	0620	24.1	30.3	340	15	14.45	Hard packed snow with good even surface.
25	5/1	1925	2025	22.2	27.7	360	13.5	12.41	Hard packed snow with good even surface.
26	5/1	2340	0040	23.1	27.7	340	14.5	14.31	Hard packed snow with good even surface.
27	5/3	1500	1600	23.9	25.1	040	13.5	11.94	Soft snow overlying hard packed surface.
28	5/3	2010	2100	23.1	25.5	030	16.5	17.35	Generally hard packed with patches of soft snow to windward of exposure site; good even surface.
29	5/4	2003	2103	20.6	23.6	030	13.5	14.03	Generally hard packed with light covering of new snow.
30	5/14	2020	2120	19.6	25.6	030	14.5	13.93	Patches of soft snow overlying the usual hard surface; area immediately upwind of mast sporting soft snow approximately 3 cm in depth.
31	5/15	0045	0245	23.2	25.7	030	15.0	13.28	Moderately soft crust covering soft snow 50% with generally hard packed snow covering remaining 50%. Ripple formations in occasional soft patches.
32	5/15	1931	2031	28.3	27.1	010	12.5	12.70	Moderately soft crust covering relatively new snow with ripple pattern on shallow dune formations; hard packed snow covering remaining 50% of area in vicinity of exposure mast.
33	5/16	0004	0134	28.2	27.9	360	11.0	11.82	Patches of soft snow overlying usual hard packed surface; area upwind of exposure mast slightly disturbed.
34	5/16	2040	2140	33.2	31.1	360	13.5	12.26	Patches of soft snow overlying usual hard packed surface; some barchan formations in area.
35	5/16	2345	0115	35.4	31.7	360	12.0	12.29	Generally hard packed with patches of soft snow.
36	5/21	1443	1543	28.3	31.1	030	16.0	15.29	Hard packed with patches of soft snow.
37	5/21	1930	2030	28.7	31.7	030	15.5	16.01	Patches of soft snow overlying customary hard packed surface; surface generally level in snow transport zone.
38	5/21	2355	0155	32.2	32.3	020	12.0	14.57	Hard packed snow with few patches of soft snow; good even surface.
39	5/25	0920	1020	39.0	36.7	020	14.0	14.07	Generally hard packed snow with isolated patches of soft snow; surface in immediate vicinity of mast slightly disturbed.

APPENDIX A. *(Continued)*

No. of Run	Date	Time		Temperatures, −°C		Wind Direction, deg	Wind Speed, m sec^{-1}	Drift Run Average Speed (10 m), m sec^{-1}	Remarks
		Start	Finish	Air (100 cm)	Snow				
40	5/25	1402	1532	31.1	35.0	040	12.5	13.46	Generally hard packed with patches of soft snow; surface in immediate vicinity of mast slightly disturbed.
41	5/25	1930	2030	27.7	33.5	040	17.5	18.02	Slight amount of soft snow overlying usual hard packed surface; tendency for soft snow to accumulate in shallow dunes.
42	5/26	0430	0500	23.4	31.7	040	21	22.43	Fair amount of soft snow overlying hard packed surface; surface relatively flat in snow transport zone.
43	5/26	0840	0900	23.8	31.0	030	21	22.88	Considerable amount of soft snow overlying hard packed surface; surface generally flat in snow transport zone.
44	5/28	1450	1630	16.1	29.9	020	14.5	13.58	Soft snow overlying hard surface; some shallow dunes in snow transport zone.
45	5/28	1935	2020	15.0	29.4	360	19.0	19.46	Numerous patches of soft snow with tendency toward wave formations upwind of mast.
46	5/29	0115	0215	16.6	28.0	030	14.0	12.68	Extensive areas of soft snow with good even surface. Slight ridge 20 yards upwind of mast.
47	5/31	0935	1135	26.1	27.9	030	12.5	12.77	Pronounced ridge upwind of mast.
48	6/5	1025	1125	25.9	32.1	030	15.0	14.89	Fresh NE breeze for the past 3 days has given the surface a good hard crust; somewhat disturbed in patches with ridges and wave formations.
49	6/5	1435	1505	25.7	31.5	030	13.0	12.96	Generally hard packed with patches of soft snow.
50	6/14	2300	0100	36.6	35.1	030	12.0	11.64	Generally hard packed with good level surface.
51	6/15	1000	1100	31.2	35.1	040	12.0	13.84	Shallow layer of soft snow overlying the usual hard packed surface.
52	6/21	2025	2225	40.0	39.4	030	15.0	14.03	Soft snow overlying hard packed; no obvious crust to soft snow; some ripples at right angles to wind.
53	6/22	0055	0255	38.6	39.3	030	11.0	11.21	Soft snow overlying hard packed; good even surface.
54	6/23	1908	2108	48.9	39.4	030	12.5	13.66	Mostly soft snow overlying hard packed; soft snow generally rippled in appearance.
55	6/24	0010	0210	46.1	40.4	030	13.0	12.19	Soft snow overlying hard packed; good even surface.
56	6/28	0955	1125	40.6	42.7	035	13.0	13.62	Generally hard packed snow with slightly roughened surface.

APPENDIX A. *(Continued)*

No. of Run	Date	Time		Temperatures, −°C		Wind Direction, deg	Wind Speed, m sec^{-1}	Drift Run Average Speed (10 m), m sec^{-1}	Remarks
		Start	Finish	Air (100 cm)	Snow				
57	6/28	1450	1620	39.8	41.8	020	14.5	14.41	Generally hard packed surface; slightly roughened.
58	6/28	2005	2105	38.3	41.5	030	16.0	15.86	Fair amount of soft snow overlying hard packed; surface slightly disturbed.
59	6/30	0530	0630	28.8	40.5	030	17.0	15.60	Fair amount of soft snow overlying hard packed; good even surface.
60	6/30	0945	1045	28.9	40.1	030	19.5	17.72	Fair amount of soft snow overlying hard packed; good level surface.
61	6/30	1520	1620	31.8	39.0	010	17.5	14.29	Soft snow overlying hard packed; good even surface.
62	7/2	0925	0955	22.8	36.7	035	18.5	15.77	Fair amount of soft snow in shallow dunes; surface generally level in undisturbed areas.
63	7/3	1426	1446	24.1	33.4	035	21.0	19.66	Snow transport zone sporting several shallow dunes of soft snow. Three low level collectors exposed on hard surface.
64	7/2	1845	1935	22.3	35.7	030	19.0	18.39	Fairly general coverage of soft snow; some shallow dunes in snow transport zone.
65	7/3	1002	1102	19.6	34.3	030	16.5	16.94	Patches of soft snow scattered throughout area; surface generally flat except for occasional shallow dunes.
66	7/3	1510	1640	25.8	33.3	010	13.5	14.07	Patches of soft snow advancing downwind; surface generally flat.
67	7/8	1440	1610	31.5	33.9	360	14.5	14.66	Generally soft snow with shallow dunes with superimposed rippled surfaces ··· 20% of surface appears to be usual hard packed snow with undisturbed crust.
68	7/16	0940	1040	41.2	36.7	020	18.5	17.48	Patches of soft snow overlying hard packed snow; some shallow dunes; surface fair to medium.
69	7/16	1400	1430	33.8	37.2	020	23.0	20.95	Shallow dunes of soft snow overlying usual hard packed surface snow; approximately 30% of area supporting hard packed snow; surface moderately flat.
70	7/16	1700	1720	33.9	37.2	015	27.0	23.94	Generally hard packed with occasional shallow dunes in snow transport zone ··· main build-up of dunes appears to be between cold room and main station.
71	7/17	0425	0455	31.3	36.5	015	22.5	22.20	Generally hard packed snow with occasional shallow dunes. Surface moderately flat.

APPENDIX A. *(Continued)*

No. of Run	Date	Time		Temperatures, −°C		Wind Direction, deg	Wind Speed, m sec^{-1}	Drift Run Average Speed (10 m), m sec^{-1}	Remarks
		Start	Finish	Air (100 cm)	Snow				
72	7/17	0926	0956	29.8	36.2	015	18.5	17.11	Generally hard packed snow with some shallow dunes of soft snow; surface moderately flat.
73	7/18	2250	2350	43.3	36.8	030	16.5	15.69	Generally hard packed with a few shallow dunes; surface slightly disturbed with isolated ridges.
74	7/19	1008	1108	37.3	37.3	020	13.5	13.12	Shallow dunes of soft snow developing after earlier precipitation period; hard packed snow covering approximately 40% of area; surface moderately flat.
75	7/20	0945	1025	35.7	37.2	030	19.5	18.20	Patches of soft snow overlying hard packed surface; surface moderately disturbed.
76	7/20	1410	1510	35.6	36.8	030	17.0	17.92	Numerous dunes of soft snow throughout area; low level collectors withdrawn due to rapidly changing surface conditions; difficult to locate the customary hard packed surface peculiar to winter season in this area.
77	7/20	1730	1800	38.3	36.6	030	15.5	16.78	Generally rough with numerous dunes and patches of soft snow.
78	7/21	1000	1100	38.3	36.7	030	17.5	15.57	Somewhat disturbed with several large dunes midst patches of soft snow.
79	7/21	1335	1435	37.8	36.7	025	17.5	16.56	Somewhat disturbed with several large dunes midst patches of soft snow.
80	7/21	1610	1725	37.4	36.6	025	14.0	13.84	Somewhat disturbed with sevveral dunes of soft snow overlying the customary hard packed surface.
81	7/22	1130	1210	35.1	37.2	030	22.0	20.96	Generally hard packed snow in vicinity of mast (several dunes downwind of cold room); surface relatively flat in snow transport zone.
82	7/22	1533	1553	33.7	36.7	025	23.0	23.51	Observations somewhat restricted due to poor visibility; however generally hard packed snow with most of the snow downwind of the snow transport zone; surface relatively flat.
83	7/24	1400	1500	31.4	36.4	360	17.5	18.42	Relatively hard packed with fair to good surface ··· this is mostly new snow with sand-like texture on surface.

APPENDIX A. *(Continued)*

No. of Run	Date	Time		Temperatures, −°C		Wind Direction, deg	Wind Speed, m sec^{-1}	Drift Run Average Speed (10 m), m sec^{-1}	Remarks
		Start	Finish	Air (100 cm)	Snow				
84	7/24	1628	1728	31.4	36.6	360	18.5	18.42	Mostly new snow but well compacted and leveled off ··· no indication of shallow dunes which featured so prominently a few days ago.
85	7/25	0950	1050	29.2	36.1	005	20.0	17.76	Moderately hard packed (new snow) with relatively good level surface.
86	7/27	1350	1650	31.8	34.6	360	12.0	11.60	Generally hard packed snow with fair to good level surface.
87	7/30	1126	1226	22.8	33.5	360	13.5	13.96	Generally hard packed snow in transport zone; some shallow dunes downwind of cold room.
88	8/5	2245	0045	41.1	41.6	010	14.5	12.90	Generally hard packed with a few shallow dunes of soft snow. Surface moderate to good.
89	8/6	0515	0645	39.9	41.2	010	15.0	12.85	Generally hard packed with a few shallow dunes of soft snow; surface moderate to good.
90	8/6	0935	1105	38.3	41.2	020	14.0	12.84	Generally hard packed with a few shallow dunes of soft snow; surface moderate to good.
91	8/6	1455	1555	30.6	40.6	010	15.5	13.81	Generally hard packed with a few shallow dunes of soft snow; area in immediate vicinity of mast hard packed and relatively undisturbed.
92	8/7	1000	1130	33.4	39.2	360	13.0	12.75	Generally hard packed with fair surface; some shallow dunes of soft snow in area (but not in immediate vicinity of exposure mast).
93	8/10	0940	1040	29.3	37.8	010	19.0	16.02	Generally hard packed snow with good even surface.
94	8/10	1440	1540	29.4	36.9	015	14.5	13.21	Generally hard packed snow with good surface.
95	8/12	0910	1010	29.3	37.1	360	20.5	18.21	Generally hard packed snow with good surface.
96	8/12	1310	1340	28.3	36.9	010	22.0	22.13	Hard surface with good level crust.
97	8/12	1545	1605	27.2	36.2	360	23.5	24.02	Hard surface with good level crust.
98	8/13	0950	1010	24.6	35.6	015	22.0	22.62	Generally hard packed with good surface.
99	8/13	1410	1440	23.9	35.3	360	18.5	19.11	Generally hard packed with good surface.
100	8/13	1603	1648	24.2	35.0	360	17.0	16.58	Generally hard packed snow with good surface.
101	8/15	0938	1108	30.6	33.4	360	14.0	14.23	Generally hard packed snow with good surface.
102	8/17	1405	1505	21.9	33.8	360	19.5	17.20	Generally hard packed snow with good surface ··· static generally below 12.5 cm.

APPENDIX A. *(Continued)*

No. of Run	Date	Time		Temperatures, −°C		Wind Direction, deg	Wind Speed, m sec^{-1}	Drift Run Average Speed (10 m), m sec^{-1}	Remarks
		Start	Finish	Air (100 cm)	Snow				
103	8/17	1628	1728	23.3	33.9	360	18.5	18.80	Generally hard packed snow with good surface ··· heavy drift near surface ··· . Static below 12.5 cm.
104	8/22	2310	0010	27.5	34.2	015	14.5	15.01	Generally hard packed and relatively flat; some shallow dunes forming in snow transport zone.
105	8/23	0545	0630	25.7	34.4	020	19.0	18.57	Generally hard packed with good even surface. All shallow dunes reported during previous observation dispersed.
106	8/23	0950	1050	24.9	33.7	015	19.0	17.51	Generally hard packed with good even surface.
107	8/24	2245	2345	23.9	32.4	050	15.0	15.91	Generally hard packed with fair surface; some shallow dunes in area.
108	8/25	0915	1000	20.6	32.2	030	18.5	17.51	Generally hard packed with appearance of soft snow overlying winter crust; good level surface with no signs of barchan or dune formation.
109	8/25	1345	1445	22.8	32.2	015	17.0	17.07	Generally hard packed with some soft snow in patches; no tendency toward dune or barchan formations.
110	8/30	1010	1155	26.6	31.7	030	13.0	12.43	Patches of soft snow overlying hard packed surface; some shallow dune formations with rippled surfaces.
111	9/28	1425	1625	37.8	40.1	010	13.0	12.66	Generally hard packed with most uneven surface; probably the roughest surface conditions since snow transport observations started.
112	9/29	1150	1450	36.6	39.7	025	12.5	11.87	Generally hard packed. Disturbed areas reported during run 111 have been whittled down slightly but area is still much disturbed.
113	9/30	1055	1140	26.6	39.4	045	13.5	17.04	Area still disturbed although drift conditions do not give much opportunity for visual check. Surface generally hard packed with patches of soft snow.
114	9/30	1525	1555	27.9	38.9	050	19.0	19.39	Generally hard packed and rough.
115	10/1	0930	1030	37.2	37.9	020	16.0	14.86	Generally hard packed with a few disturbed areas scattered throughout snow transport zone.

APPENDIX A. *(Continued)*

No. of Run	Date	Time		Temperatures, −°C		Wind Direction, deg	Wind Speed, m sec^{-1}	Drift Run Average Speed (10 m), m sec^{-1}	Remarks
		Start	Finish	Air (100 cm)	Snow				
116	10/1	1440	1540	39.7	37.8	020	15.0	14.59	Generally hard packed and much disturbed; area immediately upwind of mast relatively good.
117	10/3	0940	1040	38.9	39.1	010	17.5	16.91	Generally hard packed with occasional dunes (with thin hard crusts) scattered about snow transport zone. Area immediately upwind of mast and other exposure sites relatively flat with good hard surface.
118	10/3	1450	1535	37.0	39.0	010	20.0	18.65	Generally hard packed; some rough patches where old dunes have more or less become part of the landscape.
119	10/4	0503	0533	27.9	32.4	010	23.0	22.08	Generally hard packed; no chance to eyeball the situation due to visibility conditions.
120	10/4	0937	0957	25.6	30.7	015	21.0	19.81	Generally hard packed with patches of fresh soft snow; visibility too poor to detect presence of dunes in immediate vicinity of snow transport zone; however, dunes suspected.
121	10/4	1507	1537	23.1	27.9	030	17.5	17.79	Generally hard packed with some patches of relatively soft snow; polished crust appears to have been replaced with crust of rougher texture; area not too badly disturbed.
122	10/20	0916	1016	29.6	30.3	010	17.0	16.51	Generally hard packed with some dune formations scattered throughout snow transport zone; smooth to moderately rough.
123	10/20	1455	1625	31.1	30.3	010	14.0	12.52	Generally hard packed with some shallow dunes; surface moderate to rough.
124	10/23	1422	1622	18.9	24.4	020	14.0	13.28	Generally hard packed with moderately rough surface.
125	10/24	0942	1142	19.8	22.8	350	13.5	14.31	Generally hard packed with moderately rough surface.
126	10/25	1502	1702	20.3	24.2	020	10.5	12.10	Generally hard packed; surface definition poor and actual crust difficult to determine—assume moderate to rough.
127	11/5	0855	0955	15.1	20.6	020	17.0	16.13	Usual crust now easily shattered; surface still rather disturbed (in patches) but all collectors exposed in relatively flat areas. Some shallow dunes in snow transport zone.

APPENDIX A. (*Continued*)

No. of Run	Date	Time Start	Time Finish	Temperatures, −°C Air (100 cm)	Temperatures, −°C Snow	Wind Direction, deg	Wind Speed, m sec^{-1}	Drift Run Average Speed (10 m), m sec^{-1}	Remarks
128	11/12	2103	2203	18.9	21.7	360	18.5	17.25	Thin hard crust overlying soft snow; crust easily shattered; surface generally flat except for occasional dunes of soft snow in transport zone.
129	11/13	0937	1037	16.8	20.0	010	15.0	13.66	Thin crust overlying soft snow —crust easily broken; surface scarred with footprints (Dingle's) some shallow dunes of soft snow in area otherwise surface generally flat.

APPENDIX B. Wind Profiles for Byrd 1962

Run No.	10 m	4 m	2 m	1 m	50 cm	25 cm	12.5 cm	6.25 cm	3.125 cm	u_*	$-\log z_0$
		Observed (first line) Wind Velocity, m sec^{-1} Linear Regression on log z (second line)									
7	9.60	8.79 8.84	8.43 8.27	7.59 7.70	7.11 7.13	6.60 6.56	5.99	5.42	4.85	.329	1.0689
12	9.78	8.95 8.92	8.28	7.54 7.63	6.99	6.43 6.34	5.70	5.05	4.38 4.40	.372	0.5596
9	10.19	9.37 9.14	8.90 8.82	8.23 8.24	7.61 7.65	7.08 7.06	6.48	5.89	5.30	.339	1.2248
38	10.73	9.93 9.88	9.17 9.23	8.59	7.92 7.94	7.34 7.30	6.65	6.00 6.01	5.36	.373	1.0045
1	11.07	10.28 10.37	9.79 9.85	9.59 9.32	8.82 8.80	8.14 8.27	7.75	7.16	6.70	.303	2.3466
5	11.17	10.16 10.26	9.75 9.58	8.79 8.89	8.32 8.21	7.45 7.52	6.84	6.15	5.47	.395	0.9087
53	11.21	10.23 10.28	9.61 9.57	8.90 8.87	8.06 8.17	7.63 7.47	6.76	5.99 6.06	5.36	.406	0.7991
11	11.31	10.33 10.29	9.57 9.52	8.60 8.75	7.48	7.27 7.21	6.44	5.67 5.67	4.90	.445	0.4190
86	11.60	10.78 10.73	10.08 10.07	9.29 9.41	8.77 8.75	7.97 8.09	7.43	6.78	6.12	.380	1.3008
10	11.64	10.62 10.69	10.11 9.97	9.24 9.26	8.46 8.54	7.86 7.82	7.11	6.38	5.67	.414	0.8870
50	11.64	10.75 10.73	10.02 10.04	9.36 9.35	8.57 8.67	8.10 7.98	7.29	6.57 6.60	5.91	.397	1.0935
33	11.82	10.85 10.87	10.20 10.15	9.44	8.69 8.72	7.98 8.00	7.29	6.59 6.57	5.85	.414	0.9633

APPENDIX B. *(Continued)*

Observed (first line)
Wind Velocity, m sec^{-1}
Linear Regression on log z (second line)

Run No.	10 m	4 m	2 m	1 m	50 cm	25 cm	12.5 cm	6.25 cm	3.125 cm	u_*	$-\log z_0$
112	11.87	10.83	10.19	9.56	8.65			6.49		.423	0.8644
		10.90	10.17	9.44	8.70	7.97	7.24	6.51	5.77		
6	11.93	10.85	10.20	9.26	8.54	7.75				.454	0.5694
		10.89	10.11	9.32	8.53	7.75	6.96	6.18	5.39		
27	11.94	10.77	10.25		8.44	7.77		6.09		.458	0.5246
		10.89	10.09	9.30	8.51	7.71	6.92	6.12	5.33		
13	12.08	10.73		9.21		7.17		5.26		.532	0.0565
		10.86	9.94	9.01	8.09	7.17	6.25	5.33	4.41		
126	12.10	11.18	10.32	9.47	8.65	8.19				.441	0.8512
		11.09	10.33	9.56	8.80	8.03	7.27	6.50	5.74		
55	12.19	11.22	10.37	9.71	8.88	8.28		6.62		.436	0.8623
		11.19	10.44	9.68	8.93	8.17	7.42	6.66	5.91		
34	12.26	11.27	10.40		8.99	8.09	7.39	6.60		.446	0.7765
		11.24	10.40	9.69	8.92	8.15	7.37	6.60	5.83		
35	12.29	11.28	10.41		8.85	8.18	7.27	6.50		.456	0.6863
		11.25	10.46	9.67	8.88	8.09	7.30	6.51	5.72		
14	12.41	10.99	10.23	9.34		7.37		5.27		.555	0.1127
		11.14	10.18	9.22	8.26	7.28	6.33	5.37	4.41		
25	12.41	11.25	10.53		8.77	7.94				.484	0.4567
		11.30	10.46	9.62	8.78	7.95	7.11	6.27	5.43		
110	12.43	11.42	10.86	9.73	9.11	8.54				.433	0.8728
		11.43	10.68	9.93	9.18	8.43	7.68	6.93	6.18		
123	12.52	11.65	10.87	10.29	9.76	8.83				.390	1.8180
		11.63	10.95	10.28	9.61	8.93	8.26	7.56	6.91		
16	12.56	11.53	10.93	9.74	9.30	8.65		7.88		.426	1.1151
		11.58	10.84	10.10	9.36	8.62	7.89	7.15	6.41		
15	12.56	11.70	10.75		9.44	8.59		7.28		.421	1.1853
		11.59	10.86	10.14	9.41	8.68	7.95	7.27	6.49		
111	12.66	11.74	11.00	10.07	9.44	8.84				.425	1.5410
		11.69	10.95	10.22	9.48	8.75	8.01	7.27	6.54		
46	12.68	11.84	11.04	10.05	9.66	8.96				.412	1.3469
		11.74	11.02	10.31	9.60	8.88	8.17	7.45	6.74		
32	12.70	11.77	10.94	9.85		8.53		7.00		.454	0.8595
		11.66	10.88	10.09	9.30	8.51	7.73	6.94	6.15		
92	12.75	11.76	10.88	10.02	9.47	8.52				.455	0.8652
		11.71	10.92	10.31	9.34	8.55	7.76	6.97	6.19		
47	12.77	11.84	10.85	10.07	10.07	9.30	8.39		7.05	.458	0.8407
		11.72	10.93	10.13	9.34	8.54	7.75	6.96	6.16		
90	12.84	11.87	11.15	10.29	9.53	8.95				.430	1.1798
		11.85	11.10	10.36	9.61	8.87	8.12	7.37	6.63		
89	12.85	11.85	10.95	10.26	9.38	8.69				.455	0.9017
		11.80	11.01	10.23	9.44	8.65	7.86	7.07	6.28		

APPENDIX B. *(Continued)*

Wind Velocity, m sec^{-1}

Observed (first line)
Linear Regression on log z (second line)

Run No.	10 m	4 m	2 m	1 m	50 cm	25 cm	12.5 cm	6.25 cm	3.125 cm	u_*	$-\log z_0$
88	12.90	12.00	10.95	10.29	9.49	8.85		7.20		.449	0.9928
		11.87	11.09	10.32	9.54	8.76	7.98	7.20	6.43		
49	12.96	11.80	10.99	10.31	9.36	8.42		6.83		.483	0.6578
		11.85	11.01	10.18	9.34	8.50	7.66	6.83	5.99		
2	12.97	12.02	11.04	10.28	9.54	8.80				.458	0.9187
		11.92	11.13	10.34	9.54	8.75	7.95	7.16	6.37		
74	13.12	12.07	11.35	10.56	9.74	9.00				.447	1.0956
		12.09	11.32	10.54	9.77	8.99	8.22	7.44	6.67		
94	13.21	12.10	11.45	10.67	10.00	9.22		7.48		.443	1.1843
		12.20	11.43	10.66	9.90	9.13	8.36	7.60	6.83		
31	13.28	12.06	11.25			9.76	8.90		6.85	.493	0.6829
		12.16	11.30	10.45	9.59	8.74	7.86	7.03	6.18		
124	13.28	12.16	11.15	10.16	9.26	8.56				.525	0.7484
		12.08	11.17	10.26	9.35	8.44	7.53	6.62	5.71		
3	13.39	12.43	11.49	10.67	9.99	9.22				.457	1.0900
		12.34	11.55	10.76	9.97	9.18	8.38	7.59	6.80		
17	13.40	12.26	11.63	10.37	9.82	9.12		8.39		.467	0.9843
		12.33	11.52	10.71	9.90	9.09	8.28	7.47	6.66		
40	13.46	12.26	11.45		9.89	8.99	8.11	7.05		.493	0.3815
		12.33	11.48	10.62	9.77	8.91	8.06	7.20	6.35		
44	13.58	12.49	11.74	10.80	9.88	9.29				.477	0.9508
		12.49	11.67	10.84	10.01	9.91	8.36	7.54	6.71		
56	13.62	12.44	11.45	10.63	9.75	8.69		6.79		.526	0.4986
		12.42	11.51	10.60	9.68	8.77	7.86	6.95	6.04		
23	13.62	12.57	11.91		9.88	8.74		7.88		.480	0.9321
		12.52	11.69	10.86	10.03	9.20	8.37	7.54	6.70		
129	13.66	12.80	11.93	11.35	10.50	9.99				.407	1.8313
		12.72	12.02	11.31	10.61	9.90	9.20	8.49	7.79		
54	13.66	12.43	11.75	10.90	10.05	9.30		7.39		.485	0.8907
		12.54	11.70	10.86	10.02	9.18	8.34	7.50	6.66		
18	13.80	12.54	11.84	10.92	9.94	9.07		8.02		.510	0.6990
		12.63	11.75	10.86	9.98	9.09	8.21	7.33	6.44		
91	13.81	12.77	12.01	10.87	10.23	9.57				.472	1.0814
		12.73	11.91	11.09	10.27	9.45	8.64	7.82	7.00		
51	13.84	12.49	11.84	10.83	10.13	9.47		7.05		.513	0.6869
		12.67	11.78	10.89	10.01	9.12	8.23	7.34	6.45		
80	13.84	12.69	11.76	10.70	9.93	9.08				.522	0.6031
		12.64	11.74	10.83	9.93	9.02	8.12	7.21	6.31		
30	13.93	12.74	11.77	10.63	9.96	9.05		7.03		.541	0.4777
		12.69	11.76	10.82	9.88	8.95	8.01	7.07	6.14		
87	13.96	12.81	11.79	10.76	10.19	9.03				.529	0.5875
		12.75	11.83	10.92	10.00	9.08	8.17	7.25	6.34		

APPENDIX B. *(Continued)*

Observed (first line)
Wind Velocity, m sec^{-1}
Linear Regression on log z (second line)

Run No.	10 m	4 m	2 m	1 m	50 cm	25 cm	12.5 cm	6.25 cm	3.125 cm	u_*	$-\log z_0$
52	14.03	12.39 12.81	11.98 11.89	11.26 10.97	10.14 10.05	9.45 7.12	8.20	6.90 7.28	6.35	.533	0.5781
29	14.03	12.74 12.77	11.86 11.82	10.87	9.94 9.92	8.95 8.97	8.02	6.60 7.07	6.12	.548	0.4451
22	14.05	13.0 12.97	12.35 12.16	11.34	10.33 10.53	9.45 9.72	8.91	8.34 8.09	7.20	.469	1.1999
66	14.07	13.05 12.97	12.04 12.15	11.36 11.32	10.44 10.49	9.71 9.67	8.84	8.02 8.02	7.19	.477	1.1244
21	14.17	13.11 13.02	12.42 12.15	11.28	10.38 10.41	9.49 9.54	8.67	8.05 7.80	6.93	.502	0.9382
101	14.23	13.11 13.11	12.27 12.27	11.43	10.66 10.58	9.63 9.74	8.90	8.09 8.05	7.21	.486	1.3215
61	14.29	13.08 13.05	11.98 12.12	11.23 11.19	10.26 10.26	9.51 9.32	8.39	7.34 7.46	6.52	.538	0.6106
26	14.31	12.73 12.92	12.00 11.86	10.63 10.81	10.09 9.73	8.42 8.70	7.65	7.42 6.60	5.55	.608	0.0901
125	14.31	13.31 13.27	12.42 12.49	11.70 11.70	10.96 10.91	10.11 10.13	7.34	8.56	7.27	.454	1.7860
57	14.41	13.14 13.24	12.38 12.35	11.40 11.47	10.70 10.58	9.88 9.70	8.82	7.77 7.93	7.05	.510	0.9042
24	14.45	13.18 13.19	12.44 12.25	11.30	10.16 10.35	9.25 9.41	8.46	7.68 7.51	6.56	.546	0.5918
39	14.57	13.31 13.37	12.47 12.47	11.56	10.73 10.65	9.76 9.74	8.92 8.84	7.81 7.93	7.02	.523	0.8359
116	14.59	13.60 13.44	12.44 12.57	11.60 11.70	10.76 10.83	10.09 9.96	9.09	8.22	7.35	.502	1.2134
67	14.66	13.57 13.51	12.52 12.63	11.80 11.76	10.87 10.88	10.02 10.01	9.13	8.26	7.38	.505	1.0446
115	14.86	13.85 13.75	12.85 12.91	11.95 12.06	11.22 11.22	10.45 10.38	9.54	8.69	7.85	.486	1.6897
48	14.89	13.61 13.70	12.85 12.79	11.97 11.89	10.95 10.98	10.07 10.08	9.17	8.25 8.27	7.36	.522	0.9547
104	15.01	13.60 13.75	12.85 12.79	11.84	11.02 10.98	10.02 9.93	8.98	7.89 8.03	7.07	.550	0.8476
4	15.02	13.91 13.83	12.83 12.93	12.00 12.02	11.13 11.12	10.25 10.22	9.32	8.42	7.51	.521	1.0129
36	15.29	13.91 13.88	12.74 12.81	11.58 11.75	10.90 10.68	9.82 9.62	8.38 8.55	7.46 7.49	6.42	.615	0.3201
78	15.57	14.20 14.13	13.06 13.03	11.77 11.93	10.78 10.84	9.86 9.74	8.65	7.55	6.45	.632	0.2780
59	15.60	14.28 14.30	13.28 13.32	12.47 12.34	11.31 11.36	10.36 10.38	9.40	7.93 8.42	7.44	.566	0.7867

APPENDIX B. *(Continued)*

Observed (first line)
Wind Velocity, m sec^{-1}
Linear Regression on log z (second line)

Run No.	10 m	4 m	2 m	1 m	50 cm	25 cm	12.5 cm	6.25 cm	3.125 cm	u_*	$-\log z_0$
73	15.69	14.45	13.44	12.42	11.47	10.60				.558	0.8842
		14.41	13.44	12.48	11.51	10.54	9.58	8.61	7.64		
62	15.77	14.40	13.78	12.49	11.63	10.70				.551	0.9718
		14.51	13.55	12.60	11.65	10.69	9.74	8.78	7.83		
58	15.86	14.60	13.46	12.47	11.70	11.02		8.46		.566	0.8687
		14.57	13.59	12.61	11.62	10.64	9.66	8.68	7.70		
107	15.91	14.81	13.64		11.60	10.66		9.08		.553	0.8738
		14.64	13.68	12.72	11.77	10.81	9.85	8.89	7.93		
37	16.01	14.61	13.44	12.32	11.54	10.56		8.01		.617	0.5083
		14.60	13.53	12.46	11.39	10.32	9.25	8.18	7.11		
93	16.02	14.57	13.83	12.54	11.72	10.54				.587	0.7416
		14.67	13.66	12.64	11.62	10.61	9.59	8.57	7.56		
127	16.13	14.65	14.07	12.67	11.72	10.78				.582	0.8574
		14.80	13.79	12.78	11.77	10.76	9.75	8.74	7.77		
122	16.51	15.34	14.30	13.37	12.44	11.18				.539	1.7007
		15.28	14.34	13.41	12.48	11.54	10.61	9.67	8.74		
8	16.54	14.89	14.08	12.87	11.80	10.41				.649	0.4309
		15.06	13.93	12.81	11.69	10.56	9.44	8.31	7.19		
79	16.56	15.10	13.78	12.33	11.23	10.36				.694	0.1431
		14.47	13.76	12.56	11.36	10.15	8.95	7.75	6.55		
100	16.58	15.17	14.36	13.27	12.19	11.23				.580	0.8719
		15.25	14.25	13.24	12.26	11.23	10.23	9.22	8.22		
77	16.78	14.93	14.05	12.55	12.55	11.18	9.98			.737	0.0444
		15.09	13.81	12.54	11.26	9.98	8.71	7.43	6.15		
117	16.91	15.83	14.47	13.49		11.54		9.79		.571	1.4736
		15.60	14.61	13.62	12.63	11.64	10.65	9.66	8.67		
65	16.94	15.36	14.42	13.43	12.22	10.97		8.86		.636	0.6272
		15.48	14.38	13.28	12.10	11.07	9.97	8.87	7.77		
113	17.04	15.55	14.78	13.53	12.56	11.45				.601	0.8683
		15.66	14.62	13.57	12.53	11.49	10.45	9.41	8.36		
109	17.07	15.71	14.63	13.71	12.64	11.56				.594	0.8736
		15.71	14.68	13.65	12.63	11.59	10.56	9.53	8.51		
72	17.11	15.85	14.61	13.66	12.62	11.70				.594	1.0044
		15.75	14.72	13.68	12.66	11.63	10.60	9.57	8.54		
102	17.20	15.95	14.56	13.66	12.67	11.62				.609	0.8670
		15.80	14.75	13.69	12.64	11.58	10.53	9.67	8.42		
128	17.25	15.95	14.81	13.96	12.90		10.86			.582	1.1484
		15.91	14.91	13.90	12.89	11.88	10.87	9.86	8.86		
28	17.35	15.59	14.80	13.30	13.30		10.90		7.01	.695	0.3379
		15.75	14.55	13.35	12.14	10.94	9.74	8.53	7.33		
68	17.48	15.59	14.80	13.43	12.36	11.30		8.28		.703	0.3230
		15.87	14.66	13.44	12.22	11.00	9.79	8.57	7.35		

APPENDIX B. *(Continued)*

Observed (first line)
Wind Velocity, m sec^{-1}
Linear Regression on log z (second line)

Run No.	10 m	4 m	2 m	1 m	50 cm	25 cm	12.5 cm	6.25 cm	3.125 cm	u_*	$-\log z_0$
106	17.51	16.27	14.93	14.17	13.05	12.07				.593	1.4454
		16.15	15.13	14.10	13.07	12.04	11.01	9.99	8.96		
108	17.51	15.82	14.93	13.64		11.23		8.88		.679	0.7864
		15.96	14.78	13.61	12.43	11.25	10.08	8.90	7.72		
60	17.72	16.27	15.17	14.10	12.98	11.44		8.81		.631	0.8748
		16.27	15.18	14.08	12.99	11.89	10.80	9.71	8.61		
85	17.76	16.40	14.96	13.87	13.00	11.70				.656	0.7064
		17.26	15.12	13.99	12.85	11.71	10.58	9.44	8.31		
121	17.79	16.28	15.09	13.67	12.46	11.62				.690	0.7866
		16.21	15.02	13.82	12.67	11.43	10.24	9.04	7.85		
76	17.92	16.08	14.76	13.34	13.34	11.82	10.64			.798	0.0965
		16.09	14.71	13.33	11.95	10.56	9.18	7.80	6.42		
19	17.98	16.15	15.22		12.66	11.49		8.72		.719	0.3462
		16.34	15.09	13.84	12.60	11.35	10.11	8.86	7.63		
41	18.02	16.04	15.10	14.08	12.94	11.56	10.03	8.60		.721	0.0871
		16.37	15.12	13.87	12.62	11.37	10.12	8.87	7.62		
75	18.20	16.69	15.14	13.78	12.40	11.63				.742	0.2603
		16.50	15.12	13.93	12.64	11.36	10.07	8.78	7.50		
95	18.21	17.02	15.65	14.30		12.30		10.41		.628	1.0339
		16.77	15.18	14.59	13.50	12.41	11.32	10.23	9.15		
64	18.39	16.60	15.71	14.44	13.10	12.01		9.84		.691	0.6242
		16.81	15.61	14.41	13.22	12.02	10.82	9.63	8.43		
84	18.42	16.72	15.76	14.21	13.03	11.92				.712	0.4981
		16.97	15.56	14.33	13.10	11.87	10.63	9.40	8.16		
83	18.42	16.74	15.38	13.96	12.79	11.80				.745	0.2978
		16.71	15.42	14.12	12.84	11.55	10.26	8.97	7.68		
105	18.57	16.79	15.77		13.65	12.42		9.51		.692	0.8350
		16.99	15.79	14.59	13.39	12.11	10.99	9.79	8.59		
118	18.65	17.00	16.04	14.97	13.61	12.44				.667	0.8626
		17.12	15.97	14.81	13.66	12.50	11.35	10.19	9.04		
103	18.80	17.16	16.16	14.88	13.64	12.51				.682	0.8544
		17.23	16.05	14.87	13.69	12.51	11.32	10.14	8.96		
99	19.11	17.36	16.37		13.87	12.69		10.07		.705	0.8431
		17.49	16.27	15.05	13.83	12.61	11.38	10.61	8.94		
114	19.39	17.79	16.46		14.00	12.81				.717	0.8417
		17.75	16.51	15.27	14.02	12.78	11.54	10.30	9.06		
45	19.46	17.63	16.21	14.90	13.83	12.54		9.34		.780	0.3394
		17.67	16.32	14.98	13.63	12.28	10.93	9.58	8.23		
63	19.66	17.99	16.43	15.35	13.82	12.66				.766	0.4596
		17.90	16.58	15.25	13.92	12.60	11.27	9.94	8.62		
120	19.81	18.09	16.70	15.10		12.55		9.89		.786	0.7366
		18.01	16.65	15.78	13.92	12.56	11.20	9.83	8.47		

APPENDIX B. *(Continued)*

Run No.	10 m	4 m	2 m	1 m	50 cm	25 cm	12.5 cm	6.25 cm	3.125 cm	u_*	$-\log z_0$
		Observed (first line) Wind Velocity, m sec^{-1} Linear Regression on log z (second line)									
20	20.17	18.36	17.32		14.36	13.33		9.31		.751	0.6627
		18.45	17.14	15.84	14.54	13.24	11.94	10.63	9.33		
69	20.95	19.12	18.09	16.53	15.07	14.04				.761	0.7847
		19.21	17.89	16.57	15.25	13.93	12.62	11.30	9.98		
81	20.96	19.30	18.08	16.62	15.16	14.36				.739	0.9284
		19.26	17.98	16.70	15.42	14.14	12.86	11.58	10.30		
119	22.08	20.06	18.68	17.48	15.69	14.27				.841	0.8118
		20.15	18.69	17.24	15.78	14.32	12.87	11.41	9.95		
96	22.13	20.20	18.77		15.85	14.18		11.51		.844	0.5564
		20.20	18.73	17.27	15.81	14.35	12.89	11.42	9.96		
71	22.20	19.85	18.62	16.79	15.06	13.43				.946	0.0747
		20.03	18.39	16.75	15.11	13.49	11.83	10.19	8.55		
42	22.43	20.29	18.73	17.26	16.25	14.21	12.37	9.22		.893	0.3633
		20.39	18.84	17.29	15.74	14.20	12.65	11.10	9.95		
98	22.62	20.87	19.59	17.68	16.48	15.50				.799	0.8679
		20.79	19.41	18.02	16.64	15.25	13.87	12.48	11.10		
43	22.88	20.78	19.36	17.30	15.79	14.55	12.78	9.57		.918	0.3290
		20.78	19.19	17.60	16.00	14.41	12.82	11.23	9.64		
82	23.51	21.57	19.83	18.21	16.59	15.37				.903	0.5251
		21.44	19.88	18.31	16.75	15.19	13.62	12.06	10.49		
70	23.94	21.87	20.23	18.28	16.75	15.45				.942	0.4156
		21.78	20.15	18.52	16.88	15.25	13.62	11.99	10.36		
97	24.02	21.82	20.00	18.57	16.60	15.09				.973	0.6727
		21.79	20.10	18.42	16.73	15.04	13.36	11.67	9.97		

APPENDIX C. Rapid-Run Upper-Wind Observations, Byrd, 1962–1963

Drift Run No.	V_{10}, m sec^{-1}	Wind Maximum		Wind Minimum		Inversion Base		Height of Rapid Direction Changes, m
		Height, m	V, m sec^{-1}	Height, m	V, m sec^{-1}	Height, m	ΔT, deg	
27	13.2	180	22.5	260	14.9	450	3	280
36	15.9	100	38.5	860	14.8	550	1	430
				410	17.8			
49	13.0	220	22.5	900	11.2	450	3.5	910
63	19.9	270	38.2	850	15.0	600	4.5	600
66	14.0	380	38.0	980	6.0			
57	14.8	400	44.0	900	6.0			
67	14.7	130	25.6	950	5.0	230	4	300
61	14.9	175	29.5	770	12.0	240	1	500
76	18.2	270	30.0	580	21.0	280	5	600
80	14.8	310	27.0	850	9.0	700	3	750
82	24.7	500	80.0	420	31.0	370	4.5	640

APPENDIX C. (*Continued*)

Drift Run No.	V_{10}, m sec^{-1}	Wind Maximum		Wind Minimum		Inversion Base		Height of Rapid Direction Changes, m
		Height, m	V, m sec^{-1}	Height, m	V, m sec^{-1}	Height, m	ΔT, deg	
		360	55.0	630	10.0	600	3.7	
84	18.5	320	27.5	700	16.0	100	4	>1000
ASC 376	21.0	180	40.0	270	18.0			900
		450	40.0	900	10.0			
86	12.2	280	20.5	700	11.5	130	1.5	140
						380	3.8	
97	24.1	300	46.0	750	21.0	700	10	820
100	16.0	130	29.0	200	23.0	250	3	900
		330	40.0	450	22.0			
				1000	7.0			
103	19.0	410	40.0	800	16.0	450	3.5	800
106	18.8	250	33.0	550	10.0	650	2	800
107	16.0	450	33.0	950	18.0			750
109	17.0	270	29.0	900	14.0			900
								400
110	12.5	170	22.0	900	5.0	160	3	330
111	12.9	150	31.0	600	11.0	170	4	360
112	12.0	300	25.0	700	13.0	170	5	230
114	19.9	300	38.0	>1000	13.0	880	2	900
116	15.0	150	27.0	800	5.0	100	3	450
ASC 518	17.0	250	27.0	400	13.0	140	4	500
								(1000)
121	18.1	65	32.0	100	25.0	180	6	400
		380	41.0	700	15.0			
123	12.8	260	27.0	800	5.0	470	4	400
								600
124	13.2	350	32.0	400	20.0	390	1	
126	12.9	450	34.0	700	23.0	360	1	600
127	15.9	200	30.0	370	15.0	220	1.2	1000
ASC 599 (ascent)	10.0	250	31.0	680	10.0	580	3	800
599								

APPENDIX D. Snow Drift Densities for Byrd 1962

V_{10}, m sec^{-1}	Run No.	Drift density n_z, g m^{-3}								Fall Velocity w, m sec^{-1}	u_*, m sec^{-1}	$-\log z_0$
		4 m	2 m	1 m	50 cm	25 cm	12.5 cm	6.25 cm	3.125 cm			
9.60	7	0.076	0.122	0.175	0.331	1.232	1.800	8.084	48.406	.1606	.329	1.0689
9.78	12	0.019	0.031	0.037	0.120	0.221	1.477	6.605	39.552	.2813	.372	0.5596
10.19	9	0.111	0.176	0.251	0.271	0.660	2.000	7.201	43.119	.1479	.339	1.2248
10.73	38	0.057	0.091	0.130	0.354	0.730	2.153	10.088	60.328	.2014	.373	1.0045
11.07	1	0.136	0.230	0.264	0.541	1.172	4.889	11.726	70.216	.1454	.303	2.3466
11.17	5	0.219	0.410	0.505	0.889	1.568	2.544	11.899	53.360	.0968	.395	0.9087
11.21	53	0.082	0.205	0.380	0.791	1.691	3.861	13.290	56.035	.1992	.406	0.7991
11.31	11	0.109	0.236	0.385	0.422	1.012	5.056	30.298	135.826	—	.445	0.4190
11.60	86	0.104	0.149	0.199	0.363	0.671	2.141	5.962	30.271	.1637	.380	1.3008
11.64	10	0.105	0.226	0.424	0.855	1.794	5.527	23.073	103.467	.2144	.414	0.8870
11.64	50	0.210	0.336	0.691	1.133	2.180	4.737	14.120	49.394	.1653	.397	1.0935
11.82	33	0.046	0.074	0.278	0.429	0.936	2.978	16.463	77.293	.2635	.414	0.9633

APPENDIX D. *(Continued)*

V_{10}, m sec^{-1}	Run No.	Drift density n_z, g m^{-3} 4 m	2 m	1 m	50 cm	25 cm	12.5 cm	6.25 cm	3.125 cm	Fall Velocity w, m sec^{-1}	u_*, m sec^{-1}	$-\log z_0$
11.87	112	0.120	0.221	0.436	0.861	1.784	5.040	11.785	32.367	.1870	.423	0.8644
11.93	6	0.207	0.223	0.362	0.790	2.535	4.839	21.052	84.887	.2155	.454	0.5694
11.94	27	0.103	0.223	0.423	0.659	1.457	4.462	14.768	71.413	.2263	.458	0.5246
12.08	13	0.103	0.141	0.218	0.590	1.213	4.312	30.330	121.472	—	.532	0.0565
12.10	126	0.025	0.068	0.205	0.478	1.329	5.444	18.311	78.244	.2798	.441	0.8512
12.19	55	0.150	0.296	0.522	1.006	2.164	4.654	10.664	43.648	.1862	.436	0.8623
12.26	34	0.250	0.322	0.406	0.566	1.102	4.875	23.221	99.183	.2103	.446	0.7765
12.29	35	0.233	0.286	0.348	0.464	1.203	4.973	29.952	107.900	.2266	.456	0.6863
12.41	14	0.050	0.110	0.366	0.544	1.232	6.562	38.471	176.692	.3546	.555	0.1127
12.41	25	0.249	0.429	0.759	1.151	2.330	5.608	11.911	57.070	.1940	.484	0.4567
12.43	110	0.140	0.241	0.484	0.734	1.789	6.182	18.470	72.673	.2120	.433	0.8728
12.52	123	0.045	0.068	0.163	0.507	1.551	4.849	21.478	89.368	.2593	.390	1.8180
12.56	16	0.582	0.759	0.821	1.359	2.865	7.305	11.635	51.031	.1432	.426	1.1151
12.56	15	0.161	0.275	0.553	1.034	1.854	6.543	18.713	56.174	.1945	.421	1.1853
12.66	111	0.264	0.564	0.906	1.629	3.689	7.288	14.904	70.861	.1747	.425	1.5410
12.68	46	0.095	0.255	0.544	0.877	1.896	5.909	29.162	102.200	.2199	.412	1.3469
12.70	32	0.096	0.154	0.278	0.665	1.451	5.592	28.393	116.753	.2582	.454	0.8595
12.75	92	0.128	0.240	0.369	0.802	2.145	6.753	19.600	87.074	.2333	.455	0.8652
12.77	47	0.143	0.334	0.638	1.262	2.859	7.352	34.603	167.409	—	.458	0.8407
12.84	90	0.348	0.540	0.867	1.285	2.405	7.835	20.465	92.747	.1827	.430	1.1798
12.85	89	0.158	0.374	0.548	0.951	2.294	6.667	22.922	108.643	.2249	.455	0.9017
12.90	88	0.118	0.253	0.408	0.736	1.922	5.628	17.426	124.938	.2343	.449	0.9928
12.96	49	0.473	0.714	1.764	2.405	5.284	10.407	28.439	105.492	.1963	.483	0.6578
12.97	2	0.187	0.255	0.382	0.706	1.340	4.731	19.711	65.922	.2059	.458	0.9187
13.12	74	0.371	0.546	1.119	1.552	4.309	10.517	32.522	90.901	.1964	.447	1.0956
13.21	94	0.368	0.639	1.316	1.985	3.689	12.490	25.114	73.975	.1835	.443	1.1843
13.28	31	0.185	0.397	0.672	1.171	2.634	7.755	26.074	87.165	—	.493	0.6829
13.28	124	0.046	0.103	0.356	0.751	2.095	8.760	25.737	113.802	.3244	.525	0.7484
13.39	3	0.091	0.292	0.574	0.845	1.528	5.628	14.252	52.590	.2209	.457	1.0900
13.40	17	0.437	0.819	1.112	2.041	3.409	7.729	12.829	47.339	.1613	.467	0.9843
13.46	40	0.425	0.554	1.057	1.877	4.159	9.380	25.367	82.750	.2055	.493	0.3815
13.58	44	0.135	0.260	0.497	0.976	2.676	6.769	36.229	123.088	.2568	.477	0.9508
13.62	56	0.392	0.586	1.024	2.088	4.310	9.856	24.394	111.349	.2276	.526	0.4986
13.62	23	0.180	0.288	0.465	0.672	1.770	7.177	17.794	77.689	—	.480	0.9321
13.66	129	0.132	0.327	0.695	2.117	4.537	8.789	28.901	110.279	.2097	.407	1.8313
13.66	54	0.224	0.360	0.595	1.177	2.538	5.048	11.041	43.369	.1948	.485	0.8907
13.80	18	0.356	0.717	1.034	1.800	3.459	9.026	13.397	58.502	.1958	.510	0.6990
13.81	91	0.441	0.660	1.215	2.187	4.277	13.125	27.495	140.750	.2078	.472	1.0814
13.84	51	0.310	0.715	1.341	2.244	4.740	11.734	25.240	90.433	.2186	.513	0.6869
13.84	80	0.462	0.612	1.037	2.397	4.979	10.122	24.730	98.648	—	.522	0.6031
13.93	30	0.266	0.477	0.986	1.648	3.388	9.041	32.874	131.134	—	.541	0.4777
13.96	87	0.308	0.664	1.182	2.582	5.873	15.599	37.710	165.585	.2541	.529	0.5875
14.03	52	0.285	0.567	1.100	2.207	4.986	11.540	35.280	135.838	.2521	.533	0.5781
14.03	29	0.176	0.332	0.878	1.700	4.260	10.920	41.150	121.747	.2772	.548	0.4451
14.05	22	0.217	0.277	0.445	0.640	1.098	2.394	5.968	17.665	—	.469	1.1999
14.07	66	0.058	0.123	0.330	1.034	3.793	10.288	41.532	146.114	.3034	.477	1.1244
14.17	21	0.129	0.509	0.896	1.240	1.765	5.569	14.971	43.752	.2098	.502	0.9382
14.23	101	0.371	0.610	1.113	2.371	5.572	14.213	46.120	113.940	.2253	.486	1.3215
14.29	61	0.344	0.556	1.054	2.845	7.107	13.918	31.832	111.848	.2463	.538	0.6106
14.31	26	0.304	0.473	1.154	2.761	5.228	10.128	28.441	106.124	.2734	.608	0.0901
14.31	125	0.063	0.112	0.432	1.338	4.185	13.194	40.563	153.354	.2882	.454	1.7860
14.41	57	0.480	0.758	1.142	2.052	4.167	9.548	22.417	83.506	.2013	.510	0.9042
14.45	24	0.340	0.687	1.342	3.255	6.802	12.079	29.905	117.518	.2416	.546	0.5918
14.57	39	0.420	0.675	1.117	2.319	5.360	14.035	33.415	112.856	.2313	.523	0.8359

APPENDIX D. *(Continued)*

V_{10}, m sec^{-1}	Run No.	Drift density n_z, g m^{-3} 4 m	2 m	1 m	50 cm	25 cm	12.5 cm	6.25 cm	3.125 cm	Fall Velocity w, m sec^{-1}	u_*, m sec^{-1}	$-\log z_0$
14.59	116	0.417	0.714	1.344	2.488	5.411	15.254	36.743	88.067	.2154	.502	1.2134
14.66	67	0.194	0.356	0.541	1.514	4.188	11.847	53.194	172.729	.2775	.505	1.0446
14.86	115	0.572	1.087	2.095	4.003	8.167	20.950	44.899	96.545	.1983	.486	1.6897
14.89	48	0.205	0.351	0.614	1.330	3.175	7.101	25.728	75.819	.2450	.522	0.9547
15.01	104	0.286	0.702	1.185	2.217	4.975	14.379	34.537	144.120	.2591	.550	0.8476
15.02	4	0.262	0.561	0.819	1.724	4.259	11.064	26.918	95.017	.2356	.521	1.0129
15.29	36	0.566	0.833	1.433	2.839	6.186	16.940	48.411	200.424	.2717	.615	0.3201
15.57	78	0.675	1.292	2.447	5.386	10.778	22.391	60.898	163.195	.2748	.632	0.2780
15.60	59	0.628	1.011	1.774	3.904	8.707	17.021	52.053	183.737	.2464	.566	0.7867
15.69	73	0.545	1.170	1.889	3.316	7.030	18.753	61.942	155.780	.2464	.558	0.8842
15.77	62	0.387	0.746	1.425	2.409	5.356	14.064	40.026	150.996	.2520	.551	0.9718
15.86	58	0.463	0.909	1.870	3.478	7.228	13.482	30.528	93.832	.2281	.566	0.8687
15.91	107	0.307	0.656	1.368	2.385	5.712	12.823	34.100	130.261	.2543	.553	0.8738
16.01	37	0.538	0.830	1.667	3.253	7.235	19.907	50.718	203.429	.2864	.617	0.5083
16.02	93	0.727	1.315	2.399	4.880	11.694	24.001	54.632	169.310	.2491	.587	0.7416
16.13	127	0.114	0.285	0.659	1.717	5.113	23.492	65.261	227.172	.3577	.582	0.8574
16.51	122	0.367	0.861	1.925	3.869	9.875	28.784	75.323	249.415	.2718	.539	1.7007
16.54	8	0.410	1.088	1.621	3.458	14.088	28.307	66.142	219.014	.3186	.649	0.4309
16.56	79	0.600	1.224	2.771	6.029	12.168	27.035	73.018	241.471	—	.694	0.1431
16.58	100	0.540	1.103	1.979	4.281	10.398	21.000	53.338	167.826	.2561	.580	0.8719
16.78	77	0.521	1.382	2.507	6.382	14.401	36.094	88.402	251.504	—	.737	0.0444
16.91	117	0.720	1.383	2.515	5.601	11.430	20.558	47.538	101.724	.2220	.571	1.4736
16.94	65	0.218	0.390	1.184	2.858	8.266	18.864	66.012	227.158	.3530	.636	0.6272
17.04	113	1.195	2.304	4.468	8.781	16.482	37.033	71.910	182.744	.2339	.601	0.8683
17.07	109	0.250	0.689	1.316	2.536	5.813	13.929	29.984	107.200	.2709	.594	0.8736
17.11	72	0.855	1.526	3.037	6.030	14.095	24.151	88.930	184.458	.2538	.594	1.0044
17.20	102	0.746	1.408	2.665	4.930	10.714	22.179	51.694	130.014	.2447	.609	0.8670
17.25	128	0.353	.791	1.373	3.179	7.125	14.706	41.633	102.917	—	.582	1.1484
17.35	28	0.599	1.435	2.978	5.827	12.686	29.119	82.436	170.890	—	.695	0.3379
17.48	68	0.884	1.455	2.798	4.962	10.207	24.256	66.489	181.785	.2935	.703	0.3230
17.51	106	0.452	0.927	1.473	3.050	7.134	30.899	75.976	219.921	.2954	.593	1.4454
17.51	108	0.657	1.367	3.135	6.142	12.376	29.703	72.582	213.311	.3030	.679	0.7864
17.72	60	0.932	1.849	3.708	7.995	17.221	30.149	76.367	257.876	.2690	.631	0.8748
17.76	85	0.967	1.745	3.331	7.078	16.013	32.898	83.317	216.181	.2796	.656	0.7064
17.79	121	0.554	1.271	2.844	5.867	11.787	36.731	77.006	190.231	.3171	.690	0.7866
17.92	76	0.837	1.717	3.706	7.611	17.171	40.607	74.063	277.292	—	.798	0.0965
17.98	19	0.619	1.060	1.947	3.743	9.126	26.737	76.415	198.478	.3344	.719	0.3462
18.02	41	0.823	1.522	3.319	6.094	15.257	33.728	62.469	233.884	—	.721	0.0871
18.20	75	0.816	1.606	3.264	7.128	13.343	40.139	97.062	298.661	.3424	.742	0.2603
18.21	95	1.071	1.862	3.578	7.153	15.380	27.326	56.908	148.662	.2406	.628	1.0339
18.39	64	0.401	0.820	1.683	3.720	10.313	25.091	76.251	235.311	—	.691	0.6242
18.42	84	0.736	1.479	3.017	5.914	15.289	32.057	86.538	264.942	.3264	.712	0.4981
18.42	83	0.739	1.347	2.781	6.733	17.401	34.964	88.434	262.057	.3465	.745	0.2978
18.57	105	0.881	1.564	2.822	6.093	12.588	40.048	84.486	300.630	.3169	.692	0.8350
18.65	118	0.743	1.735	3.134	6.630	14.611	24.204	58.986	139.106	.2674	.667	0.8626
18.80	103	0.847	1.574	3.020	6.151	13.956	28.962	61.510	173.869	.2831	.682	0.8544
19.11	99	0.963	2.070	3.730	8.443	19.678	38.084	82.331	233.601	.2997	.705	0.8431
19.39	114	1.518	3.400	6.471	13.294	26.268	55.945	87.751	227.530	.2742	.717	0.8417
19.46	45	0.636	1.238	2.748	5.931	17.433	33.078	104.856	338.064	.3852	.780	0.3394
19.66	63	0.659	1.320	3.313	6.050	14.168	33.624	89.631	475.166	.3796	.766	0.4596
19.81	120	1.122	2.225	4.740	9.921	22.125	55.037	113.935	355.926	.3531	.786	0.7366
20.17	20	0.973	1.572	3.261	6.873	15.010	38.085	89.119	310.312	—	.751	0.6627
20.95	69	1.870	4.017	7.454	14.799	29.178	58.631	145.565	365.637	.3088	.761	0.7847
20.96	81	1.574	3.279	6.101	11.577	23.881	44.397	99.480	365.451	.3000	.739	0.9284

APPENDIX D. (*Continued*)

V_{10}, m sec^{-1}	Run No.	Drift density n_z, g m^{-3} 4 m	2 m	1 m	50 cm	25 cm	12.5 cm	6.25 cm	3.125 cm	Fall *Velocity* w, m sec^{-1}	u_*, m sec^{-1}	$-\log z_0$
22.08	119	1.950	3.244	7.164	15.298	32.068	62.552	141.407	406.348	.3506	.841	0.8118
22.13	96	2.335	4.975	9.947	19.601	42.095	69.074	126.437	299.297	.3127	.844	0.5564
22.20	71	2.242	4.029	7.507	16.199	36.009	63.590	160.430	382.754	—	.946	0.0747
22.43	42	1.432	2.503	5.715	11.627	28.861	80.059	168.412	371.519	.3971	.893	0.3633
22.62	98	1.944	3.210	7.009	11.943	24.407	70.792	131.307	276.904	.3192	.799	0.8679
22.88	43	1.783	3.511	6.603	13.579	30.037	89.070	189.220	543.705	—	.918	0.3290
23.51	82	2.828	6.185	11.038	21.115	41.356	72.709	136.439	505.416	.3432	.903	0.5251
23.94	70	2.861	6.686	10.367	19.057	38.101	76.172	198.899	544.596	.3728	.942	0.4156
24.02	97	2.782	5.279	10.881	21.644	44.344	80.301	151.533	348.975	.3646	.973	0.6727

APPENDIX E. Drift Contents and Transports

No.	$\bar{V}_{10}$, m sec^{-1}	$\bar{u}_*$, m sec^{-1}	$\bar{z}_0$, mm	Layer Boundaries, m 10^{-2}–0.125 Γ, g m^{-2}	Q, g m^{-1} s^{-1}	0.125–0.5 Γ	Q	0.5–2.0 Γ	Q	2.0–300.0 Γ	Q	Total 10^{-2}–300.0 Γ	Q
1	10.35	.343	.0574	26.85	89.13	0.28	2.03	0.24	2.08	2.51	29.22	29.89	122.47
2	11.42	.408	.1371	61.42	183.40	0.52	3.95	0.53	4.84	2.32	35.80	64.79	227.99
3	11.86	.429	.1574	34.43	109.74	0.62	4.91	0.54	4.55	4.61	62.16	40.21	181.35
4	12.30	.462	.2377	120.20	320.33	0.60	4.76	0.47	4.54	4.37	61.192	125.64	390.82
5	12.73	.458	.1479	22.13	83.23	0.79	6.67	0.61	6.01	4.69	67.49	28.22	163.41
6	12.86	.433	.0692	38.25	160.45	0.87	7.65	0.72	7.29	2.90	40.25	42.71	215.65
7	12.87	.455	.1217	37.14	142.26	1.10	9.60	1.04	10.81	4.61	64.36	43.89	227.02
8	13.32	.484	.1656	16.49	67.95	1.17	10.29	1.14	12.00	5.97	87.53	24.77	177.77
9	13.41	.473	.1186	30.00	124.74	1.09	9.75	0.84	9.05	5.40	80.56	37.32	224.10
10	13.79	.471	.0819	7.47	40.52	1.21	11.40	1.12	12.35	6.48	98.67	16.28	162.93
11	13.94	.528	.2590	23.01	90.71	1.73	15.66	1.58	17.47	7.60	116.72	33.93	240.56
12	14.29	.496	.0987	33.90	151.53	1.06	10.25	0.88	11.18	3.19	53.06	39.03	226.02
13	14.66	.531	.1598	19.46	92.14	1.81	17.61	1.40	16.14	8.24	135.76	30.90	261.65
14	15.05	.508	.0712	36.53	191.37	1.85	17.22	1.57	18.61	9.78	163.26	49.73	390.46
15	15.44	.577	.2244	24.90	118.62	2.48	24.91	2.19	26.64	10.55	179.17	40.12	349.33
16	15.79	.569	.1509	32.00	160.09	2.34	17.94	2.17	27.37	9.68	165.92	46.20	371.32
17	16.77	.610	.1681	40.33	219.05	3.45	38.11	2.42	31.59	5.72	100.65	51.92	389.40
18	17.12	.625	.1741	37.07	206.16	4.00	45.24	3.38	45.71	10.47	191.82	54.91	488.92
19	17.16	.615	.1424	42.13	230.76	3.19	36.51	3.01	40.92	8.21	148.84	56.55	457.03
20	18.07	.734	.5288	28.97	149.38	5.03	56.46	3.96	51.53	15.02	303.56	52.99	560.93
21	18.12	.652	.1489	45.73	274.14	4.44	53.46	3.96	53.25	17.09	339.20	71.21	720.04
22	18.61	.694	.2199	43.96	250.57	4.70	57.03	3.85	53.98	17.44	357.60	69.95	719.19
23	19.41	.710	.1785	31.48	214.03	5.66	72.39	5.22	73.10	15.97	331.41	58.33	690.93
24	20.65	.761	.1931	50.31	346.18	6.65	96.31	6.36	100.90	24.66	553.35	87.98	1096.73
25	22.58	.865	.2918	49.44	375.38	11.02	160.29	9.91	173.30	53.68	1355.13	124.05	2064.10
26	24.12	.934	.3269	57.49	453.58	13.25	203.00	13.70	257.08	45.11	1167.76	129.55	2081.42

A STUDY OF ICE ACCUMULATION AND TROPOSPHERIC CIRCULATION IN WESTERN ANTARCTICA[1]

WILLIAM W. VICKERS[2]

Technical Operations Research, Burlington, Massachusetts

Abstract. The purpose of this investigation is to determine the distribution of snow accumulation in western Antarctica and to associate it with relevant synoptic meteorological factors. The supporting evidence for the accumulation figures cited is derived primarily from tracing snow layers from areas of known stratigraphic record to areas of unknown stratigraphic record. Density and ram hardness profiles are found to be unsatisfactory as a sole means of determining accumulation because of spatial variation in regions of complex stratigraphy. Distribution of grain size within a snow layer provides moderate help for the layer tracing technique employed herein. The most favorable tools to employ for tracing layers are crusts, slabs, and icing phenomena. (This work is summarized from the parent report.) The lateral extent of the favorable features is determined by examining the areal extent of weather systems producing them and by correlating the presence of these systems with a record of the simultaneous snow surface alterations at widely separated stations. Concurrently at these stations a historic record of the snow stratigraphy is constructed, such that annual snow layers become recognizable in unknown areas by a knowledge of the recorded effects of widespread meteorological events, e.g. a drizzle crust formed on a certain date. An additional line of support for the dating of layers is sought in geochemical analyses. In this study, bomb fallout in snow samples is used to date certain snow layers. Since data are meager, the study is as much an evaluation of the technique as it is a beneficiary of the technique. Also considered (in the parent report) is the use of deuterium and oxygen isotope analyses as aids in determining accumulation. Examples of contributions to the present investigation are cited.

An analysis of IGY and post-IGY snowpit data, supported by evidence derived in the above manner, shows the annual rate of ice accumulation in western Antarctica to be 19.8 g/cm^2 for approximately the 1956–1960 time period. The distribution of accumulation is the same as the distribution of precipitation. Broadly speaking, the distribution of precipitation is governed in space and time by the interaction between inland highs and coastal circuiting maritime lows and by the occasional presence of a blocking high over Bellingshausen Sea. The snow accumulation map presented correlates well with apparent atmospheric circulation.

COMPILATION OF PRINCIPAL EVIDENCE

VARIATION OF SNOW CHARACTERISTICS WITH TIME

This study has as a primary goal the determination of the distribution of snow accumulation in western Antarctica. Investigation of time and space variations of physical properties of the snow strata was the point of departure for this effort. The initial investigation sought to determine if any change in snow properties could reliably predict the age of firn or could aid the general dating problem in any way, perhaps as a reliable strata tracer.

Continuous pits were periodically examined at Little America V, (78°10′S, 162°13′W) to establish facts about change in snow cover with time. A continuous pit is one that is periodically re-excavated, so that any physical changes with time in a given cross section of the snow can be noted. The pit wall is usually cut back slightly so as to negate the disturbance of the previous excavation. Such pits are refilled after each examination.

[1] Abridgment of Ph.D. dissertation, McGill University.
[2] Now at Mitre Corporation, Bedford, Massachusetts.

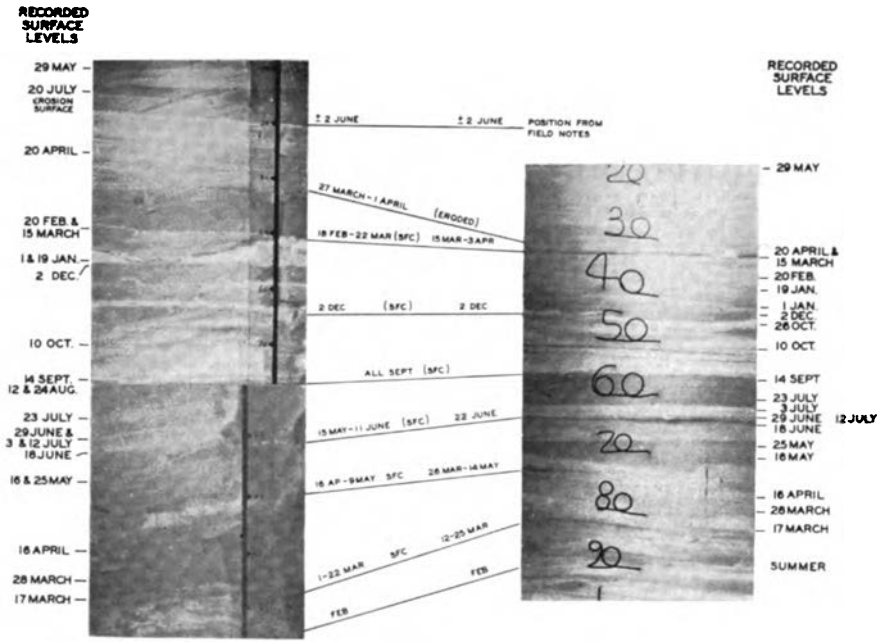

Fig. 1. Comparison of stratigraphy of Byrd (*right*) and Little America (*left*) stations.

It was found that the change of snow physical characteristics with time did not provide any ready answer to the dating of snow layers. It was of value, however, to quantify change of properties with time in order to provide a better understanding of the stratigraphy being investigated. Results of the time-change study are cited below in summary form.

1. Crustal and icing phenomena remained essentially intact for the time spans considered in this report (up to 5 years).

Sublimation layers were also lasting. Their history started with a new annual layer in November and was manifested as a decrease in density. By December identifiable crystals were evident, and by the latter part of February sublimation had reached its peak. Sublimation layers are also discernible in deep cores.

2. Ram profiles (snow hardness variation with depth) varied in magnitude by a factor greater than 2 with the change of the seasons—primarily a temperature effect.

3. Grain size history began with a 0.3-mm average size as characteristic of the winter peak. By the end of summer the size had increased to 0.8 mm. Grains several years old could grow to 7 mm. Larger grains plainly showed hexagonal habit and crystal striations, attributable to growth primarily through sublimation processes.

4. The ratio of evaporation to settling for the winter layers during the summer season was 2:3. The same ratio for summer layers during the summer season was 1:6, although magnitude of measurement and error make the summer value speculative. The net summer effect of settling in excess of evaporation on the entire annual layer was about 10% of the original quantity.

5. Apparently the faster accumulating overburden of heavy winter snowfalls influenced settling rate of winter layers more than did high summer temperature arriving at a time when much of the compaction for these layers had already occurred.

6. Settling (of the magnitude calculated herein) did not appreciably affect the stake farm records for purposes of this investigation.

In conjunction with recording the snow metamorphism with time, a compilation of the stratigraphic record was made as the snow accumulated.

Variation of Snow Characteristics with Space

The stratigraphy of a large type-pit at Little America was recorded (and photographed) in four

visibly connected sections to permit direct observation of variation in space. The observer could trace layers or key horizons laterally and determine their variation and persistence.

The same method was used with 20 pits excavated within the surrounding 35-km^2 area, an area referred to as the Little America control zone. (It was also possible to designate a similar zone at Byrd station, 80°01′S, 119°32′W, from which certain pits appear in this report.) The identity of specific layers in this zone was known, for their history had been recorded from the summer 1955–1956, indirectly, and from 1956–1957 to the summer 1958–1959 by direct measurement of stakes implanted in the snow abutting a reference ice layer. Since snow surface levels were frequently recorded on the stakes, a buried surface could be checked against its position on the stake and its time of formation noted therefrom. In this way any given surface could be traced from stake to stake, identified, and notation made as to its variation. Also, the persistence of the various features was again recorded. Those features occurring frequently (80% or more) were designated key horizons and judged most likely to appear in unknown pits excavated on the field traverses in unknown regions.

As a further test of variation of stratigraphy with space, the same procedure was followed at Byrd station, hundreds of kilometers away, where known dated layers had also been recorded. Direct correlation to the Little America control zone was found to be possible because (1) the lateral consistency of stratigraphic features (crusting and icing phenomena, large snowfalls manifested as massive layers, etc.) was maintained, and (2) the grain size within a firn layer maintained a statistically recognizable distribution, although it was frequently (about one-fifth of observations) disturbed by sastrugi (drifting snow dunes).

The following points should be noted, however:

1. The ram profile alone provided insufficient data on which to base accumulation figures, as has sometimes been done. Ram soundings displaced laterally by a matter of meters could sometimes not be correlated in areas of complex stratigraphy. Properly taken ram readings do, however, contribute to the fine detail of conventional pit interpretation.

2. The difference between density profiles from shallow pits (2 meters) was not sharp enough to allow a statistical separation of annual layers. Sastrugi effects, for example, masked the variations that would be attributable to the added accumulation of a sixth year over a fifth.

3. Density profiles from different temperature environments could not be statistically distinguished by the seasonal oscillations of the profile curve or by the slope change of density with depth, when the profiles were reduced by root mean square to straight lines. The one distinguishing characteristic was over-all increase of density with lower temperatures (offset of intercept). These regional effects of temperature were of interest but did not aid the dating problem.

Alternative inferences of the temperature effects were (*a*) the temperature effect could not be properly accounted for by the present acuity of densification formulas [*Bader*, 1960], or (*b*) the statistical population must be greatly increased to attain greater precision of analysis, or (*c*) the problem was affected by variables not considered in the calculations made.

Selecting stratigraphic features from this summary (crusts, ice layers, etc.) as the most reliable tracers, type-control pits for Little America and Byrd stations were constructed using data from many of the control pits of the respective stations.

The Little America half of Figure 1 is the compiled type-pit, intended to represent the Little America stratigraphy as it appeared at the onset of 1958–1959 summer field season. The photo is a composite of two pits, chosen because they showed the most important features found in the entire control zone study. Figure 1 also summarizes in photographic form the continuity of key horizons from the type-control pit at Little America, through the Little America control zone, to the type-control pit at Byrd station.

Very few pits at Byrd station were excavated in the immediate proximity of stakes. The few that were, however, conformed closely to those excavated at Little America. Sequence of features and dates of formation were almost identical. Differences were largely attributable to temperature effects, i.e., crusts instead of ice layers for summer horizons or complete absence of a particular snowfall. Figures 2 and 3 show several control zone pits illustrative

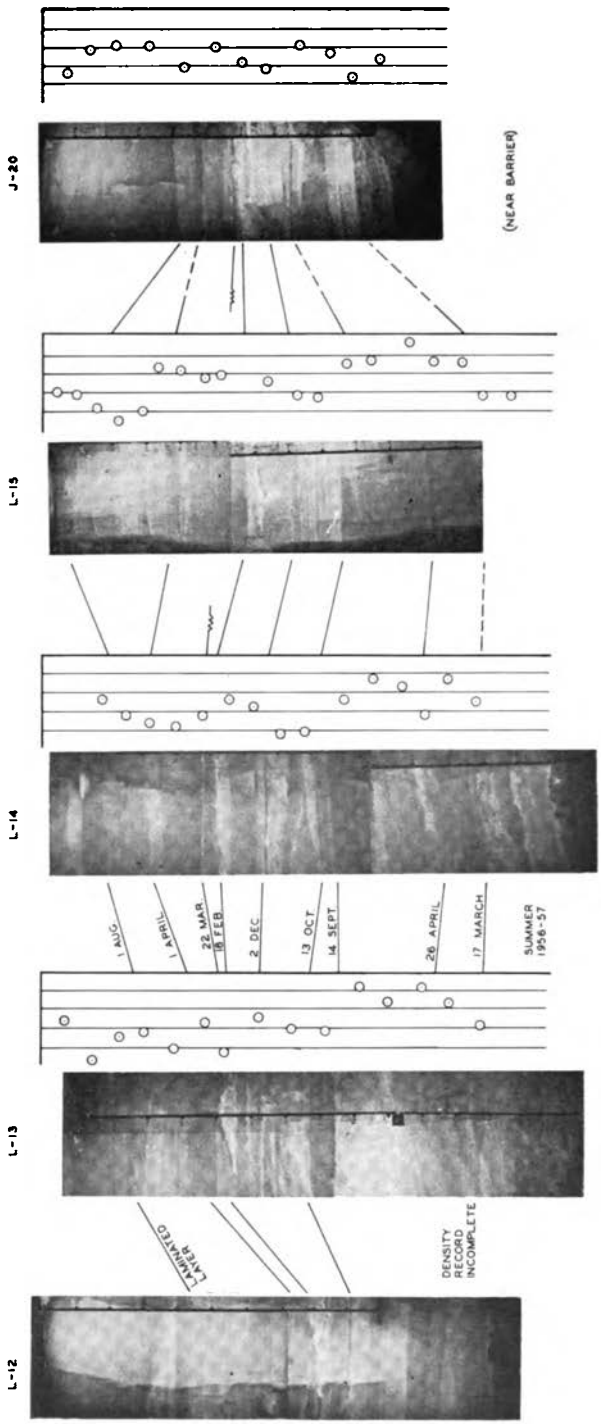

Fig. 2. Examples of Little America control pits (5 of 21).

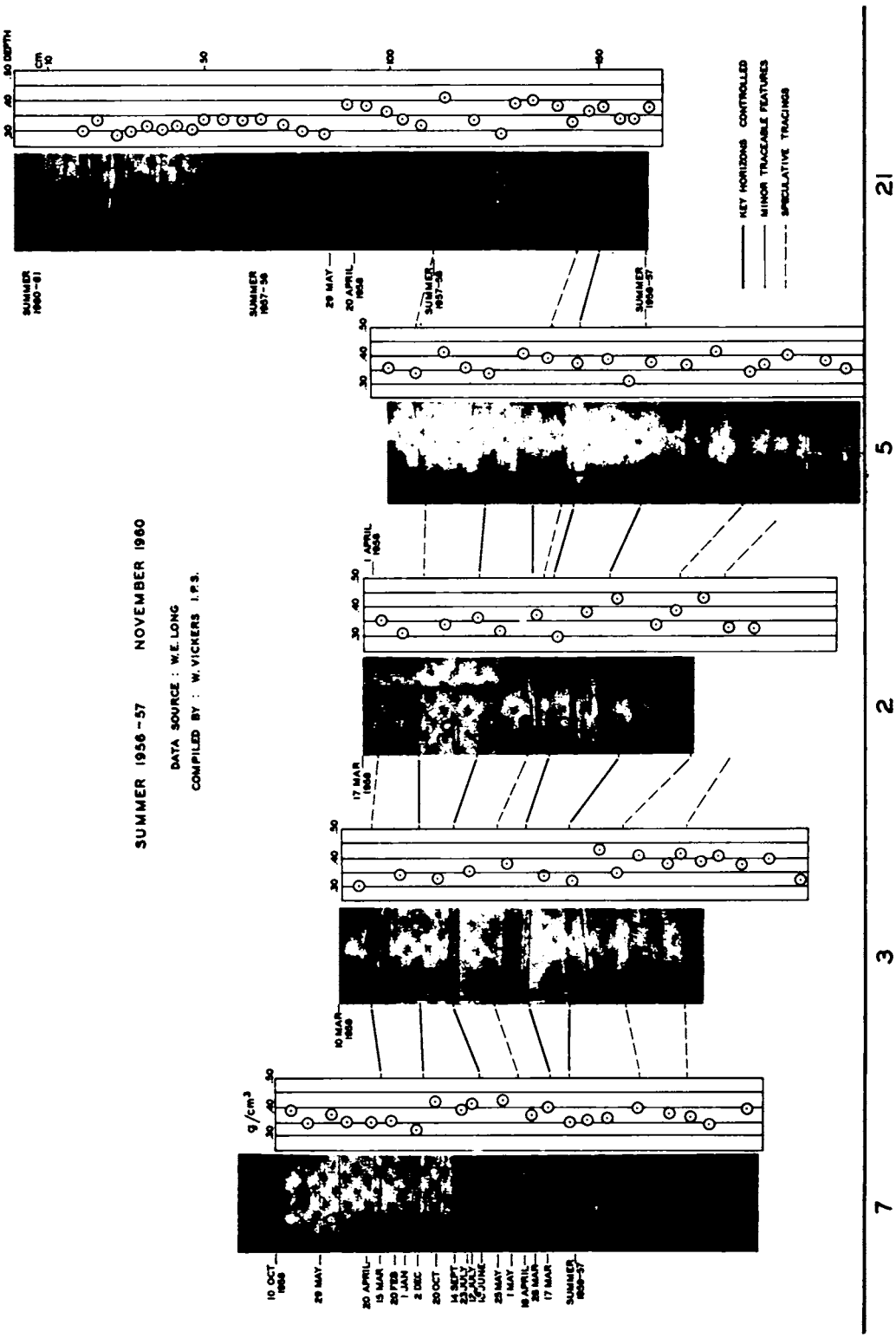

Fig. 3. Byrd station control pits.

of the variations to be expected within the respective zones.

Correlation of Synoptic Patterns, Station Accumulation Records and Type-Control Pit Stratigraphy

The next objective is to correlate storms and stable periods as depicted on 2700 surface weather charts (1957–1959), with snow surface fluctuations as depicted by station stake farms, to show that the effects of well-defined weather systems often are widespread areally and that the meteorological record directly correlates with known stratigraphy.

The observed effect of meteorological factors has already been photographically illustrated in Figure 1, where all time periods considered are identified. The accuracy of the actual surface fluctuation record is further supported by Figures 4 and 5. The surface fluctuation record shows exact dates on which snowfalls occurred (marked with snowflake symbols), as do the correlating weather maps. The surface fluctuation plot is not precisely simultaneous with weather map snowfalls because the stake farm readings, represented by the vertical offsets of the plot, were often a few days tardy owing to more urgent duties of the field crews. Erosion details in Figure 5 (a continuous pit) support the Little America surface fluctuation and meteorological records in great detail. The diagram shows surface level plotted with time, a November and February excavation with grain size and density measurements, and drizzle crust formations in May and June marked by quotation marks.

In association with the above-mentioned diagrams, Table 1 is a compilation of significant correlations of data within which the greatest store of evidence supporting this study is contained. The three columns (summarized in the following section) are intended to point out changes occurring simultaneously in tropospheric synoptic patterns,

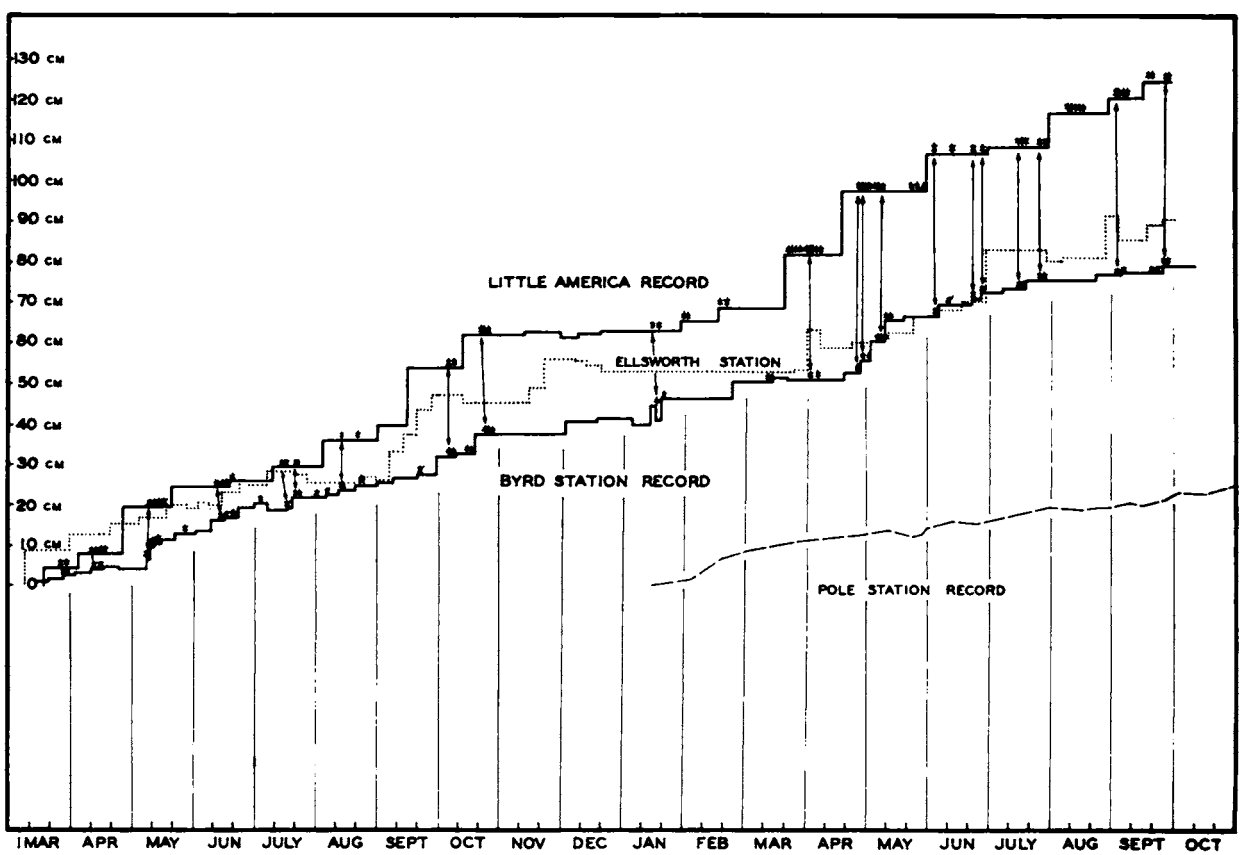

Fig. 4. Comparative accumulation: surface fluctuation plots.

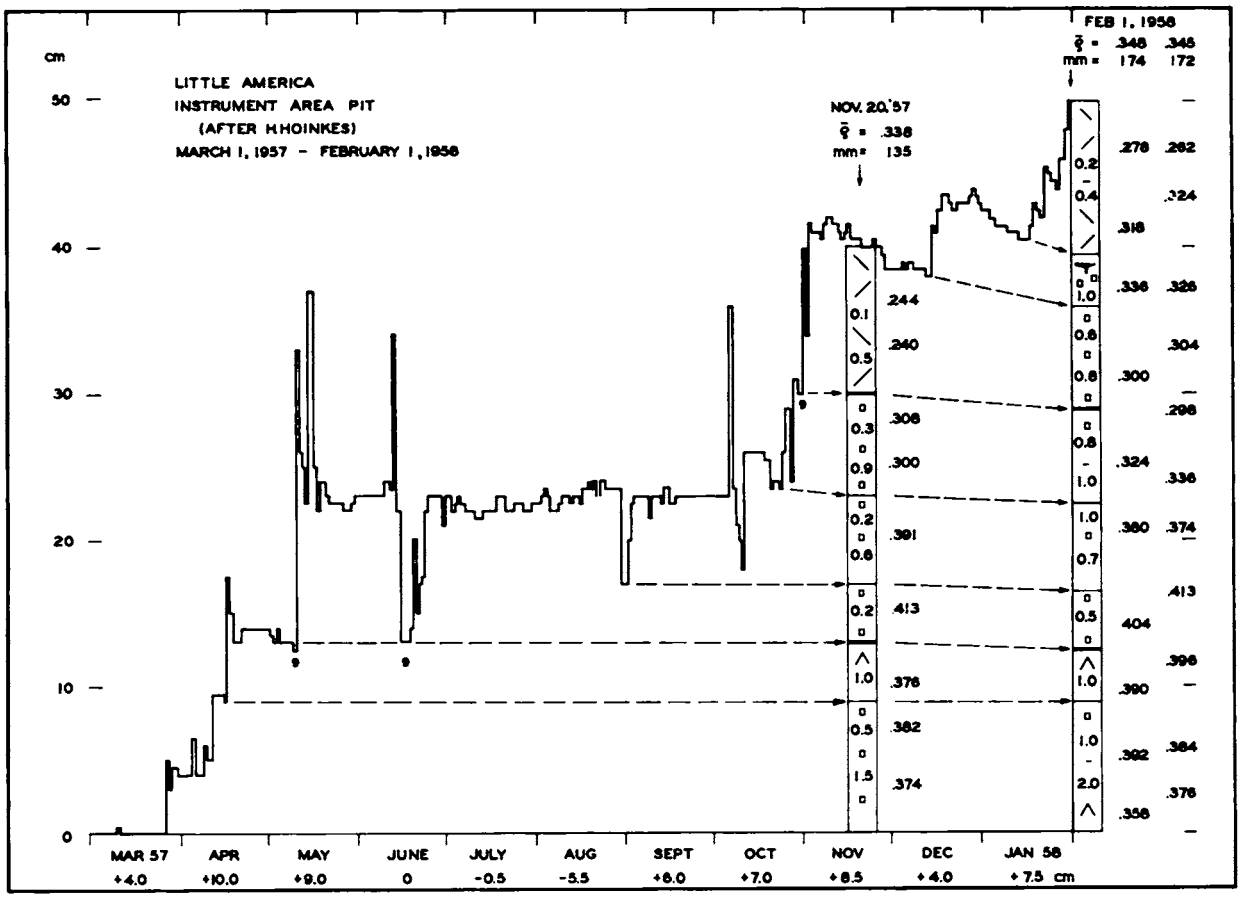

Fig. 5. Record of exact periods of scouring and filling, Little America V.

TABLE 1. Correlation of Synoptic Patterns, Station Accumulation, and Type-Control Pit Stratigraphy

Synoptic Pattern (Refer to Synoptic Charts as Directed)	Accumulation (Refer to Figure 4)	Stratigraphy (Refer to Figure 1)
MARCH 1957		
Figure 7 (0000 Mar. 27). Greatest accumulation during the last stage of occlusion. Deposited snow Little America, within last 3 hours. Actively depositing at Byrd.	Graph of Figure 4: Change in snow surface with passage of occlusion, and ensuing low pressure. Comments by Ben Harlan (monthly weather summary) indicate high winds eroded mid-March surface back to reference ice layer. Hoinkes pit, Figure 5, showed 3-cm net increase, in keeping with the main stake farm plot.	Little America records supercooled fog on Mar. 16–17. Surface, thin crusted, 1 mm, henceforward referred to as Mar. 17 surface (Figure 1).
At 0000, March 29 (chart omitted), occlusion followed by small localized low. Simultaneous precipitation at McMurdo and Little America. Later, however, larger low-pressure area lying northwest of Ross Sea, Figure 7, combined with smaller low. Reinforced system moved easterly to bring similar quantities of precipitation to Byrd station.	No stake farm data for McMurdo, although snowfall recorded in meteorology records. Accumulation at Ellsworth from independent low. Nothing in record suggests surface increase for Ellsworth Figure 4, due to Ross Sea low crossing overland from Byrd to Ellsworth.	Late March snow surface appears at 126 and 83 cm at Little America and Byrd stations, respectively. Significant effects just beneath snow surface. Time of maximum sublimation in snow cover recorded. Stratigraphic photos, Figure 1, show sublimation in lightest tone. In both photos sublimation affects March 1957 snow. Upward transition to unsublimated snow at Little America more abrupt than at Byrd. Explained by the transitional snow eroded at Little America by mid-March storm. Most significant, sublimation excellent horizon marker. Occurred in all 22 control pits.

TABLE 1 (*continued*)

Synoptic Pattern (Refer to Synoptic Charts as Directed)	Accumulation (Refer to Figure 4)	Stratigraphy (Refer to Figure 1)
APRIL 1957		
Intermittent flurries first half of month Little America and Byrd. Result of apparent back and forth migration (readings every 6 hours) of Ross Sea low between Little America and Sulzberger Bay—Hobbs Coast. Displacement perhaps controlled by inland high threatening first breakout of cold season (accomplished by end of month). Figure 8 (1800, April 26), position to which low shifted from Little America, high burst forth over western Ross Sea, drives low to Hobbs Coast. By April 28 bulge of high extended from Ellsworth to McMurdo. 1800, May 3 (omitted): Recession of high into Victoria Land. Re-establishment of low over Little America.	Accumulation small for any period at any station. Collectively, month's accumulation significant to extent indicated, surface fluctuation plot.	Accumulation bounded in stratigraphy by effects of break out of high throughout western Antarctica. Long period of stable atmosphere (strong inversion) associated with high gave ample time for undisturbed snow to crust. Crusts of this nature stand out well in stratigraphy. See Byrd pit at 74 cm; 98 cm for Little America (Figure 1). Little America crusted surface modified in early May (discussion deferred to May). Crust will henceforth be referred to as early May horizon (May 1). Very important stratum tracer.
MAY 1957		
Figure 9 (0600, May 8), precipitation starting at Byrd. High ridge over western Ross Sea (in position since April) begins recession. Intense low-pressure system northwest of Ross Sea. 1800, May 8 (chart omitted), low elongated in east-west direction bringing precipitation to most stations. Well-developed low-pressure system to northwest shifted easterly around ridge, strengthening original lows; replaced in its oceanic position by low from Wilkes coast. 0600, May 9 system intensified, Figure 10. Remained in force until May 12. Accounts for continuation of surface level surge in respective station plots, Figure 4. 0000, May 12 (omitted), Ross low still persisted; by 1200 low-pressure system regressed into Victoria Land, Figure 11. Eastern side continued to precipitate, Byrd and Pole stations. Weak low now off Cape Adare, and low to north, intensified and restarted cycle. Chart for 1800, May 13 (omitted), shows again regression into Victoria Land. May 23 (omitted), inland high again took over, succession of May snowstorms completed.	Concurrent and following circulation described for early May, biggest deposition of season occurred. Stake farm plots and monthly weather summaries show storm prevailed over most Antarctica west of Byrd-Ellsworth divide. See time correlation of Byrd and Little America plots, Figure 4. Small fluctuations of Byrd stake farm plot and Hoinkes pit, respectively, pinpoint major surface change as occurring on 8th and 9th at Byrd and lagging a day at Little America.	Weather greatly affected stratigraphy. Beginning of May high still present. Inactive surface evident in Hoinkes diagram and in Byrd stake farm plot. May 10, according to Hoinkes, drizzle at Little America; on May 11, according to meteorological record, large quantities of warm snow, $-4°$ ambient surface temperature, deposited on cold, $-17°$ snow surface. Snow fell in slush state, freezing in fused crust form. Above phenomenon not merely local. Byrd station monthly weather summary states: 'With the exception of a virtual heat wave, the temperature pattern closely resembled that of April; the coldest at the beginning and ending of the month, and the warmest during the middle of the month. With a daily mean temperature of $-60°$F and a max. of $-55.3°$F on May 1 representing the cold period, the temperature began a steady march and by the 9th had rocketed to 8° above zero. On the 10th both the max. and min. temperatures were above zero. In the period from the 9th through the 17th all the maximum temperatures were above zero. The highest temperature 19.5°F occurred on the 11th. Temperatures fell off rapidly after the 17th finally

TABLE 1 (*continued*)

Synoptic Pattern (Refer to Synoptic Charts as Directed)	Accumulation (Refer to Figure 4)	Stratigraphy (Refer to Figure 1)
	MAY 1957 (*continued*)	
		dipping to the lowest monthly temperature for May (−66.4°F on the 28th).' Heat of fresh snow enough to cause local vapor exchange (within 1–2 cm of contact). Narrow band of sublimation layer, Little America control pit (Figure 1), at ∼100 cm. Regressions of low into Victoria Land (under Synoptic Pattern) important. Snow resulting appears in Victoria Land traverse strata as thick massive layers.
	JUNE 1957	
High persisted through first week June. Intermittent one-day flurries occurred Byrd and Little America, June 8, 9, and 10, trace amounts. First widespread precipitation after recessions, June 13, 0600 (omitted). All stations recorded precipitation simultaneously. Peak precipitation 11th to 19th, Little America, and 13th to 19th, Byrd, according to monthly weather summary. June 17 (omitted), low begins to occlude. Occlusion followed by lows sporadically to end of month. Contributed to replenishment of heavy erosion, Little America, during mid-May storm.	Little America stake farm showed less gain than expected. May snow eroded and replaced with June snow. Observe extreme erosion May snow, Hoinkes' pit (Figure 5), mid-June. Surface lowered to old May 1 horizon. Figure 12 (June 14) explains: Little America wind rose shows violent onshore winds. Wherever ice shelf exposed to easterly quadrant of system, which later receded westerly, shelf eroded. No replacement material available upwind of ice front. Effect: locally diminished quantity May snow in strata. Erosion seen in Hoinkes' pit (∼3 km from ice front) much more severe than Little America stake farm. Deficit soon made up by another series heavy storms. No identifiable break in Little America stratigraphy between May and June snow. Little America-Byrd plots show Byrd's stake farm noticeably greater net accumulation, because no ice front situation comparable to above.	Significant that large snowfalls May and June comprise 'winter massive,' thick section of homogeneous winter snow. Byrd station snowfalls well bracketed by crusts, 64 and 74 cm, control pit. Early May crust well marked, Little America, 98 to 103 cm, but only possible to locate end of June by distinct marker. Missing feature appears in traverse pits, however, marked as June 18. No other traceable stratigraphic feature encountered until September. Large snowfalls of May and June poorly differentiated in strata, Little America. May 15 and June 11 surfaces congruent in type-control pit. Manifested by stake readings alongside pit.
	JULY 1957	
July 1–4: Widespread low caused precipitation, Byrd and Little America, recognizable on Byrd plot and Hoinkes' pit as 1–2 cm increase. Followed by 6 days control by high (1800, July 6 example (omitted)). Low returns July 11 as inland high weakens. Repeatedly reinforced by series of lows from Cape Adare, Figure 13 (July 14). Note lineup lows along coast of Wilkes Land. Usual to cut across Cape Adare and merge with Ross low. Reinforced low remains in Ross Sea position several days.	Low present 80% July. Resulted in cumulative increase, Byrd and Little America. Increase less at latter because onshore wind (erosion) again became intermittently operative. Note successive fill and erosion, Hoinkes' pit, slight gain at Little America stake farm, and greater though concurrent gain Byrd stake farm. Moreover, Byrd relative plus accumulation end of month. Explained by abnormal penetration of low into Byrd station, 0000, July 31 (omitted). Byrd plot, Figure 4, shows slight end July-	Other than increased accumulation, month was of minor stratigraphic importance. No important stratigraphic markers formed.

TABLE 1 (*continued*)

Synoptic Pattern (Refer to Synoptic Charts as Directed)	Accumulation (Refer to Figure 4)	Stratigraphy (Refer to Figure 1)
JULY 1957 (*continued*)		
Figure 13 also shows another preferred breakout position of inland high, Ellsworth station. Observe it holds lows offshore. Sometimes coincides with well-established low over Ross Sea. Queen Maud Land does not experience effects of inland high often; thus greater accumulation on final map for Queen Maud Land than for Ellsworth.	early August anomaly. Not known whether small low crossed divide to Ellsworth. Ellsworth plot suggests no.	
AUGUST 1957		
August: introduced new phenomenon —counterpart of blocking highs of northern hemisphere [Rex, 1950]. (See *Van Loon* [1956]; *Grandoso* [1955] for southern hemisphere observations.) Pronounced high formed in area of Antarctic Peninsula. Normal circumpolar air stream diverged around block. Effect of divergence is clear weather. Note relative flattening of Byrd accumulation plot, which also gives minimal precipitation Ellsworth, Lassiter substation, Maudheim (not shown). Figure 14 (1200, Aug. 11): Structure of blocking phenomenon. Note wind direction (diverging counterclockwise stream), clear skies Ellsworth and inland substation. Block may converge air on side adjacent Ross Sea low. Later, coupled with orographic lifting, creates highest accumulation area western Antarctica. Aug. 13: Low caused coincidental precipitation Byrd and Little America. Again Aug. 20, widespread precipitation Byrd, Little America, McMurdo, and Hallett simultaneous. All stations west of Byrd divide record snowfall.	August significant only in slight addition to earlier accumulation.	Month shares with early September (100% occurrence) crust resulting from widespread high. Crust invariably associated with break in density curve. Marker appears in Little America pit, 77 cm; and in Byrd, 56 cm (Figure 1).
SEPTEMBER 1957		
Intense low formed over Antarctic Peninsula (chart omitted). Remained stationary. Placed Ellsworth in line with easterly quadrant strong onshore, moisture-laden winds.	Surface charts and stake farms suggest little activity, except Ellsworth. Meteorology reports and stake farm here show considerable snow fall. Storm not same as storm responsible for big October accumulation rise, Little America and Byrd stake farms (see October below).	Most winter massive Ellsworth attributable to September snow. Early September crust marker, Little America and Byrd, already discussed under August.
OCTOBER 1957		
One of largest accumulations resulted from two October snowfalls. On 5th and	Increase in accumulation considerably greater at Little America than Byrd.	Crusts developed with onset summer weather; some, Little America, later

TABLE 1 (*continued*)

Synoptic Pattern (Refer to Synoptic Charts as Directed)	Accumulation (Refer to Figure 4)	Stratigraphy (Refer to Figure 1)
OCTOBER 1957 (*continued*)		
6th, Figure 15. Note all station models reported snowfall simultaneously. Third week, reoccurrence. Figure 15 illustrates areal extent of precipitation zone for many cyclonic systems.	Accumulation effect of October snowfalls well-illustrated in surface fluctuation plots.	reinforced by percolation melt water. Crusts, 68 and 71 cm, Little America, correspond to 51 and 53 cm, Byrd (Figure 1). Control pits accurately reflect increases at respective stations (depicted by stake farms).
NOVEMBER–DECEMBER 1957		
Occasional local snow flurries occurred. Ross low remained primarily near Sulzberger Bay. Temperature, as function of circulation, became focus of attention rather than precipitation.	December temperatures reached melting point, lower coastal areas. Very distinct layers in strata. Surface often settled faster than accumulated, if melting profuse. Anomaly arose between Little America, Byrd, surface fluctuation plots. Byrd snow melted; gave net increase accumulation over Little America.	Granular crust layer formed Byrd. Little America clear amorphous ice or multiple crusts fused together. Crusts seen in Figure 1.
JANUARY 1958		
Precipitation Little America, Jan. 15 and 17; Byrd, 16th and 18th; Pole, 15th and 16th (dates considered only when accumulation exceeds 3 mm).	Increased accumulation at Byrd greater than Little America, owing to previous melting and settling at latter. Accumulating snow approximately restored level of settled surface. Storms responsible for restoration concurrent at Little America, Byrd, and Pole stations.	Stratigraphic significance treated jointly with February effects.
FEBRUARY 1958		
Feb. 17 and 18: Field parties on Ross Ice Shelf and 'Victoria Plateau' record precipitation extending westward from Little America. Again Byrd no precipitation. (Independent rise on Byrd plot between Feb. 25 and Mar. 14, dates of stake measurements, actually occurs on Mar. 13 and 14.) Precipitation distribution suggests February lows entering Ross Sea retreat to southwest corner Ross Ice Shelf. Precipitation on plateau may have been heavy since inland high weakening. Figure 16, note widespread reporting of snow, especially: Fuch's field party on the 'Victoria Plateau,' lat. 82°40′S, long. 141°00′E; Liv Glacier station, lat. 83°00′S, long. 178°W.	Figure 4, Pole station stake farm record, 1958 (recorded by Giovinetto), shows February had greatest rate of accumulation for entire year. Note minimum loss recorded by individual stakes, as well as time for maximum upward surge. This is indicative of heavy snowfall where little scouring and much filling at surface. Precipitation of minor stratigraphic importance, except for pits to be excavated in high interior. (Thick layer consistently found on traverse).	Maximum sublimation observed to occur February. Little America photo record. Snow recorded between 51 and 56 cm often displays wave form seen in photo. Light tone shows snow of Jan. 15 and 17, whose wave forms formed a melt crust of fused grains. Snow rapidly sublimated beneath crust. Observed to subsequently fuse, a result of warm weather. Described author's field notes as 'rotten snow,' i.e. snow with no cohesive strength. Fused crust is visible in photo. Byrd station: High degree of metamorphism for early February snow lacking. Unlike melting snow at Little America this snow remained dry and continued drifting; it did not remain stationary long enough to sublimate. Drifting at Byrd is suggested by stake farm plot which shows slight 1.5-cm

TABLE 1 (*continued*)

Synoptic Pattern (Refer to Synoptic Charts as Directed)	Accumulation (Refer to Figure 4)	Stratigraphy (Refer to Figure 1)
	FEBRUARY 1958 (*continued*)	
		rise in February. Since no precipitation recorded, rise attributed to cumulative 'trace' reports. Six centimeters in Byrd photo between 32 and 38 cm is one place where uncertainty arises. Recorded level of Feb. 20 seems too high. Crust at 32 cm, however, in conformance with other correlated records and comparable to marker at 50 cm Little America. Little America: Darker-toned snow, within 51–56 cm limits is snow that fell Feb. 17 and filled between 'rotten snow' nodes. Section is topped by marker, 50 cm, which has high frequency occurrence, formed in first 3 weeks March.
	MARCH 1958	
Greatest effects attributable to inland high and Ross Sea low which alternate control of weather. Results clearly stated under Synoptic Patterns and Stratigraphy.	Anomalous rise of accumulation at Byrd beginning on Feb. 25, continued into March. Moreover, large accumulation occurred Little America only, during last week March, due to local concentration of Ross low. For March, therefore, the respective stake farm plots become slightly out of step with one another.	The crust at 50 cm, Little America, attributed to long still-stand (stable high present) during first three weeks March. Byrd station's counterpart is at 32 cm, although still-stand did not last so long. Snow that fell at end March, Little America, is between 43 and 50 cm. Byrd station has no accumulation counterpart. Distinctive character imparted to Little America crust 43 cm, by sleet on Mar. 31 and April 1 at $-1°C$ ambient air temperature. Elsewhere sleet crust not always present as might be expected. However, precipitation warm and sublimation slight in amount but high in frequency occurrence; manifested by a break in density curve. Referred to as April 1 position in snow strata.
	APRIL 1958	
April 9–14: Little America under influence of inland high. System affected Byrd from 8th to 17th. There is strong mid-month break. Figure 17 shows strength of high in terms of geographic extent. High temporarily replaced and slight precipitation occurred Little America on 15th–17th. Quantity reported as trace. Byrd precipitated on 18th, 19th, and 20th (not plotted). Low then pushed seaward and easterly by inland high again, as was character-	In what can be considered end-of-March weather, most of precipitation for April fell at Little America first 2 days of month from Ross low. In stake farm accumulation plot, note minimal accumulation at Byrd during this period; gave large April discrepancy between the two stations.	Crust formation for April 1 already presented under Mar. 31. Main stratigraphic significance for April was reflection of highly anomalous stake farm plots in stratigraphy (Little America vs. Byrd). Stratigraphic effect self-evident in control-pit photos. Note comparative positions (Byrd vs. Little America) of the April dates. A missing marker becomes evident here in Little America type-control pit. All other control pits distinctly show a crust and/or density break at surface

TABLE 1 (*continued*)

Synoptic Pattern (Refer to Synoptic Charts as Directed)	Accumulation (Refer to Figure 4)	Stratigraphy (Refer to Figure 1)
APRIL 1958 (*continued*)		
istic of this season for 1957. High remained until 24th, receded on 25th, advanced on 26th. Low again returned; gave widespread precipitation. Byrd experienced greatest precipitation for month, 10-cm surface rise.		level coincident with April 21. Break clearly due to high displayed in Figure 16, followed by warm snowfall which brought sublimation at cold surface contact. Same phenomenon occurred to more marked degree on May 9 of preceding year.
MAY 1958		
May again month of greatest precipitation (major storms actually include end of April). Ross low present during all but 3 days in first week. Inland high momentarily in control. As in 1957 for this period, Ross low migrated toward Sulzberger Bay area, but whether it oscillated or regressed to Little America not evident on charts (12-hour data intervals, 1958, compared with 6 hours, 1957). Surface weather maps correlate well with snow surface plots, Figure 4. After May 17, area east of Byrd divide affected by ridge extending south from blocking high over Bellingshausen Sea.	Large simultaneous rise of accumulation recorded by Byrd and Little America stake farms. However, ridge extending south from the blocking high gave minimal accumulation in Ellsworth region, confirmed by Ellsworth plot (Figure 4).	Large simultaneous rise of accumulation, Little America and Byrd stake farms, duplicated in pits. Moreover, accumulated thick layer frequently displays laminated structure seen in photos. Such characteristic appearance is consistent aid in identification of layer.
JUNE 1958		
Accumulation heavy in June 1957 but June 1958 affected more by inland high than by Ross low, accumulation low (though widespread). Weather map similar to that representing mid-May, except all lows held well to seaward by strength of inland high. Surface for this period well defined (crusted) in stratigraphy.	June accumulation not a repeat of preceding year. Byrd station will only receive another 17 cm of snow before succeeding summer, because of frequent presence of high-pressure systems. Byrd station recorded trace quantities only on days of heavier Little America precipitation. The slightly more-than-trace amount registered by Byrd stake farm was probably an accumulation of trace precipitation.	Stratigraphically caps big fall accumulation in form of high-density, cross-bedded slab. Dating of slab a bit circuitous: Two superposed cross-bedded slabs (plainly seen in photo) of type-control pit, Little America, are post-June 2. Verified by individual stake readings for other control pits. From stakes several individual records show August stake readings below June 28. June 26, however, is never below June 2. Since monthly weather summary records much blowing snow during July and August erosion during this period lowered surface to mid-June level. Erosion also indicated by truncation of cross-bedding (Little America photo between 24 and 30 cm) and in density curve by high value resulting from wind packing.
JULY 1958		
From 1st to 5th inland high present. On 6th through 10th a weak low of little importance set in. Most precipita-	Accumulation not particularly large. Moreover, Little America underwent some erosion with ensuing onshore	Effects on stratigraphy were slight.

TABLE 1 (*continued*)

Synoptic Pattern (Refer to Synoptic Charts as Directed)	Accumulation (Refer to Figure 4)	Stratigraphy (Refer to Figure 1)
	JULY 1958 (*continued*)	
tion occurred 15th through 17th during which time there was an intense low having characteristics of preceding years' intense mid-winter lows. Last week had few days of slight precipitation common to both Byrd and Little America.	winds on the 18th–19th.	
	AUGUST, SEPTEMBER, and OCTOBER 1958	
First week August characterized by return of apparent blocking high. Position this year more westerly. Effect again minimized surface change in Byrd highlands. By Aug. 10 the high shifted easterly into Bellingshausen Sea, in conformance with previous year's position. Precipitation accompanied this shift. Ross low slipped back into usual position and precipitated an anomalous quantity at Little America. Situation similar to that illustrated in Figure 17.	(See Stratigraphy.)	(Little America only.) Superposed on June–July high density slabs is 5 cm of August snow which gave a slightly perceptible break at about 18–20 cm. Balance of column is September snow. The photographic record at Byrd is poor. No great consequence, however, as period of record terminated in October.

surface snow accumulation, and resultant features formed and recorded in the snow stratigraphy. Note, for example, the cause and effect relationship for the very active month of May 1957 on the first page of the table. The very intense low pressure systems (lows) have produced the heaviest snowfall of the year almost simultaneously at several widespread stations and, owing to heat influx, have also formed a crust near the surface which can be identified in the stratigraphy throughout western Antarctica. Table 1 describes the meteorological events accompanying the formation of the entire stratigraphic column seen in Figure 1, starting with a weak occlusion on March 27 and creating some very significant stratigraphy as early as May 12.

Summation of Synoptic Pattern—Accumulation Relationships

This summation presents the essence of synoptic patterns as observed in the weather map analysis (1957–1959) and has not been modified to fit the indications of the next section on pressure comparison. It is intended that these sections remain as mutually independent as possible.

1. Comparison of weather maps and stake farms indicates that most of the large storms affect wide areas of western Antarctica almost simultaneously (± 2 days). This correlation is considered supporting evidence for later material which is based on the premise that one can trace a given meteorological phenomenon laterally in the stratigraphy over large horizontal distances.

2. Autumn and spring in Antarctica are characterized by alternating buildup (autumn) and decline (spring) of the inland high-pressure system (high) or systems; one can only say that it often appears to be a single high. The concept of the high is explained in the paragraph of the following section on pressure comparison. At maximum areal extent (winter), the high is able to check the poleward migration of maritime lows near the coast. Fall inroads by the maritime lows are coincident with times of maximum precipitation.

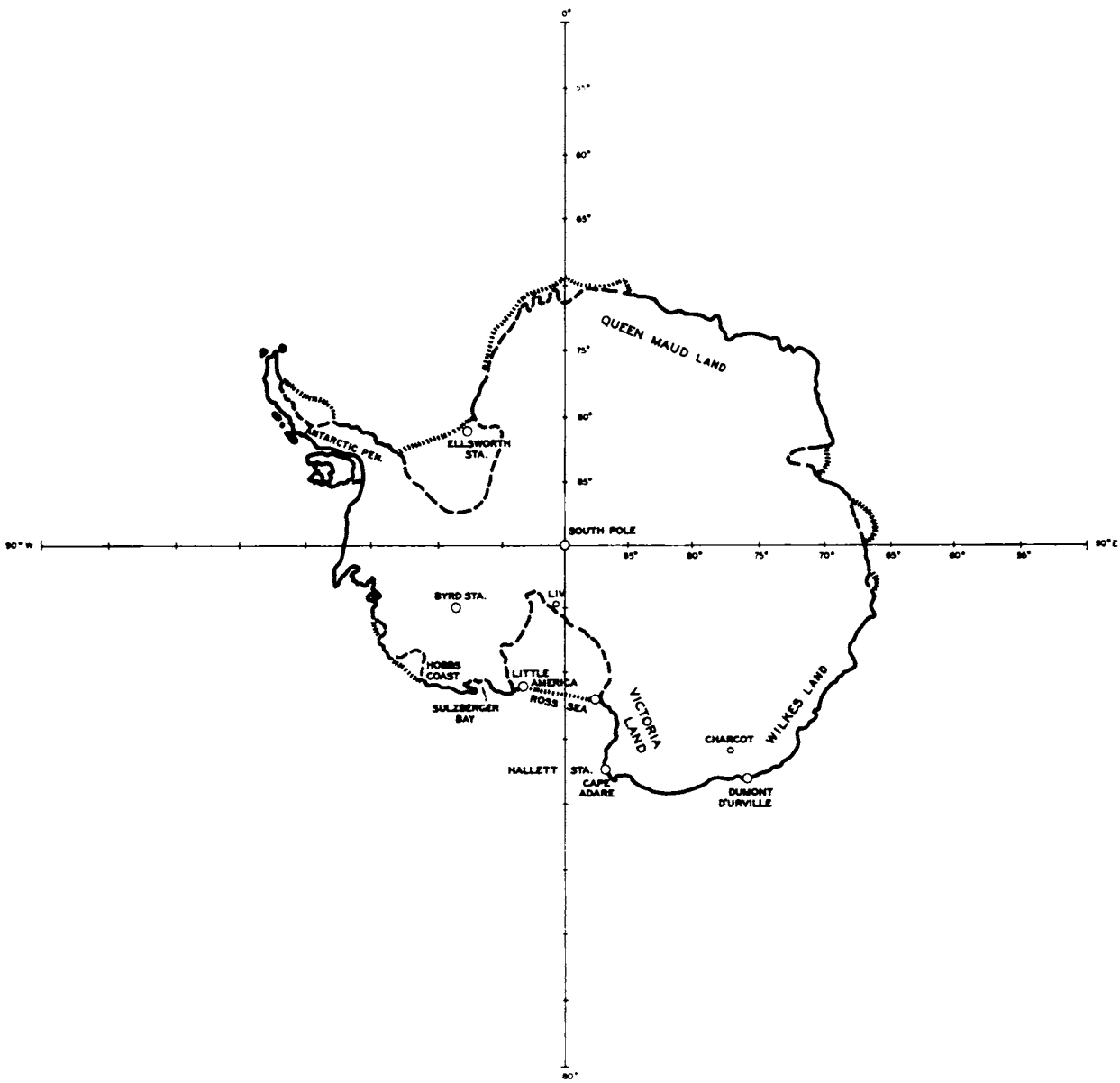

Fig. 6. Reference map for Figures 7–17.

3. Accumulation along the Ross ice front can be greatly affected by strong onshore winds from the easterly quadrant of an intensified Ross Sea low. (Such knowledge will contribute to the evaluation of drift at the end of this report.)

4. It is common for successive maritime lows along the Wilkes Land coast to cross Cape Adare and strongly reinforce a persistent low in the Ross Sea. The result is often intense and prolonged autumn storms.

5. Positive snow surface fluctuations at Ellsworth (77°43′S, 41°08′W) are at times in phase with Byrd station. However, it is not clear that this results from a continuation of the storm track across the Byrd divide to Ellsworth. A study of synoptic patterns suggests it could be a result of a pronounced weakening of the inland high which allows well-developed but separate lows to penetrate into the Ross and Weddell seas simultaneously. This agreement of snow

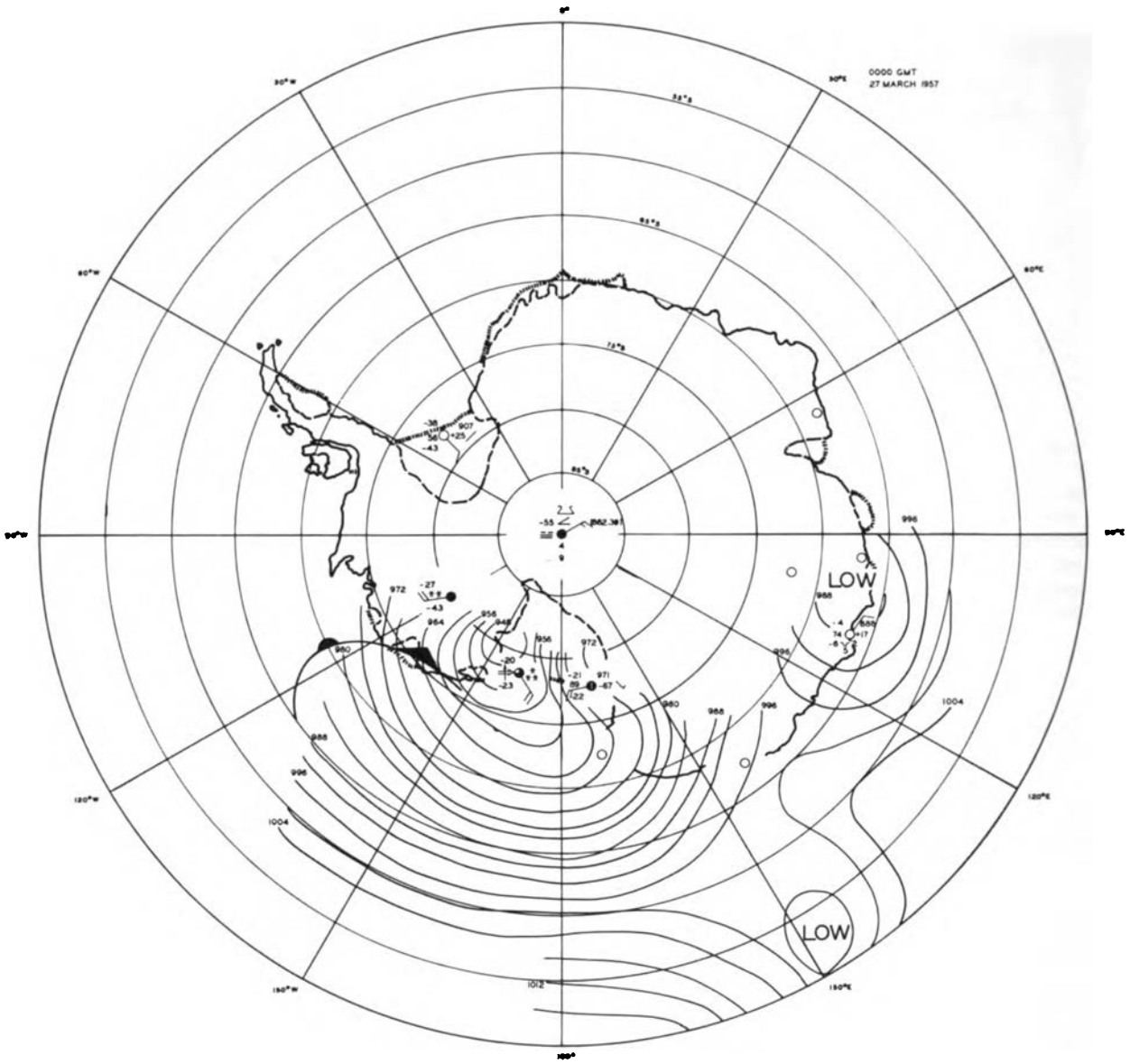

Fig. 7. 0000, March 27. Last stage of Ross Sea occlusion.

surface fluctuation is apt to be disrupted in the autumn season, if the blocking high [*Rex,* 1950; *Grandoso,* 1955; *Van Loon,* 1956] over the Antarctic Peninsula protects the Ellsworth area. It has been observed that the blocking high could protect Byrd station as well as Ellsworth station.

6. The data indicate that February may be the time of maximum precipitation on the high plateau to the south and west of the Ross Ice Shelf, although there is only a one-year documented record to support this inference. [Heavy snows at the end of summer have also been reported from the region of the Horlick Mountains (W. E. Long, personal communication, 1960)].

7. Accumulation for 1958 was generally less than for 1957, a result primarily of a nonrepeat of the heavy June and October snows of 1957. Lack of this precipitation is attributed to greater strength

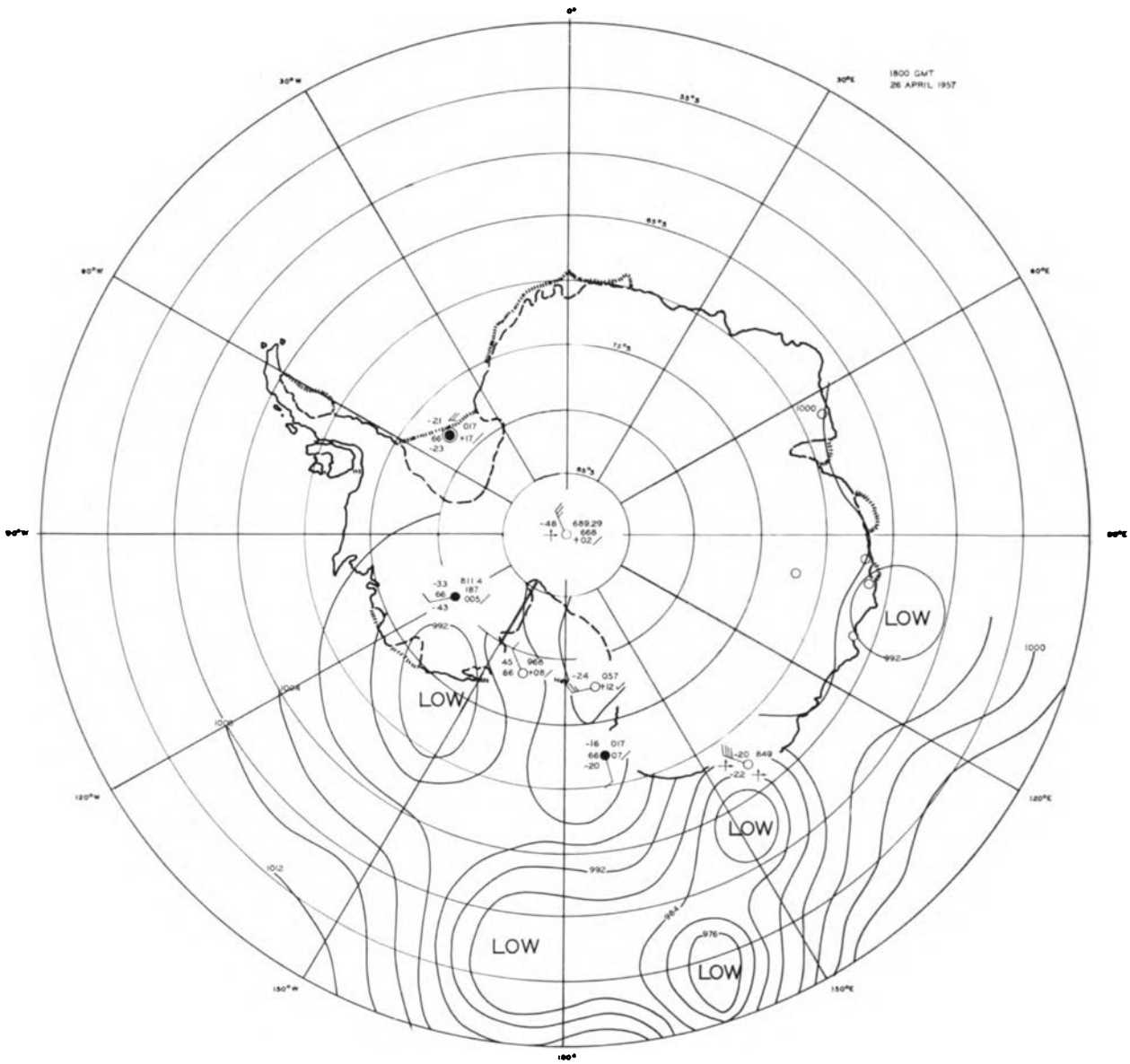

Fig. 8. 1800, April 26. Low dislodged to Hobbs Coast.

and persistence (or both) of the inland highs and protective influence of the blocking high. During 1958 the blocking high centered closer to Bellingshausen Sea than to the Antarctic Peninsula, thus strongly minimizing Byrd accumulation.

8. When the inland high is strong, the Ellsworth and Victoria Land areas are preferred positions for pressure ridges. Thus, lows are kept seaward, skirting the area, and in the case of Ellsworth come into the coast at Maudheim (71°03′S, 10°56′W). Lows at Maudheim may account for the increased accumulation at Maudheim as compared with Ellsworth. (See final accumulation map, Figure 25, for illustration of this phenomenon.)

Pressure Comparison

Figure 18 presents the trend of monthly mean pressures. Monthly deviations from the annual mean

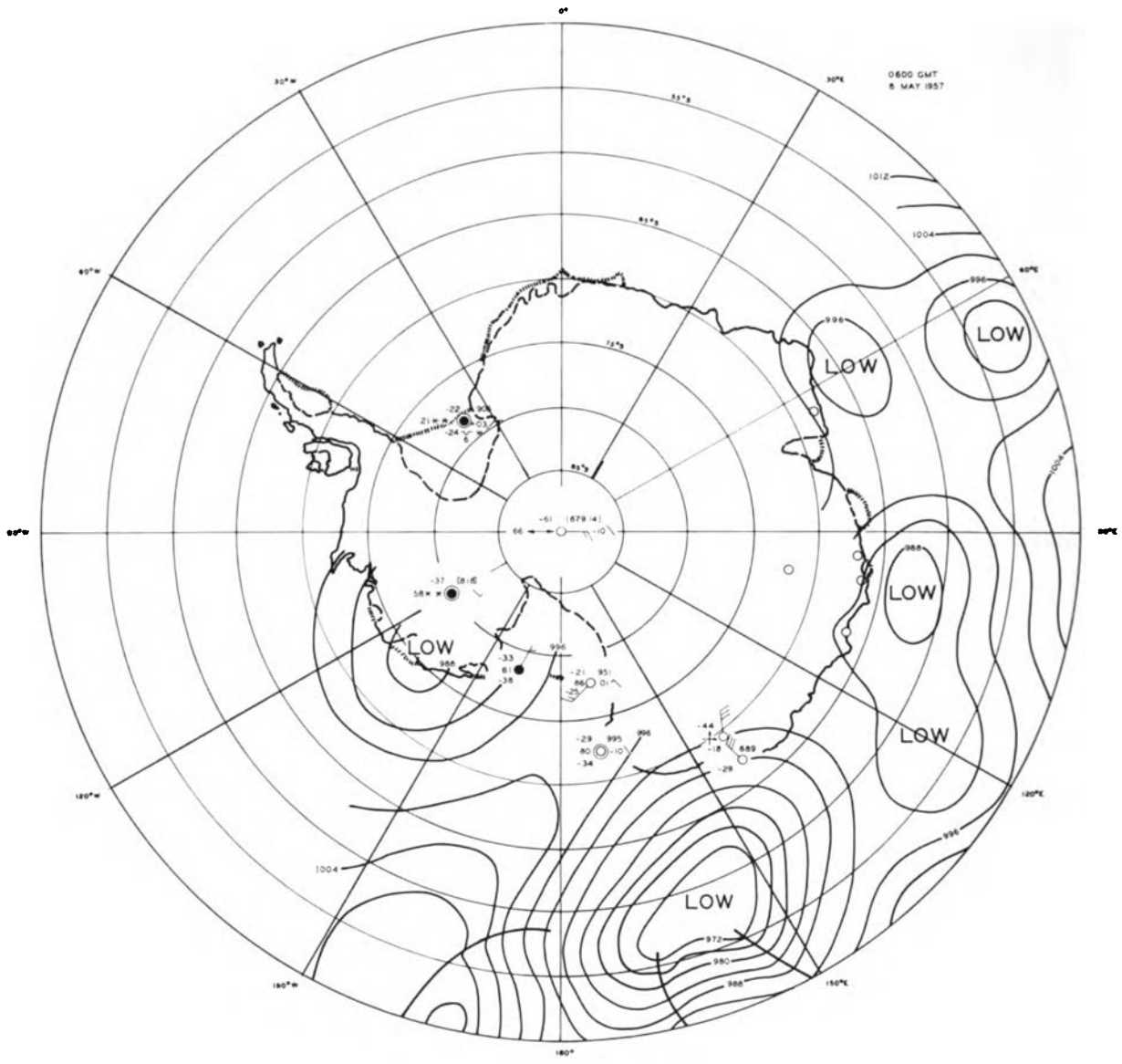

Fig. 9. 0600, May 8. Beginning of the big May storm.

have been plotted. The curves give the relative fluctuation of pressure from month to month for western Antarctica. By use of Figure 18 and Table 2 it is intended that a distinction be made between parts of the preceding description of the synoptic pattern for which support can be offered and parts for which it cannot be offered.

1. The concept of midwinter highs and autumn and spring inroads of the low-pressure system is supported but with some qualification (see item 2 of the following section on inconsistencies).

2. Table 2 has reference to ridge and nonridge areas (item 8 of the preceding synoptic summary section). Comments on the preferred high over Victoria Land are supported by the records of Hallett (72°18′S, 170°18′E), D'Urville (66°40′S, 140°01′E), and Ellsworth stations.

3. Note that Pole station and Byrd station are presented on the graph separately. The Pole sta-

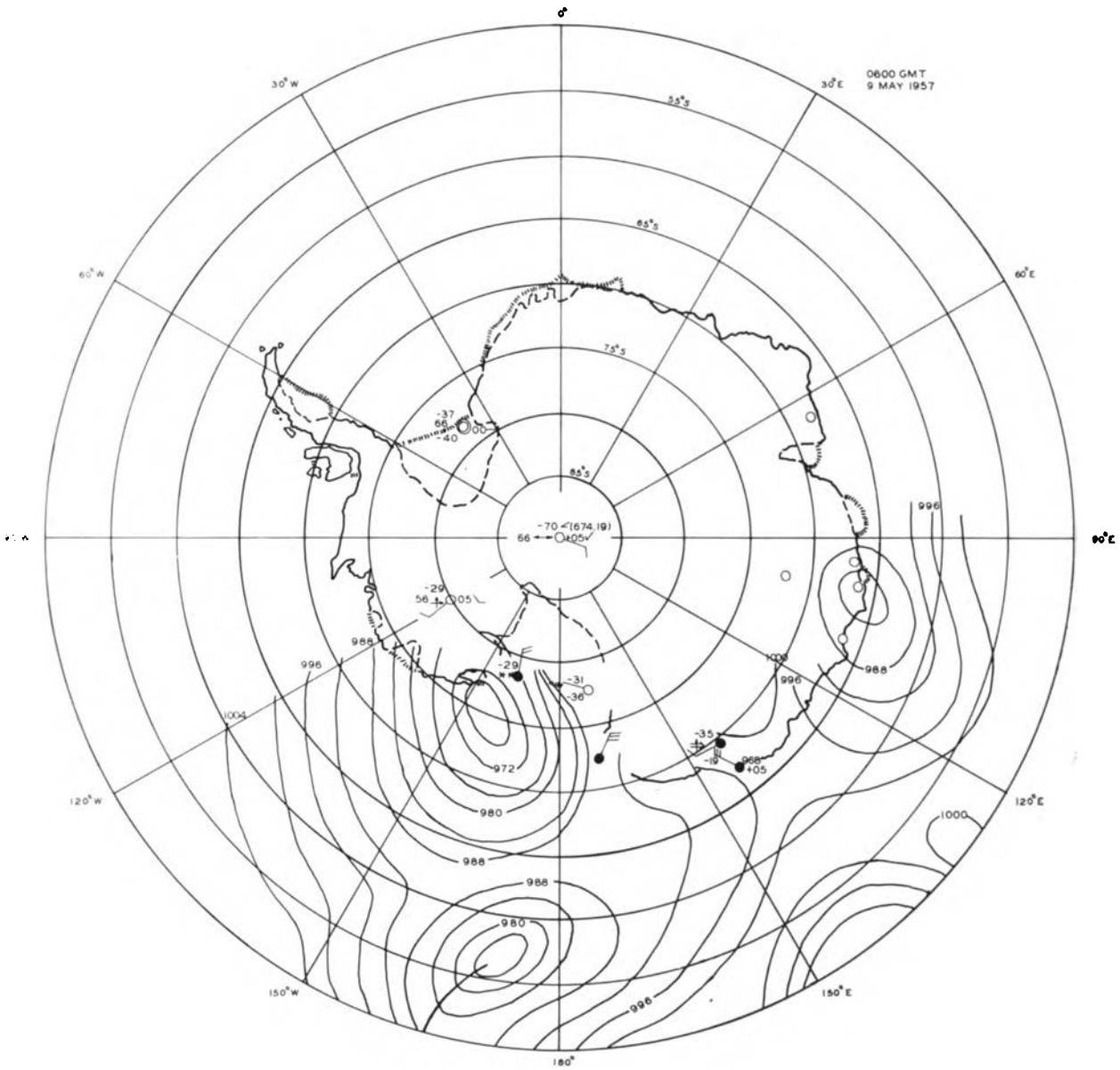

Fig. 10. 0600, May 9. Intensification of the Ross Sea low.

tion record is not necessarily out of phase with coastal stations, a question for which an answer was sought in this analysis. The midwinter high at the Pole station is of lesser magnitude (some dampening of curve is due to elevation) and actually peaks in May or early winter (see item 2 below). The peak is definitely a weak secondary maximum compared with the clearly defined summer maximum. Byrd station assumes the summer maximum of the Pole station but retains a suggestion of a secondary increase coincident with the midwinter high of the coastal stations.

Inconsistencies between the chart analysis and pressure analysis are:

1. The high-pressure period in the summer (December and January) indicated by the monthly means does not appear to an equally recognizable degree on the synoptic charts.

2. Frequency of lows in the autumn as indicated

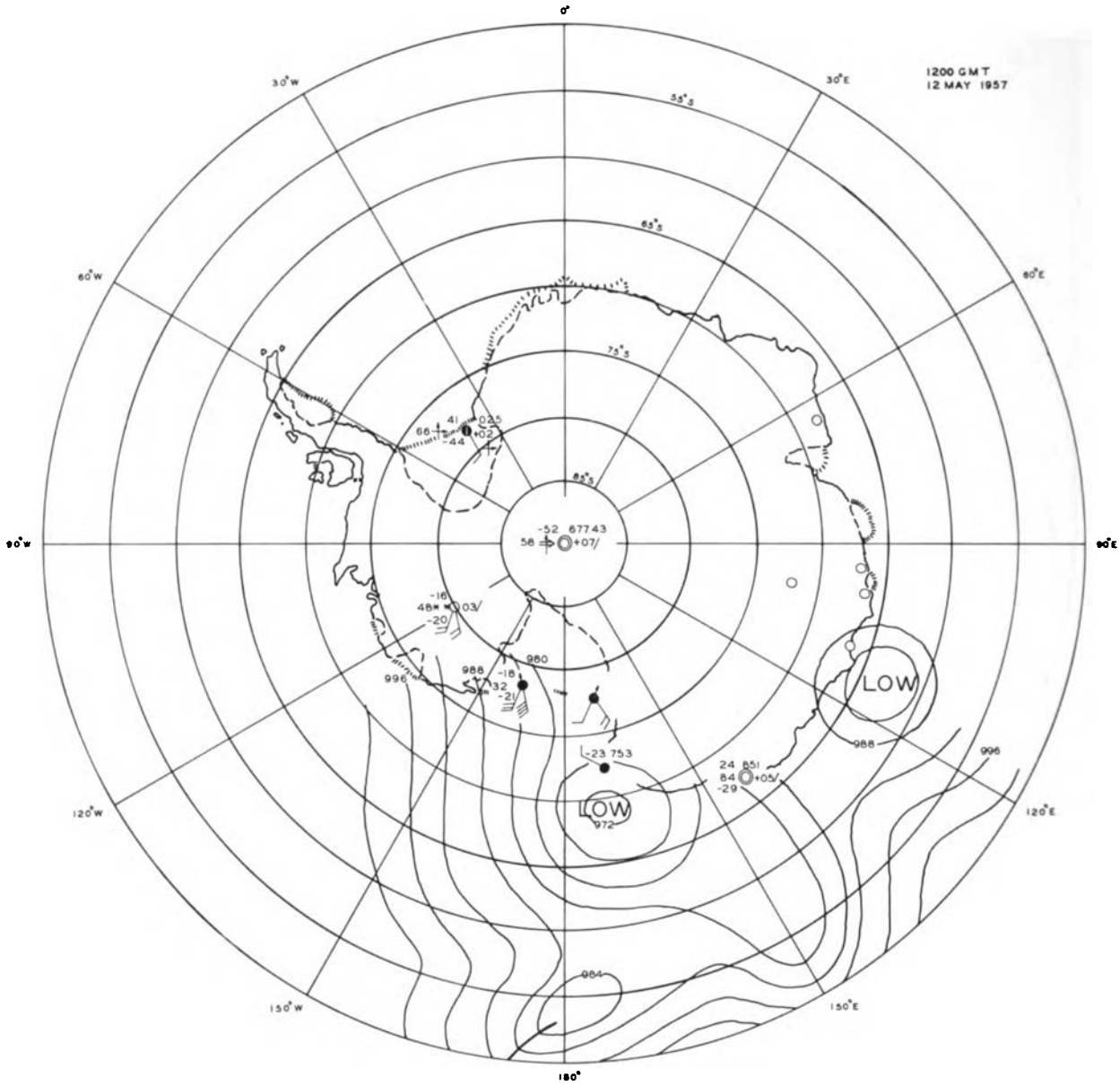

Fig. 11. 1200, May 12. Regression of the low-pressure system into Victoria Land.

by the monthly mean pressure is of a lesser magnitude than would be suggested by the charts and the snow accumulation profile (Figure 4). The winter high-pressure period of Figure 17 starts earlier and ends earlier than the charts or accumulation record suggests.

3. The idea of regressing lows (items 6, synoptic summary) precipitating on 'Victoria Plateau' in the fall is not so well supported as the assertion by *Taljaard and Van Loon* [1962, p. 5] that this is a spring phenomenon.

Stratigraphic Summation, 1957 and 1958

The composite control pit at Little America is the most informative example and can be described layer by layer upward from the 1956 to 1957 reference layer at 124-cm depth. Note Figure 1.

On February 18, 1957, the contact freezing of

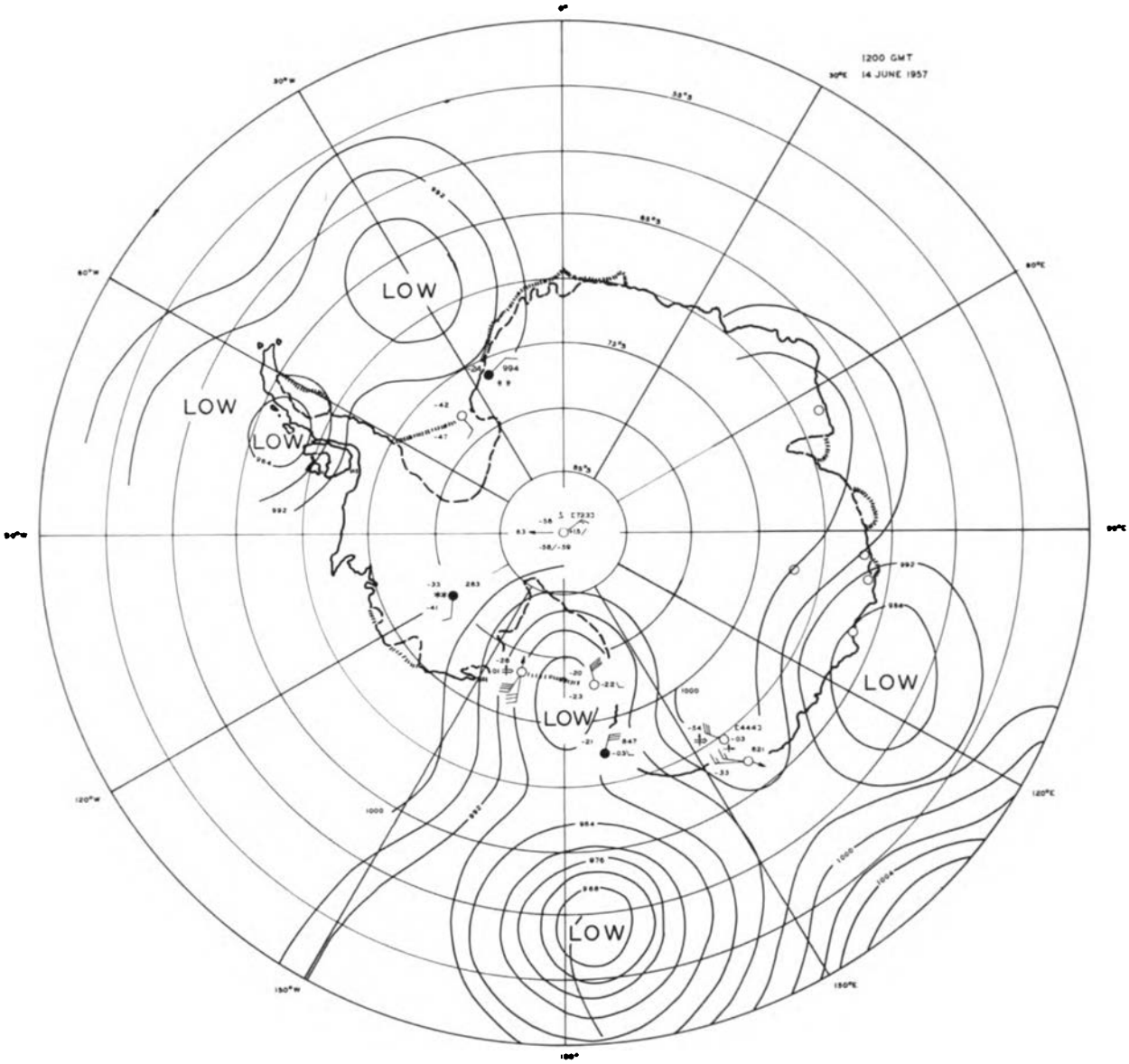

Fig. 12. June 14. Strong onshore winds from eastern quadrant of Ross Sea low.

supercooled fog droplets gave a thin, clear 2-mm ice crust visible in the photo as a wavy thin white line at 123 cm. This fog crust is not a consistent marker, being present in only 22% of the pits examined.

The next pertinent piece of weather data shown is the passage of a storm with heavy precipitation on February 20–24, followed by blowing snow and erosion up to March 1. Thereafter, the surface remained stationary until and after the stake-reading date of March 17 and acquired a crust (visible at 116 cm) with the help of two more supercooled fogs. The light gray shade below the March 17 marker is characteristic of summer sublimation layers as seen in photographs.

The meteorological record gives two separate snowfalls on March 22–28 and April 10–11. An infrequently occurring crust formed between them (not present in this photo). Of greater significance is the small sublimation layer on top of this snow at 100–102 cm. Frequency of occurrence is high.

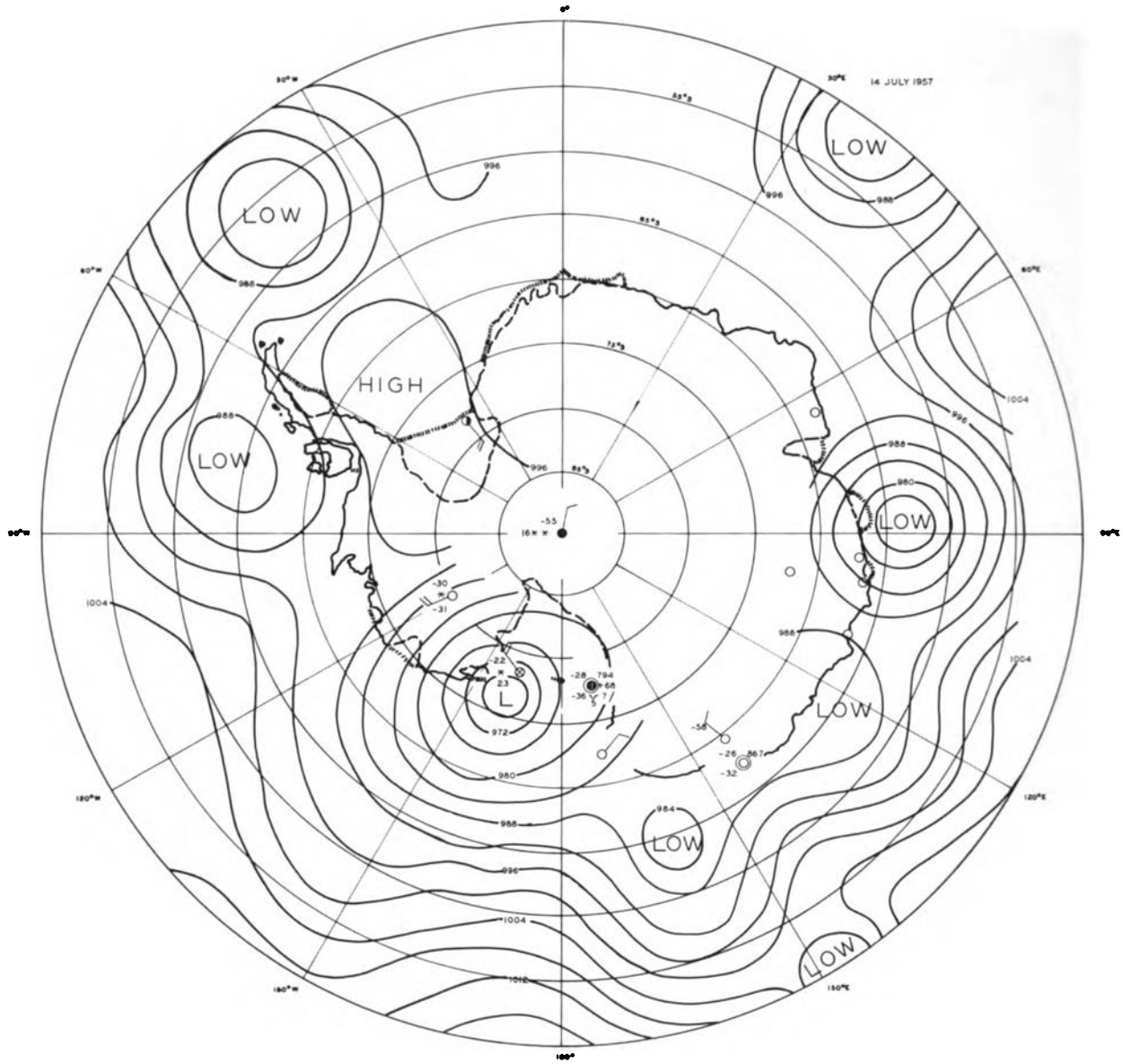

Fig. 13. July 14. Lows along the Wilkes Land coast.

The explanation and dating of the layer are as follows.

After a still-stand of 22 days the heaviest snowstorm of the season arrived. The stake farm recorded about 18 cm of new snow. This snow fell at the relatively high ambient temperature of −4°C and rested on snow of −17°C. The locally increased temperature gradient was responsible for the sublimation layer immediately beneath the late April crust at 98–100 cm. This sublimation layer occurs in about 70% of all pits, and, where the sublimation layer is weak, the April crust is more easily detected. There is reason to believe that these markers can isolate the two snowfalls of March and April in areas not well known. Their top is referred to as the early May horizon. The top of a May 8–15 snowfall is marked May 20 on the stakes and displays a very slight, infrequently occurring sublimation layer at 91 cm. The surface of this layer was exposed to a month of inactivity. There were winds up to 35 mph,

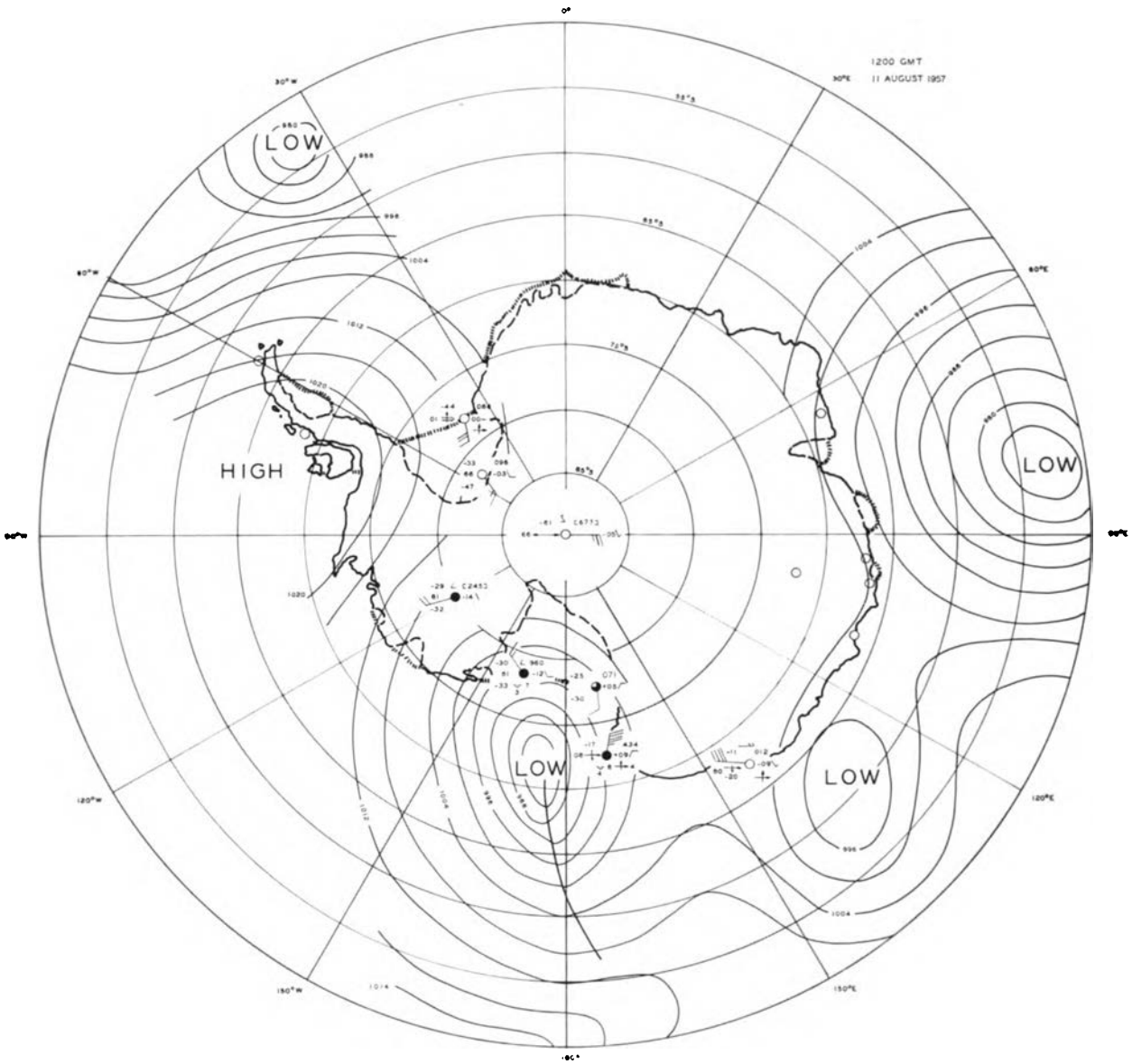

Fig. 14. 1200, August 11. Illustration of the blocking high situation.

with no record of blowing snow. Since saltation of loose snow normally begins at about 12 mph, an absence of blowing snow at 33 mph certifies presence of well-developed crust. This surface, labeled the June 18 surface, appears more distinctly in other pits.

The period from May 20 (or June 18) to the following late spring is stratigraphically uninteresting.

October 1957 was characterized, however, by precipitating and blowing snow which fell on a long inactive September surface at 77 cm (either September 14 or 21). October and September surfaces occur close together and invariably mark the break in the density profile from winter massive to summer sublimated layers. From November 1 to 4 this October activity terminated. Effects of air temperature were aided by long-wave radiation from low solid cloud cover in early November, and surface melting and drizzle are recorded. A thick

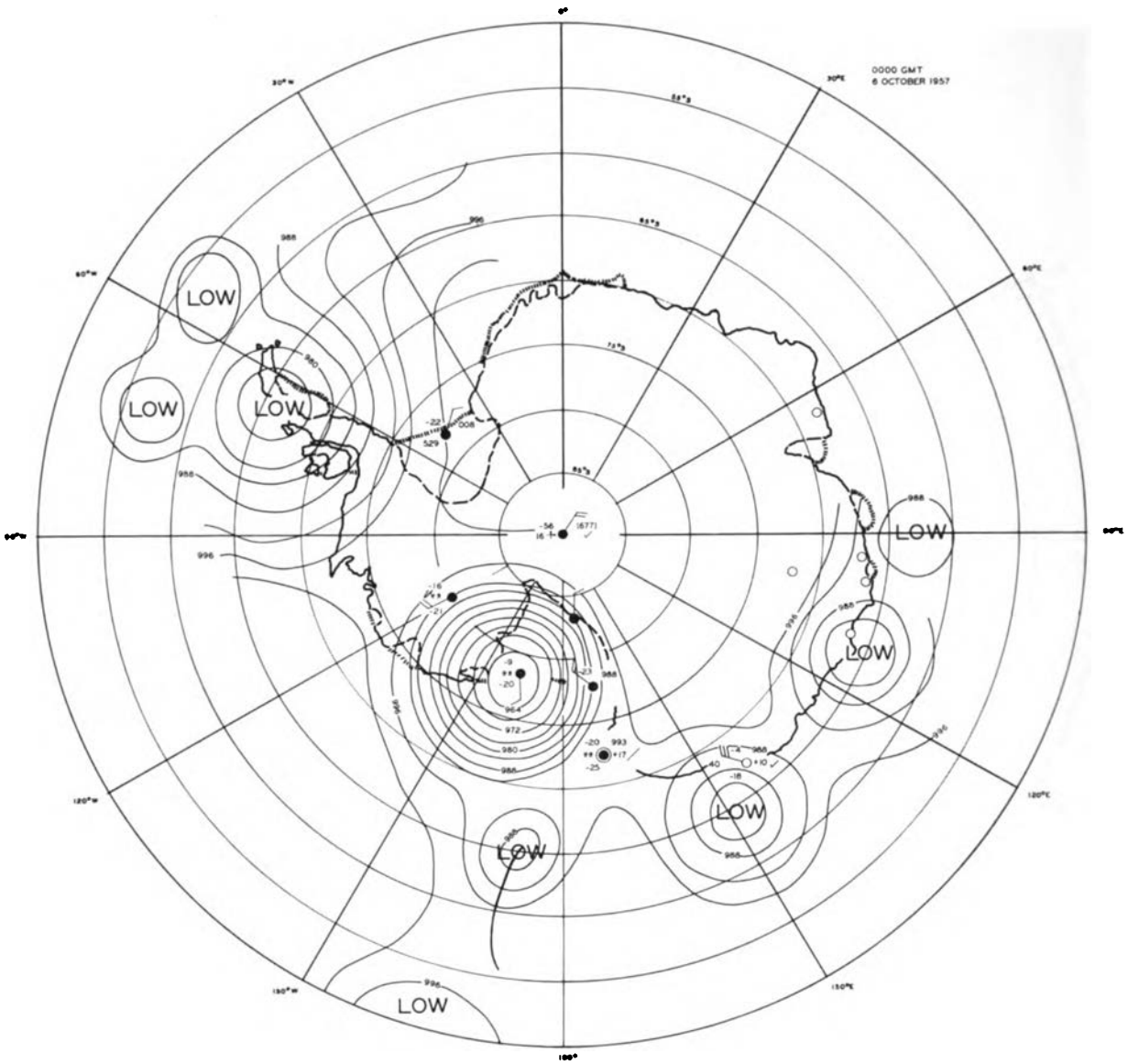

Fig. 15. October 6. Simultaneous snowfall at all stations.

granular crust where grain surfaces fused together resulted at 66-cm depth.

Another fused crust developed December 2 with the surface recorded as wet to the touch in the author's field notes. These summer dates are well bracketed in time, for stakes were read and pits dug within a few days of their occurrence. It can be shown from the data of other pits that November accumulation was so minor that the November and December crusts often became one.

In the last week of December melting became profuse. Percolating water trickled to colder depths, where it was often blocked by winter wind crusts, reinforcing such crusts to almost summer proportions in places. The last of the above-freezing temperatures for the summer season came at the end of the first week of January 1958.

For the year 1958, only phenomena of high frequency of occurrence will be mentioned. The February layer of sublimated sastrugi, 51–56 cm,

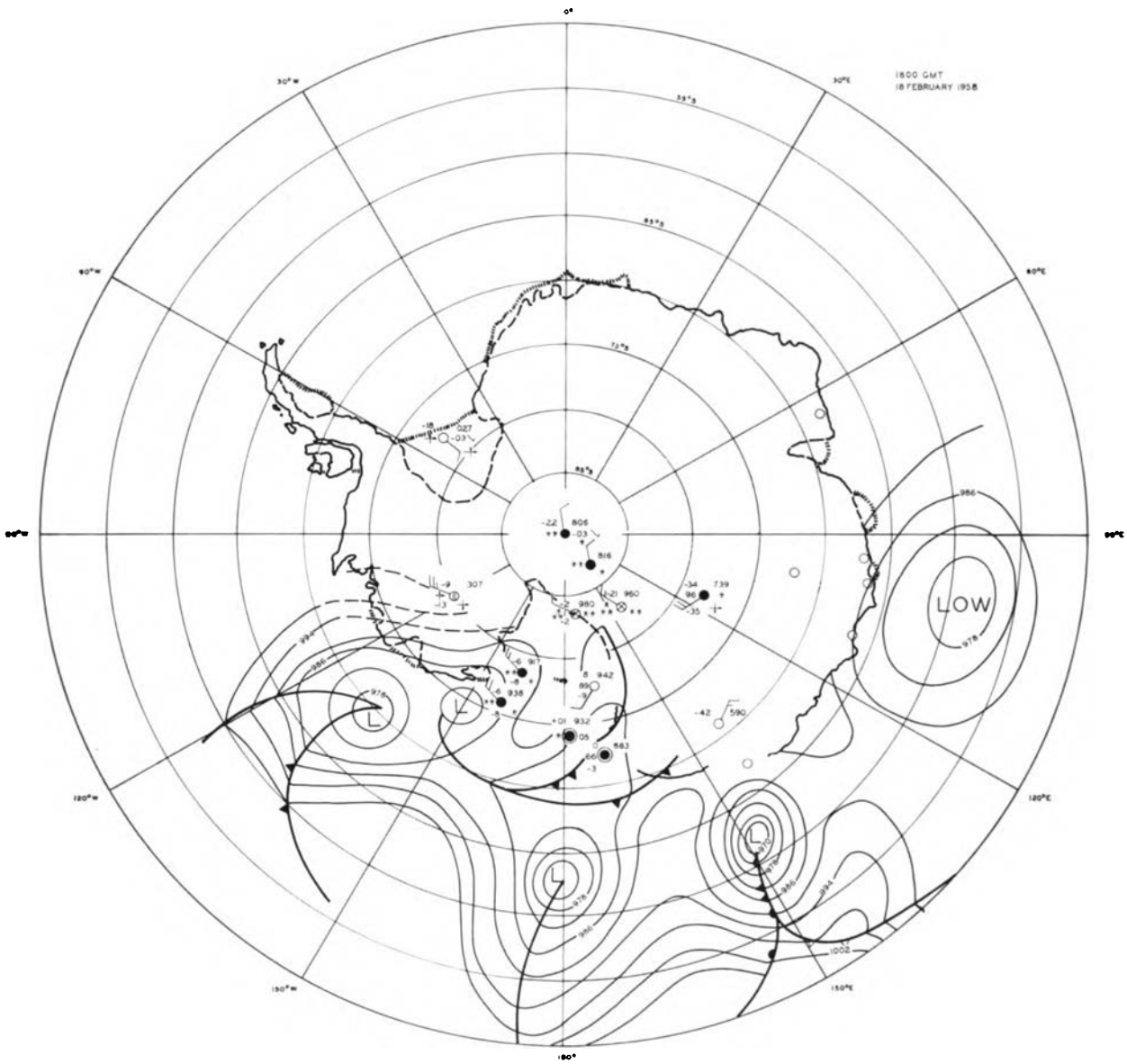

Fig. 16. Ubiquitous snowfall.

is found in all the pits, often with crescent-shaped ice glands localized by convex focusing of radiation in sastrugi pockets.

Only a 22-day inactive period can be found to account for the March 22 ice crust at 50 cm. The April 1 ice layer at 42 cm is, however, plainly a result of sleet, recorded in the meteorology log.

The laminated layer from 30 to 42 cm apparently indicates scattered snow flurries throughout the entire ensuing period. Regardless of cause, it has a high frequency of occurrence and consistently terminates with June stake readings. Its exact date cannot be determined by the meteorology log, nor can the cross-bedded slab above it, 23–27 cm. However, several accumulation stakes show August surface level readings below the June 28 reading. June 28 is never below June 2 (presumably eroded). Since the log shows a sequence of several days of blowing snow, with no appreciable new precipitation in July and August, one can assume that ero-

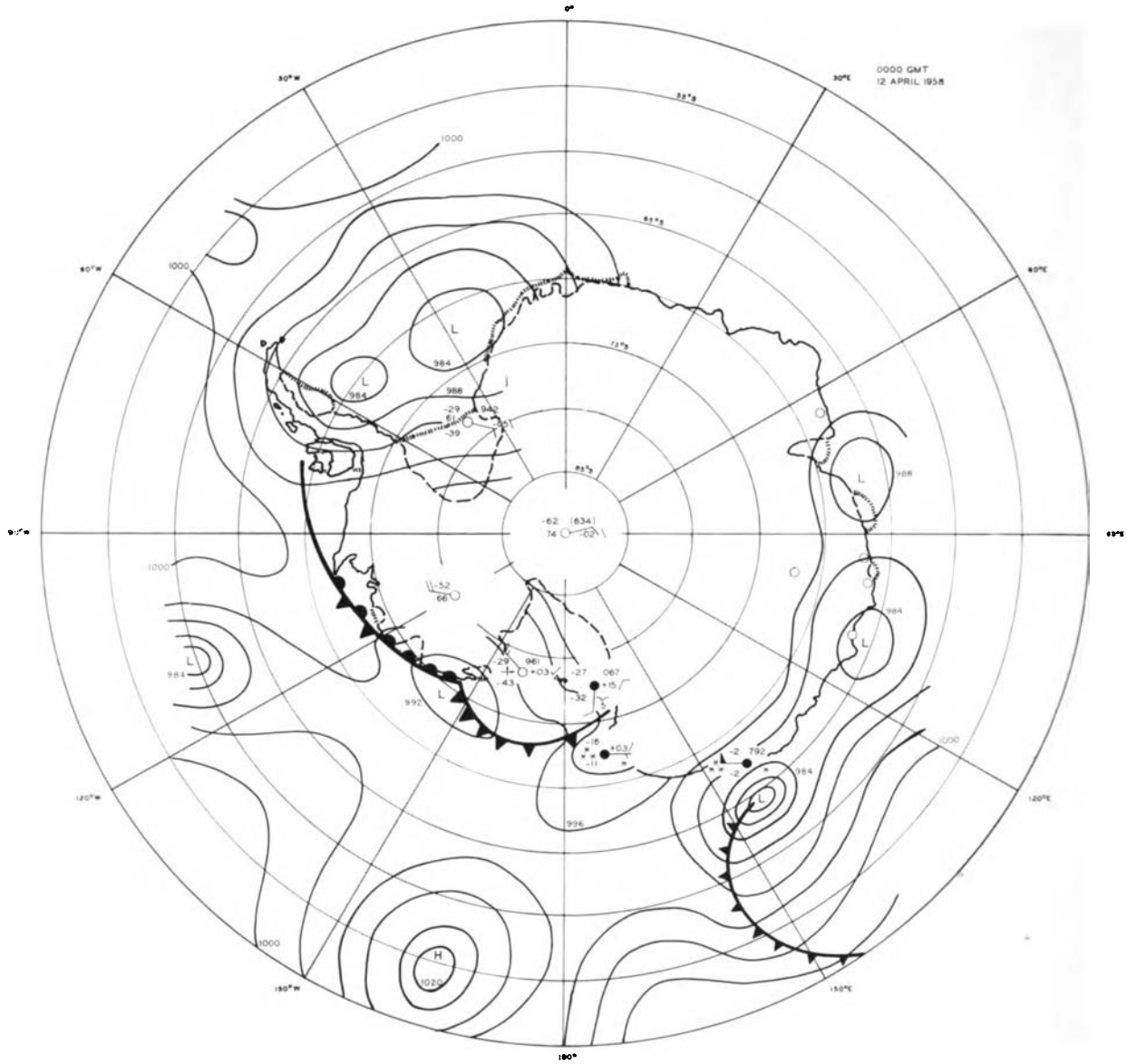

Fig. 17. Areal strength of the inland high.

sion during July and early August lowered the surface back to the mid-June level but no farther. Thus the crust at 23 cm may represent the surface existing just before the next sizeable snowfall, August 11–14. The balance of the column is September snow.

One can expect the snowfalls of March 22–28 and April 10–11, 1957, to be clearly distinguishable in the field. The year's heaviest snowfall, May 8–15, is more difficult to isolate but may well stand out where field data are plentiful. All precipitation between May 8 and August 30 can be definitely isolated. October snow is well marked at top and bottom. Markers of summer months all stand out well.

For 1958, the February sastrugi layer is reliable. The March 1–22 hiatus (crust) is fairly certain, whereas the April 1 sleet crust is decidedly certain. Anything in the laminated layer terminates in June. July and August markers could be off by a month, more or less.

The years 1955, 1956, and 1958 have various

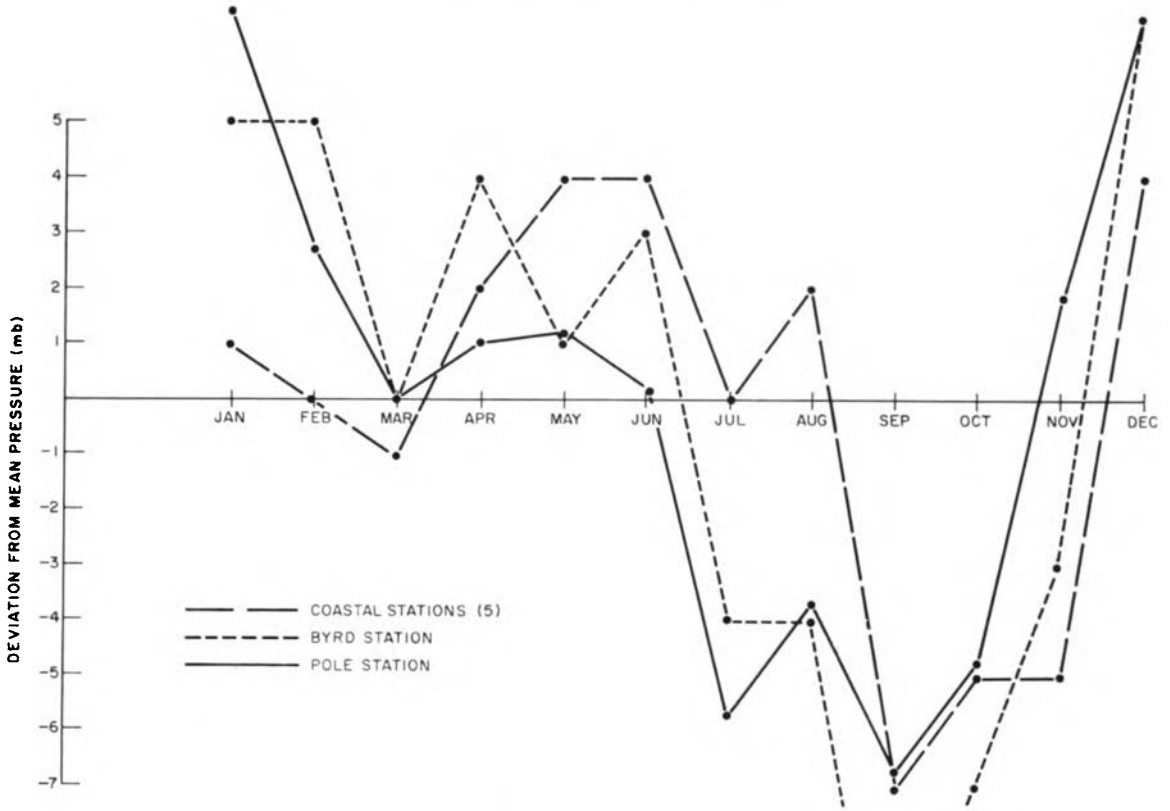

Fig. 18. Annual trend of monthly mean pressure (3-year average, 1957, 1958, 1959).

pieces of important information to contribute to the over-all reconstruction of events but are not necessary for this limited presentation. Generally, 1959 has an improved quantity of synoptic evidence from the newly established meteorological center at Melbourne. Review of 1959 data confirms the major circulation features observed in 1957–1958. Regarding 1956, the first summer melt crust below the 1957 recorded stratigraphy is verified as that of the 1955–1956 summer, thus extending reliable stratigraphy down to a year with a very characteristic ram, crusting, and sublimation profile.

Additional Comments on Comparative Accumulation Plot

Figure 4 shows the dates of actual snowfall and the surface fluctuation measurements. A few other items in this diagram regarding Ellsworth and the Pole stations are worthy of comment.

Regarding Ellsworth station, note from Figure 4 that it does not receive the heavy snowfalls common to Little America and Byrd stations in May 1957. Recall also that the effects of the blocking high (or characteristic ridge pattern) apparently cause the flat August plot for Ellsworth. The heavy spring storms begin a month earlier at Ellsworth than at Little America and Byrd stations. There is also an anomalous rise in the November surface at Ellsworth, and the July 1958 rise occurs independently of Little America and Byrd.

The dissimilarity between the snow accumulation record at Ellsworth and the other stations supports the concept that cyclonic depressions of the Ross Sea are not crossing the Byrd-Ellsworth divide. If they do, it is the rare exception, not the rule.

Note that Little America and the Pole station show simultaneous surface activity for May and the end of July 1958. Other Pole station fluctuations, however, show little concurrence with the other surface plots. It would be convenient if, through simultaneous fluctuations, a preferred moisture source were shown to exist for the Pole station either via the Ross Ice Shelf or via the Weddell

TABLE 2. Comparison of Monthly Mean Sea Level Pressure (mb) at Coastal Stations

	Ridge Areas			Nonridge Areas	
	Hallett (5 m)	D'Urville (41 m)	Ellsworth (43 m)	LAS V (44 m)	Norway (56 m)
			1957		
April	995	992	992	987	
May	996	994	995	991	no
June	994	990	991	990	record
Average	995	992	993	989	
			1958		
April	995	988	992	992	991
May	994	997	996	984	992
June	993	988	989	994	992
Average	994	991	992	990	992
			1959		
April	996	992	989		995
May	995	996	993	no	987
June	995	996	1000	record	991
Average	995	995	994		991
Average (3 yr)	995	993	993	990	991

Sea, but the data give no grounds for such assertions. In fact, the poor correlation suggests that the source of moisture is random or may lie elsewhere.

Statistical Analysis for Tracing of Firn Layers

It has been demonstrated that firn layers were traceable over considerable distance (Little America to Byrd station) by observance of their weather markings. Sedimentary beds can also be identified by noting the distribution of grain sizes within a given layer, because sediment deposited under the same environment often has its own characteristic grain distribution and is recognizable over a considerable horizontal distance. By a combination of weather markings and grain size analysis one can obtain a high degree of confidence in the tracing of firn layers. The investigation of grain size distribution is fully discussed in the full study [*Vickers*, 1965]. The following summary comments will, however, be of interest.

On a given traverse two or three pits were often unrecognizable, with good grain size correlation returning thereafter. This poor correlation may well have been in areas of very low accumulation, where it is suspected that a given layer may remain in a near-surface high-sublimation position for several seasons.

As might be anticipated, there were also problems resulting from sastrugi, much as there were with the density analysis. The advantage in the present case, however, was that a sastruga only affected one layer, not the entire profile. Nevertheless, the many gaps seen in the traverse diagrams of the original work are due to the ubiquitous presence of sastrugi. The effect of wind sorting on sand dunes, studied by *Doeglas* [1960], is applicable in many respects to sastrugi.

The assistance rendered by this study to the tracing of firn layers must be stated as moderate but with promise. Control pit and weather marking analyses, described in this report, should be made an integral part of any attempt to trace firn layers by grain size analysis.

In addition to tracing firn layers by known weather markings and grain size distribution, a further line of independent evidence was pursued. Results of geochemical dating are presented below.

Geochemical Dating

Results of geochemical dating techniques were analyzed for their present contribution and future worth to antarctic snow accumulation research. The work is summarized below with one or two sets of data analyzed to illustrate how information was used. Conclusions based on the complete analysis are cited. Results considered were those of tritium, Sr^{90}, deuterium/hydrogen, and O^{18}/O^{16}. Only bomb fallout is presented with any amplification here. Complete results of the geochemical dating investigation appear in *Vickers* [1963].

Basis for Sample Correlations, Bomb Fallout

Figure 19 shows a theoretical stratospheric inventory based on computed bomb yields modified by surface types and detonation distances above the surface. The curve shows that the May 1954 Castle shot provided the first sizeable surge in stratospheric inventory, and this date will be used in evaluating all core samples from Antarctica.

Tritium samples. Except for the one instance described below, tritium samples have been of little

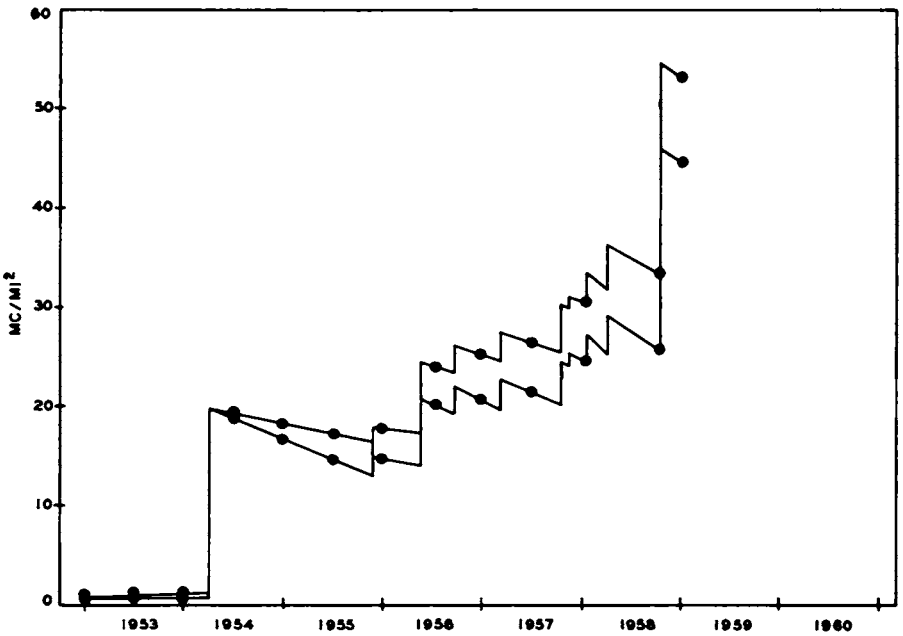

Fig. 19. Stratospheric inventory (after *Libby* [1958]).

assistance in solving the dating problem. The reason may be that tritium, which is produced from overwater shots, rapidly condenses aloft and has a very short fallout time.

Libby [1956] makes a good approximation of snow accumulation at Little America III (78°35'S, 163°50'W). He states that from tritium concentrations and the expected tritium production rate in this region he was able to determine the annual precipitation to be 7.8 in. of water (19.8 cm). Libby points out that he found 7–8 ft of snow accumulation over a tent from an earlier camp that protruded from the Ross barrier face. This accumulation represents approximately 13.5 cm yr^{-1} (water equivalent) accumulation since the establishment of the camp 7 years previously. From excavation of a campsite in the same area buried under snow for 18 years, *Vickers* [1959*b*] obtained rather positive evidence for about 16 cm accumulation in this area. It is known from stake farms at Little America V that accumulation increases rapidly as one proceeds back from the barrier face. Since the present author's campsite excavation was about 0.5 km back from the barrier, Libby's tent figure of 13.5 cm yr^{-1} at the barrier edge appears logical, and the 19.8 cm figure can be reached within the distance across the camp ground (3 km).

The above does not allow a precise evaluation of Libby's tritium analysis, but it does confirm it as being a reasonable estimate, and the rapid inland buildup of accumulation may explain the discrepancy between the tent-derived and the tritium-derived accumulation figures.

Strontium 90 samples. From equatorial shots strontium 90 (Sr^{90}) has been shown to have at least a 5-year residence time aloft. It has a radioactive half-life of 28 years. Since variation in its concentration appears repeatedly in antarctic cores, Sr^{90} should provide the principal tool for accumulation studies. During the processing of the earliest cores extracted (summers 1954–1955 and 1955–1956), interpretation was not attempted because so little was known about snow stratigraphy in Antarctica. In the light of present stratigraphic information, the author attempts this interpretation.

Libby [1956] tabulated results of samples extracted from a pit excavated February 19, 1955, at 'Admiral Byrd Bay.' A diagram of the pit from which the samples were taken appears in a report published by the *U. S. Navy Hydrographic Office* [1956]. Figure 20 shows an interpretation of the pit data in light of present knowledge on antarctic stratigraphy, and data on Sr^{90} from Libby's tables

are included for correlation. A brief discussion of the reasons for assigned dates follows.

A mid-October date is assigned for the 30-cm depth. Based on observations at Little America, the break in the density curve (Figure 20) from the high values of the winter to lower summer values occurs with the first significant daily temperature oscillations accompanying the Sun's reappearance. This produces light sublimation in the top 10 cm of snow. At Little America, for example, identifiable sublimation crystals (low density) were first observed at the end of November in the near surface layer.

A reasonable estimate of samples from 33- to 66-cm depth is 85% spring snow. This evaluation is based on the accumulation work previously presented (Table 1 and associated diagrams) in which atmospheric circulation and periods of heavy accumulation are correlated. The study shows that most accumulation occurs in the fall and spring with a mid- to late-winter break. The break occurs when the inland high has reached its maximum areal strength and manages to keep the cyclonic depressions out to sea. It is during the buildup and breakdown (fall and spring) of the inland high that the large snowfalls occur. Since stray traces of warm weather (inroads of maritime air with cyclonic depressions) often appear in spring and fall, it is likely that this upper section of the stratigraphic column is spring snow. Further evidence lies in the increase in grain size in a layer at 56-cm depth. Similarly, the snow for the fall period has a light melt crust at 87 cm. This fall indication is reinforced by a second break in the density curve. Little America stratigraphic studies show sublimation effects from dissipation of the summer's heat in the snow up to the middle of April with a maximum in February. This Sr^{90} sample, taken from 66 to 102 cm, is predominantly from fall snow. The sample from 102 to 135 cm is from fall-summer snow.

From the data given we may logically conclude that debris from the May 1954 Castle shot arrived in the austral spring, thus indicating approximately 6 months of lateral mixing time in the stratosphere. This time compares with *Martell*'s [1959] estimate of 9 months' mixing time for similar travel in the northern hemisphere.

The quantity of fallout increased toward late spring-summer. *Miyake et al.* [1962] found that the greatest specific activity in the region of Japan was coincident with the presence of the jet stream and a thaw at the 500-mb level or above in the late spring-summer. It does not seem unreasonable to expect a like correlation in the southern hemisphere, even though there is less immediate proximity of the antarctic continent to the midlatitude jet stream than in the example cited.

Similar data exist for Atka Bay (70°35′S, 08°06′W), Kainan Bay (78°10′S, 102°30′W), McMurdo Sound (77°51′S, 166°35′E), and Station C, 'Victoria Plateau' (97°22′S, 139°48′E) and has been analyzed in the above manner. The investigation afforded the following conclusions:

Present fallout and accumulation data indicate that the approximate north-south mixing time in the stratosphere is about 6 months. Spring may be the time of highest fallout rate as has been found in some other sections of the globe.

Absolute quantities of fallout in Antarctica ap-

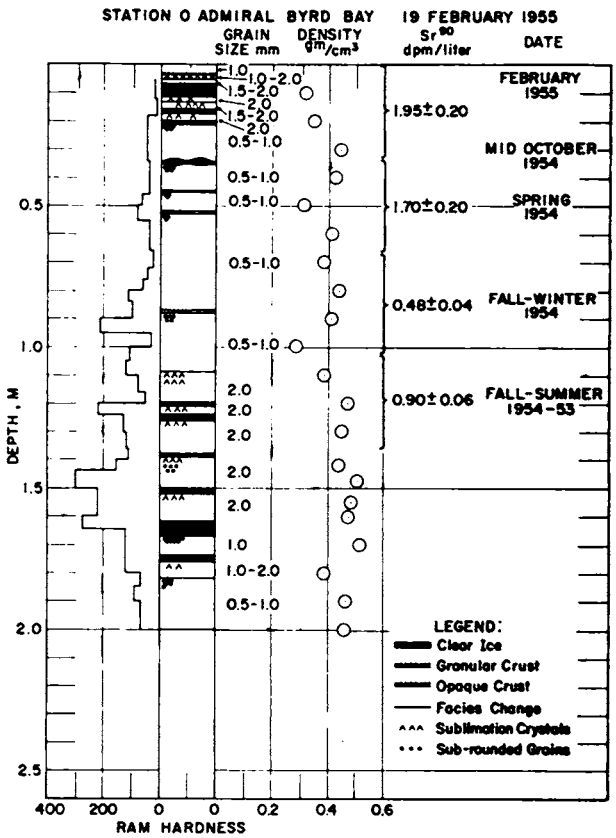

Fig. 20. Stratigraphy versus fallout values, 'Admiral Byrd Bay.'

parently vary with space. Generally high quantities for mutually distant areas do appear to have relative correlation, however, and warrant further investigation as possible dating aids. It would seem that fallout for U. S. tests in 1958 may serve as excellent stratigraphic markers for future field work.

Pit interpretations on the 'Victoria Plateau' show a reasonable conformance to 1954 debris found in the stratigraphy of less controversial accumulation areas. The 1954 layer serves as a good accumulation check in most areas investigated. Since the present investigation was completed, strong corroboration of the presence of 1954 debris has appeared in the literature [*Picciotto and Wilgain,* 1963]. Also, work by *Crozaz et al.* [1964], using the disintegration of Pb^{210} as a time measuring stick, checks well with the Pole, McMurdo, and Byrd station data presented in the parent to the present report.

The survey of isotopic work (i.e. O^{18}/O^{16}) resulted more in a definition of direction of research needed than in the fulfillment of immediate supporting evidence. Briefly, the conclusion was that the isotopic profile itself does not provide sufficient information on which to base accumulation values. However, if isotopic profiles are used in association with control zones by linking them to known profiles as well as known stratigraphy and meteorology, they could prove highly effective as stratigraphic tracers for working from known control zones into areas of unknown accumulation.

RESULTS OF TRAVERSE ANALYSES

Example of Traverse Analyses

The best support of the accumulation analysis has come from the tracing of weather markings in the pit stratigraphy. One complete traverse is presented to illustrate how the material was employed. A complete accumulation map based on all U. S. traverses in western Antarctica and relative supporting evidence is presented. Vapor transport figures are given for a few prominent storms.

General Discussion of Byrd Control Pits

Figure 3 presents selected control pits from Byrd station. They were chosen as standards against which unknown pits could be readily compared. They include almost all the variety of forms found for any given set of features.

In the Byrd pits the complexity of the year 1956 stands out in control pits 7, 3, and 2. This annual layer is often seen as a succession of closely spaced crusts interspaced with heavy sublimation. The ram profile through this layer (not shown here but well illustrated in the total body of data) is characterized by low values due to sublimation. Characteristically, the summer position is midway in this zone of low ram readings. The sublimation continues into the top of the 1955 layer. The year 1956 was apparently one of high accumulation with a warm summer which produced the heavy sublimation. The close spacing of crusts and 'narrow' ram profile of 1955–1956 is often the key point from which to begin a known-unknown correlation, owing to ease with which this year is identified. Moreover, the crust spacing and ram profile often contrast sharply with 1957, which is frequently characterized in colder snows by three superposed massive layers having a distinctly uncomplicated appearance. This is a result of the very heavy individual snowfalls of 1957 described in Table 1 (i.e., May 8–15, 1957). Note the massive layers in the top half of control 5 as an example. To emphasize the characteristic appearance of these layers, two pits lifted from the Byrd-Pole traverse (contained in the original work) are shown in Figure 21. These pits are excellent illustrations of the time-space preservation of features referred to in the early pages of this report. Note that 1956 snow is now 5 years old and that the pits are respectively 90 and 416 miles poleward from Byrd station.

Other features often repeated are the delicate crusts near the 50-cm depth of pit 7; the ragged crusts of pit 21 at 65-cm depth; the massive layers of pit 2 at 20- and 40-cm depth; and the succession of thin slabs in pit 21 between 15 and 30 cm for the year 1960.

Were there room to include a warm snow traverse (see original study), it would be seen that the features that make the best tracers in the warmer snow are not necessarily the same features that make the best tracers in the colder snow, even though many features are common to both.

A few additional aids with a high frequency of occurrence over most of western Antarctica at all elevations or temperatures are:

1953 is often the year of least accumulation.

The apparent 1954 layer has heavy icing (below the controlled stratigraphy).

1954 occasionally has abnormally large ram readings, which may be connected to change in snow compaction mechanism [*Benson*, 1960].

1955 is often the year of greatest accumulation.

1955 often has three closely spaced winter maximums in the profile of ram readings.

These are generalities, and the year designations below 1956 lack evidence. It is important to note that the vertical order or sequence of features for unknown pits should be recognizably consistent with that of the control pits. This consistency is often difficult to see until the investigator has studied many pits and begins to recognize the repetition of many of the above-listed characteristics.

Sample Traverse Tracings

In the format of the diagrams (Figures 22 and 23), key horizons are connected by a heavy solid line from pit to pit. Minor traceable features are connected with light lines. Dashed lines exist where there is poor recognition. Lines that terminate with a slight wave (broken line symbol) resume farther along the traverse; they represent instances where a layer being traced is absent or cannot be recognized in a given section but returns in later pits. The layers often display themselves as dark and light tones in the photographs. Very light tones (almost white) can be interpreted as sublimation crystals, although one can sometimes be misled when trying to correlate massive layers of dark and light tones of gray, owing to the relative placement of the photographer's light, to occasional preferred crystal orientation, or to both.

The traverse is handled in two diagrams, with the last pit of one repeated as the first pit of the next. Control pits from which to start (or terminate) are also included as either the first or last pit.

Byrd-Amundsen Sea traverse. The Byrd-Amundsen Sea traverse illustrates what occurs when the environment changes abruptly. Pits 819–963 were in an area where considerable surface melting was evident at midsummer. In Figure 22 these pits are bracketed by pit 747 and control 21, both at higher elevation. Notice prominent horizons are retained in the colder pits, but they are not quite so well defined as in pits from lower elevations. Control on stratigraphy from this traverse applies to the top 3 years.

To try a few sample tracings, note first the top

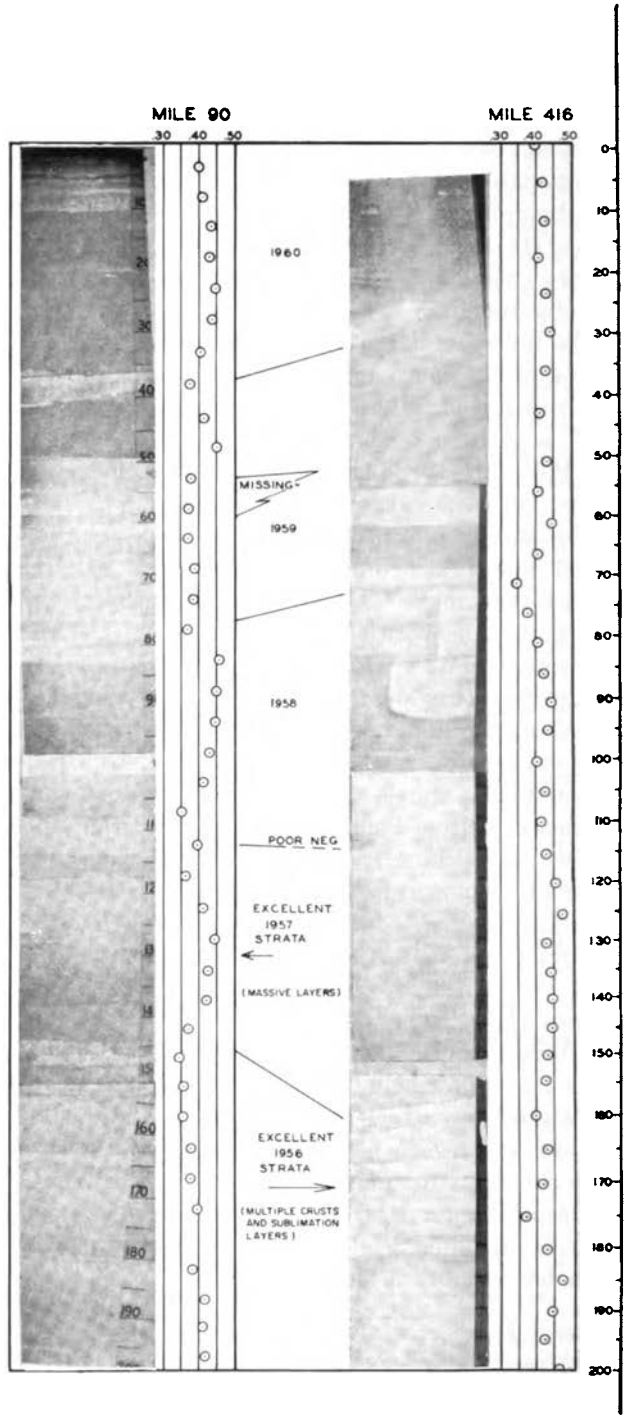

Fig. 21. Time and space preservation of stratigraphic features (Byrd–Pole traverse).

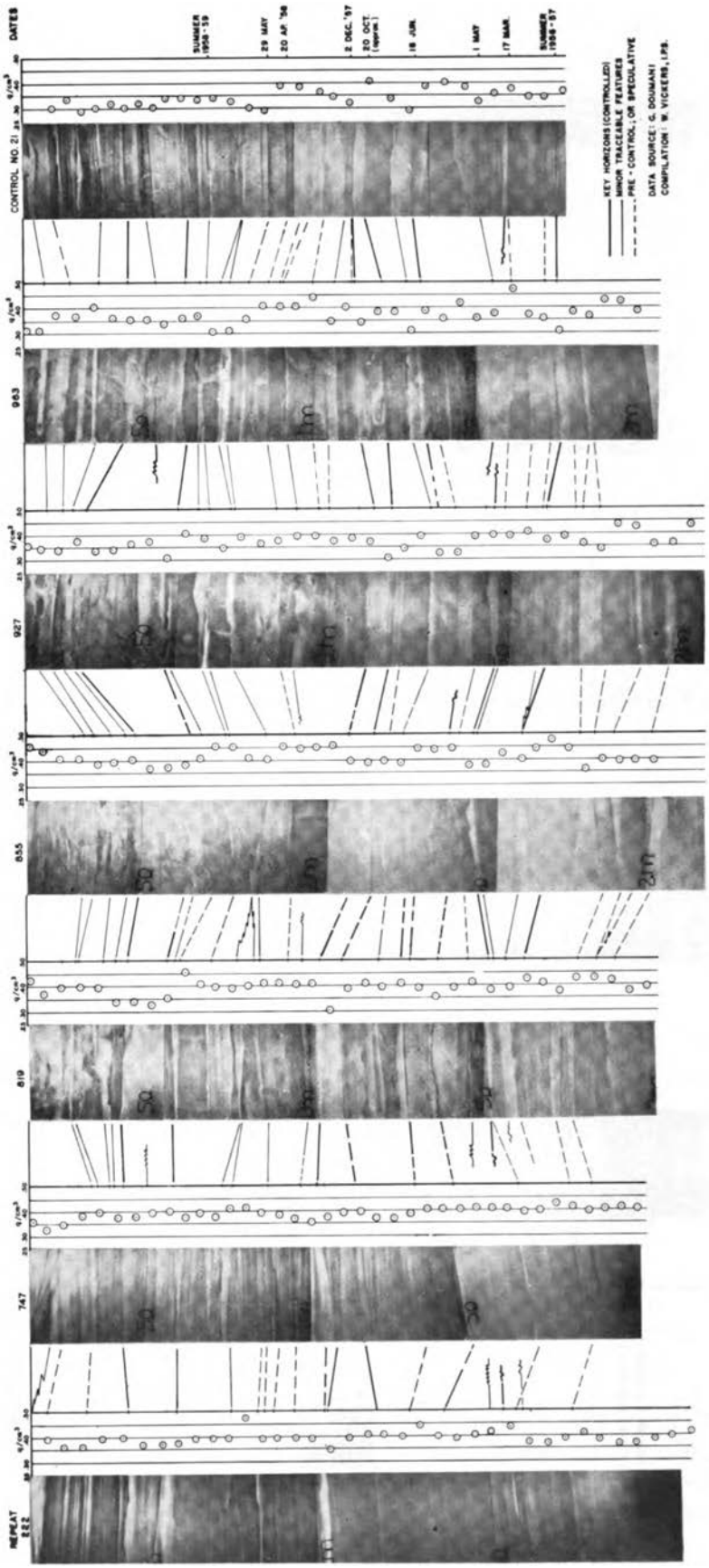

Fig. 22. Byrd–Amundsen Sea traverse (1959–1960, inbound).

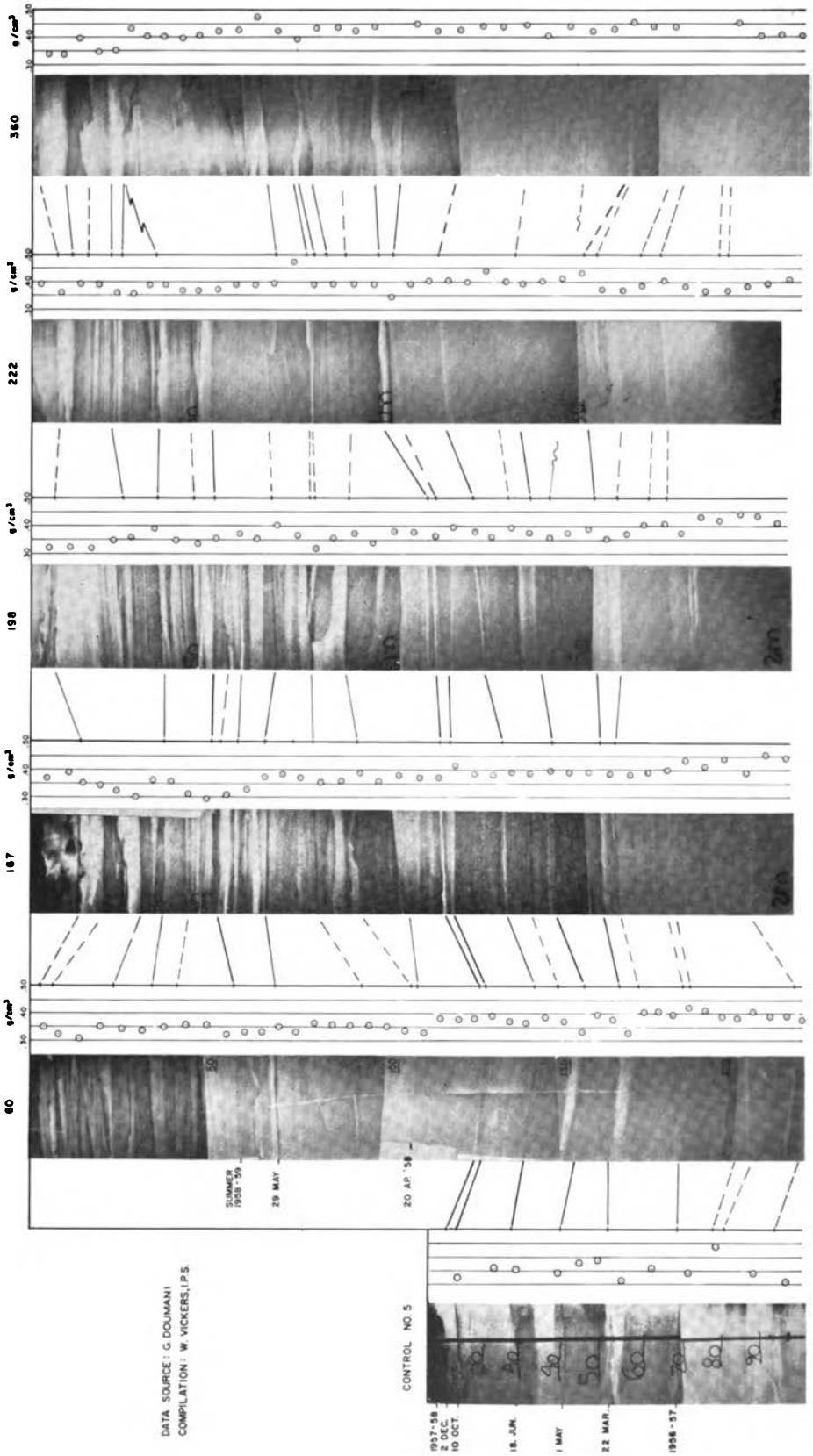

Fig. 23. Byrd–Amundsen Sea traverse (1959–1960, outbound).

60 cm of control 21, Figure 22. (Since depth markers were mistakenly clipped from the photos of control 21, assume depth markers spaced as in pits 963.) The most distinctive features are the pronounced dark and light layers and associated crusts. The easiest correlation with which to start is the ragged crust on top of the well-indurated dark-appearing slab (end of summer) at ~60-cm depth in control 21 and its continuation in pit 963 at the same depth. Note also the crusts at 42-cm depth in each column; and the repetition of the slab and sublimation layers (dark and light) in the top 25 cm of the respective columns.

Moving across the page to the left, these slabs and sublimation layers are seen to repeat themselves, although with variation, even in the cold snow pits, 747 and 222. Note also that the ragged crust loses its characteristic appearance in going from pit 963 to pit 927, probably owing to profuse melting at lower elevation producing a thicker and smoothed granular crust, 927-57. (The first number is pit identification; the second is depth to which reference is made.) The slabs in the immediate 20 cm below this crust, however, repeat distinctively. The connection from pit 855 to pit 819 is at first glance difficult. In fact, it is easier to go back to pit 963 and note that the massive layer between 40 and 60 cm with the ragged crust at its base and another crust at the top, correlates with pit 819 between ~38 and 57 cm; in fact, it continues to pit 222.

At greater depths among the warm snow pits (819–963) the 10-cm layer whose top is at 963-115, 927-111, and 819-100 repeats well. Note also the repetition of the minor surface lying at 21-128 (October 20), 963-130, 927-128, 855 unknown, and 819-125. Stratigraphy for pit 855 finally returns convincingly at ~150-cm depth, where it compares with pits 819 and 927 at approximately the same depth. The bottom quarter of pit 819 is 1956 stratigraphy, recognizable by the detail of crusts and sublimation layers. One can also see good 1957 repetition for these two pits; i.e., control 5-49 (Figure 23) and 819-145; control 5-41 and 819-137, even though control 5 is less boldly marked because of colder snow.

Thus far there has been slight reference to pits 222 and 747. These cold snow pits do not have such sharp distinctions as the warmer snow pits. Greater study is required to find correlating features. Certain features will, however, be pointed out to show that a continuation of correlation is indeed possible.

The 20-cm massive layer with the ragged crust base at ~54 cm in pit 222 has already been referred to. Attention is directed to two gross observations for pit 222. Note the three generally massive layers between 100 and 150 cm (typical 1957 stratigraphy) and the succession of complex lightly sublimated layers below 150 cm (typical of 1956 stratigraphy). The massive layers with their corresponding crusts (May 1, June 18, and approximately October 13, 1957) can be readily correlated between these two cold snow pits, but below 747-150 it becomes uncertain (dashed correlation lines to adjacent pits, and broken solid lines laterally resuming at 819-150). The bottom of pit 747 remains a mystery.

Turning now to the other cold snow pits of the outbound leg of this traverse (Figure 23), one finds pit 222 (referred to above) in its original traverse sequence. From pit 222 one can quickly trace the 1957 massive layers back to control 21 at Byrd station. One can, for example, trace 222-100, 198-110, 167-112, 60-125 to control 5-10; and 222-114, 198-125, 167-128. The breach across pit 60 is eased somewhat by the sublimation layer at 167-160 which traces well to 60-165. The 1957 massive layers are present between 125 and 200 cm in pit 60 and easily tie to control 5.

For additional inspection, there are traceable features in the upper sections of these pits as well; i.e., the crust overlain by 10 cm of sandwichlike layers at 60-67, 167-67, 198-68, and 222-68. The last section has lost the slabs but retains the crusting sequence. Pit 360 is environmentally removed from the other pits and does not seem to have undergone a similar history between 30- and 63-cm depth, apparently owing to heavy wind mixing.

Remarks. The tracing of weather markings is not the perfect answer to all problems of accumulation analysis. It does, however, provide considerable improvement over the original efforts. One goes to the field with a mental record of the meteorological events and related effects on stratigraphy.

It is to be noted that there are presently several places on the 'Victoria Plateau' with marked surfaces buried by more than 5 years of snow (Station C of the airborne traverse, 1957–1958). Five control pits at one of these sites would provide excellent knowledge of the various forms a given layer is apt

to take. Three of these stations, say, Plateau Depot (1957–1958), Station C, and the Hallett traverse's abandoned Sno-Cat (1959–1960), or Station Charcot, might provide good control zones from which to run some air-supported spot checks between stations. The effort should be one of quality rather than quantity, both in the control zone and the field. This would include carrying out the recommendations of the geochemical section as well as improved petrographic tagging of key horizons using a Rigsby stage. A 20-pit traverse without proper verification is not worth nearly so much as 3 well-substantiated pits.

The foregoing has been a presentation of the principal technique employed in the accumulation analysis. The balance of the traverses appear in the original work [*Vickers,* 1965], as do cross checks provided by geochemical samples, isolated stakes, buried camps, and the complete body of grain size tracings.

IMPLICATIONS

Snow Drift

A Consideration of Drift

A question arises as to what can be seen on the accumulation map (Figure 24). Does it actually reflect the true spatial distribution of precipitation as well as accumulation, as tacitly assumed herein? There are two points of evidence which suggest that it does.

Small-scale consideration of accumulation distribution for approximately 200 km behind the Ross ice front suggests that drift transport has a general order of magnitude of 25 km, not an order of hundreds as is sometimes opined.

Actual calculations of drift show that 15-kt winds carry about 0.15 g/sec/cm width, while snow is actively drifting. There is much qualification to be considered, however, not the least of which is crusting which limits the amount of hours of actual drift. The present author feels drift may be overrated, owing to impressive demonstrations of what the wind can do on certain occasions and in some notoriously windy areas, i.e. the Adélie Coast.

Elaboration on the foregoing points follows.

Distance Traveled by Drifting Snow

A few descriptive comments on the Ross Ice Shelf are in order before considering drift. The reasoning to follow depends on a combination of topographical and meteorological factors.

The Ross Ice Shelf is approximately triangular in map view, measuring about 600 nautical miles on a side. It is about 280 meters in thickness with essentially flat topography. Its seaward margin is marked by an abrupt ice cliff (the Ross ice front) rising about 30 meters above the water. The other margins are bordered by mountains and glaciers; the glaciers supply much of the ice of which the shelf is composed.

A rather extensive stake farm at Little America was situated near the seaward margin of the shelf a few kilometers from the Ross ice front. The Little America-Byrd trail continued landward for some 200 km from this area. Stake and pit measurements were available along this trail. The line of measurements was approximately perpendicular to the ice front. In conjunction with this topographic description, the following meteorological phenomenon is pertinent.

From the study of accumulation and circulation correlations it was learned that the easterly quadrant of the intensified Ross Sea low (Figure 12) caused considerable erosion of accumulation at Little America. Effects of this onshore wind were sharply accentuated in the Instrument Area pit shown in Figure 5. It is pointed out that equally intense offshore winds readily erode such quantities into the sea as well. For these offshore winds, however, similar replacement quantities are brought in from an infinite source upstream. The result is erosion with no replacement fill from upstream with onshore winds; and erosion with ample replacement fill for offshore winds. The fact that cold-season sea ice has sufficient snow cover to provide an infinite offshore source is negated by the fact that only a fraction of the total drift manages to 'hurdle' the Ross ice front with onshore winds.

The result of this topographic-meteorological combination is that one obtains a lateral distribution of accumulation on a line perpendicular to the ice front such as that shown in Figure 25. Accumulation at the ice front is only half what it is a few kilometers inland. Note that the peak accumulation is about 25 km in from the ice front.

Since the flat topography of the shelf does not allow orographic explanations for the above distribution (other than for small-scale undulations), it becomes reasonable to assert that the accumulation

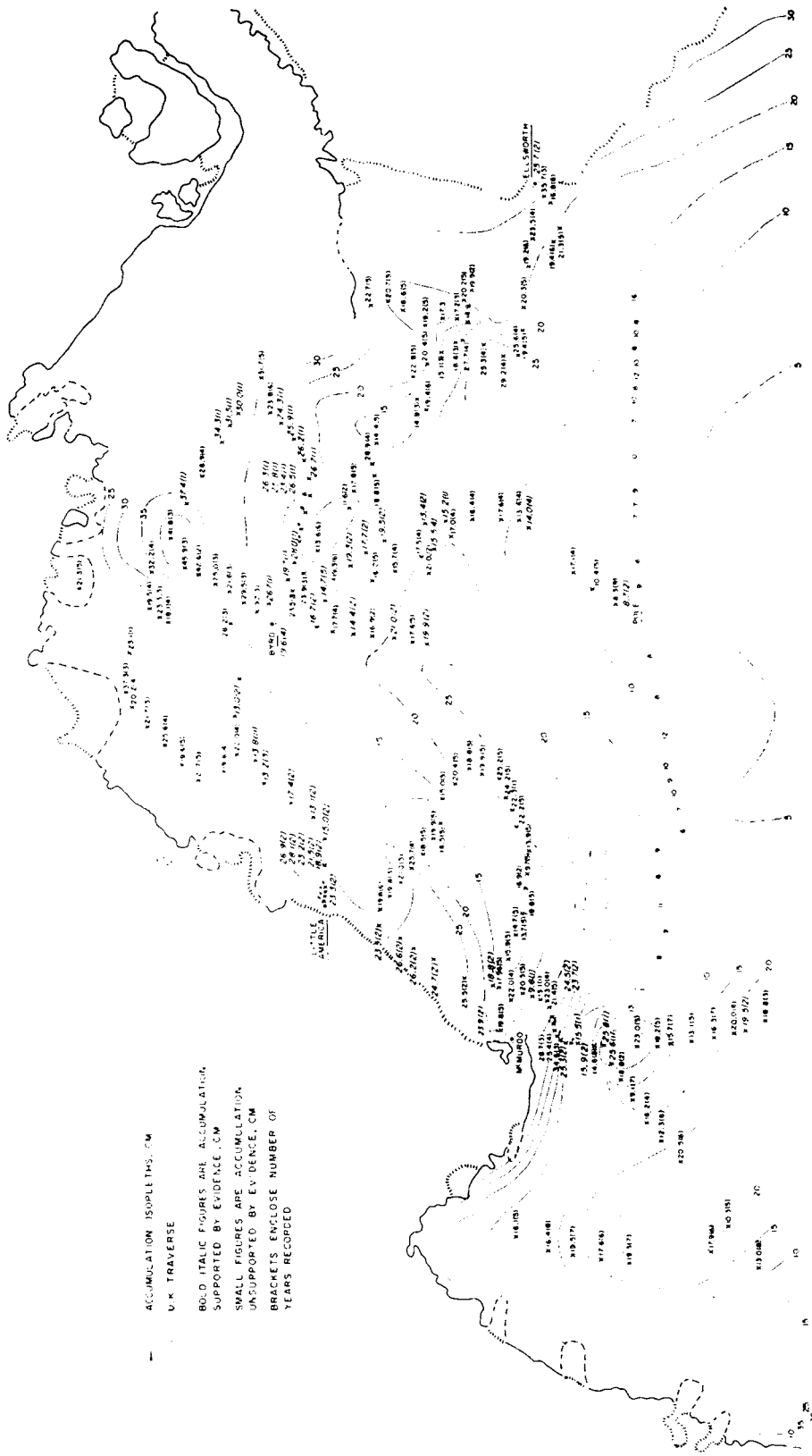

Fig. 24. Distribution of ice accumulation in western Antarctica.

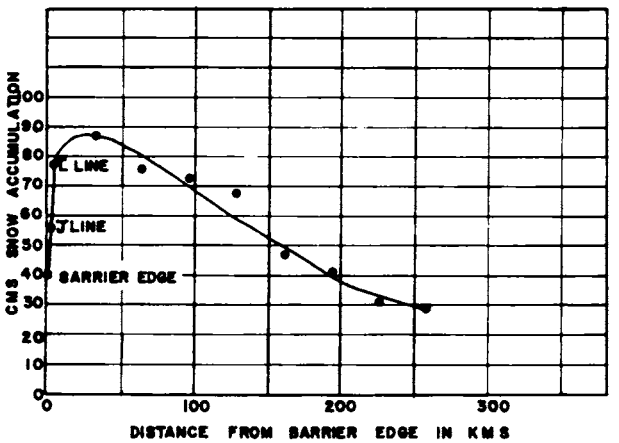

Fig. 25. Lateral accumulation profile on a line perpendicular to the Ross ice front (after *Crary* [1961]).

profile is a result of onshore winds that clean off the lip of the ice front, so to speak, and dump the load inland and fail to replenish the erosion near the ice front with a load brought in from upwind. If this reasoning is correct, it follows that drift of the order of 25 km is what one should expect in assessing the role of drift in Antarctica.

Quantitative Assessment of Drift

Shortly after return from Antarctica a quantitative approach to drift based on theoretical considerations was attempted [*Vickers*, 1959*b*] as the only way then existing to acquire working figures for the role of deflation in the calculation of mass budget. Calculations were based essentially on analogous work done by *Bagnold* [1941] on drifting sand in the Sahara Desert. The principle involved concerns the vertical profile of wind velocity. Wind profiles near the ground are normally affected by surface roughness, as are profiles of wind which are carrying a load of debris. This 'roughness' is manifested as a relative retardation of the air stream near the surface (frictional drag of the entrained debris on the air stream).

There also occurs a momentum transfer from the air stream to obstacles in the stream. For the case of entrained debris (blowing snow grains) it is possible to assess the mass of entrained material by recording the momentum change in the wind profile as the entrained debris slows the wind speed. Recent work by the French team from Adélie Coast provides rather significant corroboration of the theoretical principles originally employed. In Table 3 measurements made by *Lorius* [1962] of drifting snow quantities are seen to be in agreement with these earlier calculations.

As noted in Lorius' article, there has been considerable variation among investigators on quantities of drift obtained, perhaps due to surface or instrumentation differences. However, even more recent investigators [*Budd et al.*, 1966] corroborate Bagnold's log profile and 10-meter representative velocity level; they also corroborate the magnitude of the above figures, by data indicating 10.8 kg/m/hr transported by average winds with average drift densities at Byrd station. The existing difference between 10.8 and the values in the table could perhaps be partly accounted for by the magnitude of 'average winds' and, somewhat, by many readings at random times including events occurring when protective crusts existed at Byrd station.

Qualitative Considerations for Drift

It is well to caution that figures cited for drift quantities for various profiles are not without qualification if one is considering annual loss by deflation. There is a very effective role played by crusting of the surface which can result in high winds with relatively little load. This phenomenon in Antarctica is similar to Bagnold's observations of pebble surfaces in the desert. He observed that wind at a given height and capable of moving sand will attain a higher velocity over a pebble surface than over a sand surface. The higher velocity is reached because there is little entrainment of airborne grains over the pebble surface, since the wind strength is inadequate to start the pebbles saltating. If this same wind were then to

TABLE 3. Quantity of Drifting Snow Calculated for Various Wind Profiles Compared with Quantity Observed

The left column cites authors of reports from which wind profile data were extracted and upon which the original calculations were based. The center column represents Vickers' calculations; the right column, Lorius' measurements.

Wind Velocity at 10 m and Author of Profile, m/sec	Calculated Quantity of Drifting Snow, kg/m/hr	Measured Quantity of Drifting Snow, kg/m/hr
14.7 [*Vickers*, 1959*b*]	54	55
12.4 [*Liljequist*, 1956]	18	19.1
14.3 [*Bagnold*, 1941]	43	45.7

encounter a sand surface, its speed would be abruptly checked by loss of energy to the sand load blasted into the air. On the ice cap, the role of the pebble surface may be taken by any one of many types of surface crusts formed by radiation condensation, precipitation, or sublimation. Most common, even at very high elevations, is a 2-mm crust of either milky or clear ice. The crusts offer a cemented surface as opposed to a loose-grained surface. The type of surface, of course, determines how saturated a rising wind may become, i.e., how much loose surface material is available for entrainment. Thus one must consider the fact that crusting often sets in very rapidly in Antarctica (12 hours), once blowing snow grains have come to rest. The next increase in wind is apt to exist for considerable time before enough heavy material is broken loose to bombard and to break the crust, thus exposing the completely uncemented sublimation grains often found beneath the crusts in the warmer time of year.

Recall also that weather systems of high winds associated with heavy falls of fresh uncemented snow in colder times of year are relatively short-lived. A few days of migration at speeds much greater than those calculated above (average conditions) still do not account for much shifting of mass in terms of distance.

Regarding the present problem, the author concludes that the effects of drift on the accumulation map are not significant regarding distortion of its geographical representation of the distribution of precipitation. What the accumulation map indicates for distribution of accumulation is likely to be true for the distribution of precipitation.

Accumulation

Quantitative Assessment

1. *Calculation of the average annual accumulation rate.* The isopleths of Figure 24 have a degree of subjectivity to their plotting. Therefore, their use has been intended as a tool for description of distribution and not as a basis for quantitative calculation. The annual rate figure has been derived by a grid overlay, wherein areal increments of 100 nautical miles on a side are considered. All station values within an increment are averaged, and then a grand mean is obtained for all increment areas. This system tends to dampen the statistical weight of an area for which many pits were excavated versus an area for which only one pit may have been excavated. Examination of the map shows fairly good distribution of sampling, inland as well as coastal. The areas not sampled comprise about 30% of the total number of 100-mile squares possible.

Calculation of the annual rate of ice accumulation in West Antarctica gives a value of 19.8 g/cm^2 of water for evidence-backed figures, and 20.1 cm when all available figures are considered (including subjective pit interpretations). The latter considers a slightly larger number of years. The quantity 19.8 g/cm^2 is the preferred figure.

Rubin [1962], using an approach based on the mass budget of Antarctica, calculates 10.8–16.6 cm of accumulation. He also cites other references in which estimates range between 14.6 and 19.2 cm, varying with data and method used. One should be mindful that these estimates are for the total continent; hence they should be lower than values obtained herein, since inland plateau figures (low accumulation) would constitute a higher areal percentage of the total calculation.

2. *Calculations for an individual snowfall.* Employment of the investigative procedure used herein provides valuable detail on accumulation quantities, as well as on gross annual figures. This is obtained from an interpretation of the meteorological and stratigraphic history for the period investigated. The great snowfall commencing June 10, 1957, and capped by an early May crust has been selected as an example. It can be bracketed in the 1957 stratigraphy in 80% of pits examined. It is also known that this snowfall covered roughly all of West Antarctica west of the Byrd-Ellsworth divide. In all areas except the highlands adjacent to the Bellingshausen Sea coast, this snowfall accounted for approximately 22% of the year's accumulation based on an interpretation of traverse pits. Accordingly, one can figure about 5 g/cm^2 of water precipitated in this storm. This would give a latent heat release of 3400 cal/cm^2 of underlying surface as a contribution to the total energy of the storm system. The stratigraphy for 1957 and 1958 is sufficiently documented to calculate latent heat release for almost any period one might wish to investigate in a detailed energy study of antarctic circulatory systems.

Speculative Assessment of Accumulation Distribution

If the synoptic patterns in Table 1 are now assessed, an explanation of the distribution of accumulation becomes possible.

It was found that the annual cycle of storm activity revolved around the apparent interactions between the inland high and the coastal circuiting low-pressure systems. According to the synoptic charts the month of August represented the maximum areal strength of the inland high, whereby the continent was largely protected from maritime low invasion. (The pressure averages suggest it may occur two months earlier.) Long periods of clear stable weather were the rule for this period. However, during the buildup and decay of the high in the autumn and spring, respectively, frequent invasions by intense maritime systems became the rule. By late summer (February) weaker systems could readily invade the Polar Plateau. Recall also that the inland high may have preferred breakout positions; one over Victoria Land and possibly another over the Ronne and Filchner ice shelves. In addition to the above relationships, a large blocking high formed over, or west of, the Antarctic Peninsula during late winter (August). With these main circulatory highlights in mind, one can now examine the distribution of accumulation for apparent reasons.

Note that areas of maximum accumulation are (from east to west) the Norway station (70°S, 2°32′W) and Cape Norvegia area which is just off the right lower corner of the map (Figure 24) with 35 to 50 cm of water; the highlands adjacent to the Amundsen-Bellingshausen Sea area with up to 46 cm of water (late data, unverified, show considerable increase toward the Antarctic Peninsula, perhaps to 60 cm); and a small belt along the Adélie Coast with as much as 44 cm of water.

Minimum accumulation areas ($\approx$15 cm) are the Byrd-Ellsworth divide extending eastward toward Filchner Ice Shelf, the western Ross Ice Shelf (adjacent to Victoria Land), and the high inland plateau.

The explanation of distribution for the period of record herein lies in a combination of orographic effects and the circulation as previously described. The areas mentioned above will be considered in turn, as follows:

1. *East of the Byrd-Ellsworth divide.* The contrast between the Ronne-Filchner Ice Shelf area and Cape Norvegia ($\approx$19 cm versus 35–50 cm) is likely due to the preferred position for extensions of the inland high over these ice shelves. This ridge, according to the synoptic charts, held the maritime lows well to seaward until they hit Cape Norvegia, traveling from west to east, from the region of the Antarctic Peninsula. This seaward course was also presented in the independent studies of *Taljaard and Van Loon* [1962, p. 5]. Moreover, the Ellsworth region experienced long periods of clear diverging air from the Bellingshausen blocking high at a time when maritime lows were affecting Cape Norvegia. The result of the presence of these high-pressure systems (found as a region of few geopotential minima by *Taljaard and Van Loon* [1962, p. 7] was a twofold difference in accumulation between Ellsworth and Norway stations, both of which are coastal stations that might normally be assumed to have similar accumulation quantities. Figures 13 and 14 illustrate these meteorological situations.

2. *West of the Byrd-Ellsworth divide.* Circulation and orography account for the considerable contrast between the coastal highlands along the Amundsen-Bellingshausen Sea coast and the Byrd interior.

Regarding the role of circulation, there is evidence in Table 1 supporting the point that the prolonged presence of the blocking high is coincident with long periods of zero accumulation reaching as far westward as Byrd station. It is also known that the maritime lows frequently circuit the coast from west to east; thus they undergo direct blocking by the high and tend to become quasi-stationary in the Amundsen-Bellingshausen Sea area, contributing to the high precipitation of this area. The accumulation distribution suggests that the preferred track of storms from the Ross Sea headed eastward may be the coastal route [*Taljaard and Van Loon,* 1962, p. 6] rather than the inland Little America-Byrd track for which there are indications in early records [*Rastorguev and Alvarez,* 1958; *Alt et al.,* 1959; or *Cartwright,* 1959].

Superposed on the circulation effects are the effects due to orography. Along the Amundsen-Bellingshausen Sea coasts are abrupt mountains

providing considerable lift for onshore winds. It is of interest to note that the level of maximum accumulation, about 1500 meters, is appropriately at the lifting condensation level for this region (for 850-mb air) as presented in *Rubin and Giovinetto* [1962, p. 5168]. It appears, therefore, that there exists a combination of circulatory and orographic effects in the above region. Steep topography and a blocked maritime low can make for a maximum accumulation zone. Gentler inland slopes and more frequent protection from the inland high and the blocking high quickly minimize this trend to landward. The very high accumulation brought about by a favored circulatory-orographic situation as described above strongly suggests this region as a probable glaciation source.

3. *Western Ross Ice Shelf—Victoria Land Mountains.* On the macroscale one can readily see that the western shelf is in the lee of a large land mass as far as effects from west-east circuiting maritime lows are concerned. The regression of these storms into the southwest corner of the Ross Ice Shelf is infrequent but does occur, primarily in late summer-early fall and in spring [*Taljaard and Van Loon*, 1962]. This region is also slighted by its proximity to a favored position for extensions of the inland high over Victoria Land. It would appear, therefore, that one has no reason to expect high accumulation in this area attributable to macroscale circulation.

Regarding mesoscale effects, pits excavated on a traverse generally along the fall line of the Victoria Land mountains showed minimum accumulation within the first 100 meters of rise. This was attributed to adiabatic warming of the katabatic flow (and possibly even to the localized divergence on the downstream side of a mild form of hydraulic jump). Another factor may be the divergence of the general northeasterly wind stream as it flows off the high plateau. These factors give rise to high evaporation potential, the effects of which are seen in the stratigraphy of the Ross Ice Shelf—Victoria Land traverse, and, when coupled with a blocked supply of flowing glacier ice from the plateau (or sufficiently large upland source), becomes manifest as zero accumulation in the 'dry valleys' of Victoria Land mountains.

4. *The high interior plateau.* The accumulation of the high Victoria and Polar plateau region is slight and patchily distributed when examined in greater detail than the scale of Figure 24 allows. It approaches zero in some localized areas. The zero patches are due to wind scouring of already sparse accumulation probably resulting from the persistence of the inland high. These patches can be observed from an aircraft as surface textural changes where the orientation of a buried sastrugi layer has been exposed or a new one superposed by deposition. The distinction somewhat resembles large wind shadows and streaks as seen on a calm ocean surface from the air.

Over all, however, plateau accumulation is higher than most field workers anticipated. Recall Figure 16, where during February all stations and field parties in this area reported simultaneous snowfall from a very widespread system. Recall also the simultaneous fluctuation in surface level at Little America and the Pole station as the intense June storm of 1957 penetrated to the south pole. We consider, also, the fact that winter cyclones might enter into the antarctic upper cold low, bringing moisture in at very high levels [*Pogosjan*, 1959]. Time cross sections examined for the period covered herein show cyclonic cells extending to about 25,000 feet.

The accumulation of the high plateau region probably will receive more attention. It is suggested here that the monitoring of storm tracks by polar orbiting satellite, coupled with simultaneous atmospheric time sections and accumulation stratigraphic measurements at currently occupied ground stations, would aid greatly in the extrapolation of any traverse data acquired in the future.

Acknowledgments. I wish to thank my many antarctic colleagues whose efforts in a most unkind environment have made possible the large store of data on which this study is based.

Acknowledgment is due Albert P. Crary, who is perhaps unaware that the memos he left for the relief crew at Little America, coupled with conversations with H. Hoinkes, seeded the idea that later evolved into the main thread of this report, namely, the effects of specific meteorological variables on a specific stratigraphic section of firn.

The author is indebted to Fritz Müller and Svenn Orvig of McGill University, Richard P. Goldthwait, Fritz Loewe, Colin Bull, and Arthur Mirsky of the Ohio State University, and Carl Benson of the University of Alaska for their review and constructive criticism of this work. To Morton Rubin and William Weyant of the Environmental Science Services Administration go special thanks for very helpful discussions on antarctic circulation.

This investigation has received financial support from the National Science Foundation (grants Y/4. 10/285 and Y/21. 12/333). Work has proceeded under the facilities of the Institute of Polar Studies at the Ohio State University, Columbus, Ohio, and McGill University, Montreal. It is hoped that the report will fulfill the expectations of these institutions, as the author is most grateful for their assistance.

REFERENCES

Alt, J., P. Astapenko, and N. J. Ropar, Jr., Some aspects of the antarctic atmospheric circulation in 1958, *IGY Gen. Rept. 4*, 27 pp., 1959.

Bader, H., Theory of densification of dry snow on high polar glaciers, *SIPRE Res. Paper 69*, 8 pp., U. S. Army Corps of Engineers, Wilmette, Illinois, January 1960.

Bagnold, R. A., *Physics of Blown Sand*, Methuen, London, 1941. (Reprinted, 365 pp., 1954.)

Benson, C. S., Stratigraphic studies in the snow and firn of the Greenland ice sheet, Ph.D. dissertation, 213 pp., California Institute of Technology, Pasadena, California, 1960.

Budd, W. F., W. R. J. Dingle, and U. Radok, The Byrd snowdrift project, *this volume*, 1966.

Cartwright, G. D., Meteorological studies in the Antarctic, *IGY Bull. 24, Trans. Am. Geophys. Union, 40*, 191–195, 1959.

Crary, A. P., Glaciological studies at Little America, Antarctica, 1957 and 1958, *IGY Glaciological Report 5*, 197 pp., American Geographical Society, 1961.

Crozaz, G., E. Picciotto, and W. De Breuck, Antarctic snow chronology with Pb^{210}, *J. Geophys. Res., 69*(12), 2597–2604, June 1964.

Doeglas, D. J., Interpretation of size frequency distributions and classification of sediments, Guest lecture, Department of Geology, Ohio State University, November 3, 1960. (Published in *Geologie en Mijnbouwk*, Netherlands, May 1955.)

Grandoso, H. N., and J. Nunez, Analysis de una situación de bloqueo en la parte austral de América del Sur, *Meteoros (Buenos Aires), 5*, 35–54, 1955.

Libby, W. F., Radioactive strontium fallout, *Proc. Natl. Acad. Sci. U. S., 42*, 1956.

Libby, W. F., Radioactive fallout, *Proc. Natl. Acad. Sci. U. S. 44*, 815, 1958.

Liljequist, G. H., Wind structure in the low layer, *Norwegian-British-Swedish Antarctic Expedition, 1949–1952, Scientific Results, II*, part 1C, Norsk Polarinstitutt, Oslo, 1956.

Lorius, C., Contribution to the knowledge of the antarctic ice sheet: A synthesis of glaciological measurements in Terre Adélie, *J. Glaciol. 4*(31), 79–92, March 1962.

Martell, E. A., Atmospheric aspects of strontium 90 fallout, *Science, 129*(3357), 1197–1206, May, 1959.

Miyake, Y., K. Saruhashi, Y. Katsuragi, and T. Kanazawa, Seasonal variation of radioactive fallout, *J. Geophys. Res., 67*(1), 189–193, January 1962.

Picciotto, E., and S. Wilgain, Fission products in antarctic snow, a reference level for measuring accumulation, *J. Geophys. Res., 68*(21), 5965–5972, November 1963.

Pogosjan, H. P., Seasonal peculiarities of the temperature and atmospheric circulation regimes in the Arctic and Antarctic, *Technical Note 28*, World Meteorological Organization, 1959.

Rastorguev, V. I., and J. A. Alvarez, Description of the antarctic circulation observed from April to November 1957 at the IGY Antarctic Weather Central, Little America station, *IGY Gen. Rept. 1*, 10 pp., May 1958.

Rex, D. F., Blocking action in the middle troposphere and its effects on regional climate, *Tellus, 2*, 196–211, 275–301, 1950.

Rubin, Morton J., Atmospheric advection in the antarctic mass and heat budget, in *Antarctic Research, Geophysical Monograph 7*, American Geophysical Union, Washington, D.C., pp. 149–159, 1962.

Rubin, Morton J., and Mario B. Giovinetto, Snow accumulation in central West Antarctica as related to atmospheric and topographic factors, *J. Geophys. Res., 67*(13), 5163–5170, December 1962.

Taljaard, J. J., and H. Van Loon, Cyclogenesis, cyclones, and anticyclones in the southern hemisphere during winter and spring of 1957, *Notos, Pretoria, 11*, 3–20, 1962.

U. S. Navy Hydrographic Office, *Atka Antarctic Report*, 1956.

Van Loon, H., Blocking action in the southern hemisphere, *S. Africa Weather Bur. Notes, part I, 5*, 171–175, 1956.

Vickers, W. W., Antarctic snow stratigraphy, *IGY Bull. 23, Trans. Am. Geophys. Union, 40*, 181–184, 1959*a*.

Vickers, W. W., Wind transport of antarctic snow, *IGY Bull. 22, Trans. Am. Geophys. Union, 40*, 162–167, 1959*b*.

Vickers, W. W., Geochemical dating techniques applied to antarctic snow samples, *Publ. 61 (Berkeley Symposium), Intern. Assoc. Sci. Hydrol.*, 199–215, 1963.

Vickers, W. W., A study of ice accumulation and tropospheric circulation in western Antarctica, Ph.D. dissertation, McGill University, Montreal, Canada, 1965.

CLIMATOLOGICAL OBSERVATIONS IN ICE-FREE AREAS OF SOUTHERN VICTORIA LAND, ANTARCTICA

COLIN BULL

Institute of Polar Studies, Ohio State University, Columbus

Abstract. In the ice-free Wright and Victoria valley systems, west of McMurdo Sound, summer air temperatures are appreciably higher than temperatures on the coast of the Sound. Direction of surface winds is controlled by the topography. Easterly winds carry cool and damp air into the valleys, and the snow precipitation is greatest in the eastern ends of the valleys. Katabatic winds, from the inland ice of East Antarctica, are westerlies in the Wright Valley and northerlies or southerlies at the main observing site in the Victoria Valley system. The katabatic winds are relatively warm and dry and in the summer are confined to the western parts of the area and to the valley bottoms. Indirect evidence indicates that in the winter strong westerly winds blow throughout the valley. The annual net radiation balance in the ice-free area is positive, at about 29,000 cal cm^{-2}, whereas in neighboring ice-covered areas there is a net loss of heat energy. These conditions, with the small quantity of winter precipitation, account for the continued ice-free nature of the area.

1. INTRODUCTION

During the past seven years many geological, geophysical, geomorphological, and other studies have been made in the ice-free areas in southern Victoria Land on the west side of McMurdo Sound, Antarctica. The interest in this area has arisen largely because it is the largest accessible ice-free area in Antarctica. Detailed meteorological studies have not been reported at this writing (January 1964).

Surface weather observations for periods varying from a few days to 110 days have been made by parties working in the area. Although these observations are confined to the summer months and have been taken at several sites, they are sufficient to show some of the influences of the ice-free nature of the area on the various meteorological parameters and to indicate the problems that are worthy of detailed work.

2. PHYSIOGRAPHICAL SETTING

On the western side of the Ross Sea, McMurdo Sound, and the Ross Ice Shelf, the inland ice of East Antarctica is bounded near 160°E by the Transantarctic Mountains, which extend from 70°S to at least 83°S. Deep valleys, most of which trend east-west, have been carved through the mountain range by outlet glaciers from the inland ice.

Most of the range is ice-covered; outlet glaciers, although smaller now than previously, fill the main valleys; extensive névé fields occupy the upland areas, feeding alpine glaciers which flow into the trunk glaciers or directly into the sea or ice shelf. However, in southern Victoria Land an area of approximately 4000 km^2 is almost entirely free of ice. This area (Figure 1) lies between 77°S and 77°45′S, and 160°E and 163°E. The ice-free area comprises three major valley systems and the intervening ranges. The Victoria Valley system in the north consists of five interconnected valleys, whereas the Wright and Taylor valleys are simpler east-west valleys.The main valleys were carved by outlet glaciers from the inland ice. With a decrease in the elevation of the inland ice, resistant rock thresholds have emerged at the heads of the valleys and now seriously limit the flow from the inland ice, which is at an elevation of 2500 meters.

In the Taylor Valley the rock threshold is not high enough to cut off completely the flow of ice from the inland ice plateau. The flow is insufficient, however, to maintain a glacier to the coast. The Taylor Glacier ends 30 km inland, at an elevation of 140 meters. At the western end of the Wright Glacier only a small quantity of ice flows over the threshold, forming ice falls north and south of

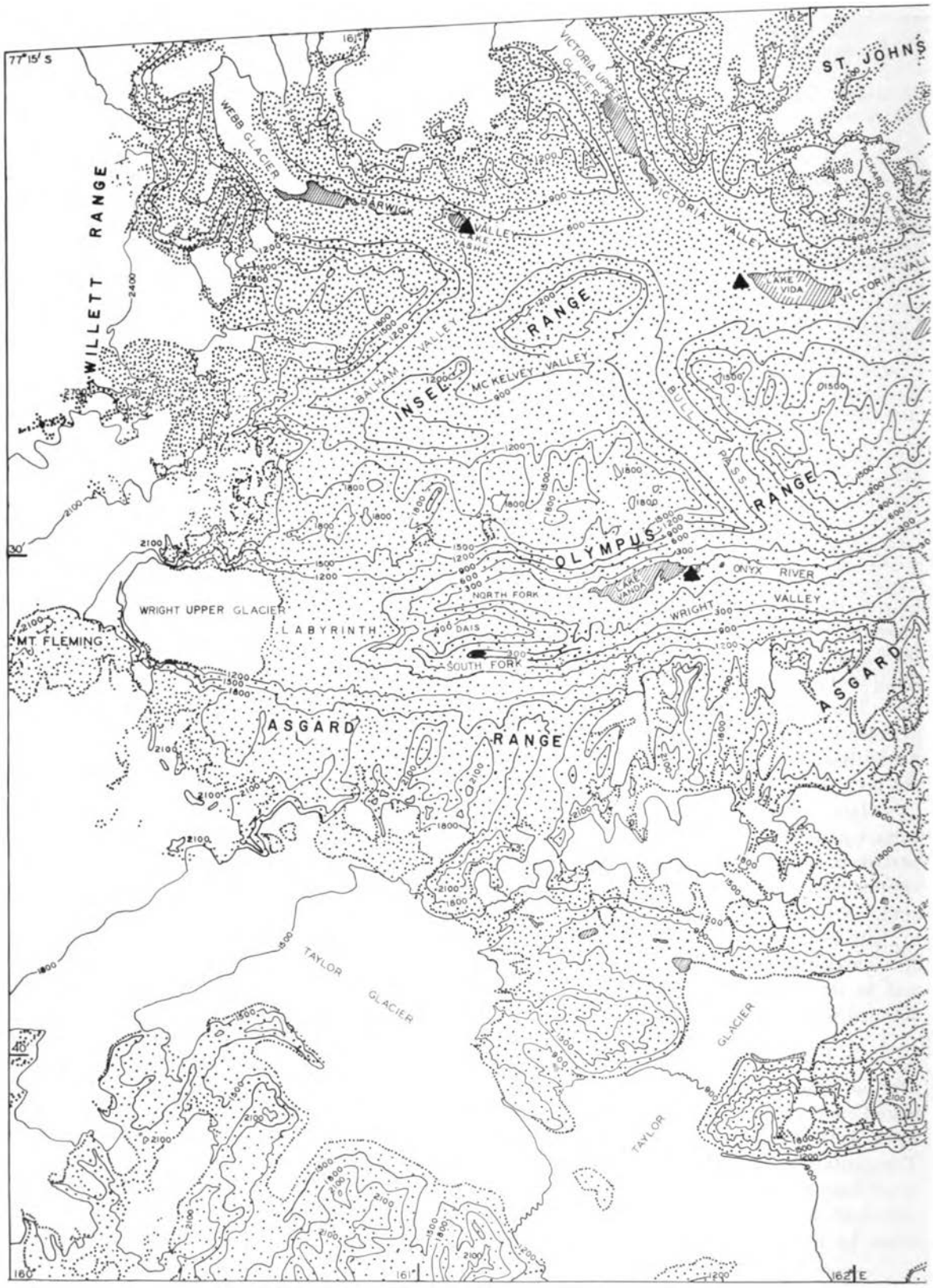

Fig. 1. Map of ice-free area in southern Victoria Land, Antarctica.

Mount Fleming. The ice flows coalesce at 1600 meters to form the thin, flat-lying Wright Upper Glacier which extends 4 or 5 km eastward.

The heads of the Balham and McKelvey valleys in the west part of the Victoria Valley system are occupied by small ice tongues from the inland ice, but the Webb Glacier, at the end of Barwick Valley, is a retreating glacier now fed almost entirely by accumulation on its own névé field. Previously, large glaciers flowed through passes in the Willett Range to join the locally fed glaciers.

In general, the elevation of the ranges bounding these valleys increases westward, from about 1000 meters near the coast to 2000 meters or more where they merge into the inland ice. At the coastal ends some of the upland areas are snow covered; small glaciers descend the valley walls, but only a few reach the valley bottoms. The western parts of the ranges are more nearly ice free.

Many lakes occupy depressions in the ice-free valleys. The largest of them, including Lakes Bonney, Vanda, and Vida, remain ice-covered throughout the year except for narrow moats that form in the summer. In midsummer the ice on Lakes Bonney and Vanda is about 4 meters thick, and the waters are 35 and 70 meters deep, respectively. Lake Vida is probably frozen nearly to the bottom [*Calkin*, 1963]. Temperatures well above 0°C have been found in many of the lakes [*Wilson and Wellman*, 1962; *Angino and Armitage*, 1963]. Various mechanisms have been suggested for the heating, but it now seems clear that the main source is the trapping of solar energy in the nonconvecting lower layers of the lakes.

3. THE OBSERVATIONS

Meteorological observations were made at sites in the fields (Figure 1) during the periods of time and with the equipment specified in Table 1. The standard time used in this report is GMT plus 12 hours; since the ice-free area is in a GMT minus 11 hours time zone, local noon in the area is at about 1300.

The observations in the ice-free area may be compared with the records from:

1. U. S. Navy Air Facility, Hut Point (referred to elsewhere as McMurdo station). The site is at 77°51′S, 166°37′E, at an elevation of about 25

TABLE 1. Field Sites at Which Meteorological Observations Were Made

Location	Period	Time of Observation	Equipment and Visual Data*	Observer
Lake Vanda (150 m)	Dec. 12, 1958–Jan. 30, 1959	6-hourly	2–10	C. Bull et al.
Lake Vashka (507 m)	Dec. 5, 1959–Jan. 31, 1960	1200, 1800 (0900, 1200)‡, §	1–6, 8–10	R. H. Balham
Lake Vida (400 m)	Dec. 4–30, 1959	...	3, 5, 10	R. H. Balham
Victoria Valley†	Oct. 23, 1960–Feb. 10, 1961	0800, 2000	1, 6, 8, 9	T. Davis and P. Calkin
Mouth of Taylor Valley	3 weeks, Nov.–Dec. 1959	...	2, 6	J. D. McCraw
Wright Valley	2 weeks, Dec. 1961	...	6, 7	F. Ugolini
Taylor Valley	2 weeks, Jan. 1963	...	6, §, ‡, ‖	Victoria Univ.
Marble Point	Nov. 15, 1958–Jan. 27, 1959	hourly	1, 3–10, §	U. S. Navy

* 1, Anemometer; 2, hand-held anemometer; 3, hygrograph; 4, barograph; 5, thermograph; 6, dry bulb thermometer; 7, wet bulb thermometer; 8, maximum thermometer; 9, minimum thermometer; 10, louvered screen.

† No fixed sites, but include east and west ends Lake Vida (410, 400 m). Bull Pass (675 m); near Lake Vashka (507 m); near Packard Glacier (750 m); Balham Valley (720 m); near Victoria Upper Glacier (446 m): Care must be taken in comparing these observations with those taken at fixed sites.

‡ Wind observation.

§ Cloud observation.

‖ Precipitation.

meters, about 2 km from the west coast of the southwest end of Hut Point Peninsula, Ross Island. Surface and upper air observations have been taken regularly since March 1, 1956, by U. S. Navy personnel.

2. Scott Base, Pram Point. Surface observations have been made regularly since March 1, 1957, by New Zealand Meteorological Office personnel. Radiation balance measurements were made during the period March 1957–February 1959. The station is located at 77°51′S, 166°48′E, about 3 km from Hut Point, 15 meters above sea level and 50 meters from the coast.

Reference also has been made to the meteorological data and notes recorded by earlier expeditions, especially on three journeys to the western mountains: January 27–March 14, 1911; September 15–28, 1911; and November 16, 1911–February 15, 1912.

4. TEMPERATURE

In general not enough readings of ambient temperature are available to allow worthwhile estimates of daily or weekly means. Mean temperatures for half-monthly periods have been obtained by taking the average of the means of the daily maximum and minimum temperatures; they are listed in Table 2. Mean temperatures calculated in this way are not likely to be in error by more than 1°C.

A minimum thermometer, left in the screen near Lake Vida, showed a minimum temperature of −62°C for the winter of 1960. The lowest temperature recorded at Hut Point in this period was −51°C [*U. S. Navy Weather Research Facility*, 1961].

The following conclusions can be drawn from the data in Table 2:

1. The highest temperature recorded, 12.3°C, at Lake Vashka on December 20, 1959, exceeds any

TABLE 2. Mean and Extreme Temperatures for 2-Week Periods at Various Sites in the Ice-Free Areas
(Temperatures in °C)

Period	Year	Days Observed	Mean	Mean Max.	Mean Min.	Range	Highest Max.	Lowest Min.	Location
Oct. 16–31	1961	8	−23.7	−15.9	−31.6	15.7	−8.9	−37.8	E. Vida
Nov. 1–15	1961	8	−14.8	−7.8	−21.8	14.0	−3.9	−28.9	E. Vida
Nov. 16–30	1961	15	−6.6	−1.8	−11.3	9.5	1.7	−10.6	Bull Pass L. Vashka
	1958	15	−7.2	−4.5	−10.0	5.5	−1.1	−16.5	Marble Pt.
Dec. 1–15	1961	9	−4.8	−0.9	−8.7	7.8	0.6	−10.6	L. Vashka Balham L.
	1959	12	−0.2	3.6	−3.9	7.5	8.3	−12.4	L. Vashka
	1958	15	−5.9	−3.5	−8.2	4.7	2.2	−13.2	Marble Pt.
Dec. 16–31	1961	15	−3.2	0.6	−7.0	7.6	2.2	−8.9	Balham L. E. Vida
	1959	16	0.7	4.1	−2.7	6.8	12.3	−5.4	L. Vashka
	1958	16	−2.7	−0.7	−4.7	4.0	1.2	−7.8	Marble Pt.
	1958	15	−0.8	1.6	−3.2	4.8	4.4	−5.3	L. Vanda
Jan. 1–15	1962	14	−1.3	1.9	−4.5	6.4	3.3	−7.2	W. Vida
	1960	15	−2.7	0.6	−5.9	6.5	3.8	−8.6	L. Vashka
	1959	15	−0.1	2.1	−2.3	4.4	4.9	−5.0	Marble Pt.
	1959	10	2.2	4.9	−0.5	5.4	8.3	−4.4	L. Vanda
Jan. 16–31	1962	16	−4.4	0.1	−8.9	9.0	3.3	−17.2	W. Vida
	1960	16	−2.5	1.3	−5.8	7.1	4.9	−10.7	L. Vashka
	1959	13	−1.4	1.0	−3.8	4.8	4.6	−6.1	Marble Pt.
	1959	15	0.3	3.3	−2.8	6.1	8.3	−4.4	L. Vanda
Feb. 1–14	1962	9	−7.4	−1.7	−13.1	11.4	0.6	−17.8	W. Vida

other temperature recorded under standard conditions in Antarctica. During four days in the 1959–1960 summer at Lake Vashka and during four days in the 1958–1959 summer at Lake Vanda, temperatures exceeded 7°C.

2. The variations in mean temperature from year to year are larger than the difference between Marble Point and the inland sites. December 1961 was 4°C colder than December 1959 in the Victoria Valley system. In 1958–1959 the western end of Wright Valley was 2°C warmer than Marble Point.

3. The temperature range (here defined as the difference between the mean of the daily maxima and the mean of the daily minima) is significantly greater in the Victoria Valley system than at Marble Point and at Lake Vanda. The low value for the range at Marble Point is due to the maritime environment. The low range at Lake Vanda is not readily explained.

4. For the period of observations, the range of temperatures is least in midsummer. At the summer solstice the maximum and minimum altitudes of the Sun are 35° and 12°. In late October the daily variation in altitude is from 23° to 0°, and hence the daily variation in the solar heating of the surface is greater then than in midsummer. Presumably the first harmonic (24-hour period) of the temperature fluctuations approaches zero in winter, as it does at other points well inside the antarctic circle.

5. Although summer temperatures in the ice-free areas are higher than on the coast or at Hut Point, the winter temperatures are much lower. In the Victoria Valley the mean temperature for the second half of October 1961 was −23.7°C; at Hut Point the mean temperature for the whole of that month was −20.4°C [*U. S. Antarctic Research Program*, 1961].

6. The monthly mean temperature exceeded 0°C in January 1959 at Lake Vanda and in December 1959 at Lake Vashka.

TABLE 3. Number of Observations of Wind from Different Directions at Lake Vanda, Summer 1958–1959

Wind Direction	Time			
	0001	0600	1200	1800
Easterly	18	3	12	13
Westerly	7	3	10	12
Calm (i.e., <5 kt)	3	6	5	5

5. WIND

Wright Valley

Wind direction. The site of observations near Lake Vanda in December 1958–January 1959 was near the lowest part of a long, narrow, and high-sided valley. Wind direction was controlled almost completely by the direction of the valley and blew either from south of west (240°–260°) or from north of east (60°–80°). Direct observations of wind direction were made at this site on 30 days. The number of observations of easterly and westerly winds and calm (<5 kt) at these times is given in Table 3.

Thus, the dominant wind during these two months was easterly, blowing from McMurdo Sound, but at 1200 and 1800 westerly winds were nearly as common as the easterlies.

Direct observation showed that the westerly wind was limited in extent. On 7 occasions when a strong westerly wind was blowing at the observing site, calm or light variable winds were experienced at elevations above 800 meters on the valley walls north or south of the site. On 19 occasions when westerly winds were observed at Lake Vanda, the wind was easterly at points in the valley more than 20 km to the east. No westerly winds have been recorded in the eastern half of the valley.

However, the easterly wind in Wright Valley is also frequently limited in vertical extent. On 15 days when a strong easterly wind was blowing at the nearest part of the valley floor, calm or light variable wind was experienced above 1200 meters on the valley walls. The vertical separation of the regions of calm and of moderate easterly winds was usually small, of the order of 100 meters.

Wind and relative humidities. The westerly winds encountered near Lake Vanda are shallow katabatic winds that originate on the ice plateau to the west or southwest of Wright Valley. The air masses involved remain in close contact with ice until they reach the eastern end of the Wright Upper Glacier, which is at an elevation of 1300 meters and about 10 km west of the site of observations. While in contact with the ice, the temperature of the air mass remains low and its relative humidity high. During its rapid descent over these 10 km, the air is heated by adiabatic compression and the specific humidity does not increase appreciably; the surface of the

TABLE 4. Dew Points for Easterly and Westerly Winds at Lake Vanda, Summer 1958–1959, with Standard Deviations
Temperatures are in °C. Figures in parentheses give the number of observations.

Direction	Time 0001	1200	1800
Easterly	(16) −5.1 ± 1.7	(10) −5.7 ± 1.5	(10) −5.2 ± 1.9
Westerly	(5) −9.6 ± 1.4	(8) −9.6 ± 1.1	(10) −8.6 ± 1.4

North and South Forks is completely dry except for two or three very minor pools; Lake Vanda remains frozen except for a moat, up to 20 meters wide, around the edges.

Consequently, the relative humidity of the westerly winds is low; during the six weeks of observations it averaged 45% at a mean temperature of 2.2°C. The extremes of relative humidity were about 5% and about 60%, with these winds.

On the other hand, the easterly winds at Lake Vanda blow from McMurdo Sound. For December 1958 and January 1959 the wind at Marble Point was dominantly southeasterly, and with these winds the mean temperature was about −2.7°C and the relative humidity about 75%. As this air mass continues westward from the coast, it is cooled by adiabatic expansion in crossing the Wilson Piedmont Glacier, elevation 600 meters, and often becomes saturated. Thus low cloud over the glacier is prevalent during easterly wind conditions, as had been noted by earlier expeditions.

For the easterly winds at Lake Vanda for the same period of observation the mean temperature was −0.5°C and the mean relative humidity was 68%.

The distinction between the easterly and westerly winds at Lake Vanda is mostly clearly shown by their dew points. Restricting analysis to the occasions when a wind of more than 5 kt had been blowing in a steady direction for more than three hours before the time of observation, the values of dew point given in Table 4 are obtained.

On some occasions the wind blew strongly for a short period in the direction contrary to that for the rest of the day. The variations of dew point for three such occasions are given in Figure 2.

The significant difference between the dew points

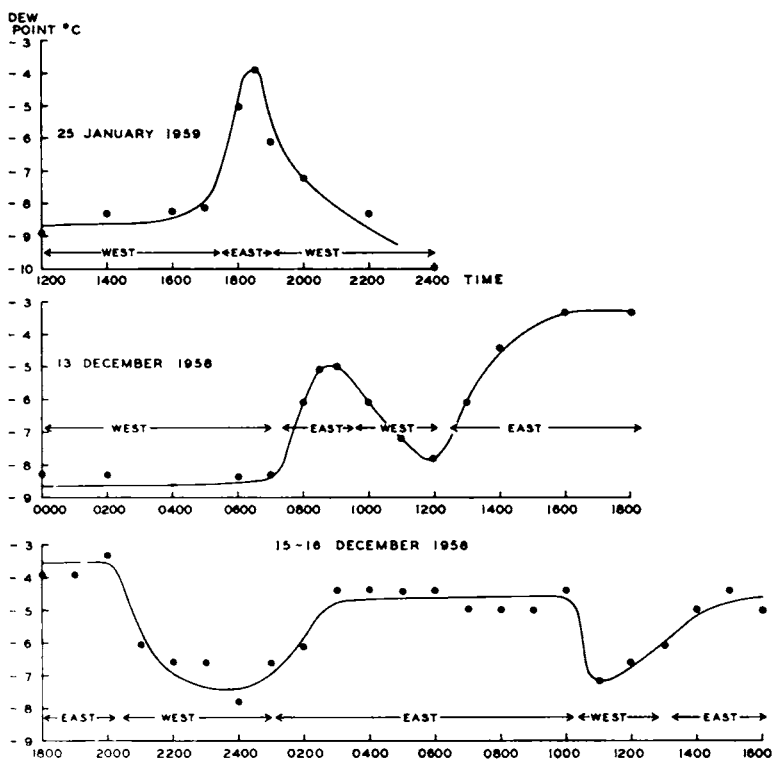

Fig. 2. Variations of dew-point temperatures with time, showing effect of wind direction. Wright Valley, near Lake Vanda.

TABLE 5. Number of Occasions of Wind from Different Directions, at Lake Vanda, Summer 1958–1959

Direction	Time 0001	0600	1200	1800
Easterly	30	24	18	21
Westerly	8	9	14	14
Calm or <5 kt	3	6	5	5
Indeterminate	11	13	15	11

with easterly and with westerly winds allows the wind direction to be inferred at the majority of times when only the temperature and relative humidity are known. The number of days with a given wind direction, either directly observed or inferred, at the four times of observation are given in Table 5.

Wind speeds. The mean wind speeds (in knots) for the period of observation at Lake Vanda are given in Table 6. There is seen to be a diurnal variation in wind velocity: with easterly winds the maximum velocity occurs at about 1800; with westerly winds the maximum occurs at about 1300.

Irregular observations were made in the eastern end of the valley on 25 days in 1958–1959. The winds, always easterly, were strongest between 1100 and 2200 and were much weaker during the 'night.' Similar observations have been made by other parties working in the area in other summers.

Wind and temperature. Air temperatures at Lake Vanda were higher with westerly winds than with easterly winds. Nearly all the differences among the mean temperatures during the half-monthly periods are due to the relative frequencies of easterly and westerly winds during the periods. The mean temperatures in the half-monthly periods, for either easterly or westerly winds alone, did not vary by more than 1.5°C.

The mean temperatures in degrees Celsius at the observing times for the different wind directions are given in Table 7. For both easterly and westerly winds the diurnal variation was about 3°C, but the maximum with westerly winds occurred at about 1630, whereas with easterlies it was at 1330, shortly after local noon.

TABLE 6. Mean Wind Speeds, in Knots, Observed at Lake Vanda, Summer 1958–1959

	0001	0600	1200	1800
All observations	11.4	8.0	11.3	14.7
With easterlies	11.5	8.2	11.7	18.3
With westerlies	12.8	10.7	16.0	13.4

TABLE 7. Mean Temperatures under Different Wind Conditions, at Lake Vanda, Summer 1958–1959 (°C)

	0001	0600	1200	1800
All observations	−0.8	−0.8	2.2	1.6
Westerly winds	1.4	1.0	3.3	4.1
Easterly winds	−1.4	−1.7	1.3	−0.1

Marble Point

Surface wind observations were taken hourly at Marble Point. The observations for the months December 1958 and January 1959 show the following features: (1) the wind patterns for the two months were similar; (2) the dominant wind was from the south and southeast; (3) northerly winds were most common at 1300 and 1900; (4) westerly wind was most common at 0100 and 0700. The percentage frequencies of wind from various directions are given in Table 8.

At Marble Point the temperature, dew point, and humidity are less clearly related to wind direction than they are at Lake Vanda. As an example, the mean values for the period December 16–31 are given in Table 9. Variations in the other half-monthly periods are of similar magnitude.

The westerly winds, which are less moist than the

TABLE 8. Frequency (in per cent) of Winds from Different Directions, Marble Point, Summer 1958–1959 (About 62 observations at each observing hour.)

Direction	Time 0100	0700	1300	1900	All Obs.
N	5	6	18	15	11
NE	...	3	5	1	2
E	3	8	8	10	8
SE	5	14	34	27	20
S	36	35	26	30	31
SW	5	4	...	3	3
W	27	13	2	8	13
NW	5	7	3	3	4
Calm	14	10	4	3	8

TABLE 9. Temperatures and Dew Point (in °C) and Relative Humidities (in per cent) for Different Wind Directions, Marble Point, December 16–31, 1958
(i. d. means insufficient data for statistical purposes.)

	0100			0700			1300			1900		
	T.	D. P.	R. H.	T.	D. P.	R. H.	T.	D. P.	R. H.	T.	D. P.	R. H.
All Obs.	−4.1			−3.4			−1.6			−2.0		
SE & S winds	−4.6	−7.6	80	−3.9	−8.1	76	−2.3	−6.1	76	−3.7	−6.3	80
W winds	−3.6	−9.5	64	−3.5	−8.3	70	i. d.	i. d.	i. d.	−0.6	−6.7	67
N winds	−3.6	−8.9	67	i. d.	i. d.	i. d.	−1.0	−7.3	63	−0.9	−5.9	69

southeasterlies, are gravity winds, as are the westerlies at Lake Vanda. However, the heating by adiabatic compression (during the descent from the Wilson Piedmont Glacier) is small compared with similar heating of the westerlies at Lake Vanda, and the reduction in the relative humidity is correspondingly smaller. The westerly winds at Marble Point are of local origin and are not directly related to those at Lake Vanda. A comparison of Tables 5 and 8 shows that the maximum frequencies of westerlies at the two sites occur about 12 hours apart.

Lake Vashka

Wind directions. The observing site at Lake Vashka resembled that at Lake Vanda in the Wright Valley by being near the lowest part of the Valley. Barwick Valley is, however, much more complicated than Wright Valley. South of Lake Vashka, Barwick Valley is joined by Balham Valley, and on the south side of Balham Valley two gaps in the Insel Range lead directly to the southwest-trending McKelvey Valley (Figure 1). For 8 km to the west of Lake Vashka, Balham Valley runs east-west and is steep-sided and narrow, but the main part of the valley then turns north and is occupied by the Webb Glacier. For 8 km east of Lake Vashka, the walls of Barwick Valley are high and continuous, but farther east this valley is joined by the Victoria and McKelvey valleys. Another difference between the surroundings of the two observing sites occurs at the edge of the inland ice. West of Wright Valley, the Olympus and Asgard ranges extend into the inland plateau, forming a funnel and thus directing katabatic winds into Wright Valley. West of Barwick Valley, the Willett Range forms a barrier to westerly winds; the lowest points in the range are west of the Balham Valley, west of the northern part of the Webb Glacier, and west of the Cotton Glacier, farther north. From this most northerly pass from the inland ice, wind can blow into the Victoria Valley system over the low pass onto the Victoria Upper Glacier.

Consequently, the wind pattern at Lake Vashka is much more complicated than at Lake Vanda. For the period December 5, 1959–January 31, 1960, observations of wind speed and direction were made at 0900, 1200, 1800, and 2100. Analyses for half-monthly periods show that no significant changes in the wind pattern occurred during these two months (Table 10).

The dominant wind was easterly, but easterlies occurred less frequently at 1200 and 1800 than at other times. In these ways the pattern resembles that at Lake Vanda. However, at Lake Vashka the wind seldom blew from the west quadrant, and, when not blowing from the east, it came from the north and northeast and from the south and southeast with about equal frequencies.

Wind and humidity. At Lake Vashka the water vapor content of the air depends on wind direction, as it does at Lake Vanda in the Wright Valley.

The values of the dew point in degrees Celsius for the various wind directions are given in Table 11.

The difference between the dew points associated with the easterly and with the southerly winds is about the same as the difference between the easterlies and westerlies at Lake Vanda, but the statistical significance of the difference is less at Lake Vashka. There is no significant difference between the dew points of the easterly and northerly winds.

The southerly winds at Lake Vashka are katabatic winds blowing from the inland ice into Bal-

TABLE 10. Number of Observations of Wind from Various Directions at Lake Vashka, December 1959–January 1960

Direction	Time				
	0900	1200	1800	2100	Total
N	1	7	3	1	13
NE	4	8	15	6	33
E	39	27	21	38	125
SE	5	6	4	3	18
S	6	9	12	7	34
SW	0	0	0	1	1
W	1	0	2	1	4
NW	1	1	0	0	2
Calm ($<\sim$2 kt)	1	0	0	0	1

ham Valley and thence, through the gap in the Insel Range, into Barwick Valley.

The origin of the northerly winds is obscure. They may be katabatic winds that blow from the inland ice into the Cotton Glacier valley, where they are deflected to the south into the Victoria Valley system over the Victoria Upper Glacier, or they may be at least partly related to unusual synoptic patterns.

Wind speeds. The mean wind speeds in knots recorded at Lake Vashka are given in Table 12. Figures in parentheses are the number of observations. Winds from the east did not exceed 20 kt at the times of observation. On only one day were northerlies recorded gusting to more than 20 kt. The southerlies were the strongest winds. At 12 times of observation, southerlies gusted to more than 20 kt, the maximum being greater than 50 kt on January 24, 1960. With these strong winds, temperatures were higher than normal for southerly winds, in similar fashion to the strong westerly winds in the Wright Valley. The higher temperatures were probably caused by the increased vertical mixing and the breakdown of the normal temperature inversion.

Simultaneous Observations at Two Sites on the Valley Floor.

The observations in the Wright Valley in 1958–1959 showed that the katabatic winds were limited in vertical and horizontal extent. An attempt was made in 1959–1960 in the Victoria Valley system to obtain more data on the problem by establishing two recording sites, one near each end of the valley floor. These sites were at Lake Vashka and at the western end of Lake Vida. Wind speed and direction recorders were not available, and only a thermograph and a hydrograph could be installed at the Lake Vida site.

The more complicated relationship between wind direction and dew point at Lake Vashka, compared with that at Lake Vanda, and small errors in the hydrograph at Lake Vida limit the quantitative value of these observations, but the following conclusions may be drawn:

a. On each of the three occasions during the simultaneous recording when the wind at Lake Vashka changed from easterly to a strong southerly, the dew point at Lake Vashka fell quickly (as it does also at Lake Vanda with the arrival of a katabatic wind), typically from —5° to about —15°C. During these periods of wind direction change at Lake Vashka the wind direction at Lake Vida remained easterly. Typically, the dew point at Lake Vida gradually fell from about —7° to —10°C during the 3-hour period, while it was falling to about —15°C at Lake Vashka, and then it fell more quickly to about —15°C. The fastest fall in the dew point at Lake Vida occurred about 7 hours after that at Lake Vashka. In situations like this one, with opposing winds blowing at the two ends

TABLE 11. Dew Points for Different Wind Directions, at Lake Vashka, Summer 1959–1960, with Standard Deviations (Temperatures are in °C; numbers of observations in parentheses.)

Month	Direction		
	Easterly	Northerly	Southerly
December 1959	(62) -9.5 ± 3.3	(16) -8.8 ± 2.3	(28) -12.9 ± 3.4
January 1960	(59) -8.5 ± 3.6	(37) -9.6 ± 2.5	(25) -14.9 ± 4.6

of the valley, the circulation pattern may be very complex. The warm, dry air mass may travel eastward down the valley until it is forced upward over the inflowing colder easterly winds and may retain its identity aloft, with little mixing. Comparing this situation with those in the detailed studies of valley and mountain wind in a more complicated topographic setting, made by *Thyer and Buettner* [1962], it appears possible that farther east the elevated westerlies may lose their momentum and be dragged into the lower level general easterly circulation. If this is the case, the 7-hour delay in the fall of the dew point at Lake Vida could represent the period of this circulatory motion.

b. On the three occasions during the simultaneous recordings when the surface wind at Lake Vashka changed from a southerly to an easterly, the dew point at Lake Vida started to rise about 3 hours sooner than did the dew point at Lake Vashka. This interval is approximately the travel time of surface winds in blowing from Vida to Vashka.

Observations of Wind Elsewhere in the Victoria Valley System

Between October 22, 1961, and February 10, 1962, wind directions were recorded twice daily, usually at 0800 and 2000. On 54 of these days, observations were made near the eastern or western end of Lake Vida, on 16 days near Lake Vashka, on 13 days near the head of Balham Valley, and on 6 days in Bull Pass. Observations were made irregularly in other places.

The observations may be summarized as follows:

1. Near Lake Vida at 2000 the wind nearly always blew from the east; calms or light variable winds were recorded on 5 days, a northerly wind on 1 day, and a southwesterly wind on 1 day. The mean wind speed for the easterlies was 10 kt. At 0800 easterly winds with a mean speed of 7 kt were observed on 39 days, calms on 12 days, westerly winds on 2 days, and a northerly wind once. On the one day (February 5, 1962) when westerly or southwesterly winds blew all day, they reached a velocity, in gusts, of 35 kt. At the same time very strong westerlies, exceeding 50 kt, were experienced in the western part of McKelvey Valley. This is the only recorded occasion on which the westerly wind extended to the eastern end of the valley system.

TABLE 12. Mean Wind Speed (in knots) at Lake Vashka, Summer 1959–1960

Month	Direction		
	Easterly	Northerly	Southerly
December 1959	(61) 5.1	(16) 5.4	(28) 8.4
January 1960	(65) 5.4	(29) 6.0	(24) 12.6

At Lake Vida the first half of January was noticeably windier than the remainder of the summer.

2. At Lake Vashka, near Balham's site, at 0800 easterly winds averaging 4 kt were recorded on 14 days, a calm once (i.e. less than about 2 kt), and a light westerly wind once. At 2100, easterly winds averaging 5 kt were recorded on 11 days, a calm once, and westerlies on 2 days.

3. At the head of Balham Valley, over a 12-day period in December 1961, all the observations at 0900 and 2100 record light to moderate westerly winds (4 to 15 kt), with the exception of 1 day of calm.

4. Near the snout of the Victoria Upper Glacier the predominant wind (for a total of about 20 days) was northerly, off the glacier.

Taylor Valley

The observations taken by several parties in various parts of the valley in the summer months can be summarized as follows:

1. In the western part of the ice-free valley, between Nussbaum Riegel and the snout of the Taylor Glacier, between midnight and 0700, the wind is usually a light easterly. Between 0700 and 1800 easterlies and westerlies occur with about equal frequency. Between 1800 and midnight westerly winds are dominant.

2. At the eastern end of Taylor Valley winds are dominantly easterly. On only one day (December 8, 1959) was a westerly wind reported. On this occasion the temperature rose rapidly from about 0° to 7°C immediately before the onset of a westerly wind which exceeded 40 kt and was sufficiently strong to lift stones of 1-cm diameter to a height of 2 meters.

It thus appears that the wind pattern in the Taylor Valley is similar to that in the Wright Valley, discussed above.

TABLE 13. Summer Cloud Cover, Expressed as a Percentage, for the Ice-Free Area and for Hut Point Peninsula
Note that these values are based on estimates of cloud cover given only in 1/8's or 1/10's.

Period	Year	Place	Total Cloud	Low Cloud
Oct. and Nov.	1961	Victoria Valley	44	18
Oct. and Nov.	1961	Hut Point	59	
Dec.	1961	Victoria Valley	63	44
Dec.	1961	Hut Point	72	
Dec.	1959	Victoria Valley	38	20
Dec.	1959	Hut Point	85	
Dec.	1958	Wright Valley	67	33
Dec.	1958	Marble Point	60	30
Dec.	1958	Scott Base	62	
Jan.	1962	Victoria Valley	40	22
Jan.	1962	Hut Point	76	
Jan.	1960	Victoria Valley	38	18
Jan.	1960	Hut Point	43	
Jan.	1959	Wright Valley	46	17
Jan.	1959	Marble Point	56	15
Jan.	1959	Hut Point	58	
Feb. (part)	1962	Victoria Valley	28	16
Feb.	1962	Hut Point	74	

6. CLOUDS

The average cloud cover, in per cent, for various periods is given in Table 13. For some of the observations it has been possible to give separately the amount of low cloud, which is considered here as cloud of less than 2000-meter altitude.

With the exception of December 1958, the ice-free area has been consistently less cloudy than the coastal parts of McMurdo Sound.

Most of the low cloud was stratus, usually producing a complete cover. A complete cover of low stratus persisted for more than 12 hours on four occasions at Lake Vanda in December 1958 and January 1959. On each occasion the clouds moved from the east, and easterly winds were experienced at the surface. On three of these occasions a complete low cloud cover was recorded at Marble Point, together with southeasterly surface winds. On the other occasion the low cloud was confined to the Wright Valley area; Marble Point experienced only medium and high clouds.

At Lake Vashka, 1959–1960, the low cloud was less clearly related to wind direction. Persistent and complete stratus cover occurred on 4 days in December and 5 days in January. Usually surface winds were light but variable in direction between northeast and south. On 1 day the low stratus was accompanied by moderate northeasterly winds, and on another by strong southerly winds. Similarly, the direction of movement of the low cloud was variable, between east and south.

High cloud over the Victoria and Wright valleys usually came from the southwest or south.

7. PRECIPITATION

The number of days on which falling snow was reported is given in Table 14.

The annual accumulation of snow near Scott Base averages 17.6 g cm^{-2} [*Stuart and Bull*, 1963]. The annual accumulation is less on the inland ice plateau west of the Skelton Glacier (70 km southwest of Lake Vanda), being about 10 g cm^{-2} according to *Lister* [1960] and about 3 g cm^{-2} according to *Giovinetto* [1963].

In the ice-free areas most of the snow comes from the east and is associated with low and middle level clouds. At the coastward ends of the Asgard, Olympus, and St. John ranges the cirques are occupied by small glaciers. At the inland ends of the ranges nearly all the cirques are empty.

Snowfall on the valley floors is also greater to the east. In mid-October 1961, snow 8–10 cm deep covered half the eastern end of Victoria Valley, while Barwick, Balham, and McKelvey valleys were much clearer. Photographs in other years indicate that the snowfall in the winter of 1961 was unusually heavy. Nearly all the snow on the valley floor had disappeared (mainly by sublimation) before mid-November 1961, and all the area at elevation less than 1300 meters was snow-free by mid-December. In 1957, 1958, and 1959 all the area at elevation less than 1500 meters was clear of snow by early December.

8. RADIATION

Direct measurements of radiation balance for the summer months of 1962–1963 have been made in the Wright Valley by R. A. Ragotzkie and G. E. Likens but had not been published at the time of writing. However, detailed investigations have been made by *Thompson and MacDonald* [1962] at Scott Base, 77°51′S, 166°46′E. Their findings can be used to estimate the radiation balance in the ice-free areas as follows:

TABLE 14. Days and Total Amount of Snow Fall in the Ice-Free Area and at Hut Point

Period	Year	Place	Days	Amount Snow (water equivalent)
Oct. 22–Nov. 30	1961	Victoria Valley	2	0.8 cm at 1000-m altitude
Nov.	1961	Hut Point		0.3 cm
Dec.	1961	Victoria Valley	6	1.4 cm
Dec.	1961	Hut Point		1.1 cm
Dec.	1959	Victoria Valley	8	1.0 cm
Dec.	1959	Hut Point		2.5 (?) cm
Dec. 10–31	1958	Wright Valley	5	1.3 cm at 1200-m altitude
Dec. 10–31	1958	Marble Point	7	4.0 (?) cm
Jan.	1962	Victoria Valley	6	0.6 cm at 600-m altitude
Jan.	1962	Hut Point		1.5 cm
Jan.	1960	Victoria Valley	7	
Jan.	1959	Wright Valley	3	0.3 cm
Jan.	1959	Marble Point	0	

1. *Incoming short-wave radiation.* Since the latitude and elevation of Scott Base differ very little from those of the bottoms of the ice-free valleys, differences in incoming short-wave radiation are due principally to differences in cloud cover and in the obstruction of insolation by mountains. Direct comparison of cloud cover for December 1958 and January 1959 is given in Table 13. For other months of the summer 1958–1959 the direct comparisons are not available, but from the comparable observations in 1961–1962 it may be concluded that the mean cloudiness in the ice-free areas for the summer 1958–1959 was about 10% less than at Scott Base. Using Thompson and MacDonald's empirical curves for the variation of short-wave radiation with cloudiness and their direct measurements of this radiation, it is estimated that the total incoming short-wave radiation at Lake Vanda for the year February 1958–January 1959 is about 94,000 cal cm^{-2}.

2. *Reflected short-wave radiation.* The observing site at Scott Base was almost completely snow-covered until about December 20, 1958. The snow cover decreased to zero about January 15, 1959, and remained low until mid-February. Thereafter it increased to 50% at the end of the month.

The mean albedos at Scott Base for November, December, January 1–15, and January 16–31 were 71, 67, 32, and 14%, respectively. The surface rock at Scott Base is very dark volcanic debris, whereas most of the surface in Wright Valley is lighter colored granitic material. On similar terrain at Oazis (66°16′S, 100°45′E), measured values of the albedo in January, February, March, and April were 15, 18, 24, and 27%, respectively [*Soviet Antarctic Expedition,* 1962]. The albedo of the surface rocks in Wright Valley is assumed to be 20%.

The valley floors remain almost snow-free for the entire summer. In mid-October 1961, after the snowiest winter of recent years, only 30% of the floor area of the Victoria Valley system was snow-covered. In November 1961 the snow cover for the land below 1000 meters was less than 20%. For 1958–1959 the snow cover was less, but in the absence of quantitative estimates the mean albedos for October, November, and the rest of the summer are taken as 40, 35, and 20%, respectively. On the basis of the monthly incoming short-wave radiation figures, given by Thompson and MacDonald and modified for the estimated cloud amounts, the net absorbed short-wave radiation for the year is estimated as 65,500 cal cm^{-2}.

3. *Long wave radiation balance.* The net loss of radiative energy from the surface depends mainly on the ground temperature, the water vapor distribution above the surface, the cloud amount, and the temperature of the cloud base. Thompson and MacDonald established empirical relations between the outgoing radiation and the cloud amount and between the outgoing radiation and the mean of the screen temperature and the maximum tropospheric temperature.

In the absence of any measurements it is assumed that the winter cloud cover in the ice-free area is the same as at Scott Base. Average winter air temperatures are probably about 5°C lower than at Scott Base; summer temperatures are about 4°C higher. Applying these changes to the net long-wave radiation balance at Scott Base, calculated from Thompson and MacDonald's figures and tables, the yearly loss is estimated at about 36,000 cal cm^{-2}.[1]

4. *Radiation balance.* The annual net balance of radiation from these calculations is a gain of about 29,000 cal cm^{-2} per year; at Scott Base the gain is about 18,000 cal cm^{-2} per year. Oazis station is situated in similar ice-free terrain but is 11 degrees of latitude farther north. Here the annual balance is a gain, quoted as 26,700 cal cm^{-2} [*Soviet Antarctic Expedition,* 1962] and as 37,600 cal cm^{-2} [*Rusin,* 1961].

All stations in permanently snow-covered areas of Antarctica record a net heat loss by radiation, typical figures being 8800 cal cm^{-2} per year at Maudheim (71°03′S, 10°56′W) [*Liljequist,* 1956], 7400 cal cm^{-2} at Pionerskaya (69°44′S, 95°30′E) [*Rusin,* 1961], 6800 cal cm^{-2} per year at Little America V (78°33′S, 164°00′W) [*Hoinkes,* 1961] and 13,000 cal cm^{-2} per year at South Pole station [*Hanson and Rubin,* 1962].

9. OTHER EVIDENCE OF CLIMATE

Ventifacts. The deposits left by earlier glaciers cover most of the floors of the Taylor, Wright, and Victoria valley systems. Ventifacts are common throughout the area; the best developed ones are formed of very fine-grained dolerite and very fine-grained orthoquartzite. The ventifacts range in size from 1 cm to boulders 4 meters across. The small ones are common on the older surfaces; the large ones are most common on the youngest surfaces.

An extensive examination of wind-cut stones in the Victoria Valley system has been made by G. Haselton and P. Calkin [*Calkin,* 1963] and less thorough studies in the Wright and Taylor valleys have been made by the author and J. D. McCraw (unpublished studies).

The important conclusions from these studies are as follows: (1) throughout the Victoria Valley system, including the area around Lake Vida, the cutting action of winds from the southwest is greater than that from the east; (2) in the Wright Valley ventifacts cut by westerly winds are found as far east as the entrance to the valley of the Clark Glacier; (3) in the Taylor Valley ventifacts cut by westerly winds occur throughout the length of the valley; (4) these ventifacts, cut by westerly winds, are being formed today.

Because westerly winds are rarely observed at the eastern ends of these valleys during the summer, it follows that they must be a winter phenomenon. The abrasion of rocks is caused mainly by wind-blown sand, but wind-blown ice also is effective; wind-polished boulders occur on the outcrops immediately east of the inland ice plateau.

Pebble ridges. Ridges of pebbles are common on the sandy parts of the floors of the Victoria Valley system, the Wright Valley, and elsewhere in the ice-free areas of south Victoria Land. The best-developed ones occur in Barwick Valley, in Wright Valley (east of Bull Pass), and in the Salmon and Marshall valleys, north of the Koettlitz Glacier.

The ridges are dominantly transverse to the wind but slightly concave toward the strongest wind direction. The coarsest material is found on the crests. Dolerite pebbles with dimensions of $6 \times 4 \times 3$ cm are common on the crest of the ridges in Barwick Valley; in the other places cited the maximum size is less. For the Barwick Valley ridges, *Calkin* [1963], following *Bagnold* [1942], has calculated that the required wind velocity to produce these ridges, with the $6 \times 4 \times 3$ cm pebbles at their crests, is about 24 knots at 1 cm above surface level or 111 knots at 3 meters above the surface.

In Wright Valley the required wind velocity is less, but it still greatly exceeds the highest wind velocities measured in the summer.

Calkin considers the ridges with the biggest pebbles to be stable because the undersides of the pebbles are salt encrusted. However, the ridges with slightly smaller pebbles are not stable and are forming at present. The following conclusions are made: (1) stronger westerly winds blew in the recent past than they do now, and (2) westerly

[1] One reviewer has pointed out that the yearly loss could be increased to 41,000 cal cm^{-2}, if the rock surface in summer averages 5°C higher than air temperature. By varying the other assumptions I have made (on albedo and incoming short-wave radiation), he obtains an annual balance as a gain of about 6000 cal cm^{-1}. This seems to be at the lower limit of 'reasonable values,' and 29,000 cal cm^{-2} per year is at the upper limit.

winds in the winter in the Barwick and Wright valleys are much stronger than those in the summer.

Sand dunes. A belt of sand dunes covers about 4 km^2 of the north side of the lower Victoria Valley east of Lake Vida. The ridges and barchans are up to 15 meters high. Smaller areas of sand dunes occur in Bull Pass and in the Taylor Valley.

The dunes in Victoria Valley are formed by easterly winds. During one month of the summer, when the surface layers of the dune were thawed, the slip faces advanced westward with an average velocity of about 5 cm per day [*Calkin*, 1963].

A 1.5-meter section of a dune south of the snout of the Packard Glacier shows parallel and interbedded layers of sand (up to 35 cm thick) and snow (up to 7–8 cm thick) dipping 24°E (G. Gibson and A. Allen, Victoria University of Wellington, New Zealand, unpublished studies). Snowfall in December and January is usually accompanied by calm conditions, and the snow seldom remains on the valley floor for more than a few hours. Hence it is concluded that the interbedded snow and sand is formed at other times of the year, and, because the source of sand lies to the east, the interlayering must be produced by easterly winds.

Some of the dunes, formed by easterly winds, are in areas where ventifacts display abrasion facets produced by westerly winds. *Calkin* [1963] has argued that most of the strong westerly winds occur when the dunes are frozen.

Temperatures. On January 23, 1962, Calkin measured the temperature in deep cracks at an elevation of 825 meters on the Packard Glacier. At 6-meter depth the temperature was —22.0°C, and at the bottom of a 7-meter crack it was —24.5°C.

Neglecting the effects of percolating meltwater and convection in the air column, the temperature at a depth of 7 meters in glacial ice in late January should be about 2°C lower than the mean annual temperature at that depth [*Cameron and Bull*, 1962]. Percolation of meltwater and air convection may raise both the instantaneous and the mean annual temperature at that depth but cannot lower them. Because the mean annual temperature of the ice at depths of 4–16 meters is otherwise very nearly the same as the mean air temperature, it is concluded that the maximum value for the mean annual air temperature here is —22.5°C.

Allowing only for the adiabatic temperature gradient, the corresponding mean annual temperature at Lake Vashka (elevation 507 meters), 300 meters lower, should be about —20°C. This compares with a mean annual air temperature of —18°C at McMurdo station, for the five years following 1957 [*U. S. Navy Weather Research Facility*, 1961].

Snow accumulation and ablation on glaciers. The annual snow accumulation on two glaciers has been determined from an examination of texture, hardness, and density of snow strata as revealed in pits. The results are as follows.

On the Wilson Piedmont Glacier, at a site about 2 km from the McMurdo Sound coast and at an elevation of 350 meters, the mean annual accumulation for the three years 1956–1959, was about 8 g cm^{-2}.

At a site on the Wright Lower Glacier, at an elevation of 450 meters, about 10 km west of the previous one, the mean annual accumulation for the same years was probably about 6 g cm^{-2}. This site is west of the highest part of the piedmont glacier system.

Calkin [1963] dug eight pits on the Packard Glacier, four at an elevation of 1040 meters, and four near 800 meters. Two pits at each location were dug early in the summer and the other two at the end of January. The net accumulation for the year February 1960–January 1961 varied between 5 and 7 g cm^{-2}. Probably the firn limit on this glacier is normally at about 1000 meters on the west side and 900 meters on the east side, but for the summer of 1961–1962 the east side remained snow-covered almost to the snout, which is at an elevation of 600 meters. In December 1957 the lowest 3 km of the glacier was clear of snow. In Calkin's pits hard and dirty ice was reached at depths varying from 46 to 106 cm, indicating that the last few years had been unusually snowy.

Between early November 1961 and the end of January 1962, stakes at elevations above 1000 meters in the névé basin of the Packard Glacier showed a snow accumulation varying from 0.1 to 1.1 g cm^{-2}. Below 1000 meters the surface generally lowered in this period by amounts varying from 1 to 7 cm. In addition, in three of the four pairs of pits the mean density of the top 30 cm of snow decreased by about 10% over the two and one-half months. This decrease suggests that most of the ablation is by subli-

mation. Similarly, the sections in the pits showed many sublimation layers, and very little water was seen on the surface of the glacier except very close to the snout.

These values of snow accumulation are not representative of the valley bottoms, because Packard Glacier is sheltered from the strongest winds. The average depth of snow on the ice of Lake Vida was about 10 cm in early October, and this value probably does represent the winter's accumulation. Some of this snow remained until late November.

For the same two and one-half month period in summer 1961–1962, ablation at stakes on the tongue of the Victoria Lower Glacier (500-meter elevation) varied between 0.3 and 2.0 g cm^{-2}.

The annual accumulation of snow on the glaciers in the western part of the ice-free area is much less than in the eastern part. In early December 1958 and in October 1961 the Webb Glacier was almost completely free of snow up to an elevation of 770 meters. The ablation is also higher on this glacier than on the ones farther east and amounts to 5.8 g cm^{-2} (of ice) for the two and one-half month period in summer 1961–1962 [*Calkin*, 1963].

The low accumulation in the west is due to less precipitation than in the east and greater loss by deflation by strong westerly winds. The increased ablation in the west is mainly due to sublimation produced by the warm, dry, katabatic winds. As described above, during the summer these winds are confined largely to the western part of the ice-free area.

Lake levels. Lake Vanda in Wright Valley and Lake Vida in Victoria Valley are fed in the summer by meltwater from surrounding glaciers and snow banks. Neither lake has an outlet. The quantity of meltwater varies greatly from year to year. In the summers of 1957–1958 and 1958–1959, substantial streams from the Victoria Upper and Lower glaciers flowed into Lake Vida; in 1961–1962 the only meltwater that reached the lake came from local snow banks.

During the period late October 1961 to early February 1962, the level of Lake Vida dropped by at least 50 cm. A small part of this drop represents a change in volume caused by the melting of ice around the edge of the lake, but most of it represents the loss by evaporation and sublimation.

Very nearly all the inflow of Lake Vanda is the Onyx River, most of which is meltwater from the Wright Lower Glacier. Flow in this stream is greater than in streams in the Victoria Valley, largely because the Wright Lower Glacier is lower than the Victoria Upper and Lower glaciers. On January 19, 1962, the Onyx River, south of Bull Pass, was flowing at 1 meter sec^{-1} in a stream 25 meters broad and 30 cm deep in the middle, while the stream courses from the Victoria Lower Glacier, 300 meters higher, were dry.

The inflow into Lake Vanda was measured on four days in the summer of 1958–1959; the depth and width of the stream at the same point were measured regularly. Considerable extrapolation is required to calculate the total season's inflow, but the figure obtained for the expected rise in the lake (18 cm) greatly exceeds the observed rise (9.5 cm). The difference is attributable to evaporation and sublimation.

Other lakes without outlets in the valleys also show evidence of rapid loss. Near Lake Vanda one fresh lake that was 1 meter deep and 40 meters across in late January 1959 had disappeared completely by January 1962.

Lake Balham, situated at the head of Balham Valley, remained ice-covered to the edges in the summers of 1958–1959 and 1961–1962, but the level had dropped in this time by 170 cm.

Other phenomena demonstrating aridity.

1. The existence of the undrained lakes indicates that evaporation exceeds precipitation [*Nichols*, 1963]. The ratio of the area of the catchment basin to that of Lake Vanda exceeds 50:1; this may be compared with ratios of 24:1, 36:1, and 29:1 for the Lahontan Basin of Nevada, the Great Salt Lake, and the Dead Sea, respectively [*Nichols*, 1963].

2. Thick subsurface and surface accumulations of soluble salts are common throughout the ice-free area. The evaporation of lakes that occupied depressions in the moraine has produced deposits of salts as much as 10 cm thick. The principal salts found are $CaCO_3$, NaCl, $MgSO_4$, and $CaSO_4$. Some of the deposits are associated with lakes that probably dried up several thousand years ago [*Péwé*, 1960].

The underside of almost every pebble and boulder on the stable moraines is covered with a thin veneer

of salts; the predominant salt is calcite. Many of the ventifacts have a well-developed 'desert varnish.'

3. The excess of evaporation over precipitation results in a gradual increase with time of the depth to icy permafrost in the glacial deposits and an increase in the salt content in the surface layers [*Ugolini*, 1963; *Calkin*, 1963].

10. THE ICE-FREE NATURE OF THE AREA

Simultaneous weather studies are required in the ice-free valleys and in neighboring ice-filled valleys of similar topography to determine directly the effects of the ice-free nature of the area on the various meteorological elements.

It is apparent that the high temperatures and low humidities of the westerly winds are a consequence of the lack of ice in the western parts of the Wright Valley and Victoria Valley system. In valleys that are similar but ice-filled, heat and vapor transfer between the ice and the descending air mass reduces air temperatures and increases specific humidities above those in the ice-free valleys. The surface temperature of glaciers is limited to 0°C, but surface temperatures of the ground in the area have been measured as high as 24°C at Marble Point [*Kelly and Zumberge*, 1961] and 27°C at Hallett station [*Rudolph*, 1963].

These differences are a result of the ice-free nature of the area and are not a direct cause of it. The glacial history of the Wright and Victoria valleys includes early periods when the area was inundated with ice flowing from the inland ice plateau followed by periods when much of the valley floor area was occupied by glaciers flowing from the east [*Nichols*, 1961; *Bull et al.*, 1962; *Bull*, 1962; *Calkin*, 1963]. A similar history is shown in neighboring ice-free areas north of the Mackay Glacier [*Calkin*, 1963] and north of the Koettlitz Glacier [*Péwé*, 1960; *Blank et al.*, 1963].

In other parts of the Transantarctic Mountains the outlet glaciers from the inland ice plateau are still very active. The differential starvation of the glaciers from the plateau into the Wright and Victoria valleys was due to the existence of high rock thresholds at the heads of these valleys [*Bull et al.*, 1962]. The thresholds are lower in the valleys of the Taylor and Mackay glaciers and may be completely absent in other valleys. With a reduction of the height of the inland ice, the flow of ice into the Wright and Victoria valleys was completely disrupted, but the flow into valleys with lower thresholds was reduced only a small amount.

The most extensive westward-flowing glaciers probably originated in the McMurdo Sound area. With a decrease in worldwide sea level (perhaps coinciding with a maximum of glaciation in the northern hemisphere), the Ross Ice Shelf grounded, so that subsequently its surface attained an approximately parabolic profile [*Hollin*, 1962]. The elevation of the surface east of the Wright and Victoria valleys may have been 1500 meters, high enough for the ice to override the threshold (400 meters high) at the eastern end of the Wright Valley [*Bull*, 1960].

The end of the most active phase of this glaciation was probably produced by the melting of the Wisconsin ice sheets of the northern hemisphere, the consequent increase in sea level, and the disappearance of the grounded ice sheet in the McMurdo Sound area. *Hollin* [1962] has suggested that the Wilson Piedmont Glacier is a relic of this grounded ice sheet.

At its maximum, the west-flowing glacier in Wright Valley extended west of Bull Pass where it was 300 meters thick [*Calkin*, 1963]. In the Victoria Valley it was thinner. In neither valley did the glaciers cover the ranges north and south of the valleys, although the cirque glaciers and névé fields were more extensive than at present [*Calkin*, 1963].

There are many interrelated reasons why the ice has disappeared from the valley floors while it has remained on the Wilson Piedmont Glacier. The snowfall is greater in the coastal area of the Piedmont Glacier than it is farther inland. The inland region containing the valleys has at all times contained extensive upland areas that would remain snow-free under the influence of strong winds. In these areas the radiation balance remained positive, so that the extent of the glaciers gradually decreased. The area of the Wilson Piedmont Glacier contains only a limited number of small nunataks. In the immediate area of the nunataks the ablation is high, but elsewhere the radiation balance is negative, and the amount of summer melting is small.

Acknowledgments. I am grateful to the many individuals mentioned in the text for permission to use their unpublished meteorological records and to the U. S. Weather Bureau for microfilm copies of the daily records from Marble Point and McMurdo station. Miss Vanessa Wical read the microfilms; Miss Mary Meadowcroft helped

considerably with the analysis of the records. I wish to thank R. W. Balham, P. Calkin, F. Loewe and M. Rubin for their useful criticisms of the manuscript.

The work was supported by National Science Foundation grant G-20473 (Ohio State University Research Foundation project 1396).

Note added (June 1965). In the last two years additional climatological data have been obtained by several parties working in these ice-free areas, notably in the Taylor Valley by R. F. Black and T. E. Berg, Department of Geology, University of Wisconsin. Direct measurements of radiation in the Wright Valley have been made by R. A Ragotzkie, Department of Meteorology, University of Wisconsin and by G. E. Likens, Department of Biological Sciences, Dartmouth College. However, as far as the author knows, none of this material has yet been published.

Further work has been carried out on the chemical and physical properties of the lakes [e.g., *Shirtcliffe,* 1964; and *Wilson,* 1964], and other considerations have been made of the climatic changes since the area became ice-free [e.g., *Ugolini and Bull,* 1965].

REFERENCES

Angino, E. E., and K. B. Armitage, A geochemical study of Lakes Bonney and Vanda, Victoria Land, Antarctica, *J. Geol., 71,* 89–95, 1963.

Bagnold, R. A., *The Physics of Blown Sand and Desert Dunes,* New York, William Morrow, 1942.

Blank, H. R., R. A. Cooper, R. H. Wheeler, and I. A. G. Willis, Geology of the Koettlitz-Blue Glacier region, southern Victoria Land, Antarctica, *Trans. Roy. Soc. New Zealand, 2,* 79–100, 1963.

Bull, C., Gravity observations in the Wright Valley area, Victoria Land, Antarctica, *New Zealand J. Geol. Geophys., 3,* 543–552, 1960.

Bull, C., Quaternary glaciations in southern Victoria Land, Antarctica, *J. Glaciol., 4,* 240–241, 1962.

Bull, C., B C. McKelvey, and P. N Webb, Quaternary glaciations in southern Victoria Land, Antarctica, *J. Glaciol., 4,* 63–78, 1962.

Calkin, P. E., Geomorphology and glacial geology of the Victoria Valley system, southern Victoria Land, Antarctica, Ph.D. dissertation, Geology Department, Ohio State University, 1963.

Cameron, R. L., and C. B. Bull, The thermal properties of Wilkes glacial ice, in *Antarctic Research, Geophysical Monograph 7,* pp. 178–184, American Geophysical Union, Washington, D. C., 1962

Giovinetto, M., Glaciological studies on the McMurdo-South Pole traverse, 1960–1961, *Inst. Polar Studies Rept. 7,* 1963.

Hanson, K. J., and M. J. Rubin, Heat exchange at the snow-air interface at the south pole, *J. Geophys. Res., 67,* 3415–3424, 1962.

Hoinkes, H. C., Studies in glacial meteorology at Little America V, Antarctica, *Symposium on Antarctic Glaciology, IASH Publ. 55,* pp. 29–48, 1961.

Hollin, J. T., On the glacial history of Antarctica, *J. Glaciol., 4,* 173–195, 1962.

Kelly, W. C, and J. H. Zumberge, Weathering of a quartz diorite at Marble Point, McMurdo Sound, Antarctica, *J. Geol., 69,* 433–446, 1961.

Liljequist, G. H., Long-wave radiation and radiation balance: *Norwegian-British-Swedish Antarctic Expedition, 1949–1952, Scientific Results,* vol. 2, part 1B, 1956.

Lister, H., Glaciology, 1, Solid precipitation and drift snow, *Trans-Antarctic Expedition 1955–1958, Scientific Report 5,* London, 1960.

Nichols, R. L., Multiple glaciation in the Wright Valley, McMurdo Sound, Antarctica, *Abstracts of the 10th Pacific Science Congress, Honolulu,* p. 317, 1961.

Nichols, R. L., Geologic features demonstrating aridity of McMurdo Sound area, Antarctica, *Am. J. Sci., 261,* 20–31, 1963.

Péwé, T. L., Multiple glaciation in the McMurdo Sound region, Antarctica—A progress report, *J. Geol., 68,* 498–514, 1960.

Rudolph, E. D., Vegetation of Hallett station area, Victoria Land, Antarctica, *Ecology, 44,* 585–586, 1963.

Rusin, N. P., Solar radiation in Antarctica, in *Results of the Conference Summarizing the International Geophysical Year (1960) and Meteorological Studies of Antarctica (1959),* Moscow, 1961.

Shirtcliffe, T. G. L., Lake Bonney, Antarctica: Cause of the elevated temperatures, *J. Geophys. Res., 69,* 5257–5268, 1964.

Simpson, G. C., *Reports of the British Antarctic Expedition, 1910–1913, Meteorology,* vol. 3, Harrison and Sons, London, 1923.

Soviet Antarctic Expedition, *Works of the Soviet Antarctic Expedition,* vol. 16, *Third Continental Expedition 1957–1959,* Leningrad, 1962.

Stuart, A. W., and C. Bull, Glaciological observations on the Ross Ice Shelf near Scott Base, Antarctica, *J Glaciol., 4,* 399–414, 1963.

Thompson, D. C., and W. J. P. MacDonald, Radiation measurements at Scott Base, *New Zealand J. Geol. Geophys., 5,* 874–909, 1962.

Thyer, N., and K. J. K. Buettner, On valley and mountain winds, *Dept. Atmospheric Sci. Univ. Washington, Final Rept., AF contract 19(604)-7201,* 1962.

U. S Antarctic Research Program, *Status Report 34,* October 1961.

U. S. Department of Commerce, Weather Bureau, Climatological data for Antarctic Stations, July 1957–December 1958, Number 1, Washington, D. C., 1962.

U. S. Navy Weather Research Facility, Climatology of McMurdo Sound, *Rept. NWRF 16-1261-052,* Norfolk, Virginia, 1961.

Ugolini, F., Pedological investigations in the lower Wright Valley, Antarctica, paper presented at the International Conference on Permafrost, Purdue University, November 1963.

Ugolini, F., and C. Bull, Soil development and glacial events in Antarctica, in *Quaternaria VII,* pp. 251–269, 1965.

Wilson, A T., Evidence from chemical diffusion of a climatic change in the McMurdo dry valleys 1200 years ago, *Nature, 201,* 147–149, 1964.

Wilson, A. T., and H. W. Wellman, Lake Vanda: An antarctic lake, *Nature, 196,* 1171, 1962.

A PHYSICAL CLIMATOLOGY OF THE ANTARCTIC PLATEAU

PAUL C. DALRYMPLE

Quartermaster Research and Engineering Center, Natick, Massachusetts

Abstract. This study presents a regional climatic classification for the interior of Antarctica and discusses the microclimatology of this region. Based on data from nine scientific stations (Byrd, South Pole, South Ice, Sovietskaya, Vostok, Komsomolskaya, Vostok I, Pionerskaya, and Charcot) between the years 1957 and 1965, a climatic classification is derived for the study area, a physiographic region called the Antarctic Plateau. Four climatic regions are delimited: Cold Central Core, Cold Interior, Cold Katabatic, and Cold Transitional. Differences in climatic extremes are the basis for distinguishing regions. The climatography presents a comprehensive review of climatic data for all stations during the International Geophysical Year and the International Geophysical Cooperation; the eight-year climatic data for Byrd and South Pole are presented in tables and discussed. Interrelationships of climatic elements consider surface inversions, katabatic winds, and windchill. Windchill, a measurement of the cooling power of the atmosphere, is presented as the most important climatic element on the Antarctic Plateau, and windchill data are listed for all stations. The microclimatology presents certain features of the micrometeorological observations of temperature and wind speed measured by the author at South Pole in 1958. Logarithmic wind speed profiles characterize midsummer conditions, and small surface inversions of temperature are featured in most of the eight-month period of 'winter.'

INTRODUCTION

Antarctica (Figure 1), a snow-covered continent of approximately 13,375,000 km², has 90% of the world's snow and ice. It has the highest average elevation of any continent; 55% of its area is over 2000 meters, 43% is over 2500 meters, and 25% is over 3000 meters. (Areal measurements are computed from the 1962 American Geographical Society map of Antarctica, using a compensating polar planimeter.) Its geographical position, its high elevation, and its areal extent make it a true polar continent—one whose climate is unparalleled in the Arctic.

In this report, the conventional terms of West Antarctica and East Antarctica are used to denote major division of Antarctica by the Transantarctic Mountains. West Antarctica is basically an archipelago of islands covered with great amounts of ice and snow. It lies entirely in the western hemisphere. East Antarctica has a considerable amount of its bedrock well above sea level. All but a small portion of it lies in the eastern hemisphere.

Cross sections of Antarctica show that it is essentially a high elevation plateau, which is appreciably higher in East Antarctica than in West Antarctica (Figure 2). Nearly everywhere the surface of Antarctica ascends steeply to a vast interior plateau having gentle slopes. The plateau is a physiographic unit including parts of the Rockefeller Plateau and all of the Horlick-Kenyon and South Polar plateaus, as well as the inland parts of Queen Maud Land and Wilkes Land. The plateaus more or less merge into one another and are therefore considered here as a single plateau called the Antarctic Plateau.

The Antarctic Plateau was delimited on the basis of slope[1] (less than 1 degree) and elevation (above 1500 meters in West Antarctica and above 2000 meters in East Antarctica). The higher elevations and greater coastal slope in East Antarctica necessitated raising the lower boundary in this region. The merging of the two different contours was accomplished by (1) following the 1-degree slope south of the mountainous areas in Queen Maud Land and (2) following the 1-degree slope south of the mountainous arc extending from the Horlick Mountains to Victoria Land.

[1] A 1-degree slope is approximately 17.5 meters per kilometer, which is frequently expressed as 0.0175 or as 2×10^{-2}.

The Antarctic Plateau, 87% as large in area as the United States, is, for the most part, a featureless expanse of snow with relatively little local relief. It is a desert, a cold desert comparable in size to the largest deserted areas of the world, the Sargasso Sea and the Sahara. All maximum temperatures are below freezing, and the annual precipitation, as determined by the net accumulation, is very low.

Estimates based on seismic reflection and seismic refraction shots [*Robin*, 1962] indicate that the average thickness for the whole continent is be-

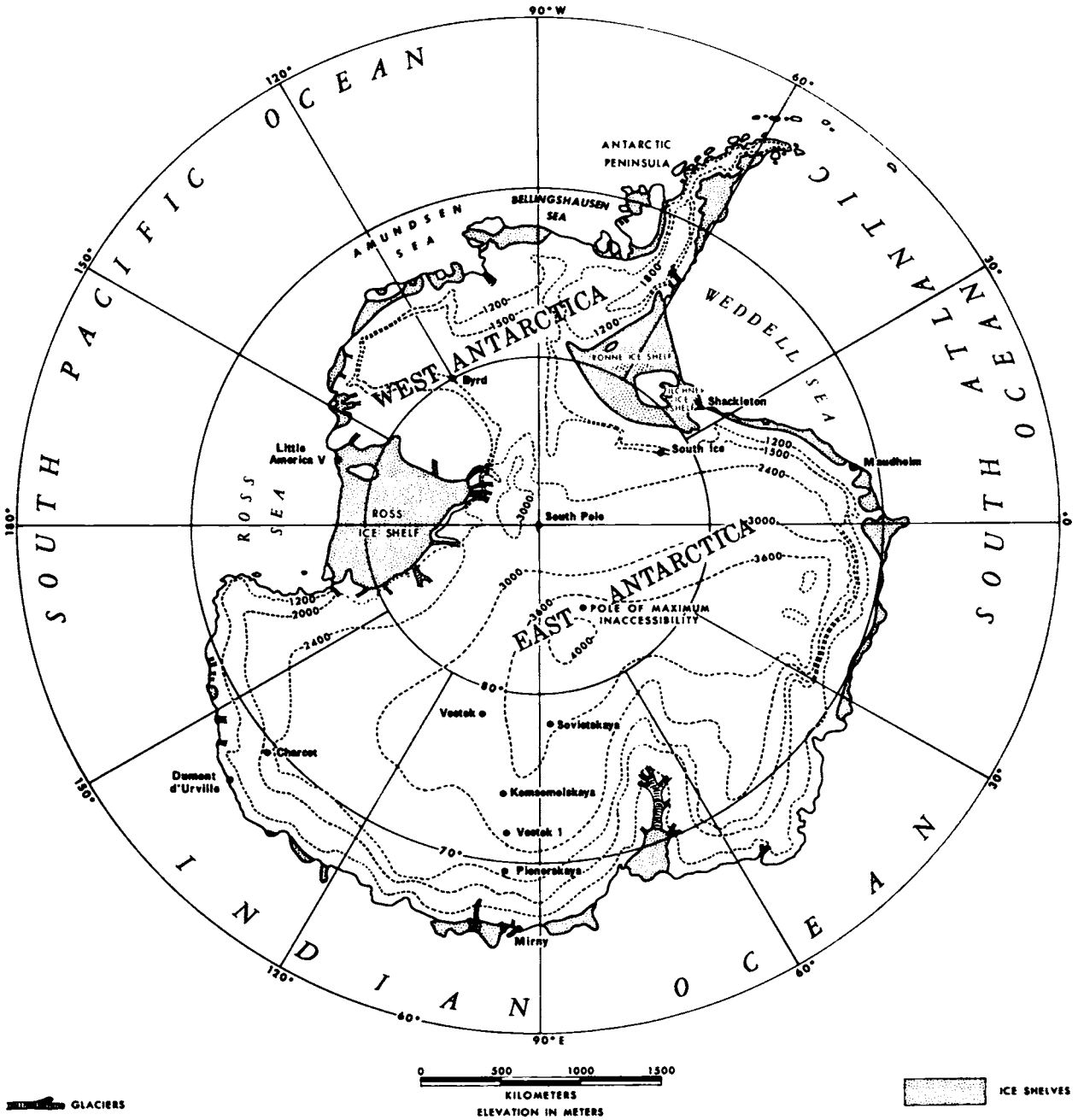

Fig. 1. Antarctica.

tween 2000 and 2500 meters. It is believed that the snow and ice on the Antarctic Plateau may be several hundred meters thicker than the average. The total volume of snow and ice in Antarctica is considerable; *Crary* [1962] estimates 29×10^6 km^3, and *Gow* [1965] estimates 30×10^6 km^3. If we assume that the average depth on the Antarctic Plateau is 2500 meters and that its area is 8.13×10^6 km^2, then 20.32×10^6 km^3 of snow and ice cover the Antarctic Plateau. This amount is comparable to the Laurentide ice sheet, which covered a large part of North America during the Quaternary.

LOCATION OF STATIONS

Nine scientific stations, at one time or another, have been established on the Antarctic Plateau (Table 1). Although the sites for the stations were selected for their over-all desirability for the various geophysical sciences, they were particularly well suited to meteorological purposes. Three stations, Charcot, Pionerskaya, and South Ice, were located in the zone of strong winds associated with katabatic flow off the Antarctic Plateau, and Vostok I was located on the interior margin of the katabatic flow. Vostok, Komsomolskaya, Sovietskaya, and South Pole were all located so that they provided data representative of the Cold Interior. Byrd, in central West Antarctica, was established in an area in West Antarctica subject to frequent cyclonic storms moving between the Ross and Weddell seas. Byrd and South Pole have remained in operation since their establishment and are the only two stations on the Antarctic Plateau with continuous records. Vostok was reopened in 1963 and is still operative. Komsomolskaya is occasionally occupied during the summer months.

GEOGRAPHICAL INFLUENCES

The most important control of climate in the polar regions is the position of the Earth in its elliptical orbit around the Sun. The Earth is approximately 3 million miles closer to the Sun during the antarctic summer than during the antarctic winter. At the geographical south pole, the period during which there is no part of the Sun visible is longer by about three days because of the longer path the Earth takes to aphelion; however, the closer po-

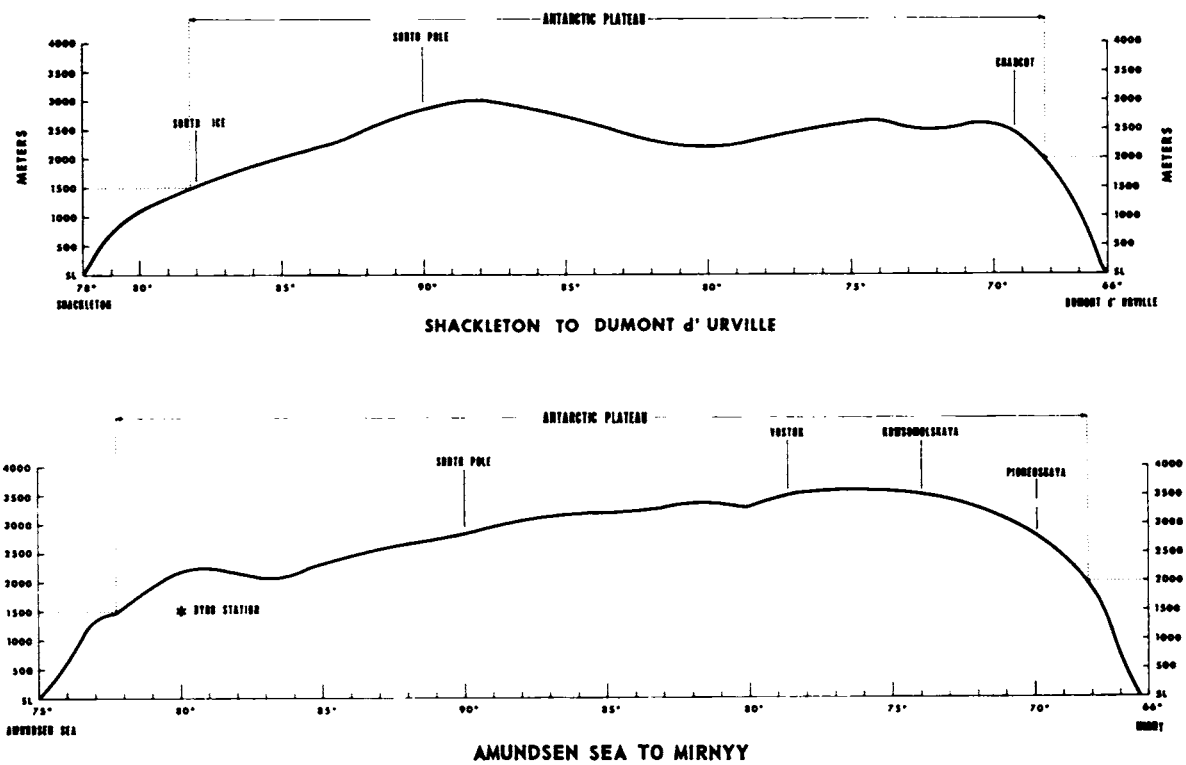

Fig. 2. Cross sections of Antarctica.

TABLE 1. Climatic Stations*

Station	Nation	Latitude, S	Longitude	Elevation, m	Sunset†	Sunrise†	Distance from Coast,‡ km	Depth of Snow,§ m	Period of Record
South Pole	US	90°00′		2800	Mar. 22	Sept. 22	1235	2810	Jan. 9, 1957, to date
Byrd	US	80°00′	120°00′W	1515	April 17	Aug. 26	675	2615	Jan. 9, 1957, to Feb. 18, 1962
		80°01′	119°32′W	1530					Feb. 18, 1962, to date
Vostok	USSR	78°28′	106°48′E	3488	April 24	Aug. 18	1265	3700	Dec. 16, 1957, to Jan. 21, 1962
									Jan. 24, 1963, to date
Pionerskaya	USSR	69°44′	95°31′E	2741	May 29	July 15	350	2050	May 27, 1956, to Jan. 15, 1959
Charcot	France	69°22′	139°01′E	2401	May 26	July 18	295	2890	Feb. 1, 1957, to Dec. 31, 1958
Komsomolskaya	USSR	74°06′	97°30′E	3498	May 7	Aug. 4	830	3320	Nov. 6, 1957, to Jan. 10, 1959
Sovietskaya	USSR	78°24′	87°32′E	3662	April 25	Aug. 19	1050	1830	Feb. 16, 1958, to Jan. 3, 1959
South Ice	UK	81°56′	29°30′W	1500	April 12	Aug. 31	450	540	Feb. 4, 1957, to Jan. 6, 1958
Vostok I	USSR	72°09′	96°37′E	3252	May 15	July 27	575	2900	April 12, 1957, to Nov. 30, 1957

* Data presented in this table were taken from reports published by countries maintaining stations.

† Dates (supplied in part by Harvard Observatory) of last seasonal sunset and first seasonal sunrise are computed for the center of the Sun disk on the horizon. Appropriate allowance is made for refraction, which tends to accelerate sunrise and to retard sunset.

‡ Maximum distance, 1515 km; minimum distance, 65 km.

§ Maximum measured, 4335 m; minimum measured, 320 m.

sition of the Earth to the Sun during the antarctic summer compensates for the longer period without Sun. Table 1 shows the periods without Sun for the stations included in this study.

Station elevations (Table 1) account in large part for the degree of coldness in the interior of Antarctica. The maximum elevation measured on the Antarctic Plateau is 4270 meters, whereas the minimum, in terms of the criterion established for this discussion, is 1500 meters.

The distance from the coast (Table 1) is another climatic factor of importance, as much of interior Antarctica is a region relatively free of cyclonic disturbances that transport heat and moisture from lower latitudes.

The difference in the mean annual temperature between South Pole and Vostok for their two years of comparable data, 1958 and 1959, was 6.6°C. A dry adiabatic lapse rate (1°C per 100 meters) accounts for the temperature difference between the two stations. *Cameron et al.* [1959] showed a 0.9°C lapse rate for each 100 meters on the coastal slopes near Wilkes. *Mellor* [1961] plotted *Bogoslovsky's* [1960] firn temperatures at 15 meters versus station height and versus distance from the coast. He found a lapse rate of approximately 1.27°C per 100 meters at stations between 2000 and 3300 meters; above 3300 meters the lapse rate increased considerably. It is quite evident from Figure 3 that the mean annual temperature, firn temperature at 10 or more meters, elevation, and distance from the coast are closely related.

Slope is both a local and regional climatic control, as winds are related to the direction and degree of slope of the snow surface. Three stations, South Ice, Pionerskaya, and Charcot, have strong katabatic flow, as they lie near the edge of the Antarctic Plateau. Although Komsomolskaya, Sovietskaya, South Pole, and Vostok are interior stations, their prevailing wind is also downslope. Recent analyses by *Lettau* [1963] have shown that the winds at South Pole are of a thermal nature, and this may also prove to be true at other interior sites.

The entire surface of the Antarctic Plateau has a near-uniform snow surface which returns over 80% of the incoming short-wave radiation during the antarctic summer. The difference in the depth of snow is not a significant climatic control because the minimum snow depths are still appreciable (Table 1). The minimum measured snow depth is 320 meters, although there are no doubt sites with less snow. The most extensive area of deep snow lies in the interior core of East Antarctica.

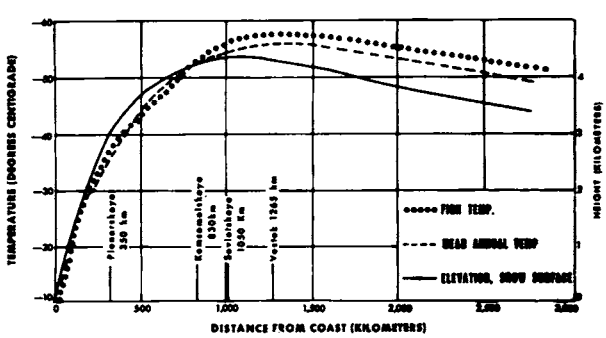

Fig. 3. Temperature correlations.

CLIMATIC REGIONS

Several climatic classifications [*Alt*, 1960; *Bugaev*, 1960; *Dolgushin*, 1961; *Sabbagh*, 1962, 1963] have been applied recently to portions of Antarctica, but none has distinguished between regions on the basis of degrees of severity. This classification presumes that (1) subfreezing temperatures occur throughout the year, (2) the mean annual temperature is below −17.8°C, (3) the net accumulation from all sources is less than 45 cm of water, and (4) the mean annual windchill is greater than 1800 kg cal/m²/hr. The boundary of the Antarctic Plateau circumscribes the core area meeting these criteria.

The climatic classification criteria used in this study are shown in Table 2, and the climatic regions are presented in map form in Figure 4. The greatest emphasis is on the mean annual temperature, maximum and minimum temperatures, and mean annual wind speed. It is rather reassuring, after using several elements to delimit climatic regions, to have one element reunite the area into a whole. This was accomplished through windchill, where higher winds near the periphery compensated for the higher temperature and resulted in windchill values that were comparable to those obtained in the interior.

CLIMATOGRAPHY

Circulation and fronts. The antarctic circulation pattern [*Rastorguev and Alvarez*, 1958; *Alt et al.*, 1959; *Astapenko*, 1960] has four main features in the middle and lower troposphere: two areas of higher pressures (central East Antarctica and eastern Byrd Land) and two areas of lower pressures (Ross and Weddell seas). The most prominent of the four is the anticyclone over East Antarctica. The best guide to the existence and intensity of this anticyclone is its presence on the 500-mb map, as most of East Antarctica is above the 700-mb level. There are two main circulation tracks at the surface, one from Queen Maud Land to Victoria Land to the Antarctic Peninsula, and the other from Byrd Land to Wilkes Land. There are more storms in West Antarctica than there are in East Antarctica, with the main tracks between the two depressions in the Ross and Weddell seas. Multiple cyclonic depressions are often found on the surface map around the periphery of the continent, but most of these storms do not penetrate deeply into interior Antarctica.

Frontal passages in the interior of Antarctica are difficult to recognize and are often detectable only on upper-air charts. Weaker fronts are not able to destroy the semipermanent surface inversion that exists on the Antarctic Plateau during the winter. *Astapenko* [1960] noted that 41 fronts were observed at South Pole during four months in 1958, with 11 each in July, October, and December, and 8 in September. Thirty-four of these fronts were observed at the 400-mb level; six of the seven

TABLE 2. Climatic Classification Criteria for the Antarctic Plateau

	Cold Transitional	Cold Katabatic	Cold Interior	Cold Central Core
Mean annual temperature	−25° to −40°C	−30° to −40°C	−40° to −50°C	<−50°C
Minimum temperature	−50° to −70°C	−55° to −70°C	−70° to −80°C	<−80°C
Maximum temperature	0.0° to −10°C	−5° to −20°C	−10° to −20°C	<−20°C
Mean annual wind speed	7 to 10 m/sec	9 to 12 m/sec	5 to 7 m/sec	3 to 5 m/sec
Drifting snow frequency (%) (wind speed >7 m/sec)	55 to 65	75 to 90	30 to 55	5 to 20
Blowing snow frequency (%) (wind speed >12 m/sec)	10 to 20	25 to 50	0 to 10	less than 2
Mean annual precipitation (cm of water)	10 to 35	0 to 45	0 to 30	0 to 15
Mean annual windchill (kg cal/m²/hr)	1800 to 2200	2000 to 2400	2300 to 2500	2200 to 2600
Maximum monthly windchill (kg cal/m²/hr)	2100 to 2500	2500 to 2800	2500 to 3000	2500 to 3200
Stations	Byrd	South Ice Charcot Pionerskaya	South Pole Vostok I	Komsomolskaya Vostok Sovietskaya

fronts observed below 400 mb occurred in the months of October and December. The average temperature differential across the atmospheric fronts for the four months is shown in Table 3. Temperature differentials across fronts are generally greater in winter than in summer.

Barometric pressure. *Bugaev* [1960] pointed out that there is a general correlation of lower pressures with colder temperatures at the Soviet stations. The high pressures in East Antarctica are occasionally replaced by a cold cloudless cyclone which extends to the stratosphere; e.g., with a low-pres-

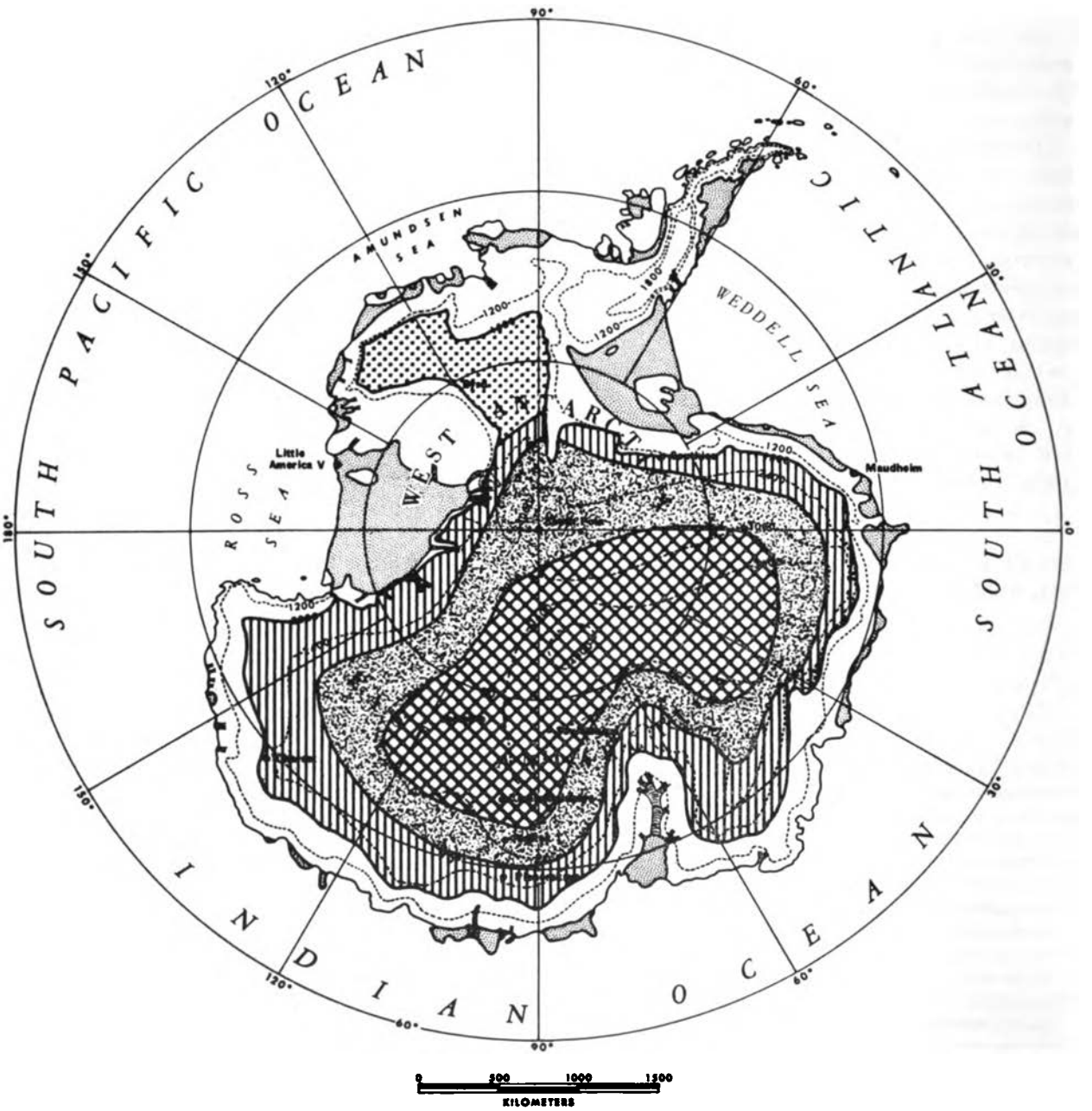

Fig. 4. Climatic regions of Antarctica: dotted area, Cold Transitional; striped area, Cold Katabatic; flecked area, Cold Interior; and hatched area, Cold Central Core.

TABLE 3. Frontal Temperature Differential (in °C), South Pole, 1958

Level, mb	Dec.	Sept. to Oct.	July
300	...	...	2.7
400	2.3	3.0	4.2
500	2.2	2.7	4.5
600	2.7	3.1	2.6

sure cell over East Antarctica from August 21 to 25, 1958, temperatures dropped to —78°C at Sovietskaya and to —80°C at Vostok and Komsomolskaya. IGY microcard data do not reveal any other periods with extreme cold temperatures occurring with low pressures. Monthly minimum temperatures were all measured when an anticyclone predominated over East Antarctica.

Tables 4 and 5 show that the highest monthly mean pressures at South Pole and Byrd tend to occur during the summer months of December and January, with the lowest monthly pressures generally after the winter solstice.

Temperature. Temperature is the most important climatic element in the interior of Antarctica. It is an element which is extremely hard to measure over snow with any precision during the summertime. Absolute temperature measurements in the polar regions in midsummer require both shielding and aspiration of the thermometer, or the use of a sensor that compensates for radiation errors. Radiation errors can be as much as several degrees Celsius close to the snow surface during midsummer. *Portman* [1961] has shown in wind tunnel tests that errors in temperature readings increase as one approaches the surface, as wind speeds decrease, as the wind direction becomes parallel to the sensor, and as the solar intensity increases.

Temperature frequencies were prepared for each month of 1958 for Vostok, Sovietskaya, Komsomoskaya, South Pole, Pionerskaya, Charcot, and Byrd, and for South Ice for 1957 (Figure 5). High frequencies of extreme cold temperatures occur in the Cold Central Core and the Cold Interior. For example, at Vostok 66% of its 3-hourly observations were below —50°C, 48% were below —60°C, 16% were below —70°C, and 2% were below —80°C. These extreme cold temperatures are, for the most part, centered in the coreless winter months of April through September. An examination of this period showed that in 1958 both Vostok and Sovietskaya had 82% of their observations below —60°C and South Pole had 49% below the same value. It will be pointed out later that over a period of years mean monthly temperatures for March through October are lower than the mean annual temperatures for the stations in the Cold Central Core and the Cold Interior. When 1958 temperature observations are examined for this period, it is found that 72% of those for Vostok, 71% of those for Sovietskaya, and 40% of those for South Pole were below —60°C. The value of —60°C may have some significance insofar as human activity and productivity are concerned, as it is approximately at the lower threshold, with light winds, when outside activities can be performed in comfort for extended periods. As these stations normally have light winds, they thus assume some importance.

Monthly mean and annual temperatures for all stations are shown for the years 1957 and 1958 in Table 6. At most stations, both years showed colder months after the solstice. The South Pole tempera-

TABLE 4. South Pole Monthly Values, Based on Data from 1957 to 1965

	Jan.	Feb.	Mar.	April	May	June	July	Aug.	Sept.	Oct.	Nov.	Dec.	Year
Mean station pressure (mb)	687.5	686.0	679.3	680.8	682.3	682.2	676.7	677.9	674.8	675.8	681.9	687.5	681.0
Mean temperature (−°C)	28.9	40.0	54.3	58.6	57.2	56.1	59.5	58.8	59.4	51.2	38.9	27.9	49.3
Maximum temperature (−°C)	14.7	21.4	28.1	31.7	32.3	30.9	34.9	32.5	37.2	29.4	19.0	18.9	14.7
Minimum temperature (−°C)	40.9	56.2	70.6	72.9	73.6	74.4	80.7	77.8	78.6	67.2	54.4	38.9	80.7
Prevailing wind (degrees)	360	360	022	022	022	022	022	022	022	022	022	022	022
Mean wind speed (m/sec)	4.4	5.7	6.5	6.6	7.1	7.7	7.7	7.5	7.4	7.0	5.1	4.2	6.4
Maximum wind speed (m/sec)	22	22	17	18	24	19	19	23	20	19	15	14	24
Mean cloud cover (tenths)	5.3	5.2	4.9	2.8	2.8	3.3	2.9	3.4	4.5	5.3	3.8	4.5	4.1

TABLE 5. Byrd Station Monthly Values, Based on Period 1957–1965

	Jan.	Feb.	Mar.	April	May	June	July	Aug.	Sept.	Oct.	Nov.	Dec.	Year
Mean station pressure (mb)	813.9	812.8	805.9	807.5	806.3	808.0	801.7	801.0	798.2	803.4	805.6	816.2	806.7
Mean temperature (−°C)	15.5	19.8	28.7	29.9	32.1	34.3	35.4	36.7	36.5	30.8	21.3	15.1	28.1
Maximum temperature (−°C)	0.8	3.3	8.9	7.2	6.9	10.6	5.3	13.2	15.6	11.2	4.4	2.7	0.8
Minimum temperature (−°C)	29.6	38.9	53.3	56.7	61.7	59.7	63.2	62.2	62.0	58.3	41.1	29.9	63.2
Prevailing wind (degrees)	360	360	360	022	022	360/022	360	022	22/45	45	360/022	360	360
Mean wind speed (m/sec)	6.1	7.2	8.0	9.1	9.4	9.6	9.9	9.8	10.2	9.2	7.8	6.5	8.5
Maximum wind speed (m/sec)	20	30	27	32	31	39	35	35	33	28	30	26	39
Mean cloud cover (tenths)	6.8	7.5	7.1	6.1	4.6	4.8	5.0	5.3	5.8	7.0	6.6	7.0	6.1

ture regime appears to be independent of the Soviet stations in East Antarctica. In each year, when South Pole was experiencing its coldest month (September in 1957 and April in 1958), the other stations were having near 'normal' temperatures. It appears that there will be small deviations from the mean annual temperatures. In 1957 and 1958 a difference of only 0.2°C existed in the annual mean temperature at South Pole, and Vostok had the same annual mean temperature (—55.4°C) in 1958 and 1959. For its first nine years of record, the mean annual temperature at South Pole was —49.3°C, with the warmest year being 1963 (—48.7°C) and the coldest 1964 (—49.9°C).

The 'kernlose' or coreless winter with temperature reversals was found at South Pole, Vostok I,

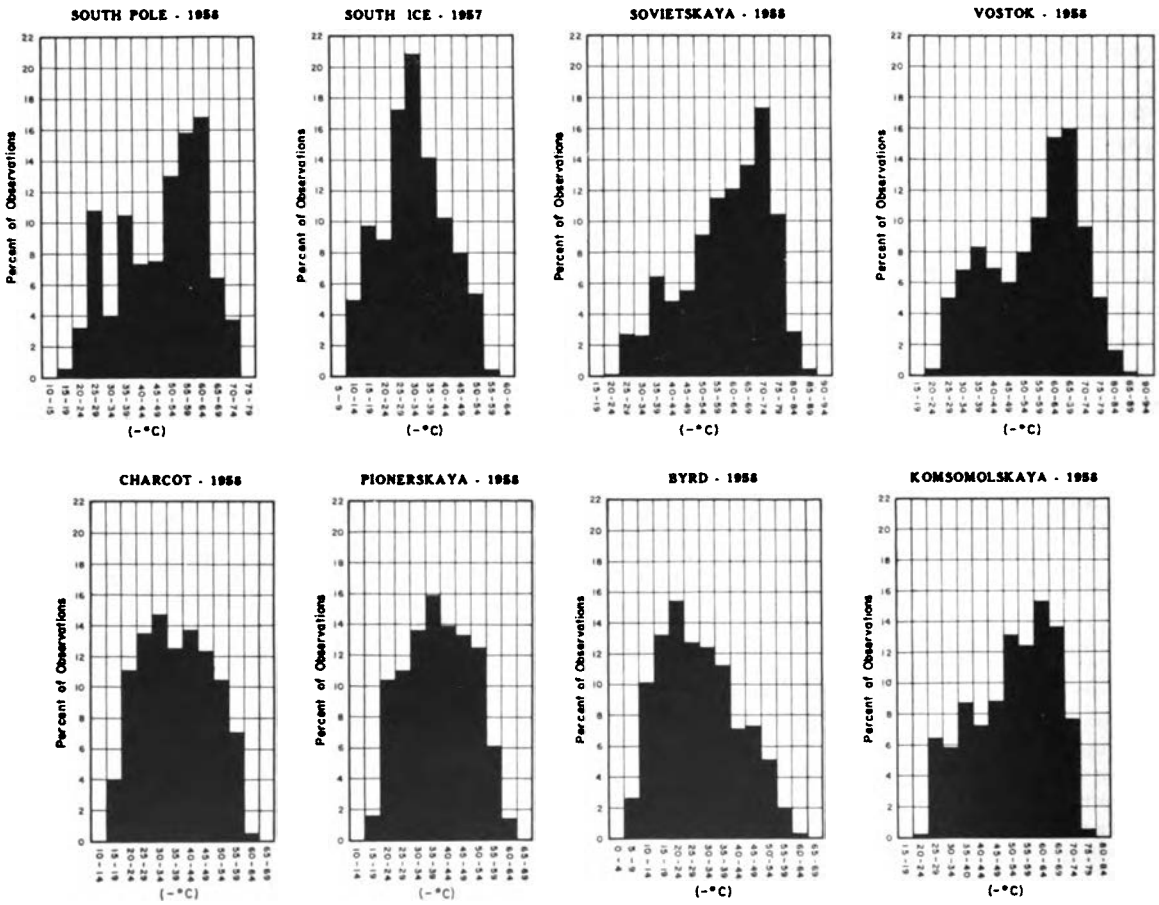

Fig. 5. Annual temperature frequencies at the Antarctic Plateau stations.

TABLE 6. Mean Temperatures (in −°C)

	Jan.	Feb.	Mar.	April	May	June	July	Aug.	Sept.	Oct.	Nov.	Dec.	Annual
1957													
Komsomolskaya											43.0	32.9	
Vostok I				48.0	52.7	51.7	58.0	53.0	48.7	43.3	36.7		
South Pole	27.8*	38.2	53.7	56.4	55.7	56.4	60.9	58.2	62.3	52.7	37.1	25.1	48.7
South Ice		21.3	34.3	29.7	39.1	34.7	41.0	41.1	42.1	29.0	23.2	15.2	
Pionerskaya	22.6	31.3	39.2	38.2	43.8	44.0	48.9	44.4	41.9	36.5	31.0	22.2	36.8
Charcot				40.6	41.5	47.2	48.7	46.4	43.9	37.4	30.3	21.3	
Byrd	15.5	21.2	30.5	35.8	35.8	33.5	40.7	28.8	30.6	26.1	20.6	12.1	27.6
1958													
Vostok	31.3	44.6	55.9	64.0	62.9	67.9	65.3	71.8	66.3	58.8	43.2	33.4	55.4
Sovietskaya		48.1	53.8	58.7	67.3	69.6	69.4	71.9	66.5	59.9	43.7	33.7	
Komsomolskaya	31.6	44.8	51.7	57.1	59.2	64.7	61.9	65.3	61.7	55.4	42.3	33.8	52.5
South Pole	25.0	35.3	54.0	62.1	56.9	61.1	55.1	61.7	56.2	49.2	38.5	31.2	48.9
Pionerskaya	23.8	34.4	36.5	41.2	40.7	50.8	45.4	49.4	48.2	41.7	31.9	25.7	39.1
Charcot	22.4	30.6	34.4	38.5	41.4	49.8	41.7	43.2	51.6	39.7	30.5	23.7	37.3

* January 9–31.

Pionerskaya, South Ice, and Byrd in 1957, and at Vostok, Komsomolskaya, South Pole, Charcot, Pionerskaya, and Byrd in 1958. Figure 6 shows a plot of the average monthly temperatures for Byrd, Charcot, Pionerskaya, South Pole, and Vostok for 1958. The kernlose winter is particularly noticeable at Vostok and South Pole. Each station experienced two temperature reversals during the year. Over a period of years, the temperature reversals occur in different months and tend to cancel one another, resulting in a broad U-shaped temperature curve with a wintertime minimum occurring in July and August. This is evident from Tables 4 and 5 which present the monthly mean temperatures for South Pole and Byrd 1957–1965.

The annual mean temperature is generally warmer than the mean monthly temperature for at least seven months of the year. At South Pole, during eight of the first nine years, the monthly mean temperatures were below the annual mean temperature for the eight-month period March through September. Vostok also had eight months that were colder than its annual mean temperature in two of its first three years of record. The much

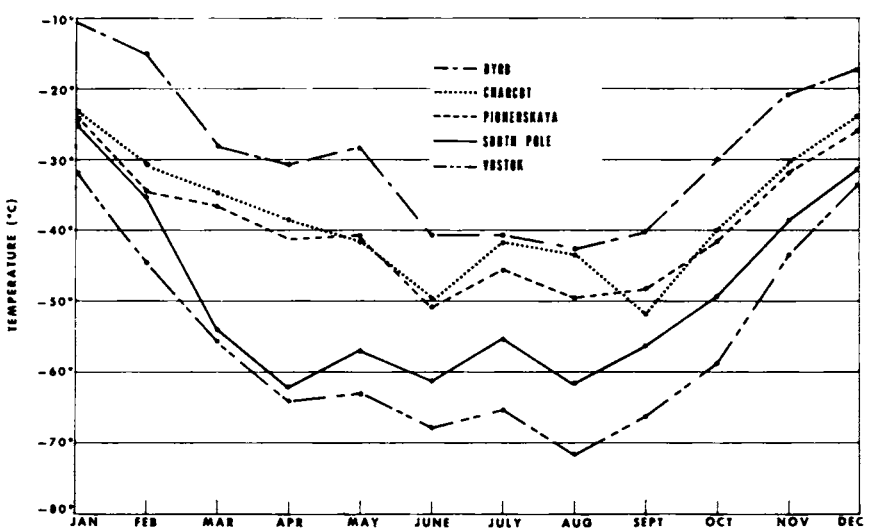

Fig. 6. Average monthly temperature in 1958, showing kernlose pattern and reversals.

longer winter is definitely confined to the Cold Interior and to the Cold Central Core and is a function of continentality rather than latitude. Byrd, the closest permanent station to South Pole, at 80°S, has had from five to eight months that were colder than the mean temperature for individual years.

The coldest month frequently occurs during or following the month when the Sun returns above the horizon. When the Sun returns above the horizon, it is so low in the sky and above the horizon for such short periods that it has little opportunity to destroy the stable conditions established during the long period without Sun. There is a singularity in that one of the season's extreme cold periods precedes the return of the Sun and helps to account for the late winter minimum of mean annual temperature. This was the case during the first three years at South Pole, when the temperature was below —74°C during the week preceding the return of the Sun above the horizon. The third lowest temperature recorded to date for South Pole also occurred during this period. Twelve consecutive days were below —75°C at Vostok in 1958 prior to the date when the Sun returned above the horizon. The annual minimum at Vostok during the three years of record occurred shortly after the Sun returned.

There are no climatic seasons on the Antarctic Plateau such as are experienced in the midlatitudes. Basically there is a period with Sun, a period without Sun, and, except for South Pole, periods with both. Common usage has, however, assigned the period with Sun as summer and the period without Sun as winter. In actuality, the stations in the Cold Central Core and Cold Interior (Vostok, Sovietskaya, Komsomolskaya, and South Pole) have an abbreviated two-month 'summer' in December and January, transitional climates in February and November, and an eight-month winter from March through October. Although it is difficult to imagine a 'summer' month with a monthly mean temperature of —36.2°C, as occurred at Vostok in January 1959, one must realize that the low wind speed, low amount of sky cover, and high solar radiation occurring during this period create a rather pleasant environment.

TABLE 7. Comparison of Firn Temperatures and Mean Annual Temperatures

Station	Firn Temperature, −°C	Air Temperature, −°C	Period of Record, yr
Vostok	57.3	56.4	3
Komsomolskaya	53.9	52.5	2
South Pole	50.9	49.2	7
Pionerskaya	39.4	38.0	2
Byrd	28.3	28.4	7

Firn temperature measurements in the snow and ice at approximately the 10-meter depth have small amplitudes and are a close approximation to the mean annual air temperature for that site (Table 7). At the Antarctic Plateau stations, the firn temperature is generally lower than the air temperature, since it is a function of the snow surface temperature, and a temperature inversion is generally present at plateau stations during most of the year. Over 200 firn measurements were plotted on a map (Figure 7), and isotherms were drawn for the Antarctic Plateau. As one would expect, there is a strong correlation between the isotherms and contour lines. Additional maps of the mean annual temperatures, based on firn measurements, have been drawn by many others, including *Cameron and Goldthwait* [1961] and *Rubin* [1962].

Temperature extremes. Continuously subfreezing temperatures on the Antarctic Plateau have produced a biogeographical desert in the area. The writer believes that the absolute minimum that could be experienced on the Antarctic Plateau would be about —95°C. There is an absolute temperature range for the whole region of approximately 95°C. The large annual temperature ranges on the Antarctic Plateau are comparable with those experienced in midlatitude deserts.

Maximum temperatures on the Antarctic Plateau (Table 8) are usually associated with frontal passages. Although most of the fronts are only detected on upper-air charts, the more intense ones are observed at the surface. Frontal passages occasionally break through a strong anticyclonic circulation and interrupt a cold spell. This happened at all of the Soviet stations in the Cold Central Core in late August 1958. The most pronounced effect was at Sovietskaya, where the temperature rose 31°C in a 6-hour period. The temperature was —85°C prior to the frontal pas-

sage, so that the subsequent warming to —37°C in 30 hours only resulted in a less cold temperature. During the same month, Vostok had a maximum temperature of —55°C. This temperature is the coldest monthly maximum measured on the Antarctic Plateau. Twenty-four hours preceding this monthly maximum, the temperature was 17°C colder (—72°C).

Although South Pole is 1235 kilometers from the nearest coast, advection of warm air associated with a midsummer blizzard in January 1958 raised the temperature to —14.7°C. This occasion is the

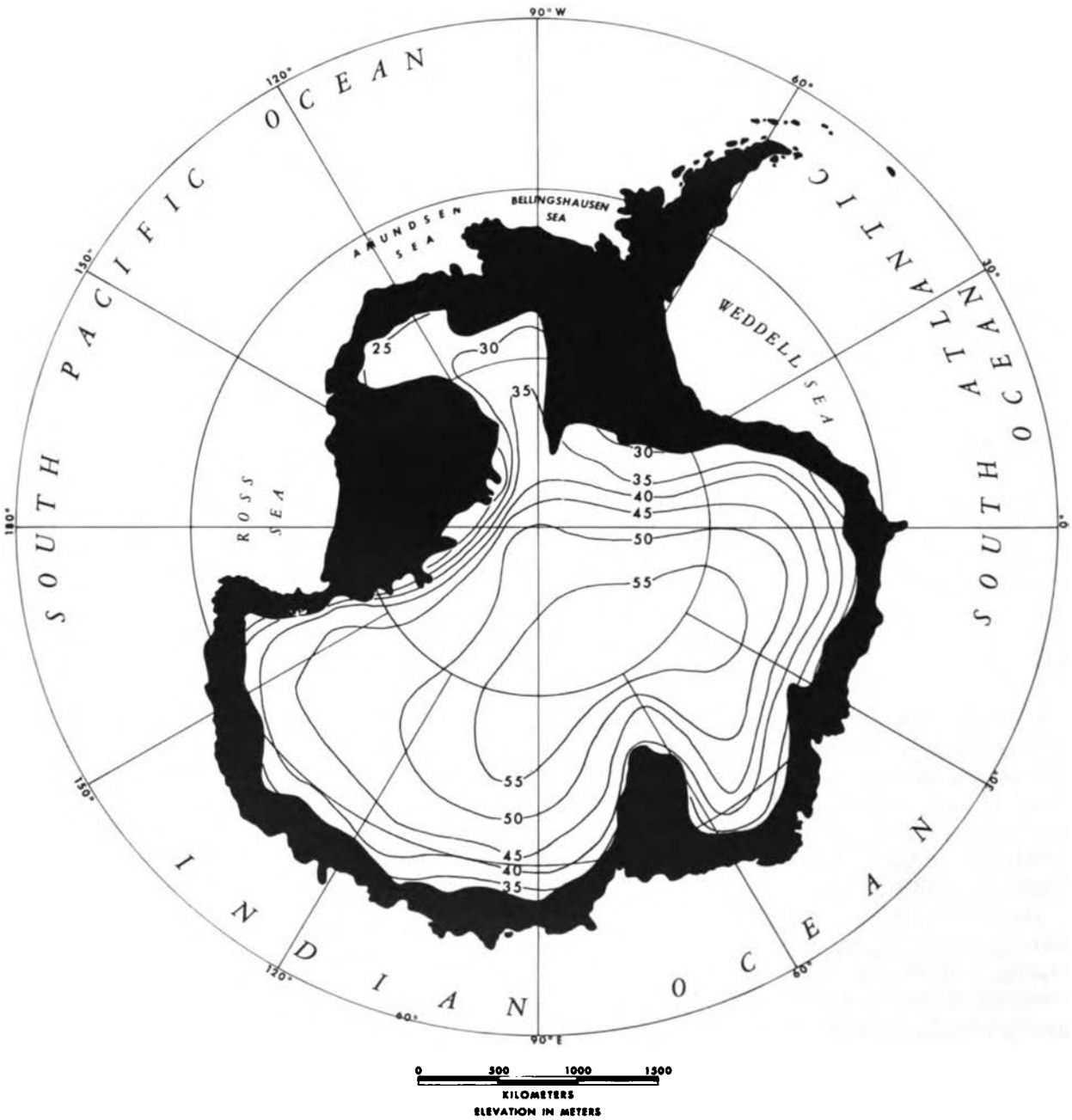

Fig. 7. Firm temperatures (in degrees Celsius) on the Antarctic Plateau.

TABLE 8. Maximum Temperatures (in −°C)

	Jan.	Feb.	Mar.	April	May	June	July	Aug.	Sept.	Oct.	Nov.	Dec.	Year
1957													
Komsomolskaya											25	19	
Vostok I				35.8	34.9	30.5	40.5	35.3	30.1	28.1	23.4		
South Pole	21.1†	27.8	37.2	32.0	34.5	41.3	40.4	43.0	49.8	43.0	19.0	18.9	18.9
South Ice*		(9.2)	(23.8)	(14.6)	(19.5)	(25.9)	23.8	23.7	17.4	18.6	9.4	8.2	
Pionerskaya	15	17	24	25	25	38	36	27	23	21	18	13	13
Charcot				22.5	26.5	29.9	28.0	30.6	24.3	23.6	15.2	9.8	
Byrd	5.4	11.4	18.3	17.7	6.9	15.8	20.6	13.2	17.0	11.2	4.4	4.4	4.4
1958													
Vostok	23	29	47	43	43	47	44	22	45	41	34	26	23
Sovietskaya		34	40	43	44	49	38	48	48	45	31	24	
Komsomolskaya	22	30	30	40	28	46	41	47	44	42	30	25	22
South Pole	14.7	21.4	37.6	48.8	46.1	39.3	34.9	48.7	37.6	33.7	26	23	14.7
Pionerskaya	15	24	25	24	17	39	26	28	32	33	20	19	15
Charcot	10.7	20.4	15.0	21.0	14.0	27.0	17.6	19.6	40.9	16.9	20.3	17.1	10.7
Byrd	4.6	7.0	13.4	9.2	11.1	19.8	10.3	17.3	21.1	15.0	12.0	2.7	2.7

* February to June, based on hourly observations.
† January 9–31.

only one in the station record when the maximum temperature has gone over −18.9°C; the seasonal maximum has been several degrees colder in the ten years of record.

Maximum temperatures at the stations closest to the coast (Charcot, 295 kilometers; Pionerskaya, 350 kilometers; and South Ice, 450 kilometers) are relatively low considering their geographical location. These stations are all in the Cold Katabatic zone, and turbulence associated with the katabatic flow brings colder air from the interior of the continent to the surface at these stations, thus preventing warm maximum temperatures from occurring. There is a tendency for the katabatic wind flow to become weaker or nonexistent during the summer, and during periods with no katabatic flow the temperatures may warm to around −10°C (South Ice, −8.2°C; Charcot, −9.8°C; and Pionerskaya, −13°C).

The station with the highest maximum temperatures on the Antarctic Plateau is Byrd (Table 5). During a midwinter blizzard in May 1957 the temperature rose to −6.9°C at Byrd, showing the destruction of the surface inversion and the advection of relatively warm air from over the Ross Sea to Byrd. On January 30, 1961, Byrd experienced a temperature of −0.8°C, which was 1.9°C warmer than the previous station maximum recorded in 1958. No other station has recorded a temperature within 8°C of 0°C.

Minimum temperatures (Table 9) are not associated with frontal passages but are the result of a prolonged period without warm air advection, strong outgoing radiation, little or no sky cover, and light winds. Although *Bugaev* [1960] has pointed out that extreme cold conditions can exist with a cold cyclonic circulation, nearly all the monthly minimum temperatures in winter were recorded during periods dominated by surface anticyclonic circulation.

Minimum temperatures observed in Antarctica have been far lower than any minimums experienced in the northern hemisphere, where the absolute minimum of −67.7°C occurred at Oimyakon, U.S.S.R. All the Cold Central Core and Cold Interior stations experienced temperatures below −73.4°C except Vostok I which had a minimum temperature of −73.2°C. Extreme minimum temperatures were recorded at Vostok and Sovietskaya and, to a lesser degree, at Komsomolskaya. All these stations in the Cold Central Core experienced temperatures below −80°C. The absolute minimum temperature measured (through 1962) was −88.3°C at Vostok on August 24, 1960. During August 1958 the absolute minima recorded at Sovietskaya and at Komsomolskaya were −86.8°

TABLE 9. Minimum Temperatures (in −°C)

	Jan.	Feb.	Mar.	April	May	June	July	Aug.	Sept.	Oct.	Nov.	Dec.	Year
1957													
Komsomolskaya											57	46	
Vostok I				58.5	70.1	67.8	73.2	65.4	63.4	61.4	52.6		
South Pole	34.3†	56.2	63.6	67.3	73.6	71.7	72.7	73.2	74.5	65.6	48.1	29.7	74.5
South Ice*		(38.4)	(46.1)	(42.8)	(53.1)	(43.9)	57.3	53.3	55.2	38.9	35.0	24.1	
Pionerskaya	35	48	53	54	57	60	59	58	60	53	42	35	60
Charcot				57.0	56.0	56.9	62.0	57.0	58.0	50.0	43.1	32.4	
Byrd	29.6	37.1	45.6	55.6	54.7	56.9	56.6	46.3	51.9	48.2	33.6	25.2	56.9
1958													
Vostok	41	60	67	73	78	80.7	81	87.8	82	71	60	44	87.4
Sovietskaya		62	67	73	79	81.2	83	86.8	79	73	59	49	86.8
Komsomolskaya	43	58	64	69	74	74	76	81	77	66	60	46	81
South Pole	31.1	46.7	67.4	72.9	67.9	74.3	71.6	73.4	74.3	63.6	49	38	74.3
Pionerskaya	34	47	49	53	55	57	63	63	63	58	43	35	63
Charcot	34.0	44.2	48.8	55.2	54.9	61.5	61.5	60.2	61.6	55.7	42.0	33.5	61.6
Byrd	23.9	19.8	47.3	54.1	54.8	59.7	63.2	62.2	53.9	45.1	33.4	29.9	63.2

* February to June, based on hourly observations.
† January 9–31.

and −80.8°C, respectively. The absolute minimum temperature for South Pole is −80.7°C, which occurred on July 21, 1965 (Table 4).

Minimum temperatures for Vostok for 1958 are shown in Table 10. Sixteen days had minimum temperatures below −80.0°C, and 111 days during the year had temperatures below −70.0°C. Of the days between June 1 and September 23, 74% had temperatures below −70.0°C. In August, minimum temperatures were below −70.0°C on 27 days. For Vostok's three years of record, 1958–1960, August 1958 was the coldest month, the monthly mean minimum was −77.0°C, and the monthly mean temperature was −71.8°C. The mean wind speed for this month was 4.7 m/sec, and the average sky cover was 2.8; neither of these means was abnormal. Minimum temperatures in the Cold Katabatic zone were milder than in the interior because of the turbulence associated with the katabatic wind flow. *Bugaev* [1960] refers to the katabatic zone as 'the climatic zone of continual snowstorms.' Clouds of blowing snow, 50–100 meters thick, were observed 25–29 days during each winter month and 15–20 days during each summer month at Pionerskaya. The absolute minimum for the three stations in the Cold Katabatic zone, −63°C, is the same as the absolute minimum for Byrd (Table 5).

The annual temperature range was larger at the interior stations than in the zone of katabatic wind flow (Table 11). This difference is to be expected, as the consistently higher winds of the Cold Katabatic zone keep the temperatures from reaching extremes. Byrd station has the largest temperature ranges because of the frequent frontal passages. The smallest monthly range for any station during 'winter' was 18°C for Pionerskaya (June 1958); the largest monthly range for any month was 52.9°C for Byrd (July 1958). South Pole had the smallest range (10.8°C) for a midsummer month (December 1957).

Wind. Wind is the second most important climatic element on the Antarctic Plateau, and there are times, particularly in the Cold Katabatic zone, when it is the most critical. The cooling power of low temperatures becomes more severe when wind speeds are moderate or high. One of the more surprising features discovered during the IGY about the climate of interior Antarctica was the fact that winds are more or less continuously blowing during 'winter' at a higher speed than anticipated.

Wind directions on the plateau tend to be related to the slope of the snow surface. Although much of the interior of East Antarctica has never been surveyed, it is believed that the average slope is less than 1 degree. *Dolgushin* [1961] estimates the

TABLE 10. Vostok, 1958, Minimum Temperatures (in −°C)

	Jan.	Feb.	Mar.	April	May	June	July	Aug.	Sept.	Oct.	Nov.	Dec.
1	38.6	39.6	59.7	61.8	76.6	74.6	71.6	74.6	72.6	66.6	57.6	41.6
2	37.6	42.7	60.7	64.7	78.9	74.7	71.7	77.8	74.9	68.6	59.6	40.6
3	37.6	43.6	60.7	62.8	72.7	71.7	66.9	64.6	72.7	66.8	50.7	42.6
4	39.6	47.6	59.7	66.7	71.6	63.6	63.6	67.6	66.6	70.6	43.7	44.6
5	36.7	49.6	57.9	67.7	71.7	67.9	67.9	68.6	70.9	73.6	54.9	43.6
6	34.6	50.6	59.6	69.6	71.6	66.6	67.9	77.6	70.6	71.9	51.6	41.6
7	31.9	50.6	59.7	68.6	71.7	68.6	65.7	84.6	67.6	71.6	51.6	42.6
8	37.6	51.6	56.7	68.8	67.9	73.9	56.6	84.7	69.8	62.6	52.6	39.9
9	38.6	49.6	59.7	62.7	65.8	72.7	58.8	79.9	66.6	67.6	54.6	39.6
10	36.6	51.6	62.7	64.7	68.6	70.7	71.6	78.7	73.9	68.6	54.6	37.9
11	36.7	52.6	62.6	66.7	68.7	69.6	70.7	75.6	70.6	70.6	53.6	36.9
12	27.9	53.6	62.7	67.8	65.7	72.6	66.6	75.8	68.9	69.6	52.6	35.6
13	33.6	54.6	62.7	59.7	64.6	79.8	67.7	75.6	81.6	68.6	53.6	38.6
14	35.6	56.6	67.7	62.6	70.6	78.6	72.9	76.8	82.6	69.6	53.6	40.6
15	36.6	55.6	66.7	68.7	71.7	81.9	72.7	78.6	82.7	64.7	51.6	39.6
16	35.6	54.6	61.8	70.6	62.7	79.9	66.6	82.9	81.7	68.6	51.7	36.9
17	37.6	54.7	60.7	71.7	61.6	79.6	71.8	81.8	78.6	69.9	50.6	34.6
18	40.6	53.7	58.6	70.7	62.7	80.7	72.6	72.7	78.6	63.7	45.7	37.6
19	40.7	44.6	66.7	71.7	61.6	74.7	74.9	71.9	78.6	63.9	43.6	38.6
20	37.9	45.6	67.7	72.8	63.7	60.7	70.7	75.9	72.6	65.6	44.9	37.6
21	37.7	52.7	66.8	68.7	58.7	65.6	72.6	73.7	78.6	65.7	44.9	40.6
22	40.6	51.6	64.7	71.6	52.9	68.6	77.6	74.6	78.6	64.6	50.9	38.6
23	40.6	55.6	63.8	73.6	60.6	72.6	83.9	81.9	71.7	66.6	45.6	38.6
24	38.7	55.6	61.7	71.8	64.6	74.6	77.9	83.9	61.7	67.6	46.6	38.6
25	36.6	54.7	61.8	71.9	68.8	75.9	76.9	87.8	58.9	63.9	46.6	36.6
26	34.6	54.6	58.7	57.7	66.6	73.7	73.7	82.7	53.6	61.6	45.6	35.6
27	35.6	59.6	65.7	64.7	69.9	68.7	73.7	78.9	59.6	55.7	44.6	36.6
28	37.6	60.6	67.7	71.7	70.6	73.6	73.7	80.6	64.9	52.9	44.6	38.6
29	39.6		66.8	73.6	72.8	75.8	68.6	79.7	67.6	54.7	46.6	35.6
30	40.6		60.7	73.6	69.7	68.7	68.7	66.7	67.7	54.6	44.9	37.9
31	40.7				66.7		67.7	70.9		54.9		38.9
Mean	37.3	51.7	62.4	68.0	67.5	72.7	70.1	77.0	71.5	65.4	49.8	38.9

slope to be 10^{-3}, which is less than a slope of 1 degree (2×10^{-2}). Because of the gentle slope of the high interior of East Antarctica, the winds behave as in fluid flow, and the dominant wind direction tends to be downslope. Wind speeds increase as they approach the slope of the Antarctic Plateau and become more consistently from the same direction. There is a tendency for the katabatic winds to be more pronounced during the sunless period than during midsummer.

Wind roses were determined from the sum of the monthly wind direction frequencies prepared for each station (Figure 8). These diagrams show most vividly the katabatic winds at South Ice, Pionerskaya, and Charcot. The most unusual distribution is for South Ice, which shows two predominating wind directions 40° apart; both are from the high interior of East Antarctica.

Frequencies of winds from predominating directions are shown in Table 12. The most noticeable feature is the large percentage of winds from a relatively small sector, especially for stations in the Cold Katabatic zone. Prevailing winds at all stations are downslope.

The prevailing wind directions for all stations on the Antarctic Plateau for 1957–1958 are presented in Table 13. Prevailing directions for South Pole and Byrd for 1957 through 1962 are shown in Tables 4 and 5, respectively. As all directions at South Pole are north, directions are presented in compass directions, with Greenwich considered as being at 0°.

TABLE 11. Temperature Range (in °C)

	Jan.	Feb.	Mar.	April	May	June	July	Aug.	Sept.	Oct.	Nov.	Dec.	Year
1957													
Komsomolskaya											32	27	
Vostok I				22.7	35.2	37.3	32.7	30.1	33.3	33.0	29.2		
South Pole	13.2†	38.4	26.4	35.3	39.1	30.4	32.3	30.2	24.7	22.6	29.1	10.8	55.6
South Ice*		(18)	(34)	(28)	(22)	(29)	33.5	29.6	37.8	20.3	25.6	15.9	49.1
Pionerskaya	20	31	29	29	32	32	23	31	37	32	24	22	47
Charcot				34.5	29.5	27.0	34.0	26.4	33.7	26.4	27.9	22.6	52.2
Byrd	24.2	25.7	27.3	37.9	47.8	41.1	36.0	33.1	34.9	37.0	29.2	20.8	52.5
1958													
Vostok	18	31	20	30	35	34	37	32	37	30	26	18	65.4
Sovietskaya		28	27	30	35	32	45	39	31	28	28	25	62.4
Komsomolskaya	21	28	34	29	46	28	35	34	33	24	30	21	59
South Pole	16.4	25.3	29.8	24.1	21.8	35.0	36.7	24.7	36.7	29.9	23	15	59.6
Pionerskaya	19	23	24	29	38	18	37	35	31	25	23	16	48
Charcot	23.3	23.8	33.8	34.2	40.9	34.5	43.9	40.6	20.7	38.8	21.7	16.4	50.9
Byrd	19.3	12.8	33.9	44.9	43.7	39.9	52.9	44.9	32.8	30.1	21.4	27.2	60.5

* February to June, based on hourly observations.
† January 9–31.

Uniformity is the one word which best describes the climate of the Antarctic Plateau, as diurnal and weekly changes are very small. Wind speed, which is relatively moderate and consistent on the plateau, is particularly uniform. There are very few calms and very few winds over 20 m/sec, with a great concentration around the mode (Figure 9). The higher wind speeds at the stations in the Cold Katabatic zone are in great contrast to the low winds of the Cold Central Core. One of the interesting sidelights of the month of April 1958 was the large number of calms at Sovietskaya (41 hours), which exceeded the highest frequency (23 hours) for any wind speed for the month (4 m/sec). (Calm data can sometimes be misleading, since large 3-cup anemometers in cold environments often remain immobile at speeds up to 1.5 m/sec.)

Wind speeds on the Antarctic Plateau are related to the distance from the coastal slope and cyclonic tracks. The average wind speed for the Cold Central Core is of the order of 4 m/sec [Vostok, 5.1; Sovietskaya, 3.6; and Komsomolskaya, 3.8 m/sec (Table 14)]. The maximum wind speed measured at Sovietskaya was 12 m/sec; at Vostok, 25 m/sec; and at Komsomolskaya, 17 m/sec (Table 15).

Wind speeds at South Pole in the Cold Interior are somewhat higher than speeds in the Cold Central Core, averaging 6.4 m/sec (Table 6). July 1963 was the windiest month during the first seven years of record and had a mean wind speed of 9.7 m/sec. The mean monthly wind speed increases with each month from December through July and then drops off as the winter passes into summer. The maximum wind speed (24.2 m/sec) on record at South Pole occurred in May 1957 (Table 4). The most 'famous' wind was the blizzard of January 1958, when the temperature rose to —14.7°C, 4.2°C warmer than the next highest maximum. Winds peaked to 21.6 m/sec in this storm.

Both mean and maximum wind speeds in the Cold Katabatic zone are approximately twice those in either the Cold Central Core or the Cold Interior. The mean annual wind speed in the Cold Katabatic zone is close to 10 m/sec. South Ice was the windiest of the three stations, and its average wind speed for the six winter months from April through September was 13.4 m/sec. This is higher than in comparable winter periods from the other two katabatic stations, Pionerskaya and Charcot. Pionerskaya had a mean annual wind speed of 10.7 m/sec, and Charcot's mean wind speed for 1958 was 9.2 m/sec. Pionerskaya's maximum speed was 32 m/sec in February 1958; Charcot's maximum wind speed was also 32 m/sec in April 1957.

Byrd station in West Antarctica has wind speeds

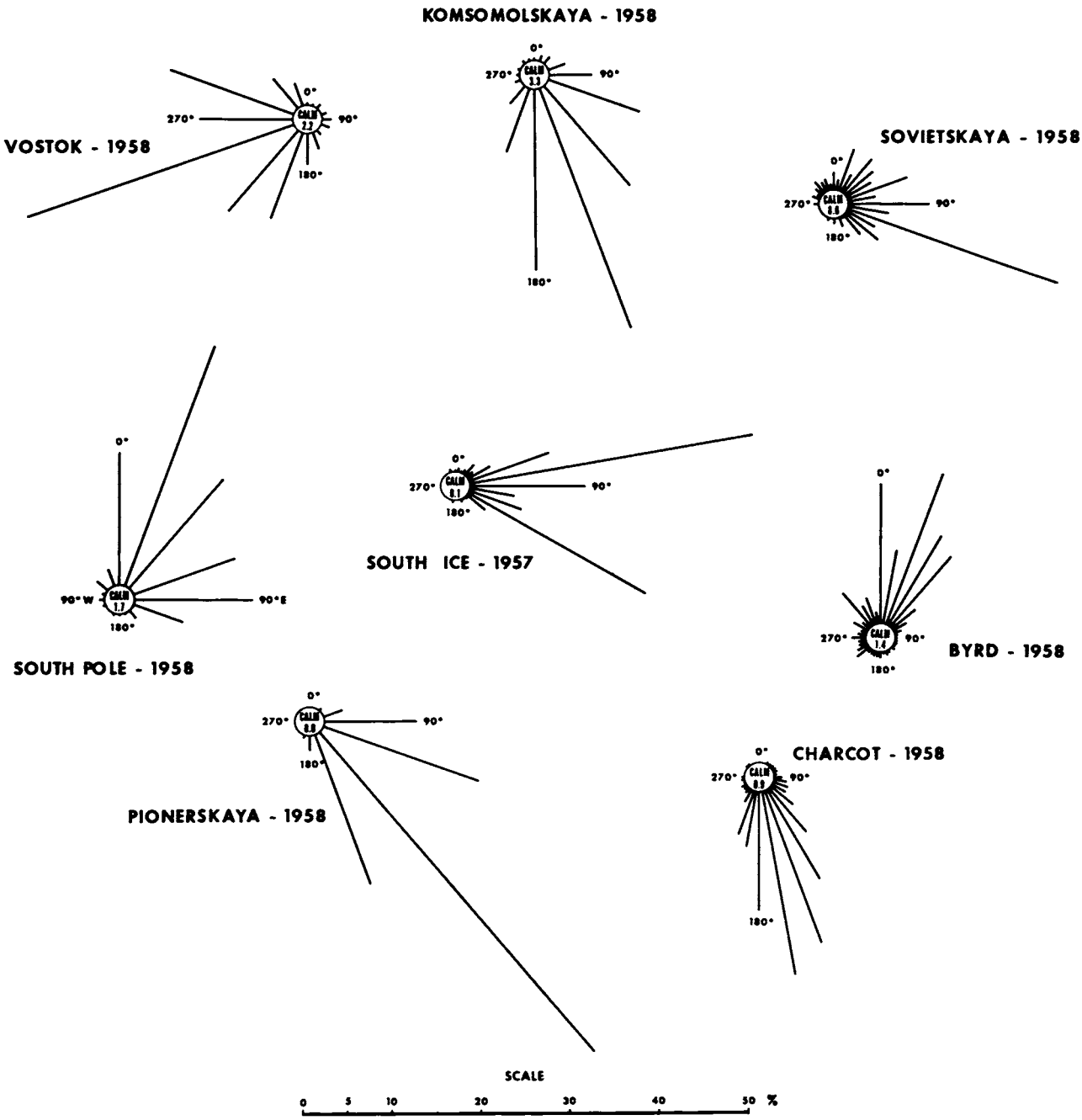

Fig. 8. Annual wind direction frequencies at Antarctic Plateau stations.

that are higher than those at South Pole and lower than those in the katabatic zone. Its average wind speed is 8.5 m/sec (Table 5) and its absolute maximum, 39 m/sec, occurred on June 30, 1965 (Table 5). High wind speeds at Byrd are usually associated with cyclonic activity.

The maximum wind speed for any station in the Cold Central Core and Cold Interior occurred at Vostok on June 20, 1958, when the wind speed reached 25 m/sec from the prevailing wind direction of 250 degrees (Table 16). As with most monthly maximum wind speeds, this was associated

TABLE 12. Frequencies of Winds from Predominant Directions

Station	Wind Direction	Percentage
	Central Cold Core	
Sovietskaya (1958)	015 to 135	76
Vostok (1958)	190 to 300	89
	210 to 280	62
Komsomolskaya (1958)	100 to 190	76
	130 to 190	65
	Cold Interior	
South Pole (1958)	350 to 100	86
	Cold Katabatic	
Pionerskaya (1958)	080 to 170	95
	100 to 170	85
Charcot (1958)	125 to 205	87
South Ice (1957)	065 to 125	89
	West Antarctica	
Byrd (1958)	355 to 045	75

with a frontal passage. The barometric pressure and the temperature started to fall on the eighteenth, and the wind started to increase slowly on the nineteenth. The storm occurred during the winter solstice following the coldest temperatures ever recorded to that time. The effects of the storm were more severe at Vostok, owing to the great increase in wind speed, but were also noted at other stations (Table 17).

Vostok was the only station to have abnormally high winds, as its prevailing winds were reinforced by the cyclonic winds. The degree of warming at Vostok and Sovietskaya, both at approximately the same latitude, was identical (32°C). The storm came from the west and passed from the interior toward the coast. The degree of warming downslope was of lesser magnitude because of the warmer surface temperatures at the lower elevation. The resultant temperatures at all stations were in the —40's.

Wind speeds on the Antarctic Plateau may seem light in comparison with the high speeds (>50 m/sec) measured at coastal stations in East Antarctica, although mean wind speeds at all stations are comparable. South Pole has a higher mean wind speed than many of the coastal stations.

Precipitation. Accurate measurement of the amount of precipitation in polar regions is practically impossible. The net accumulation can be determined with reasonable accuracy from a network of accumulation stakes. Precipitation, in water equivalent terms, can be determined from glaciological pit studies. The average net accumulation for Antarctica has been estimated by *Rubin* [1962] to be 14.5 cm of water. This estimate is based on snow stake measurements and pit stratigraphy studies and is considered to be the minimum value for precipitation, which could amount to an additional 5 cm if larger values were ascribed to

TABLE 13. Prevailing Wind Direction (in degrees)

	Jan.	Feb.	Mar.	April	May	June	July	Aug.	Sept.	Oct.	Nov.	Dec.	Year
1957													
Komsomolskaya											140	160	
Vostok I					140	140	140	140	140	160	140		
South Pole	360	360	020	020	020	040	020	040	020	020	360	090	020/360
South Ice							080	120	120	080	080	080	
Pionerskaya	120	140	140	140	140	140	140	110	110	140	140	110	140
Charcot					160	160	160	160	175	180	180	175	
Byrd	360	360	040	020	020	360	020	030	050	020	030	360	020/360
1958													
Vostok	200	250	200	250	250	250	250	250	250	250	250	250	250
Sovietskaya		090	120	Calm	110	110	110	110	110	110	110	Calm	110
Komsomolskaya	180	160	160	160	160	180	180	160	160	160	160	140	160
South Pole	360	090	020	090	020	040	020	040	020	020	360	090	020
Pionerskaya	110	140	140	140	140	160	140	140	140	140	140	110	140
Charcot	160	180	160	150	170	170	180	170	170	170	160	150	170
Byrd	360	360	360	020	020	360	360	020	020	020	040	040	020/360

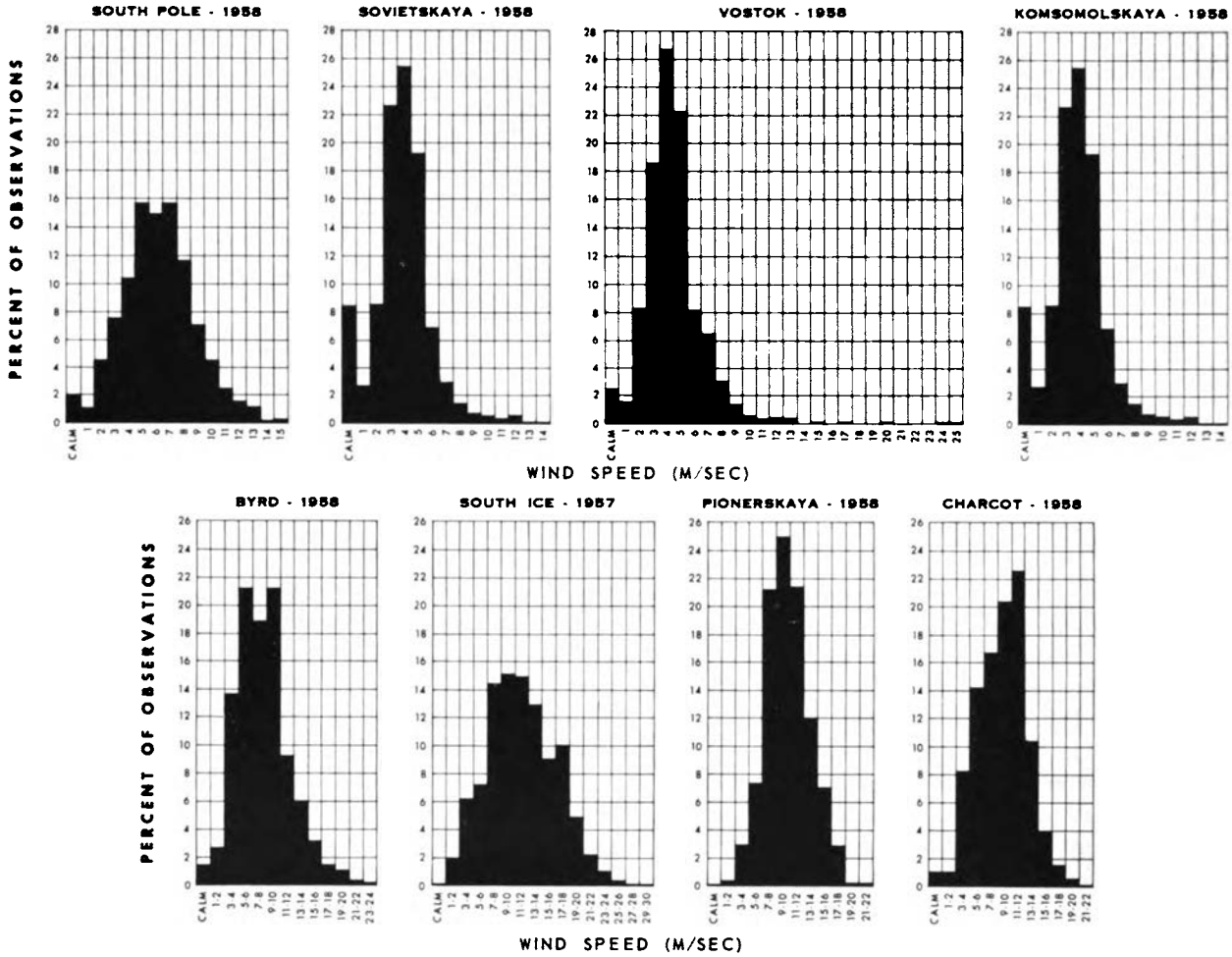

Fig. 9. Annual wind speed frequencies at the Antarctic Plateau stations.

TABLE 14. Mean Wind Speed (in m/sec)

	Jan.	Feb.	Mar.	April	May	June	July	Aug.	Sept.	Oct.	Nov.	Dec.	Annual
1957													
Komsomolskaya											3.3	3.9	···
Vostok I				8.1	6.3	6.3	5.3	6.0	7.9	5.7	5.7		···
South Pole	5.0	5.0	5.8	7.7	7.7	8.6	7.9	8.1	6.5	7.1	4.7	3.7	6.5
South Ice		6.6	9.3	12.0	15.5	14.4	11.8	14.1	12.6	8.4	10.2	7.7	11.1*
Pionerskaya	12.4	13.1	12.0	13.3	9.0	9.9	9.2	13.5	12.9	11.2	9.4	9.0	11.2
Charcot					12.0	13.1	9.0	9.2	9.5	10.5	9.1	7.4	···
Byrd	5.4	6.4	8.9	8.9	8.5	8.0	9.8	12.1	11.5	7.7	8.5	6.9	7.8
1958													
Vostok	4.6	3.7	5.1	4.0	5.2	4.9	5.0	4.7	5.4	4.0	4.2	3.8	4.6
Sovietskaya		1.4	3.6	3.3	3.9	4.6	4.4	4.6	4.6	3.8	3.4	2.5	3.6*
Komsomolskaya	5.5	3.8	3.0	3.8	4.1	4.3	4.1	2.7	4.2	3.5	3.3	2.9	3.8
South Pole	5.7	4.3	5.8	5.7	8.1	7.2	8.8	6.3	6.6	7.1	3.9	4.2	6.1
Pionerskaya	9.0	9.3	10.1	11.7	10.8	10.4	11.1	9.6	11.1	10.6	9.6	8.8	10.2
Charcot	9.4	8.9	10.8	10.9	8.0	11.9	8.4	8.1	10.5	8.7	7.8	6.9	9.2
Byrd	6.7	9.6	7.2	7.7	10.0	6.3	8.0	8.2	9.8	9.1	8.1	6.4	8.1

* ~11 months.

TABLE 15. Maximum Wind Speed (in m/sec)

	Jan.	Feb.	Mar.	April	May	June	July	Aug.	Sept.	Oct.	Nov.	Dec.	Year
1957													
Komsomolskaya											17	13	
Vostok I				22	17	12	12	13	14	11	16		
South Pole			14	17	24	17	19	17	19	17	14	10	
Pionerskaya	20	22	22	26	22	17	20	24	23	24	25	25	26
Charcot				32	25	25	28	18	23	25	17	16	
Byrd	13	14	19	19	15	21	20	28	21	20	19	22	28
1958													
Vostok	14	9	10	10	15	25	13	13	13	12	13	11	25
Sovietskaya		3	9	8	12	11	10	12	12	9	12	6	
Komsomolskaya	10	9	8	15	13	11	9	10	10	10	8	8	15
South Pole	22	13	16	13	17	15	21	14	13	14	12	11	22
Pionerskaya	16	32	17	21	21	20	28	17	19	18	17	18	32
Charcot	24	15	26	26	20	29	23	27	26	24	20	26	29
Byrd	14	26		23	27	20	28	27	26	23	26	18	28

losses due to drifting, evaporation, and surface melting. Another method of estimating precipitation takes into account all the snow and ice that leaves the continent, whether it be from melting, evaporation, calving, or blowing snow. The total figure obtained by *Rubin* [1962] for this estimate was 10.8–16.6 cm of water. *Rubin and Giovinetto* [1962] studied snow accumulation in West Antarctica, and their general conclusions were that the annual accumulation increases from west to east and from south to north. The distribution was explained by the interaction of cyclonic systems with topographic features.

The net accumulation map (Figure 10) is from *Rubin* [1962]. Most of the Cold Central Core lies within the 5 cm of water isohydropleth, with the Sovietskaya area having about 3 cm of water. The Cold Interior averages about 10 cm of water, with South Pole about 7 cm of water. This value was verified by *Picciotto and Crozaz* [1964] using two methods (beta activity and Pb-210 isotopes). They determined water equivalent values of 6–7 cm for South Pole. The Cold Katabatic zone has from less than 5 to over 40 cm of water; the Cold Transitional has from 5 to 35 cm of water, with Byrd having about 18 cm of water.

A deep core of snow-firn-glacier ice was obtained from the Antarctic Plateau at Byrd, where the U.S. Army Cold Regions Research and Engineering Laboratory (1959) bored 309 meters into the snow. Below 60 meters, the temperature appears to have stabilized at about −28.3°C, which is exactly the same as the mean annual temperature for Byrd. Below 120 meters, the temperature decreases by less than 0.01°C per 30 meters. A detailed study of the

TABLE 16. Weather Conditions, June 20–21, 1958, Vostok

Date	Hour	Wind Dir., deg	Wind Speed, m/sec	Temp., °C	Sky Cover
June 20	00	250	7	60	Cloudless
	06	250	24	51	Sky obscured
	12	250	25	48	Sky obscured
	18	250	18	47	Sky obscured
June 21	00	220	20	48	Sky obscured
	06	220	11	55	Cloudless
	12	220	12	59	Cloudless

TABLE 17. Frontal Temperatures, June 18–21, 1958

Station	Date	Hour	Temp., °C	Temp. Rise, °C
Vostok	18	00	−79	
	20	18	−47	32
Sovietskaya	19	00	−81	
	20	06	−49	32
Komsomolskaya	19	06	−73	
	21	12	−46	27
Pionerskaya	19	12	−54	
	21	06	−41	13

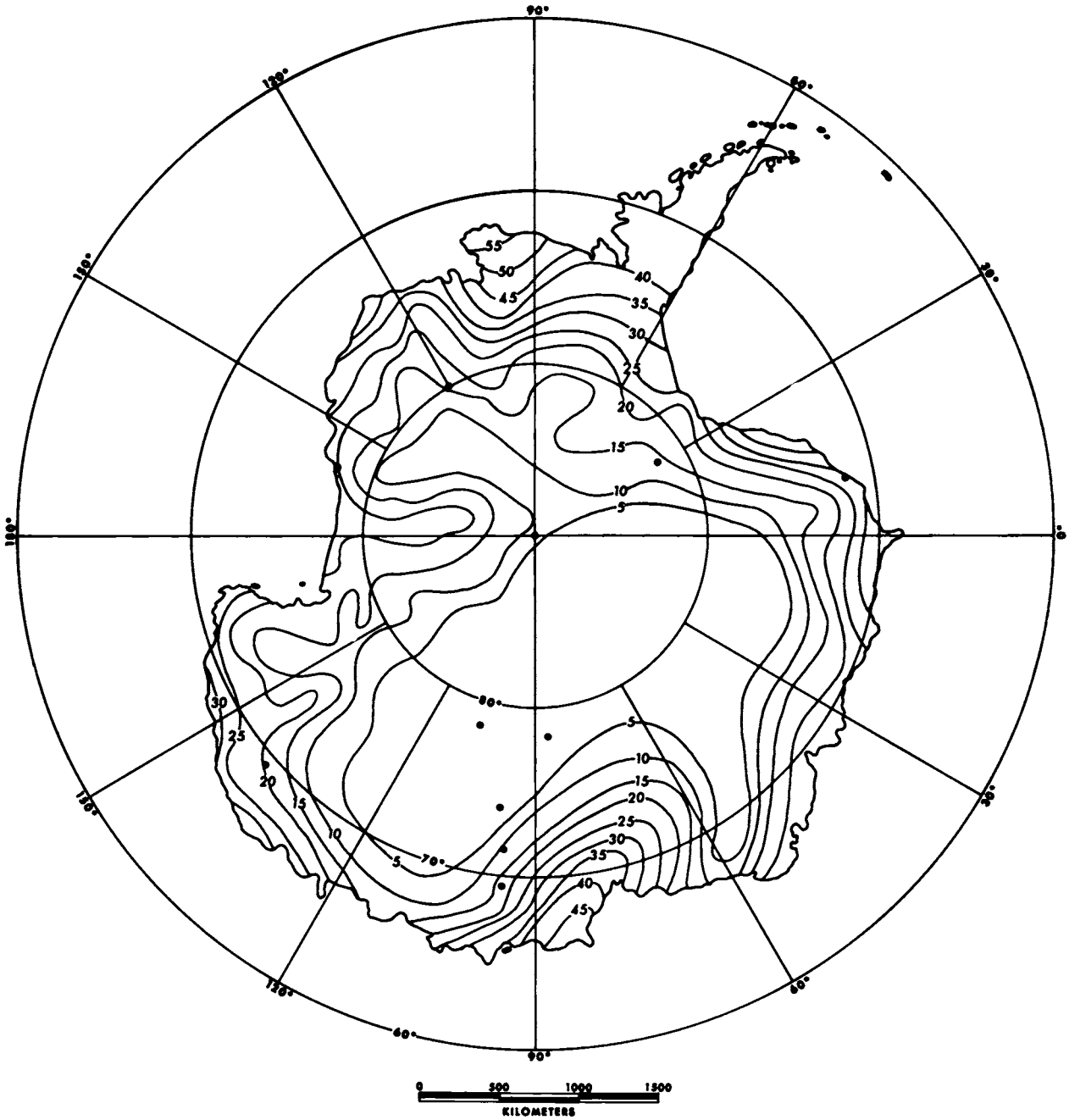

Fig. 10. Annual accumulation of precipitation (in cm of H_2O).

stratigraphy was made of the first 19 meters which date back to 1893. The average rate of accumulation at Byrd since this date is equivalent to 14.4 cm of water per year. The greatest annual accumulation was 24.4 g/cm² in 1896 (40-cm annual layer), and the smallest annual accumulation was 8.6 g/cm² in 1942 (18-cm annual layer). *Wexler* [1961] discussed the growth and thermal structure of the deep ice near Byrd and estimated that the climate at Byrd, based on annual accumulations of 10 or 20 cm of ice, has warmed 1.528°C, or 1.556°C per 1000 years.

TABLE 18. Sky Cover (in tenths)

	Jan.	Feb.	Mar.	April	May	June	July	Aug.	Sept.	Oct.	Nov.	Dec.	Annual
1957													
Vostok I				6.5	4.5	4.2	3.9	6.4	7.8	6.6	5.0		
South Pole	5.8	4.9	6.6	3.0	3.0	1.5	2.0	2.6	2.8	4.2	3.2	4.4	3.7
South Ice		3.6	2.0	3.2	2.0	1.0	1.7	1.2	2.6	4.7	3.2	5.0	
Pionerskaya	7.6	5.8	6.7	8.6	7.5	6.9	6.9	8.9	8.6	6.6	5.5	6.8	7.2
Byrd	8.5	7.8	7.1	4.8	4.2	4.6	4.0	6.6	6.5	8.4	6.3	7.1	6.3
1958													
Vostok	3.9	2.6	4.2	2.6	5.2	2.1	2.5	2.8	4.1	3.2	2.9	2.7	3.2
Sovietskaya			3.6	2.3	1.3	1.1	1.1	1.0	1.4	1.9	2.7	3.9	2.0
Komsomolskaya	3.6	2.3	3.4	2.6	2.0	0.8	2.7	3.6	3.7	3.4	3.9	3.2	2.9
South Pole	5.4	6.1	5.0	1.5	2.7	2.4	4.7	3.5	5.7	6.5	6.3	3.8	4.5
Pionerskaya	4.2	2.2	4.1	4.9	4.5	3.2	5.9	4.3	3.8	4.3	4.5	5.2	4.3
Byrd	6.9	8.1	7.6	6.4	6.6	4.7	5.8	5.8	6.3	7.2	6.5	7.0	6.6

Sky cover. Accurate cloud observations are among the most difficult observations to make, particularly in the higher latitudes of the polar regions where prolonged periods without Sun add to the difficulties. In addition to the problem of identifying clouds during darkness, there is also the problem of obscuration from blowing snow.

The interior of Antarctica is a fair-weather region, less cloudy than coastal areas. The Cold Central Core has the smallest amount of cloudiness, as determined by observations in tenths of sky cover [Sovietskaya about 2.5, Komsomolskaya about 4.0, and Vostok about 4.2 (Table 18)]. Komsomolskaya had an average sky cover in June 1958 of less than one-tenth. The first thirteen days of the month were completely cloudless and represent the longest cloudless period on the Antarctic Plateau during the IGY. Sovietskaya had a mean cloudiness of about 1.5 for the six-month period, May–October 1958.

South Pole, in the Cold Interior, has an average sky cover of 4.1 (Table 4). There is less cloudiness during the period without Sun, 2.9–3.3 for the months April through August. The months with the highest amount of cloudiness were October and February. The average number of clear days in May (1957–1962) is 20, with 8 partly cloudy and 3 cloudy days. In contrast, for the same six-year period, February averages 9 clear, 9 partly cloudy, and 10 cloudy days.

There are no cloud data for South Ice or Charcot on the WMO microcards; Pionerskaya, the other Cold Katabatic station, had a higher amount of cloudiness, approximately 5.3 sky cover, than the other stations in East Antarctica on the plateau.

Byrd had the greatest amount of cloudiness, averaging 6.1 sky cover (Table 5). This is to be expected, as the station is between four large seas (Ross, Amundsen, Bellingshausen, and Weddell). There is the same general pattern, with a minimum of cloudiness during the period without Sun and a maximum during the transitional periods between 'summer' and 'winter.'

Cloud types on the Antarctic Plateau are confined primarily to high and middle clouds, e.g. Table 19.

These data are probably representative of cloud conditions over most of the Antarctic Plateau. The predominating clouds are high clouds (cirrus and cirrostratus), with some middle clouds, particularly altostratus. The cirrus clouds are usually thin, and generally only a small part of the sky is opaque.

Stratocumulus clouds are the most important cloud types, since whiteout conditions can occur with an overcast of stratocumulus. The reflection between the base of the clouds and the snow surface can be so intense as to wash out the horizon. The presence of a stratocumulus overcast does not, however, always presage a whiteout.

Radiation. Although radiation measurements are not comparable in all respects because of different observational procedures and instrumentation, a comparison of the results of some radiation measurements at different stations can be instructive.

Table 20 presents the mean hourly total radiation (Sun plus sky) for stations with continuous meas-

TABLE 19. Frequency of Cloud Types

	High Clouds			Middle Clouds		Low Clouds				
	Ci	Cc	Cs	Ac	As	Cu	Sc	St	Frst	Frcu
Komsomolskaya (1958)	432	7	302	37	37	1	25	4	1	1
Vostok I (1957)	283	27	195	7	129	...	...	...	...	...
Pionerskaya (1957)	112	17	322	41	253	...	13	...	...	...

urements, and a breakdown of these data into direct and diffuse radiation for the Soviet stations. Radiation values are high, owing to the position of the Earth in relation to the Sun during the antarctic summer and to the high elevation of the Antarctic Plateau. *Rubin* [1962] states that about 7% more solar energy reaches the top of the antarctic atmosphere than at the north pole in midsummer because the Earth is at perihelion and the Sun's rays have 30% less air mass to traverse because of the high elevations.

The daily total radiation of Sun and sky on a horizontal surface for South Pole in 1958 is shown in Table 21. These values are particularly high for the month of December, averaging 917 calories per cm^2. December of that year was probably a near 'normal' December, with a mean sky cover of 4.4, with 14 clear, 10 partly cloudy, and 7 cloudy days. During the month of December 1957, a total of 28,427 calories per cm^2 was received at South Pole. This total is approximately 79% of the radiation reaching the top of the atmosphere. About 76% of the radiation received at the surface in midsummer is immediately reflected into space. Maximum normal incidence radiation values are available from *Kopanev* [1960] for the Soviet stations on a monthly basis (Table 22). Normal incidence measurements were taken at South Pole for selected periods. Values (in langleys) for 1957–1958 were 1.53 to 1.56 for December 25–29; 1.51 to 1.47 for January 2–27; 1.47 to 1.31 for February 2–21; 1.13 to 0.50 for March 2–14; 1.21 for October 19; and 1.45 to 1.47 for November 6–17. These values are comparable to those obtained by *Hoinkes* [1960] in the European Alps at 3000 meters in December.

Albedo measurements were taken at most of the stations, and the mean monthly albedo at the Soviet stations is shown in Table 23. Highest values at those stations were obtained in early summer, which would seem to indicate a smooth snow surface following winter. In contrast, at South Pole the albedo values calculated by *Hanson* [1960] are lower at the end of winter than they are at the end of summer (Table 24). This distinction is due in part to the smoothing of the sculptured winter surface

TABLE 20. Monthly Mean Hourly Radiation Data, 1958* (in cal/cm^2/hr)

	Jan.	Feb.	Mar.	April	May	Aug.	Sept.	Oct.	Nov.	Dec.
					Total Radiation					
Vostok	27.2	18.5	5.3	0.4	...	...	6.4	10.3	22.4	31.1
Sovietskaya	...	...	4.7	0.4	...	...	2.9	12.2	23.7	32.8
Komsomolskaya	31.2	17.1	9.2	1.6	0.3	0.6	4.7	14.4	24.8	29.5
South Pole	32.1	19.8	4.5	...	...	...	0.4	11.3	29.0	38.2
Pionerskaya	26.6	18.2	...	...	...	0.9	3.8	10.8	19.8	25.4
					Diffuse Radiation					
Vostok	6.0	2.6	2.0	0.2	...	...	1.1	3.5	4.0	6.7
Sovietskaya	...	...	1.8	0.2	...	...	1.2	3.0	4.4	7.1
Komsomolskaya	8.8	4.2	3.2	0.7	...	0.5	2.7	5.0	7.0	7.3
Pionerskaya	11.2	7.2	5.0	1.3	...	0.8	2.5	6.8	9.4	11.7
					Direct Radiation					
Vostok	21.2	15.9	3.3	0.2	...	...	5.3	6.8	18.4	24.4
Sovietskaya	...	...	2.9	0.2	...	...	1.7	9.2	19.2	25.7
Komsomolskaya	22.4	12.9	6.0	0.9	...	0.1	2.0	9.4	17.8	22.3
Pionerskaya	15.4	11.0	...	...	...	0.1	1.3	4.0	10.4	13.7

* Data shown only for months with observations.

TABLE 21. Daily Total Radiation (Sun and Sky), South Pole, 1958 (in cal/cm²/day)

1958	Jan.	Feb.	Mar.	Sept.	Oct.	Nov.	Dec.
1	925	446	249	...	59	526	940
2	896	701	294	...	71	426	950
3	886	485	276	...	129	456	912
4	M	M	247	...	171	454	920
5	875	578	226	...	89	599	938
6	910	522	252	...	167	639	952
7	956	594	130	...	226	M	954
8	938	632	147	...	234	642	969
9	874	588	126	...	209	698	982
10	685	564	135	...	133	668	984
11	810	605	87	...	M	683	993
12	662	597	92	...	M	725	963
13	766	579	109	...	222	M	895
14	686	576	M	...	267	735	857
15	645	559	M	...	321	757	755
16	625	536	80	...	353	773	832
17	782	273	66	...	245	780	737
18	797	267	41	...	333	664	801
19	808	301	30	...	384	633	914
20	857	283	23	...	357	M	951
21	860	401	17	6	270	M	980
22	853	314	15	5	349	646	882
23	752	311	13	8	375	764	M
24	692	355	12	12	372	768	M
25	683	225	7	14	326	792	919
26	587	226	4	20	288	866	910
27	752	227	2	35	364	828	919
28	650	240	...	46	320	819	954
29	596	...	...	54	337	870	968
30	729	...	...	59	375	908	936
31	575	...	...	...	527	...	937

M = missing data.

and, in February and March, to the higher values that are obtained with the Sun at lower solar angles and thus at a lower angle of incidence. *Hoinkes* [1960] took a series of 100 albedo measurements within 1 kilometer of South Pole between December 5, 1957, and January 4, 1958. These midsummer observations were under cloudless skies for 73 series and overcast skies for 27 series; the albedo values at South Pole are presented in Table 25. These values are considerably higher than those obtained by the Weather Bureau at South Pole, probably due to the fact that Hoinkes had portable equipment that enabled him to walk away from camp and be selective in his sites.

Monthly mean radiation balance data are shown from *Kopanev* [1960] and from USWB data made available by the Polar Meteorology Research Project (Table 26).

Relative humidity. The relative humidity values are of little consequence because of the small amount of moisture that the atmosphere can hold at the cold temperatures experienced in the Antarctic. There is little deviation in mean monthly values, and they are consistently high (Table 27).

INTERRELATIONSHIPS OF CLIMATIC ELEMENTS

Surface inversions. One of the most interesting phenomena existing on the Antarctic Plateau is the surface inversion, a permanent feature of 'winter' over most of the Antarctic Plateau. A study of all upper-air soundings at Vostok for the years 1960 and 1961 showed that a permanent surface inversion existed on all soundings from February through November and that a semipermanent inversion existed in December and January.

Surface inversions in the polar regions are formed by both long-wave and short-wave radiation of energy away from the surface. Cloudless or partly cloudy skies and low winds combine to make conditions favorable for the formation and continuation of surface inversions. Turbulence created by strong winds can destroy inversions in a relatively short time. They reform quickly, however, as soon as winds decrease below 10 m/sec and skies become partly cloudy to cloudless. The one element that appears to be the controlling factor in determining

TABLE 22. Maximum Normal Incidence Measurements, 1958 (in cal/cm²/min)

	Jan.	Feb.	Mar.	April	Aug.	Sept.	Oct.	Nov.	Dec.
Vostok	1.39	1.26	1.30			1.27	1.48	1.50	1.50
Sovietskaya			1.60	1.08	0.44	1.44	1.72	1.83	1.82
Komsomolskaya	1.82	1.59	1.48	1.32	0.96	1.46	1.72	1.60	1.77
Pionerskaya		1.70	1.27	0.97	0.45	1.49	1.53	1.66	1.70

TABLE 23. Monthly Mean Albedo, 1958 (%)

	Jan.	Feb.	Mar.	April	May	June	July	Aug.	Sept.	Oct.	Nov.	Dec.
Vostok	75	79	75						90	90	82	84
Sovietskaya									87	82	80	77
Komsomolskaya	78	83	75	74				89	85	80	81	82
Pionerskaya									86	90	81	82

the height and intensity of the inversion is wind speed. Stations with low wind speeds have larger and deeper surface inversions.

Upper-air observations were analyzed for surface inversion data for the IGY (July 1957–December 1958); for Vostok, 1960–1961; and for South Pole and Byrd, 1959–1961. The main purpose was to determine the depth and the intensity (temperature difference) of the surface inversion. Data on the depth of the inversion are presented in Table 28. These data show that (1) the depth of the inversion is greater in East Antarctica than it is in West Antarctica, (2) the depth of the inversion is greatest in the Cold Central Core, where stations are at higher elevations, and (3) the inversions are much deeper in 'midwinter' than they are in 'midsummer.'

The intensity of these surface inversions, in tenths of degrees Celsius, is shown in Table 29. The inversion intensity seems to follow the same general pattern as the inversion depth: (1) the intensities are greater in East Antarctica than in West Antarctica, (2) the intensities are greatest in the Cold Central Core, where stations are at higher elevations, and (3) the inversions are much greater in 'midwinter' than they are in 'midsummer.'

Mean monthly surface inversion data were computed for Vostok for 1958 and 1960–1961 and for South Pole and Byrd stations for November 1958–October 1961 (Table 30). These data, averaged for three-year periods, show more vividly the difference between a high-elevation station in East Antarctica and a low-elevation station in West Antarctica. The mean annual surface inversion depth for Vostok (848 meters) is 1.7 times that for Byrd (498 meters), and the mean annual surface inversion intensity for Vostok (17.0°C) is nearly twice that for Byrd (8.6°C).

Some of the more intense inversions have occurred during either the cold months or at the end of a cold period. April was the coldest month of 1958 at South Pole, and the largest surface inversion of the year, 33.4°C (Figure 11), occurred on April 21. One of the steepest inversions close to the surface at South Pole occurred on April 2, 1958, when a temperature differential of 25.7°C occurred in the first 140 meters from the surface. The largest inversion at Vostok during 1960–1961 was one of 34.6°C on August 24, 1961. This inversion (Figure 11) extended through 1150 meters, although most of the inversion (33.7°C) was in the lowest 580 meters.

Wind speeds were averaged for the surface and the top of the inversion for South Pole for 1958 and for Vostok for 1960 (Table 31). These data, based on daily soundings, show that the wind speed at the top of the inversion is considerably higher than that observed at the surface. Soundings taken at Pionerskaya during the 'summer' months showed that the wind speeds aloft do not decrease within 3000 meters of the surface, which is well above the top of the inversion.

The surface inversion is a semipermanent characteristic of conditions in the planetary boundary layer of the Antarctic Plateau. An analysis of the 1960–1961 Vostok data revealed that the surface inversion was permanent for ten months (February through November), and an analysis of the 1958

TABLE 24. Bimonthly Albedo, South Pole, 1957–1958 (%)

	Cloudless	Overcast
Oct.–Nov.	77	84
Dec.–Jan.	74–83	80–88
Feb.–Mar.	87	93

TABLE 25. Midsummer Albedo, South Pole, 1957–1958 (%)

	Mean	Max.	Min.
Overcast	88	91	84
Cloudless	89	93	84

TABLE 26. Monthly Mean Radiation Balance of Short-Wave and Long-Wave Radiation, 1958 (in cal/cm²/hr)

	Jan.	Feb.	Mar.	April	May	June	July	Aug.	Sept.	Oct.	Nov.	Dec.
Vostok	0.3		−0.6	−0.6	−1.3	−0.9	−1.3	−0.9	−0.7	−0.6	0.6	1.6
Sovietskaya			−1.0	−0.8	−0.9	−1.1	−0.9	−1.3	−1.1	−0.8	0.7	1.8
Komsomolskaya	0.4	0.8	−0.3	−1.2	−2.4	−3.0	−2.8	−2.2	−2.4	0.8	0.8	1.7
Pionerskaya	2.0	1.1	−0.4	−1.1	−1.6	−1.7	−1.4	−1.6	−1.6	−1.2		1.5
South Pole	−1.5	−1.3	−2.6	−2.2	−2.3	−2.3	−2.4	−2.9	−1.2	−1.2	0.6	

South Pole data showed that the inversion was destroyed only once between January 26 and October 30. Figure 11 presents a sequence of four South Pole upper air temperature soundings (surface to 400-mb level) showing the destruction and reformation of the surface inversion in late July 1958. There was a 20°C surface inversion on July 25 at 2300 hours, when the wind speeds began to increase at the surface. The inversion had been destroyed by 0300 hours on July 28 as surface wind speeds reached a peak of 19 m/sec. The cold front passed the station on July 29 and the inversion quickly reformed.

This storm also passed over the four Soviet stations on the plateau. The temperature contrasts with the frontal passage were strong at those stations as well as at South Pole. There was a 24°C warming at South Pole, 27°C warming at Sovietskaya, 12°C warming at Vostok, 17°C warming at Komsomolskaya, and 20°C warming at Pionerskaya. With the passing of the cold front, the surface temperatures decreased by 13°C at South Pole.

Katabatic winds. The vertical thickness of katabatic winds extends to the top of the inversion. *Ball*'s [1960] nomogram for determining the katabatic force in terms of inversion strength and surface slope shows that katabatic forces exceed pressure gradient forces when the slope exceeds 2×10^{-3}. This is a slope of approximately 2.0 meters in a kilometer which is less than the delimiting value (1.75×10^{-2}) we have assigned to the Antarctic Plateau. *Tauber* [1960] believes katabatic wind speeds are 2 to 2½ times the pressure gradient wind. These figures appear to be of the proper magnitude when data from the Cold Katabatic and the Cold Central Core stations are compared.

There are several distinctive features about katabatic winds. The wind direction backs as one goes aloft into the inversion, and at the top of the inversion, which is also the top of the katabatic wind flow, winds are approximately 45 degrees from the surface wind direction. Katabatic winds may exhibit a great deal of gustiness. They also show a diurnal and seasonal effect, being much stronger and more frequent during the 'winter' than in 'summer' and at night than in day during the periods with daylight and darkness. Although cyclones infrequently penetrate the Antarctic Plateau, their passage along the coast can influence winds over the continent. Katabatic wind flow increases at most places after cyclones have advanced along the coast.

There is a definite foehn effect associated with the

TABLE 27. Monthly Mean Relative Humidity (%)

	Jan.	Feb.	Mar.	April	May	June	July	Aug.	Sept.	Oct.	Nov.	Dec.	Annual
Vostok (1958)	78	74	73	73	74	73	73	71	72	73	75	76	74
Sovietskaya (1958)	···	···	56	56	55	54	54	53	55	55	56	58	
Komsomolskaya (1958)	67	64	63	64	73	77	77	76	80	62	69	72	73
Vostok I (1957)	···	···	···	73	74	73	71	73	74	74	76	···	
Charcot (1958)	75	64	73	75	75	73	76	76	72	71	66	58	71
Pionerskaya (1957)	81	76	70	78	79	81	79	80	83	80	77	79	79
South Ice (1957)	···	···	80	80	81	84	85	74	74	78	71	72	
Byrd (1957–1959)	67	70	66	66	65	57	62	61	62	61	62	69	64

TABLE 28. Monthly Mean Depth of Surface Inversion (in meters)*

	Jan.	Feb.	Mar.	April	May	June	July	Aug.	Sept.	Oct.	Nov.	Dec.
1957												
Vostok I	...	...	...	...	...	...	810	686	778	816	883	...
1958												
Vostok	680	920	890	660	840	920	720	980	840	840	760	510
Sovietskaya	...	...	883	840	962	933	999	851	908	1018	697	494
South Pole	376	605	707	686	623	650	665	648	617	588	604	330
Pionerskaya	...	...	1012	857	...	...	...	...	...	950	800	620
Byrd	347	398	437	545	510	698	570	719	697	494	427	179
1959												
South Pole	414	529	697	624	719	620	584	578	602	556	...	...
Byrd	317	274	496	351	685	667	537	621	564	895	...	...
1960												
Vostok	582	909	854	910	981	1058	931	918	1030	844	739	432
South Pole	342	643	619	798	654	702	629	696	717	673	412	331
Byrd	433	472	520	424	561	556	678	656	550	506	452	258
1961												
Vostok	638	860	916	1081	1122	1031	903	1118	883	886	867	467
South Pole	294	659	718	714	630	602	687	629	739	568	...	...
Byrd	290	382	429	426	621	485	589	599	566	543	...	...

* Data presented as available.

TABLE 29. Monthly Mean Intensity of Surface Inversions (in °C)*

	Jan.	Feb.	Mar.	April	May	June	July	Aug.	Sept.	Oct.	Nov.	Dec.
1957												
Vostok I	...	...	...	...	...	...	19.8	16.0	11.7	8.0	5.3	...
1958												
Vostok	3.2	10.3	18.8	20.5	22.2	22.9	22.3	24.5	20.0	18.4	6.2	2.1
Sovietskaya	...	...	14.3	19.7	25.6	22.4	25.0	22.9	23.5	20.6	7.2	2.7
South Pole	3.2	9.0	19.9	25.8	19.2	23.2	16.6	22.7	18.1	15.1	7.9	3.1
Pionerskaya	...	...	11.6	11.0	...	...	...	...	...	8.7	4.4	2.4
Byrd	3.8	5.9	8.7	11.4	8.3	14.2	13.0	15.3	13.5	7.3	5.4	2.7
1959												
South Pole	3.5	9.7	20.7	21.1	20.8	23.6	22.1	20.8	22.5	15.7	...	...
Byrd	4.6	5.1	6.2	6.6	12.1	11.8	11.2	12.1	10.4	10.6	...	...
1960												
Vostok	3.7	12.3	19.4	24.6	23.6	24.6	22.8	26.7	22.6	15.0	7.9	3.0
South Pole	3.0	12.2	21.4	21.1	20.4	21.7	20.2	23.6	19.1	16.6	6.8	2.2
Byrd	5.7	6.6	8.7	12.4	11.3	8.7	9.3	13.6	11.4	7.9	4.3	4.1
1961												
Vostok	3.3	10.8	19.6	25.0	24.6	22.0	23.3	24.6	24.8	17.5	8.7	2.4
South Pole	4.1	11.4	22.0	25.8	23.8	18.7	20.9	20.9	22.1	14.7	...	...
Byrd	3.2	7.6	7.9	9.3	13.7	11.3	5.9	11.3	11.5	11.5	...	...

* Data presented as available.

TABLE 30. Mean Monthly Surface Inversion Data

	Jan.	Feb.	Mar.	April	May	June	July	Aug.	Sept.	Oct.	Nov.	Dec.
						Depth, m						
Vostok*	633	896	887	884	981	1003	851	1005	918	857	789	470
South Pole†	357	609	685	706	657	644	641	638	669	596	546	319
Byrd†	347	382	470	437	594	602	594	649	594	610	441	259
						Intensity, °C						
Vostok*	3.4	11.1	19.3	23.3	23.5	23.2	22.8	25.3	22.5	17.0	7.6	2.5
South Pole†	3.4	10.6	20.0	23.5	21.1	21.8	20.0	22.0	20.5	15.5	7.7	2.3
Byrd†	4.3	6.3	7.9	9.9	11.4	11.5	9.9	13.1	11.7	9.3	4.8	3.3

* 1958, 1960, 1961.
† Nov. 1958–Oct. 1961.

downslope movement of katabatic winds, since they warm according to the dry adiabatic lapse rate. East Antarctica is probably one of the best areas (and definitely the largest) in the world in which to study katabatic winds. During the IGY there was a line of stations (South Pole, Sovietskaya, Vostok, Komsomolskaya, Vostok I, Pionerskaya, and Mirnyy) extending from the geographical south pole to the coast. There is an elevation difference of 3660 meters from Sovietskaya to the coast, a distance of 1050 kilometers. Light downslope winds exist throughout the year at the three stations in the Cold Central Core. There is a slight katabatic wind at Komsomolskaya, which becomes more pronounced by the time it reaches Pionerskaya.

Pionerskaya had strong katabatic winds throughout the year. Forty-eight per cent of the winds were from 140°, and the mean annual wind speed was around 10.7 m/sec. South Ice also had strong katabatic winds from January through October, but they decreased in speed and frequency during the midsummer months of November through January. Charcot had a much greater spread of wind directions, as katabatic conditions broke down periodically throughout the year. This was particularly true of July 1958. During that month winds were recorded from 030° to 320°, owing, no doubt, to the closeness of Charcot to the coast (295 kilometers) and its position near one of the major storm tracks into the interior of the continent.

Wind direction versus temperature frequency distributions show the association of colder temperatures with winds from the higher elevations. This association was noticed during the year at South Pole (Table 32) and proved to be true at the other stations. South Pole temperatures during the sunless period were 10° to 15°C colder with winds blowing from the higher elevations in East Antarctica than when they were blowing from lower elevations in West Antarctica.

Windchill. Windchill is presented in this section on the interrelations of climatic elements, even though it is a single element as measured by the Davos Frigorimeter. There were no frigorimeters for measuring the cooling power of the atmosphere in the Antarctic during the IGY, although one has since been installed at South Pole. The limitation of this method is readily acknowledged, as it fails to consider radiation in any form. However, it presents a relatively good index of the severity of the antarctic climate during midwinter, when the Sun is below the horizon and there is no incoming shortwave radiation.

Windchill was computed from the Siple-Passel formula

$$K_0 = [(v \times 100)^{-1/2} + 10.45 - v](33 - T_A)$$

where K_0 is expressed in kilogram calories per m^2 per hour, v is wind speed in m/sec, and T_A is the ambient temperature of the air in degrees Celsius. This equation results in unrealistically small increases in windchill between 16 and 25 m/sec and even in decreasing windchill values after winds go above 25 m/sec. As Table 15 shows, however, maximum winds on the Antarctic Plateau are generally below this value.

Maximum windchills for the period of the IGY

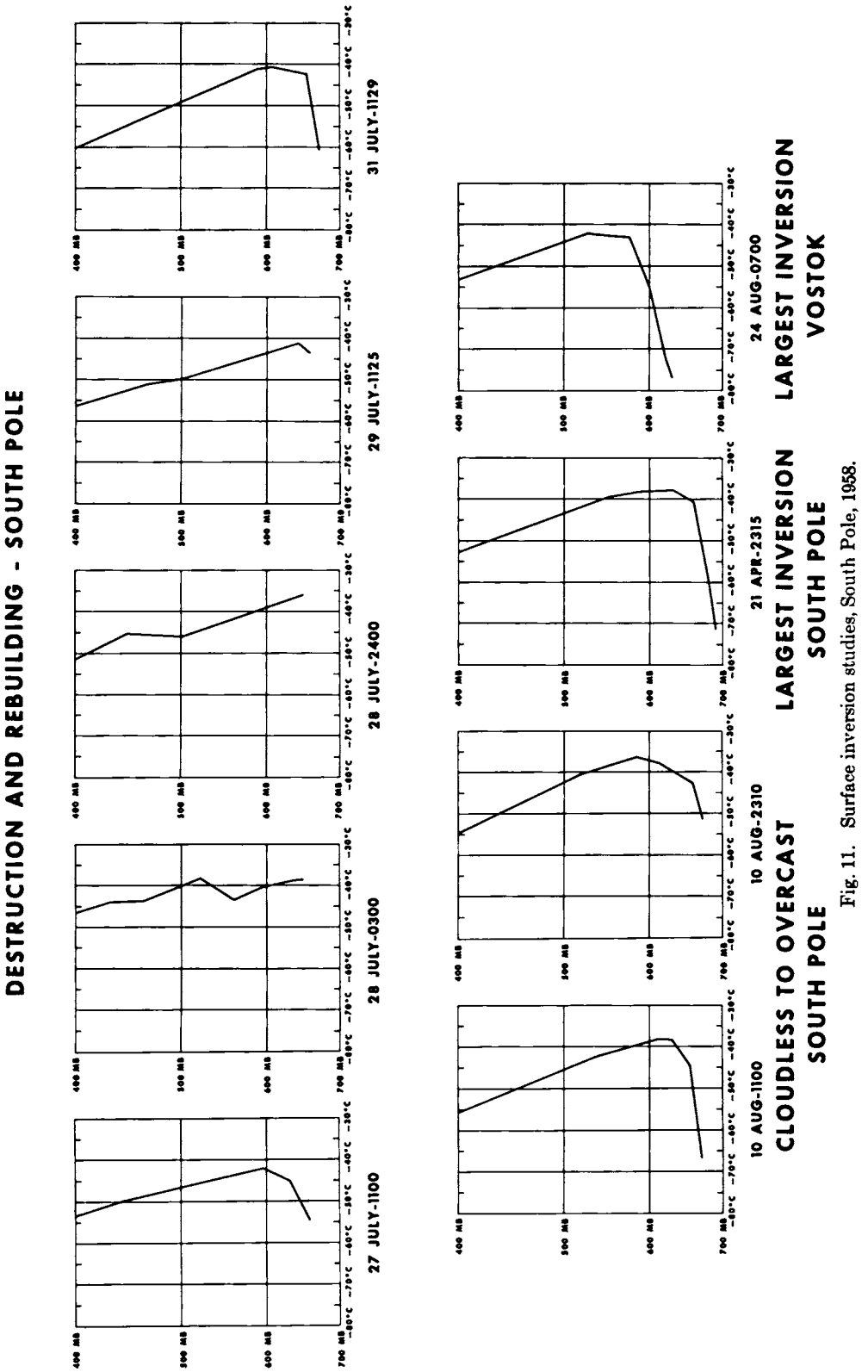

Fig. 11. Surface inversion studies, South Pole, 1958.

TABLE 31. Monthly Mean Inversion Wind Speed (in m/sec)

	Jan.	Feb.	Mar.	April	May	June	July	Aug.	Sept.	Oct.	Nov.	Dec.
South Pole, 1958												
Base of Inversion	4.9	4.5	6.0	5.8	8.4	6.8	8.4	6.5	6.4	7.0	4.3	3.9
Top of Inversion	8.5	7.2	7.8	6.9	10.9	1.1	11.9	9.1	11.6	9.0	7.0	4.3
Vostok, 1960												
Base of Inversion	4.8	6.0	6.3	5.1	4.5	5.1	4.6	4.8	5.3	5.8	4.4	5.3
Top of Inversion	8.2	6.0	8.4	6.7	8.2	9.1	10.2	9.1	8.1	9.0	4.9	7.5

are shown in Table 33. These windchills are much larger than any computed for any sites in the northern hemisphere, where the maximum computed windchill is 2650. The two low-elevation stations (South Ice at 1500 meters and Byrd at 1530 meters) have relatively low maxima, but the other stations have maxima between 3200 and 3400. The small variance in windchill maxima for stations on the Antarctic Plateau helps to substantiate the homogeneity of the area as a climatic region.

MICROCLIMATOLOGY OF THE SOUTH POLE[2]

Program. Temperature and wind profile measurements were taken by the writer in the Antarctic at Little America V in 1957 and at South Pole in 1958 as part of the USNC-IGY glaciology program. Wind speeds were measured by small 3-cup anemometers at six heights (25, 50, 100, 200, 400, and 800 cm), and temperature was measured by fine-gage thermocouples at nine heights (3, 6, 12, 25, 50, 100, 200, 400, and 800 cm), at surface, and at seven depths (−2, −5, −10, −25, −50, −250, and −800 cm). The top six heights were instrumented with both temperature and wind sensors, so that micrometeorological profile analyses could be made on the characteristics of the profile. Subsurface depths were selected so as to provide the necessary data for the computation of the heat flux in the snow.

Wind speed profiles. Lightweight plastic 3-cup anemometers with low starting and stalling speeds (around 0.2 m/sec) were used to measure wind speeds. A total of 1409 wind profiles, mostly of a

TABLE 32. Mean Temperatures for Observed Wind Directions at South Pole, Sunless Period, 1958

Wind Direction, °Long.	Frequency, %	Mean Temperatures, °C
67° W	0.1	−45.2
45 W	0.4	−46.3
22 W	1.1	−45.8
0	10.9	−52.2
22 E	32.5	−55.7
45 E	17.9	−58.1
67 E	14.1	−61.4
90 E	14.2	−62.4
112 E	7.0	−64.8
135 E	1.1	−64.3
157 E	0.1	−61.1
180 E	0.1	−54.9
135 W	0.1	−53.5
Calm	0.5	−57.2

[2] See *Dalrymple et al.* [1966].

TABLE 33. Maximum Windchill

Station	Hourly Temperature, °C	Hourly Wind Speed, m/sec	Hourly Windchill, kg cal/m²/hr
Vostok	−64	13	3250
	−74	7	3200
	−87	4	3174
Sovietskaya	−69	8	3134
	−77	6	3183
	−83	5	3226
Komsomolskaya	−74	7	3200
South Pole	−71	9.8	3323
	−71	10.3	3353
South Ice	−53	20.6	3031
Pionerskaya	−62	14	3218
Charcot	−60	18	3254
Byrd	−55	10.3	2837

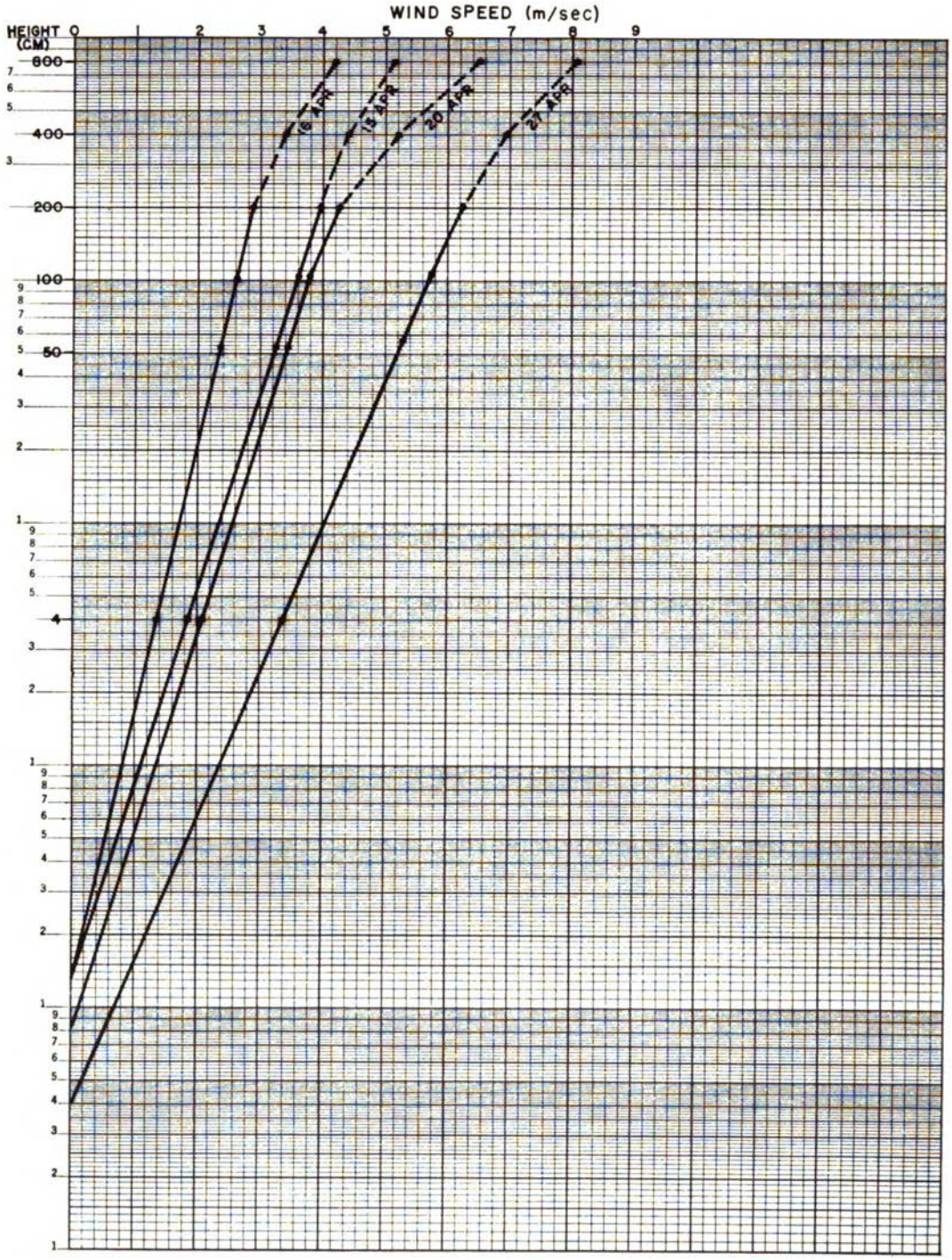

Fig. 12. Selected wind profiles.

TABLE 34. Monthly Mean Wind Speed Profiles (height, cm; speed, cm/sec)

	No. of Profiles	Ht.	Speed	Ht.	Speed	Ht.	Speed	Ht.	Speed	Ht.	Speed
Jan.	67	49.1	529.0	99.1	577.1	199.1	619.6	399.1	666.1	799.1	712.8
Feb.	83	44.0	296.8	94.0	328.0	194.0	359.7	394.0	398.8	794.0	458.0
Mar.	83	43.3	344.2	93.3	382.7	193.4	422.3	394.1	483.8	797.3	569.9
April	83	53.8	340.6	103.8	373.1	203.8	412.8	404.8	479.0	804.0	573.6
May	70	56.0	553.0	106.0	600.1	206.0	651.8	406.0	719.0	806.0	797.2
June	96	49.0	470.9	99.0	519.9	199.0	575.4	399.0	636.2	799.0	728.7
July	106	49.2	589.5	98.7	649.7	198.7	705.5	390.1	774.3	790.1	858.5
Aug.	129	47.9	417.3	99.2	464.7	194.4	515.3	385.1	573.6	785.6	663.0
Sept.	137	44.7	530.8	96.5	554.8	189.5	660.5	381.1	694.8	781.4	779.4
Oct.	133	42.6	517.8	92.6	559.8	185.6	605.9	382.6	670.9	776.6	755.0
Nov.	86	47.4	369.4	97.4	398.8	194.7	431.5	393.5	469.1	791.2	514.8

1-hour duration, were measured at South Pole in 1958. These were broken down into 5 m/sec classes as follows: 0–5 m/sec (as determined at 8-meter height), 317 profiles; 5–10 m/sec, 919 profiles; 10–15 m/sec, 166 profiles; and 15–20 m/sec, 7 profiles. The distribution of profiles is representative of the Cold Interior but is not representative of the Cold Central Core (lower winds) or the Cold Katabatic or the Cold Transitional (both having higher winds). The number of profiles measured was governed by the wind speed, shape of the profiles, and total revolutions of the counters. (The wind counter system utilizing Sodeco counters was the first one engineered by Beckman and Whitley, and there were some doubts as to the life expectancy of the counters.) There was good climatological coverage; profiles were measured on 303 of the 326 days between January 1 and November 28, 1958. Daily observations were measured on 201 consecutive days between May 5 and November 22. Altogether there were 1214 hours of simultaneous wind temperature profiles; only 670 of these were selected for micrometeorological analyses. The Quartermaster Research and Engineering Command has published a data report [*Dalrymple*, 1961] which includes 1163 hourly wind profiles from South Pole.

Midsummer profiles were logarithmic from the lowest level to the top. Logarithmic profiles were obtained during midwinter when the lowest set of cups was as low as 4 cm. The logarithmic nature of the profile decreased as stability increased with 'winter,' and profiles were only logarithmic to about 2 meters. Individual plots are shown in Figure 12. The curvature of the profile plot above 2 meters indicates the existence of a strong surface inversion. Profiles under lapse conditions in winter tend to return to a logarithmic relationship.

Monthly mean wind speed profiles were computed for all runs of 1 hour or more when all wind channels were functioning properly. These data are shown in Table 34. Monthly mean wind profiles were plotted on semilog paper for four of these months (January, February, April, and July) in 1958 (Figure 13). January is an example of a 'midsummer' month with logarithmic conditions to 8 meters; February is an example of a transition month with logarithmic conditions extending only to 4 meters; April is an example of strong stability and shows the profile curvature at around 2 meters; July is an example of a windy month when the stable conditions were not so pronounced. Individual hourly profiles with light winds may find the maximum wind speeds (<4 m/sec at 8-meter height) at 4 meters or even at 2 meters. Monthly mean profiles show, however, a systematic increase in wind speeds for all heights. One can estimate with a fair degree of accuracy which months were the coldest and the warmest in winter from the mean wind speeds. During 1958, April had a monthly mean temperature of $-62.1°C$, May of $-56.9°C$, June of $-61.1°C$, July of $-55.1°C$, and August of $-61.7°C$. In all these months, there is a definite relationship between wind speed and temperature, with the lowest temperature being associated with the lightest wind speed and the higher temperature with the highest wind speed.

The approximate roughness length of the snow

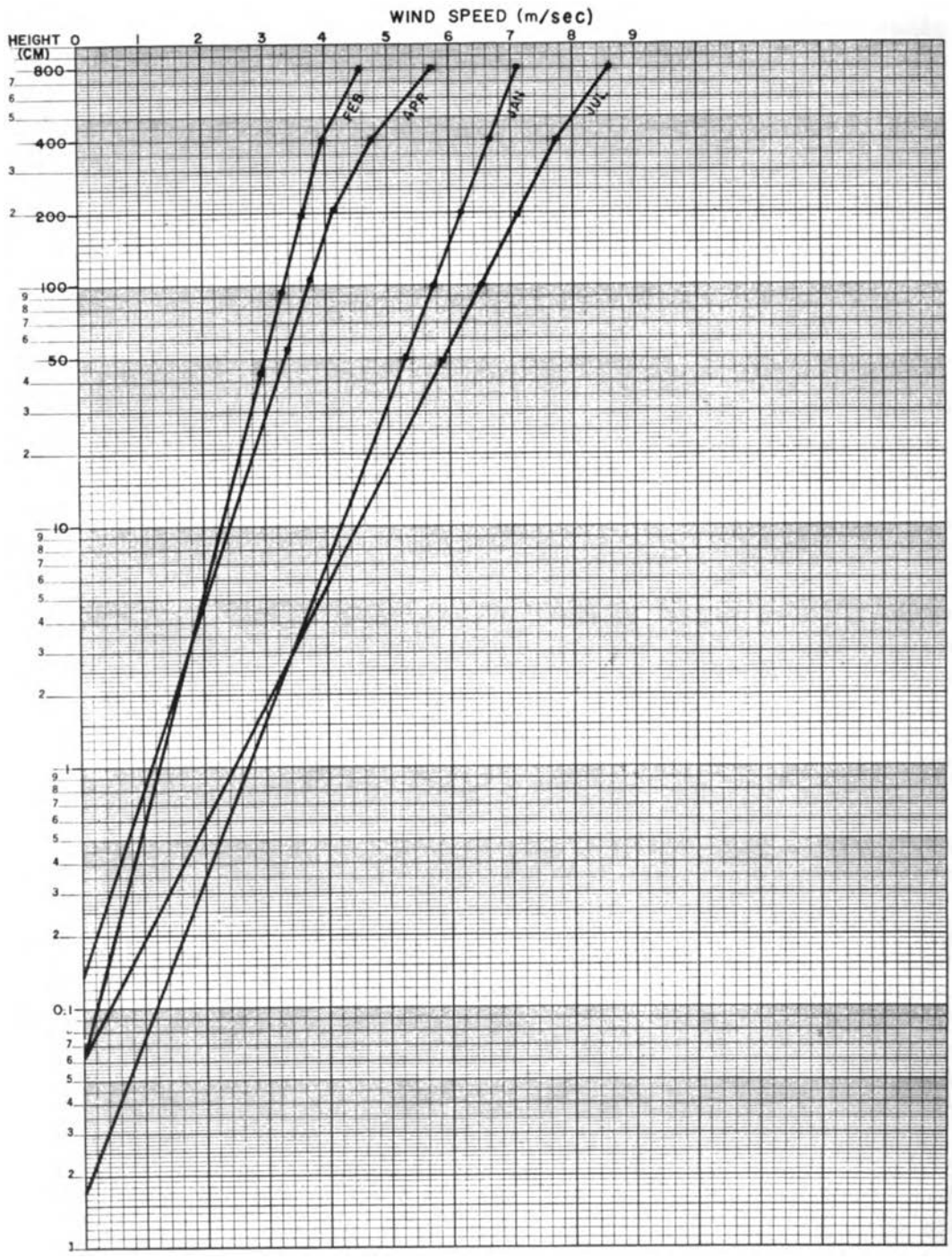

Fig. 13. Monthly mean wind profiles.

TABLE 35. Monthly Mean Temperatures at South Pole, 1958 (in −°C)

	Surface and Above, cm									
	Surface	3	6	12	25	50	100	200	400	800
Feb.	36.20°	36.03°	36.18°	36.37°	36.47°	36.45°	36.40°	36.38°	36.23°	35.95°
Mar.	56.05	55.70	55.68	55.63	55.59	55.56	55.39	55.25	54.92	54.29
April	64.11	63.66	63.57	63.50	63.44	63.36	63.23	63.09	62.80	62.00
May	59.78	59.03	58.60	58.40	58.34	58.18	58.02	57.88	57.61	57.03
June	63.29	63.10	62.16	61.80	61.68	61.58	61.42	61.30	61.03	60.53
July	59.43	58.95	58.82	58.66	58.57	58.45	58.32	58.19	57.99	57.53
Aug.	63.95	63.33	63.12	62.92	62.81	62.71	62.58	62.42	62.18	61.43
Sept.	60.72	60.18	59.21	58.72	58.52	58.39	58.27	58.08	57.75	56.99
Oct.	49.97	49.34	49.56	50.06	50.01	49.96	49.91	49.77	49.61	49.23
Nov.	37.71	38.64	38.99	39.17	39.20	39.18	39.11	39.10	39.03	38.95

	Subsurface, cm						
	−800	−250	−50	−25	−10	−5	−2
Feb.	51.79°	43.56°	35.90°	35.89°	36.16°	36.58°	36.75°
Mar.	51.41	44.16	48.38	49.59	52.64	54.80	56.16
April	50.69	47.03	57.40	58.61	61.20	62.93	63.88
May	50.28	50.23	56.95	57.88	58.69	59.10	59.31
June	50.16	51.52	59.03	61.11	62.03	62.56	62.87
July	50.25	52.75	56.89	57.31	57.58	57.86	58.05
Aug.	50.37	53.28	59.30	62.00	63.01	63.34	63.87
Sept.	50.56	53.94	57.63	58.33	58.85	59.44	59.72
Oct.	50.56	53.71	53.44	51.75	51.28	50.94	50.83
Nov.	50.98	52.98	46.13	42.14	40.69	39.77	39.22

surface is given by the height of the intersection of the wind profile plot on the ordinate. Roughness lengths are known to vary from approximately 0.001 cm for very smooth surfaces such as ice and mud flats to as much as 9 cm for thick grass 50 cm high. *Liljequist*'s [1956, 1957] average value for Maudheim for 1950–1951 was 0.012 cm. A mean roughness length of 0.014 cm was computed mathematically for South Pole.

Temperature profiles. Temperature profiles were recorded on a more or less continuous basis. A certain amount of record was lost when subsurface thermocouples had to be reset in the snow, when arms had to be raised on the mast, when charts had to be changed, when the range and zero of the recorder had to be checked, when the ice bath had to be refreshed, and during electronic maintenance. From the time when the recorder was officially put into operation (1900 hours, February 3, 1958) until it was secured (2336 hours, November 22, 1958), it was operative 83.5% of the time. The data collected have all been reduced, and mean hourly and mean daily temperatures for all depths and for all heights have been computed and published by the Quartermaster Research and Engi-

TABLE 36. Maximum Monthly Inversions, 1958

	8 Meters, °C	Raobs, °C
January	M	11.3
February	8.1	16.9
March	9.4	30.0
April	14.7	33.4
May	10.2	28.8
June	10.8	28.9
July	11.0	27.8
August	13.0	30.1
September	14.1	30.2
October	8.9	24.6
November	8.9	14.7

M = missing data.
Raobs = radiosonde observations.

neering Command [*Dalrymple*, 1961]. These data were carefully screened, and all questionable data were rejected. The wind and temperature profiles represent the only set of such data ever obtained in the interior of Antarctica.

Monthly mean temperature profiles (Table 35) were computed for all depths, surface, and nine heights, February through November. Over 1,790,000 temperature values were recorded during the year. The month of March had 12,599 or more observations for all depths or levels. The minimum number of observations used for any monthly mean was 5,464 observations (3 cm in September). There were fewer observations for the surface, 3 cm, and 6 cm, as these were the levels most frequently overrun by sastrugi and drifting snow, and such cases have been thrown out. Approximately 27% of the surface and 3-cm observations in September were rejected for this reason. The profiles for the sunless period are considered good to excellent; profiles for the period with Sun, particularly November and February, readily show the influence of solar radiation below 25 cm. The radiation error seemed to be confined to surface, 3, 6 (all unshielded), and 12 (shielded) cm, although one must remember that there were no 'midsummer' observations in December and January.

The subsurface mean temperatures appear to be quite good throughout the 10 months of record. The two deep thermocouples (—250 and —800 cm) were left in place throughout the year, and the depths of the other thermocouples were regulated to maintain their original established depths. This was made possible by the use of long-stemmed protected rod probes which could be easily set at the correct depths while still maintaining close contact with the snow.

The temperature profiles for the seven months

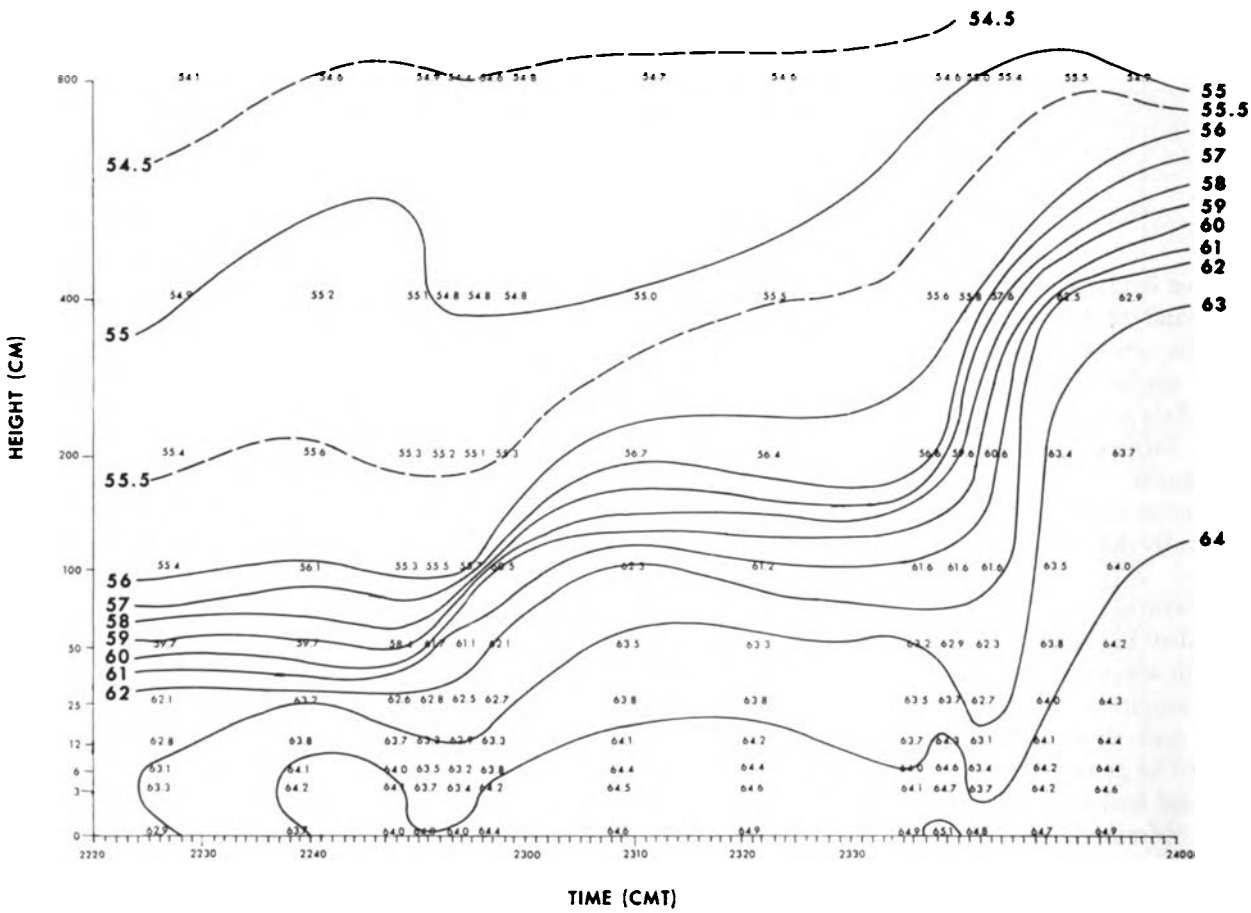

Fig. 14. Upward progression of temperature inversion, South Pole, May 7, 1958.

that have no Sun or only a short period of Sun (March through September) are all colder at the surface and show a gradual warming with height. September, the second coldest month, shows the largest temperature differential between the surface and 800 cm, 3.73°C. As one would expect, July, the windiest month in 1958, had the smallest temperature increment, 1.90°C. The greatest temperature differences were (1) between the surface and 3 cm, where the surface temperature reading tended to reflect that of the snow and the 3-cm reading that of the air layer immediately above the snow, and (2) between 400 and 800 cm where the main part of the inversion appeared to be concentrated. Temperatures to a depth of —50 cm reflected conditions at the surface. The deeper thermocouple readings experienced a pronounced temperature lag, with the coldest temperature at —250 cm occurring in September and at —800 cm during midsummer.

A detailed study of temperature in the environmental layer of the atmosphere allows a closer inspection of the inversion where the rate of warming is at its maximum. (Environmental layer is defined by the writer as that part of the atmosphere next to the snow surface in which man and his vehicles must operate.) Relatively steep surface inversions occurred within 8 meters of the surface from February through October. The largest monthly inversions measured on the mast and also from radiosonde observations are shown in Table 36. There were three inversions greater than 11°C in the first 8 meters: 14.7°C in April, 14.1°C in September, and 13.0°C in August. Temperature changes in the first meter generally were small, being less than 1°C most of the year. There were noticeable exceptions, however; e.g., in an early May inversion, there was a 4.2°C warming from 25 to 50 cm and, 3 minutes later, a 10.3°C warming from 50 to 100 cm. Occasionally, very steep gradients existed close to the snow surface. In June, during a period with 8 m/sec of wind at 2 meters, a 2.6°C difference (warming) occurred between the surface and 3 cm.

Inversions within the lowest 8 meters are most interesting, and the steepest inversions often occur during cold periods when there are rapid temperature changes at all heights in the environmental layer. There appear to be no set criteria for the formation or destruction of inversions. Inversions usually form slowly over a period of hours or even days but can be destroyed in a matter of minutes by high winds or in a few hours by the advancement of an overcast. The only total destruction of the surface inversion at South Pole during the 1958 'winter' occurred during the strongest frontal passage of the winter (see Figure 11). There was a 20°C inversion on July 25 at 2300 hours, when the wind speeds began to increase at the surface. The inversion had been destroyed by 0300 hours on July 28 as winds reached a peak at 19 m/sec. The cold front went through on July 29, and the inversion quickly reformed. A surface inversion was partly destroyed when a cloudless sky became overcast in a half-day (Figure 11). An 8-meter inversion of 9.4°C was reduced to an inversion of 1.1°C in one

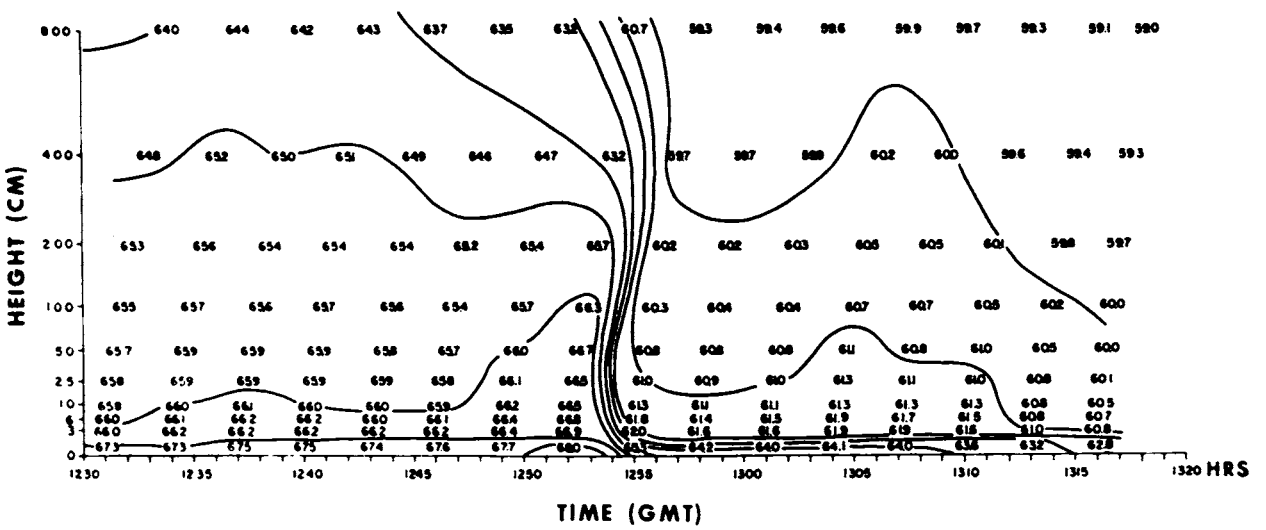

Fig. 15. Rapid change of temperature (in —°C), South Pole, May 8, 1958.

hour in early March when a cloud cover moved over the station. An 8-meter inversion of 3°C existed for several days in May, when winds were as high as 11 and 12 m/sec.

The first indication of the formation of an inversion is generally a warming at the 8-meter height. Subsequent warming occurs at lower levels as the inversion strengthens. There are few instances where temperature differences greater than 5°C existed between levels below 50 cm. There were, however, many inversions that strengthened in the lower levels and then progressed upward to 8 meters. One such instance was on May 7 (Figure 14). The square root of the height of the thermocouples is used for the vertical scale, and the horizontal scale is a linear time scale. The total 8-meter inversion at 2355 hours was 10.0°C. Conversely, there are relatively few instances of large temperature differentials at 8 or 4 meters descending toward the surface.

Rapid temperature changes in the lowest 8 meters are relatively common, and one of the most rapid occurred in early May during inversion conditions (Figure 15). Sixteen complete profiles are shown of above-surface temperature readings covering a 46-minute period. The abrupt temperature change was experienced at all levels on the micrometeorological mast. A 5°C warming occurred from 3 to 200 cm in approximately 3 minutes. The rapidity of this warming made it all the more interesting. The rapid response of thermocouples, plus a multipoint recorder, resulted in an excellent record of this rapid temperature change. There were no changes in sky condition, wind direction or speed, or barometric pressure. It is believed that this rapid change was the result of subsidence.

REFERENCES

Alt, J., Some general considerations of meteorology in the Antarctic (in French), in *La Météorologie*, pp. 18–41, 1960.

Alt, J., P. Astapenko, and N. J. Ropar, Some aspects of the antarctic atmospheric circulation in 1958, in *IGY Gen. Rept. 4*, National Academy of Sciences, World Data Center A, Washington, D. C., 1959.

Astapenko, Paul D., *Atmospheric Process in the High Latitudes of the Southern Hemisphere* (in Russian), 282 pp., Academy of Sciences, USSR, Moscow, 1960.

Ball, F. K., Winds on the ice slopes of Antarctica, in *Antarctic Meteorology*, pp. 9–16, Pergamon Press, New York, 1960.

Bogoslovsky, V. N., Temperature regime and movement of antarctic ice sheet (in Russian), in *Second Continental Expedition, 1956–1958*, vol. 10, pp. 114–140, Leningrad, 1960.

Bugaev, V. A., Climatic zones of Eastern Antarctica and the Southern Ocean (in Russian), *Meteorol. i Gidrol., 3*, 3–10, 1960.

Cameron, Richard L., and Richard Goldthwait, The U.S.-IGY contribution to antarctic glaciology, *IUGG Publ. 55*, pp. 7–13, Gentbrugge, 1961.

Cameron, Richard L., Olav Løken, and John Molholm, USNC-IGY antarctic glaciological data, field work, 1957 and 1958, unpublished report, 1959.

Crary, Albert P., The Antarctic, *Sci. Am., 207*, 60–73, 1962.

Dalrymple, Paul C., South Pole micrometeorology program, 1, Data presentation, *U. S. Army, Quartermaster Research and Engineering Tech Rept. ES-2*, pp. 1–388, 1961.

Dalrymple, Paul C., Heinz H. Lettau, and Sarah H. Wollaston, South Pole micrometeorology program: Data analysis, *this volume*, 1966.

Dolgushin, L. D., Zones of snow accumulation in Eastern Antarctica, *IUGG Publ. 55*, pp. 63–70, Gentbrugge, 1961.

Gow, Anthony J., The ice sheet, in *Antarctica*, edited by T. Hatherton, New Zealand Antarctic Society, Methuen, London, 1965.

Hanson, Kirby J., Radiation measurements on the antarctic snowfield, A preliminary report, *J. Geophys. Res., 65*, 935–946, 1960.

Hoinkes, Herfried, Studies of solar radiation and net radiation in the Antarctic, *Arch. Meteorol. Geophys. Bioklimatol. B, 10*, 175–181, 1960.

Kopanev, I. D., *Snow Cover of the Antarctic* (in Russian), 142 pp., Hydrometeorologic Press, Leningrad, 1960.

Lettau, Heinz H., A case study of katabatic flow on the Antarctic Plateau surrounding the south pole, Symposium on Polar Meteorology, McGill, University, July 7–19, 1963.

Liljequist, Gosta H., Energy exchange of an antarctic snowfield, part A; Short-Wave radiation, part B; Long-Wave radiation and radiation balance, part C; Wind structure in the low layer, part D; in *Surface Inversions and Turbulent Heat Transfer*, pp. 1–298, Norsk Polarinstitütt, Oslo, 1956, 1957.

Mellor, Malcolm, *The Antarctic Ice Sheet*, pp. 1–50, U.S. Army CRREL, Hanover, 1961.

Piciotto, E., and G. Crozaz, Rate of accumulation of snow at the south pole as determined by radioactive measurements, *Nature, 203*(4943), 393–394, 1964.

Portman, D. J., Some heat transfer characteristics of two thermocouple probes, unpublished report, University of Michigan, 1961.

Rastorguev, Vladimir J., and J. A. Alvarez, Description of the antarctic circulation observed from April to November 1957 at the IGY Antarctic Weather Central Little America Station, *IGY Gen. Rept. 1*, pp. 1–10, World Data Center A, National Academy of Sciences, Washington, D. C., 1958.

Robin, Gordon de Q., The ice of the Antarctic, *Sci. Am., 207*, 132–146, 1962.

Rubin, Morton J., Atmospheric advection and the antarctic mass and heat budget, in *Antarctic Research, Geophysical*

Monograph 7, pp. 149–159, American Geophysical Union, Washington, D. C., 1962.

Rubin, Morton J., and Mario Giovinetto, Snow accumulation in central West Antarctica as related to atmospheric and topographic factors, *J. Geophys. Res., 67*, 5163–5170, 1962.

Sabbagh, Michael E., A preliminary regional dynamic climatology of the antarctic continent, *Erdkunde, 16*(2), 94–111, July 1962.

Sabbagh, Michael E., Seasonal and regional variations of temperature over the antarctic continent during 1958, *Geografiska Ann., 45*(1), 1963.

Tauber, G. M., Characteristics of antarctic katabatic winds, in *Antarctic Meteorology*, pp. 52–64, Pergamon Press, New York, 1960.

Wexler, H., Growth and thermal structure of the deep ice in Byrd Land, Antarctica, *J. Glaciol, 3*(30), 1075–1087, 1961.